UNIVERSITY OF SOUTHAMPTON

FACULTY OF NATURAL AND ENVIRONMENTAL SCIENCES

Chemistry

Polyphosphate Kinase from Intracellular Pathogens as a Novel Antibacterial Target

by

Mariacarmela Giurrandino

Thesis for the degree of Doctor of Philosophy

May 2017

UNIVERSITY OF SOUTHAMPTON

ABSTRACT

FACULTY OF NATURAL AND ENVIRONMENTAL SCIENCES

Chemistry

Thesis for the degree of Doctor of Philosophy

Polyphosphate Kinase from Intracellular Pathogens as a Novel Antibacterial Target

Mariacarmela Giurrandino

To circumvent the established mechanisms of bacterial resistance towards the available antibiotics, previously unexploited pathways critical for bacterial survival and pathogenicity must be targeted. Polyphosphate metabolism plays a crucial role in bacterial survival, in the expression of several virulence factors, in bacterial persistence and in the adaptation to stress conditions. The bacterial enzyme polyphosphate kinase (PPK) catalyses the reversible synthesis of polyphosphate by the transfer of a phosphate unit from ATP onto the growing polyphosphate chain. The presence of PPK in the genome of many pathogens and the attenuation of virulence observed in *ppk* deletion mutants make the PPK a potential target for the development of a new class of antibiotics.

The objective of this project has been the biochemical characterization of PPK2 from *Francisella tularensis* (*Ft*PPK), the discovery of potential inhibitors and their evaluation as antibacterial agents. Using recombinant *Ft*PPK and firefly luciferase, a coupled assay was developed to measure the *Ft*PPK activity and further optimised to produce a robust assay in a format suitable for high throughput screening (384 well plate, Z'=0.70). The optimised *Ft*PPK- luciferase coupled assay was used to characterize the kinetic properties of *Ft*PPK and for the screening of two small libraries: a protein kinase inhibitor library (Protein Kinase Inhibitor Set, released by GSK), and a nucleotide analogue library (Reynolds library). The

screening yielded 27 and 34 initial hits, respectively. The hits were validated by independent luminescence assay, thermal shift assay and HPLC assay. The most potent hit was re-synthesised for detailed characterization. IC_{50} and preliminary mode of inhibition have been investigated and, in conjunction with some preliminary SAR and with the modelling in the *Ft*PPK active site, provide a starting point for later medicinal chemistry optimisation.

.

Table of Contents

List of tables

List of figures

Declaration of Authorship

I, Mariacarmela Giurrandino, declare that this thesis and the work presented in it are my own and has been generated by me as the result of my own original research:

Polyphosphate Kinase from Intracellular Pathogens as a Novel Antibacterial Target

I confirm that:

1. This work was done wholly or mainly while in candidature for a research degree at this University;
2. Where any part of this thesis has previously been submitted for a degree or any other qualification at this University or any other institution, this has been clearly stated;
3. Where I have consulted the published work of others, this is always clearly attributed;
4. Where I have quoted from the work of others, the source is always given. With the exception of such quotations, this thesis is entirely my own work;
5. I have acknowledged all main sources of help;
6. Where the thesis is based on work done by myself jointly with others, I have made clear exactly what was done by others and what I have contributed myself;
7. None of this work has been published before submission

Signed:

Date:

Acknowledgements

I would like to thank Prof. Peter Roach, my supervisor, to whom I am deeply grateful for giving me the chance to turn timid ambitions into fulfilments. I would like to thank him for the guidance and the criticisms, all of which have contributed to my scientific and personal growth, and also for being capable of providing warm moral support when the journey toughened.

I would like to thank Prof. Petra Oyston, for the fascinating insights into the microbiology world, and Prof. Bruno Linclau for the greatly appreciated advice on the chemistry. A big thank you goes also to the members of the Roach group, with whom I have shared this adventure. Particularly, to Alice Parnell and Pedro Dinis, who were there from the very beginning to the very end.

And then to the heart. Words could never adequately express my gratitude to Jack Hardwick, for giving me strength and confidence in fighting to reach my goals, for pulling me together in moments of crisis, for introducing me to beer, for delighting me every single day with bubbly cheerfulness and extraordinary wit (often to my expense).

And finally to the soul, who has never left the island and never will. Short but incredibly essential have been the therapeutic and refreshing retreats to the island, embraced by the endlessly care of my family. Thank you to my untie Maria, who is a never ending source of sweetness and love, to my grandma Pippina, who seeded in the child I was the love for the studies, to my brother Daniele who is always caringly ready to provide support by all possible means.

I owe who I am and what I have become to Franco and Pinuccia, my parents, who have devoted their life to mine and my brother's accomplishment. It is most precious to me their unconditional trust and no days go without the appreciation of how generous they were in encouraging me to chase my ambitions, despite the expensive price of the distance.

The greatest pride I take in graduating as a *Philosophiae Doctor* comes from the pride that this gives to my family, who is my safe harbour. This work is dedicated to them.

Definitions and Abbreviations

2x YT	2x Yeast extract and Tryptone
^{31}P-NMR	Phosphorous Nuclear magnetic resonance
Abs	Absorbance
CAN	Acetonitrile
APS	Ammonium persulfate
ADP	Adenosine diphosphate
ATP	Adenosine triphosphate
BSA	Bovine serum albumin
cca.	*circa* or approximately
DAPI	4',6-diamidino-2-phenylindole
DI	De-Ionisised
DMHA	Dimethylhexylamine
DTT	Dithiothreitol
E. coli	*Escherichia coli*
EDTA	Ethylenediaminetetraacetic acid
Eq	Equivalent
Eq.	Equation
FLuc	thermostable *Photinus pyralis* firefly luciferase
FP	Fluorescence polarisation
FPLC	Fast Protein Liquid Purification
FRET	Förster resonance energy transfer
*Ft*PPK	*Francisella tularensis* polyphosphate kinase
F. tularensis	*Francisella tularensis*
His6-tag	Polyhistidine tag
HGT	Horizontal gene transmission
HPLC	High Pressure Liquid Chromatography
HTS	High Throughput Screening
kDa	kilo Dalton
K_d	Dissociation constant
K_i	Dissociation constant
K_m	Michaelis-Menten constant

kw	kinetic window
IDA	Iminodiacetic acid
IPTG	Isopropyl-◎-D-thiogalactopyranoside
ITC	Isothermal titration calorimetry
LC	Liquid chromatography
LC-MS	Liquid chromatography–mass spectrometry
MDR	Multidrug resistant
min	minute
mol	mole
M. ruber	*Meiothermus ruber*
*Mr*PPK	*Meiothermus ruber* polyphosphate kinase
MRSA	Methicillin resistant Staphylococcus aureus
MS	Mass spectrometry
MSC	Microbiology safety cabinet
MWCO	Molecular weight cut-off
NMR	Nuclear Magnetic Resonance
μmol	micromole
nmol	nanomole
PBP	Penicillin-binding protein
P_i	Inorganic phosphate
PKIS	Published Kinase Inhibitor Set
PolyP	Polyphosphate
PPX	Polyphosphate exopolyphosphatase
P. pyralis	*Photinus pyralis*
P. aeruginosa	*Pseudomonas aeruginosa*
R_f	Retention factor
RFU	Relative fluorescence units
RL	Reynolds library
RLU	Relative luminescence units
RP	Reverse phase
SD	Standard deviation
SDS	Sodium dodecyl sulphate

SDS-PAGE	Sodium Dodecyl Sulphate Polyacrylamide Gel Electrophoresis
sec	seconds
SHX	Serine Hydroxamate
S meliloti	*Sinorhizobium meliloti*
*Sm*PPK	*Sinorhizobium meliloti* polyphosphate kinase
SOC	Super optimal broth with catabolic repressor
SPR	Surface plasmon resonance
st	standard
S75	Superdex 75 resin
TAE buffer	Tris Acetate EDTA buffer
TBAH	Tetrabutyl ammonium hydroxide
TBAHS	Tetrabutyl ammonium hydrogen sulfate
TEA	Triethyl ammonium hydrogen sulfate
TEAA	Triethyl ammonium acetate
TEMED	Tetramethylethylenediamine
TLC	Thin layer chromatography
T_m	Melting temperature
UHPLC	Ultra high pressure liquid chromatography
V_{max}	Maximum velocity
VRE	Vancomycin resistant enterococci
XDR	Extensively drug-resistant
+ve cntr	Positive control
-ve cntr	Negative control

Chapter 1

Introduction

1.1. Antibiotics: the Need to Fill the Void

Antibiotic resistance has been declared as one of the three major threats to public health by the World Health Organization (WHO),[1] which has called for a joint international action to safeguard the resources available and to promote research for the development of new antibacterial agents.[2,3] Resistance has been detected for all the classes of available antibiotics,[4] with the phenomenon evolving in many cases in multi-drug resistance (MDR, Table 1.1).[5–7] Diseases that were eradicated, or considered to be under control, are now re-emerging and an increasing number of infections caused by MDR bacteria that cannot be treated has been registered.[8] Widespread antibiotic resistance not only impacts the duration of illness and the increase in mortality, but also significantly affects the cost of public health and threatens the prevention of infections during various medical practices, such as invasive surgery, the use of immunosuppressive drugs and organ/tissue transplants.[8–10]

Bacteria resistance can be attributed to genetic mutations that provide advantages for survival under selective pressure, such as in the presence of antibiotics.[7] The appearance of resistance pre-dates the discovery of antibiotics, as proven by the identification of resistance genes in the genomes of ancient microorganisms.[11] Nonetheless, the spread of bacteria resistance has been boosted by massive exposure to antibiotics,[12] due to the extensive use and misuse not only in the public health sector but also in farming and agriculture.[8,13,14]

The problem is being exacerbated by the limited success of the pharmaceutical industry in delivering new classes of antibiotics in the past decades, despite the promises held by

advances in recombinant DNA technology, structural biology and high throughput technology.[10,15–20]

Table 1.1: Multidrug resistant bacteria

	Notorious MDR bacteria responsible for common nosocomial infection
Gram positive	Methicillin-resistant *Staphylococcus aureus* (MRSA), vancomycin-resistant enterococci (VRE), *Clostridium difficile*[21]
Gram negative	MDR *Pseudomonas aeruginosa, Acinetobacter baumannii, Escherichia coli* and *Klebsiella pneumoniae*[6,9,22,23]
Mycobacteria	MDR and the extensively drug-resistant (XDR) *Mycobacterium tuberculosis* [24,25]

Because of the high costs of these unsuccessful campaigns, industry has mainly withdrawn from the field or shifted to safer strategies such as focusing on "best-in-class" drug development, which consists of improving the potency of existing antibiotics or enlarging the spectrum by modification of known compounds active on consolidated targets.[26,27] The latter approach provides very little potential for the development of new antibacterial agents capable of circumventing bacteria resistance, which has emerged towards all the mechanisms targeted by all classes of antibiotics currently in use.[28] Therefore, despite the greater challenges and the high risk of failure, the development of new-target antibiotics (first class antibiotics) remains the best option to address the problem of bacteria resistance.[14,29]

1.1.1. Antibiotics: mechanisms of action, discovery and development

Current antibiotics target a limited number of pathways involved in the structural integrity of the bacteria cell during growth and replication (Figure 1.1, Table 1.2),[30] resulting in either a bactericidal (bacteria death) or bacteriostatic effect (growth suppression or attenuation).[31] The latter distinction is often not binary, and some bactericidal antibiotics may display bacteriostatic effects towards either some specific microorganisms or at lower concentrations.[31] Antibiotics disrupting biosynthesis of the cell wall (β-lactams, vancomycin, fosfomycin, bacitracin), or interfering with the integrity of the cell membrane (polymyxins, daptomycin), tend to exert a bactericidal effect.[32] Other antibiotics with bactericidal properties are the quinolones, which form a stable complex with the topoisomerase and the cleaved DNA, eventually leading to the arrest of the DNA replication machinery and the activation of stress responses and to compromised viability.[32] Bacteriostatic activity is instead mostly displayed by antibiotics targeting protein synthesis, such as tetracyclines, macrolides and chloramphenicol.[10,31] A notable exception is the aminoglycoside family, which cause alteration of the membrane structural integrity due to the generation of cytotoxic mistranslated peptides.[33,34]

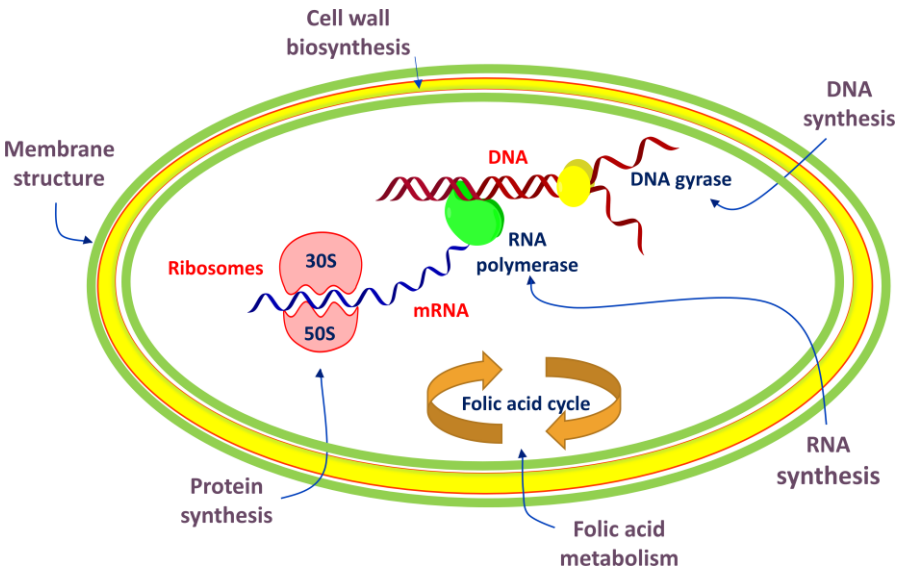

Figure 1.1: Target of antibiotics

The cartoon depicts a bacteria cell and the respective pathways targeted by antibiotics: cell wall biosynthesis, membrane integrity, nucleic acid biosynthesis, protein biosynthesis, folic acid metabolism. Adapted from Chellat[28] and Lewis.[30]

Table 1.2: Antibiotics, chemical scaffolds, targets and mechanism of resistance

Antibiotic class	Target	Resistance
β-lactams 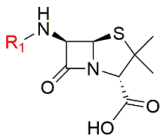 Penicillins 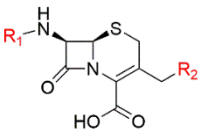 Cephalosporins 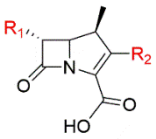 Carbapenem	Cell wall biosynthesis	β-lactamase PBP2a (reduced affinity for β-lactams) Efflux pump Porin loss[22]
Glycopeptides (Vancomycin) Cyclic peptides (Bacitracin)		Altered peptidoglycan[35]
Cyclic lipoproteins (Daptomycin) Polymixins (Polymixin B)	Cell membrane	Interference with target interaction (not well understood)[36] Modification of the outer membrane structure[37]
Sulfonamides (Sulfamethoxazole) 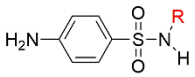	Folate synthesis	Efflux pump Altered dihydropteroate synthase (DHPS)[38]
Trimethoprim 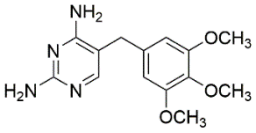		Efflux pump Altered dihydrofolate reductase (DHFR)[38]
Tetracyclines (Doxycycline, Tigecycline) 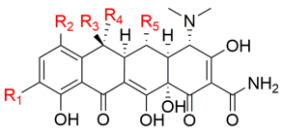 Tetracyclines	Protein synthesis: 30S subunit	Efflux pump Ribosomal protection Drug modification[39,40]
Aminoglycosides 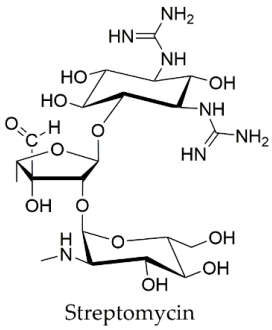 Streptomycin 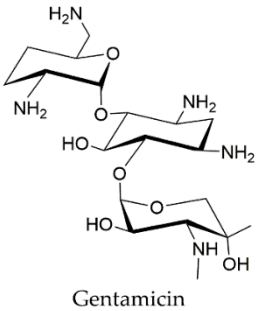 Gentamicin		Drug modification Ribosomal modification Efflux pump[41]

Antibiotic class	Target	Resistance
Macrolides (Azithromicin, Erythromicin) 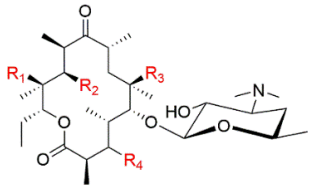		Ribosomal modification Efflux pump Drug modification[42]
Oxazolidinones (Linezolid) 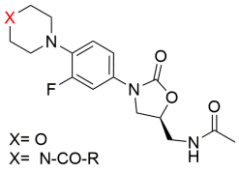 		Ribosomal modification[43]
Lincosamides (Clindamycin) 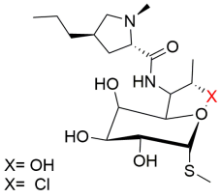 	Protein synthesis: 50S subunit	Ribosomal modification Efflux pump Drug modification[42]
Choramphenicol 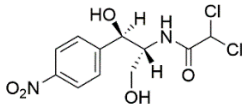		Drug modification Efflux pump[44]
Streptogramins (Streptogramin A and B)		Ribosomal modification Efflux pump Drug modification[45]
Quinolones (Ciprofloxacin, Levofloxacin) 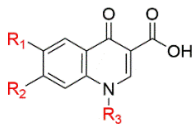	Topoisomerase II (gyrase) and topoisomerase IV	Altered topoisomerase II or IV Efflux pump[46]
Rifamycins (Rifampicin) 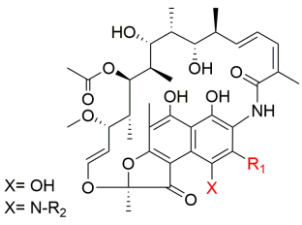 	RNA polymerase	Altered RNA polymerase[47]

The majority of current antibiotics are natural products or their semisynthetic derivatives, developed to improve the spectrum of action and to overcome resistance.[48] Their discovery can be dated back to the so-called Golden Age (1940-1960), when extensive screening of fermentation broths and microorganism extracts, mostly of soil-derived *Actinomycetes* (Waksman platform), were conducted in search of antimicrobial activity (Figure 1.2).[30] In the 1960s, the appearance of clinical resistance prompted the medicinal chemistry optimisation of the existing classes, resulting in newer generations of semisynthetic antibiotics which maintain the core chemical scaffold but exhibit improved properties.[48] The quinolones, a synthetic class of antibiotics, are an exception to this, and were accidentally discovered as side products during the synthesis of antimalarials.[49] No new classes of antibiotics have been discovered since the 1960s. Antibiotic classes developed over the last two decades were actually discovered much earlier (Figure 1.2).[20,48]

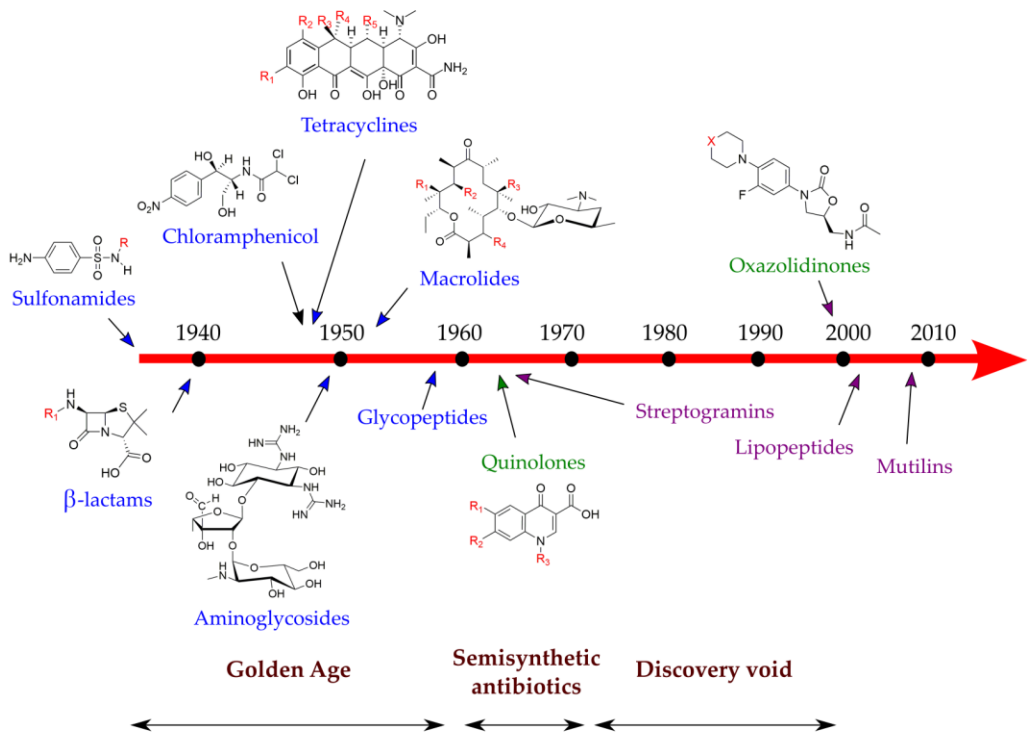

Figure 1.2: Time scale of antibiotic drug discovery

The majority of current antibiotics were discovered during the Golden Age, including the recently FDA-approved streptogramins (discovered in 1960s), oxazolidinones and mutilins (both discovered in 1950s).[50] The lipopeptide daptomycin was instead discovered in the 1980s. Blue: from natural products, later medicinal chemistry optimisation produced newer generations; green: synthetic; purple: recently approved although previously discovered. Adapted from Fischbach[48] and Lewis.[20]

1.1.2. Bacterial resistance and persistence, a threat to antibiotic efficacy

1.1.2.1. Resistance acquisition

Resistance occurs through a variety of mechanisms that prevent, or negatively affect, the interaction of the antibiotic with the respective target. Resistance can be intrinsic, acquired following an adaptive response, developed on genetic bases upon either chromosomal mutation (endogenous resistance) or via horizontal gene transmission (HGT, exogenous resistance).[4,51]

Intrinsic resistance is linked to some peculiar features of bacteria that preclude antibiotic susceptibility, such as the lack of the antibiotic target or the presence of some structural elements that prevent the antibiotic from reaching the target (e.g. an outer membrane).[51]

Adaptive responses entail transcriptional changes in response to environmental stimulation. Under particular conditions, such as temperature, osmolality, or in the presence of sub-lethal concentrations of antibiotics,[12] mechanisms that mediate resistance are supported and bacteria transiently become resistant.[52] Unlike genetic-based resistance, adaptive resistance is not transferred to the daughter cells.

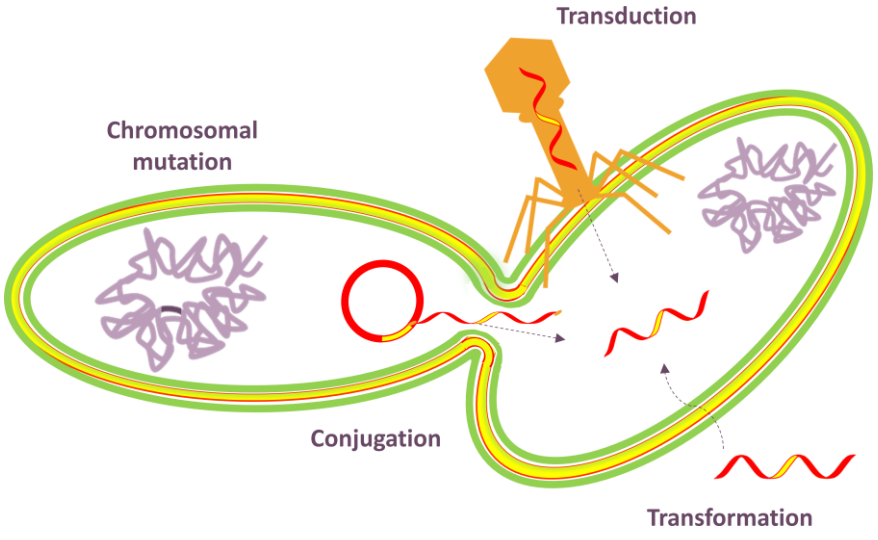

Figure 1.3: Mechanism of genetic resistance acquisition

The cartoon illustrates the mechanism of resistance acquisition arising from chromosomal mutation (endogenous) or from the acquisition of external genes by transformation (naked DNA), conjugation (the DNA is directly transferred from bacteria to bacteria), transduction (mediated by bacteriophage infection). Adapted from Levy[4] and Chellat.[28]

Endogenous resistance arises from random genetic mutations caused by error-prone DNA synthesis, which allow bacteria to develop phenotypes that enable survival under antibiotic pressure (Figure 1.3).[51] Although these mutations are often not advantageous for growth and virulence, cell fitness and virulence are usually restored by the appearance of compensatory mutations in the following generations.[53] Exogenous resistance instead originates from the acquisition of mobile genetic elements derived from other bacteria, even of different taxonomic groups (horizontal gene transfer, Figure 1.3).[54]

Resistance genes, carried by naked DNA, transposons, plasmid or bacteriophages, are taken up via mechanisms such as transformation (naked DNA and plasmids), conjugation (transposons and plasmids) and transduction (bacteriophages). By means of horizontal gene transmission, resistance developed in a specific microorganism can rapidly spread to other bacteria and MDR bacteria can arise by accumulation of genes responsible for resistance towards different antibiotics.[54]

1.1.2.2. Mechanisms of resistance

Three recurrent mechanisms of resistance can be distinguished: alteration of cell permeability and active efflux, genetic or post-translational modification of the target, and enzymatic modification of the antibiotic.[51] The permeability to some antibiotics is mediated by porin proteins, which allow the crossing of small hydrophilic compounds through the cell membrane in a non-specific manner.[55] For these antibiotics, mutations leading to loss of porin channels, alteration of their structure or down-regulation of their expression, result in the reduction of permeability with the consequent failure in reaching adequate cellular antibiotic concentration (Figure 1.4).[56] Subjected to porin-dependent resistance are β-lactams, tetracyclines, fluoroquinolones and chloramphenicol.[56] The other mechanism interfering with delivery in cells is the active efflux of antibiotic, which is mediated by the efflux pumps (Figure 1.4). The role of the efflux pumps in the bacteria is linked to the removal of possible toxins from the cytoplasm.[56] More recently, their involvement in quorum sensing has also been hypothesized.[56] Efflux pumps actively expel antibiotics. Even though some efflux pumps have shown a high specificity for their substrates (e.g. for tetracyclines), they are mostly not specific and as such contribute to the development of MDR bacteria.[55]

Efflux pump-mediated resistance is observed upon their over-expression, although in some cases it can be linked to an increase in affinity for the antibiotic.[56] The level of expression of genes encoding for efflux pumps is controlled by some regulators, either global regulators, involved in the control of broad pathways, or by local regulators, located alongside the efflux pump genes.[51,56] Resistance arises either as a consequence of mutations within these regulators or upon adaptive responses to environmental signals.[51,56] The result of reduced permeability or active export of antibiotics causes a significant decrease in the intracellular concentration of antibiotics. Drugs such as aminoglycosides, fluoroquinolones, β-lactams and tetracyclines are typically subjected to efflux pump-mediated resistance.[56]

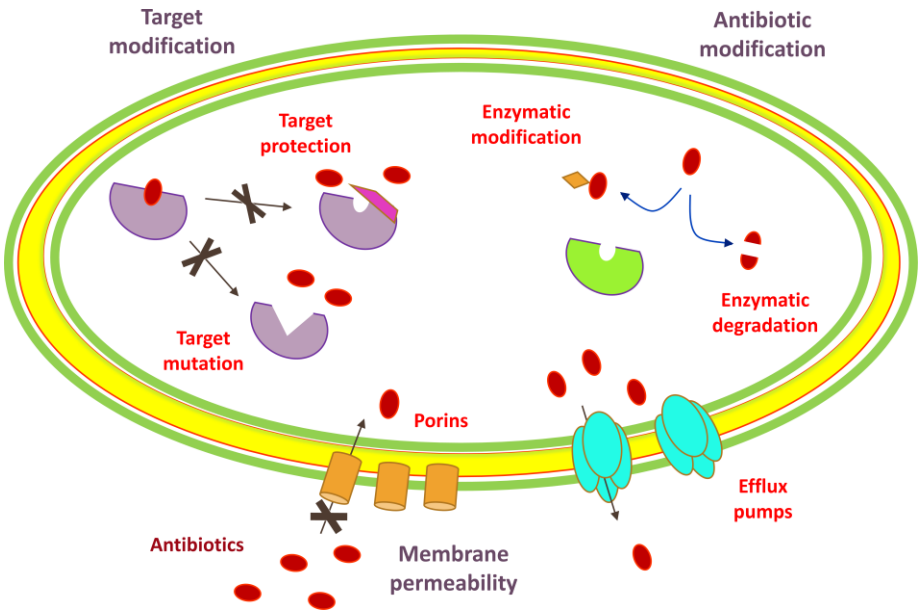

Figure 1.4 Mechanisms of antibiotic resistance

The cartoon illustrates the strategies that bacteria have evolved to exert resistance to antibiotics. These mechanisms can be summarised as follow: interference with the antibiotic penetration in cells, inactivation of the antibiotics by enzymatic modification, neutralization of the antibiotic activity by preventing the interaction with the target. Adapted from Levy,[4] Chellat[28] and Lewis.[30]

Another widespread mechanism of resistance involves alteration to the interactions between an antibiotic and its target, which occurs as a consequence of structural modification of the target (Figure 1.4).[57,51] The latter can arise either from genetic mutation of the target gene or from target protection by enzymatic modification. In the first case, the mutated allele expresses for a target with lower affinity for the antibiotic. For example, the *mecA* gene

expresses for PBP2a, a penicillin-binding protein with lower affinity for β-lactams, responsible for methicillin resistance of MRSA.[58] In the second case, the target becomes inaccessible to the antibiotic due to an enzymatic modification of the active site. Examples include the methylation of either 16S or 23S rRNA subunits which, by preventing the binding to the target, cause resistance to aminoglycosides, macrolides, chloramphenicol, lincosamines, streptogramins and oxazolidonones.[59] A similar mechanism is responsible for resistance to fluoroquinolones, due to a peptide binding to the targets topoisomerase IV and DNA gyrase,[60] and to polymyxins, whose affinity for the lipopolysaccharide (LPS), their target, is reduced as a consequence of the attenuation of LPS negative charges, caused by the binding of a phosphoethanolamine.[61]

A third common mechanism of resistance consists in the enzymatic modification, which either inactivates the antibiotic or prevents its interaction with the target (Figure 1.4).[51,62] Antibiotic inactivation is mostly based on enzymatic hydrolysis, a classic example of which is the hydrolysis of β-lactams by β-lactamases.[63] Resistance by enzymatic modification, such as acylation, phosphorylation or transfer of nucleotidyl or ribitoyl groups, arises by preventing binding due to steric hindrance.[51] Antibiotics with exposed hydroxyl or amino groups, such as aminoglycosides, macrolides, lincosamides and rifamycins, are particularly susceptible to this mechanism of resistance.[62]

1.1.2.3. Persistence

An alternative means of bacterial survival to antibiotic treatment is provided by the appearance of persistence, which is described as a physiological state characterised by a very slow growth, often defined as *dormant* state.[64,65] Persistent cells stochastically originate from a fast growing colony, from cells in the stationary phase or from biofilms.[66,67] It has been hypothesized that bacteria develop persistency as a way of dealing with unexpected stress.[68–70] While the population with the fast growing phenotype is susceptible to antibiotic treatment, the subpopulation of persistent cells, caught in a state of dormancy in which the antibiotics targets of are not available, survive the treatment.[65] As opposed to genetically-derived resistance, the persistent trait is not heritable. The appearance of persister cells provides a means for bacteria to circumvent the antibiotic treatment and propagate the

infection. Indeed, persistent cells can reverse back to a normal fast-growing phenotype, from which a normal population can derive.[64] Furthermore, the persistence-mediated endurance of the infection can facilitate the appearance of resistance traits, either resulting from mutations or from horizontal acquisition.[12,65]

1.1.3. Filling the void, the quest for new antibiotic targets

In response to the threat of the increasing spread of bacteria resistance, exacerbated by the lack of success in the past decades in delivering first-in-class antibacterial agents, new strategies must be implemented to fill the void in the antibiotic pipeline. Among some of the approaches that have been suggested to discover new antibiotics, such as to address the problem of cell permeability (the major cause of failure of HTS and rational design based campaigns) with adequate attention to physicochemical properties,[30,71] and a return to screening of natural products,[20,30] a most logical approach could be pursuing the identification of novel targets.[10] Current antibiotics target only a limited number of pathways, which are essential for bacterial growth and survival (section 1.1.1 and Table 1.2). Resistance mechanisms are well established to oppose the disruption of these pathways. Therefore, the development of antibiotics hitting conventional antibacterial targets would be likely to suffer from the emergence of cross-resistance eventually.[20] It has been reported that the "essential genes" for *in vitro* growth in rich media (the conditions used for Waksman platform, section 1.1.1), typically targeted by the available antibiotics, constitute only 7% of the *E.coli* genome.[10] More genes have been found to be essential for growth under stress conditions (such as nutrient depravation or chemical stress)[72] and many more have been identified from *in vivo* models as essential for survival in the host cells and for pathogenicity (virulence genes).[10,73] Targeting these *in vivo* essential genes constitutes an alternative approach for the development of new antibiotics.[71] Attenuated bacteria, upon treatment with antivirulence agents, could be easily cleared by the immune system. Examples of *in vivo* pathways with potential as new antibacterial targets are pathways involved in toxin-mediated virulence, pathways such as quorum sensing, that regulates and coordinate the expression of virulence factors, and pathways involved in the colonization of the cells host (e.g. adhesion mediated by pili).[71,74,75] An hypothesized advantage of this strategy could be

a lower likelihood of resistance development. In particular, the latter scenario may be envisaged for antibacterial agents strictly targeting the interactions with the host and virulence factors, where mechanisms essential for growth would not be disrupted and therefore bacteria would not be exposed to selective pressure.[71] A possible drawback of this approach could be a narrower spectrum of activity, because of the species specificity of the mechanisms involved in bacteria-host interaction and the specificity of virulence factors.[71]

1.2. Drug Discovery by High Throughput Screening: the Screening Cascade

In the past 25 years, the most common approach in early drug discovery consisted of screening campaigns of large libraries on highly conserved targets. A success rate of about 50-60% has been estimated,[76,77] with many drug candidates failing due to poorly validated targets, non-appropriated physical-chemical properties,[78] lack of adequate animal model and unpredictable safety concerns emerging during clinical trials (due to both off target-effects and on-target toxicity).[77,79] A long time is required from the target selection and the launch of screening campaigns until the approval of a new drug (about 13.5 years),[80] hence the limited success rate is more representative of the efficiency of earlier, rather than current, HTS campaigns.

Nowadays, drug discovery projects benefit not only from advances in screening technology, but also from a more rigorous approach within the drug discovery cascade to the steps both upstream and downstream of the HTS campaigns (Figure 1.5).[81] The very first critical step for the success of a screening campaign consists in the target identification and validation.[82] Bioinformatics approaches are often applied for target identification,[83] alternatively targets are identified by phenotypic screenings.[82] Once a potential target has been selected, further investigation is required to build confidence in the target-disease relationship (e.g. by siRNA, proteomics, transgenic animal models)[82] and to evaluate the target's druggability.[82]

Further to the improvements in automation and robotics, that have allowed greater miniaturization and throughput, significant efforts are directed towards the development and optimisation of the assays, of which the quality is evaluated not only by statistical analysis (Z'-factor)[84] but also by the ability to capture a greater variety of chemical scaffold, including weak inhibitors.[81] Alongside the classic approach of using either *in vitro* biochemical assays or cell-based assays, screening by biophysical assays is becoming more common.[85] The choice of one or the other method is dictated by factors such as the target and the library characteristics but also the throughput. Particular efforts have also been directed towards the improvement of compound libraries, often considered to be the main reason for screening campaign failure.[78] Libraries generated by combinatorial chemistry are now available, characterised by a better exploration of the chemical space, to boost the

potential for the identification of new chemical entities, by compounds with drug-like physicochemical properties and filtered to remove known promiscuous compounds (PAINS)[81,86] Alongside diverse chemical libraries, screening of target-based libraries and fragment libraries are increasingly applied, the first being collections of target substrate analogues, the second collections of low molecular weight molecules.[78,81,87]

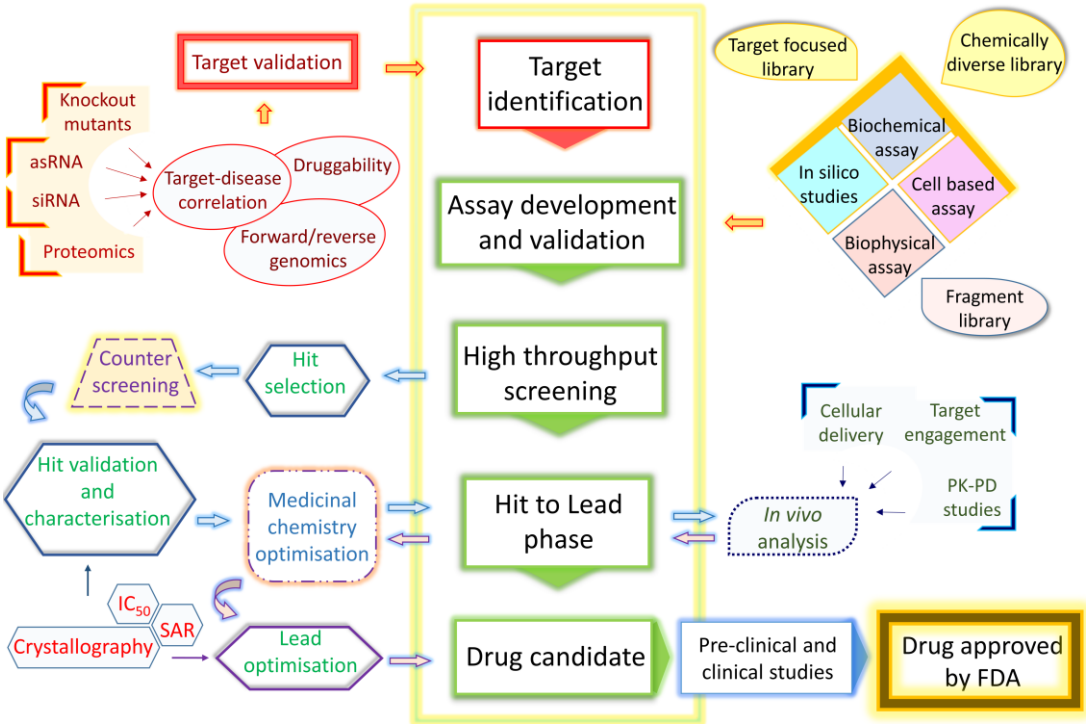

Figure 1.5: Drug discovery screening cascade

The screening cascade describes the different steps for the progression towards the development of a new drug. The tools and the investigations required to allow the progression to the next stage were illustrated in the figure.

After HTS, the activity of compounds that scored as "hits" is tested in secondary assays (or orthogonal assays). Both biochemical assays and biophysical methods (e.g. NMR, SPR, ITC) can be used as orthogonal assays, often in association.[88] Orthogonal assays are aimed at confirming the activity of genuine hits and identifying and discarding possible spectroscopic artefacts (interference with the assay readout and format) and chemical artefacts (due to compound aggregation under the assay conditions).[81] The compounds that are found to specifically modulate the activity of the target, independently from the method of investigation, are subjected to kinetic characterization and selectivity profiling (when

possible) and then advanced to the medicinal chemistry optimisation stage, where preliminary investigation of SAR is conducted.[82] Previously, the selection of hits to follow up was based mainly on synthetic accessibility, affinity and functional behaviour (mechanism and selectivity), while the evaluation of other properties was postponed. This approach resulted in compounds with fully-optimised potency and selectivity, though at the expense of solubility, permeability and metabolic stability (poor ADME). Learning from the past, nowadays physicochemical properties favourable for ADME are taken in consideration from the early stage of the hit selection for follow up.[81,82] The preliminary medicinal chemistry phase aims to define general SAR and to biochemically characterize the hits. This is followed by the hit-to-lead phase, in which more intense and systematic SAR studies are conducted, aided by structural information (X-crystallography, NMR, molecular modelling).[82] The lead compounds are subjected to careful physicochemical properties profiling and the activity is investigated in relevant biological models to prove target engagement in complex biological systems.[89,90] Compounds with optimal properties are advanced to pre-clinical studies, where PK/PD studies,[91,92] ADME investigation,[93,94] and efficacy and toxicity studies in animal models are conducted.[82] Finally, compounds with a favourable efficacy/toxicity profile are admitted to clinical studies.

1.3. Polyphosphate Kinase from Intracellular Pathogens as a Novel Antibacterial Target

1.3.1. Polyphosphate metabolism

Polyphosphate (polyP) is an inorganic linear polymer comprising tens to hundreds of phosphate units (P_i), linked by phospho-anhydride bonds with energy comparable to those of ATP (Figure 1.6).[95–100] PolyP was initially isolated from yeast[101–103] and later identified in various microorganisms subjected to nutrient starvation.[104,105] Widely distributed among bacteria, including some major pathogens,[97,106] polyP can also be found in archaea, fungi, plants, insects and mammals.[99,107]

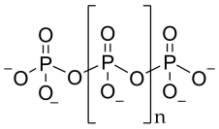

Figure 1.6: Inorganic polyphosphate

In bacteria, the enzyme responsible for the synthesis of polyP is the polyphosphate kinase (PPK). The first bacterial PPK to be purified to homogeneity, cloned and well characterised was the PPK from *E. coli*, which catalyses the synthesis of long polyP chains (about 750 phosphate units), by transfer of the γ-phosphate of ATP onto polyP with a processive mechanism (Figure 1.7).[108,109]

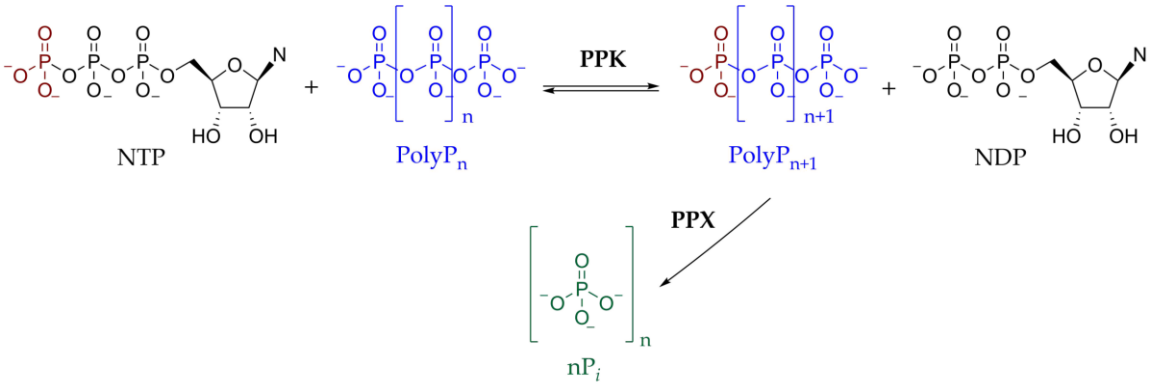

Figure 1.7: PolyP synthesis and degradation

PPKs reversibly catalyze the synthesis and the degradation of polyP, using nucleotides either as phosphate donor or acceptor, respectively. The polyP can be also degraded by PPX, which catalyzes the hydrolysis of polyP into phosphate units.

PPK can also catalyse the reverse phosphorylation of nucleoside diphosphates (NDP) using polyP as a phosphate donor (Figure 1.7).[108,110]

Following the identification of the *ppk* gene[111] and the construction of *ppk* deletion mutants, it became clear from the detection in mutants of residual polyP that the latter could be synthesised in the *ppk*-knockout mutants by alternative sources.[112,113] Later, a new phylogenetically distinct family of polyphosphate kinase was identified in *Pseudomonas aeruginosa*,[114] which was designated as PPK2, to distinguish it from the previously characterised and non-homologous PPK (denominated PPK1). Like PPK1, PPK2 catalyses both the synthesis and the degradation of polyP, with a preference for the polyP-driven phosphorylation of NDP (section 1.3.3.1).[115] PPK1 and PPK2 are widely conserved in microorganisms, including pathogens. In some cases, both of them can be found in the microbial genome, either in single or multiples copies. In other cases only the one or the other is present, and in some other cases none.[97,114]

Another enzyme involved in polyP metabolism, responsible for polyP degradation, is the exopolyphosphatase (PPX).[116] PPX catalyses the hydrolysis of polyP into P_i units with a processive mechanism.[117] Variation in the catalytic efficiency towards polyP of different chain length and in the extent of polyP hydrolysis has been observed for PPX from different microorganisms.[116,118] For instance, the *E.coli* PPX hydrolyses long polyP chains more efficiently while displaying a low activity towards small chains.[117,118] In *E.coli*, the *ppx* gene is part of the *ppk* operon,[108,111,117] suggesting co-regulation of their transcription (although not always this is the case).[119] The *E.coli* PPX activity is subjected to inhibition by competitive binding of the metabolite guanosine-5'-diphosphate,3'-diphosphate (ppGpp, Figure 1.8), leading to accumulation of polyP.[120]

The modulation of PPK and PPX activity, based on the phase of the growth cycle or in response to environmental variations, is the main mechanism for the regulation of the polyP content in most bacteria.[116] Other enzymes have been reported to catalyse polyP-dependent reactions, although they are not widely represented in many bacteria. An extensive description can be found in the review *Enzymes of inorganic polyphosphate metabolism*, by Kulakovskaya and Kulaev.[116]

1.3.2. Polyphosphate role in bacteria survival and pathogenicity

Initially regarded just as a fossil biopolymer, various other functions have been attributed to polyP, according to the organism of interest, the localization within the cell and the phase of the cellular cycle.[95,121] PolyP has been regarded as a reservoir of phosphate, an available source of energy and a chelator for metal ions. Its involvement in the formation of channels for bacteria competence and in RNA processing and degradation has also been reported.[95,99,109,122] More recently, the role of polyP in the expression of virulence factors of many pathogens and in the regulation of the response to stress conditions and to nutrient starvation has been widely investigated.[95,97,109,121,123] It has become clear that the latter are the most common and important functions of polyP, in view of their effect on microorganism viability and pathogenicity.

1.3.2.1. Stationary phase adaptation and stress responses in bacteria

Under adverse conditions, including various forms of stress and nutrient deprivation, bacteria enter the stationary phase, which allows them to survive for long periods without growth.[109] The transition from the exponential growth phase to the stationary growth phase entails important changes in the physiology and morphology of the bacterial cell.[110] At the transcriptional level, a switch is observed from the expression of the genes required during the growth phase to the expression of genes that allow long term survival in the stationary phase and development of resistance to physical and chemical stress (hence preventing cell damage).[124–129] In *E.coli*, the transcriptional switch is mediated by the gene *rpoS,* which encodes for the RNA polymerase (RNAP) sigma factor σ^S (also known as σ^{38} or RpoS).[129–131] In the late stage of the exponential growth or in the occurrence of stress, the binding of the σ^S factor to the RNAP is favoured over then binding of the housekeeping sigma factor σ^{70} (which promotes the expression of genes essential for growth).[130,132,133] As a consequence, the expression of the genes controlled by σ^S factor is induced and the transition to the stationary phase occurs.[134] The genes activated by the σ^S code for proteins involved in morphological changes, in the prevention and repair of DNA damage, in the resistance to

osmotic, thermal and oxidative stress, in the survival under nutrient starvation, and in the modulation of virulence.[129,135]

Both the cellular concentration of the σ^S factor and the interaction with the RNAP are mainly regulated by the alarmone ppGpp (Figure 1.9), the primary mediator of bacteria response to nutritional starvation (stringent response, section 1.3.2.3).[136–139] A certain degree of modulation on the expression of the *rpoS* gene is also exerted by polyP (Figure 1.9).

1.3.2.2. PolyP and the modulation of the *rpoS* gene: resistance to oxidative, thermal and osmotic stress.

An increase of the polyP content has been detected in the stationary phase,[109] and this has been linked to the positive modulation of polyP on the *rpoS* gene expression.[112,140,141] Mutants, constructed by either deletion of *ppk* and/or overexpression of *ppx*,[108,111,117] resulting in a phenotype containing low concentration of polyP, were used to investigate the role of polyP in the stationary phase.[112,140,141] No significant differences in phenotype were observed between the wildtype and mutants during the exponential growth phase.[112] On the other hand, the long term survival in the stationary phase significantly decreased for the polyP-deficient phenotypes.[112,140] Mutants were also subjected to oxidative stress by exposure to H_2O_2 and to the quinone menadione (which generates oxygen radicals), to thermal stress by exposure to heat (55°C, 2 min) and to osmotic stress by exposure to high salt concentration (2.5 M NaCl for 21 h).[140,141] A significant increase in sensitivity to the three forms of stress was observed for the polyP-deficient phenotypes. In each case, sensitivity comparable to the wildtype was restored by complementation with plasmids bearing the *ppk* gene. This observation validated the link between resistance to stress and polyP concentration (Figure 1.9).[140,141]

It did not go unobserved that the increase of the resistance to thermal, oxidative and osmotic stress is a common feature that appears during the stationary phase. Indeed, the expression of the genes involved in the activation of responses to these forms of stress is promoted by the σ^s factor.[129,135] When the complementation of the polyP-deficient mutants with a plasmid carrying the *rpoS* gene resulted in the restoration of resistance to stress, it became clear that the mutant's increased sensitivity actually resulted from low expression of the

rpoS gene, which in turn was a consequence of low polyP concentration.[140,141] Mutant studies also suggested a possible involvement of polyP in the inhibition of the binding of σ^{70} factor to the RNAP while favouring the σ^{S} binding,[121,142] although no further confirmation from following studies has been reported in the literature.

1.3.2.3. Stringent response

In the occurrence of nutrient starvation, the arrest of the exponential growth and the transition into the stationary phase is triggered by the activation of an adaptive mechanism known as *stringent response*. The stringent response is coordinated by the alarmones guanosine-3'-diphosphate-5'-triphosphate (pppGpp) and guanosine-3',5'-diphosphate (ppGpp), which are together referred to as (p)ppGpp (Figure 1.8).[136,143–147]

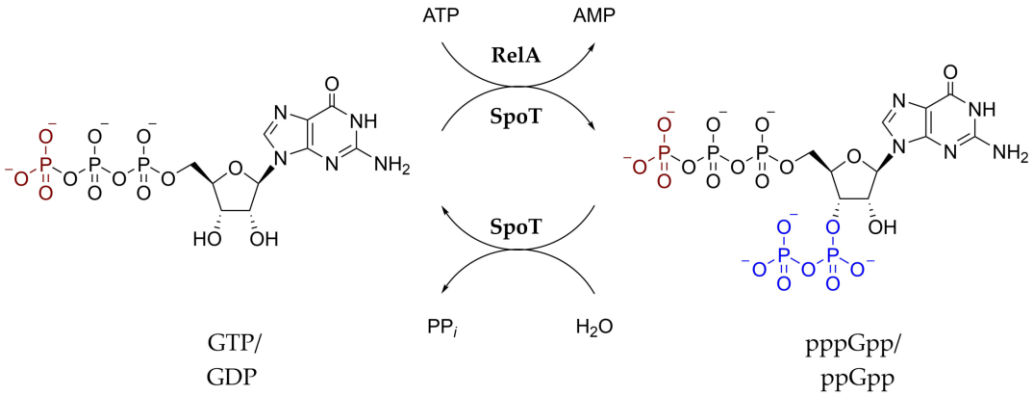

Figure 1.8: Synthesis and degradation of (p)ppGpp

The synthesis of (p)ppGpp is catalysed by both RelA and SpoT, by transfer of a pyrophosphate unit from an ATP molecule onto either a GTP or a GDP molecule. The SpoT is capable of catalysing also the degradation of (p)ppGpp by hydrolysis. Under normal conditions SpoT exerts only hydrolase activity while RelA is inactive. Under starvation, RelA and the synthetase activity of SpoT are turned on.

In *E.coli*, (p)ppGpp is synthesised by either the RelA or SpoT, which catalyse the phosphorylation of GTP or GDP using ATP as pyrophosphate donor (Figure 1.8). The SpoT is a bifunctional synthetase-hydrolase and catalyses also the degradation of (p)ppGpp into the corresponding guanosine nucleotides by hydrolysis of the 3'-pyrophosphate group (Figure 1.8).[148] The cellular content of (p)ppGpp is regulated by the integrated activity of RelA and SpoT, which are activated by shortage of nutrients. In particular, amino acid starvation leads to (p)ppGpp accumulation mediated by RelA activity, stimulated by stalled

ribosomes (caused by uncharged t-RNA).[149–151] Under normal conditions SpoT principally exerts hydrolase activity, maintaining the concentration of (p)ppGpp to basal levels.[152] However, the synthetase activity is enhanced, supporting the increase of (p)ppGpp levels,[152–154] in the occurrence of fatty acid starvation,[155–157] carbon starvation,[148] phosphate starvation[158] and iron starvation.[159]

During the exponential growth phase, ppGpp is present in basal level and is involved in the control of the growth rate and in the homeostasis of guanosine nucleotides.[145,160,161] The increase of the cellular content of (p)ppGpp, caused by starvation, promotes the switch of bacteria physiology from the growth transcription profile to the stress adaptation profile.[136,146,162] The ppGpp-mediated transcriptional change is promoted by the positive modulation of the expression of the *rpoS* gene and by the regulation of the RNAP activity (Figure 1.9).[145]

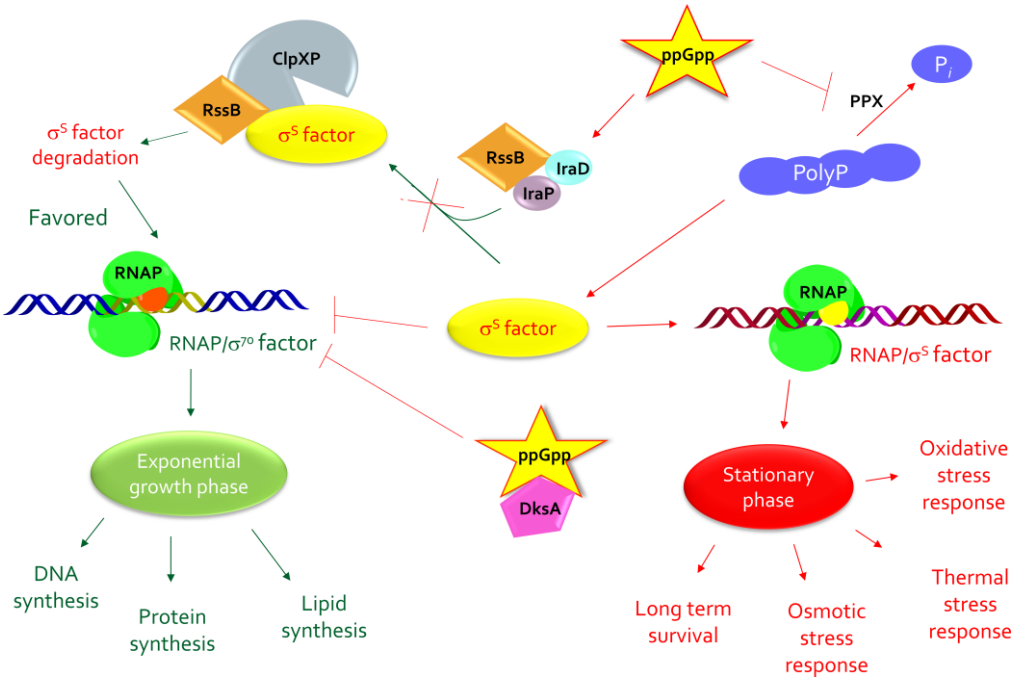

Figure 1.9: Role of ppGpp in the transition from growth phase to stationary phase

PpGpp positively modulate the concentration of the σ^S factor by stimulating the expression of IraP and IraD, which prevent the association of RssB to the σ^S factor. Therefore, the degradation of the σ^S factor by ClpXP does not occur and the concentration of the σ^S factor increase. A positive modulation of the σ^S factor is also exerted by polyP. The σ^S factor favours the expression of the stationary phase genes. The latter is also supported by the inhibitor control that the complex ppGpp/DskA exerts on the binding to the RNPA of the σ^{70} factor.

The *rpoS* gene is expressed during exponential growth, but the cellular concentration is maintained at a low level due to its association with an adaptor protein, RssB, which directs the σ^S to the proteasome ClpXP for degradation.[134,163] PpGpp stimulates the expression of anti-adaptor proteins, IraP and IraD, which bind to RssB blocking its activity and therefore leading to an increase of σ^S cellular concentration.[136] For the modulation of the RNAP activity, ppGpp requires the participation of the co-factor DksA.[164,165] The complex ppGpp/DksA can operate either by destabilizing (promoters with GC-rich region) or favouring (promoters with TA-rich region) the formation of some RNAP-promoter complexes,[145,166] or by altering the RNAP affinity for sigma factors (disfavouring the binding of sigma factor σ^{70} while favouring the binding of σ^S factor).[134,138,167,168]

A connection between the stringent response and polyP metabolism was first observed in bacteria exposed to a nutritional downshift from a rich to a minimal medium, in which accumulation of polyP was observed.[105,169] Later, the increased concentration of polyP was linked to the inhibition exerted by pppGpp, and to a lower extent also by ppGpp, on the PPX activity (Figure 1.9).[120] The role of polyP within the stringent response was investigated by means of *ppk/ppx* mutants, which in comparison to the wildtype showed an extended lag phase of growth following nutrient starvation.[170] The mutants were also defective in protein degradation, which is promoted by the stringent response to increase the pool of free amino acids.[170] It has been known since long time that in *E. coli* the degradation of stable proteins to provide free amino acids, together with the (p)ppGpp-mediated downregulation of tRNA and rRNA, is characteristic of the adaptation response to amino acid starvation.[171,172] In *E. coli*, the ATP-dependent proteases responsible for protein degradation are the Clp protease (ClpAP and ClpXP) and the Lon protease.[173] A link between protein degradation and polyP was confirmed upon construction of *clp* and *lon* gene deletion mutants, which yielded a similar phenotype as the *ppk/ppx* mutants when subjected to nutritional downshift, and by co-purification of polyP with the Lon protease.[174] Further investigation showed that the binding of polyP to Lon protease stimulates the Lon-dependent degradation of ribosomal proteins.[174,175] The derived pool of free acids allows the

biosynthesis of the enzymes necessary to endure the starvation and later to resume the growth.

1.3.2.4. DNA damage

The polyP-deficient mutants have also been used to investigate possible involvement of polyP in the regulation of SOS gene expression. The SOS response is activated when DNA damage occurs.[176] The expression of the SOS regulon is controlled by the gene *umuDC*, of which the transcription is repressed by the LexA protein and induced upon LexA degradation by the activated RecA protein.[177–179] The viability of polyP-deficient mutants was tested upon exposure to mitomycin C and UV, as a model for DNA damage.[180] The sensitivity of polyP-deficient mutants was significantly higher compared to the wildtype and was restored upon increase of polyP cellular concentration by complementation with the *ppk* gene.[180] Reduction of the expression of both *umuDC* and of *recA* genes was detected for the mutant phenotypes. The decreased expression of *umuDC* was not dependent on a possible polyP interference with the activation of the protein RecA but was a consequence of the low expression of the *recA* gene (Figure 1.10).[180]

A regulatory effect of polyP was also reported for another protein involved in DNA damage, the polymerase IV (Pol IV), which is responsible for adaptive mutation. Pol IV belongs to the family of Y-family of DNA polymerase, or error-prone polymerase, which are capable of functioning even in the presence of DNA lesions, inserting incorrect nucleotides at high frequency.[181] Pol IV is expressed as part of the LexA-controlled SOS regulon, which is in turn activated by the stall of a normal polymerase (Pol III) at a DNA lesion. The activity of Pol IV results in a high mutation rate, which allow the bacteria to restore growth under non-lethal selective conditions (adaptive mutation). PolyP-deficient mutants showed a significant decrease in the adaptive mutation, which persisted when the concentration of polyP was significantly increased, suggesting that an optimal polyP concentration is required for the correct functioning of Pol IV.[182] Despite the link of Pol IV with the RecA protein, in the absence of which no adaptive mutation occurs, and with RpoS, which controls the expression of Pol IV, the alteration of the adaptive mutation in polyP mutants was not dependent on the effect that polyP has on *recA* and *rpoS* expression. It appeared instead

that polyP dos not modulate the level of expression of Pol IV but does affect Pol IV activity although the mechanism remains unknown (Figure 1.10).[182]

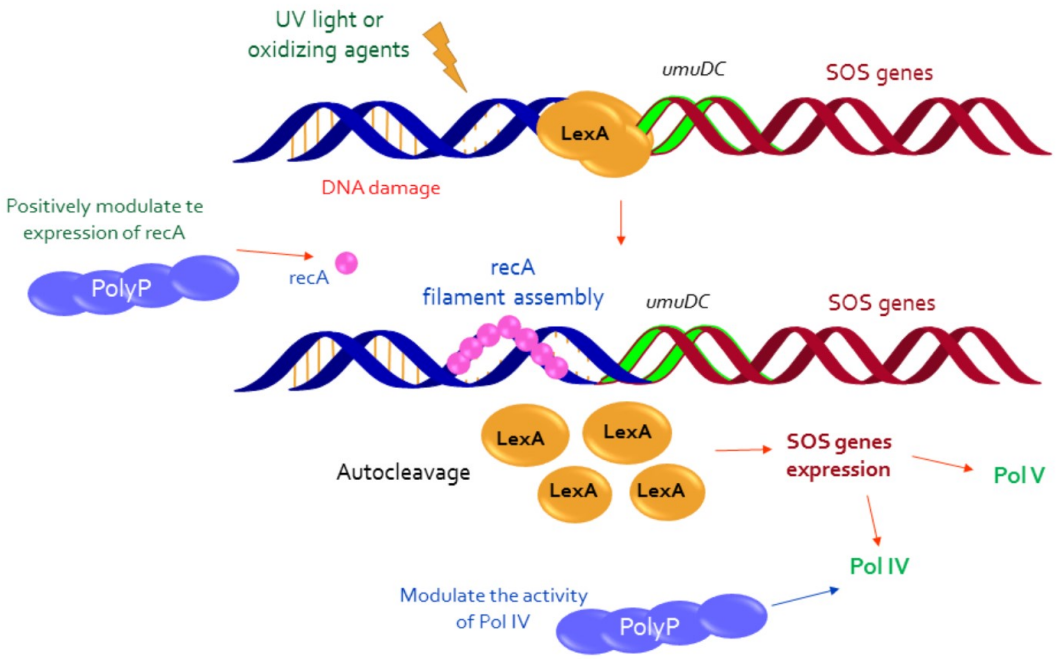

Figure 1.10: PolyP and the SOS response activation

The expression of *umuDC*, which controls the SOS genes, is repressed by the transcriptional repressor LexA. When DNA damage occurs, binding of the RecA proteins to the single DNA strands causes activation of LexA autocleavage. The expression of the *umuDC* operon leads to the activation of the SOS response, including the error-prone polymerases IV and V.[183] PolyP positively modulates the expression of RecA and the activity of Pol IV.

1.3.2.5. Persistence

The molecular mechanisms at the base of the persistence physiology are currently being investigated.[184] The persistence phenotype was first linked to the gene *hipA*, which encodes for a kinase that is the toxin component of a toxin-antitoxin module. (TA module). A toxin-antitoxin system is described as a complex of a stable protein, the toxin, that when free can disrupt an essential cellular function, and a degradable antitoxin component (RNA for antitoxin type I and III, protein for antitoxin type II), which suppresses the toxin activity upon binding to it.[185] The locus *hipAB*, which codes for HipA toxin and the correspondent

HipB antitoxin,[186] was found to be under the control of (p)ppGpp (Figure 1.11).[66,187] Later, the involvement of polyP by activation of the Lon protease was elucidated (Figure 1.11).[66,188] A total number of 11 TA modules was identified as being involved in the activation of persistence. Further to the type II toxin-antitoxin *hipAB* locus, the remaining 10 type II TA modules code for mRNAases.[184,188–190] The activation of these toxins, by degradation of the correspondent antitoxin, leads to the appearance of a phenotype in a bacteriostatic condition, characterised by a very slow growth rate (mediated by HipA), by the arrest of translation (mediated by the mRNAases) and by antibiotic tolerance. The resurrection from the persistent state is reversed by inactivation of the toxin upon binding of the respective antitoxin.[191]

The switch to a persistence phenotype is considered a consequence of a stochastic increase of ppGpp in a very small percentage of the bacteria population (about 0.01%).[66] Two of the functions exerted by ppGpp contribute to the appearance of the persistence phenotype: the growth control[160] and the inhibition of PPX.[120] Following an increase in ppGpp concentration, bacterial growth rate is significantly reduced and the accumulation of polyP, due to PPX inhibition, occurs. PolyP in turn activates the Lon protease, which degrades the antitoxin components of the TA modules.[190] The activation of HipA mediates a positive feedback effect on the ppGpp concentration. Indeed, HipA inactivates glutamyl tRNA synthase (GltX) by phosphorylation, which results in the accumulation of deacylated tRNAs.[192,193] The latter cause stalling of the ribosomes and consequent stimulation of RelA, leading to the accumulation of a greater concentration of ppGpp. The further increase of ppGpp concentration reinforces the persistence phenotype by supporting the activation of the Lon protease. The proteolytic activity is exerted not only on the antitoxin HipB but also on the antitoxins of mRNAase toxins, which promotes the disruption of translation. Persistence and drug tolerance were observed either in mutants overexpressing HipA or in mutants lacking HipA but overexpressing the mRNAase TA. No drug tolerance but only a slow growth phenotype was observed in mutants overexpressing HipA but lacking mRNAase TA.[194] Cells accumulating ppGpp were drug tolerant only in the presence of mRNAase TA, suggesting that the role of ppGpp is to mediate the activation of toxin while the expression of a drug tolerant phenotype is to be attributed to the mRNAases.[194]

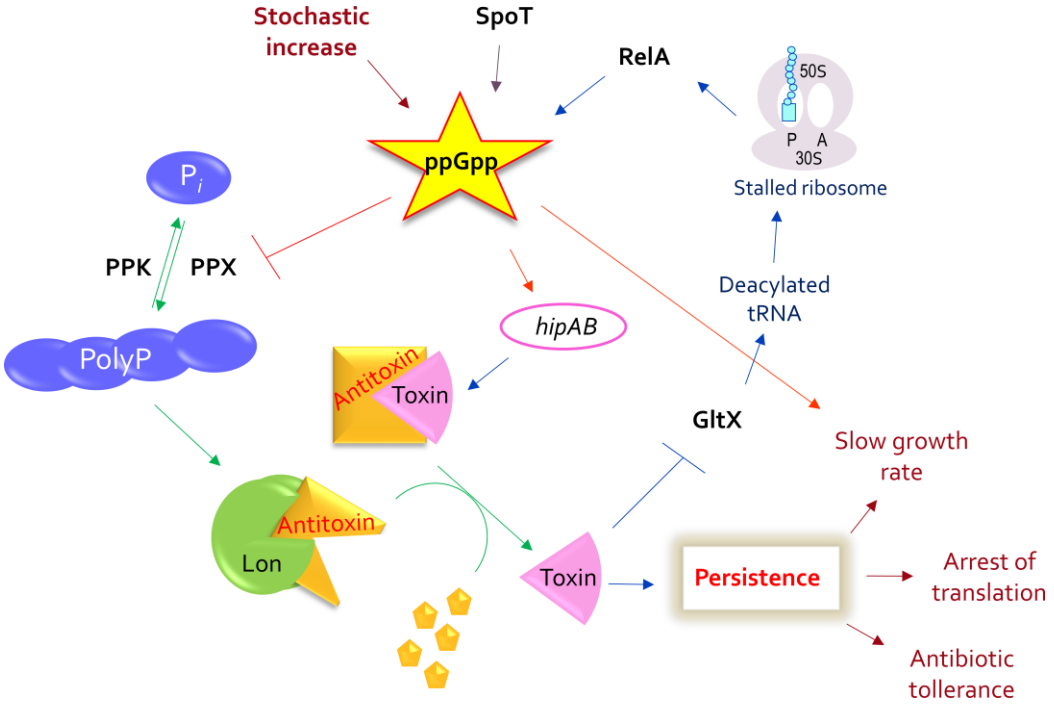

Figure 1.11: The role of ppGpp and polyP in bacteria persistence

ppGpp is involved in the activation of persistence. Stochastic increase of ppGpp leads to the expression of the *hipAB* locus, which codifies for a toxin-antitoxin module. ppGpp also induces increase of polyP concentration, which in turn activates the Lon protease. Upon degradation of the antitoxin by the Lon protease, the free toxin induces appearance of the persistence state, by promoting the arrest of the translation and slow growth. Toxin also exerts a positive control on ppGpp, by inducing activation of RelA mediated by inhibition of GltX, which results in stalled ribosomes.

Recently, the involvement in the activation of persistence of a type I TA module, *hokB/sokB*, has been reported.[195,196] The toxin HokB is a membrane protein that causes a reversible, although severe, decrease of the membrane potential. The respective antitoxin, the sokB-RNA, is an antisense RNA that inhibits the translation of the *hokB* mRNA. The activation of HokB is mediated by the widely conserved GTPase Obg, by a mechanism dependent on ppGpp.[196]

The mechanism involved in the switch of the persistent cells to normal phenotype has not been confirmed yet. It has been hypothesized that normalization of the ppGpp concentration occurs by interruption of the positive feedback loop, which may be achieved either by self-inhibition of HipA upon auto-phosphorylation or by SpoT–mediated degradation of ppGpp.[194,197]

Despite the fact that much more remains to be discovered about the molecular mechanism of persistence, and the possible involvement of alternative regulator molecules or TA modules, it seems clear that ppGpp is a key mediator in the activation and coordination of persistence. PolyP in turn, is directly involved in the degradation of antitoxin and as such is essential for the implementation of persistence.

1.3.2.6. PolyP and the expression of virulence factors

For many pathogens, the role of polyP in pathways leading to the expression of virulence factors, and therefore pathogenicity, has been reported. The link between polyP metabolism and virulence has been investigated by construction of both *ppk1* and *ppk2* mutants and has been well characterised for the opportunistic pathogen *P. aeruginosa*. In particular, *ppk1* mutants of *P. aeruginosa* resulted in impaired motility, quorum sensing and biofilm formation.[113,198,199]

Motility is a virulence factor required by many pathogens for their colonization and invasive capacity, and therefore for their ability to cause infection. Quorum sensing is a form of cell-to-cell communication, mediated by the release of molecules called autoinducers.[200,201] The sensing of autoinducers in the environment allows a single bacteria cell to detect the presence of other cells and to implement a coordinated response. At a concentration of autoinducers beyond a certain threshold, the activation-repression of genes responsible for biofilm formation,[200] virulence[202] and antibiotic resistance is triggered. Both motility and quorum sensing are required for the formation of biofilms. Biofilms are bacterial communities in which the cells adhere to a solid surface and to each other, eventually forming a three dimensional structure supported by an extracellular polysaccharide matrix.[203] The first step of biofilm formation consists of the migration of free bacteria onto an abiotic site and their attachment to a surface by using flagella or pili, which requires the correct functioning of motility.[204] Subsequently, small micro-colonies are formed which then differentiate into the biofilm by means of the coordinated biofilm gene expression, mediated by quorum sensing.[200] The biofilm bacteria cells are then cemented by a matrix made of exopolysaccharides. In *P. aeruginosa* alginate is the major component of the exopolysaccharide matrix.[205] A link between the synthesis of alginate and PPK2 activity has been established. For the synthesis

of alginate GTP is required, and this in turn is in large part synthesised by PPK2.[115,206] The disruption of the biofilm formation mediated by PPK1 and PPK2 is of particular relevance, given the role that biofilms have in bacterial survival under adverse conditions, in their tolerance to antibiotic treatment and in the development of antibiotic resistance.[123,207,208] The attenuation of the *P. aeruginosa* virulence in polyP deficient phenotypes was confirmed in ocular and burned-mouse models.[198,209] Furthermore, a greater susceptibility to the treatment with antibiotics was observed for both *ppk1* and *ppk2* mutants.[210,211]

A similar phenotypic profile has also been reported for mutants of the enteric intracellular pathogens *Shigella flexneri* and *Salmonella typhimurium*, which reportedly exhibited increased sensitivity to low pH, high temperature and antibiotics, and were impaired in biofilm formation and motility [212,213]

The *ppk1* deletion mutants of *Campylobacter jejuni,* another gastric pathogen, were defective in survival during osmotic shock and under stringency conditions, although not affected with respect to motility, oxidative and thermal stress,[214] and their virulence attenuation was confirmed in an intraepithelial cell infection model.[214] Impairment of host invasion and intracellular survival was also observed for *ppk2* mutants of *C. jejuni.*[215]

A massive accumulation of polyP was detected during the infection stage of *Helicobacter pylori*[216] and a decrease of the fitness was observed in *ppk1* mutants.[217] Although the mutants growth was not impaired, in association with the decrease of motility, the ability to colonize the mouse gastric mucosa was significantly reduced[218] and the involvement of polyP in maintaining viability under anaerobic conditions was observed.[216]

Further to the commonly observed effects on motility, biofilm formation and increased sensitivity to antibiotic, a role of polyP in the sporulation process was reported for the Gram positive *Bacillus cereus,* which is commonly used as a model of the highly pathogenic *Bacillus anthracis.*[219]

A role of polyP in the pathogenicity of *Mycobacterium tuberculosis*, known for its ability to persist for long periods within infected tissues with a decreased susceptibility to antibiotics, has also been reported. *M. tuberculosis* possesses both a *ppk1* and a *ppk2* gene. The PPK1 is involved in the regulation of the stress induced *mprAB-sigE-rel* signaling pathway, which

is responsible for the activation of the stringent response in *M tuberculosis*.[220] In particular, polyP controls the expression of the two component system histidine kinase gene *mprAB,* which is involved in the regulation of the expression of the sigma factor σ^E. This in turn regulates *rel* expression, therefore affecting the ppGpp synthesis.[220] On the other hand, the PPK2 was reported to affect the intracellular pool of GTP and to be involved in the activation of responses to survive low pH, hypoxic and thermal stress.[221] Increased tolerance to isoniazid, impaired growth during macrophages infection were observed for the *ppk2* mutants.[221,222] Interestingly, an increase of the expression of IL-2 and IL-10 cytokine was observed in the microphages infected with *ppk2* mutants, suggesting a certain involvement of PPK2 in the interaction of *M. tuberculosis* with the host and in the activation of the immune response.[222]

The involvement of polyP in pathogenicity has also been reported for the bacteria *Vibrio cholerae*, *Burkholderia pseudomallei* and *Francisella tularensis*, which are classified as biowarfare agents. Attenuation of motility and biofilm formation was reported for *ppk* mutants in both *V. cholerae*[223] and *B. pseudomallei*, with the latter also presenting higher susceptibility to oxidative stress.[224] In *F. tularensis*, polyP has been reported to modulate the transcriptional regulator MglA, from which the activation of the stringent response, the resistance to oxidative stress, and the regulation of virulence gene depends.[225,226] Furthermore, *ppk* mutants of *F. tularensis* reportedly exhibit defects in intracellular growth and resulted attenuated in virulence.[227]

1.3.3. Polyphosphate kinase 2 as a potential new antibiotic target

1.3.3.1. Polyphosphate kinase 2

The PPK2 enzymes belong to the large superfamily of P-loop (phosphate binding motif) NTPase kinases.[228] P-loop kinases typically hydrolyse the β-γ bond of nucleotide triphosphates and are structurally characterised by two conserved motifs, the Walker A and the Walker B motif, which bind the β and the γ phosphate and a magnesium ion. PPK2 enzymes do not share any sequence similarity with the PPK1 enzymes and were initially identified in *P. aeruginosa*.[114] Homologues of PPK2 have been found in 34 species, including Gram-positive and Gram-negative bacteria[114] and 722 PPK2-like sequences have been identified in the database of sequenced microbial genomes.[229] Both PPK1 and PPK2 catalyse the transfer of a phosphate unit from a nucleotide onto the polyP chain and *vice versa*, with a processive mechanism. *E. coli* PPK1 preferentially catalyses polyP synthesis using exclusively ATP as substrate, while for polyP driven phosphorylation, all NDPs are used in the following order of preference: ADP>GDP>CDP>UDP.[110] On the other hand, PPK2 typically has a remarkable preference for the polyP degradation. The PPK2 from *P. aeruginosa,* the first to be characterised, showed a preference for GDP over ADP in the polyphosphate driven phosphorylation, whilst GTP and ATP are used equally well for the polyP synthesis.[115] In the genome of *P. aeruginosa* a two-domain PPK2, which phosphorylates AMP (or GMP) rather than ADP (or GDP), was also identified.[229] The successive identification of a single domain phylogenetically distinct PPK2, capable of phosphorylating AMP and then ADP,[229–232] led to the proposition of a sub-classification of the PPK2 in three sub-classes. The distinction was made based on the ability to synthesize nucleoside triphosphate from either di- or monophosphates.[232] Belonging to class I are PPK2 enzymes with one-domain, which catalyse the formation of nucleoside triphosphates from nucleoside diphosphate. PPK2 enzymes with two-domains instead catalyse the synthesis of nucleoside diphosphates from their monophosphates and are classified as class II. And finally, PPK2s with one-domain, capable of catalysing the synthesis of nucleoside triphosphates both from their mono- and diphosphates, were classified as class III.[232,233]

1.3.3.2. The biowarfare agent *Francisella tularensis* as a model for intracellular pathogens

1.3.3.2.1. Biowarfare agents

The term bioterrorism designates the intentional use of biological agents as a means for mass destruction.[234,235] During the early twentieth century, research programs for the development of bioweapons were undertaken by many countries.[234,236,237] Bioterrorism is still considered to remain a serious threat to public health and safety.[234] Potential biowarfare agents have been grouped in three categories.[238] Category A includes agents that can be easily transmitted or spread from person to person and that have a potential for high mortality. The pathogens included in the category A are *Bacillus anthracis*, *Yersinia pestis* and *Francisella tularensis*.[238] Category B includes agents which are moderately easy to disseminate and that have a moderate morbidity and a low mortality rate. The pathogens that belong to this category are *Brucella spp.*, *Burkholderia mallei* and *pseudomallei*.[238] Finally a third category, the category C, includes emerging pathogens that could be engineered for mass dissemination because they are easily available, easy to produce and have a potential for high morbidity and mortality rate.[238] The current measures against potential biowarfare agents consist of vaccination, passive antibody therapy and antibiotic therapy.[239] However, neither vaccination nor antibody therapy are well-suited to face a bioterrorism event.[234,239] Only the use of antibiotics, if administered early enough, can be sufficiently effective to treat infections caused by some of the biowarfare agents.[239,240] However, this resource is threatened by the emergence of resistance, either naturally occurring or potentially produced by bioengineering technologies. Resistant strains have been reported for *B. anthracis*, *Y. pestis* and *B. pseudomallei* (appropriate susceptibility tests are not available for *F. tularensis*).[240] As a consequence, the development of antibacterial agents with a new mode of action, as a possible alternative for the treatment of resistant strains, is highly sought after.

1.3.3.2.2. Francisella tularensis

Francisella tularensis, a Gram-negative bacillus, is the causative agent of tularaemia,[241] a rodent infection that can spread to humans.[242] Humans are accidental hosts, and are usually infected via exposure to contaminated water or meat, by tick bites and by inhalation of

contaminated dust.[242] No human-to-human transmission has been observed.[243] However, *F. tularensis*, which is highly pathogenic and infectious (inoculation dose of only 10 microorganisms) is regarded as a biowarfare agent.[243] Exposure by inhalation is most likely to be exploited for a terrorist attack, by releasing *F. tularensis* in aerosols.[243]

F. tularensis is a facultative intracellular pathogen that multiplies in microphages. The infection occurs via skin, mucous membranes, gastrointestinal tract and respiratory airways.[243] At the site of inoculation, lesions and pus arise, eventually leading to ulcerations. As part of the inflammatory response, macrophages migrate to the site of entrance, in which *F. tularensis* replicates. Following this, bacteria spread to the nearby lymph nodes, where they further replicate, and then spread to other organs in the body.[243] Swelling of the lymph nodes at the site of inoculation and fever are general characteristic symptoms of tularemia. Five forms of tularemia can be distinguished based on the exposure: ulceroglandular and glandular (swelling with and without ulceration) from skin exposure; oculoglandular from eye exposure; oropharyngeal from ingestion; pneumonic from inhalation.[241] The latter is the most severe form, with development of haemorrhagic inflammation of the airways, which can progress to bronchopneumonia.[241,243]

No licensed vaccine is available for the prophylaxis of tularemia, although a live vaccine strain was developed and is effective against administration of a low infection dose. The vaccine does not provide protection to high infection doses and cases of reversed virulence have been observed, which make the vaccine not safe for public use.[244] Historically the antibiotic of choice for the treatment of tularemia has been the aminoglycoside streptomycin,[245] which could also be replaced by gentamicin (another aminoglycoside). However, due to their nephrotoxicity and ototoxicity, aminoglycosides are only used in the most severe cases.[244] Chloramphenicol and tetracycline are also active on tularemia, but problems of hematopoietic toxicity and relapses may arise, respectively.[243] The current drug of choice is the fluoroquinolone ciprofloxacin.[244,246]

F. tularensis is phagocytosed by macrophages and during the initial part of its life cycle resides in the phagosome. Here, by means of the acid phosphatase protein AcpA, *F. tularensis* inhibits the release of reactive oxygen species, activated to neutralize

phagocytosed particles or bacteria (respiratory burst).[247] *F. tularensis* also causes arrest of the phagosome maturation. The increase of acidity in the phagosome leads to the burst and release of bacteria in the macrophage cytoplasm.[248] Eventually, *F. tularensis* induces macrophage apoptosis and bacteria are freed.[249]

For survival, intracellular pathogens have developed the ability to adapt to the different conditions encountered in the phagosome (reactive oxygen species, low pH, low nutrients) and in the cytoplasm (competition with the host cell for nutrients).[250] One of the most important genes for the intra-macrophage growth and for virulence of *F. tularensis* is *mglA*, which codes for the macrophage locus protein A (MglA).[251] MglA is involved in the activation of the general stress response, heat/cold shock response, oxidative stress and stringent response[226] and in the regulation of the pathogenicity islands (FPI).[252,253] The FPI are a group of genes that code for virulence factors and for the type VI-like protein secretion system, which is required for intra-macrophage growth.[254,255] MglA forms an heterodimer complex with the stringent starvation protein A (SspA), and the complex binds to the RNAP, promoting the expression of the FPI genes (Figure 1.12).[252] A third component, FevR (in some cases named PigR), a DNA-binding protein, and ppGpp also seem to be involved in the positive modulation of the gene expression mediated by the complex MglA-SspA-RNAP.[256] It was proposed that FevR directly interacts with the MglA-SspA complex, bound to RNAP, and that this interaction is promoted by ppGpp (Figure 1.12).[256,257] The latter has been shown to be required for virulence by *relA* mutant studies, in which bacteria lacking ppGpp resulted attenuated in macrophages.[258] A clear link between environmental and nutrient stress experienced in the host cell and FPI gene expression has been identified. The activation of stress responses and stringent response leads to the increase of ppGpp, which in turn results in the activation of the FPI genes by positive modulation of the FevR-MglA-SspA-RNAP complex (Figure 1.12).[259] The ppGpp-dependent promotion of the FPI genes can be linked to the regulation of the polyP concentration, which in the presence of ppGpp increases due to inhibition of PPX.[225] PolyP is involved in a direct interaction with the MglA-SspA complex, on which it exerts a stabilizing function, hence favouring the FPI gene expression (Figure 1.12).[225] MglA seems also to modulate the expression of PPK2 in

F. tularensis. This may explain the positive effect on the activation of stress responses, which in bacteria is commonly mediated by polyP (section 1.3.2.2 and 1.3.2.3).[225]

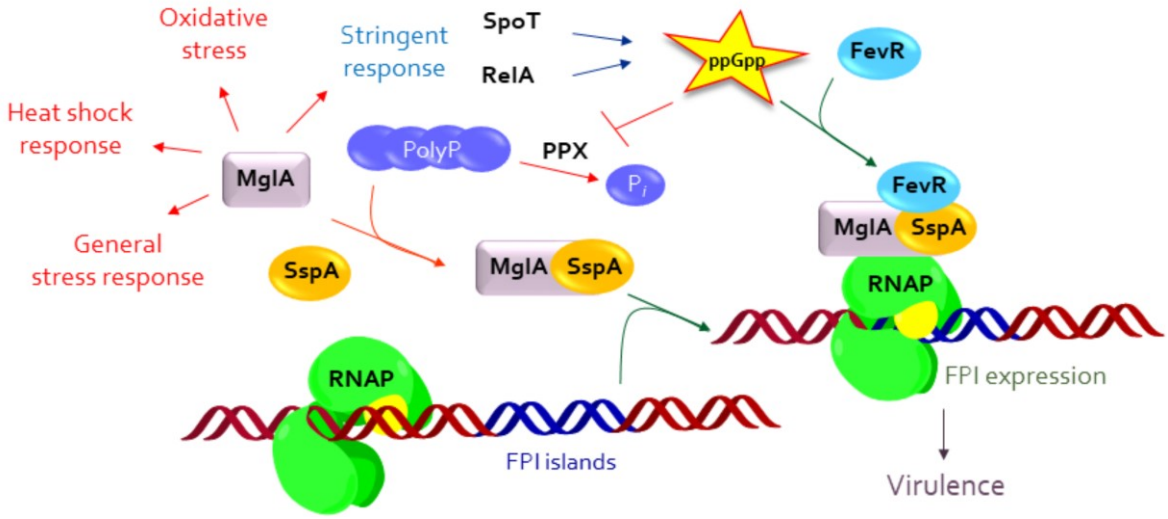

Figure 1.12: *F. tularensis* pathogenicity island expression

MglA exerts a control on the expression of *F. tularensis* pathogenicity islands (FPI), by formation of a complex with SspA and FevR. The complex MglA-SspA-FevR directly interacts with RNAP leading to the expression the FPI. The formation of the complex MglA-SspA-FevR is favoured by ppGpp, which directly promotes the aggregation of FevR to the MglA-SspA and indirectly promotes the formation of the MglA-SspA complex, via positive modulation of polyP. The latter is involved in the stabilisation of the MglA-SspA complex. Alongside the effect on the FPI expression, MglA is also involved in the activation of different stress responses.

1.3.3.2.3. Virulence attenuation of *F. tularensis ppk2* deletion mutants

The relevance of polyP in the pathogenicity of *F. tularensis* has been investigated by the construction of *ppk* (FTT1564 gene) deletion mutants of *F. tularensis*, subspecies *tularensis* (strain SCHU S4).[227] The *ppk* mutants, in which no polyP production was observed, were tested for intracellular growth in macrophages and for virulence attenuation in mice.[227] By comparison with the wild type, growth defects in macrophages were observed after 24 h from inoculation and were even more significant after 48 h (Figure 1.13*a*). To test for virulence attenuation, mice were injected with two doses of wild type and mutants. Upon injection of the wild type (2×10^2 and 2×10^4 c.f.u.), no mice survived the challenge. On the other hand, all the mice survived when the lower dose of mutant (4.5×10^2 c.f.u.) was

administered, although some died at the higher dose (4.5×10^4 c.f.u., Figure 1.13*b*).[227] Alongside growth defects and attenuated virulence, the *ppk* deletion mutants also showed an increased sensitivity to the antibiotics that have been used for the treatment of *F. tularensis* infections (Figure 1.13*c*).[260]

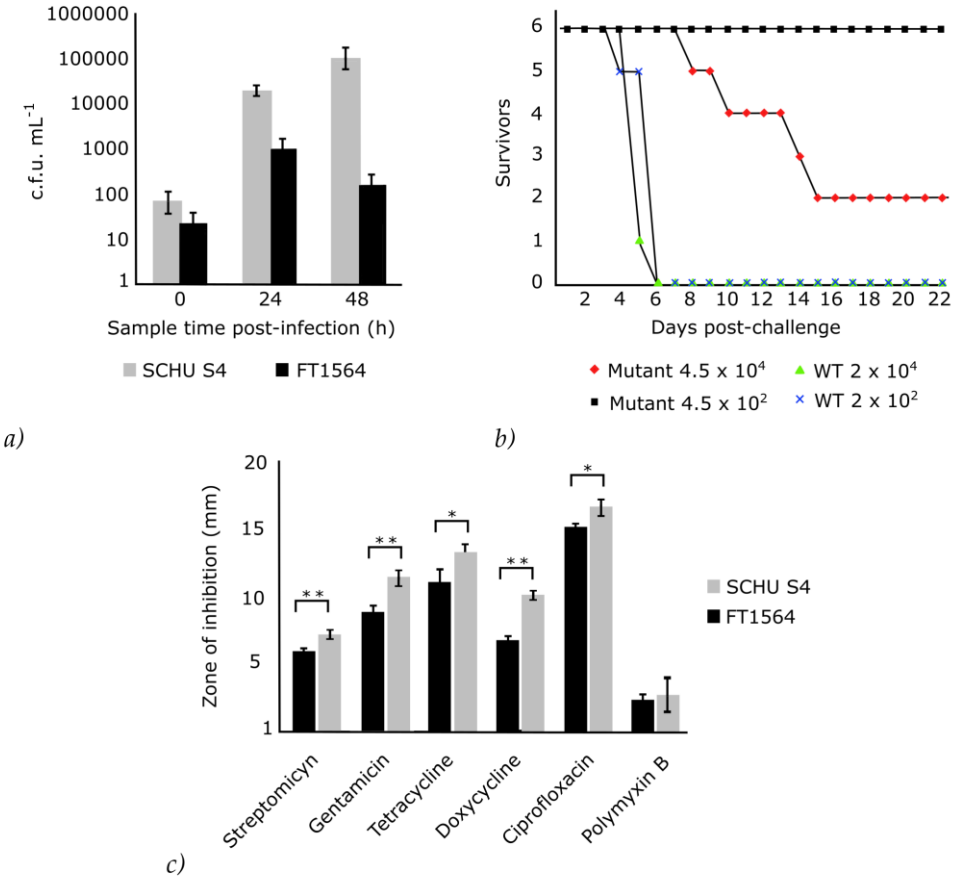

Figure 1.13: *In vivo* validation of *Ft*PPK as potential target for antibiotics

a) Comparison of wildtype *F. tularensis* (SCHU S4) and *Δppk* mutants (FT1564) growth in macrophages. *b*) Virulence of wildtype and *Δppk* mutant at different doses in mice model. *c*) Comparison of wildtype *F. tularensis* (SCHU S4) and *Δppk* mutants (FT1564) antibiotic sensitivity. The figure was adapted with permission from Richards *et al.*[227]

1.3.3.2.4. *F. tularensis* polyphosphate kinase

The genome of *F. tularensis* contains a single copy of a polyphosphate kinase gene (FTT1564 gene). The *F. tularensis* PPK (*Ft*PPK) has been characterised as a class I PPK2-like enzyme.[260] Catalytic activity was observed when using nucleoside di- or triphosphates, while

nucleoside monophosphates were not accepted as substrates.[260] *Ft*PPK showed substrate specificity for purine nucleotides, with no activity observed on the pyrimidine nucleotides. Unlike other PPKs characterised, no significant preference for the polyphosphate driven phosphorylation of nucleosides diphosphates over the polyP synthesis was observed when using GDP or GTP as substrate. A slight preference was instead detected for ADP over ATP. The efficiency in catalysing reactions from GDP or ADP was comparable.[260] Divalent ions, either Mg^{2+} or Mn^{2+}, and an optimal pH of 8 were required for activity.[260] No binding of nucleotides was observed in the absence of polyP, which is probably required for the acquisition of an active confirmation.[260]

1.4. Project Aims

The involvement of polyP in different adaptation responses and in pathways related to virulence and the activation of persistence suggests that the PPK enzymes may constitute suitable new antibacterial targets. Due to the widespread occurrence in the genome of various pathogens (e.g. *P. aeruginosa*, *M. tuberculosis*), PPKs could serve as a target for a broad spectrum antibiotic, although some limitations may arise for pathogens owning both a PPK1 and a PPK2.[114] In humans, polyP is involved in blood clotting.[261,262] To date, the human enzyme responsible for polyP synthesis or enzymes with sequence similarities to the bacterial PPKs have not been identified.[263] Thus, a potential antibiotic targeting PPK would be likely to have little or no toxicity.

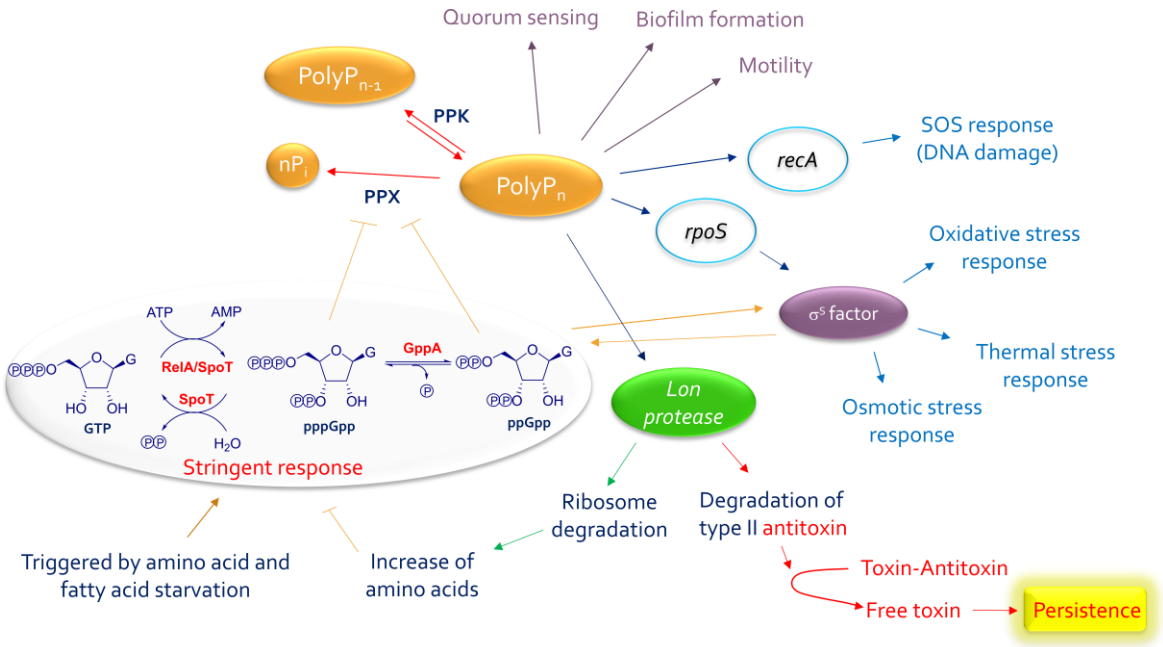

Figure 1.14: Involvement of PolyP in adaptation responses, virulence and persistence

PolyP exerts an integrated control on adaption responses, contributing to the activation of stress responses and the SOS damage response, by positively modulating the expression of the *rpoS* and *recA* gene, respectively. Upon stimulation of the Lon protease activity, polyP indirectly contributes in restoring the free amino acids pool and to the appearance of persistence. In many pathogens, polyP is also involved in the mechanisms that regulate motility, quorum sensing and biofilm formation.

For the project reported herein, PPK from *F. tularensis* was used as a target for the development of a new class of antibiotics. The biowarfare agent *Francisella tularensis* possesses a single copy of a PPK2 enzyme (*Ft*PPK). The *Ft*PPK has been cloned and

kinetically characterised (section 1.3.3.2.4).[260,264] Structural information are also available, both of the apo-form and in complex with polyP and with a non hydrolysable analogue of ATP (section 5.2.4).[264,265]

The link between polyP and *F. tularensis* virulence has been confirmed by *ppk* deletion mutant studies (section 1.3.3.2.3).[266] In the absence of polyP, *F. tularensis* reportedly exhibited growth defect and attenuated virulence. The involvement of polyP in *F. tularensis* virulence was also confirmed by the discovery of a direct interaction between polyphosphate and the MglA/SspA complex, which in *F. tularensis* regulates the expression of virulence genes (section 1.3.3.2.2).[225]

The investigation of *Ft*PPK as a target served the purpose, in the first place, of identifying a new chemical scaffold that could be further developed into a novel antibiotic for the treatment of *F. tularensis*. Given the potential as biowarfare agent, the development of a new antibiotic against *F. tularensis* is required as an alternative to the current drugs of choice, in case resistance arise. Possible antibiotics hitting antivirulence targets have been reported to have the potential of being used for prophylaxis.[71] Hence, an antibiotic targeting PPK might also be used in the event of a bioterrorist attack. .

Despite the main purpose of developing a new antibiotic for the *F. tularensis*, the potential for a broader spectrum of action remains, given the presence of PPK2 enzymes in various pathogens. In particular, the prospective of exploiting PPK2 as antibiotic target has been envisaged for important pathogens such as *M. tuberculosis*[267,268] and *P. aeruginosa*.[211]

The objective of the research project was to identify an inhibitor of the polyphosphate kinase 2 from the biowarfare agent *Francisella tularensis* (*Ft*PPK) and to evaluate its potential as an antibacterial agent. To pursue this goal, a high throughput screening approach was adopted. The optimisation of a primary assay to a standard suitable for HTS was required in conjunction with the development of alternative formats (secondary assays) to validate the inhibitors identified with the screening. Some preliminary investigation of the mode of inhibition was also undertaken.

Chapter 2

Development and Optimisation of a Luminescence Coupled Assay for the *Francisella tularensis* Polyphosphate kinase

2.1. Introduction

When a target is selected for a screening campaign, the biochemical characterization of the target, including the investigation of the optimal conditions for catalysis and detailed kinetics analysis, provides a significant support to assist the design of a rigorous biochemical assay for high throughput screening (HTS). The choice of the biochemical assay to develop for HTS must take into account factors such as the assay throughput, hence the ability to deliver speed and adaptability to automation and miniaturization, but also factors such as sensitivity and the potential for accurate and reproducible measurement of enzyme activity.[269] Another factor that cannot be ignored, especially for larger screening campaigns, is the cost.[269] Assays with spectroscopic detection methods tend to fulfil the stated criteria and are the dominant assay formats applied for HTS.[269,270] The design and optimisation of the biochemical assay, to ensure that the assay readout signal provides an accurate measure of the target activity, constitutes a non-trivial and critical step to the success of a screening program. This chapter describes the optimisation of a luminescence coupled assay to measure the *Ft*PPK activity and its validation by kinetic characterization of the *Ft*PPK is reported.

2.1.1. Principles of Enzyme Kinetics

Enzymatic reactions are described in terms of rate of the catalysed reaction. For a general enzymatic reaction in which E is the enzyme, S the substrate, ES the enzyme-substrate complex, and P the reaction product, the kinetic characterization is conducted under the steady-state conditions, that is at a constant concentration of ES.[271–273] The latter is a consequence of the balance between ES formation and ES disappearance, which is due to both dissociation back to E plus S and to the chemical conversion of ES into P and the free enzyme.[271]

$$E + S \underset{k_{-1}}{\overset{k_1}{\rightleftharpoons}} ES \xrightarrow{k_2} E + P$$

Eq. 2.1: Enzyme kinetics, the steady-state model

k_{-1} and k_1 are the dissociation and association rate constants of the complex ES, of which the ratio corresponds to the equilibrium constant K_d (or K_s); k_2 is a first order kinetic rate constant for the conversion of ES into P, which for a simple reaction is equal to the catalytic constant K_{cat}.

For the steady state conditions to apply, the following assumptions are made: the enzyme is in catalytic amount ([E]<<[S]); the concentration of S is in large excess compared to the concentration of E; the rate is measured under the initial rate conditions (approximately, less than 10% substrate consumption). Under these conditions, the concentration of S can be considered constant and the reverse reaction rate negligible. Therefore, the rate is exclusively a function of the ES concentration and as such is constant and proportional to the E concentration.[271,272]

The progress of an enzymatic reaction in the presence of an initial substrate concentration S_0, can be monitored by means of a *time course*, that is by measuring either the substrate concentration or the product formation at a series of selected time points. While in theory monitoring either one should not make any difference, in practice it is more accurate measuring a small increase in concentration of product rather than a small decrease in a large concentration of substrate. During the initial phase of the reaction, the product increases linearly with time and the rate is constant (initial rate, v_0). With the progress of the reaction, this trend is broken due to the decrease of the substrate concentration, which leads to a decrease in rate. Eventually, the equilibrium with the backward reaction is

reached, at which point the rate is equal to zero.[272] To allow for the deviation of the rate from perfect linearity, the increase of the product with time can be modelled as a pseudo-first order process[a] and is described by an exponential one-phase equation:

$$P = P_{max}(1 - e^{-kt})$$

Eq. 2.2: One phase pseudo-first order association equation[b]

P is the product concentration a t time, P_{max} is the product concentration at t_∞ (which is equal to S_0) and k is the rate constant.[271,274]

By fitting points from a complete time course plot to Eq. 2.2 (which may include data ranging from the initial phase to the equilibrium phase of the reaction), the value of the rate constant k can be determined. The latter can in turn be used to calculate the apparent initial rate v_0^{app} for the simplified enzyme reaction S → P according to the equation:

$$v_0^{app} = k[S_0]$$

Eq. 2.3: Apparent initial rate

k is the rate constant and S_0 is the concentration of substrate at $t = 0$. [271,274]

Alternatively, if, rather than points from a complete time course which deviates from strict linearity, only time points in the initial nearly linear phase of the reaction progress have been measured, the apparent initial rate v_0^{app} can be defined as the slope of the linear regression of product concentration against time (Eq. 2.4).[272]

$$y = y_0 + ax$$

Eq. 2.4: Linear regression equation

When applied for the determination of the v_0^{app}, y is the reaction product, y_0 is the intercept to the y axis and under steady state condition is expected to be equal to 0, a is the slope of the linear regression and a measure of v_0^{app}, x is time.

[a] A reaction with two substrates follows a second-order kinetics, however if one of the two substrates is in very large excess the kinetics can be approximated to a pseudo-first-order kinetics

[b] Eq.2.3 corresponds to $S = S_0(e^{-kt})$, which describes the substrate consumption with time.

As a rule of thumb, the upper limit of the linear phase of a reaction corresponds to 10% of substrate depletion. Below this limit only a small amount of substrate has been depleted, therefore it is possible to consider the substrate concentration approximately constant.

Under steady-state conditions and at a fixed concentration of E (catalytic concentration), the initial rate v_0 varies with the S concentration. At low concentration of S, a linear increase of v_0 with S is observed. Once again, the trend breaks down at higher concentration of S due to the increasing saturation of E, eventually leading to a maximum velocity ($V_{\max}$), at which the enzyme is fully saturated. For a single substrate enzyme, the relation between v_0 and S is described by the Michaelis-Menten equation:

$$v = \frac{V_{max}[\mathrm{S}]}{K_\mathrm{m} + [\mathrm{S}]}$$

Eq. 2.5: Michaelis Menten equation

v is the reaction rate at the substrate concentration S, V_{max} is the maximum rate under saturating conditions of S, K_m is the Michaelis-Menten constant which is equal to the substrate concentration at which half of the V_{max} is observed.[275,276]

The value of K_m and $V_{\max}$ can be derived by fitting a plot of initial rate against substrate concentration to the Michaelis-Menten equation (Eq. 2.5), and $V_{\max}$ in turn can be used to derive the value of the catalytic constant k_{cat} according to the following equation:

$$V_{max} = k_{cat}[\mathrm{E}]$$

Eq. 2.6: V_{max} equation

V_{max} is the maximum rate under saturating conditions of S, k_{cat} is the catalytic constant and E is the enzyme concentration.

The K_m is often considered a measure of the affinity of S to E and is therefore comparable to the dissociation constant K_d.[271,273] However, this is true only in the special case where $k_2 \ll k_{-1}$. The original Michaelis-Menten equation does not strictly apply to the steady-state model but was based on the assumption that the ES complex was in equilibrium only with E and S ($k_2 \ll k_{-1}$). The relationship between K_m and K_d is better described by the Briggs-Haldane equation.[271,273,277] The latter was derived from the elaboration of the steady-state

theory, hence taking into account the disappearance of the ES complex due to chemical conversion to P:[277]

$$v = \frac{k_2\,[\mathrm{E}][\mathrm{S}]}{\left(\frac{k_{-1} + k_2}{k_1}\right) + [\mathrm{S}]}$$

Eq. 2.7: Briggs-Haldane kinetics equation

k_{-1} and k_1 are the association and dissociation rate constant of ES and k_2 is the rate constant of the conversion of ES into P.

The Michaelis-Menten equation (Eq. 2.5) and the Briggs-Haldane equation (Eq. 2.7) have the same form and by comparison it is possible to derive Eq. 2.8, which defines the K_m for all the enzymatic mechanisms.[271]

$$K_\mathrm{m} = \left(\frac{k_{-1} + k_2}{k_1}\right)$$

Eq. 2.8: Relation between K_m and ES formation and disappearence of rate constant

K_m is the Michaelis-Menten constant, k_{-1} and k_1 are the association and dissociation rate constant of ES and k2 is the rate constant of the conversion of ES into P.

The Eq. 2.8 can be re-written as Eq. 2.9, which describes the relation between K_m and the dissociation constant K_d.[271]

$$K_\mathrm{m} = K_\mathrm{d} + \frac{k_2}{k_1}$$

Eq. 2.9 Relation between K_m and K_d

K_m is the Michaelis-Menten constant, k_{-1} and k_1 are the association and dissociation rate constant of ES and k_2 is the rate constant of the conversion of ES into P.

2.1.2. Biochemical assays: Direct Assays and Coupled Assay

Biochemical assays are experimental protocols developed to measure the properties of biomolecules. For enzymes, these properties usually relate to their catalytic activity (activity assays) or to their ability to bind ligands (binding assays). In the first case, the enzymatic reaction is monitored by direct or indirect measurement of substrate consumption or of product formation. In the second case, the binding of a ligand is measured by displacement for competitive binding of a labelled ligand of known affinity. Spectroscopic techniques (e.g. fluorescence, luminescence, UV-vis absorbance) or analytical techniques (HPLC, mass spectrometry, LC-MS) are used as readout methods based on the properties of the analyte of interest, which can be measured either in a continuous format or in a discontinuous format. In the first case, the progress of the reaction can be monitored in real time by direct measurement of the readout signal, which is generated during the reaction without the need for additional operations. In contrast, for discontinuous assays the reaction must be stopped to allow analyte analysis by appropriate methods. Continuous assays are spectroscopic-based and are characterised by high throughput and by a greater versatility with regard to the format design. Discontinuous assays are mostly based on analytical techniques, and as such entail a low throughput, and are used to analyse compounds that are not spectroscopically active.

An alternative to the direct measurement of the analyte of interest by either spectroscopy or by analytical techniques (direct assay), consists in the coupling to a secondary process that causes a detectable change in the system, or that converts the product of the reaction of interest into a second detectable analyte (indirect assay). Examples include the variation of the signal observed when the analyte displaces a spectroscopically-active ligand from binding with an enzyme or an antibody,[272,278] or the chemical reaction of the analyte with a reagent resulting in a spectroscopically-active compound.[272,278] Another special example involves the conversion of the analyte into a detectable compound by means of an enzyme-catalysed reaction, known as coupled assay.[272,278]

A coupled assay is a system constituted by a primary assay, in which the target of interest catalyses the formation of the respective product, and by a secondary assay, in which a

secondary enzyme catalyses the conversion of the product of the first reaction into a second product.[272,274,278–280] A coupled assay can be described by the model:

$$\mathrm{A} \xrightarrow{v_1} \mathrm{B} \xrightarrow{v_2} \mathrm{C}$$

Eq. 2.10: Coupled assay model

Primary assay or reaction of interest: conversion of A into B, with rate equal to v_1, secondary assay or coupled assay: conversion of B into C, with rate equal to v_2.

The purpose of a coupled assay is to measure the rate of formation of B by detection of C, therefore for an ideal system the condition $v_2 = v_1$ must apply. Under this condition, the concentration of B will be constant because of the balance between the formation, catalysed by the primary enzyme, and the depletion, catalysed by the secondary enzyme (steady-state condition). This is possible only if the primary reaction is rate limiting, hence $v_1 \ll v_2$, which ensures the immediate conversion of B into C. The rate measured by monitoring the production of C will therefore reflect the rate of formation of B. To ensure that v_2 is proportional to B, the primary assay condition should be adjusted so that the steady state concentration of B is lower than the K_m of the coupled enzyme for B ($K_{\mathrm{m}2}$). The Michaelis-Menten model applies to the secondary reaction and, for $\mathrm{B} < K_{\mathrm{m}2,}$ the dependence of v_2 on B follows a first order kinetics. On the other hand, if the condition $v_2 \ll v_1$ applies, the product B will accumulate because of the slower conversion of B into C, of which the observed rate (measured as the accumulation of C) will no longer reflect the activity of the primary enzyme.

The right relationship between v_1 and v_2 can be established by optimisation of the enzyme concentration, utilizing catalytic amounts for the primary enzyme and an excess of the secondary enzyme. A lag phase is typically observed at the beginning of a coupled assay when the secondary enzyme concentration is not fully optimised.[272,274,278,279] This lag phase can be explained with the dependence of the coupled assay rate v_2 on the concentration of B, which during the initial phase is building up towards steady state concentration and therefore is not sufficient to sustain v_2 at the same rate as v_1. However, as time progresses, the accumulation of B reaches the steady state concentration when $v_2 = v_1$. The time required for v_2 to match v_1 corresponds to the lag phase observed.[279]

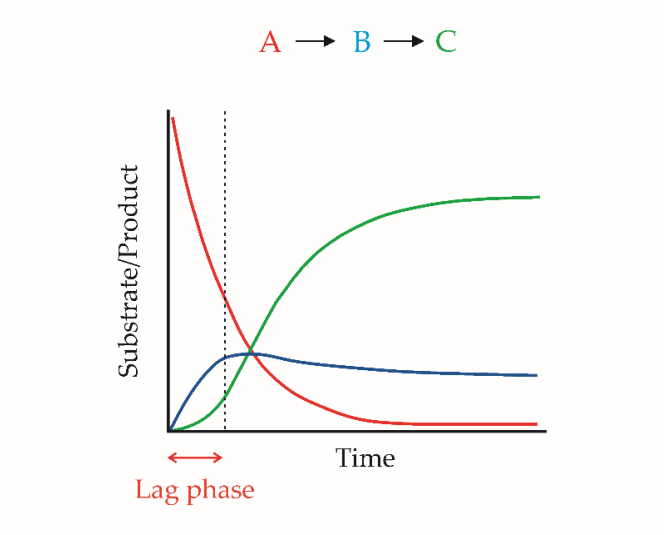

Figure 2.1: Coupled assay time course

Representation of a coupled assay time course with the respective variation of the concentration of A, B and C until equilibrium is approached. The substrate A exponentially decreases with time, while the primary reaction product B initially builds up until a steady state concentration is reached. The primary reaction product B is converted into the secondary reaction product C. A lag phase is observed in the early stages when the concentration of B is not enough to allow v_2 to match v_1. Further accumulation of B eventually leads to the establishment of the relation $v_2 = v_1$, at which steady state concentration of B is achieved and the production of C follows a pseudo first order kinetic model. The figure was adapted from Fersht, A. (1985).[281]

It is of critical importance for the reliability of the coupled assay that the steady-state ($v_2 = v_1$) is reached while the primary reaction is still within the linear phase, hence while v_1 is constant.[274] Therefore, the lag phase must be minimized as much as possible. This can be achieved by increasing the concentration of the coupled enzyme so that it can catalyse the formation of C from low concentrations of B more quickly. The Michaelis-Menten model can be applied to the secondary reaction; hence, the V_{max} of the coupled reaction (V_{max2}) is proportional to the concentration of the coupled enzyme. The concentration of the coupled enzyme required to remove the lag phase can be theoretically calculated by means of an equation, derived by Storer and Cornish-Bowden (Appendix, section A2 1).[278] Alternatively, experimental optimisation can be conducted by measuring the rate at increasing concentrations of the coupled enzyme while maintaining the primary enzyme concentration constant. For a fixed concentration of primary enzyme, observing no variation of the rate when varying the secondary enzyme suggests that an adequate excess of the secondary enzyme has been applied.

2.1.3. Development of a Luminescence Coupled Assay for *Francisella tularensis* Polyphosphate Kinase

When developing an assay for high throughput screening (HTS), the appropriate detection method should be selected taking in consideration the ability to develop an homogeneous assay format and to deliver speed, accuracy and sensitivity and the adaptability to automation and miniaturization (section 3.1.2). Spectroscopic techniques based on photon emission (fluorescence and chemiluminescence) are the dominant methodology applied for HTS, due to their easy adaptation to different targets and because they allow assays to be developed in a continuous format.[269]

For the development of a *Ft*PPK assay, it was decided to monitor the polyP degradation in the presence of ADP, resulting in the formation of a shorter polyP chain and ATP. A luminescence coupled assay was chosen as the readout method to measure the ATP production (Scheme 2.1).

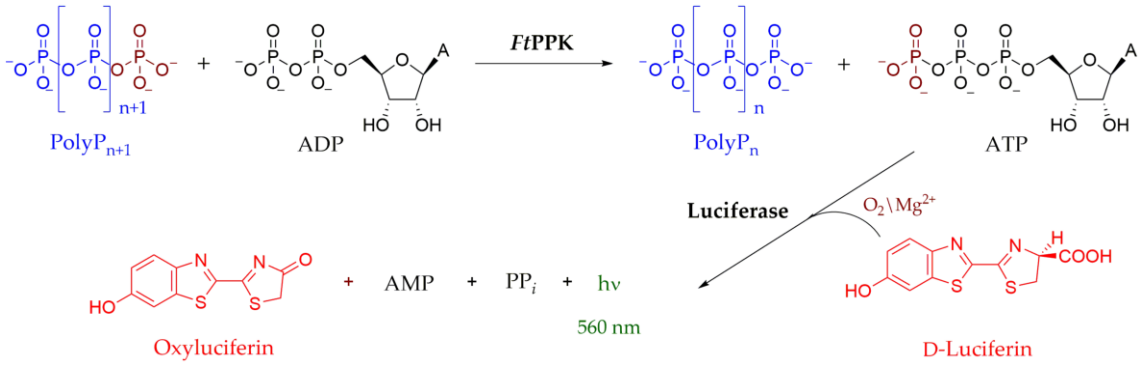

Scheme 2.1: *Ft*PPK luminescence coupled assay reaction

The *Ft*PPK catalyses the transfer of a phosphate unit from the polyP chain onto ADP (kinase reaction). The produced ATP can then be quantified by a secondary reaction catalysed by the luciferase (luminescence reaction). The ATP is consumed by the luciferase for the oxidation of the luciferin, which is accompanied by emission of light (560 nm). The intensity of the light emitted is proportional to the concentration of ATP.

The same assay was previously used by Ault-Riché in an early investigation of the PPK activity under stress conditions.[169] The luminescence assay is based on the bioluminescence reaction catalysed by the *Potinus pyralis* firefly luciferase. In the presence of magnesium ions and molecular oxygen, the luciferase oxidizes the luciferin to oxyluciferin.[282–285] The reaction requires ATP and is accompanied by emission of light (λ_{max} 560 nm). Under

optimised conditions, the intensity of the light emitted is proportional to the concentration of ATP. Hence, by coupling the luminescence assay to the *Ft*PPK reaction, the production of ATP can be monitored as a function of the light emitted. For kinase reactions, ATP constitutes the usual source of phosphate, hence reactions are often monitored in a substrate depletion format (ATP consumption). For the *Ft*PPK, it was possible to design a format based on product formation.[286] Because of the great sensitivity of the luminescence assay, which allows accurate detection of small variation of ATP concentration, it was possible to measure the enzyme activity strictly applying initial rate conditions (less than 10% substrate consumption). A great advantage provided by the luminescence assay is the inherent low background signal. Indeed, for luminescence, the transition to an excited state is not generated by absorption of light but is promoted by energy derived from an exothermic chemical reaction.[287–291] For the same reason, when luminescence assays are applied for the screening of compound libraries, possible signal interference due to spectroscopically-active compounds is strongly reduced (termed the inner-filter effect).[292] Nonetheless, a potential source of compound-mediated signal interference can derive from possible effects exerted on the luciferase. The latter is the main drawback of using a luminescence coupled assay for high throughput screening.[293] The problem can be adequately addressed by application of an orthogonal luciferase-independent assay (counter-screening).

2.1.3.1. Luminescence assay: mechanism and kinetics of light emission

Bioluminescence is a form of chemiluminescence, in which the light emitting reaction is catalysed by the enzyme luciferase. It is a widespread phenomenon that has been observed in many organisms including bacteria, fungi, insects, mollusks and fishes.[294] Luciferase enzymes from various organisms have been isolated and studied.[294,295] All the luciferases catalyse the oxidation of their substrate, known as luciferin, accompanied by the emission of light.[296] The structures of luciferins for different luciferases are quite diverse, as are the mechanisms of the reaction catalysed.[296,297] Nevertheless, a common pattern can be identified, which consists in the oxidation of luciferin by means of molecular oxygen, followed by the formation and the breakage of a four-member ring dioxetanone-intermediate resulting in the release of CO_2 and in the formation of a carbonyl compound in an

electronically excited state (Scheme 2.2). Light emission eventually results from the relaxation of the excited state.[296]

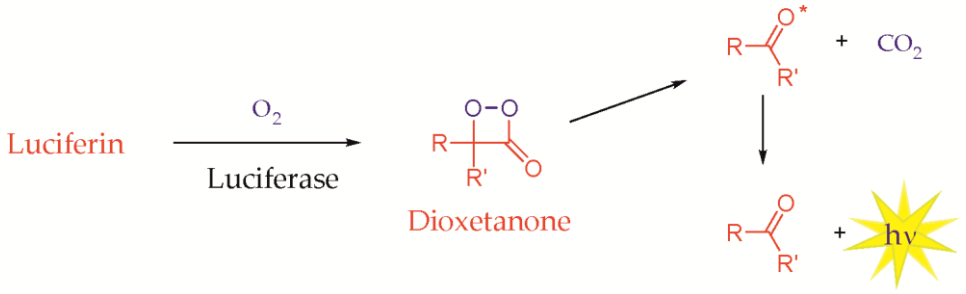

Scheme 2.2: General scheme for the luminescence reaction mechanism

Luciferase from the beetle *Photinus pyralis*, also known as Firefly luciferase (FLuc), is the luciferase that the most has found application for bioassays. The luminescence assay has been used, in particular, as an analytical method for detection and quantification of ATP, both in biochemical assays and in cell-based assays.[286,287,298–301] Another widespread application of FLuc has been as a gene-reporter, either on its own or in conjunction with other luciferases with a different spectroscopic profile (e.g. with *Renilla reniformis* luciferase).[287,298,302–305]

FLuc is a member of the ANL family of the adenylating enzymes superfamily (the Acyl-CoA synthetases, the NRPS adenylation domains, and the Luciferase enzymes),[306] which also includes the acyl- and aryl-CoA synthetases and the adenylation domains of non-ribosomal peptide synthetase.[283,306–308] The family is characterised by a shared two-step mechanism, involving a first step of carboxylate activation by adenylation, yielding an acyl-AMP intermediate. The seconds step consists of either the formation of a thioester or, for the luciferase, an oxidation step.[306]

The FLuc is a monomeric enzyme constituted by a 550 amino acid residues (62 kDa).[309,310] The monomer folds in two distinct domains: the N-terminal domain (1-436 aa) and a small C-terminal domain (440-550 aa), linked by a flexible loop.[311–313] The active site is located between the surfaces of the two domains, where residues conserved among the adenylating enzymes have been identified.[311] A characteristic of FLuc, as well as other enzymes belonging to the ANL family, is the C-terminal loop rotation of ~140° during catalysis, which orients

different faces of the same domain to the active site, depending on whether the first step or the second step are being catalysed.[313]

The substrate firefly luciferin, simply known as D(-)-Luciferin (D-LH_2), is a benzothiazolyl-thiazoline derivative, with S stereochemistry at the position 4 (Figure 2.2).[282,283,314,315]

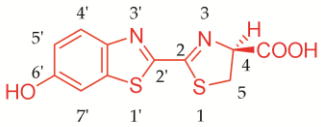

D-Luciferin

Figure 2.2: Structure of D-Luciferin

Luciferin is formally the (S)-2-(6′-hydroxy-2′-benzothiazolyl)-2-thiazoline-4-carboxylic acid. The stereochemistry is commonly reported using the denomination of D-Luciferin.

The mechanism of the bioluminescence reaction catalysed by FLuc entails two distinct steps: the adenylation of D-LH_2, leading to the formation of the luciferase-bound intermediate luciferin-acyl adenylate (FLuc:D-LH_2-AMP complex), and the oxidation of the latter to the complex FLuc:Oxyluciferin in an electronically excited state, of which the relaxation induces emission of light (Scheme 2.3).

$$\text{FLuc} + \text{D-LH}_2 + \text{ATP-Mg}^{2+} \rightleftharpoons \text{FLuc:D-LH}_2\text{-AMP} + \text{PP}_i\text{-Mg}^{2+} \qquad a)$$

$$\text{FLuc:D-LH}_2\text{-AMP} + \text{O}_2 \longrightarrow \text{FLuc:Oxyluciferin*} + \text{AMP} + \text{CO}_2 \qquad b)$$

$$\text{FLuc:Oxyluciferin*} \longrightarrow \text{Oxyluciferin} + h\nu \qquad c)$$

Scheme 2.3: Mechanism of the FLuc bioluminescent reaction

The luciferin adenylation occurs *via* a phosphoryl transfer mechanism. The nucleophilic attack by the carboxylic function in position C4 of the D-LH_2 thiazoline ring, on the electrophilic α-phosphoryl moiety of ATP, results in the displacement of the good leaving group PP_i and in the formation of the D-LH_2-AMP intermediate (Scheme 2.4).[282,316–318] The Mg^{2+} ion forms a complex with the β- and the γ-phosphate of the ATP, contributing to the neutralization of the negative charges, controlling the orientation of the ATP phosphate groups and activating the PP_i leaving group. The stereochemistry at the C4 of D-LH_2 is

crucial to the luminescence reaction. Although FLuc catalyses the adenylation of the other enantiomer, L(+)-Luciferin (L-LH_2), no luminescence is generated.[282,283,319]

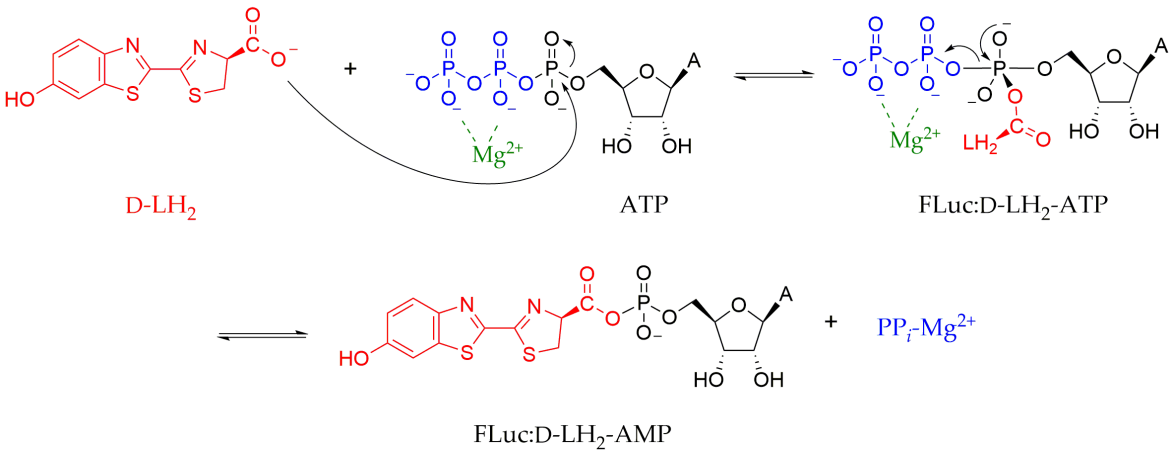

Scheme 2.4: Bioluminescence mechanism, D-LH_2-adenylation

The adenylation step occurs even in the absence of oxygen. The latter is required in the second step for the formation of the key intermediate luciferin-dioxetanone (Scheme 2.5), which breaks down via an oxidative decarboxylation of luciferin with concomitant emission of light (Scheme 2.6).

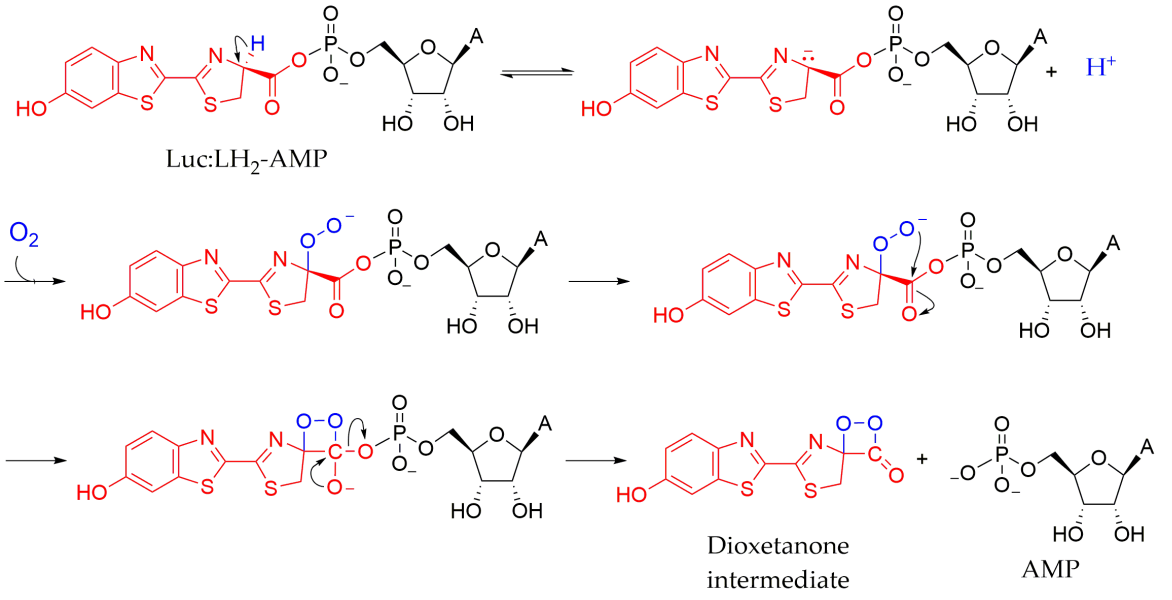

Scheme 2.5: Bioluminescence mechanism, D-LH_2-AMP oxidation to the dioxetanone intermediate

The addition of the AMP moiety to the luciferin has the effect of increasing the acidity of the H in position C4, allowing the generation of a very reactive carbocation intermediate that reacts by nucleophilic attack with O_2 (Scheme 2.5)[282,320] The resulting hydroperoxide intermediate in turn exerts an intramolecular nucleophilic attack on the carbonyl group, causing the displacement of the AMP moiety and the formation of the highly strained four-membered ring luciferin-dioxetanone (Scheme 2.5).[282,321–323] The spontaneous breakdown of the strained dioxetanone intermediate generates CO_2 and oxyluciferin (Scheme 2.6).[282,324–328] The process is accompanied by the release of a large amount of energy, which promotes the transition of the oxyluciferin to the excited singlet state.[282,329,330] The subsequent decay to the ground state results in the release of a photon with yellow-green emission (λ_{max} 560 nm, pH=7.8).

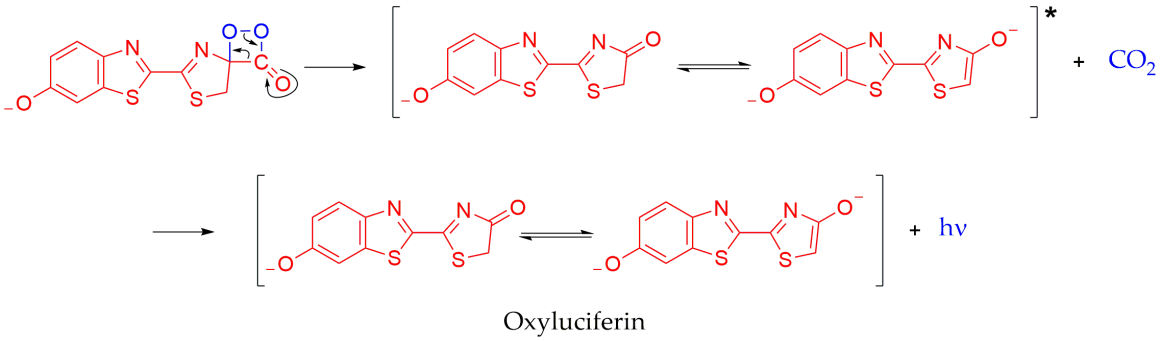

Scheme 2.6: Bioluminescence mechanism, dioxetanone intermediate breakdown and light emission

Factors such as the pH, the temperature and heavy metal cations can cause a redshift of the emission spectrum (up to λ_{max} 620 nm).[328,331,332] It was initially hypothesized that the colour modulation could be attributed to the enzyme-assisted keto-enol tautomerism of oxyluciferin (red emission from the keto-form, yellow-green emission from the enol form).[328,331,333] However, this hypothesis was dismissed when emission of yellow-green light was observed from an oxyluciferin analogue constrained in the keto-form.[334] Later, it was found that the anionic keto-form constitutes the only light emitter and that different colour emission could be ascribed to different oxyluciferin conformations derived from the twisting around the C2-C2' bond.[335,336] Recent papers have proposed that not just the oxyluciferin conformation but also conformational changes affecting the whole active site microenvironment influence the colour emission.[337,338]

According to early reports, luciferase catalyses the light emitting reaction with a very high efficiency; the ratio of photons emitted per D-LH_2 molecule consumed, or quantum yield, was reported to be 88%.[332] However, a recent study revised this value to 41%.[339] The FLuc light emission kinetics has a characteristic flash pattern. The peak of light intensity is reached after 0.3 sec, followed by an initial fast decay (0.8 sec to reach 50% inhibition) and then a slow decay with emission of low intensity light that may last for hours.[340] This characteristic kinetic pattern has been explained by product inhibition.[282,283,341,342] Indeed, the FLuc is inhibited by oxyluciferin, with a competitive mechanism (K_i = 0.5-2 µM), and by the dehydro-luciferyl-AMP (L-AMP), which is the product of a side reaction (20% of D-LH_2 is converted into L-AMP).[341] Further to the luminescent reaction, the FLuc catalyses side reactions that do not result in the emission of light and are therefore called dark reactions. The most important of these reactions is the oxidation of the D-LH_2-AMP into D-L-AMP by reaction with O_2 (Scheme 2.7).[318,343–345]

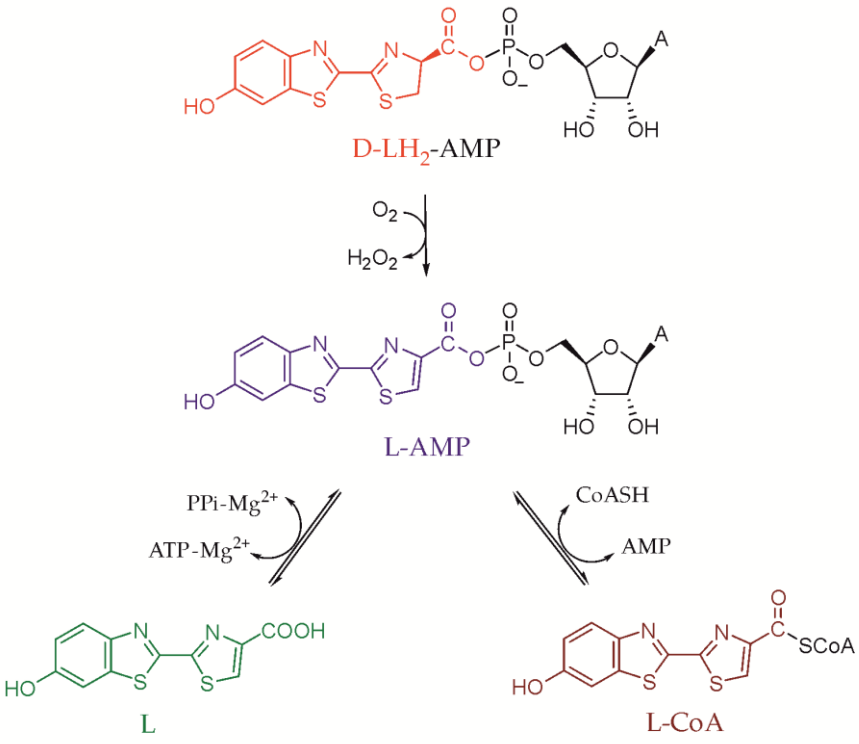

Scheme 2.7: Luciferase dark reactions

L-AMP is a powerful inhibitor, for which a profile as a tight binding competitive inhibitor has been reported (K_i = 3.8 nM).[318,341] By reaction with the PP_i-Mg^{2+} released during the

luminescence reaction or with CoA, the L-AMP is converted into dehydroluciferin (L)[346,347] or into the dehydroluciferyl-CoA (L-CoA),[348,349] respectively (Scheme 2.7). The inhibitor effect of oxyluciferin and L-AMP has been proposed to be responsible for the rapid decay of light emission. The subsequent attenuation of light decay was instead attributed to the conversion of L-AMP into L or L-CoA, which are weaker inhibitors and as such more easily subjected to displacement by competition with D-LH_2. [282,346]

2.1.3.2. Thermostable *Photinus pyralis* Firefly Luciferase

The main issue encountered when working with FLuc is rapid and irreversible inactivation of the enzyme. The consequent variation in the catalytic activity can significantly compromise the accuracy and the sensitivity of the assay and cause discrepancies in the ATP detection throughout the course of the experiment. Stabilizing additives can help to preserve the activity of the enzyme during ongoing experiments and over a relatively long time at -80°C. Nonetheless, the wildtype form of FLuc remains highly susceptible to heat inactivation. To address problems with thermo-instability, it is common practise to engineer the wild-type enzyme by insertion of mutations which confer greater stability at higher temperatures. A major concern in this case is retention of the catalytic efficiency, which can be compromised by the mutations.[350] For the *Ft*PPK-luminescence coupled assay, a thermostable form of *P. pyralis* firefly luciferase, engineered by insertion of four point mutations (E354K, T214A, I232A, F295L), has been chosen.[351] An increase of about 7°C in the thermostability for the four-point mutation FLuc (4mutFLuc) compared to the wildtype (wtFLuc) has been reported.[351] No variation of the bioluminescent spectrum and of the kinetics of light emission have been observed. The K_m for ATP was approximately the same (wtFLuc: 73 μM; 4mutFLuc: 79 μM) while a five-fold increase of the K_m for luciferin (wtFLuc: 10 μM; 4mutFLuc: 50 μM) and a decrease of catalytic efficiency (wtFLuc: 7800 RLU/nmole; 4mutFLuc: 4350 RLU/nmole) were reported.[351] The variation observed are not significant enough to disfavour the use of the four point mutation FLuc for luminescence assay. Indeed, it is possible to account for the increased K_m of luciferin by appropriately adjusting the luciferin concentration; on the other hand, the increased stability of the

luciferase compensates to some degree for the attenuation of the catalytic activity, which would equally be observed for the wildtype luciferase due to inactivation.

2.2. Results and Discussion

To measure the activity of the *Ft*PPK, a luminescence-based coupled assay was developed and optimised. The FLuc and the *Ft*PPK were expressed *in E. coli* (BL21 DE3) with an N-terminal His_6-tag to allow Ni-affinity chromatography purification. The luminescence assay was optimised to maximize the luminescence signal, the assay dynamic range defined and then coupled to the *Ft*PPK reaction. The coupled assay conditions were gradually optimised and carefully balanced to ensure that the luminescence signal was exclusively a function of the *Ft*PPK activity. A format that enabled the measurement of *Ft*PPK activity consistently and in high throughput was established. The optimised assay was then validated by application to kinetics characterization of the *Ft*PPK. For the avoidance of confusion and to maintain the logical progression of the assay optimisation process, in the following sections the experiments are reported in chronological order, including some experiments that led to a miscalculation of the *Ft*PPK kinetic parameters, which were later amended following further optimisation of the assay conditions.

2.2.1. Expression and Purification of FLuc and *Ft*PPK

2.2.1.1. Thermostable *P. pyralis* Firefly Luciferase expression and purification

The FLuc expression plasmid (pET16b::*luc,* Figure 2.3) was prepared by J. Docherty, who also investigated the optimal conditions for the expression and the purification of FLuc.[352]

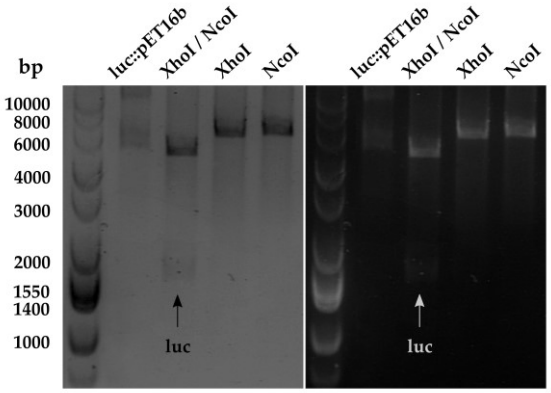

Figure 2.3: FLuc plasmid restriction digest

1% agarose gel of the pET16b::*luc* plasmid showing: unrestricted plasmid (7325 bp), double digested plasmid and corresponding restricted *luc* gene (1688 bp), single digested plasmid restricted with either *Xho*I or *Nco*I enzyme.

For protein expression, the plasmid was transformed into *E.coli* BL21 (DE3) Rosetta. Expression studies revealed that a better yield was obtained from freshly transformed cells by induction with 400 µM IPTG at 0.6 OD_{600} and overnight growth at 27°C.[352] Under these conditions 7.87 ± 1.5 g/L of cell paste were recovered from a 5 L culture. The N-terminal His_6-tagged FLuc (62 kDa) was purified by immobilized Ni^{2+} affinity chromatography (Figure 2.4).

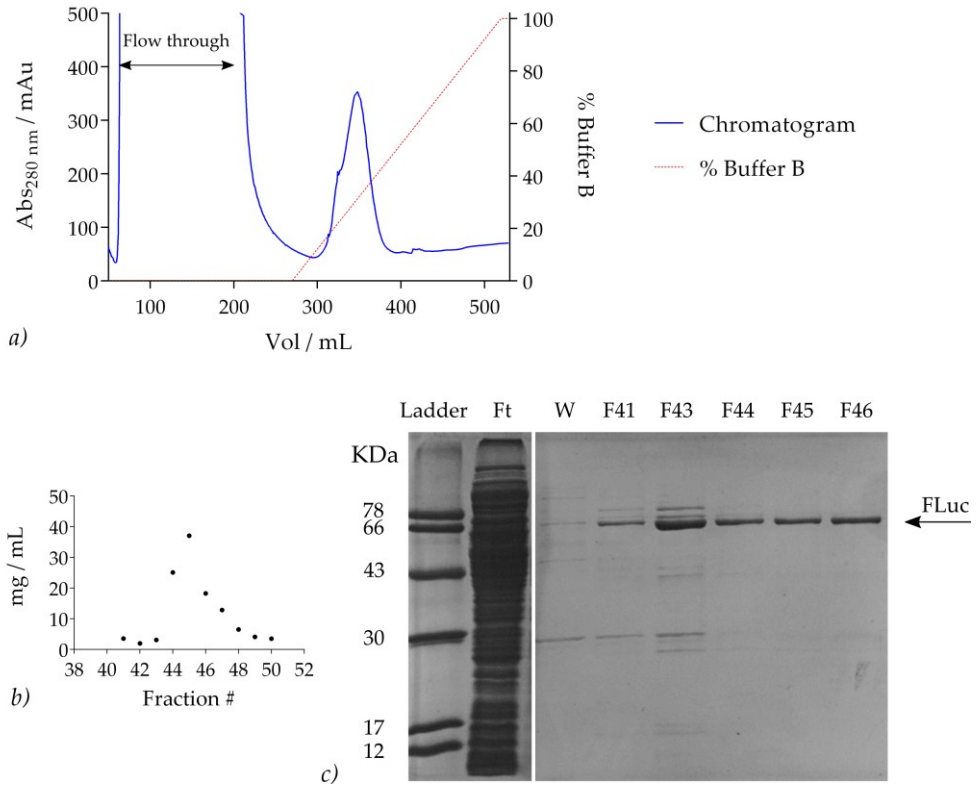

Figure 2.4: FLuc purification

a) Ni-affinity chromatography: UV-vis chromatogram recorded at 280 nm. The FLuc (62 kDa) was eluted by imidazole gradient (Buffer A: 50 mM Imidazole, Buffer B: 500 mM Imidazole). The FLuc eluted between 10% and 45% buffer B; *b*) Bradford analysis of fractions 41-50; *c*) SDS-PAGE analysis: Ft: flow through. W: washing, F#: fraction number. The concentration of the fractions loaded on the SDS-PAGE was adjusted to 1 mg/mL.

The lysis buffer was supplemented with lysozyme and with protease inhibitor to facilitate cell lysis and reduce luciferase proteolysis during purification.[353] To favour elution of loosely but not specifically bound proteins, NaCl, NaH_2PO_4 and a low concentration of imidazole (50 mM) were included in the purification buffers (section 7.4.1.3).[352] Following a washing

step with the low imidazole buffer, the FLuc was eluted by imidazole gradient (50 mM to 500 mM imidazole) over 250 mL volume. SDS-PAGE analysis of the fraction showed that a good degree of purity with only minor apparent impurities was achieved (Figure 2.4*c*). The FLuc was dialyzed in storage buffer (Table 7.28). The latter was supplemented with $(NH_4)_2SO_4$, ethylene glycol, glycerol, EDTA and DTT, which have been reported to stabilize the luciferase for long term storage at -80°C.[354–358] Typically, the yield of the FLuc purification was 17.6 ± 2.3 mg per grams of cell paste.

2.2.1.2. *Francisella tularensis* Polyphosphate kinase expression and purification

The expression plasmid for *Ft*PPK (pET16b:*Ftppk*, 6476 bp) was prepared by L. Batten[264] and includes the *F. tularensis* (*subspecies tularensis SCHU S4*) *Ft*PPK gene (FTT1564) on a *NcoI/PstI* fragment that encodes an N-terminal His_6 tag (Figure 2.5).

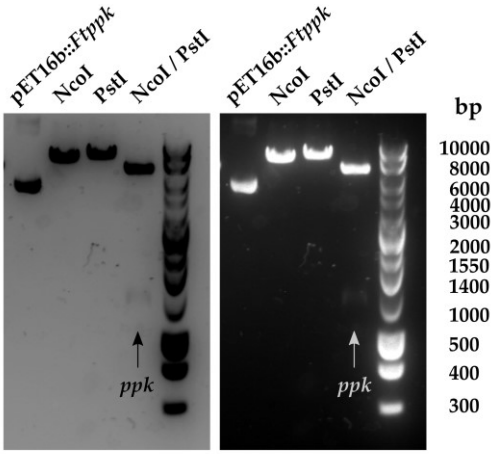

Figure 2.5: *Ft*PPK plasmid restriction digest

1% agarose gel of the pET16b::*Ftppk* plasmid showing: unrestricted plasmid (6476 bp), double digested plasmid and corresponding restricted *Ftppk* gene (1236 bp), single digested plasmid restricted with either *Nco*I or *Pst*I enzyme.

Batten went on to investigate the expression and purification of *Ft*PPK.[260,264] *Ft*PPK codon analysis revealed abundance of codons deemed rare in *E. coli*, hence the *Ft*PPK was expressed in *E. coli* BL21 Rosetta™ pLysS (DE3),[264] optimised for heterologous expression.[359,360] Optimal conditions for *Ft*PPK expression have been identified as induction by 400 μM IPTG at 0.6 OD_{600} followed by overnight growth at 27°C,[260,264] typically yielding

8.1 ± 0.9 g/L of cell paste. The insertion of the His_6 tag allowed purification of the *Ft*PPK (33 kDa) by Ni affinity chromatography (Figure 2.6*a*).

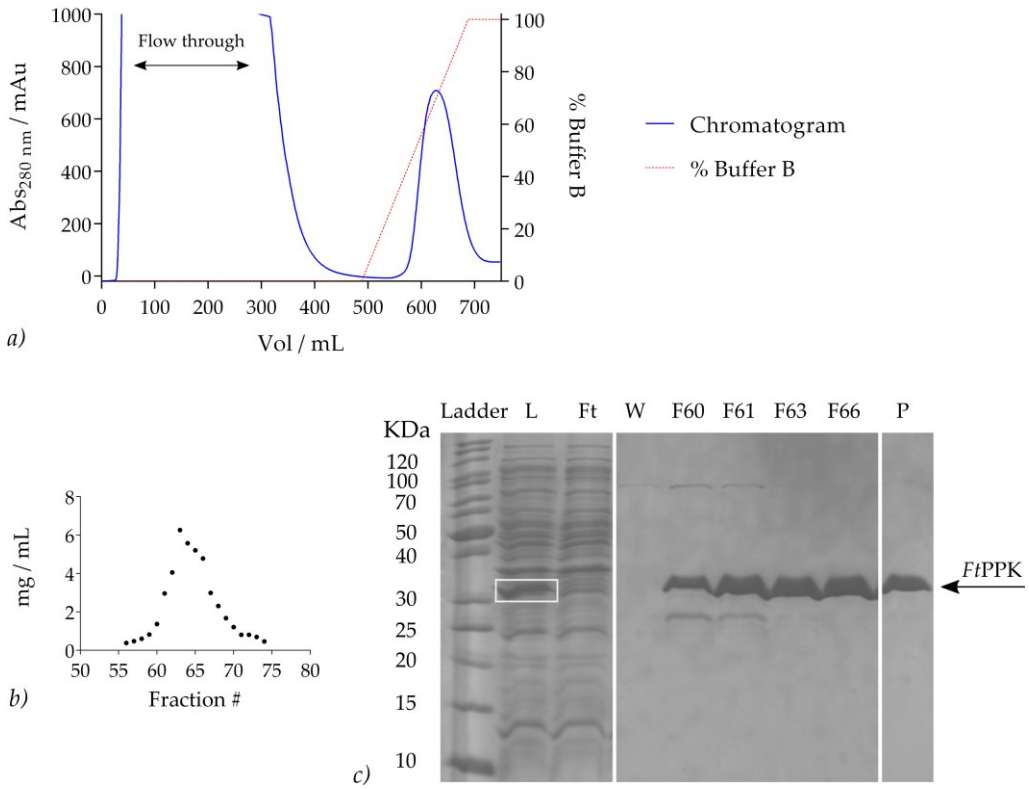

Figure 2.6: *Ft*PPK purification – Ni affinity chromatography

a) Ni-affinity chromatography: UV-vis chromatogram recorded at 280 nm. The F*t*PPK (33 kDa) was eluted by imidazole gradient (Buffer A: 50 mM Imidazole, Buffer B: 500 mM Imidazole). The *Ft*PPK eluted between 40% and 100% buffer B; *b*) Bradford analysis of fractions 55-75; *c*) SDS-PAGE analysis: L: lysate, Ft: flow through, W: washing, F#: fraction number, P: pooled fractions. The concentration of the fractions loaded on the SDS-PAGE was adjusted to 1 mg/mL.

The *Ft*PPK was eluted by a gradient of imidazole from 50 mM to 500 mM. The degree of *Ft*PPK purity was typically very high with few minor proteins observed at low concentration co-eluting in the first fractions (Figure 2.6*c*). To remove imidazole, the *Ft*PPK was dialyzed into the storage buffer containing 300 mM NaCl and 20% glycerol (Table 7.32). The yield of the *Ft*PPK purification was 3.15 ± 0.8 mg/g of cell paste. For crystallography, the *Ft*PPK was further purified by size exclusion chromatography. The first *Ft*PPK batch used for the optimisation of the *Ft*PPK-luminescence couple assay, kindly donated by A. Parnell, had been purified for crystallography purposes and therefore gel filtered. For the sake of consistency, it was decided to extend this practice to all the *Ft*PPK batches later produced.

The *Ft*PPK (33 kDa) was gel filtered in storage buffer (Table 7.32) using the resin Superdex 75 (S75). The elution volume of pure *Ft*PPK was about 130 mL (Figure 2.7).

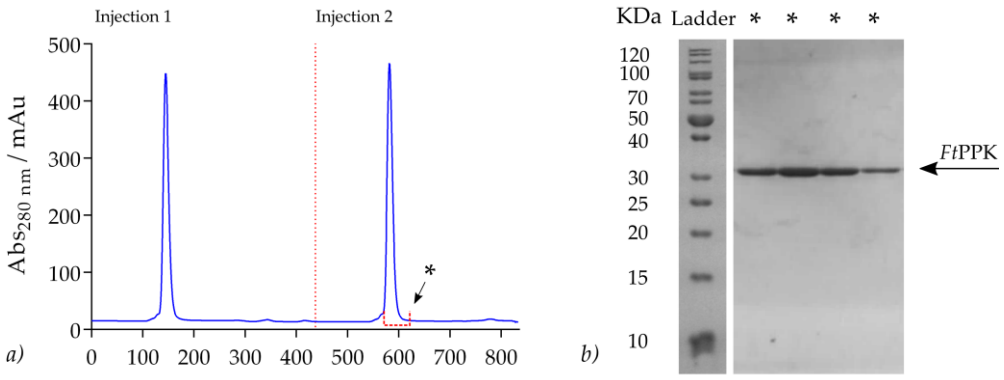

Figure 2.7: *Ft*PPK purification – size exclusion chromatography

a) Size exclusion chromatography: UV-vis chromatogram recorded at 280 nm. Two consecutive injections of *Ft*PPK (3 mL, about 10 mg/mL). *b*) SDS-PAGE analysis of fractions corresponding to the section indicated by the asterisk on the adjacent UV chromatogram. *Ft*PPK: 33 kDa. The fractions loaded on the SDS-PAGE were diluted four fold; the ratio of concentration was maintained as eluted from the column.

2.2.2. Optimisation of the Luminescence Assay

2.2.2.1. Preliminary luminescence assay conditions

A preliminary investigation of the in-house expressed thermostable FLuc activity was undertaken by J. Docherty,[352] using the buffer previously adopted by L. Batten for the *Ft*PPK characterization studies.[264] The same buffer was adopted for the optimisation of the luminescence assay and its composition was: 50 mM Tris-HCl, 10 mM $MgCl_2$, 0.3 M NaCl, 80 mM $(NH_4)_2SO_4$ and 20% glycerol at pH 7.8. The FLuc activity was tested at the concentration of 1 μM in the presence of 7.5 μM luciferin and a range of ATP concentrations (150 μM – 5 mM), conditions arbitrarily chosen as the starting point for the luminescence assay optimisation. The assays were manually prepared in triplicate in a 96 well plate full area (200 μL volume). The FLuc was incubated at 37°C in the presence of luciferin and the assays started by addition of ATP. The luminescence signal was measured after 30 seconds from the initiation of the assays.

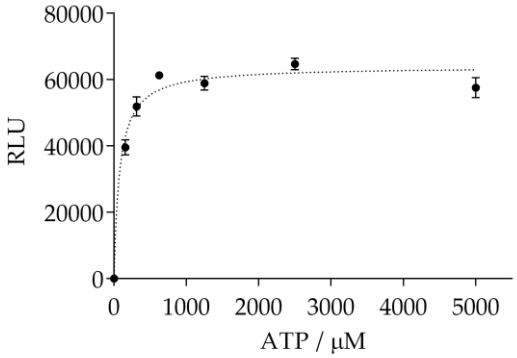

Figure 2.8: Luminescence assay – preliminary conditions

The luminescence signal reached saturation in the presence of concentration of ATP above 1 mM. Preliminary assay conditions: 200 μL assay volume, 1 μM FLuc, 7.5 μM luciferin, 150 μM – 5 mM ATP, 37°C. Gain: 2050.[c]

Increase of the luminescence signal was observed up to 600 μM ATP, above which enzyme saturation occurred (Figure 2.8). The activity of the recombinant FLuc, expressed and purified according to the method developed by J. Docherty,[352] was confirmed and the

[c] The gain is a parameter that can be adjusted to regulate the sensitivity of the POLARstar Omega BMG plate reader to the luminescence signal. A higher gain would result in amplification of the signal, a lower gain would reduce the intensity of the signal recorded.

arbitrarily defined assay conditions were adopted as the starting point for a step by step optimisation of the luminescence assay.

2.2.2.2. Luminescence assay: optimisation of FLuc to rate limiting concentration

One of the basic principles of enzymology is the requirement of only catalytic amounts of enzyme for the enzymatic reactions to occur. In the presence of an excess of substrate the rate of the reaction and therefore the concentration of product at t time is proportional to the concentration of the enzyme. Hence a higher concentration of FLuc in the assay would be expected to give a higher intensity of the luminescence signal. Practical consideration concerning the cost of the luciferin reagent and the time required to express and purify FLuc should be taken into account when optimizing the FLuc concentration. Ideally, the lowest concentration of both FLuc and luciferin that does not compromise the signal intensity should be used.

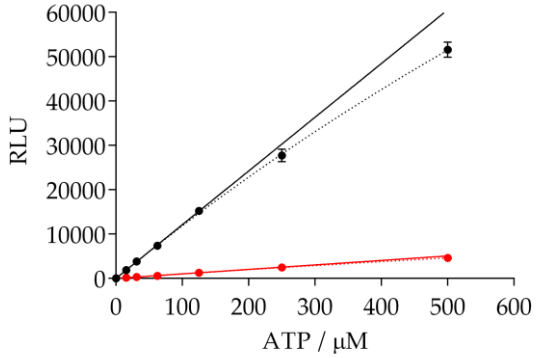

Figure 2.9: Luminescence assay – preliminary FLuc concentration

Comparison of the luminescence signal produced by 1 µM FLuc (black circles) and 100 nM FLuc (red circles). The data up to 150 µM ATP were fitted to a linear regression equation (Table 2.1). Assay conditions: 200 µL assay volume, 1 µM or 100 nM FLuc, 7.5 µM luciferin, 15.6 – 500 µM ATP, 37°C. Gain: 2550.

Table 2.1: Preliminary FLuc concentration optimisation

FLuc	RLU/ATP (RLU µM^{-1})	R^2
1 µM	121.1 ± 0.8	0.99
100 nM	10.1 ± 0.1	0.99

Under the preliminary assay conditions, the concentration of FLuc was in the same order of magnitude as the luciferin (section 2.2.2.1). The first step towards the optimisation of

the luminescence assay was to reduce the FLuc concentration by one order of magnitude while the luciferin concentration (7.5 μM) was unchanged. To identify a range of concentration at which the luminescence signal was proportional to the ATP concentration, the latter was reduced as well by one order of magnitude (15.6 – 500 μM ATP). A ten-fold decrease of the light emission rate was observed with the decrease of the FLuc concentration, showing that under the applied conditions the FLuc was rate limiting (Figure 2.9 and Table 2.1). The range of linearity between luminescence signal and ATP concentration was defined by fitting the data to the linear regression equation (Eq. 2.4). The data were corrected by subtraction of the background signal, hence the constraint $y_0 = 0$ was applied according to the assumption that an ATP concentration of 0 μM, no emission of luminescence occurs. A relation of proportionality between luminescence and ATP was observed up to 150 μM ATP, above which deviation from linearity occurred (Figure 2.9). The concentration of 100 nM FLuc was adopted as standard for the following optimisation steps.

2.2.2.3. Luminescence Assay Buffer: pH and Additives

Optimal conditions for activity have been extensively investigated to improve the efficiency of luciferase application for analytical purposes.[361–364] Buffers such as Tris, tricine and glycylglycine have been reported to favour the activity of the luciferase while HEPES and phosphate buffer exert an inhibitory effect.[361] The optimal pH for activity has been reported to be 7.75,[362] preferentially adjusted by acetic acid, which exerts the least inhibitory effect on the luciferase activity.[363,364] In the preliminary work of J. Docherty[352] and L. Batten,[264] Tris acetate was used for the FLuc storage buffer (Table 7.28) while for the assay buffer chloride was adopted as a counter ion to adjust the pH to 7.8. The same buffering systems and pH were adopted for the luminescence assay without any further experimental optimisation, given the correlation with literature reports.

One of the major issues when developing a luminescence assay is the precarious stability of the luciferase and its inactivation with time. These properties are due to the high content of hydrophobic amino acids, resulting in a high tendency to aggregate,[365,366] and to the presence of several thiol groups, two of which essential for catalysis, being susceptible to oxidation thereby leading to loss of activity.[367] To improve stability, DTT and EDTA at

0.5-1 mM concentration are commonly included in luciferase buffers.[354,355,358] These additives are routinely added to protein buffers to prevent protein disruption due to non-site-specific oxidation and metal-induced site-specific oxidation of cysteine, respectively.[368] EDTA is also included to prevent activity of metal-dependent proteases that may be present in the system.[358] The FLuc storage buffer (Table 7.32) was supplemented with 5 mM DTT and 2 mM EDTA. To prepare a FLuc solution at the working concentration (10x stock of the final assay concentration), the FLuc storage buffer was used for dilution (section 7.4.3.9), hence it was decided not to further supplement the assay buffer with these additives.

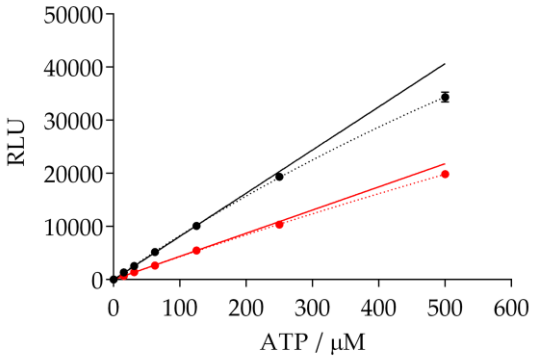

Figure 2.10: Luminescence assay – BSA effect

Comparison of the luminescence signal produced in the presence of BSA (black circles) and in the absence of BSA (red circles). The data up to 150 µM ATP were fitted to a linear regression equation (Table 2.2). Assay conditions: 200 µL assay volume, 100 nM FLuc, 7.5 µM luciferin, 15.6 – 500 µM ATP, 37°C. Gain: 2250.

Table 2.2: Luminescence assay: effect of BSA

BSA	RLU/ATP (RLU µM^{-1})	R^2
0.1 mg/mL	81.3 ± 0.4	0.99
No BSA	43.6 ± 0.3	0.99

To address the hydrophobicity problem and the consequent loss of activity due to aggregation or adhesion to the labware surfaces, BSA has been included as stabilizing agent in luciferase buffers.[355,356,358] The effect of BSA on the activity of FLuc was directly investigated by comparison of the luminescence produced in the presence of 0.1 mg/mL (1.3 µM) BSA and in its absence. To derive the rate of light emission, data up to 150 µM ATP were fitted to the liner regression equation (Eq. 2.4). When BSA was added to the assay

solution, a significant increase of the signal intensity produced for a given concentration of ATP (Figure 2.10 and Table 2.2). Therefore, BSA was adopted as a standard component of the luminescence assay.

2.2.2.4. Luminescence assay: luciferin optimisation

To maximise the luminescence signal, the optimal concentration of luciferin was investigated. Initially, a range of luciferin concentration between 0.19 µM and 50 µM was tested in the presence of 31.25, 62.5 and 125 µM ATP. The luminescence signal was measured 30 seconds after the start of the assays and the data were reported in terms of rate of light emission (RLU sec^{-1}) against concentration of luciferin (Figure 2.11*a*).

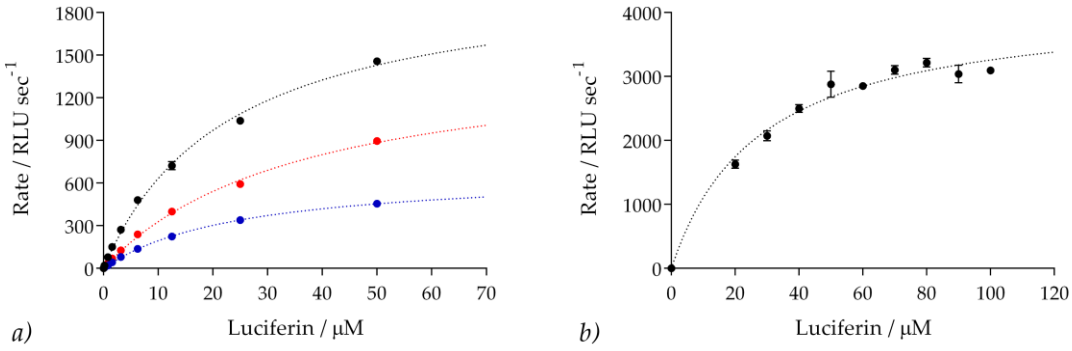

Figure 2.11: Luminescence assay – Luciferin optimisation

a) Rate of light emission at 0.19 – 50 µM luciferin in the presence of: 125 µM ATP (black circles), 62.5 µM ATP (red circles), 31.25 µM ATP (blue circles). The rate was measured in end point format, 30 sec after the start of the luminescence assay. *b*) Rate of light emission at 20-100 µM luciferin in the presence of: 300 µM ATP. The rate was measured in end point format, 52 sec after the start of the luminescence assay. Assay conditions: 200 µL assay volume, 100 nM FLuc, 1.3 µM BSA, 0.19-50 µM luciferin and 31.25-125 µM ATP or 20-100 µM luciferin and 300 µM ATP, 37°C. Gain: 1650.

Table 2.3: Luminescence assay: luciferin optimisation

Luciferin	ATP	K_m (µM)	R^2
0.19-50 µM	125 µM	22.9 ± 1.1	0.99
0.19-50 µM	62.5 µM	36.6 ± 2.9	0.99
0.19-50 µM	31.25 µM	25.1 ± 1.4	0.99
20-100 µM	300 µM	27.70 ± 3	0.98

The data were fitted to the Michaelis-Menten equation (Eq. 2.5). The K_m values for luciferin in the presence of increasing concentrations of ATP were comparable (Table 2.3), suggesting

that maximum luminescence signal should be observed above 60 μM luciferin. To confirm this hypothesis the experiment was repeated using a higher range of luciferin concentrations (20 – 100 μM) in the presence of 300 μM ATP, a wide excess in comparison to the expected ATP concentration produced by the optimised *Ft*PPK assay. The luminescence signal was measured after 52 seconds and the data were fitted to the Michaelis-Menten equation (Eq. 2.5). The estimated K_m was comparable to the values obtained at lower concentrations of ATP and accordingly the rate of light emission did not increase significantly beyond the luciferin concentration of 70 μM (Figure 2.11*b* and Table 2.3). In accordance with the data obtained and in consideration of the luciferin reagent cost, it was decided not to use an excess of luciferin but just the concentration required to reach saturation of the luminescence signal. Hence, the standard concentration of luciferin adopted for the luminescence assay was 70 μM.

2.2.2.5. Luminescence assay: temperature optimisation

The rate of enzymatic reactions is greatly affected by temperature. An increase of the catalytic efficiency is observed with the increase of temperature. However, above a certain temperature, enzymes become subject to denaturation.[272,274,369] An optimal temperature can be experimentally defined at which the catalytic activity reaches its maximum and beyond which a decline is observed. The luminescence assay was initially measured at 37°C, the temperature applied for the *Ft*PPK characterisation by L. Batten.[260,264] A range of temperatures (20°C, 25°C, 30°C, 35°C, 36°C and 37°C) were investigated by J. Docherty in her preliminary studies of the FLuc activity, according to which the intensity of the luminescence signal was higher at 30°C.[352] Because good quality data were reported by J. Docherty, the experiment was repeated testing only the following three temperatures: 25°C, 30°C, 37°C. The assay volume was reduced to 100 μL and the FLuc activity measured at a range of ATP concentrations between 3.9 and 62.5 μM, following incubation at the temperature of interest for 20 minutes. The luminescence was recorded after 43 seconds and the data, reported in terms of rate against concentration of ATP, were fitted to a linear regression equation (Eq. 2.4), where $y_0 = 0$. A higher FLuc activity was observed at 30°C (Figure 2.12). This temperature was adopted as standard for the luminescence assay.

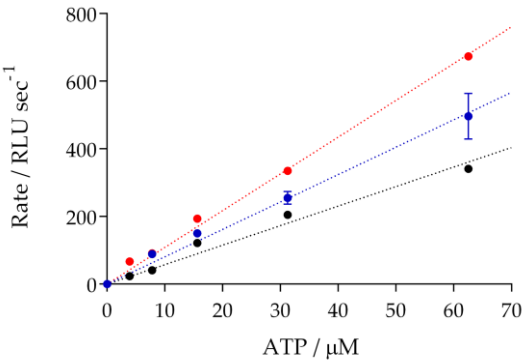

Figure 2.12: Luminescence assay – temperature optimisation

Comparison of the luminescence signal produced at the following temperatures: 37°C (black circles), 30°C (red circles), 25°C (blue circles). The rate was measured in end point format, 43 sec after the start of the luminescence assay, the data were fitted to a linear regression equation (Table 2.4). Assay conditions: 100 µL assay volume, 100 nM FLuc, 1.3 µM BSA, 70 µM luciferin, 3.9-62.5 µM ATP, 25°C, 30°C and 37°C. Gain: 1500.

Table 2.4: Luminescence assay: temperature effect

T	v/ATP (RLU sec^{-1} μM^{-1})	R^2
37°C	5.7 ± 0.2	0.96
30°C	10.9 ± 0.2	0.99
25°C	8.1 ± 0.3	0.97

2.2.2.6. Luminescence assay: ATP standard curve

Following optimisation of the luminescence assay conditions, the relation between luminescence and ATP was investigated over a wide range of ATP concentrations (9.37-2000 µM). To explore such a wide range of concentrations without compromising on the accuracy of the ATP sample preparation, and therefore trying to reduce as much as possible the experimental error, three ATP standard curves were prepared by two-fold serial dilution from 2000 µM, 1600 µM and 600 µM ATP. To monitor for the possible variation of the signal between standard curves and hence to determine whether the data could be merged, one ATP sample from the first standard curve was included in the second and in the third standard curve. The luminescence signal was measured after 14 seconds from the start of the luminescence assay. The data from the three standard curves were consistent and therefore merged and analysed as a single data set (Figure 2.13). The upper limit of the

luminescence assay dynamic range was defined by fitting the data up to 100 µM ATP to a linear regression equation (Eq. 2.4), where $y_0 = 0$. As previously observed (section 2.2.2.2), a relation of proportionality was observed between ATP concentration and light emitted up to 150 µM ATP (R^2 0.99), above which deviation from linearity occurred (Figure 2.13*b*).

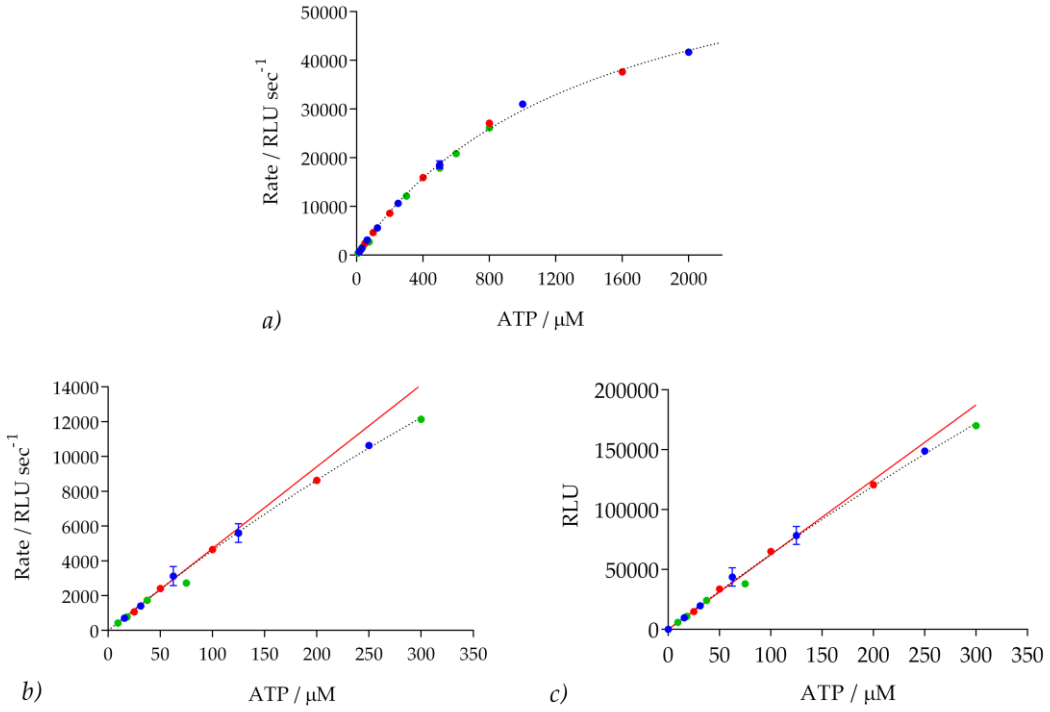

Figure 2.13: Luminescence assay – ATP standard curve

a) Standard curve 1 (15.6-2000 µM ATP, blue circles), standard curve 2 (25-1600 µM ATP, red circles) and standard curve 3 (9.37-600 µM ATP, green circles). *b*) and c) same data reported in *a*) showing the range of linearity (9.37-150 µM) reported in terms of rate of luminescence emission and RLU versus ATP concentration. Assay conditions: 100 µL assay volume, 100 nM FLuc, 1.3 µM BSA, 70 µM luciferin, 9.37-2000 µM ATP, 30°C. Gain: 1500.

A decrease of the luminescence signal with time was detected, in accordance with the luciferase flash-pattern kinetics (Figure 2.14*a*). The latter is characterised by a very quick increase of light intensity, followed by a rapid decay that later becomes more gentle.[340,370–373] As well as the intensity of light emitted, the light decay, which is due to product inhibition, is more pronounced at higher concentration of ATP (Figure 2.14*a*).[301] Upon fitting the ATP standard curve full data set to the Michaelis-Menten equation (Eq. 2.5) the value derived for the apparent K_m (K_m^{app}) for ATP was 1371 ± 64.73 µM, a value about 20

fold higher than what reported for the recombinant wildtype luciferase or for the four-mutations luciferase (K_m for ATP: 73 μM and 79 μM, respectively).[351]

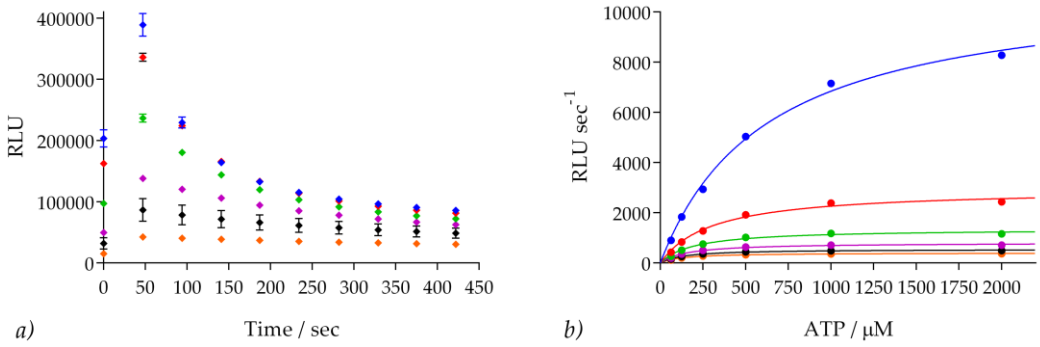

Figure 2.14: Luminescence assay – ATP standard curve, light decay.

a) Light decay with time reported for each concentration of ATP included in the standard curve 1: 2000 μM (blue rhombus), 1000 μM (red rhombus), 500 μM (green rhombus), 250 μM (purple rhombus), 125 μM (black rhombus), 62.5 μM (orange rhombus). The decay was steeper up to 250 sec after which it becomes gentler. *b*) Light decay per each ATP concentration of the standard curve 1 after the following delays from the start of the assay: 47 s (blue circles), 94 s (red circles), 141 s (green circles), 187 s (purple circles), 234 s (black circles), 282 s (orange circles). The data were fitted to the Michaelis-Menten equation (Eq. 2.5, Table 2.5). Assay conditions: 100 μL assay volume, 100 nM FLuc, 1.3 μM BSA, 70 μM luciferin, 62.5-2000 μM ATP, 30°C. Gain: 1500.

Table 2.5: Luminescence assay: ATP standard curve kinetics

Time	K_m^{app} (RLU sec^{-1} μM^{-1})	R^2
14 s	1371 ± 64.7	0.99
47 s	624.5 ± 50.1	0.99
94 s	303.3 ± 28.3	0.98
141 s	199.6 ± 16.9	0.97
187 s	156.5 ± 14.8	0.97
234 s	135.7 ± 11.9	0.97
282 s	124.7 ± 10.3	0.97

The initial high K_m^{app} can be justified by product inhibition, which according to the kinetics of competitive inhibitors[272,274,369] has the effect of shifting the K_m^{app} towards higher concentrations. On the other hand, the decrease of the K_m^{app} with time reflects the displacement of the inhibitor dehydro-luciferyl-AMP from the active site and conversion into dehydroluciferin, to which the lower decay rate can be attributed (section 2.1.3.1 and

Figure 2.14*b*). The decay of light emission is a feature of the luminescence assay that potentially could interfere with the correct determination of the ATP concentration on the basis of the signal intensity. Both the light decay and the established luminescence assay dynamic range (upper limit: 150 μM ATP) should be taken into account during the optimisation of the coupled assay to ensure the relation of proportionality between the concentration of ATP produced and the luminescence signal.

2.2.3. Development and Optimisation of the *Ft*PPK Coupled Assay

The possibility of using a luminescence coupled assay to measure the activity of the *Ft*PPK has been previously explored by L. Batten, who developed a *Ft*PPK coupled assay using a commercially available luciferin-luciferase reagent, which was then applied for validation of the *Ft*PPK kinetics parameters.[264] The conditions of the optimised independent luminescence assay (section 2.2.2) were adopted as starting point for the development of the *Ft*PPK coupled assay with the in-house expressed luciferase (FLuc), and were integrated with the *Ft*PPK assay components. The coupled assay was step-by-step optimised until a format was obtained that allowed to reproducibly and accurately measure the *Ft*PPK activity. The *Ft*PPK-FLuc coupled assay was validated by kinetic characterization of the *Ft*PPK and was later optimised for high throughput screening.

2.2.3.1. *Ft*PPK-FLuc coupled assay: preliminary conditions

For the preliminary *Ft*PPK-FLuc coupled assay, no changes were made to the assay buffer (50 mM Tris-HCl, 10 mM $MgCl_2$, 80 mM $(NH_4)_2SO_4$, 0.3 M NaCl, 20% glycerol, pH 7.8), of which the composition had been in the first place defined by L. Batten to favour the activity of the *Ft*PPK, according to literature.[264] The concentration of the *Ft*PPK (300 nM) and the concentration of the substrates (200 μM $polyP_{25}$, 1 mM ADP) were arbitrarily chosen. The conditions for the luminescence assay were 100 nM FLuc, 70 μM luciferin, 1.3 μM BSA, as defined upon optimisation (section 2.2.2). In its preliminary format ADP and polyP were added to the assay buffer, the primary assay was initiated by addition of *Ft*PPK and the coupled assay by addition of a mixture of FLuc-BSA-luciferin. ATP standard curves were prepared in parallel to the coupled assay to convert the luminescence in concentration of ATP produced and to account for possible variation of the FLuc activity. To measure the *Ft*PPK activity, a continuous assay and a discontinuous assay format were compared. For the continuous format, the luminescence assay was started 15 seconds after the *Ft*PPK assay was initiated and the luminescence signal measured every 3 seconds (Figure 2.15*a*). While for continuous assay the activity is monitored by measuring the variation of the signal produced by a single assay, in a discontinuous format multiple assays are stopped at the desired time points and the signal measured. Various methods can be used to quench assays:

the enzyme activity can be disrupted by either denaturation (by heat, by addition of an acid or of an organic solvent) or by addition of a metal chelator (such as EDTA), which captures the ions required for catalysis. None of these quenching methods could be applied to the *Ft*PPK-FLuc coupled assay because the FLuc, on which activity the assay readout depends, would be quenched in addition to *Ft*PPK. A virtual quenching method was used by L Batten for her *Ft*PPK-luminescence coupled assay, where the luciferin-luciferase reagent was added to the *Ft*PPK reaction after variable delays and the luminescence signal measured.[264] Accordingly, a similar format based on the principle of a delayed addition of the FLuc, rather than a real quenching step, was developed and optimised for the *Ft*PPK-FLuc coupled assay. Following the start of the *Ft*PPK assay, a mixture of FLuc-BSA-luciferin was added after a variable delay (according to the time point to measure) and the luminescence signal measured after the same delay from the start of the luciferase assay (Figure 2.15*b*).

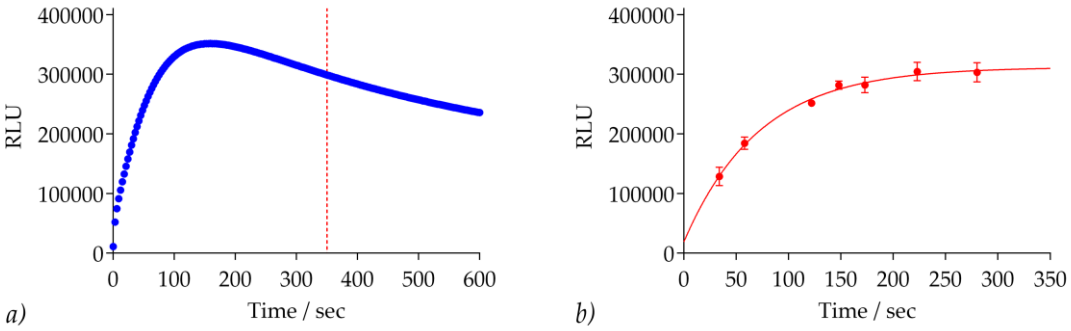

Figure 2.15: *Ft*PPK-FLuc coupled assay: continuous and discontinuous format comparison

a) *Ft*PPK time course measured by a continuous assay format. The dotted line corresponds to 350 sec. *b*) *Ft*PPK time course measured by a discontinuous assay format. Assay conditions: 100 µL assay volume, 300 nM *Ft*PPK, 200 µM $polyP_{25}$, 1 mM ADP, 100 nM FLuc, 1.3 µM BSA, 70 µM luciferin, 30°C. Gain: 1500.

The data from both the continuous format and the discontinuous format were comparable, with a peak of luminescence obtained after approximately 150 seconds, in correspondence to the maximum concentration of ATP produced (Figure 2.15). As reported in section 2.2.2.6, two factors affect the intensity of the luminescence signal: the concentration of ATP and the kinetics of light decay. For the continuous format, although masked during the initial part of the time course due to the ATP concentration increasing with time, the decay

effect became obvious after the ATP production reached the plateau. No measures could be taken to account for the light decay, with the consequence that the relationship luminescence-ATP, as defined by the standard curve, was less likely to be maintained and the signal measured would not exclusively reflect the *Ft*PPK activity. For the discontinuous format, while the delay between the initiation of the *Ft*PPK assay and the initiation of the FLuc assay allowed to build up ATP, the consistent delay between the start of the luciferase reaction and the luminescence measurement, which was applied to the same extent as for the ATP standard curve, allowed to account for the light decay kinetics. Indeed, the signal from the coupled assay was directly comparable to the signal from the standard curve and therefore any variation could be attributed only to the ATP concentration. The discontinuous format was adopted as standard and later further optimised. The signal produced by the coupled assay under the preliminary conditions was well above the range of linearity of the ATP standard curve (Figure 2.13). Hence, although validating the possibility of using a discontinuous format for the measurement of the *Ft*PPK activity, the data reported in Figure 2.15*b* were not representative of a real *Ft*PPK time course.

2.2.3.2. *Ft*PPK-FLuc coupled assay: temperature effect

The optimal temperature for luciferase activity was defined as 30°C (section 2.2.2.5 and J. Docherty).[352] On the other hand, the temperature applied by L. Batten for the HPLC-based kinetic characterisation of the *Ft*PPK was 37°C.[264] Before further optimising the concentration of the assay components, the performance of the *Ft*PPK-FLuc coupled assay was tested at 30°C and 37°C, applying the preliminary conditions and the discontinuous format as described in section 2.2.3.1. The data were fitted to the one phase-association equation (Eq. 2.2). A decrease of the luminescence signal was observed when the temperature was raised to 37°C while the rate constant k and the half-time $t_{1/2}$ were comparable (Figure 2.16 and Table 2.6). Hence, the temperature had a greater effect on the FLuc activity, to which the increase was detrimental, while it did not significantly affect the rate of ATP production catalysed by *Ft*PPK. In view of these results, a temperature of 30°C was maintained as standard parameter for the *Ft*PPK-FLuc coupled assay.

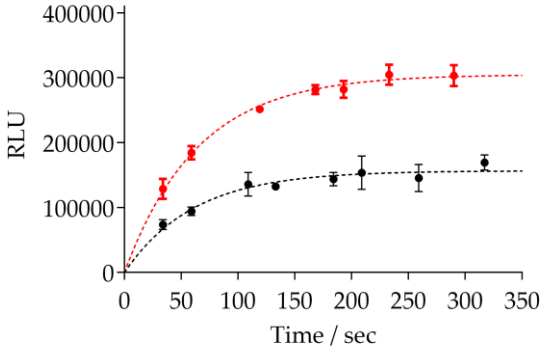

Figure 2.16: *Ft*PPK-FLuc coupled assay: effect of the temperature

Comparison of the *Ft*PPK-FLuc coupled assay performance at 30°C (red circles) and 37°C (black circles). No significant changes were observed on the *Ft*PPK activity (same k and $t_{1/2}$) while a significant decrease of luminescence occurred. The data were fitted to the one-phase association equation Eq. 2.2. Assay conditions: 100 µL assay volume, 300 nM *Ft*PPK, 200 µM $polyP_{25}$, 1 mM ADP, 100 nM FLuc, 1.3 µM BSA, 70 µM luciferin. Gain: 1500.

Table 2.6: *Ft*PPK-FLuc coupled assay: effect of the temperature

T (°C)	P_{max} (x 10^4 RLU)	k (s^{-1})	$t_{1/2}$ (s)	R^2
30	30.5 ± 0.5	0.015 ± 0.001	44.65 ± 4.9	0.96
37	17.67 ± 0.5	0.016 ± 0.002	42.12 ± 8.6	0.80

2.2.3.3. *Ft*PPK-FLuc coupled assay: preliminary optimisation of the *Ft*PPK concentration

Two issues were encountered when measuring the *Ft*PPK time course under the arbitrarily chosen preliminary conditions (300 nM *Ft*PPK, 200 µM $polyP_{25}$, 1 mM ADP): firstly, only two time points (30 seconds and 50 seconds) could be measured at the mid-late region of the apparent linear phase of the time course, and secondly, the luminescence signal produced was well above the upper limit of the dynamic range of the ATP standard curve (150 µM ATP). As a consequence, the initial phase of the time course, critical for a correct determination of the apparent initial rate (v_0^{app}), was not accurately measured and the relation of proportionality between the luminescence signal and the ATP concentration did not apply. To address these problems the concentration of the *Ft*PPK was reduced to slow down the reaction rate and consequently produce less ATP within the time frame investigated. Three time courses were measured at 300 nM, 100 nM and 30 nM *Ft*PPK, maintaining the concentration of the other components unchanged. The data were fitted to

the empirically chosen one-phase association equation (Eq. 2.2) and from the resulting parameters the v_0^{app} was derived according to the first order kinetic rate equation (Eq. 2.3). As opposed to the experiment previously described (section 2.2.3.2) and in line with the reduction of the *Ft*PPK concentration, a decrease of the luminescence signal in parallel to a decrease of the apparent initial rate (v_0^{app}) and of the half-time ($t_{1/2}$) was observed (Figure 2.17 and Table 2.7). The variation of the RLU at the estimated plateau was not proportional to the variation of *Ft*PPK concentration when the concentration was decreased from 300 nM to 100 nM (Figure 2.17*a*).

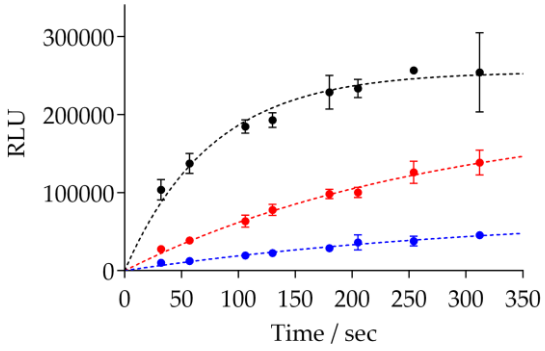

Figure 2.17: *Ft*PPK-FLuc coupled assay: *Ft*PPK concentration preliminary optimisation

The *Ft*PPK time course measured at the 300 nM (black circles), 100 nM (red circles) and 30 nM *Ft*PPK (blue circles). A decrease of the luminescence signal and of the v_0^{app} was observed in parallel to the decrease of the *Ft*PPK concentration. The data were fitted to the one-phase association equation (Eq. 2.2). Assay conditions: 100 µL assay volume, 300 nM or 100 nM or 30 nM *Ft*PPK, 200 µM polyP$_{25}$, 1 mM ADP, 100 nM FLuc, 1.3 µM BSA, 70 µM luciferin, 30°C. Gain: 1500.

Table 2.7: *Ft*PPK concentration preliminary optimisation

***Ft*PPK (nM)**	**P_{max} (x 10^4 RLU)**	***k* (x 10^{-3} min^{-1})**	**v_0^{app} (x 10^3 RLU s^{-1})**	**$t_{1/2}$ (s)**	***R*²**
300	25.5 ± 0.9	13 ± 1.3	33.5 ± 0.1	52.77 ± 9.4	0.90
100	20.43 ± 2.6	3.6 ± 0.7	0.736 ± 0.1	192.4 ± 54.7	0.95
30	7.37 ± 1.7	2.9 ± 1	0.220 ± 0.05	231.8 ± 95.5	0.89

A proportional decrease of the RLU at plateau and of the v_0^{app} was instead observed when the concentration was lowered from 100 nM to 30 nM *Ft*PPK, consistent with the hypothesis that at the latter concentration range the *Ft*PPK was rate limiting. It was concluded from these results that a concentration of 30 nM was appropriate as the standard *Ft*PPK

concentration. At this concentration the *Ft*PPK appeared to be rate limiting, furthermore the intensity of the luminescence signal was well within the dynamic range of the ATP standard curve, ensuring that a relation of linearity between signal detected and concentration of ATP produced would be maintained.

2.2.3.4. *Ft*PPK-FLuc coupled assay: effect of the BSA

In view of the improvement to the luminescence signal obtained in the presence of BSA, the effect on the *Ft*PPK activity was investigated. The addition of BSA to prevent adsorption onto the vessel surfaces which results in decrease of the active enzyme concentration is a common practise.[270] In addition to the BSA included in the preparation of the FLuc-luciferin mixture, BSA was also added to the *Ft*PPK stock solution. A time course was measured in the presence and in the absence of additional BSA.

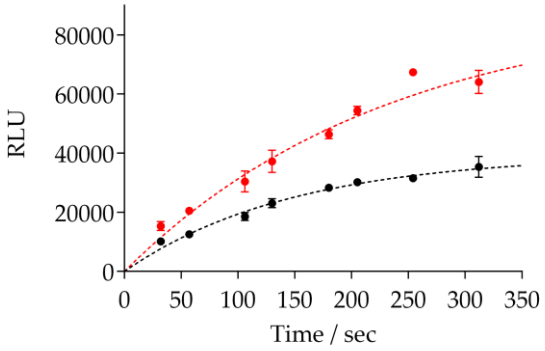

Figure 2.18: *Ft*PPK-FLuc coupled assay: BSA effect

Comparison of the *Ft*PPK time course without further addition of BSA (black circles) and following addition of further BSA to the *Ft*PPK solution (red circles). An improvement in the luminescence signal was observed when the *Ft*PPK reagent was supplemented with 1.3 μM BSA. Assay conditions: 100 μL assay volume, 30 nM *Ft*PPK /± 1.3 μM BSA, 200 μM polyP$_{25}$, 1 mM ADP, 100 nM FLuc/1.3 μM BSA, 70 μM luciferin, 30°C. Gain: 1500.

The luminescence signal was further enhanced by the addition of BSA, although it was not possible to deconvolute whether the activity of the *Ft*PPK was favoured or whether the BSA further improved the performance of the FLuc (Figure 2.18). The extra addition of BSA was adopted as part of the standard assay procedure, and the overall concentration of the BSA in the *Ft*PPK-FLuc coupled assay was 2.3 μM (0.2 mg/mL), half of which was

included in the preparation of the FLuc-luciferin reagent and the remaining half in the preparation of the *Ft*PPK solution.

2.2.3.5. *Ft*PPK-FLuc coupled assay: *Ft*PPK time course measurement

The optimised conditions described in the previous sections (30 nM *Ft*PPK, 100 nM FLuc, 70 μM luciferin, 2.6 μM BSA, 30 °C, section 2.2.3.1 to 2.2.3.4) were applied for the measurement of a long *Ft*PPK time course in the presence of 200 μM poly P_{25} and 1 mM ADP. Alongside the time course assays, an ATP standard curve was prepared and measured in parallel. The latter became a standard practice, not only to be able to report the *Ft*PPK activity in terms of ATP produced but also to monitor the FLuc activity (e.g. control experiments to account for the day-to-day activity variability or possible FLuc inactivation-with time). The time course data were reported in terms of RLU and in terms of ATP concentration, extrapolated by means of the ATP standard curve (Figure 2.19). The data were fitted to the one phase-association equation (Eq. 2.2) and v_0^{app} derived according to Eq. 2.3. Despite the correction of the data by subtraction of the background signal, the intercept to the y axis of time course was not zero, which suggested that possibly the protocols applied for the assay measurement required further optimisation (e.g. the actual time point measured was later than intended compared to the initiation of the *Ft*PPK assay) or that the conditions applied for the control assay should be modified.[d] A proportional increase of the signal with time was observed up to 300 seconds and the corresponding ATP produced was within the dynamic range of the ATP standard curve ($<$ 150 μM ATP, section 2.2.2.6). On the other hand, the ATP concentration derived from the luminescence signal produced at the time points measured after 300 seconds was higher than the upper limit of the luminescence assay dynamic range. Given that the v_0^{app} could be measured in the presence of 1 mM ADP without exceeding the ATP standard curve dynamic range, the coupled assay was applied for a preliminary kinetic characterisation of the *Ft*PPK.

[d] At this stage, the control assays were prepared by taking out the ADP, which was subsequently found to contain ATP traces.

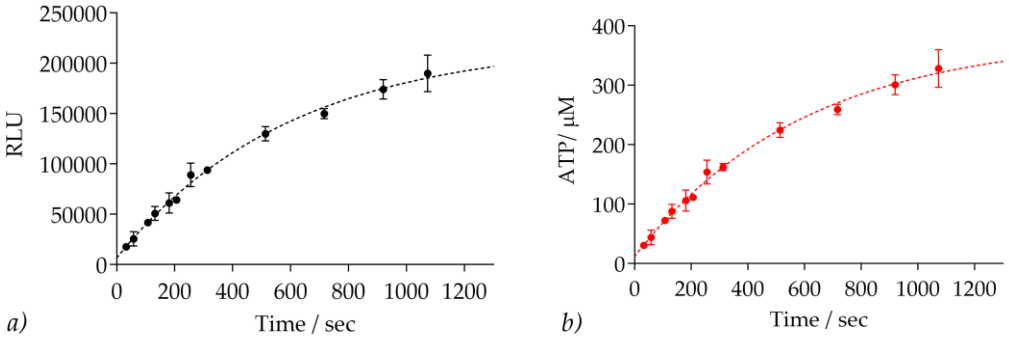

Figure 2.19: *Ft*PPK-FLuc coupled assay: time course

a) *Ft*PPK time course reported in terms of RLU; *b*) *Ft*PPK time course reported in terms of ATP concentration. The data were fitted to an exponential one phase-association equation (Eq. 2.2) and the v_0^{app} derived according to Eq. 2.3. Assay conditions: 100 µL assay volume, 30 nM *Ft*PPK /1.3 µM BSA, 200 µM polyP$_{25}$, 1 mM ADP, 100 nM FLuc/1.3 µM BSA, 70 µM luciferin, 30°C. Gain: 1500.

Table 2.8: *Ft*PPK time course

***Ft*PPK (nM)**	**P_{max} (µM)**	**k (x10^{-3} s^{-1})**	**v_0^{app} (µM s^{-1})**	**R^2**
30	382.5 ± 22	1.67 ± 0.2	0.64 ± 0.04	0.98

2.2.3.6. *Ft*PPK-FLuc coupled assay: preliminary *Ft*PPK kinetics investigation

The use of the coupled assay for the investigation of the *Ft*PPK kinetics parameters served two purposes: the validation of the coupled assay itself and the determination of the K_m in view of the development of a format for high throughput screening. Kinetics characterisation of the *Ft*PPK was carried out by L. Batten by means of an HPLC-based assay and by means of a luminescence coupled assay using a commercially available luciferin-luciferase reagent.[260,264] While the HPLC assay was not adequate to reliably determine the K_m for polyP$_{25}$ and some reservations were kept on the value obtained by the luminescence assay (5.35 ± 1.84 µM), the K_m for ADP was defined by both assays as 369 ± 70 µM and 286 ± 14 µM, respectively.[260,264] The agreement of these values with the parameters determined by the *Ft*PPK-FLuc coupled assay would allow validation of the coupled assay and counter-validate the characterisation done by L. Batten. It is particularly important for the success of a screening campaign that the correct kinetic parameters for the enzyme of interest are known. Indeed, to increase the chances of identifying inhibitors of all modalities, K_m

concentration of substrates is preferably used for HTS (section 3.1.2).[270,374] To determine the K_m, the apparent initial rate is measured over range of substrate concentrations between 0.2-5 K_m.[272,274,374] For an enzymatic reaction involving more than one substrate, the K_m for the substrate of interest is determined maintaining the other substrate at a saturating concentration. To measure the K_m for ADP the concentration of polyP$_{25}$ was set at 200 µM and the concentration of ADP was varied between 7.8 µM and 2400 µM. To measure the K_m with polyP$_{25}$, the latter was titrated between 6.25 µM and 600 µM while the ADP concentration was maintained at 1500 µM. The ADP concentration to use for the K_m with polyP$_{25}$ was experimentally defined as saturating concentration by measuring a time course at 1000 µM, 1500 µM, 2000 µM and 3000 µM ADP, in which a comparable luminescence was obtained at 1500 µM and 2000 µM ADP and inhibition observed at 3000 µM ADP (Appendix, section A2 4). Short time courses (30 – 110 seconds) were prepared and the apparent initial rate (v_0^{app}) was defined by fitting the data to a linear regression equation (Eq. 2.4) where y was the ATP produced, x was the time point measured and the slope ax was a measure of the v_0^{app}. To determine the kinetics parameters the v_0^{app} was plotted against ADP concentration and the data fitted to the Michaelis-Menten equation (Eq. 2.5). Similar values of V_{max} and K_m were obtained in repeat experiments (on different days) for both ADP and PolyP$_{25}$ (Figure 2.20 and Table 2.9). The K_m for ADP (759.8 ± 55.47 µM and 711.5 ± 55.44 µM) was found to be approximately two-fold higher than that determined by L. Batten.[264] Similarly, the K_m for polyP$_{25}$ (30.53 ± 3.23 µM and 31.13 ± 6.3 µM) was six-fold higher. Two different values of V_{max} were obtained for the polyP$_{25}$ characterisation, the second of which was in accordance with the V_{max} obtained from the experiment to determine the K_m for ADP (Table 2.9). It is likely that the lower V_{max} obtained was a consequence of inactivation of the FLuc. Two different formats were used for these experiments, the second of which was improved in the time required for the kinetic measurement.

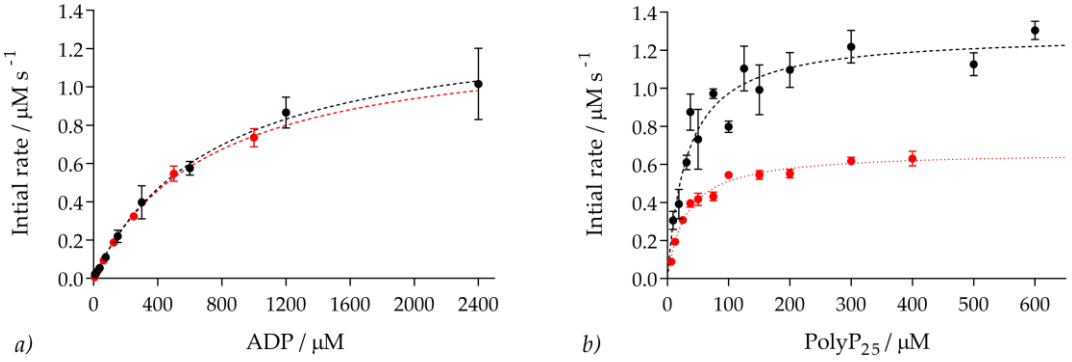

Figure 2.20: *Ft*PPK-FLuc coupled assay: preliminary kinetic characterisation

a) Determination of K_m for ADP, measured varying the ADP concentration between 7.8 µM and 2400 µM, while the polyP$_{25}$ was 200 µM. *b*) Determination of K_m for polyP$_{25}$, measured varying the polyP$_{25}$ concentration between 6.25 µM and 600 µM, while the ADP was 1500 µM. In both cases the data were produced using two different formats differing for the *Ft*PPK addition step (section 7.4.3.6.1 and 7.4.3.6.2): Exp1 (black circles), Exp2 (red circles). The data were fitted to the Michaelis-Menten equation (Eq. 2.5). Assay conditions: 100 µL assay volume, 30 nM *Ft*PPK /1.3 µM BSA, 8.7-2400 µM ADP for K_{mADP} or 1500 µM for K_{mPolyP}, 200 µM polyP$_{25}$ for K_{mADP} or 6.25-600 µM for K_{mPolyP}, 100 nM FLuc/1.3 µM BSA, 70 µM luciferin, 30°C. Gain: 1500.

Table 2.9: Preliminary kinetics characterisation of *Ft*PPK

Substrate	K_m (µM)	V_{max} (µM s^{-1})	k_{cat} (s^{-1})	R^2
ADP (*Exp1*)	759.8 ± 55.5	1.36 ± 0.04	45.3 ± 1.3	0.99
ADP (*Exp2*)	711.5 ± 59.9	1.27 ± 0.1	42.33 ± 2	0.99
PolyP$_{25}$ (*Exp1*)	30.53 ± 3.2	0.67 ± 0.02	22.3 ± 0.7	0.98
PolyP$_{25}$ (*Exp2*)	31.13 ± 6.3	1.29 ± 0.1	43 ± 2	0.91

Although in line with K_m values reported in literature for other PPK2-like enzymes (e.g. K_m with ADP for *P. aeruginosa* PPK2 was 750 µM;[115] K_m with polyP for *Sinorhizobium meliloti* PPK2 was 21 ± 3.9 µM),[375] the K_m values measured with the *Ft*PPK-FLuc coupled assay exceed the values previously determined by L. Batten.[264] Two factors could potentially be accounted for the differences observed: either the coupled assay was not fully optimised in terms of relative concentrations of the primary and secondary enzymes or the format used for the time courses was not accurate in the measurement of the time points. In both cases, the likelihood of the measurement of a distorted initial rates would be high. Hence, further optimisation of the assay format and of the assay conditions was pursued.

2.2.4. *Ft*PPK-FLuc Coupled Assay Optimisation: Towards an HTS Format

Following the development of a coupled assay to measure the *Ft*PPK activity, further optimisation was aimed to improve the assay quality to a level suitable for HTS. The optimisation process was guided by the statistical parameter Z'-factor,[84] defined by the following equation:

$$Z' = 1 - \left(\frac{3\sigma_{c+} + 3\sigma_{c-}}{|\mu_{c+} - \mu_{c-}|} \right)$$

Eq. 2.11: Z' factor

$\mu_{c+/c-}$ is the mean and $\sigma_{c+/c-}$ the standard deviation of the signal from the positive and negative control assays, respectively.

In other words, the Z' is a coefficient that takes into account the assay dynamic range and the variability of the signal: the first corresponding to the signal window between the positive control and the negative control band ($|\mu_{c+} - \mu_{c-}|$), the second represented by the amplitude of the variation band (defined as $\mu \pm 3\sigma$). The greater is the dynamic range and the smaller the variation band, the higher the Z' value would be. Assays with a Z' ≥ 0.5 are considered suitable for HTS, assays with Z' ≥ 0.7 are considered excellent. Particularly critical for the achievement of a good Z' and therefore for obtainment of a good screening window is the width of the variation band $\mu \pm 3\sigma$. Hence, to improve the assay quality, the problem of the data variability should be addressed. On the other side, reducing the background signal and intensifying the luminescence signal can help to increase the screening window. The experiments reported in the section below were aimed at increasing the assay quality by developing a format that achieved lower data variability across the microplate as well as increased the dynamic range. Further assay optimisation was done in the presence of DMSO (library solvent), of which a concentration compatible with the assay was determined. To reduce the data variability, a new assay format was investigated, while to improve the dynamic range, the background signal was reduced by purification of ADP (to remove traces of contaminating ATP) and the assay signal intensified by increasing the concentration of the FLuc.

2.2.4.1. *Ft*PPK-FLuc coupled assay: effect of the library solvent (DMSO).

DMSO is the solvent most commonly used for HTS libraries due to its propensity to dissolve relatively hydrophobic compounds while remaining miscible with aqueous solutions.[374,376] This optimisation step is required, as in the presence of an organic solvent, the activity of enzymes may be attenuated. In view of the application of the coupled assay for HTS, it was decided to investigate the effect of the DMSO earlier during the optimisation process to allow further optimisation in the presence of all the assay components. To determine the optimum concentration of DMSO, to ensure adequate solubility of the library without significantly compromising the activity of the enzymes, the tolerance of the *Ft*PPK and of the FLuc to DMSO was experimentally determined (Figure 2.21).

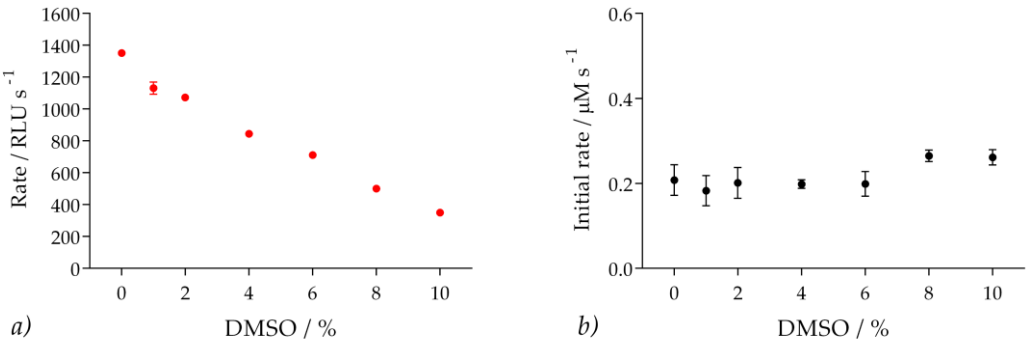

Figure 2.21: *Ft*PPK-FLuc coupled assay: effect of DMSO

a) Effect on the FLuc activity reported as variation of the rate of light emitted with the increase of the DMSO concentration; *b*) Effect on the *Ft*PPK activity reported as rate of ATP production with the increase of the DMSO concentration. Assay conditions: 100 µL assay volume, 35 nM *Ft*PPK /1.3 µM BSA, 700 µM ADP, 30 µM polyP$_{25}$, 100 nM FLuc/1.3 µM BSA, 70 µM luciferin, 30°C. Gain: 1700.[e]

DMSO was titrated between 0 and 10% v/v final concentration in *Ft*PPK-FLuc coupled assays and in ATP standard curves prepared alongside. A significant decrease of the FLuc activity was observed, while the activity of the *Ft*PPK appeared constant with the increase of the DMSO concentration (Figure 2.21). As a compromise between compound solubility

[e] A new batch of *Ft*PPK was used for the experiments. Because of the concentration of the new stock and for the sake of consistency, it was easier to prepare a *Ft*PPK solution yielding a 35 nM final concentration.

and FLuc activity, a concentration of 5% v/v DMSO was chosen as standard for the coupled assay.

2.2.4.2. *Ft*PPK-FLuc coupled assay: format optimisation and incubation time

Various factors can negatively contribute to the data variability. A major role may be played by suboptimal performance of the instruments used to prepare the assays (liquid handling workstation and plate reader) or by imperfect programming of the operation protocols for the assay measurement (plate reader control protocols). On the other hand, data variability could also result from the assay format and conditions that may affect the enzyme activity. To address the issues falling into the first category, an extensive investigation of the performances of the plate reader and of the liquid handling workstation was conducted, alongside the design of various control protocols until a format was defined that enabled measurement of the *Ft*PPK time course in a precise and reproducible manner. Of equal significance to the achievement of a more reliable format was the correction of the assay format regarding the preparation of the assay solution and its initiation. Previously the *Ft*PPK assays were started by addition of the *Ft*PPK to the assay solution in which both the substrates were included. In the new protocol, the *Ft*PPK was added to the assay solution while the ADP was left out and later injected to initiate the assays. This allowed the incubation of the *Ft*PPK with $MgCl_2$, $polyP_{25}$ and the other components of the assay solution added as stabilising agents. The choice of incubating the *Ft*PPK with the $polyP_{25}$ and not with the ADP was dictated by some experiments done by A. Parnell showing that incubation with $polyP_{25}$ favoured the *Ft*PPK activity while no ADP binding was observed in the absence of $polyP_{25}$.[265] Furthermore, the new format developed allowed a better equilibration of the enzyme to the assay temperature, the latter being a potential additional source of data variability if not uniform across the microplate. Hence, incubation steps of various lengths of time prior the start of the *Ft*PPK assay were investigated to ensure equilibration of the plate at the assay temperature (30°C). The newly optimised format and the following conditions were applied: 35 nM/1.3 μM *Ft*PPK/BSA, 700 μM ADP, 30 μM poly P_{25}, 100 nM/1.3 μM FLuc/BSA, 70 μM luciferin, 5% v/v DMSO. Optimisation of the plate reader control protocols allowed to monitor the time course during the early phase

(the earliest time point that could be measured was 12 seconds), resulting into a more accurate measurement of the apparent initial rate (v_0^{app}, Table 2.10). Within the interval of time investigated (70 seconds) a linear increase of the ATP concentration with time was observed, which was preceded by a lag phase (Figure 2.22*a* and *b*). The latter was probably either a format artefact (e.g. a mixing effect) or was due to the time required to the *Ft*PPK to build up ATP to a steady state concentration (section 2.1.2).[301]

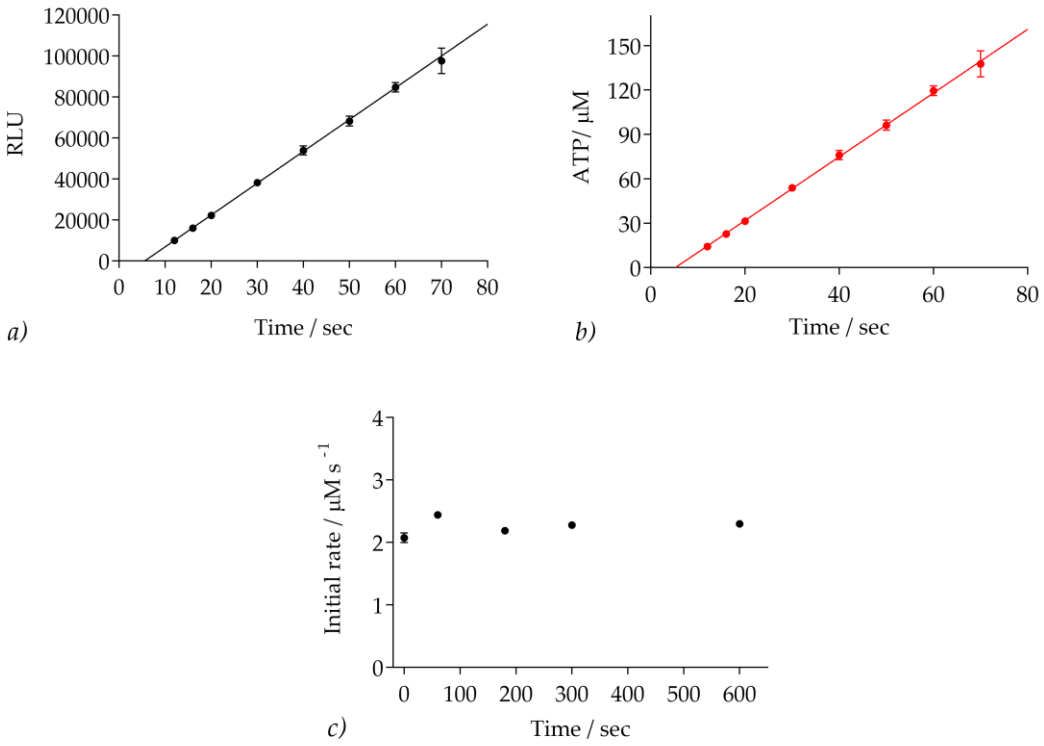

Figure 2.22: *Ft*PPK-FLuc coupled assay, new format: time course and incubation time

*Ft*PPK-FLuc time course measured after being incubated for 3 min at 30°C. *a*) time course reported in terms of RLU; *b*) time course reported in terms of ATP produced. The initial rate was determined by fitting the data below 60 seconds to the linear regression equation Eq. 2.4. *c*) Effect of the incubation prior assay initiation (0 s, 60 s, 180 s, 300 s, 600 s). Assay conditions: 100 µL assay volume, 35 nM *Ft*PPK /1.3 µM BSA, 700 µM ADP, polyP$_{25}$ 30 µM, 100 nM FLuc/1.3 µM BSA, 70 µM luciferin, 5% DMSO, 30°C. Gain: 1700.

Table 2.10: Effect of the incubation time on the initial rate

Incubation time	v_0^{app} (µM s^{-1})	R^2
0 min	2.07 ± 0.07	0.98
1 min	2.44 ± 0.06	0.99
3 min	2.19 ± 0.03	0.99
5 min	2.23 ± 0.05	0.99
6 min	2.3 ± 0.04	0.99

Overall, a very low variation of the data for each triplicate was observed, suggesting that the optimisation of the format was effective towards improving the data reproducibility. For each time course the v_0^{app} was defined by fitting the data up to 60 seconds to the linear regression equation Eq. 2.4, where y was the ATP produced, x was the time point measured and the slope ax was a measure of the v_0^{app}. The v_0^{app} was then plotted against the incubation time (Figure 2.22*c*). No significant variation in the assay rate was observed when the incubation time was increased, hence 5 minutes was adopted as standard incubation time prior to initiation of the coupled assay measurement.

2.2.4.3. *Ft*PPK-FLuc coupled assay: optimisation of the FLuc concentration

Widening the assay dynamic range by increasing the difference between the signal produced by assays in which full activity is observed (positive control assays) and assays in which no activity is observed (negative control assays) can positively contribute towards the improvement of the Z' factor (Eq. 2.11). This task can be accomplished by minimizing the background signal, namely the signal that can not be attributed to the *Ft*PPK activity, but also by further intensifying the luminescence signal by increase of the FLuc concentration. A relatively significant luminescence was detected from control assays in which ADP and $polyP_{25}$ but not *Ft*PPK were present. This was tracked down to ATP impurities in the commercial ADP sample. The issue was addressed by purification of ADP by anion exchange chromatography (DEAE sepharose) to reduce the ATP contaminants (Appendix, A2 5). To intensify the luminescence signal, the concentration of the FLuc was optimised. In addition to improve the screening window, an increase of the FLuc concentration, hence of the ratio between secondary and primary enzyme, would ensure that the primary enzyme (the *Ft*PPK) is rate limiting, overall improving the reliability of the coupled assay (section 2.1.2). To define a new optimal FLuc concentration, the *Ft*PPK time course was measured by coupling to a range of FLuc concentrations between 50 and 330 nM. Due to precipitation occurring above 330 nM, it was not possible to investigate any higher FLuc concentration. The coupled assay rate was reported for each concentration of FLuc, both in terms of RLU sec^{-1} and in terms of ATP sec^{-1} (Figure 2.23*a* and *b* respectively). In the latter case, the

luminescence was converted into ATP concentration by means of ATP standard curves prepared at the respective FLuc concentration.

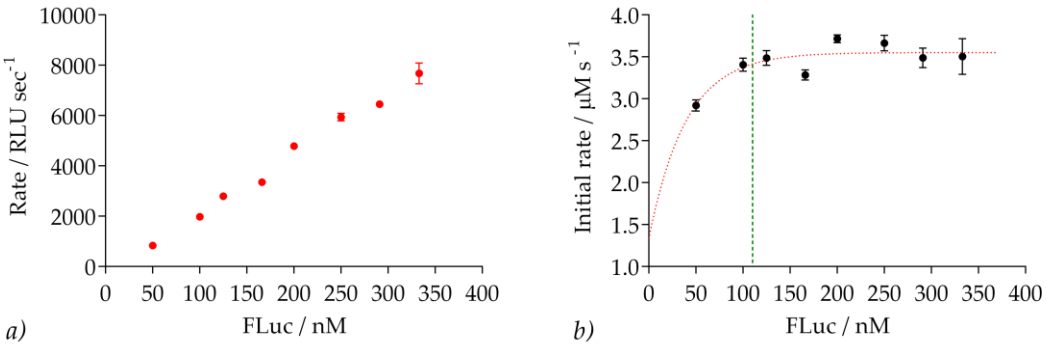

Figure 2.23: *Ft*PPK-FLuc coupled assay: optimisation of the FLuc concentration

a) *Ft*PPK-FLuc coupled assay: rate of light emission. A linear increase of the rate was observed with the increase of the FLuc concentration. *b) Ft*PPK-FLuc coupled assay: rate of ATP production. Above the concentration of 100 nM FLuc the rate was constant regardless the increase of the FLuc concentration. Assay conditions: 100 µL assay volume, 35 nM *Ft*PPK /1.3 µM BSA, 700 µM ADP, 30 µM polyP$_{25}$, 50-333 nM FLuc/1.3 µM BSA, 70 µM luciferin, 5% DMSO, 30°C. Gain: 1700.

Table 2.11: Effect of the FLuc concentration on the rate of ATP production

FLuc (nM)	v_0^{app} (µM s^{-1})	R^2
50	2.9 ± 0.06	0.99
100	3.4 ± 0.08	0.99
125	3.4 ± 0.09	0.99
165	3.3 ± 0.06	0.99
200	3.7 ± 0.05	0.99
250	3.6 ± 0.09	0.99
300	3.5 ± 0.1	0.99
330	3.5 ± 0.2	0.98

A linear increase of the rate of light emission was observed with the increase of the FLuc concentration (Figure 2.23*a*) while the rate of ATP production was constant, within error, in the presence of a FLuc concentration above 100 nM (Figure 2.23*b* and Table 2.11). The data obtained showed that the increase of the FLuc concentration produced the desired increase of the luminescence signal and confirmed that when applying a concentration of FLuc above 100 nM, the rate measured was exclusively a function of the *Ft*PPK activity.

The latter was not true when the concentration of FLuc was below 100 nM, in which case a lower rate of light emission corresponded to a lower rate of ATP production (Figure 2.23*b*).

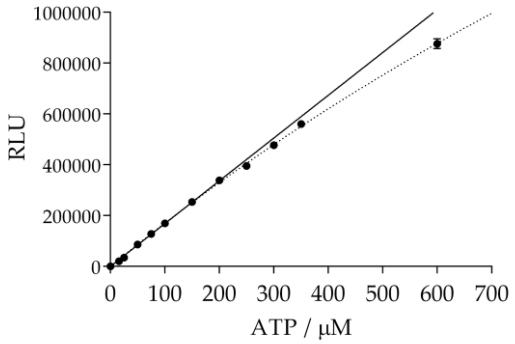

Figure 2.24: ATP standard curve in the presence of 300 nM FLuc

Linear relation between luminescence and ATP concentration up to 150 µM ATP (luminescence assay dynamic range). Assay conditions: 100 µL assay volume, 300 nM FLuc/1.3 µM BSA, 70 µM luciferin, 15.6-600 µM ATP 5% DMSO, 30°C. Gain: 1700.

To maximise the signal, a concentration of FLuc equal to 300 nM was chosen as standard for the coupled assay. An extended ATP standard curve and a *Ft*PPK time course were measured in the presence of 300 nM FLuc. Being determined by the FLuc kinetics, no variation of the ATP standard curve dynamic range was observed, of which the upper limit was confirmed to be 150 µM ATP (Figure 2.24).

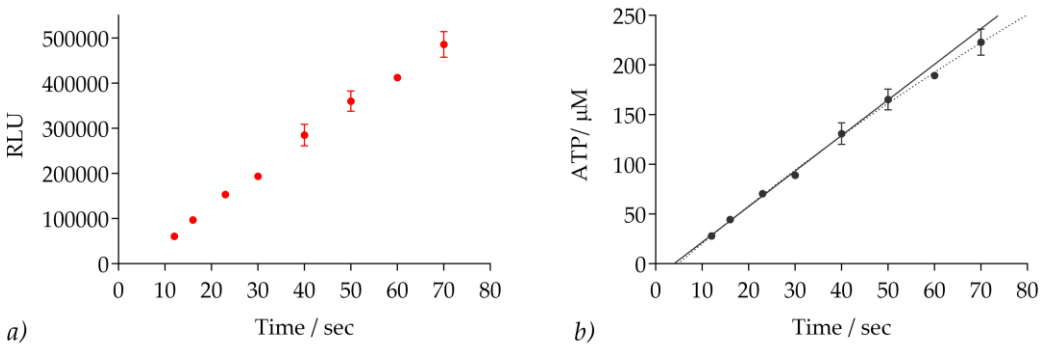

Figure 2.25: *Ft*PPK-FLuc coupled assay: time course measured by 300 nM FLuc

a) time course reported in terms of RLU; *b*) time course reported in terms of ATP produced. A linear increase of the ATP produced with time was observed up to 50 s. Assay conditions: 100 µL assay volume, 35 nM *Ft*PPK /1.3 µM BSA, 700 µM ADP, 30 µM polyP$_{25}$, 300 nM FLuc/1.3 µM BSA, 70 µM luciferin, 5% DMSO, 30°C. Gain: 1700.

Although the coupled assay signal increased linearly with time, the corresponding ATP produced by 35 nM *Ft*PPK (in the presence of 30 μM $PolyP_{25}$ and 700 μM ADP) at time points later than 40 seconds, exceeded the dynamic range of the ATP standard curve. Therefore, the v_0^{app} could be determined by fitting the data to the linear regression equation (Eq. 2.4) only up to 50 seconds (Figure 2.25). The obtained data suggested that a further optimisation of the *Ft*PPK concentration was required, to ensure that the concentration of the ATP produced during the measured initial phase of the time course would be within the ATP standard curve dynamic range. The improvement would allow a more accurate measurement of the *Ft*PPK apparent initial rate and therefore a more reliable investigation of the *Ft*PPK kinetics.

2.2.4.4. *Ft*PPK-FLuc coupled assay: optimisation of the *Ft*PPK concentration

The optimisation of the primary and secondary enzyme concentration is a critical step for the development of a coupled assay, in which the rate measured is exclusively a function of the primary enzyme catalysis (section 2.1.2). The concentration of the *Ft*PPK adopted so far, following a preliminary optimisation (section 2.2.3.3), has proven to be rate limiting in the presence of varying concentrations of FLuc (section 2.2.4.3). However, the ATP produced during a 70 seconds time course exceed the experimentally defined upper limit of the luminescence assay dynamic range (section 2.2.4.3). The second requirement for a well optimised coupled assay is that the secondary enzyme immediately catalyses the turnover of the primary enzyme product into detectable signal. To fulfil this condition not only the secondary enzyme needs to be in excess but the concentration of the primary enzyme should be optimise so that the product concentration does not exceed the relative K_m of the secondary enzyme. At this stage of the project, it was realized that the content of NaCl in the assay buffer (300 mM) had a deleterious effect on the activity of the FLuc. The optimisation of the NaCl concentration (to 25 mM, Appendix, section A2 6), resulted in a significant increase of the luminescence signal. As a consequence, the assay sensitivity to low concentration of ATP was further improved, therefore favouring the investigation of the coupled assay at lower *Ft*PPK concentration. To investigate the optimal *Ft*PPK concentration, the luminescence assay (300 nM FLuc) was coupled to a range of *Ft*PPK

concentration between 1.5 nM and 50 nM and the respective time courses measured (Figure 2.26).

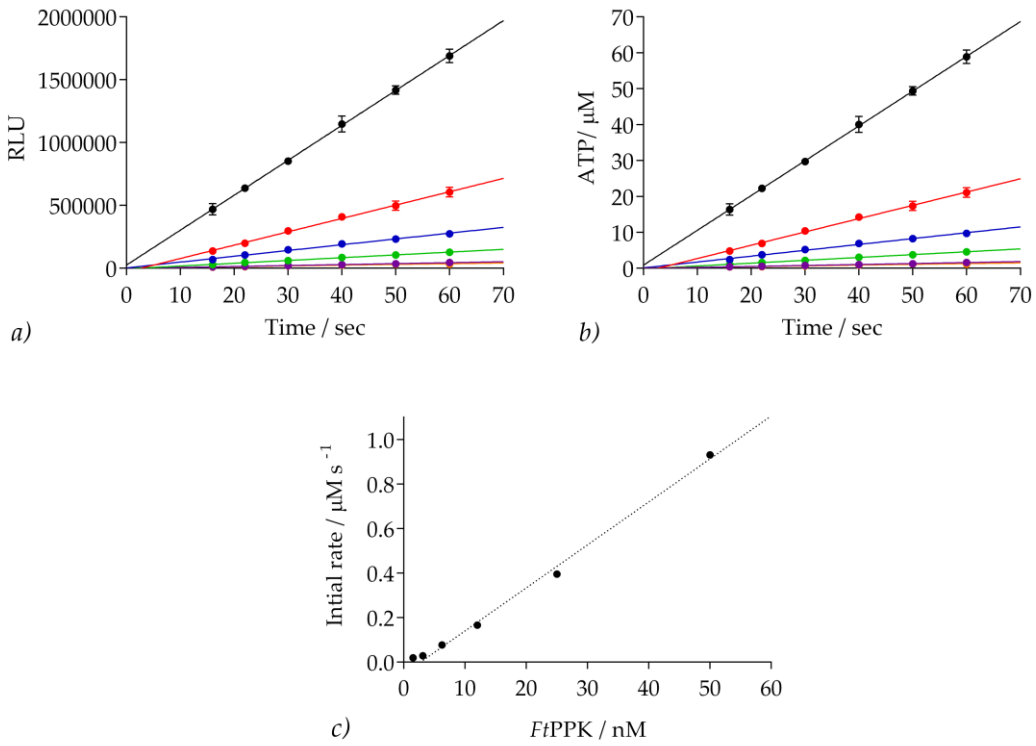

Figure 2.26: *Ft*PPK-FLuc coupled assay: optimisation of the *Ft*PPK concentration

a) *Ft*PPK time course reported in terms of luminescence signal; *b*) *Ft*PPK time course reported in terms of ATP produced. The concentration of *Ft*PPK investigated were: 50 nM (black circles), 25 nM (red circles), 12.5 nM (blue circles), 6.25 nM (green circles), 3.12 nM (purple circles), 1.5 nM (orange circles). *c*) v_0^{app} of ATP production plotted against *Ft*PPK concentration. A linear relation was observed between rate measured and *Ft*PPK concentration between 3 and 50 nM. Assay conditions: 100 µL assay volume, 1.5 - 50 nM *Ft*PPK /1.3 µM BSA, 700 µM ADP, 30 µM $polyP_{25}$, 300 nM FLuc/1.3 µM BSA, 70 µM luciferin, 5% DMSO, 30°C. Gain: 1700.

Table 2.12: Effect of the *Ft*PPK concentration on the rate of ATP production

***Ft*PPK (nM)**	**v_0^{app} (µM s^{-1})**	**R^2**
50	0.93 ± 0.008	0.99
25	0.4 ± 0.007	0.99
12.5	0.16 ± 0.004	0.99
6.2	0.07 ± 0.001	0.99
3.1	0.03 ± 0.001	0.99
1.5	0.02 ± 0.001	0.93

A relation of linearity was observed between the *Ft*PPK concentration and the rate measured, which decreased proportionally to the decrease of the *Ft*PPK concentration (Figure 2.26*c*). The trend was broken below 2 nM *Ft*PPK, supposedly in correspondence of the lower limit of the luminescence assay dynamic window. The experiment confirmed that at the range of *Ft*PPK concentrations tested and under the applied optimised coupled assay conditions the *Ft*PPK was rate limiting. To ensure that within the time frame measured (0-70 seconds) the ATP production proceeds linearly with time and at a concentration well below the FLuc K_m (79 μM ATP),[351] the concentration of *Ft*PPK adopted as standard for the coupled assay was 10 nM.

2.2.4.5. *Ft*PPK-FLuc coupled assay: kinetic characterisation of *Ft*PPK applying the optimised coupled assay conditions

Following the further optimisation of the coupled assay, the kinetic characterisation of the *Ft*PPK was re-attempted applying the following conditions: 10 nM *Ft*PPK, 300 nM FLuc and 70 μM luciferin. To measure the K_m for ADP, time courses were prepared at 200 μM $polyP_{25}$ while the ADP was varied between 9.9 μM and 2500 μM, the same conditions applied for the preliminary kinetics investigation (section 2.2.3.6). The data were fitted to the Michaelis-Menten equation (Eq. 2.5) and the derived K_m for ADP was 407.2 ± 50.9 μM (Figure 2.27*a* and Table 2.13). The new K_m value was about two-fold lower than what previously determined (759.8 ± 55.47 μM and 711.5 ± 59.88) and therefore better in accordance with what reported by L. Batten (369 ± 70 μM and 286 ± 14 μM).[264] The difference between the two measurements was probably due to the further optimisation of the *Ft*PPK and of the FLuc concentration and to the optimisation of the assay format (section 2.2.4.3 and 2.2.4.4), which allowed a more accurate measurement of v_0^{app}. The K_m for $polyP_{25}$ was also investigated maintaining the ADP concentration at 2500 μM while the $polyP_{25}$ was varied between 1.5 and 400 μM. Substrate inhibition was observed at $polyP_{25}$ concentrations higher than 50 μM (Figure 2.27*b*). The data were fitted to the substrate inhibition equation:[272,273]

$$v = \frac{V_{max}[S]}{K_m + [S] + \left(1 + \frac{[S]}{K_i}\right)}$$

Eq. 2.12: Substrate inhibition

v is the reaction rate, V_{max} is the maximum rate, [S] the concentration of substrate, K_m the Michaelis-Menten constant and K_i the substrate dissociation constant.

The following kinetic parameters were derived: K_m 1.4 ± 0.26 μM, V_{max} 0.45 ± 0.02 μM s^{-1}, K_i 621 ± 128 μM (Table 2.13). The measurement of the K_m for ADP was repeated in the presence of 30 μM $polyP_{25}$, at which V_{max} was approached but no inhibition observed (Figure 2.27*c*). A further decrease of the K_m and a higher value for V_{max} were obtained (206 ± 30.9 μM and 0.3 ± 0.01 μM s^{-1} respectively, Table 2.13). Because a slight inhibition was observed at 2500 μM ADP (Figure 2.27*c*), the K_m measurement for $polyP_{25}$ was repeated once more at 1500 μM ADP and the range of $polyP_{25}$ concentration extended to lower concentrations (0.78 – 400 μM). Inhibition above 50 μM $polyP_{25}$ was confirmed and the kinetics parameters obtained were comparable to the previous measurement: K_m 1.27 ± 0.15 μM, V_{max} 0.52 ± 0.01 μM s^{-1}, K_i 606 ± 108 μM (Figure 2.27*d* and Table 2.13). To investigate whether the *Ft*PPK activity or the FLuc activity was inhibited by high concentration of substrates, ATP standard curves were prepared in the presence of the same amount of ADP and $polyP_{25}$ used for the K_m measurements. Increasing concentration of ADP did not significantly affect the activity of the FLuc at concentrations below 1000 μM while above this value a mild inhibition was observed (Figure 2.28*a*). The effect of $polyP_{25}$ on the FLuc activity reflected the pattern observed in the K_m measurement, with the inhibition becoming more significant above 50 μM $polyP_{25}$ (Figure 2.28*b*). The differences in the rate of light emission observed between the set of experiments in which either ADP or $polyP_{25}$ was titrated (Figure 2.28*a* and *b*) could be explained with the use in the second case of a fixed concentration of 1500 μM ADP, at which a mild inhibition of the FLuc occurs, according to the data reported in Figure 2.28*a*. To correct for the FLuc inhibition, the *Ft*PPK kinetic characterisation was repeated alongside ATP standard curves containing the corresponding concentration of ADP and $polyP_{25}$. However, due to the extension of the time required to prepare and measure

the experiments, in conjunction with the FLuc instability with time, it was not possible to produce data of a satisfactory quality.

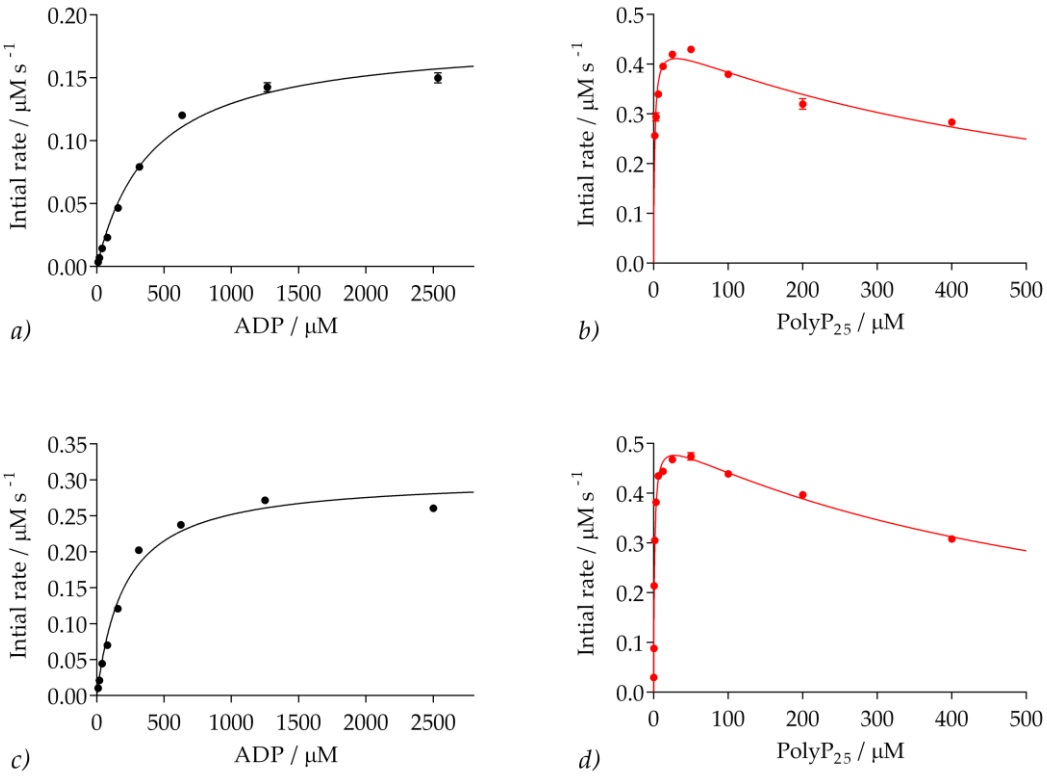

Figure 2.27: *Ft*PPK-FLuc coupled assay: optimisation of the *Ft*PPK concentration

a) K_m for ADP, measured varying the ADP concentration between 9.76 µM and 2500 µM, while the polyP$_{25}$ was 200 µM. *b*) K_m for polyP$_{25}$, measured varying the polyP$_{25}$ concentration between 1.5 µM and 400 µM, while the ADP was 2500 µM. *c*) K_m for ADP, measured varying the ADP concentration between 9.76 µM and 2500 µM, while the polyP$_{25}$ was 30 µM. *d*) K_m for polyP$_{25}$, measured varying the polyP$_{25}$ concentration between 0.78 µM and 400 µM, while the ADP was 1500 µM. The data were fitted to the Michaelis-Menten equation (Eq. 2.5) and to the substrate inhibition equation (Eq. 2.12). Assay conditions: 100 µL assay volume, 10 nM *Ft*PPK /1.3 µM BSA, ADP and polyP$_{25}$ as per respective experiment, 300 nM FLuc/1.3 µM BSA, 70 µM luciferin, 30°C. Gain: 1700.

Table 2.13: Kinetics characterisation of *Ft*PPK by coupled assay

Substrate	Fixed substrate	K_m (µM)	V_{max} (µM s^{-1})	k_{cat} (s^{-1})	R^2
ADP (*Exp1*)	200 µM polyP$_{25}$	407.2 ± 50.9	0.18 ± 0.01	18 ± 0.8	0.99
ADP (*Exp2*)	30 µM polyP$_{25}$	206 ± 30.9	0.3 ± 0.01	30 ± 1	0.98
PolyP$_{25}$ (*Exp1*)	2500 µM ADP	1.4 ± 0.3	0.45 ± 0.02	45 ± 2	0.93
PolyP$_{25}$ (*Exp2*)	1500 µM ADP	1.27 ± 0.1	0.52 ± 0.01	52 ± 1	0.98

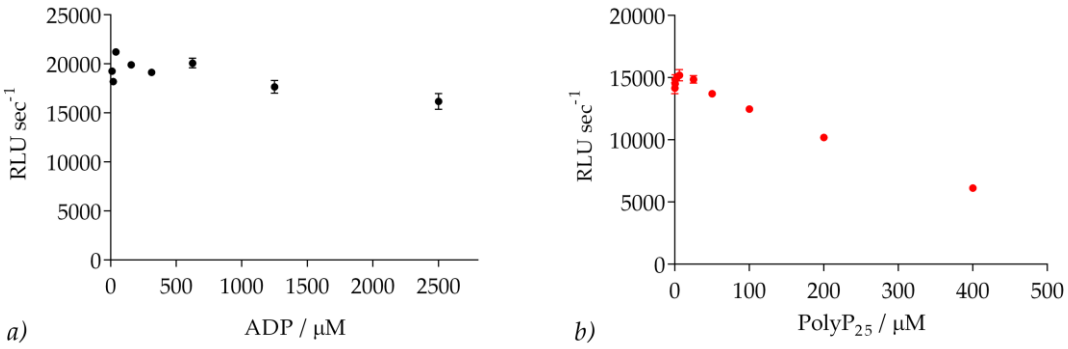

Figure 2.28: Effect of ADP and polyP$_{25}$ on the FLuc activity

a) Effect of ADP (9.76 µM and 2500 µM) in the presence of 30 µM polyP$_{25}$ on the FLuc activity; *b*) Effect of PolyP$_{25}$ (0.19 µM and 400 µM) in the presence of 1500 µM ADP on the FLuc activity. Assay conditions: 100 µL assay volume, 300 nM FLuc/1.3 µM BSA, 3.9-31.2 µM ATP, 70 µM luciferin, ADP 9.76-2500 µM and 30 µM polyP$_{25}$ or 0.19-400 µM polyP$_{25}$ and 1500 µM ADP, 30°C. Gain: 1700.

Although, in the presence of polyP$_{25}$ at concentrations higher than 50 µM, the inhibition of the FLuc activity may interfere with the correct determination of the concentration of ATP produced, and therefore with the measurement of V_{max}, it is believed that the determination of the K_m values would not be significantly affected. Indeed, the FLuc inhibition becomes significant only at substrate concentrations that would not greatly affect the data fitting to the Michaelis-Menten equation or to the substrate inhibition equation.

2.3. Summary

The methods developed by J. Docherty[352] and L. Batten[264] were adopted without any further optimisation for the heterologous expression of the thermostable FLuc and of the *Ft*PPK and for the subsequent purification by Ni-affinity chromatography (followed by gel filtration for the *Ft*PPK). Starting from some preliminary conditions derived from J. Docherty[352] and L. Batten's[264] work, the luminescence assay was optimised and then coupled to the *Ft*PPK assay. The assays were prepared in a buffer supplemented with $MgCl_2$ (required for catalysis) and $(NH_4)_2SO_4$ (which favours the *Ft*PPK activity) with the following composition: 50 mM Tris HCl, 10 mM $MgCl_2$, 80 mM $(NH_4)_2SO_4$, 300 mM NaCl, 20% glycerol, pH 7.8.[264]

The initial optimisation, aimed to develop a format suitable for the measurement of a *Ft*PPK time course, entailed:

i. the determination of the optimal concentration of luciferin to maximise the luminescence signal;
ii. the effect of BSA on both FLuc and *Ft*PPK activity and the determination of the optimal temperature for the coupled assay;
iii. a preliminary adjustment of the enzymes concentration to produce ATP within the dynamic range of the luminescence assay and the development of a preliminary format for the measurement of the *Ft*PPK time course.

The preliminary optimisation process resulted in the following assay conditions: 30 nM *Ft*PPK /1.3 μM BSA, 100 nM FLuc/1.3 μM BSA, 70 μM luciferin, 30°C. These were applied for a preliminary kinetic characterisation of the *Ft*PPK to validate the coupled assay format. However, the kinetic parameters derived were exceeding the values previously determined by L Batten,[264] suggesting that some further optimisation of the coupled assay was required.

In view of the application of the coupled assay for HTS, the effect of DMSO on the enzymes activity was tested. While the *Ft*PPK was not affected by DMSO, a decrease of the FLuc activity was observed with the increase of the DMSO concentration. A concentration of 5% DMSO provided the best compromise between enzyme activity and solubility of possible hydrophobic compounds. To improve the assay quality for HTS, the assay optimisation was

aimed to maximise the screening window by reducing the signal from the negative control assays and by intensifying the signal from the positive control assays. The first goal was achieved by ion-exchange purification of the ADP to remove ATP impurities. The second goal was achieved by increasing the concentration of the FLuc and by optimisation of the content of NaCl in the assay buffer, which proved to be detrimental for the activity of the FLuc (optimum NaCl: 25 mM). The optimisation of the FLuc concentration, in conjunction with the further optimisation of the *Ft*PPK concentration, allowed to establish an optimal ratio between primary and secondary enzyme, at which the *Ft*PPK proved to be rate limiting and the ATP produced (time course: 16 - 70 seconds) was well within the luminescence assay dynamic range.

The newly optimised conditions (10 nM *Ft*PPK /1.3 μM BSA, 300 nM FLuc/1.3 μM BSA, 70 μM luciferin, 5% DMSO, 30°C; 25 mM NaCl in the assay buffer; ADP purified by ion-exchange), together with a further optimised format, allowed the accurate and reproducible measurement of the *Ft*PPK activity and were applied for the kinetic characterisation of the *Ft*PPK. The K_m values obtained (K_m for ADP: 206 ± 30.9 μM, K_m for $polyP_{25}$: 1.27 ± 0.15 μM) were better comparable to the values reported by L. Batten (K_m for ADP: 369 ± 70 μM and 286 ± 14 μM, measured by HPLC assay and luminescence assay respectively; K_m for $polyP_{25}$: 5.35 ± 1.84 μM, measured by luminescence assay).[264] Substrate inhibition was observed within the experiments for the K_m determination for $polyP_{25}$, due to the inhibition of the FLuc activity (above 50 μM $polyP_{25}$). A mild inhibition of the FLuc activity caused by high concentration of ADP (above 2000 μM ADP) was also observed. Although probably altering the measurement of V_{max}, it is believed that the K_m determination was not significantly affected by the FLuc inhibition. Indeed, no measurable FLuc inhibition occurred below 1500 μM ADP and 30 μM $polyP_{25}$, concentrations used for the K_m measurements.

Chapter 3

High Throughput Screening

3.1. Introduction

The purpose of conducting a screening campaign is to identify chemical entities that inhibit the target of interest (hit compound), to be later progressed to the lead state by medicinal chemistry optimisation and ultimately leading to the development of a compound with drug-like physical chemistry profile and appropriate toxicology profile, that can eventually be advanced to clinical studies. Following the development of an assay to measure the activity of the target of interest, it is of critical importance to transfer the assay to a format suitable for high throughput screening (HTS) and conveniently optimised to allow the identification of active compounds.

3.1.1. Inhibition modality

An inhibitor (I) is defined as a molecule that reduces the catalytic activity by formation of a complex with the enzyme (EI complex). It is possible to classify inhibitors based on their mode of action.[273,377,378] A first distinction can be made between inhibitors that reversibly bind to the enzyme (reversible inhibitors) and inhibitors that covalently bind to the enzyme (irreversible inhibitors). While irreversible inhibitors can not be displaced from the EI complex, reversible inhibitors form dynamic complexes and their interaction with the enzyme can be described in terms of equilibrium dissociation constant (K_i, inhibitor constant) and in terms of free energy of binding ($\Delta G_{binding}$):[272,274,281,374]

$$K_i = \frac{k_{off}}{k_{on}} = \frac{[E][I]}{[EI]}$$

Eq. 3.1: Inhibitor dissociation constant

[EI], [E] and [I] are: the concentration of the enzyme-substrate complex, the concentration of the free enzyme and the concentration of the free inhibitor, respectively; k_{on} and k_{off} are the association and the dissociation rate constant of the inhibitor to the enzyme.

$$\Delta G_{binding} = \Delta H - T\Delta S = RT\ln(K_i)$$

Eq. 3.2: Relation between $\Delta G_{binding}$ and K_i

ΔH is the enthalpy of binding and ΔS the entropy of binding at the temperature T.

Reversible inhibitors can be further classified in three different categories based on the effect reciprocally exerted by inhibitor (I) and substrate (S) to the respective binding affinity for the enzyme (E).[272–274,281,374] The binding affinity of the substrate (S) to the enzyme (E) is quantified by the dissociation constant K_d. Likewise, the affinity of an inhibitor (I) for the enzyme is expressed by the inhibitor dissociation constant K_i (Figure 3.1*a*). If substrate and inhibitor bind simultaneously to the enzyme, both the substrate K_d and the inhibitor K_i are modified to an extent that is defined by the constant α (Figure 3.1*a*). The constant α can have the following values: equal to 1 when the binding of the substrate to the enzyme does not affect the inhibitor binding affinity; equal to infinite when the binding of the substrate to the enzyme prevents the binding of the inhibitor; < 1 when the binding of the substrate to the enzyme favours the binding of the inhibitor. In most cases, when the inhibitor is bound to the enzyme at saturating concentration no product formation is observed and β, which is a constant referring to the inhibitor effect on the catalysis rate, is equal to 0. The models described define the three most common inhibition modality of reversible inhibitors: competitive, non-competitive and uncompetitive inhibition. Competitive inhibitors are characterised by exclusive binding to the enzyme, competing with the substrate for the active site ($\alpha = \infty, \beta = 0$, Figure 3.1*b*). An increase of K_m for the substrate to which the inhibitor competes is observed in the presence of increasing concentration of competitive inhibitor, because of substrate displacement from the active site. On the other hand, the V_{max} is not affected, since increasing concentration of substrate can displace back

the inhibitor from active site, leading to the restoration of full enzyme activity. Due to the competition for the same site, the apparent K_i increases with the increase of the substrate concentration.

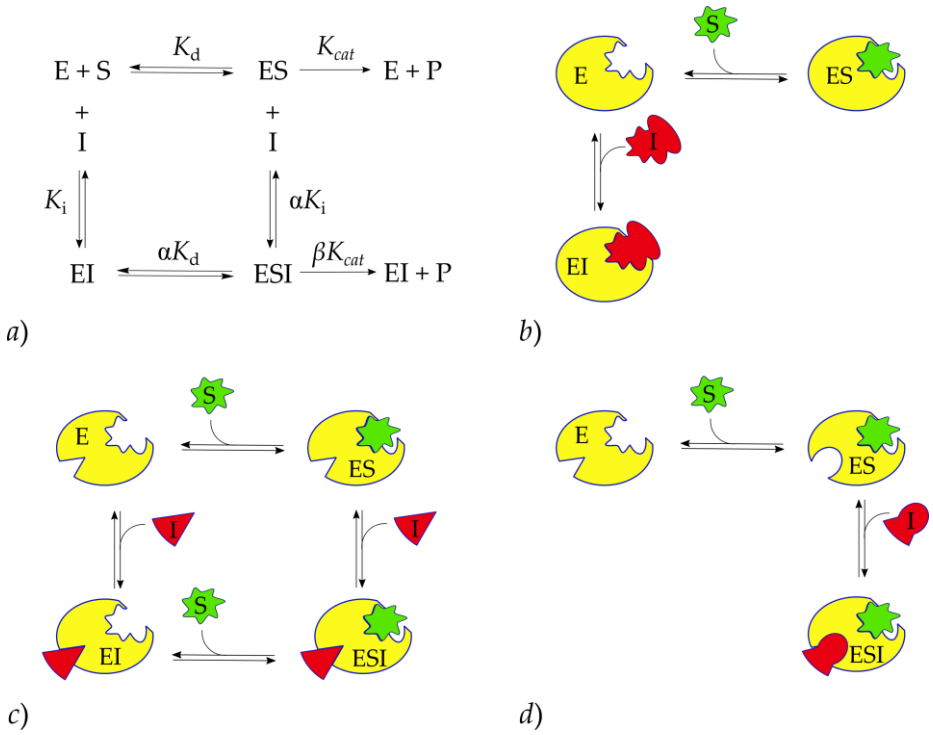

Figure 3.1: Inhibition modality

a) Schematic describing the inhibitor (I) modality based on the effect on the substrate (S) binding affinity to the enzyme (E): competitive inhibitor, $\alpha = \infty$; non-competitive inhibitor, $\alpha = 1$; uncompetitive inhibitor, $\alpha < 1$. β provides a measure of the inhibitor effect on the rate of catalysis: $\beta = 0$, enzyme activity blocked; β 0 <1, enzyme activity partially blocked; $\beta > 1$ enzyme activity enhanced. *b*) Cartoon describing the competitive inhibition: either S or I can bind to the active site. *c*) Cartoon describing the non-competitive inhibition: I and S binds to different sites without affecting the respective affinity. *d*) Cartoon describing the uncompetitive inhibition: I can bind only to the complex ES. Adapted from Copeland.[374,379]

Non-competitive inhibitors bind to a different site than the active site, independently from the substrate ($\alpha = 1, \beta = 0$, Figure 3.1*c*). No variation of K_m, hence of the affinity of the substrate to the enzyme, is observed in the presence of non-competitive inhibitors. Likewise, the inhibitor K_i is not affected by the substrate concentration. Because no displacement of the inhibitor can be exerted by increasing the concentration of the substrate, a lower V_{max} is observed in the presence of non-competitive inhibitors. Previous binding of the substrate to the enzyme is instead required for the uncompetitive inhibitors, which exclusively bind

to the enzyme-substrate complex ($\alpha < 1$, $\beta = 0$, Figure 3.1*d*). Both a variation of the apparent K_m and V_{max} is observed in the latter case, alongside to a lower K_i with the increase of the enzyme-substrate complex concentration.

Further to the three inhibition models described, which are well characterised in relation to the ES complex formation, the following inhibitor types, which present distinct additional features, have been identified: partial inhibitors, allosteric inhibitors, tight-binding inhibitors and time-dependent inhibitors.[272,273,380] A partial inhibitor is defined as molecule that reduces the rate of product formation allowing the persistence of some residual activity ($0 < \beta < 1$) even in the presence of saturating concentration of inhibitor. Partial inhibitors are rare and often apparent partial inhibition is actually due to problems of inhibitor solubility.[272,380] Allosteric inhibitors bind to a different site than the active site and cause a change of the enzyme conformation that negatively affect either the formation of the enzyme-substrate complex or the catalytic process. Allosteric inhibition is therefore due to the stabilization of the enzyme in an inactive conformation.[381] Tight-binding inhibitors are compounds with a very high affinity for the enzyme and as such dissociate very slowly and could be mistaken for irreversible inhibitors. Tight-binding inhibitors may display competitive, non-competitive and uncompetitive binding mode and are characterised by an apparent K_i very close to the enzyme concentration.[272] Slow binding inhibitors instead are characterised by a small association constant (k_{on}) and by a small dissociation constant (k_{off}). As a result of the slow association step, the inhibition will increase with the reaction time, resulting in a non linear initial rate.[272] Often slow binding inhibitors are also tight-binding compounds.[382] The same phenotype as for a non-competitive inhibition modality is displayed by these inhibitors and more detailed analysis is required to define the right type of inhibition.[272]

3.1.2. HTS: considerations for the format development and optimisation

The design of a rigorous biochemical assay constitutes a key factor for the success of a screening program.[374] Equally important is the adjustment of the assay condition to increase the assay sensitivity for the identification of active compounds. Ideally, the identification of as many active compounds as possible, including weaker compounds, and different inhibition

modalities is desirable. The apparent potency displayed by an inhibitor is affected by assay conditions such as enzyme and substrate concentration or by the measurement of the enzyme activity at an earlier or later time point of a time course.[270,379]

Except for the special case of partial inhibitors (including some allosteric partial inhibitors), the activity of an enzyme in complex with an inhibitor (EI) is completely blocked, while the activity of the remaining free enzyme (E) is unmodified. This results in attenuation of the overall rate of catalysis, although the reaction will continue until the substrate has been depleted. The most significant difference between the rate measured in the presence and in the absence of an inhibitor is detected during the initial phase of the reaction (initial rate v_0), when the product formation is linear with time (less than 10% substrate depletion).[374,379] To favour throughput and data handling, assays for HTS are measured in end point format, for which a time point that is a measure of v_0 is ideally selected. A variable that strongly affects the displayed potency of inhibitors with different modalities is the substrate concentration,[272,273,379] and the optimisation of this can be crucial for the success of the HTS. The relation between the potency (IC_{50}) of inhibitor of different modalities and the ratio between the substrate concentration (S) the respective K_m is illustrated in Figure 3.2*b*.

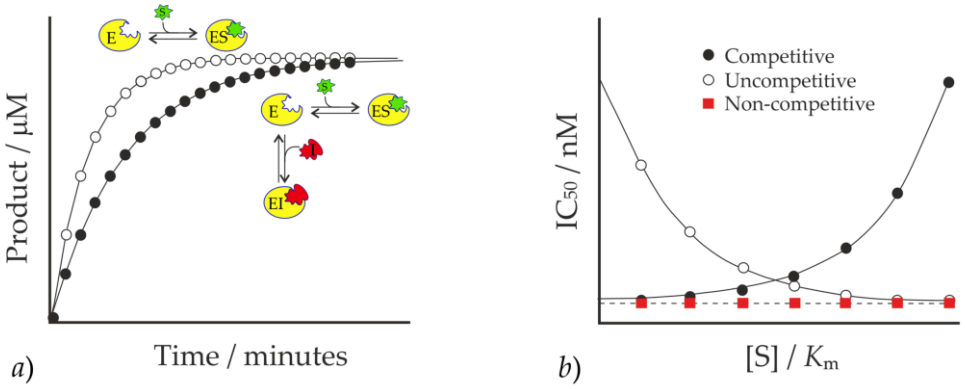

Figure 3.2: Behaviour of competitive, uncompetitive and non-competitive inhibitors

a) Time courses in the absence (open circles) and in the presence of a competitive inhibitor (full circles). Eventually the reaction will reach equilibrium and the whole substrate will be converted into product. *b*) Variation of the apparent inhibition (IC_{50}) with the increase of the substrate concentration (ratio S/K_m) for different inhibition modes. Adapted from Copeland.[379]

Non-competitive inhibitors are not sensitive to variation of the substrate concentration, due to their ability to bind both to the free enzyme E and to the ES complex (Figure 3.1*c*). In

contrast, the apparent potency of competitive inhibitors and uncompetitive inhibitors is significantly affected by the concentration of the complex ES. At $[S] = K_m$ ($[S]/K_m = 1$) the concentration of the free E and of the complex ES is equivalent. For $[S] < K_m$ the concentration of free E available for the formation of EI complex is greater than the concentration of the ES complex and competitive inhibitors will display a greater potency. The opposite occurs for $[S] > K_m$ when the substrate competition for the binding to the free E results in a higher concentration of ES complex over the EI complex. On the contrary, uncompetitive inhibitors, which binds only to the complex ES, will display a greater potency in the presence of a higher concentration of ES over the free E. Hence, the identification of competitive inhibitors will be favoured by the ratio $[S]/K_m < 1$ while uncompetitive inhibitors by the ratio $[S]/K_m > 1$. To permit unbiased identification of inhibitors displaying all inhibition mode, the substrate concentration in HTS format is often set to K_m.[379] However, due to issues with sensitivity, to improve the signal:noise ratio and therefore the screening window, it may be required to either adjust the substrate to higher concentration or to delay the assay measurement to a higher substrate consumption. In both cases, the detection of weaker inhibitors, particularly with competitive modality, can be compromised.[270,379,383]

For the adaptation of the *Ft*PPK-FLuc coupled assay for HTS format, these principles were taken into account. The initial investigation of a format suitable for HTS and the final optimisation phases of the *Ft*PPK-FLuc coupled assay were conducted simultaneously. Hence, assay conditions that were not fully optimised were used in the preliminary phases of the HTS format development and later replaced by optimal parameters. The optimisation of format and assay conditions were guided by the statistical parameter Z'-factor (section 2.2.4, Eq. 2.11), used to monitor the assay quality at each stage of the development process.

3.1.3. HTS: monitoring the assay performance during the screening

If the Z' factor allows to assess the assay quality during the format optimisation, the Z factor is the corresponding coefficient derived from monitoring the assay performance during the screening, calculated by taking into account the effect of the compound library on the

assay.[84] The same equations used to derive the Z' (Eq. 2.11) is applied for the Z factor, with the terms μ_{c-} and σ_{c-} exchanged for μ_s and σ_s, as reported below:

$$Z = 1 - \left(\frac{3\sigma_s + 3\sigma_c}{|\mu_s - \mu_c|} \right)$$

Eq. 3.3: Z-factor

μ_s and σ_s are the mean and the standard deviation of the signal from the assays containing the library compounds and μ_c and σ_c are the mean and the standard deviation of the control assays.

To calculate the Z factor for inhibition format, assays producing a signal comparable to 100% activity inhibition are used, that is either assays in which a known inhibitor was added or assays in which no activity is observed due to the lack of the targeted enzyme or of a substrate. In comparison to the Z' factor obtained during the format development, a lower Z factor is usually observed during the screening due to the effect of the library on the assay.

3.1.4. HTS: data normalization

The application of a correct data processing is a critical factor for the success of an HTS program and to reduce the inherent incidence of false positive (hits that are not real inhibitors) and false negative (genuine inhibitors failed to be identified).[384–386] The latter arise from the interference of experimental and technical errors from which data variation, leading to a misrepresentation of the assay performance, derives.[384–386] While it is easier to rule out false positives by testing the library in replicates and by means of a secondary screen, the only tool that can be used to reduce the rate of false negatives is the application of statistical analysis to correct for the effect of possible error on the data variability.[384–386] It is possible to distinguish between two types of data variability. The first is randomly generated variability, whereas the second is derived from technical factors such as the assay format, poor instrument performances or failure (liquid handling workstation or plate reader), row or column bias (edge effect) or unintended differences in library compound concentrations.[384–386] Data variation can be observed within the same microplate or from plate to plate. In both cases, normalization of the raw data allows homogenization of the data which therefore become more meaningfully comparable. The normalization methods

most commonly applied for HTS data processing are the *Normalized Percentage Inhibition* (*NPI*) method, the *Z-score* method and the *B-score* method.[384] The first two methods allow minimization of unspecific variability while the third method allows correction for systematic errors. The *Normalized Percentage Inhibition* method is a control-based normalization method that allows normalization of plate to plate variability based on control assays prepared in each microplate. Data can be normalized by *NPI* according to the following equation:

$$NPI = \left(\frac{c_- - x_i}{|c_- - c_+|} \right) \times 100$$

Eq. 3.4: Normalized percentage inhibiton

x_i is the signal from the assay containing the potential inhibitor and c_- and c_+ are the signal from the negative control assays (high intensity signal, comparable to 0% inhibition) and from the positive control assays (low intensity signal, comparable to 100% inhibition).

To monitor for the variation of the signal between plates, it is common practice to include control assays, usually assays containing a weak inhibitor, an inactive compound or simply DMSO. For practical reasons, control assays are commonly prepared on external columns or rows of the plate. However, an important caveat of this arrangement of controls is that the external wells are commonly subjected to bias due to factors such as a quicker evaporation, uneven equilibration to the assay temperature or consistent faults in the reagent pipetting/delivery. Hence, the downside of using the *NPI* method is that possible errors introduced in the control assays can affect the whole data normalization, leading to possible attribution of a higher or lower activity than actually observed for the compounds screened, ultimately creating false positive or false negative. On the other hand, the application of a control-based normalization method is advantageous when many active samples are screened within the same microplate.[385]

The other normalization method commonly applied is the *Z-score* method, a non-control based method which relies on the assumption that assays containing a library compound can be regarded as negative controls, given that most of the library compounds would not display any target activity. *Z-score* normalization can be applied according to the following equation:

$$Z\text{-}score = \frac{x_i - \bar{x}}{\sigma_x}$$

Eq. 3.5: Z-score

x_i is the signal from the assay containing the potential inhibitor, $\bar{x}$ is the mean of the whole population of assays containing library compounds and σ_x the respective standard deviation.

The *Z-score* is a method that identifies hits as outliers with respect to the normal distribution of the population.[385] The advantage of using a non-control-based normalization method is the possibility to neutralize signal shift from plate to plate due to possible day-to-day variability of the enzyme activity in response to slight variation of the experimental conditions (e.g. reagents and assay preparation). The major problems encountered with the application of the *Z-score* consist in the lack of sensitivity towards positional effects (as well as the *NPI*) and in the susceptibility to many outliers (e.g. many active compounds) which would alter the mean distribution and the standard deviation, potentially resulting in the generation of many false negatives.[385] To normalize the data taking into account positional effects, the *B*-score method has been developped.[385] As for the Z-factor, the *B*-score exploits the plate population as the normalization control, therefore neutralizing plate-to-plate variability, but in addition a robust statistical analysis[387] is applied to reduce the sensitivity to the outliers, and a two-way median polish, which helps to account for row and column effect (Appendix, section A3 2).[388] Usually, both the *Z-score* and the *B-score* methods are considered more appropriate for data normalization than the control-based *NPI* method.[384,385] It has been shown that the *B-score* method performs better when systematic variation occurs, otherwise it is preferable to apply the *Z-score* method.[385] Because of the complexity of the *B*-score calculations (powerful statistical software are required), the method was not applied for the *Ft*PPK screening. However the screening data were processed by both the *Z-score* and the *NPI* method, to counter-balance for the respective limitation and therefore to reduce the rate of both false positive and false negative.[385] To reduce the sensitivity to the outlier effects and to the commonly observed deviation of the data from a normal distribution,[389] a robust statistical analysis[387] was applied to both methods. Hence, the mean ($\bar{x}$) and the standard deviation (σ_x) were substituted with the

corresponding terms in robust statistic: median ($\tilde{x}$) and median absolute deviation (MAD_x) respectively. The *robust Z-score* (Z_R-*score*) normalization was applied according to Eq. 3.6:

$$Z_R\text{-}score = \frac{x_i - \tilde{x}}{MAD_x}$$

Eq. 3.6: Robust Z-score

x_i is the signal from the assay containing the potential inhibitor, $\tilde{x}$ is the median of the whole population of assays containing library compounds plus the negative control assays containing only 5% DMSO (activity comparable to 0% inhibition) and MAD_x is the median absolute deviation of the whole population of assays.

Because data variation within the negative control assays, ascribable to systematic error, was observed during the PKIS screening (section 3.2.2.1), for the normalization with the *NPI* method the term $c\_$ (Eq. 3.4) was substituted by the median of all the assays in which full activity of the target would be observed ($\tilde{x}$), namely the negative control assays and the assays containing the library compounds.[f] Hence, the *robust NPI* (NPI_R) normalization was applied according to Eq. 3.7:

$$NPI_R = \left(\frac{\tilde{x} - x_i}{|\tilde{x} - \tilde{c}_+|}\right) \times 100$$

Eq. 3.7: Robust Normalized Percentage Inhibiton

x_i is the signal from the assay containing the potential inhibitor, $\tilde{x}$ is the median of the whole population of assays containing library compounds plus the negative control assays containing only 5% DMSO (activity comparable to 0% inhibition) and $\tilde{c}_+$ is the median of the positive control assays (activity comparable to 100% inhibition).

3.1.5. Hit selection

The aim of an HTS campaign is to identify starting points, *hits*, for drug Optimisation efforts. A *hit* is defined as a compound for which a variation of activity beyond a defined threshold (selection criterion) is observed.[84,374,384,390] The criteria for hit declaration can be arbitrarily established based on the screening performance and on practical considerations, such as capacity limitations.[374,384] The hit selection threshold limit is usually set to ≥ 3

[f] Negative control assays (no library compound but only 5% DMSO): 0% inhibition; Assays containing the library compound: comparable to % 0 inhibition, based on the assumption that most of the library compounds will not display activity.

standard deviation of the mean of the signal from assays containing the library compounds,[84,374,384] which statistically provides a 99.73% confidence of diversity.[84] If a low hit rate is obtained, the hit threshold can be adjusted to ≥ 2 standard deviation, in which case the confidence of diversity is reduced to 95%.[84] Hence, it is common practise to either increase or reduce the hit threshold according to the hit rate, with the unavoidable consequences of either increasing the false positive or the false negative rate.[374,384] For the *Ft*PPK-FLuc coupled assay the hit threshold applied was equal to ≥3 MAD[g] computed with respect to the median of the normalized data.

[g] The MAD is the term used in robust statistical analysis, corresponding to the standard deviation of the classic statistical analysis.

3.2. Results and Discussion

3.2.1. Coupled Assay Optimisation for HTS

3.2.1.1. HTS format development: preliminary investigation of assay quality

The development of a format suitable for HTS started with the design of a preliminary format based on the measurement of *Ft*PPK rate by means of short *Ft*PPK activity time courses (3 time points), prepared in replicates on a 96 well microplate. The format was applied for the evaluation of the assay quality after the purification of ADP and the optimisation of the FLuc concentration (section 2.2.4.3) but prior to the optimisation of the *Ft*PPK concentration and of the NaCl content of the assay buffer (section 2.2.4.4). The substrate concentration applied were equal to the K_m values obtained from the preliminary kinetic investigation (section 2.2.3.6). A total number of 18 sets of *Ft*PPK time course assays (positive control assays, time point measured in triplicate: 16 s, 23 s, 30 s) and 6 sets of negative control assays (lacking *Ft*PPK, each measured in triplicate) were prepared per microplate.[h] ATP standard curves (3 sets) were included as well to monitor the activity of the FLuc with time. To validate the effect of the FLuc concentration on the screening window, the *Ft*PPK assay was coupled to both 100 nM FLuc and to 300 nM FLuc (FLuc concentrations used as standard prior and after FLuc optimisation). For each set of assays the *Ft*PPK apparent initial rate (v_0^{app}) was defined by fitting the three time points to the linear regression equation (Eq. 2.4). The assay quality was then assessed by calculating the Z' factor according to Eq. 2.11. Excellent Z' values were obtained for both the assays coupled to 100 nM FLuc (Z' = 0.75) and for the assays coupled to 300 nM FLuc (Z' = 0.84), which was due in both cases to the low variability of the positive control assays and negative control assays ($\mu_{+/-c} \pm 3\sigma_{+/-c}$). The screening window ($|\mu_{+c} - \mu_{-c}|$) of the assays coupled to 300 nM FLuc was further improved due to the higher intensity of the luminescence signal, confirming the positive effect exerted on the assays quality by the optimisation of the FLuc concentration (Figure 3.3).

[h] Within the optimisation process of the HTS format it was referred as positive control assays to those assays in which full activity was observed (including all the assay components) and negative control assays to those assays in which no activity was observed (no *Ft*PPK included).

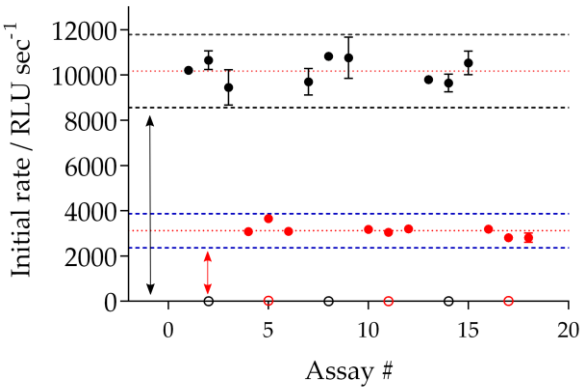

Figure 3.3: HTS preliminary format, rate measurement

Screening window and Z' factor comparison between *Ft*PPK assays coupled to 300 nM FLuc (Z' 0.84) and to 100 nM FLuc (Z' 0.75). The data were reported as initial rate versus assay number. *Ft*PPK assays coupled to 300 nM FLuc were shown as: black circles, v_0^{app} from positive control assays; black open circles, rate from negative control assays; *Ft*PPK assays coupled to 100 nM FLuc were reported as equivalent in red circles. Dashed lines, $\pm 3\sigma_{+c}$, dotted lines: μ_{+c}; black arrow: screening window corresponding to Z' 0.84; red arrow: screening window corresponding to Z' 0.75. Assay conditions: 100 µL volume, 35 nM *Ft*PPK /1.3 µM BSA, 700 µM ADP, 30 µM $polyP_{25}$, 300 nM or 100 nM FLuc/1.3 µM BSA, 70 µM luciferin, 5% DMSO, 30°C. Gain: 1700.

3.2.1.2. Development of an end-point format in 384 well plate

Following the assessment of the assay quality using a preliminary format, a new format in which the assays were measured in end-point mode was developed. The *Ft*PPK activity was measured by a single time point (32 seconds), chosen within the linear phase of the time course and therefore a function the initial rate. A total number of 80 *Ft*PPK-FLuc assays were prepared on a 96 well plate: 40 positive control and 40 negative control assays. In addition, 2 sets of ATP standard curve assays were included, to monitor the FLuc activity with time. The Z' for this plate was 0.88, which confirmed the good quality of the assay (Figure 3.4). The application of the end-point mode to the HTS format allowed a significant increase in throughput, improving both the number of compounds that could be screened per plate and the time required to measure the whole microplate.

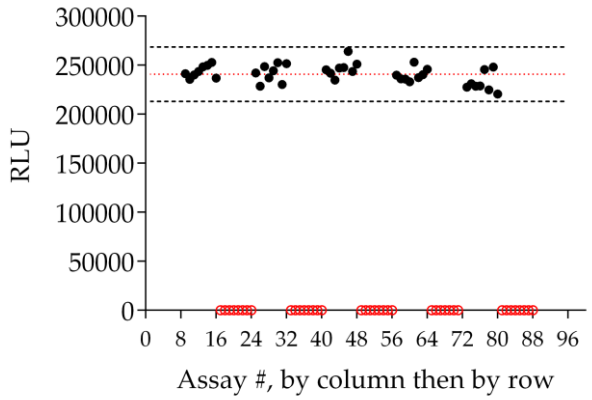

Figure 3.4: HTS format, end-point mode in 96 well microplate

A single time point (32 s) within the linear phase of the time course was measured (Z' = 0.88). Black circles: positive control assays; red open circles: negative control assays; black dashed lines: $\pm 3\sigma_{+c}$; red dotted line: μ_{+c}. The data were reported as signal measured from each assay plotted against position on the microplate (column 1, then column 2, etc.). The positive control assays and the negative control assays were prepared in alternating columns. Assay conditions: 100 µL volume, 35 nM *Ft*PPK /1.3 µM BSA, 700 µM ADP, 30 µM polyP$_{25}$, 300 nM FLuc/1.3 µM BSA, 70 µM luciferin, 5% DMSO, 300 seconds incubation, 30°C. Gain: 1700.

To further improve the throughput, the end-point format was transferred to a 384 well microplate, although the final assay volume was not changed (100 µL volume). The 384 well microplate was divided in four subsections, each prepared and measured as the 96 well plate (section 1 or quarter 1: wells AH1-12; section 2: wells AH13-24; section 3: wells IP1-12; section 4: wells IP13-24). A total number of 320 *Ft*PPK assays were prepared, 160 positive controls and 160 negative controls assays, and 8 sets of ATP standard curve assays. The signal, and therefore the activity of the enzymes, was overall consistent during the entire experiment (40 minutes required to measure the whole plate of assays), except for a slight decrease of the intensity in the last quarter of the plate measured (IP13-24). Despite using the same protocols for the assay preparation and measurement (section 7.5.1.2), a greater data variability ($\mu_{+/-c} \pm 3\sigma_{+/-c}$) was observed in comparison to the 96 well format (Figure 3.5), perhaps caused by the smaller well size of the 384 well microplate (which might have affected both the performance of the liquid handling robot and the accuracy of the signal measurement). The Z' measured for the 384 well microplate was 0.73, well above the 0.5 limit required to ensure a good separation of the positive control and negative control assay

bands.[84] The end-point format in 384 well microplate was adopted as standard for the high-throughput screening.

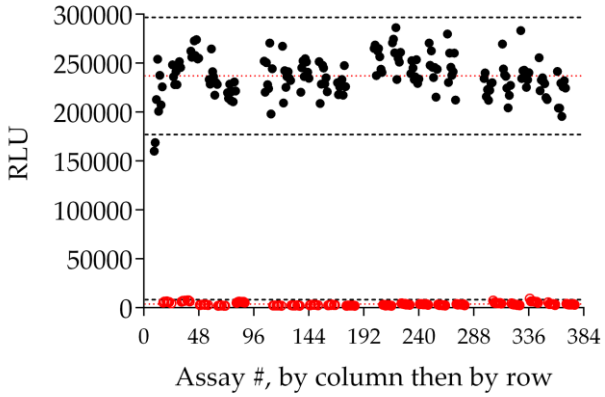

Figure 3.5: HTS format, end point mode in 384 well microplate

Measurement of a single time point (30 s) within the linear phase of the time course (Z' = 0.73). Black circles: positive control assays; red open circles: negative control assays; upper black dashed lines: $\pm 3\sigma_{c+}$; upper red dotted line: μ_{c+}; lower black dashed lines: $\pm 3\sigma_{c-}$; lower red dotted line: μ_{c-}; The data were reported as signal measured from each assay plotted against position on the microplate: the data from # 1 to 96 corresponded to the wells AH1-12 (column 1, then column 2, etc.); the data from # 97 to 192 corresponded to wells AH13-24, the data from # 193 to 288 corresponded to well IP1-12; , the data from # 289 to 384 corresponded to well IP13-24. Assay conditions: 100 µL volume, 35 nM *Ft*PPK /1.3 µM BSA, 700 µM ADP, 30 µM $polyP_{25}$, 300 nM FLuc/1.3 µM BSA, 70 µM luciferin, 5% DMSO, 300 seconds incubation, 30°C. Gain: 1700.

3.2.1.3. HTS format development: plate layout to apply for HTS and Z' reproducibility

The next step in the development of a format suitable for HTS was the designation of a screening layout and the assessment of the assay day-to-day variability. For each 384 well microplate 280 *Ft*PPK-FLuc assays were prepared: 40 assays to be used as negative control (no variation of the signal, comparable to 0% inhibition); the remaining 240 assays to screen 80 library compounds in triplicate. A total of 40 positive control assays (no *Ft*PPK, maximal variation of the signal, comparable to 100% inhibition) and 8 sets of ATP standard curve assays were also included (section 7.5.1.3). To reduce the data variability potentially due to the introduction of experimental errors during the preparation of the assays due to multi injections steps, the latter were reduced in number by adjusting the assay preparation protocols (section 7.5.1.3). To reduce the signal drifting across the microplate potentially

due to uneven equilibration to the same temperature (30°C), various incubation times prior assay initiation were investigating, resulting in an optimum of 20 minutes (Appendix, section A3 3.1.1). To assess the Z' reproducibility, screening simulations were repeated on different days. Based on 5 independent experiments prepared on 5 different days, a Z' approaching 0.70 was obtained in average (Figure 3.6 and Appendix, section A3 3.1.1,)[i]

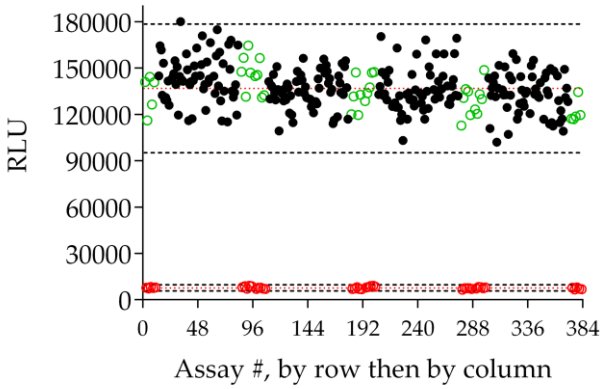

Figure 3.6: HTS format, end point mode in 384 well microplate, screening layout

Measurement of a single time point (32 s) within the linear phase of the time course (Z' = 0.70). Green open circles: screening negative control assays (0% inhibition); black circles: assays due to contain the library compound; red open circles: positive control assays (100% inhibition); upper black dashed lines: $\pm 3\sigma_{-c}$; upper red dotted line: μ_{-c}; lower black dashed lines: $\pm 3\sigma_{+c}$; lower red dotted line: μ_{+c}; The data were reported as signal measured form each assay plotted against position on the microplate: the data from # 1 to 96 corresponded to Q1, wells AH1-12 (row1, then row 2, etc.); the data from # 97 to 192 corresponded to Q2, wells AH13-24; the data from # 193 to 288 corresponded to Q3, well IP1-12; the data from # 289 to 384 corresponded to Q4, well IP13-24. Assay conditions: 100 µL volume, 35 nM *Ft*PPK /1.3 µM BSA, 700 µM ADP, 30 µM polyP$_{25}$, 300 nM FLuc/1.3 µM BSA, 70 µM luciferin, 5% DMSO, 20 minutes incubation, 30°C. Gain: 1700.

The Z' was also measured with respect to individual plate subsections (or quarter, resembling the 96 well plate format). In the latter case, the Z' values oscillated above and below 0.70 based on the position of the quarter on the microplate and on the sequence of the assay measurements (Appendix, section A3 3.1.1). A general trend was identified: a larger data variability was observed for quarter 1 (Q1, wells AH1-12) and quarter 3 (Q3, wells IP1-12) and a slightly lower intensity of the signal was observed for the last quarter

[i] The lower intensity of the luminescence signal compared to the experiment reported in Figure 3.5 was due to the use of a new batch of FLuc which resulted less active.

measured (Q4, wells IP13-24), possibly due to a slow inactivation of the enzymes. Overall, the performances of the format were judged suitable for screening and therefore applied for the screening of the PKIS library (section 3.2.2.1), although later the coupled assay conditions were further optimised and significantly improved (section 3.2.1.4).

3.2.1.4. End-point format in 384 well plate, optimal coupled assay conditions

Following the optimisation of the FLuc concentration (section 2.2.4.3), the assay quality was initially considered satisfactory and the end point format in 384 well microplate was applied for the screening of the PKIS library (section 3.2.1.3 and 3.2.2.1, respectively). However, a later further investigation of the coupled assays conditions, particularly the effect of the NaCl on the FLuc activity (Appendix, section A2 6) and optimisation of the *Ft*PPK concentration (section 2.2.4.4), led to a superior assay quality. The newly optimised conditions were adopted for the kinetics characterization of the *Ft*PPK yielding two different and more reliable values of K_m (K_m for ADP: 206 ± 30.9 μM, K_m for polyP$_{25}$: 1.27 ± 0.15 μM, section 2.2.4.5). The optimised conditions and the newly derived K_m values (10 nM *Ft*PPK/1.3 μM BSA, 200 μM ADP, 1.5 μM polyP$_{25}$, 300 nM FLuc/1.3 μM BSA, 70 μM luciferin, 5% DMSO, 20 minutes incubation, 30°C) were adopted for the HTS format and the Z' factor investigated. To compensate for the possible detrimental effect on the Z' caused by the lower *Ft*PPK and substrates concentration, a format in which the *Ft*PPK activity was measured after 60 seconds was developed alongside the 30 seconds end-point format. Despite the significantly lower intensity of the signal produced by the 30 seconds end-point format, the two Z' factors were comparable (30 seconds format: Z' = 0.78; 60 seconds format: Z' = 0.76, Figure 3.7). Due to the advantage provided in terms of the shorter time required to measure the whole microplate, the 30 seconds end-point format was initially chosen as standard and the Z' factor day-to-day reproducibility investigated. On average, the Z' was mostly above 0.7 for the single quarters while it was approaching 0.65 when computed for the whole microplate, due to the widening of the variation band ($\mu_{-c} \pm 3\sigma_{-c}$) caused by the signal drift across quarters (Appendix, section A3 3.1.2).

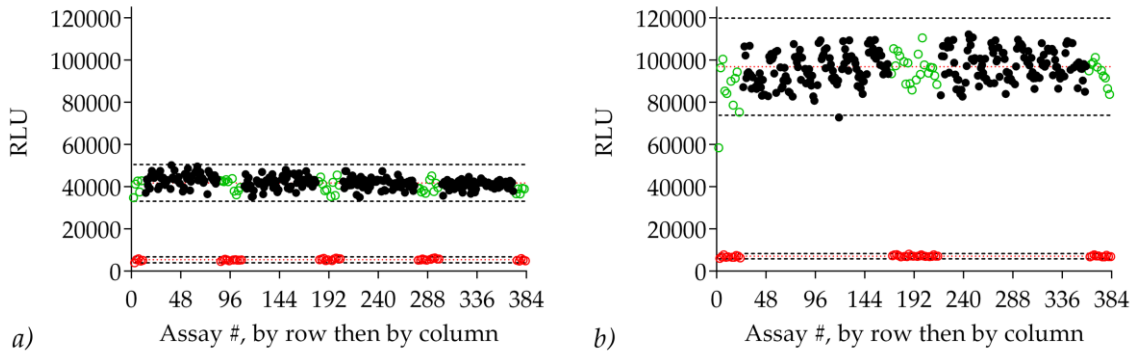

Figure 3.7: HTS end point format, 384 well microplate, optimal conditions

Z' comparison between HTS format to which the fully optimised coupled assay was applied and the *Ft*PPK activity was measured after either 30 seconds (*a*, Z' = 0.78) or after 60 seconds (*b*, Z' = 0.76). Green open circles: screening negative control assays (0% inhibition); black circles: assays due to contain the library compound; red open circles: positive control assays (100% inhibition); upper black dashed lines: $\pm 3\sigma_{-c}$; upper red dotted line: μ_{-c}; lower black dashed lines: $\pm 3\sigma_{+c}$; lower red dotted line: μ_{+c}. The data were reported as described in the legend of Figure 3.6. Assay conditions: 100 µL volume, 10 nM *Ft*PPK /1.3 µM BSA, 200 µM ADP, 1.5 µM polyP$_{25}$, 300 nM FLuc/1.3 µM BSA, 70 µM luciferin, 5% DMSO, 20 minutes incubation, 30°C. Gain: 1700.

The small window between the negative control assays signal and the positive control assays signal ($|\mu_{-c} - \mu_{+c}|$), a consequence of the low luminescence derived from the ATP produced after 30 seconds, negatively impacted the Z' particularly in the occurrence of a greater data variation (example reported in Appendix, section A3 3.1.2, Figure A3 7*d*). This, and the deterioration of the Z' observed during the screening of the PKIS library, led to the investigation of alternative conditions to improve the quality and the reproducibility of the HTS format.

Since it was not possible to reduce the data variability, due to the inherent experimental errors derived from the performance of the liquid handling workstation and the performance of the plate reader, it was attempted to improve the screening window by increasing the signal from the negative control assays (no inhibition), by either changing the concentration of the substrates or by further extending the time point measured. Because of the characteristics of the Reynolds library, a collection of nucleoside analogues (section 3.2.2.2) therefore are likely to compete with ADP rather than with polyP$_{25}$, it was decided to increase the concentration of polyP$_{25}$ to 30 µM (saturating concentration, section 2.2.4.5) while maintaining ADP at K_m concentration. In parallel, the effect of extending the

measurement of the *Ft*PPK activity to 90 seconds (which was well within the linear phase of the time course)[j] while maintaining the concentration of both substrates at K_m was investigated. The expected increase of the luminescence signal from the negative control assays was observed in both cases and a better Z' was obtained for the format in which the *Ft*PPK activity was measured after 90 seconds (Z' = 0.72) compared to the format in which the concentration of $PolyP_{25}$ was raised to 30 μM (Figure 3.8). Once again, the Z' value was affected by the downward drift of the signal, which for the experiment with 30 μM $polyP_{25}$ more severely broadened the negative control band (no inhibition), defined by considering all the assays on the entire microplate (Figure 3.8*a*).

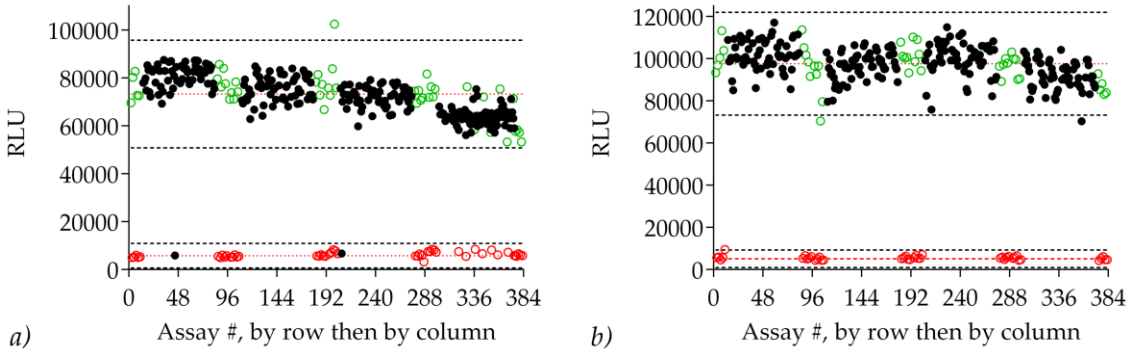

Figure 3.8: HTS end point format, optimal conditions, improvement of the screening window

Z' comparison between HTS format: *a*) 30 μM $polyP_{25}$, 30 seconds, Z' = 0.65; *b*) 1.5 μM $polyP_{25}$, 90 seconds, Z' = 0.72. Green open circles: screening negative control assays (0% inhibition); black circles: assays due to contain the library compound; red open circles: positive control assays (100% inhibition); upper black dashed lines: $\pm 3\sigma_{-c}$; upper red dotted line: μ_{-c}; lower black dashed lines: $\pm 3\sigma_{+c}$; lower red dotted line: μ_{+c}. The data were reported as described in the legend of Figure 3.6. Assay conditions: 100 μL volume, 10 nM *Ft*PPK /1.3 μM BSA, 200 μM ADP, 1.5 or 30 μM $polyP_{25}$, 300 nM FLuc/1.3 μM BSA, 70 μM luciferin, 5% DMSO, 20 minutes incubation, 30°C. Gain: 1700.

Since a good Z' factor and a comparable luminescence signal was obtained from both formats, it was decided to adopt as standard the format in which the concentration of both substrates was maintained at K_m value and the *Ft*PPK activity was measured after 90 seconds. In the attempt to attenuate the downward drift of the signal, which most probably was the consequence of enzyme inactivation, the incubation time at 30°C of the microplate

[j] Proven by investigation of the *Ft*PPK activity by HPLC assay under the applied conditions (10 nM *Ft*PPK, 200 μM ADP and 1.5 μM $polyP_{25}$ (section 4.2.3.1.2, Figure 4.13).

prior initiation of the assays was reduced from 20 minutes to 15 minutes (Figure 3.9). Applying a 20 minutes incubation, a wide decrease of the signal was observed when the HTS format was repeated (Figure 3.9*b*). Oh the other hand, although the problem was not completely solved, an attenuation of the signal drift was observed when the incubation time was reduced to 15 minutes (Figure 3.9*a*). The latter parameter was adopted as a new standard for the HTS format.

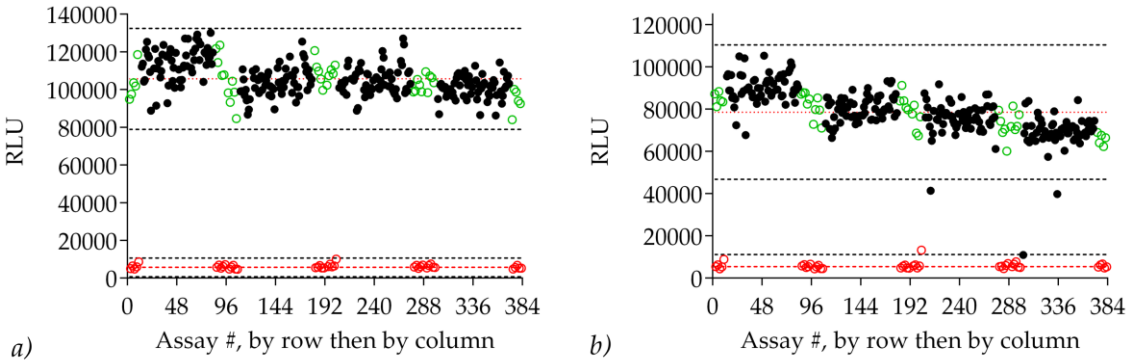

Figure 3.9: HTS end point format, optimal conditions, incubation time

Z' comparison between HTS format with the following incubation times: *a*) 15 minutes, Z' = 0.71; *b*) 20 minutes, Z' = 0.55. Green open circles: screening negative control assays (0% inhibition); black circles: assays due to contain the library compound; red open circles: positive control assays (100% inhibition); upper black dashed lines: $\pm 3\sigma_{-c}$; upper red dotted line: μ_{-c}; lower black dashed lines: $\pm 3\sigma_{+c}$; lower red dotted line: μ_{+c}. The data were reported as described in the legend of Figure 3.6. Assay conditions: 100 µL volume, 10 nM *Ft*PPK /1.3 µM BSA, 200 µM ADP, 1.5 µM $polyP_{25}$, 300 nM FLuc/1.3 µM BSA, 70 µM luciferin, 5% DMSO, 30°C. Gain: 1700.

3.2.2. High Throughput Screening

Typically, library containing between 10,000 and 100,000 compounds have been used for large screening campaigns.[77] Despite the library size, the poor structural diversity as well as inappropriate physicochemical properties have been considered one of the major factors for the limited success of HTS programmes.[391] More recently efforts have been directed towards the improvement of the library quality, favouring a wider exploration of the chemical space, therefore increasing the chemical diversity and the chance for novelty, as well as favouring compounds with lead-like properties.[391] Another approach has also emerged, consisting in the development of focused libraries, that is a collection of compounds that could better match the properties of a specific class of targets.[87] These small libraries are usually designed based on target, substrate or known ligand properties, often by various substitutions of few chemical scaffolds.[87] Despite being detrimental for diversity and novelty relative to bigger unbiased libraries, the screening of small target-focused libraries usually yields a higher hit rate. Furthermore, structure activity relationship (SAR) information can be derived by comparison of the activity of analogues of the same chemotypes contained in the library.[87]

The *Ft*PPK-FLuc coupled assay was applied for the screening of two small focused libraries: the PKIS library[392] and the Reynolds library,[393] the first a collection of kinase inhibitors, the second a collection of nucleoside analogues.

3.2.2.1. PKIS library

The PKIS (Published Kinase Inhibitor set) library is a collection of 358[k] protein kinase competitive inhibitors and corresponding inactive analogues, released by GlaxoSmithKline and available for public use. The inhibitors are competitive for ATP and as such could potentially bind to the luciferase, which is commonly used for kinase assays. Characterization of the PKIS library with respect to the activity on *Photinus pyralis* luciferase in the presence of 10 μM ATP and 10 μM luciferin has confirmed that 10% of the library (35 compounds) inhibit the luciferase, in some cases with potency below 1 μM.[392]

[k] The number of compounds provided with the library stock microplates was 358, although in the paper[392] related to the activity on the FLuc is reported that the library contains 367 compounds.

3.2.2.1.1. PKIS library screening: assay performance

For the screening of the PKIS library, the end-point assay format on a 384 well microplate of the *Ft*PPK-FLuc coupled assay was applied under the conditions reported in Table 3.1. At the stage of the PKIS screening, the coupled assay was considered well optimised (section 2.2.4.3) and the assay quality suitable for HTS (section 3.2.1.3). However, later the assay conditions and the format were further improved (section 2.2.4.4 and 3.2.1.4). The PKIS library was screened at the concentration of 10 μM in 5% DMSO. 80 compounds were screened per plate in conjunction to 40 negative control assays (containing 5% DMSO) and 40 positive control assays (no *Ft*PPK, containing 5% DMSO), prepared in alternate wells beside the assays containing the library compounds (Appendix, section A3 1.2.1 and A3 1.2.2). A total number of 354 compounds was screened (4 x 80 compounds per plate + 1 x 34 compounds per plate). Each compound was screened in triplicate. The use of replicates provides a more precise estimation of the real compound activity (duplicates reduce the measurement imprecision by 29%, triplicates by 42%) and positively impacts on the reduction of the false positive rate and in the detection of low active but potentially interesting compounds (rate of false negative).[384] The assay performance during the PKIS screening was monitored by measuring the Z' factor (Eq. 2.11) and the Z factor (Eq. 3.3) for each plate. A general pattern was observed, consisting in a lower variability within the plate subsections resembling a 96 well microplate (quarters) and a higher variability across the whole microplate from quarter to quarter (raw data in the Appendix, section A3 3.2 and Figure A3 8). Hence the Z' factor and Z factor were also derived for each quarter other than for the whole 384 well microplate (Appendix, Table A3 9). On a visual inspection of the raw data, numerous outliers, either real inhibitors or just caused by error, were identified. To reduce the impact of the outliers on the assessment of the screening performance, both the Z' factor and Z factor were calculated applying a robust statistic (median and MAD). Because of the data variation across quarters within the same microplate, the overall plate Z' and Z factor were in some cases just approaching 0.40, however the values for the individual quarters were typically higher. The measurement of the Z' factor was mostly negatively affected by systematic error (control assays prepared at the edges of the 96 well subsection) as clearly deducible by comparison with the other assay from the same

subsection. The value of the Z factor was instead affected by the many outliers, which could be potentially judged as hits since reproducibly was observed within the triplicates (Appendix, section A3 3.2, Table A3 9, Figure A3 8).

Table 3.1: PKIS screening conditions

Component/parameter	**Condition**
Buffer	50 mM Tris HCl, 10 mM $MgCl_2$, 300 mM NaCl, 80 mM $(NH_4)_2SO_4$, 2.6 μM BSA, 20 % glycerol, pH 7.8
Enzyme concentration:	*Ft*PPK (primary enzyme): 35 nM FLuc (secondary enzyme): 300 nM
Substrate concentration:	30 μM poly P_{25}, 700 μM ADP 70 μM luciferin
Library concentration	10 μM
DMSO concentration	5%
Assay temperature	30°C
Incubation time	20 minutes
Time point measured	30 seconds
Assays set up per plate	
Library compound	80 (in triplicate)
Negative control	40 (no library compound, 5% DMSO, 100% activity)
Positive control	40 (no *Ft*PPK, no library compound, 5% DMSO 100% inhibition)

3.2.2.1.2. PKIS library screening: data normalization and hit selection

The raw data were normalized applying the Z_R-*score* method (Eq. 3.6) and the NPI_R method (Eq. 3.7), which facilitated comparison of the data from different microplates (Figure 3.10). While the *Z-score* normalization method takes into account the distribution of the population and its variability across the microplate, the *NPI* method is a control based method and the normalization is done with respect to assays in which full activity and no activity is observed (control assays). As a consequence, applying the Z_R-*score* normalization,

the data variability is re-scaled allowing direct comparison of the data from different microplates.

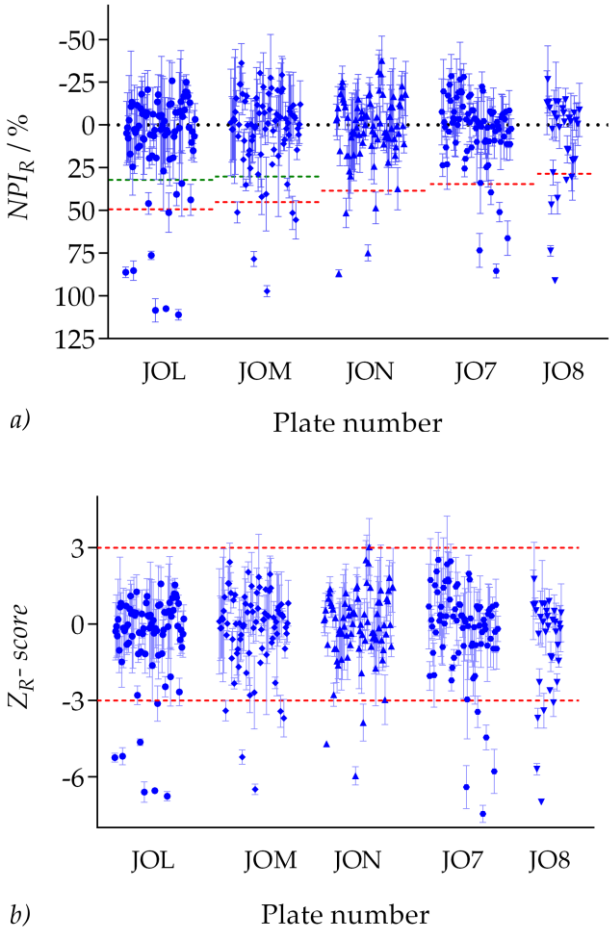

Figure 3.10: PKIS screening, data normalization and hit selection

a) PKIS screening data normalized by NPI_R. Red dashed line: 3 MAD hit threshold (plate JOL 49% NPI_R, plate JOM 45% NPI_R, plate JON 37% NPI_R, plate JO7 34% NPI_R, and plate JO8 28%. NPI_R); green dashed line: 2 MAD hit threshold (plate JOL 32% NPI_R, plate JOM 30% NPI_R). *b*) PKIS screening data normalized by Z_R-*score*. Red dashed line: 3 MAD hit threshold (-3 Z_R-*score*). The data were reported as average of the triplicate and respective error bar and were plotted against plate, and within the plate against compound number (# 1 to 80). Assay conditions: 100 µL volume, 35 nM *Ft*PPK /1.3 µM BSA, 700 µM ADP, 30 µM $polyP_{25}$, 300 nM FLuc/1.3 µM BSA, 70 µM luciferin, 10 µM library compound, 5% DMSO, 20 minutes incubation, 30°C. Gain: 1700.

The same is not observed when the NPI_R method is applied, in which case the original degree of variability in comparison to the data from other microplate is maintained (for example, refer to the relation between the variability of plate JOL and JO8 when the data were normalized by NPI_R and by Z_R-*score*, Figure 3.10*a* and *b*, respectively). As a

consequence, while the same hit selection threshold could be applied to the whole screening data set normalized by Z_R-*score*, a different threshold was calculated plate-wise for the data normalized by NPI_R to avoid missing potential inhibitors demonstrating weaker but still interesting activity. In both cases the hit criterion was set to median ± 3 MAD of the normalized data, which corresponded to -3 Z_R-*score* and to the following NPI_R values: plate JOL 49%, plate JOM 45%, plate JON 37%, plate JO7 34%, and plate JO8 28%. Reassuringly, the same compounds were selected as hits by both normalization methods applying the hit criterion of 3 MAD. However, by visual inspection of the data obtained from plate JOL and JOM, it appeared that the high hit selection NPI threshold was due to the presence of many outliers in the microplates. Hence for these two plates the NPI hit selection criterion was lowered to 2 MAD (late JOL 32%, plate JOM 30%). Compounds with value of mean plus standard deviation of the triplicate measurement beyond or across the threshold limit were declared hits (Appendix, Table A3 10). A hit rate of $<$1% and ~5-10% is usually scored from the screening of unbiased libraries and from target-focused libraries, respectively.[374] For the PKIS screening a hit rate of 8.6% (31 compounds) was obtained by selection based on the Z_R-*score* while hit selection based on the NPI_R yielded 11.1% hit rate (40 compounds). As previously mentioned, some of the library components (10%) have been reported to be FLuc inhibitors,[392] which may help to rationalize such a high hit rate.

3.2.2.2. Reynolds library

The Reynolds library is a collection of nucleoside and nucleotide analogues (736 compounds), kindly donated by Prof Robert Reynolds (Chemistry, University of Alabama). The library is mostly composed by adenosine and uridine analogues but includes also some guanosine, thymine and peptidyl nucleoside analogues.[393–396] Subsets of the library have been screened against a various range of biological assays aiming to identify chemical entities to be progressed towards the development of antibiotics, antimalarial drugs and anti-cancer drugs. Biological activity has been reported for some components of the library, particularly among the adenosine-5'-carboxamide and sulfanilamide derivatives[394] and the peptidyl-uridine derivatives[395]

3.2.2.2.1. Reynold library screening: assay performance

The Reynold library (RL) was screened against the fully optimised *Ft*PPK-FLuc coupled assay (section 2.2.4.4) applying the end-point format in 384 well microplate (section 3.2.1.4), according to the conditions reported in Table 3.2. The library was screened at the concentration of 10 μM in 5% DMSO. 80 compounds were screened per plate in conjunction to 40 negative control assays (containing 5% DMSO) and 40 positive control assays (no *Ft*PPK, containing, 5% DMSO) prepared in alternate wells beside the assays containing the library compounds (Appendix, A3 1.2.1 and A3 1.2.2). A total number of 736 compounds (7x 80, 1x 67, 1x 70 and 1x 39 compounds per plate) were screened in triplicate to reduce the rate of false positives and false negatives. The assay performance during the RL screening was monitored by measuring the Z factor (Eq. 3.3) for the whole microplate and for individual quarters within the same microplate (Appendix, Table A3 11). The Z-factor was calculated from the raw data (Appendix, Figure A3 14 and Figure A3 15), applying both classical statistical analysis (Z_C-factor, computed based on mean and standard deviation) and robust statistical analysis (Z_R-factor, computed based on median and MAD). By comparison between the Z_C-factor and the Z_R-factor it was possible to identify the plates with potential inhibitors, in which case the Z_C-factor was below 0.5 and considerably lower than the Z_R-factor. Overall, the screening performance was very good with the Z_R-factor computed for the whole 384 microplate above 0.6. The only exception was constituted by

plate 8 in which the Z_R-factor was 0.44, which however could be justified by the occurrence of 6 potential inhibitors (Table A3 11 and Figure A3 15). The very good performance of the screening was also reflected in the Z_R-factor calculated for individual quarters which was mostly approaching 0.8 unless potential inhibitors were included.

Table 3.2: Reynolds library screening conditions

Component/parameter	Condition
Buffer	50 mM Tris HCl, 10 mM MgCl2, 25 mM NaCl, 80 mM $(NH_4)_2SO_4$, 2.6 µM BSA, 20 % glycerol, pH 7.8
Enzyme concentration:	*Ft*PPK (primary enzyme): 10 nM FLuc (secondary enzyme): 300 nM
Substrate concentration:	1.5 µM poly P_{25}, 200 µM ADP 70 µM luciferin
Library concentration	10 µM
DMSO concentration	5%
Assay temperature	30°C
Incubation time	15 minutes
Time point measured	90 seconds
Assays set up per plate	
Library compound	80 (in triplicate)
Negative control	40 (no library compound, 5% DMSO, 100% activity)
Positive control	40 (no *Ft*PPK, no library compound, 5% DMSO 100% inhibition)

3.2.2.2.2. Reynolds library screening: data normalization and hit selection

To correct for intra-plate and inter-plate signal variability the raw data were normalized applying the Z_R-*score* method (Eq. 3.6) and the NPI_R method (Eq. 3.7). In comparison to the PKIS screening, a better degree of uniformity was obtained between inter-plate data not only following normalization by Z_R-*score* but also when the NPI_R method was applied, probably due to the better performance of the coupled assay during the RL library screening (Figure 3.11).

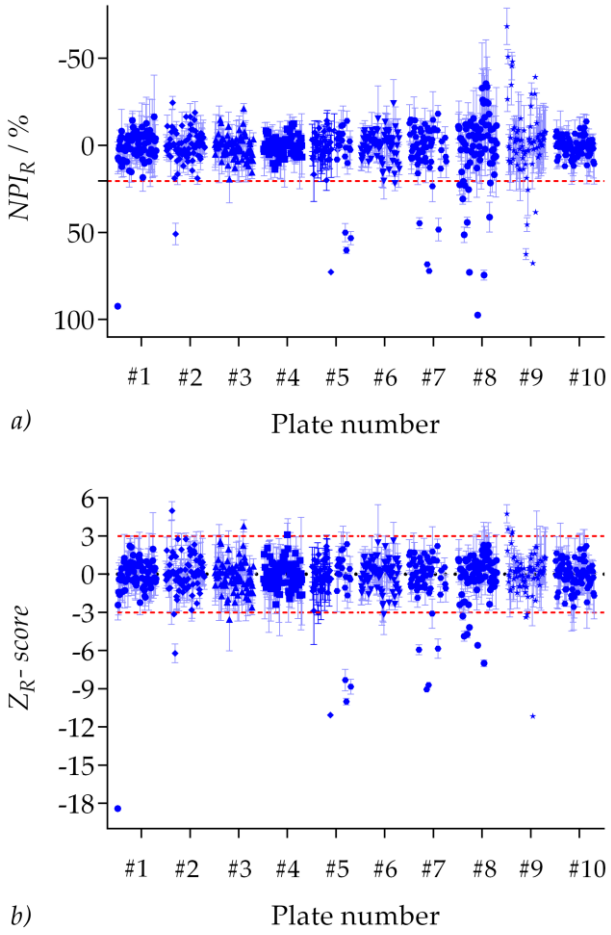

Figure 3.11: Reynolds library screening , data normalization and hit selection

a) RL screening data normalized by NPI_R. Red dashed line: 3 MAD hit threshold (20.5 % NPI_R); *b*) RL screening data normalized by Z_R-*score*. Red dashed line: 3 MAD hit threshold (-3 Z_R-*score*). The data were reported as average of the triplicate and respective error bar and were plotted against plate number, and within the plate against compound number (e.g. RT13-PL2, compound # 13, plate 2 from RL). Assay conditions: 100 µL volume, 10 nM *Ft*PPK /1.3 µM BSA, 200 µM ADP, 1.5 µM $polyP_{25}$, 300 nM FLuc/1.3 µM BSA, 70 µM luciferin, 10 µM library compound, 5% DMSO, 15 minutes incubation, 30°C. Gain: 1700.

Hence, as well as for the Z_R-*score* normalized data, the same hit selection threshold could be applied to the whole set of NPI_R normalized data. As described for the PKIS screening, the hit selection criterion was set to median ± 3 MAD of the normalized data, corresponding to –3 Z_R-*score* and 20.5% NPI_R. Compounds of which the mean plus the standard deviation of the triplicate measurement fell beyond or across the threshold limit were declared hits. Once again, the hit selection from the data normalized by the two different methods was intended to reduce the false negative rate. Indeed, some compounds missed by the Z_R-*score*-

based hit selection threshold were declared hits by NPI_R-based selection, and *vice versa* (Figure 3.12). The molecules selected by both or either the Z_R-*score* or the NPI_R method were declared hits (Appendix, Table A3 12). For the Reynold library screening a hit rate of 4.5% was obtained. In total a number of 33 compounds were declared hits, of which 23 were selected by both normalization methods while 3 more compounds were selected only by the Z_R-*score* method and 7 more by the NPI_R method (Appendix, Table A3 12).

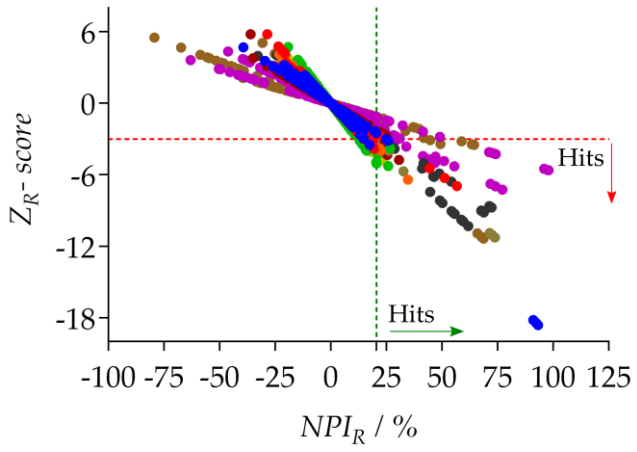

Figure 3.12: *ZR-score* and *NPIR* hit selection comparison

For each compound the *ZR-score* normalized data were plotted against the *NPIR* respective value. *ZR-score*-based hit selection threshold (-3 *ZR-score*): red dashed line; *NPIR*-based hit selection threshold (20.5% *NPIR*): green dashed line. Some compounds were selected as hits only by either one or the other selection threshold.

3.3. Summary

A format suitable for HTS screening was developed and optimised. The preliminary investigation of the HTS format preceded the final stage of the coupled assay optimisation, hence the following *Ft*PPK assay condition were applied: 35 nM *Ft*PPK /1.3 μM BSA, 300 nM/1.3 μM BSA, 70 μM luciferin, 5% DMSO, 30°C. To favour the identification of inhibitors of all modalities (competitive, non-competitive, uncompetitive) the substrate concentrations were adjusted to 700 μM ADP and 30 μM $polyP_{25}$, which were estimated as K_m applying the coupled assay under the pre-optimised conditions. A preliminary HTS format was designed on a 96 well microplate based on the measurement of v_0^{app} from a three time point time course. The format yielded a screening window suitable for HTS (Z' = 0.7-0.8), well within the assay conditions broadly considered adequate for HTS (Z' > 0.5).

To increase the throughput an end-point format was developed, in which the activity of the *Ft*PPK was measured by a single time point (30 seconds) within the linear phase of the time course. Originally developed in 96 well microplate, the end-point format was adapted to a 384 well microplate to permit further increase of the throughput. The day-to-day signal variation was investigated and the problem of the signal drifting across the microplate addressed by optimisation of the plate incubation time at the assay temperature. A format for HTS in 384 well plate with the Z'-factor reproducibly approaching 0.7 was obtained. Having concluded this was both sufficiently sensitive and with adequate throughput, the coupled assay was applied for the screening of the PKIS library.

The PKIS library, a collection of kinase inhibitors (358 compounds), was screened against the *Ft*PPK-FLuc coupled assay, in the presence of 35 nM *Ft*PPK, 300 nM FLuc, 70 μM luciferin and at the ADP and $polyP_{25}$ concentrations of 700 μM and 30 μM, respectively. Each compound was screened in triplicate at the concentration of 10 μM and the data normalized by Z_R-*score* and NPI_R method to reduce the rate of false positive and false negative. The hit selection criterion applied was 3 MAD, corresponding to -3 Z_R-*score* and variable NPI_R. For two plates of which the performance was strongly affected by the data variation and by the presence of potential genuine inhibitors (confirmed by the triplicate)

the hit selection criterion was adjusted to 2 MAD for the data normalised by NPI_R. The hit rate was 11.1% (40 compounds, 9 of which were selected only by NPI_R method).

Following the PKIS screening, the *Ft*PPK-FLuc coupled assay condition and format were further investigated, leading to a better optimised assay in which the concentration of the *Ft*PPK was reduced to 10 nM and the format improved to allow a more accurate measurement of the *Ft*PPK activity. The optimal coupled assay was applied for the kinetic characterization of *Ft*PPK resulting in more reliable measurements of the K_m: 200 μM for ADP and 1.5 μM for $polyP_{25}$. Hence, the PKIS library was actually screened under saturating concentrations of substrates, which most likely prevented the identification of real *Ft*PPK inhibitors with competitive mode of action. Due to the limited availability of PKIS library material, it was not possible to repeat the PKIS screening under optimal conditions. On this basis, it seems reasonable to conclude that it may be worthwhile rescreening this library in the future.

The performance of the end-point HTS format was tested applying the optimal *Ft*PPK-FLuc coupled assay conditions (10 nM *Ft*PPK /1.3 μM BSA, 300 nM/1.3 μM BSA, 70 μM luciferin, 5% DMSO, 30°C) and *Ft*PPK substrate concentration at K_m (200 μM for ADP and 1.5 μM for $polyP_{25}$). The decrease of the *Ft*PPK concentration and the consequent production of ATP at lower concentration resulted in a reduction of the assay dynamic range ($|\mu_{c+} - \mu_{c-}|$). This made the format more subject to worsening of the assay performance due to data variation (drop of the Z'-factor). To address the problem, two options were investigated: the extension of the measured time point to 90 seconds; the increase of the $polyP_{25}$ concentration to 30 μM (saturating concentration). Formats of comparable quality were obtained, hence it was decided to maintain the concentration of $polyP_{25}$ at K_m. The performance of the 90 seconds end-point format in experiments to assess the day-to-day reproducibility (Z'-factor around 0.7) was judged adequate for HTS and the format was applied for the Reynold library screening.

The Reynolds library, a collection of nucleoside and nucleotides analogues (736 compounds), was screened against the *Ft*PPK-FLuc coupled assay, in the presence of 10 nM *Ft*PPK, 200 μM ADP, 1.5 μM $polyP_{25}$, 300 nM FLuc, 70 μM luciferin, 5% DMSO at 30°C. Each

compound was screened in triplicate at the concentration of 10 μM and the data normalized by Z_R-*score* and NPI_R method. The hit selection criterion applied was 3 MAD, corresponding to -3 Z_R-*score* and 20.5% NPI_R. The hit rate was 4.5% (33 compounds, 23 identified by both methods, 3 only by Z_R-*score* and 7 only by NPI_R).

Chapter 4

Hit Validation and Characterization

4.1. Introduction

Within the flow chart of a drug discovery cascade (Figure 1.5), the step following the identification of hit compounds consists in the confirmation of the identified hits. The occurrence of false positive compounds, which caused attenuation of the assay signal by interference with the assay format or by unspecific interaction with the target of interest, is extremely common during a screening campaign. Compounds that are spectroscopically active (e.g. light-absorbing compounds) may interfere with the signal intensity, causing either attenuation or enhancement.[374] Compounds with detergent-like properties, or tending to aggregate, or particularly reactive, could inhibit the enzymes by unspecific interactions, hence leading to false positive hits.[86,397,398] When a coupled assay is used, false positives can originate from the inhibition of the secondary enzyme rather than the target of interest. Under analogous conditions to the primary assay, in terms of assay reagents and concentrations, real inhibitors should display activity towards the target of interest independent of the assay format. Hence, to confirm the hits selected with the primary screening, alternative biochemical assays (secondary activity assays) and/or biophysical analysis can be applied.

The first step for the identification of false positives within the active compounds selected by the *Ft*PPK-FLuc coupled assay, was a counter screen with an independent FLuc activity assay (i.e. in the absence of *Ft*PPK but including ATP as a reagent), to identify possible FLuc inhibitors. Binding to the *Ft*PPK and *Ft*PPK inhibition was then investigated by thermal shift assay and by an alternative biochemical assay, respectively. In addition, the

development of an absorbance-based PPX-Malachite green coupled assay to detect polyP formation or consumption, to be used as a secondary assay, was attempted but was judged not suitable for hit identification (Appendix, section A4 2). Eventually, an HPLC-based assay was developed and optimised, which allowed direct monitoring of the *Ft*PPK activity, minimizing the occurrence of possible artefacts.

4.1.1. Thermal shift assay

The thermal shift assay, also known as differential scanning fluorimetry (DSF), is a biophysical technique that in recent years has found increasing application for hit validation in the workflow of drug discovery programs.[85,399–403] The technique allows the investigation of protein-ligand interactions on the basis of an increase of the protein melting temperature observed upon ligand binding.[401] The stability of a protein is related to the Gibbs free energy of unfolding (ΔG_{unf}), which is defined as the difference in energy between the unfolded state and the native state and is a function of temperature (Eq. 4.1).[404,405]

$$\Delta G_{\mathrm{unf}} = G_{\mathrm{u}} - G_{\mathrm{n}}$$

Eq. 4.1: Gibbs free energy of unfolding

ΔG_{unf} is the protein Gibbs free energy of unfolding, G_u is the energy of the protein in its unfolded state and G_n is the energy of the protein in the native state.

For $\Delta G_{unf} > 0$, the protein is mainly in its folded state and therefore stable. With the increase of temperature, the ΔG_{unf} decreases and with it the protein stability. When ΔG_{unf} reaches 0 an equilibrium between the native state and the unfolded state occurs. Further increase of the temperature causes a shift of the equilibrium towards the unfolded state. The temperature at which $\Delta G_{unf} = 0$ is known as melting temperature (T_m). The latter can be experimentally measured by exploiting the increased hydrophobicity of the environment as a consequence of the progressive exposure of the protein hydrophobic cores upon denaturation. Environment sensitive fluorescent dyes, which are quenched in a hydrophilic environment but in contrast are fully fluorescent in a hydrophobic environment, can be used to probe the temperature induced denaturation.[400,406] In the presence of the dye and upon increase of the temperature, an increase of the fluorescence signal will be observed, due to

the partitioning of the fluorescent dye into the increased hydrophobic environment produced by protein denaturation. Protein melting curves can be derived by plotting the variation of the fluorescence signal against the temperature, where the midpoint of the melting curve corresponds to T_m. In the presence of a ligand that binds to the protein, the binding energy contributes to stabilize the protein in the native conformation by raising the energy of the native state and therefore the $\Delta G_{unf.}$ As a consequence, a shift of T_m to higher temperature (ΔT_m) is observed in correlation to the binding affinity and to the ligand concentration.[400,407–411] K_d and thermodynamic parameters can be derived from the ΔT_m.[399,412,413],[414] However, a direct comparison of ligand potency can not be made on the basis of the ΔT_m, which is affected to a different extent by entropic and enthalpic contribution to the binding energy.[401,405,415,416] For example, for a similar K_d a greater shift of the T_m would be observed for binding based on entropically driven interaction. *Vice versa*, compounds causing a similar ΔT_m are unlikely to have the same K_d, as a result of various possible combination of entropic/enthalpic contributions.[403] The influence of the binding entropy and enthalpy on the ΔT_m has also been credited with explaining the anomalous behaviour of some validated inhibitors that have failed to cause any temperature shift.[403] The interpretation of the thermal shift assay data might be further complicated by factors such as the ligand affinity for both the native and the unfolded state, the use of an excess of dye (which could compete with the ligand for the binding to the protein) and a high fluorescence signal observed before temperature increase (which may be attributed to either protein aggregation or to the presence of hydrophobic molecules that favour the dye emission).[403] Furthermore, a negative shift of the T_m in the presence of small molecules has often been observed and attributed to factors such as the ligand binding to the protein unfolded state, covalent modification of the protein and destabilization of the chelation of ions required by the protein.[403]

A protein melting curve measured by thermal shift assay is described by a sigmoidal curve, obtained by plotting the fluorescence signal versus the temperature variation. Initially, a slight decrease of the signal is observed due to the dissociation of the dye from the exposed hydrophilic residues. To follow, the signal proceeds approximately horizontally until the increase of temperature begins to cause protein unfolding. When the T_m is approached, a

rapid increase of the fluorescence signal is observed due to the rapid denaturation of the protein. In the final phase, a decrease of the fluorescence signal occurs because of the dissociation of the dye from the protein, which may aggregate and/or precipitate. The T_m corresponds to the inflection point of the curve and can be defined by fitting the curve to the Boltzmann equation:[401]

$$F_{\mathrm{T}} = F_{\mathrm{n}} + \frac{(F_{\mathrm{u}} + F_{\mathrm{n}})}{1 + \exp\left(\frac{T_{\mathrm{m}} - x}{a}\right)}$$

Eq. 4.2: Boltzmann equation for T_m determination

F_T is the fluorescence intensity at temperature T, F_n is the fluorescence measured when the protein is in the native state (minimum intensity), F_u is the fluorescence measured when the protein is in the unfolded state (maximum intensity) and a is the slope of the curve.

Alternatively, the T_m can be derived by extrapolation of the lowest point of the curve generated by plotting the negative first derivative of fluorescence intensity against temperature ($-dRFU/dT$).[401]

4.1.2. Nucleotide analysis by reversed-phase ion-pair chromatography

Reversed-phase ion-pair (RP IP) HPLC methods have been widely applied for nucleotide analysis.[417–437] Due to their polarity, nucleotides are weakly retained on a reverse phase column. However, their retention time can be increased by supplementing the aqueous and the organic phases with ion pairing agents, cationic molecules that neutralise the nucleotide negative charges (Figure 4.1). The consequent attenuation of the nucleotide polarity results into a greater retention time, with the nucleotide monophosphate eluting first, followed by nucleotide diphosphates and then nucleotide triphosphates (in order of the resulting degree of polarity). Further to the lower polarity, the retention of the nucleotides is also mediated by the interactions of the alkyl chains of the ion pairing agent with the C18 chains of the stationary phase (Figure 4.1). Methods with different alkyl ammonium salts as ion pairing agents have been developed for nucleotide analysis.[417–437] The choice of the ion pairing agent is dictated by the sample composition (e.g. complex mixture of nucleotides with similar retention time), the degree of resolution required and by the analytical technique applied

(HPLC *versus* LC-MS systems). For HPLC analysis coupled to UV detection, the tetrabutyl ammonium hydroxide (TBAH), or the correspondent hydrogen sulphate salt (TBAHS), has been used as ion pairing agent.[417–424] For LC-MS systems, requiring volatile compounds to improve the compatibility of the LC with the MS detection, chromatographic methods containing as ion pairing agents salts of hexylamine (HA),[425,426] triethylamine (TEA)[427–431] and dimethylexylamine (DMHA)[432–437] have been used for nucleotide analysis.

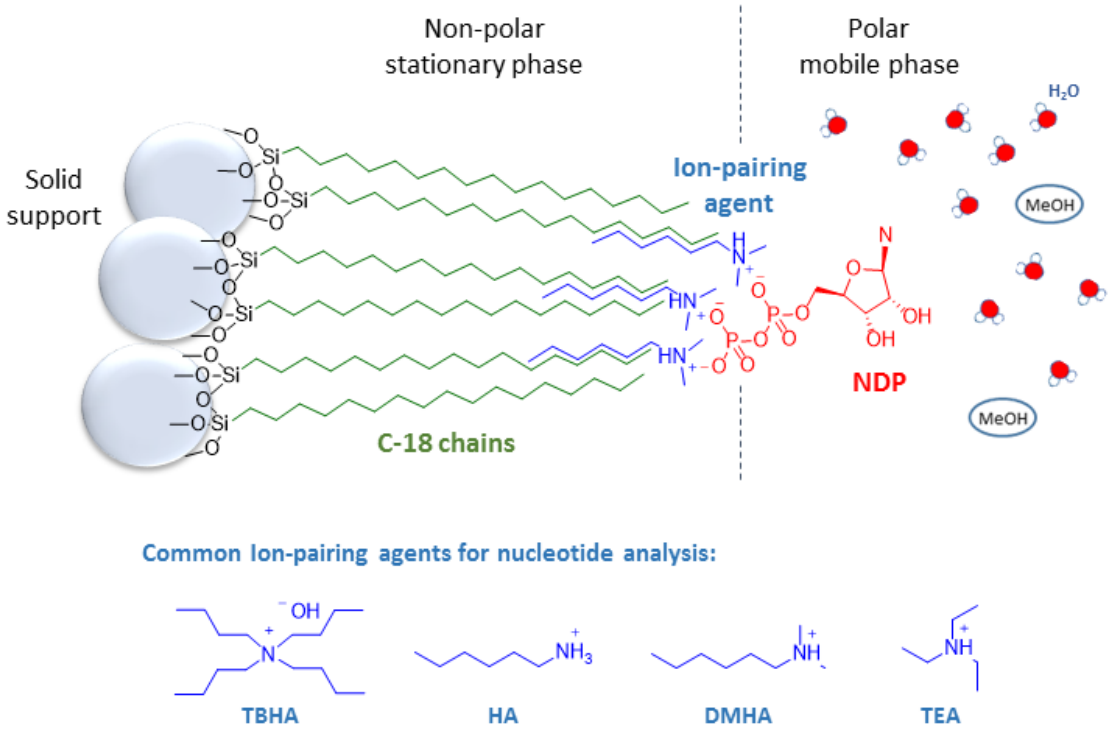

Figure 4.1: Principles of ion pairing reverse phase chromatography for nucleotides

Beads coated with C-18 chains, which confer non-polar character, constitute the matrix of the stationary phase. The mobile phase is constituted by a polar system (e.g. buffer with low percentage of organic solvent) supplied with an ion pairing agent. The nucleotide charge is neutralized by the ion-pairing agent. The nucleotide-ion pairing agent complex is retained by interaction of the hydrophobic tail with the C-18 chains. Elution is driven by decrease of the mobile phase polar character, upon increase of the organic solvent content. TBHA: tetrabutyl ammonium hydroxide; HA: hexylamine; DMHA: dimethylhexylamine; TEA: triethylamine.

4.2. Results and discussion

4.2.1. Hit validation: Counter Screening by Independent Luminescence Assay

To assess the potential activity towards the FLuc, the identified hits were tested using an independent luminescent assay. The same conditions applied for the coupled assay were adopted: 300 nM FLuc and 70 μM luciferin. The concentration of ATP was set to 10 μM, which correlates approximately to the amount of ATP produced by *Ft*PPK at the time point measured for the HTS end-point format. The hits were tested in triplicate at the concentration of 10 μM. Negative control assays (0% FLuc inhibition), in which either only DMSO or inactive library compounds were included, and positive control assays (100% FLuc inhibition), in which no FLuc was added, were prepared. The data were reported in terms of RLU and were normalized by the Normalized Percentage Inhibition (*NPI*) method (section 3.1.4, classical statistic, Eq. 3.4), where x_i was the signal from the assay containing the hit tested, c_- was the average of the signal measured from the negative control assays[l] and $c_+$was the average of the signal from the positive control assays.[m] The normalization allowed comparison of each compound in the independent luminescence assay and in the coupled assay.

Since ATP is not only the product of the polyP degradation but also a substrate in the opposite polyP synthesis, it is reasonable to expect that some molecules functioning as FLuc inhibitors could also inhibit the *Ft*PPK activity (and *vice versa*). Hence, it was decided not to discard any hits on the basis of the independent luminescence assay. However, the comparison of the data from the two inhibition screens (*Ft*PPK coupled assay and independent FLuc uncoupled assay) did allow the identification of molecules that selectively inhibited *Ft*PPK activity, when a significant difference was observed.

4.2.1.1. PKIS hits

The PKIS library has been characterised with respect to the activity on the *Photinus pyralis* firefly luciferase, revealing a 10% hit rate for inhibition.[392] To identify possible FLuc

[l] Including both the assays containing DMSO and the assays containing an inactive library compound
[m] While for the screening data normalization the modified NPI_R method was applied, for the normalization of the independent luminescence assay the classic NPI method was applied.

inhibitors, the PKIS hits were tested with the independent luminescence assay. As expected, some degree of FLuc inhibition was observed for most of the hits (Figure 4.2). By comparison between the inhibition of the independent luminescence assay and the inhibition of the coupled assay, the latter appeared to be mostly a reflection of the FLuc inhibition (Figure 4.3).

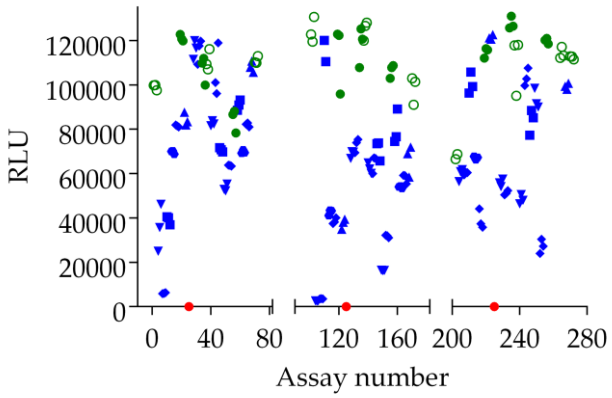

Figure 4.2: PKIS hits, independent luminescence assay counter screen

Luminescence signal (RLU) generated by independent luminescence assay: blue symbols, assays with the PKIS hits; green open circles, assays with DMSO; green full circles, assays with inactive PKIS compound; red circles, assays with no FLuc. The hits (40 compounds) were tested in triplicates (same symbol for triplicate assays). Assay conditions: 100 µL volume, 300 nM FLuc/2.6 µM BSA, 70 µM luciferin, 10 µM ATP, 10 µM library compound, 5% DMSO, 15 minutes incubation, 30°C. Gain:1700

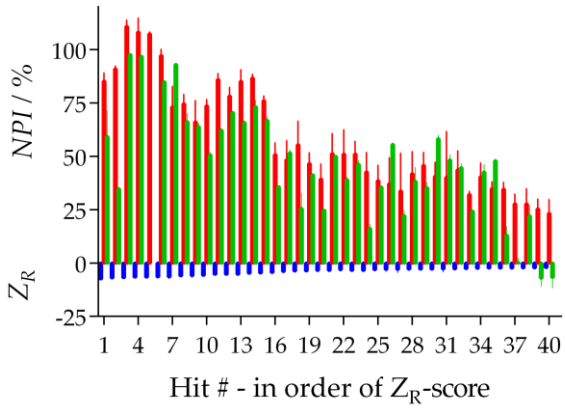

Figure 4.3: PKIS hits, comparison between coupled assay NPI and luminescence assay NPI

For each compound the *Z_R-factor* (blue bar), the coupled assay *NPI_R* (red bar) and the independent luminescence assay *NPI* (green bar) were reported. The data were plotted in order of *Z_R-factor*, from the compound with higher *Z_R-factor* value (left) to the compound with lower *Z_R-factor* value (right).The data for compound n°5 was missing.

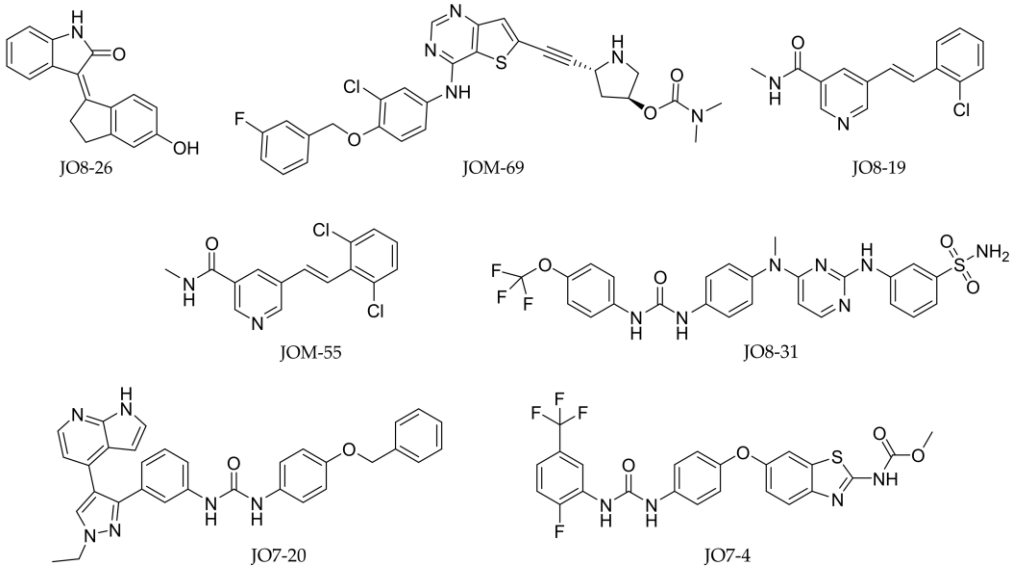

Figure 4.4: Structures of the PKIS hits that did not show significant activity towards the FLuc.

Table 4.1: Performance of the PKIS library hits that did not inhibit the FLuc

Ranked*	Plate position	*ZR-score*	Coupled assay *NPIR*	FLuc assay *NPIR*
2	JO8-26	-6.99 ± 0.1	90.9 ± 1.4	34.7 ± 0.8
18	JOM-69	-3.7 ± 0.74	55.4 ± 11	25.5 ± 7.3
24	JO8-19	-3.4 ± 0.68	42.7 ± 9.2	16.1 ± 2.1
Hit Selected only by NPI method				
36	JOM-55	-2.31 ± 0.22	34.6 ± 3.3	13 ± 4.2
37	JO8-31	-2.29 ± 0.33	27.8 ± 4.5	0.2± 2.3
39	JO7-20	-2.21 ± 0.41	25.3 ± 4.7	-7.1 ± 3.9
40	JO7-4	-2 ± 1.26	22.9 ±14.5	-6.6 ± 5.1

*Ranking based on the *ZR-score*

Only a small minority of compounds showed a significant difference between the observed *NPI* of the coupled assay and the *NPI* of the independent luminescence assay (Table 4.1). Among these compounds, it is likely that compounds JO8-31, JO7-20 and JO7-4 scored as hits in the coupled assay only because they are weak inhibitors of the FLuc. Indeed, careful comparison shows that they are structural analogues of compounds for which significant inhibition of the FLuc was observed in the independent luminescence assay (Appendix, section A3 3.2). Further investigation of the remaining compounds to assess their ability to inhibit the *Ft*PPK was required.

4.2.1.2. Reynolds library hits

The hits identified from the Reynold library screening were counter-screened with the independent luminescence assay to identify FLuc inhibitors. A significant or modest activity towards the FLuc was observed for most of the hits, with only few reporting a mild activity or being inactive against FLuc (Figure 4.5).

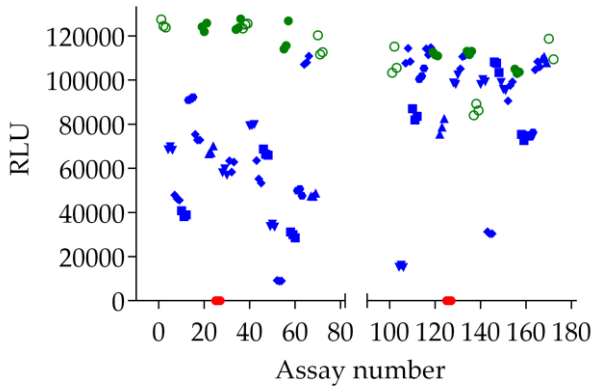

Figure 4.5: RL hits, independent luminescence assay counter screen

Luminescence signal (RLU) generated by independent luminescence assay: blue symbols, assays with the RL hits; green open circles, assays with DMSO; green full circles, assays with inactive RL compound; red circles, assays with no FLuc. The hits (34 compounds) were tested in triplicates (same symbol for triplicate assays). Assay conditions: 100 µL volume, 300 nM FLuc/2.6 µM BSA, 70 µM luciferin, 10 µM ATP, 10 µM library compound, 5% DMSO, 15 minutes incubation, 30°C. Gain: 1700.

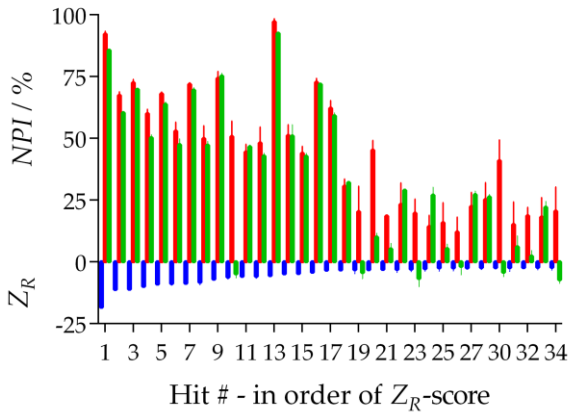

Figure 4.6: RL hits, comparison between coupled assay NPI and luminescence assay NPI

For each compound the *ZR-factor* (blue bar), the coupled assay *NPIR* (red bar) and the independent luminescence assay *NPI* (green bar) were reported. The data were plotted in order of *ZR-factor*, from the compound with higher *ZR-factor* (left) to the compound with lower *ZR-factor* (right).

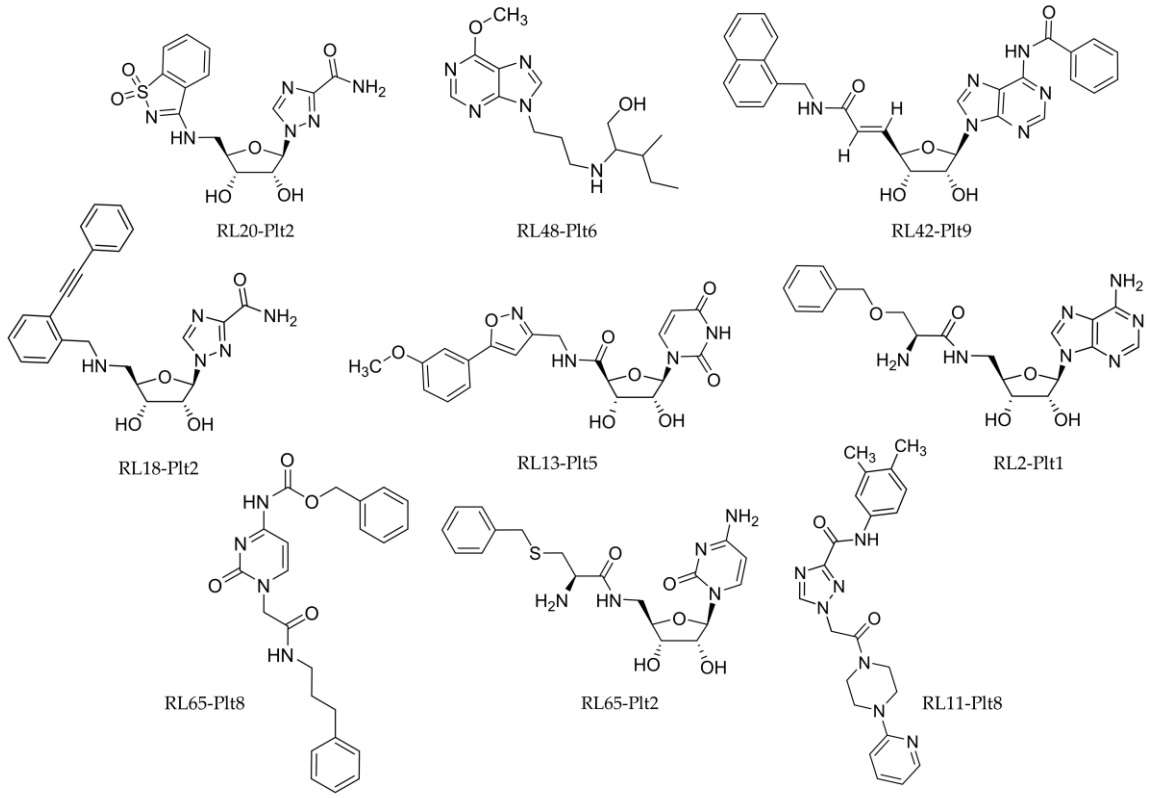

Figure 4.7: Structures of the RL hits that did not show significant activity towards the FLuc.

Table 4.2: Performances of the RL library hits that did not inhibit the FLuc

Ranked*	Plate position	*ZR-score*	Coupled assay *NPIR*	FLuc assay *NPIR*
10	RL20-PLT2	-6.2 ± 0.7	50.8 ± 6.1	-4.9 ± 1.6
19	RL48-PLT6	-3.2 ± 1.6	20.4 ± 10.2	-4.3 ± 2.6
20	RL42-PLT9	-3.1 ± 0.4	45.3 ± 3.8	10 ± 1.6
21	RL18-PLT2	-3.1 ± 0.04	18.6 ± 0.2**	5.2 ± 2.3
23	RL13-PLT5	-3. ± 0.9	19.8 ± 5.6	-6.7 ± 3.3
26	RL2-PLT1	-2.4 ± 1.2	12.2 ± 5.9**	-1.8 ± 3.3
Hit Selected only by NPI				
29	RL65-PLT8	-2.35 ± 0.48	40.97 ± 8.39	-4.2 ± 1.8
31	RL65-PLT2	-2.29 ± 0.4	18.73 ± 3.26	2.3 ± 2.2
33	RL11-PLT8	-2.20 ± 1.04	20.54 ± 9.75	-7.2 ± 1.4

*Ranking based on the *ZR-score;* ** selected only by *ZR-score*

By comparison of the inhibition of the independent luminescence assay with the inhibition of the coupled assay, it appeared that most of the hits from the Reynolds library were likely to be false positives (Appendix, Table A4 2). Nonetheless, a few compounds were identified

for which a significant difference was observed (Table 4.2). With the exception of compound 10 (RL20-Plt2), these compounds scored as weak inhibitors of the coupled assay, indeed their Z_R-*score* or NPI_R was very close to the hit selection threshold. Although the activity towards the FLuc was assessed, the results were not considered conclusive for hit validation. To exclude the possibility of having performed as false positive independently from the FLuc inhibition, or to investigate the possible inhibition of the *Ft*PPK in conjunction to the inhibition of the FLuc, a direct investigation of the activity towards the *Ft*PPK was still required.

4.2.2. Hit Validation by Thermal Shift Assay

4.2.2.1. Thermal shift assay protocol optimisation

A range of environment sensitive fluorescent dyes have found application for thermal shift assay.[400,403] Among them, SYPRO Orange has become the most popular because of its optical profile (excitation 470 nm, emission 596 nm), in particular the emission in the far red, which reduces the likelihood of background fluorescence interference from small molecules or proteins.[401,438–440]

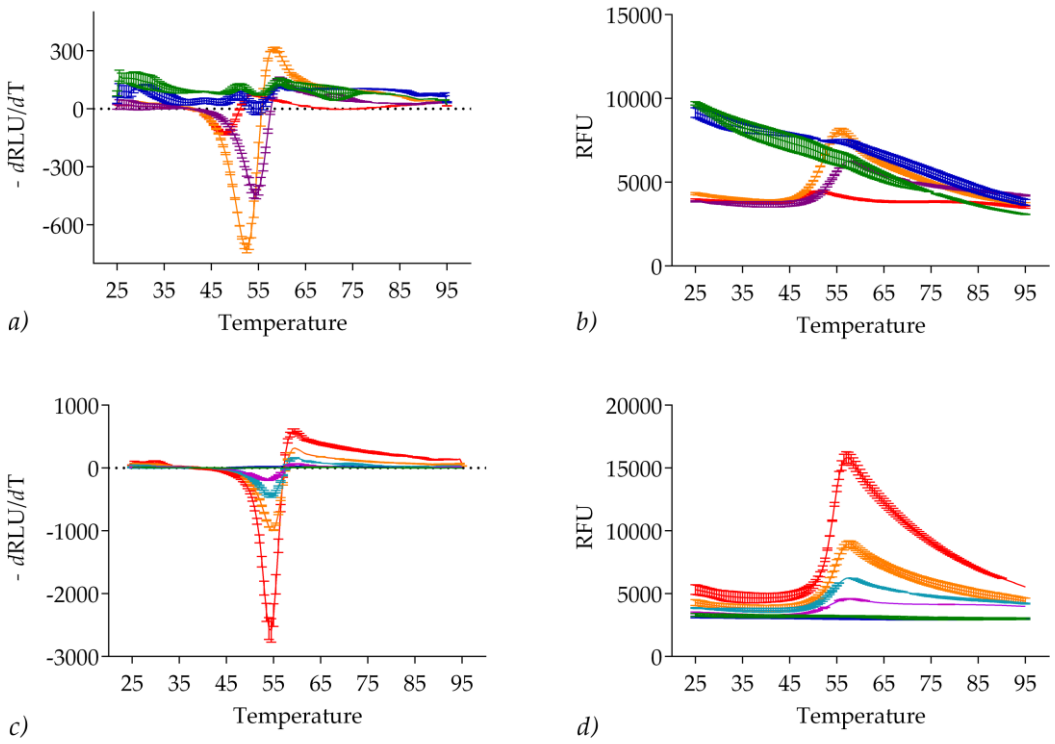

Figure 4.8: *Ft*PPK and SYPRO Orange concentration optimisation

a) and *b*) Melting curves derived in the presence of 1 µM *Ft*PPK and variable concentrations of SYPRO Orange:1x SYPRO Orange (green), 2x SYPRO Orange (blue), 5x SYPRO Orange (purple), 10x SYPRO Orange (orange), 20x SYPRO Orange (red). *c*) and *d*) Melting curves derived in the presence of 5x SYPRO Orange and variable concentrations of *Ft*PPK: 0.5 µM *Ft*PPK (purple), 1 µM *Ft*PPK (light blue), 2 µM *Ft*PPK (orange), 5 µM *Ft*PPK (red), only *Ft*PPK without dye (green), only SYPRO Orange (blue) The data were reported as the negative first derivative of fluorescence intensity (RFU) versus temperature (*a* and *c*) and as florescence intensity (RFU) against temperature (*b* and *d*). Assay conditions: 0.5 – 5 µM *Ft*PPK, 1x - 20x SYPRO Orange, 5% DMSO. Temperature increase: 25-95°C, rate 0.5°C/min.

Following this trend, SYPRO Orange was adopted for measuring the protein melting curve of *Ft*PPK. To define optimal assay conditions, a range of *Ft*PPK concentrations and SYPRO

Orange concentrations were screened in parallel. Assay solutions were prepared with 1x, 2x, 5x, 10x and 20x SYPRO Orange[n] and each of them was tested with 0.5 µM, 1 µM, 2 µM and 5 µM *Ft*PPK (Appendix, section A4 1.1, Figure A4 1). To measure background fluorescence (not due to protein denaturation), control assays with only *Ft*PPK or SYPRO Orange were also prepared. Melting curves were measured by FRET channel, applying a gradient of temperature from 25 ° C to 95 ° C at the rate of 0.5 ° C/min.[441,442] An increase of the fluorescence signal was observed with the increase of both the *Ft*PPK and the SYPRO Orange concentration. The melting curve was more pronounced and better defined for *Ft*PPK $>$ 1 µM and SYPRO Orange $>$ 5x, while below 1 µM *Ft*PPK and 2x dye solution it was not possible to observe a distinct melting curve. The maximum signal intensity was recorded in the presence of 10x SYPRO Orange, however the T_m was slightly shifted towards lower temperature in comparison to what observed for the other assay conditions (Figure 4.8*a*). A strong T_m downshift, in conjunction to a lower signal intensity, was observed in the presence of 20x SYPRO Orange (Figure 4.8*a*). The high concentration of SYPRO Orange seemed to be detrimental for the stability of the *Ft*PPK, possibly as a consequence of dye aggregation.

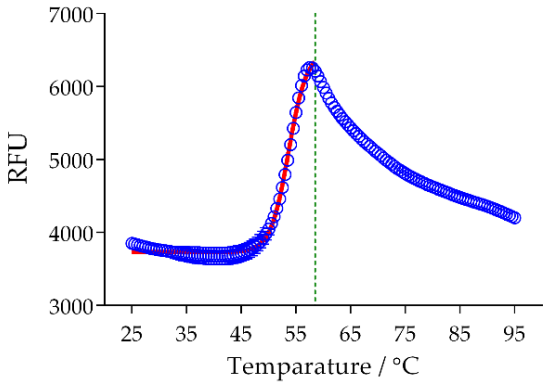

Figure 4.9: *Ft*PPK melting curve under optimal conditions

*Ft*PPK melting curve (blue open circles). Green line: the data beyond were not considered for the fitting to Eq. 4.2; Red line: curve derived from fitting to Eq. 4.2 (R^2 = 0.98). T_m : 53.64 ± 0.11 °C. Assay conditions: 1 µM *Ft*PPK, 5x SYPRO Orange, 5% DMSO. Temperature increase: 25-95°C, rate 0.5°C/min.

[n] Due to proprietary rights, the concentration of the SYPRO orange is not specified but the dye solution is sold as a 5000x stock.

A distinct and well defined melting curve was instead observed at the concentration of 5x SYPRO Orange, which was chosen as standard for the thermal shift assay (Figure 4.8*b*). For the *Ft*PPK, the concentration of 1 μM appeared to be a good compromise between protein consumption and signal intensity (Figure 4.8*c* and *d*), hence it was adopted as standard. Under the defined standard conditions (1 μM *Ft*PPK, 5x SYPRO Orange, 5% DMSO) the *Ft*PPK T_m was estimated to be 53.64 ± 0.11 °C (Figure 4.9). The T_m was derived by fitting the data to the Boltzmann equation (Eq. 4.2). Because of the rapid decrease of the signal after the maximum fluorescence intensity was reached, only the data up to the third measurement after the peak of fluorescence were flitted to Eq. 4.2.[416]

4.2.2.2. PKIS hit validation by thermal shift assay

The thermal shift assay was applied for the validation of the hits obtained from the screening of the PKIS library (section 3.2.2.1). The hits were tested in duplicate at the concentration of 100 μM applying the optimised conditions: 1 μM *Ft*PPK, 5x SYPRO Orange, 5% DMSO, temperature increase from 25 to 95°C (rate 0.5°C/min). Control assays were prepared alongside to measure the melting curve of the *Ft*PPK and to measure the background signal due to the library compound. The T_m was derived by fitting the melting curve to the Boltzmann equation (as described in section 4.2.2.1). For each compound the ΔT_m was calculated according to Eq. 4.3.

$$\Delta T_{\mathrm{m}} = T_{\mathrm{m}}^{\mathrm{h}} - T_{\mathrm{m}}^{\mathrm{d}}$$

Eq. 4.3: Calculation of the T_m shift (ΔT_m)

T_m^h was the melting temperature of the *Ft*PPK in the presence of the hits and T_m^d was the melting temperature of the *Ft*PPK in the presence of 5% DMSO.

A $\Delta T_m > 3$ standard deviation from the average of the *Ft*PPK T_m measured in the presence of 5% DMSO was considered significant. The *Ft*PPK T_m variation observed from plate to plate was on average equal to 0.26°C. To calculate the ΔT_m and the threshold of the variation significance, it was considered the average of *Ft*PPK T_m derived from the assays prepared within the same microplate as the hit of interest.

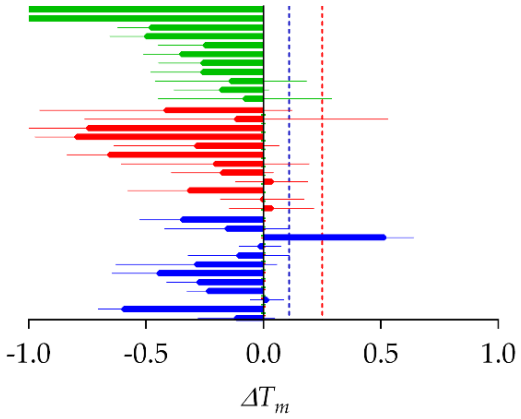

Figure 4.10: PKIS hits tested by thermal shift assay

*Ft*PPK melting temperature variation observed in the presence of the PKIS library hits. The ΔT_m of hits tested within the same microplate were reported with bars of the same colour. The dashed lines indicate the variation significance threshold for the data set of the corresponding colour, calculated as 3SD of the mean of the *Ft*PPK T_m measured in the presence of 5% DMSO. Assay conditions: 1 μM *Ft*PPK, 5x SYPRO Orange, 100 μM hit, 5% DMSO. Temperature increase: 25-95°C, rate 0.5°C/min.

Most of the PKIS library hits caused a decrease in T_m of *Ft*PPK (Appendix, Table A4 1). Only in three cases a positive shift of the T_m was observed and this was significant only for compound JO8-3 ($\Delta T_m = 0.5 \pm 0.1$ °C, blue bar in Figure 4.10). However, a better analysis of the data showed an unusual behaviour of the *Ft*PPK melting curve in the presence of JO8-3. In comparison to the other assays, a very low fluorescence signal was observed in the presence of JO8-3, suggesting that some interference with the dye, possibly aggregation, caused quenching of the signal. None of the PKIS screening hits were confirmed on the basis of the thermal shift assay, and overall these results were considered inconclusive.

4.2.2.3. RL hit validation by thermal shift

The thermal shift assay was applied for the validation of the Reynolds library hits under the same conditions as for the PKIS hit validation: 1 μM *Ft*PPK, 5x SYPRO Orange, 5% DMSO, temperature increase from 25 to 95°C (rate 0.5°C/min). For a ligand binding to the respective target, an increase of the T_m with the increase of the ligand concentration is expected.[401,411] Because of the higher availability of the Reynolds library compounds, each hit compound was tested in triplicate at three different concentrations: 10 μM, 50 μM and 100 μM.

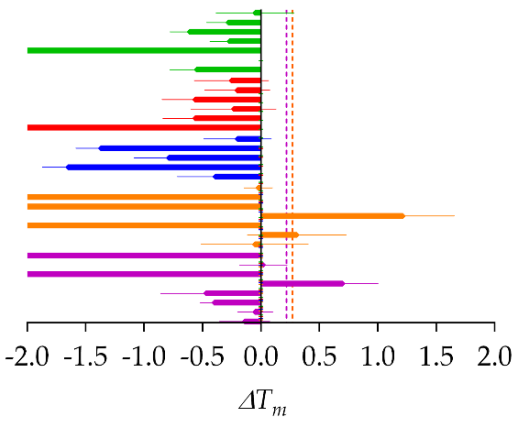

Figure 4.11: RL hits tested by thermal shift assay

*Ft*PPK melting temperature variation observed in the presence of the Reynolds library hits (100 µM). The ΔT_m of hits tested within the same microplate were reported with bars of the same colour. The dashed lines indicate the variation significance threshold for the data set of the corresponding colour calculated as 3SD of the mean of the *Ft*PPK T_m measured in the presence of 5% DMSO. Assay conditions: 1 µM *Ft*PPK, 5x SYPRO Orange, 10 µM or 50 µM or 100 µM hit, 5% DMSO. Temperature increase: 25-95°C, rate 0.5°C/min.

Control assays were prepared in the same microplate to measure the *Ft*PPK T_m and the background signal due to the library compound. As for the PKIS hits, the T_m was derived by fitting the melting curve to the Boltzmann equation (Eq. 4.2, as described in section 4.2.2.1), the ΔT_m calculated according to Eq. 4.3 and the criterion for variation significance set to > 3 standard deviation of the average of the *Ft*PPK T_m measured within the same microplate. The data obtained in the presence of 100 µM hit were reported in Figure 4.11. Once again, most of the hits produced a negative shift of the T_m, which was more pronounced with the increase of the hit concentration (Appendix, Table A4 2). A positive but mild shift of the T_m was observed in the presence of compounds RL60-Plt7 ($\Delta T_m = 1.2 \pm 0.4$ °C), RL37-Plt7 ($\Delta T_m = 0.7 \pm 0.3$ °C) and RL20-Plt2 ($\Delta T_m = 0.3 \pm 0.4$ °C). A slight increase of the T_m was observed from 10 µM to 50 µM, although the trend was broken at 100 µM (Appendix, Table A4 2). Because of the mild T_m shift detected, and given the lack of a strong correlation between ligand concentration and respective ΔT_m, the data were judged not enough robust to validate compounds RL60-Plt7, RL37-Plt7 and RL20-Plt2 as real hits of the *Ft*PPK, but support from other methods was sought.

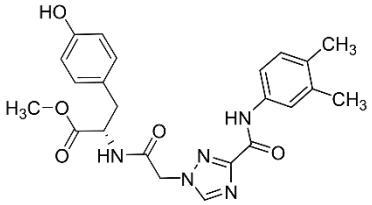

RL60-Plt7

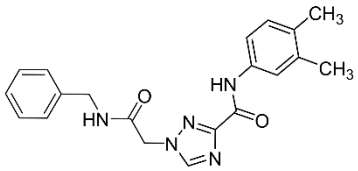

RL37-Plt7

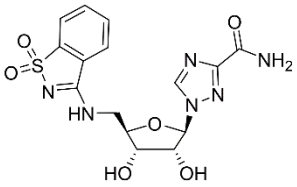

RL20-Plt2

Table 4.3: RL library hits, ΔT_m at different concentrations

Compound	10 µM, ΔT_m (°C)	50 µM, ΔT_m (°C)	100 µM, ΔT_m (°C)
RL60-PLT7	0.8 ± 0.6	1.4 ± 0.3	1.2 ± 0.4
RL37-PLT7	0.02 ± 0.5	0.8 ± 0.8	0.7 ± 0.3
RL20-PLT2	0.20 ± 0.1	0.4 ± 0.3	0.3 ± 0.4

4.2.3. Hit Validation: HPLC Assay

4.2.3.1. *Ft*PPK HPLC based assay optimisation

Since the thermal shift assay proved unsuitable as a method for validation of the *Ft*PPK hits, an HPLC-based assay was developed. A great advantage provided by an HPLC based assays is the direct quantification of the analyte of interest, although issues of sensitivity may arise for the detection of low analyte concentrations. The *Ft*PPK activity was investigated by detection of ATP formation and ADP consumption (Scheme 4.1), using reversed-phase ion-pair (RP IP) chromatography.

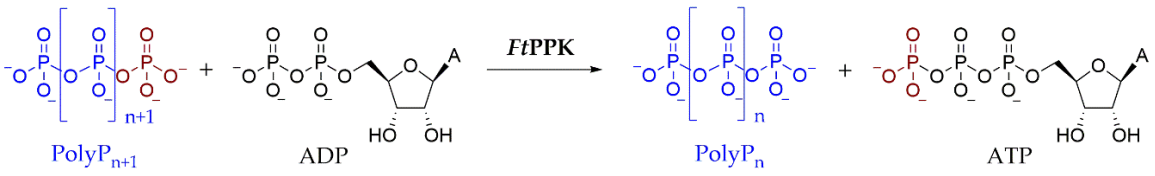

Scheme 4.1: *Ft*PPK-HPLC based assay

4.2.3.1.1. Method optimisation for *Ft*PPK assay quenching and HPLC analysis

A RP IP method with *N*,*N*-Dimethylhexylamine (DMHA) as ion pairing agent on a C18 column was previously used by L. Batten for the investigation of the *Ft*PPK activity and was adopted as a starting point for the development of an HPLC-based assay suitable for hit validation.[264] For the nucleotide elution the mobile phase was constituted by water and methanol supplemented with the ion pairing agent. The aqueous mobile phase (mobile phase A) composition was: 15 mM DMHA, 5% MeOH in water, pH 7; the organic mobile phase (mobile phase B) composition was: 15 mM DMHA, 80% MeOH in water, pH 7. The nucleotides were eluted by a gradient of low to high percentage of organic mobile phase, applying the following program: 0 min 25% B, 5 min 25% B, 27 min 60% B, 28 min 100% B (DMHA method 3). In comparison to the original method applied by L. Batten,[264] the DMHA method was optimised to improve the resolution between ADP and ATP (Appendix, section A4 3.1). To stop the *Ft*PPK reaction for time courses preparation, three methods were investigated: quenching by formic acid (1 M), quenching by heat (95°C, 5 min), quenching by EDTA (50 mM). While the first two methods rely on protein denaturation

upon exposure to harsh conditions, the third method relies on the chelation of ions required for catalysis ($MgCl_2$, for the *Ft*PPK).

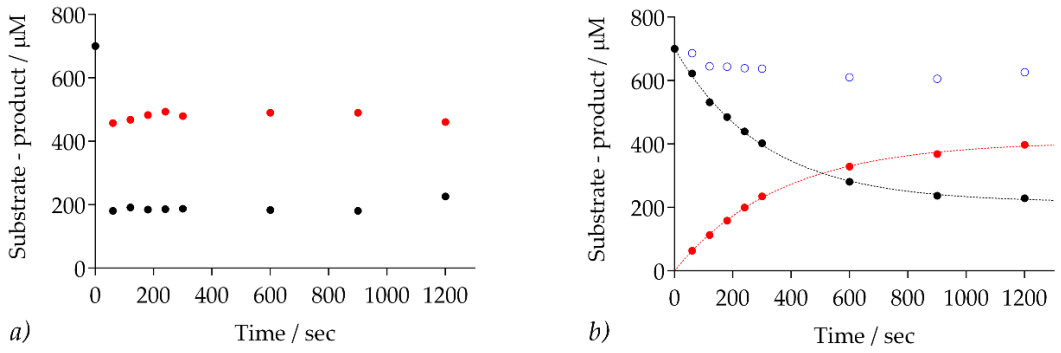

Figure 4.12: Comparison of the *Ft*PPK assay quenched by heat and by EDTA

*Ft*PPK time course prepared by heat quenching (95°C, 5 min); *b*) *Ft*PPK time course prepared by EDTA quenching (50 mM). ADP: black circles; ATP: red circles. Sum of [ADP] + [ATP]: blue open circles. The data were fitted to Eq. 2.2 and v_0 calculated according to Eq. 2.3. Assay conditions: 100 µL assay volume, 35 nM *Ft*PPK, 700 µM ADP, 30 µM $polyP_{25}$, 2.6 µM BSA, 5% DMSO, 30°C. HPLC analysis method: DMHA method 3 (Experimental, Table 7.53).

Table 4.4: *Ft*PPK time course, assays stopped by EDTA

	k (x 10^{-3} sec^{-1})	R^2
ADP consumption	3.27 ± 0.12	0.99
ATP formation	2.78 ± 0.12	0.99

The possibility of using formic acid as a quenching agent was ruled out because of the interference with the HPLC analysis (Appendix, section A4 3.1). Both heat denaturation and addition of EDTA proved to be compatible with the nucleotide analysis by DMHA method (Appendix, Figure A4 14) and their effectiveness in stopping the *Ft*PPK assay was tested by preparation of a time course. Upon heat quenching the same amount of ATP was produced at each time point, showing that the method was not adequate to stop the *Ft*PPK reaction, which proceeded to completion in each sample (Figure 4.12*a*). An increase of the ATP concentration and a corresponding decrease of ADP with time was instead observed by quenching the *Ft*PPK assay with EDTA (Figure 4.12*b*). In view of the obtained results, quenching by EDTA was adopted a standard method to stop the *Ft*PPK reaction for HPLC analysis.

4.2.3.1.2. HPLC based-*Ft*PPK assay: investigation of the conditions to apply for end-point format assay

For hit validation, ideally the same conditions applied for HTS (enzyme and substrate concentration) should be adopted. For the *Ft*PPK screening the concentration of the substrates was set to K_m values (200 µM ADP and 1.5 µM polyP$_{25}$), which resulted in the production of ATP below 20 µM at the time point chosen for the coupled assay end-point format.

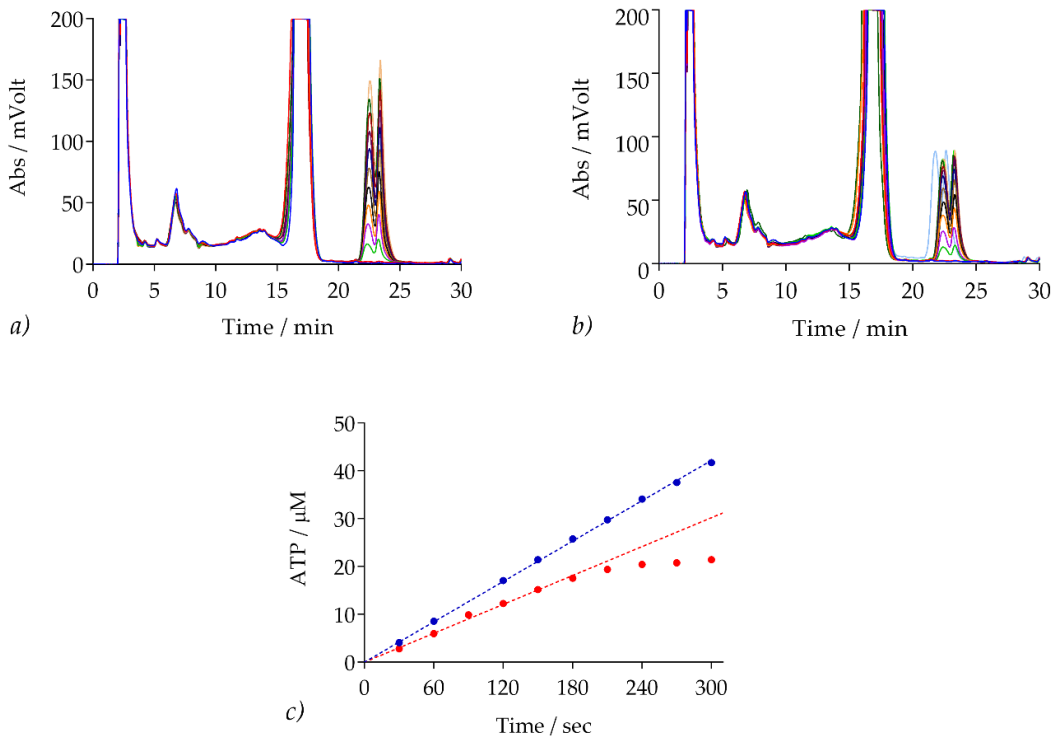

Figure 4.13: *Ft*PPK time course in the presence of 1.5 µM and 30 µM polyP$_{25}$.

HPLC chromatograms of the time points measured for the *Ft*PPK time course: *a*) in the presence of 30 µM polyP$_{25}$; *b*) in the presence of 1.5 µM polyP$_{25}$; *c*) comparison of the ATP concentration produced during the time course with 30 µM polyP$_{25}$ (blue circles) and with 1.5 µM polyP$_{25}$ (red circles). To determine $\boldsymbol{v_0}$ the data below 190 sec were fitted to Eq. 2.4. Assay conditions: 100 µL assay volume, 10 nM *Ft*PPK, 2.6 µM BSA, 200 µM ADP, 1.5 µM or 30 µM polyP$_{25}$, 5% DMSO, 30°C. HPLC analysis method: DMHA method 3 (Experimental, Table 7.53).

Table 4.5: *Ft*PPK time course

[PolyP$_{25}$]	v_0 (µM sec^{-1})	R^2
30 µM	0.14 ± 0.0001	0.99
1.5 µM	0.10 ± 0.001	0.99

The same conditions were applied for the HPLC-based *Ft*PPK assay. A time course was measured to define the reaction linear phase and determine the time point at which to stop the *Ft*PPK assay for the end point format. In the presence of 1.5 μM $polyP_{25}$, which provided only about 37.5 μM of P_i units, a limited amount of ATP could be produced. Therefore, in anticipation of possible issues of poor sensitivity at low micromolar concentration, and consequent issues in accurate and reproducible measurements, the *Ft*PPK time course was also investigated in the presence of 30 μM $polyP_{25}$ (saturating concentration). Overall, the two time courses were prepared in parallel applying the following condition: 10 nM *Ft*PPK, 200 μM ADP and either 1.5 μM $polyP_{25}$ or 30 μM $polyP_{25}$. In the presence of 30 μM $polyP_{25}$ the product formation was linear up to 300 seconds while in the presence of 1.5 μM $polyP_{25}$ a linear regression was observed up to 180 seconds (Figure 4.13). For the end point format, the last time point well within the linear phase was chosen, to ensure that *Ft*PPK activity was measured as a function of apparent initial rate (critical for the identification of competitive inhibitors) and in the attempt to address possible issues of sensitivity. For the *Ft*PPK assays prepared with 1.5 μM $polyP_{25}$ this time point was 180 minutes. For the *Ft*PPK assays prepared with 30 μM $polyP_{25}$, the time point was extended to 300 minutes.

4.2.3.1.3. HPLC based-*Ft*PPK assay: end point format optimisation

Although successfully applied for *Ft*PPK activity measurement, the DMHA method was not optimal for the analysis of nucleotides in the *Ft*PPK buffer. Issues were encountered in particular with the lack of baseline resolution between the AMP and ADP peaks, and an irregular and high background signal in the region corresponding to the ATP retention time. In addition, a wide and double peak (as opposed to a single and sharp peak) was observed for ATP elution (Figure 4.13*a* and *b*). With the aim of improving the sensitivity for small amounts of analyte, which could be partially achieved by solving these issues, an alternative method for RP IP chromatography was investigated. In particular, a method in which DMHA was substituted by trimethylamine ammonium acetate (TEAA) as the ion pairing agent was developed (TEAA method), which provided a significant decrease of the base line signal and an improved resolution and peak shape of AMP/ADP/ATP (for the TEAA method development refer to Appendix, section A4 3.2).[428,431] The mobile phases

composition for the TEAA method was: mobile phase A, 0.1 M TEAA in water, pH 7; mobile phase B: 0.1 M TEAA in 20% water/ 80% MeOH, pH 7. The elution program was: 0 min 5% B, 24 min 5% B, 25 min 10% B, 35 min 10% B, 36 min 100% B.

The suitability for hit validation of the HPLC-based *Ft*PPK assay in end point format was assessed by investigating the screening window and the data variability, based on replicates of the *Ft*PPK assays prepared at K_m concentration of ADP (200 μM) and at either 1.5 μM $polyP_{25}$ (K_m for $polyP_{25}$) or 30 μM $polyP_{25}$ (saturating concentration). The assays were quenched by EDTA (50 mM) after 180 sec or 300 sec, respectively. A total number of 12 replicates were prepared per experiment, which was repeated on four different days to investigate day-to-day variability. To evaluate the assay quality at each concentration of $polyP_{25}$, the whole data set was considered for statistical analysis. The data variability was measured in terms of mean (μ) and standard deviation (σ or SD) and by the coefficient of variation (CV):

$$\mathrm{CV} = \frac{\sigma}{\mu} \times 100$$

Eq. 4.4: Coefficient of variation

Negative control assays were prepared in which no *Ft*PPK was added and using ADP purified by anion exchange chromatography (Appendix, section A2 5). At the ADP concentration used for the assays (200 μM) no ATP traces were detected by HPLC. Hence, no signal was generated by the negative control assays and the screening window was marked only by the edge of the data variation band, which was set to the mean + 2SD. For the assays with 30 μM $polyP_{25}$ the upper limit of the screening window corresponded to 19.1 μM ATP, for the assays with 1.5 μM $polyP_{25}$ the upper limit was 10.3 μM (Figure 4.14). A common trend was identified in both assay formats: for each set of experiments a decrease of the activity (lower ATP produced) in the order of assay measurement was detected. As a consequence, a substantial data variation was observed which strongly compromised the potential for hit identification. It was anticipated that this issue could be addressed by shortening the time required to complete the measurement of a set of assays. Although the CV observed was lower for the assays measured in the presence of 1.5 μM $polyP_{25}$ (an

observation that could not be readily rationalized), the screening window was higher for the assays measured in the presence of 30 μM polyP$_{25}$ due to the higher concentration of ATP produced.

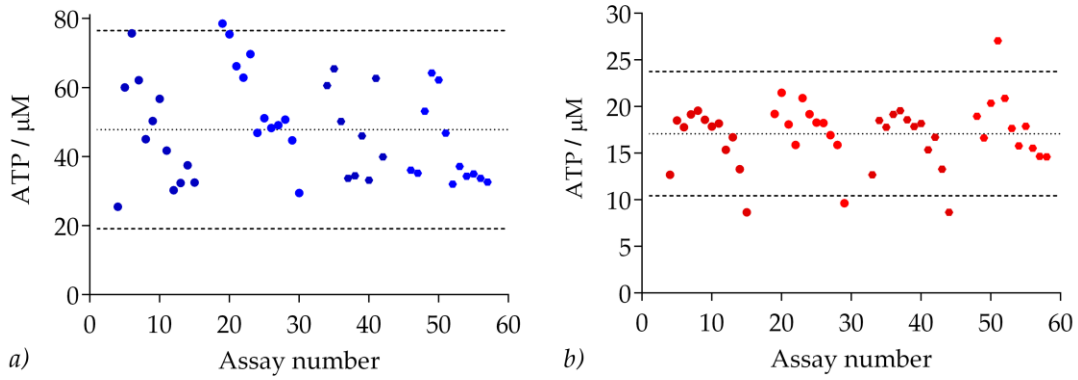

Figure 4.14: HPLC based *Ft*PPK assay in end point format

Screening window and data variation of the HPLC based *Ft*PPK assay: *a*) 30 μM polyP$_{25}$, assays quenched after 300 sec; *b*) 1.5 μM polyP$_{25}$, assays quenched after 180 sec. Dotted line: mean; dashed line: mean ± 2 SD. For each condition 4 sets of assays were tested. For each set of assays (group of 12, in the graph sharing the same colour shade) the data were reported from left to right in order of measurement. Assay conditions: 100 μL assay volume, 10 nM *Ft*PPK, 2.6 μM BSA, 200 μM ADP, 1.5 μM or 30 μM polyP$_{25}$, 5% DMSO, 30°C. HPLC analysis method: TEAA, water/methanol system.

Table 4.6: Statistical evaluation of the HPLC based *Ft*PPK assay in end point format

Parameter	30 μM polyP$_{25}$	1.5 μM polyP$_{25}$
Mean ± SD	47.8 ± 14.3 μM	17.1 ± 3.3
CV	30%	19.5%
Hit validation (mean + 2SD)	< 19.1 μM	< 10.3 μM

Compounds that displayed > 20.5% inhibition were selected as hits. Therefore, for the purpose of validating possible weak but real inhibitors, a 20% decrease of activity should be accurately detected by the HPLC based assay, which corresponds to a variation of about 10 μM ATP for the assay format with 30 μM polyP$_{25}$ and about 3.5 μM ATP for the assay format with 1.5 μM polyP$_{25}$.[o] Because of the low sensitivity of the HPLC analysis, while it

[o] Calculated as 20% variation from the average of ATP produced by the assays format with the respective concentration of polyP$_{25}$ (Table 4.6).

was judged possible, although subjected to the reduction of the data variability, to measure a variation of about 10 μM ATP, it was considered unlikely that a variation in the range of ± 3 – 4 μM ATP could be accurately measured and discriminated from the control assays. Hence, the HPLC-based *Ft*PPK assay format with 1.5 μM $polyP_{25}$ was discarded.

4.2.3.1.4. HPLC based-*Ft*PPK assay: establishing final conditions for the end-point format for hit validation

Despite efforts to improve the chromatography of analytes, issues of sensitivity imposed a deviation from the ideal conditions for hit validation, in which both substrates would be maintained at K_m concentration. In particular, the $polyP_{25}$ concentration was adjusted to saturating concentration (30 μM), which potentially disfavours the identification of possible polyP competitive inhibitors. The ADP concentration was instead maintained at K_m (200 μM), keeping the potential for the validation of inhibitors competitive with ADP. The accurate measurement of the *Ft*PPK time course under these conditions was the first step towards the establishment of a definitive assay format for hit validation (Figure 4.15). To allow measurement of initial rate, a critical requirement for the detection of competitive inhibition, the time point chosen for the end-point format was 7 minutes (420 sec), which approximately corresponded to the top end of the linear phase (Figure 4.15*a*). On the other hand, the higher concentration of ATP produced at this time point (81.1 ± 2.6 μM) resulted in an improvement of the assay screening window. To evaluate the possible sensitivity of the assays towards detection of inhibition, the chromatograms of the assay quenched after 7 minutes (80.8 μM ATP produced) was compared with the chromatogram of assays quenched at 3 min and at 5 min time points. The ATP produced at 3 min (40 μM ATP) and 5 min (64 μM ATP) corresponded to the ATP produced if 50% inhibition or 20% inhibition of the activity observed at 7 min had occurred, respectively (Figure 4.15*b*). The difference in the peak area of ATP produced in the absence of inhibition and in the occurrence of 20% inhibition was judged sufficient to identify possible weak inhibitors, assuming that a low data variability was achieved.

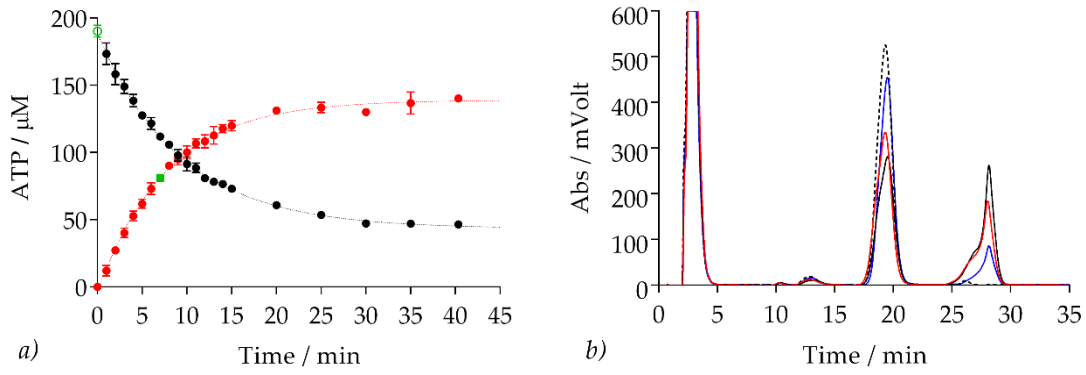

Figure 4.15: HPLC based *Ft*PPK time course for hit validation format

*a) Ft*PPK time course (in triplicate), time points measured over 40 minutes, initially at 1 minute interval, later every 5 minutes: ADP, black circles; ATP red circles; ADP in control assay, green open circle; time point chosen for end point format (7 min), green square. *b*) HPLC chromatogram corresponding to: control assay (no *Ft*PPK, 0 µM ATP), black dashed line; 100% activity measured at 7 min time point (81 µM ATP), black line; peaks corresponding to ~80% activity (64 µM ATP), red line; peaks corresponding to ~50% activity (40 µM ATP). Assay conditions: 100 µL assay volume, 10 nM *Ft*PPK, 2.6 µM BSA, 200 µM ADP, 30 µM $polyP_{25}$, 5% DMSO, 30°C. Assays quenched by EDTA (50 mM). HPLC analysis method: TEAA, water/80% methanol system. ADP retention time: 17-22 min; ATP retention time: 25 min-30 min.

Table 4.7: *Ft*PPK time course, conditions for hit validation

	k (min^{-1})	R^2
ADP consumption	0.11 ± 0.003	0.99
ATP formation	0.13 ± 0.004	0.99

A protocol was optimised to apply the *Ft*PPK assay in end-point format for hit validation (assay conditions: 10 nM *Ft*PPK, 200 µM ADP, 30 µM $polyP_{25}$). For each set of experiments, a total number of 3 hits were tested in duplicate at the concentration of 10 µM (same concentration applied for HTS). The experiment included 4 *Ft*PPK assays with 5% DMSO to monitor the activity of the *Ft*PPK, 2 negative control assays in which no *Ft*PPK was added, and a control assay for each hit compound tested to monitor the hit retention time (no *Ft*PPK added). Each assay was independently started by addition of ADP and quenched after 7 min by addition of EDTA. To attenuate the data variability due to inactivation, the assay protocol was optimised to reduce as much as possible the interval of time between the first and the last assay measured. To monitor possible data variability due to loss of activity, a *Ft*PPK assay with DMSO was measured before and after the assay

duplicates containing the hit. This format was applied for the validation of both the PKIS library hits and the Reynolds library hits.

Table 4.8: Hit validation by HPLC assay

Component/parameter	Condition
Buffer	50 mM Tris HCl, 10 mM $MgCl_2$, 25 mM NaCl, 80 mM $(NH_4)_2SO_4$, 2.6 μM BSA, 20 % glycerol, pH 7.8
Enzyme concentration:	*Ft*PPK (primary enzyme): 10 nM
Substrate concentration:	200 μM ADP, 30 μM $polyP_{25}$
Library concentration	10 μM
DMSO concentration	5%
Assay temperature	30°C
Incubation time	20 minutes
Time point measured	7 minutes (quenched by EDTA 50 mM)
Assays set up per experiment	
Hit compound	3 (in duplicate)
Negative control	4 (no library compound, 5% DMSO, 100% activity)
Positive control	2 (no *Ft*PPK, no library compound, 5% DMSO 100% inhibition)
HPLC analysis	
Mobile phase A	0.1M TEAA, water, pH 7
Mobile phase B	0.1M TEAA, 80% MeOH in water, pH 7
Elution method	0 min 5%B, 24 min 5%B, 25 min 10%, 35 min 10%B
Retention time	ADP: 19-24 min; ATP: 28-31 min.

4.2.3.2. PKIS hit validation by HPLC assay

The PKIS library hits (Appendix, Table A4 1) were tested in duplicate at the concentration of 10 µM applying the HPLC based *Ft*PPK assay in end-point format (Table 4.8). For the statistical analysis the whole set of data was considered, that is both control assays (5% DMSO) and assays with the hit compounds.

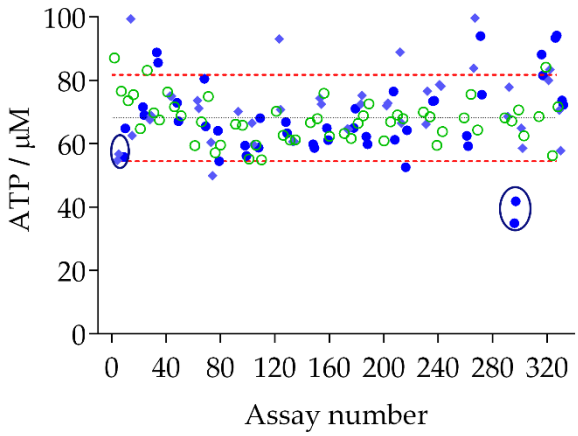

Figure 4.16: PKIS hit validation

The *Ft*PPK assay control (5% DMSO, green open circles) and the *Ft*PPK assays containing the hit compounds (alternating light blue rhombus and dark blue circles, same colour and shape for duplicates) were plotted as ATP produced against number of assay. Black dotted line: median, red dashed line: hit validation criterion (median ± MAD). The data highlighted with the blue circles corresponded to the assays containing the selected hit compounds. Assay conditions: 100 µL assay volume, 10 nM *Ft*PPK, 2.6 µM BSA, 200 µM ADP, 30 µM $polyP_{25}$, 10 µM hit compound, 5% DMSO, 30°C. Assays quenched after 7 min by EDTA (50 mM).

Table 4.9: Statistical evaluation of PKIS hit validation

Mean ± SD	CV	Median ± MAD	Hit validation (median - 2MAD)
69.4 ± 10.9 µM	15.9%	68.2 ± 6.8 µM	54.6 µM

Both classic and robust statistical analysis was applied (means and SD and median and MAD, respectively). A noticeable improvement of the CV was observed in comparison to that observed before protocol optimisation (Table 4.6). A certain degree of consistency was observed for the control assays while a greater variation was observed for the assays containing the hit compounds. To attenuate the effect of the experimental error, robust statistical analysis was applied for the determination of the hit validation criterion which

was defined as median – 2MAD, corresponding to a concentration of ATP produced equal to 54.6 µM ATP. Two compounds were selected as possible real hits: compound J07-4 (55.7 ± 1.4 µM ATP produced) and compound JOM-69 (38.4 ± 4.9 µM ATP produced).

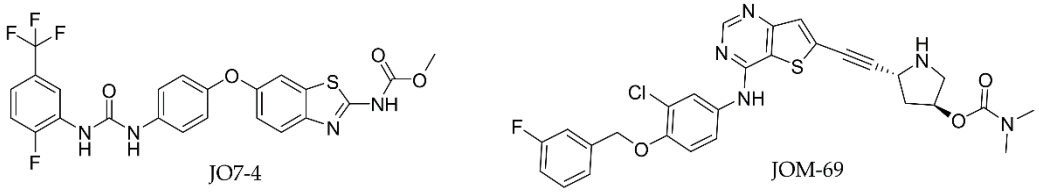

Table 4.10: PKIS hits JO7-4 and JOM-69 performance

Performance	JO7-4	JOM-69
Z_R-score*	-2 ± 1.3	-3.7 ± 0.7
NPI_R%*	2.9 ± 14.5	55.4 ± 11
FLuc NPI_R%*	2.7 4 ± 11.1	25.6 ± 7.3
ΔT_m **	n/a	-0.20 ± 0.39
HPLC NIP_R%*	17.6 ± 0.5 %	43.3 ± 7.2 %

*10 µM concentration; **100 µM concentration

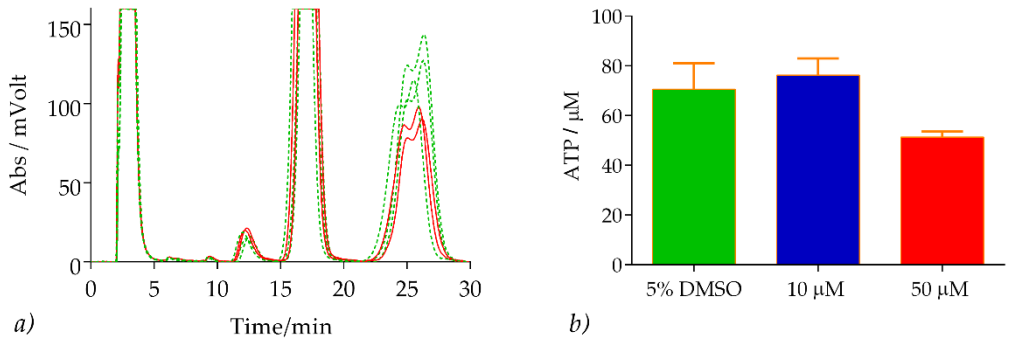

Figure 4.17: PKIS hit, JO7-4 compound

a) HPLC chromatogram showing the UV trace of the *Ft*PPK assays measured in the presence of 5% DMSO (dashed green line) and the *Ft*PPK assays measured in the presence of 50 µM JO7-4 (red line). *b*) Comparison of the ATP produced by the *Ft*PPK control assays and by the assays containing the hit compound JO7-4. Assay conditions: 100 µL assay volume, 10 nM *Ft*PPK , 2.6 µM BSA, 200 µM ADP, 30 µM $polyP_{25}$, 10 or 50 µM hit compound, 5% DMSO, 30°C. Assays quenched after 7 min by EDTA (50 mM).

While compound JO7-4 was selected as a hit of the *Ft*PPK-FLuc coupled assay only on the basis of the $NPI_R\%$ hit selection criterion, compound JOM-69 scored as hits according to both the Z_R-*score* and the $NPI_R\%$ hit selection criterion (Table 4.10). Unfortunately, no more of compound JOM-69 was available for further investigations. Compound JO7-4 instead was re-tested at 10 μM and at 50 μM (Figure 4.17). At the latter concentration, a 24.3 ± 3.3% inhibition was observed, suggesting that compound JO7-4 could potentially be a weak inhibitor of the *Ft*PPK.

4.2.3.3. RL hit validation by HPLC assay

As for the PKIS hits, the HPLC based *Ft*PPK assay in end format (Table 4.8) was applied for the validation of the Reynolds library hits. Each compound (Table A4 2) was tested in duplicate at the concentration of 10 µM (Figure 4.18).

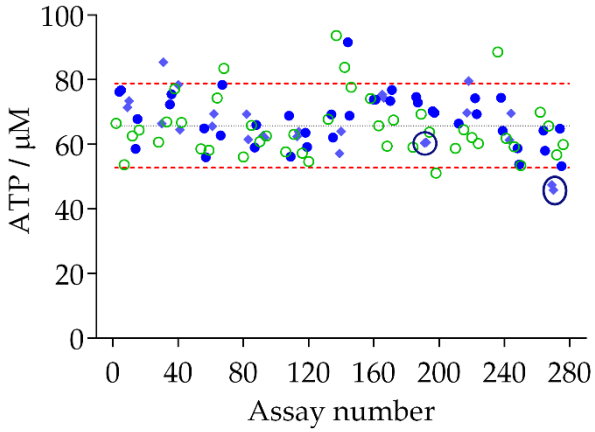

Figure 4.18: RL hit validation

The *Ft*PPK assay control (5% DMSO, green open circles) and the *Ft*PPK assays containing the hit compounds (alternating light blue rhombus and dark blue circles, same colour and shape for duplicates) were plotted as ATP produced against number of assay. Black dotted line: median, red dashed line: hit validation criterion (median ± MAD). The data highlighted with the blue circles corresponded to the assays containing the selected hit compounds. Assay conditions: 100 µL assay volume, 10 nM *Ft*PPK, 2.6 µM BSA, 200 µM ADP, 30 µM $polyP_{25}$, 10 µM hit compound, 5% DMSO, 30°C. Assays quenched after 7 min by EDTA (50 mM).

Table 4.11: Statistical evaluation of RL hit validation

Mean ± SD	CV	Median ± MAD	Hit validation (median - 2MAD)
68.9 ± 14.2 µM	20.7%	65.8 ± 6.5 µM	52.8 µM

To evaluate the assay performance, the same statistical analysis as for the PKIS hit validation was applied (Table 4.11). The derived hit validation criterion (median – 2MAD) corresponded to a concentration of ATP produced equal to 52.8 µM. The only compound selected by the hit validation criterion was RL42-Plt9 (46.7 µM ± 1.1 µM ATP produced). On a careful visual inspection of the data, it was noticed that for another compound, RL41-Plt8, the activity of the *Ft*PPK, although comparable with the activity observed in the

control assays containing 5% DMSO, was significant lower in comparison to the activity observed in the presence of the other hit compounds tested within the same experiment (Figure 4.18).

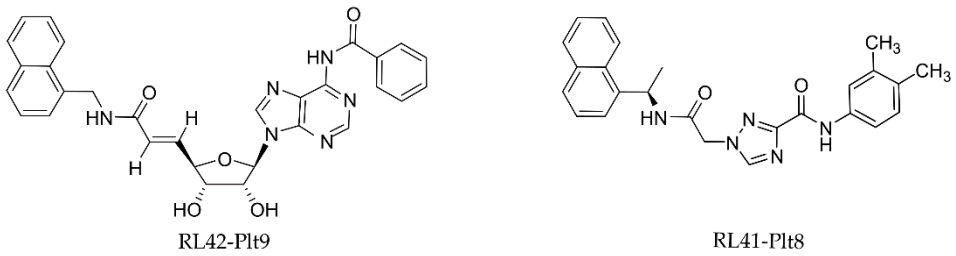

Table 4.12: RL hits RL42-Plt9 and RL41-Plt8 performance

Performance	RL42-Plt9	RL41-Plt8
Z_R-score*	-3.1 ± 0.3	-5.6 ± 0.1
NPI_R%*	45.3 ± 3.8	97.2 ± 1.2
FLuc NPI_R%*	10.1 ± 1.6	92.5 ± 0.1
ΔT_m **	-0.2 ± 0.3	-17.2 ± 0.3
HPLC NIP_R%*	29.1 ± 1.7 %	8.1 ± 1.5 %

*10 µM concentration; **100 µM concentration

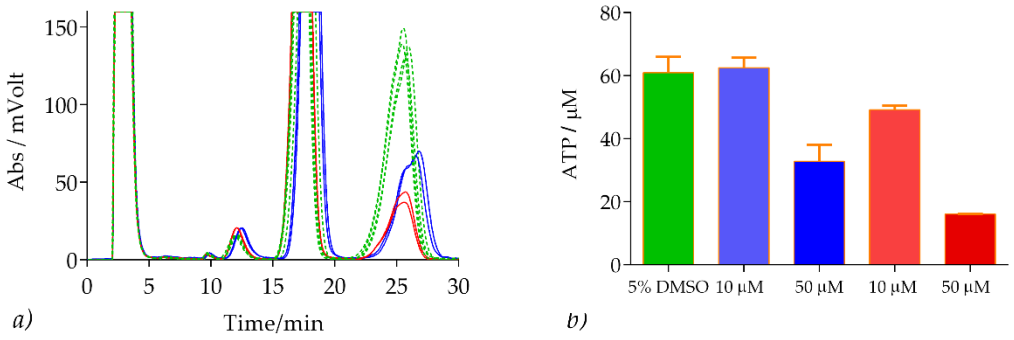

Figure 4.19: RL hit, RL42-Plt9 and RL41-Plt8

a) HPLC chromatogram showing the UV trace of the *Ft*PPK assays measured in the presence of 5% DMSO (dashed green line) and the *Ft*PPK assays measured in the presence of 50 µM RL41-Plt8 (blue line) and of 50 µM RL42-Plt9 (red line). *b*) Comparison of the ATP produced by the *Ft*PPK control assays (green block) and by the assays containing the hit compound RL41-Plt8 (10 µM light blue block, 50 µM dark blue block) and the hit compound RL42-Plt9 (10 µM light red block, 50 µM dark red block). Assay conditions: 100 µL assay volume, 10 nM *Ft*PPK , 2.6 µM BSA, 200 µM ADP, 30 µM $polyP_{25}$, 10 or 50 µM hit compound, 5% DMSO, 30°C. Assays quenched after 7 min by EDTA (50 mM).

In conjunction with compound RL42-Plt9, selected by the validation threshold, it was decided to further investigate the activity of compound RL41-Plt8 as well (Table 4.12), which interestingly had some structural features in common with compound RL42-Plt9. Both compounds were re-tested at the concentration of 10 μM and at 50 μM. For compound RL41-Plt8 no significant reduction of the *Ft*PPK activity was observed in the presence of 10 μM concentration, however when the concentration was increased to 50 μM a 46 ± 8.6 % inhibitions was observed (Figure 4.19). For compound RL42-Plt9 the inhibition observed in the presence of 10 μM compound was confirmed (19.1 ± 2%) and a 73.5 ± 0.1% inhibition was detected in the presence of 50 μM. In light of time constraints, it was decided to focus on further investigation of the activity of compound RL42-Plt9, which of these two appeared to be the most active.

4.2.3.4. Structure confirmation of compound RL42-Plt9

To allow characterization with respect to the binding affinity, mode of binding and mechanism of action by both biochemical analysis and co-crystallization with the *Ft*PPK, it was necessary to re-synthesize compound RL42-Plt9. Before engaging in the synthesis, the chemical identity of the compound was investigated. The low amount available did not allow analysis of the compound by NMR. The identity and the purity of the RL42-Plt9 library stock was investigated by electrospray ionization (ESI) mass spectrometry in positive mode. Two peaks were observed on the RP UHPLC chromatogram: a peak with 0.23 min retention time and a peak with 1.73 min retention time. For the first peak an ion with 157.09 m/z was observed, which could be attributed to DMSO (equal to $(2m+H)^+$). For the second peak, ions corresponding to 551.27 m/z and 552.25 m/z were observed, which could be attributed to $(M + H)^+$ of RL42-Plt9 (RL42-Plt9 calculated Mw: 550.58). The mass spectrometry analysis provided one piece of data supporting the chemical identity of compound RL42-Plt9 and indicated that no other major component was observable under these conditions.

4.3. Summary

For the validation of real *Ft*PPK inhibitors and the identification of false positives, the *Ft*PPK-FLuc coupled assay hits were counter screened by the independent luminescence assay. Comparison between the inhibition of the coupled assay and the inhibition of the luminescence assay identified strong FLuc inhibitors, likely to be false positive hits, and also possible genuine hits. Because of the possibility that FLuc inhibitors could also inhibit the *Ft*PPK, further validation by thermal shift assay and by secondary biochemical assay was sought.

The conditions for the thermal shift assay were optimised by testing a range of concentrations for the *Ft*PPK and SYPRO Orange dye. Optimal conditions were identified as: 1 μM *Ft*PPK and 5x SYPRO Orange. Both the PKIS library hits and the RL hits were tested with the thermal shift assay. Among the PKIS hits, a significant T_m shift was observed only for compound JO8-3. However, due to some anomalies of the melting curve, the data were judged inconclusive. Among the RL library hits, which were tested at three different concentrations (10 μM, 50 μM, 100 μM), a significant shift of the T_m was observed for compounds RL37-Plt7, RL60-Plt7 and RL20-Plt2. However, the expected correlation between increase of the T_m shift and increase of the concentration was not observed for any of the three compounds.

The thermal shift assay proved inadequate to provide a definitive validation of the PKIS and of the RL library hits. Although the obtained data could simply reflect the lack of real or sufficiently potent *Ft*PPK inhibitors, it is also possible that the thermal shift assay might have not been sufficiently sensitive to detect binding to the *Ft*PPK. It has been observed that some proteins (e.g. not globular proteins or multi-domain protein) are not responsive to the thermal shift assay.[443] On reflection, the suitability of the thermal shift assay to investigate *Ft*PPK binding should have been validated beforehand, by testing the effect of the binding of any of the substrates as a positive control. Furthermore, the thermal shift assays were prepared without including the *Ft*PPK substrates. Possible conformational changes occurring in the presence of the substrates and potentially relevant for the binding of any of the identified hits, may explain why no significant T_m shift was observed.

Eventually, the adaptation of an HPLC-based method for hit validation was considered. An important caveat when applying HPLC analysis during inhibitor discovery projects is that the throughput is relatively low (compared, for example, to HTS with 384 wells). Use of HPLC methods are therefore best applied after an initial high throughput stage, when validation of a relatively small number of hits is required. For *Ft*PPK, a RP IP method, using DMHA as ion pairing agent, was optimised for ADP and ATP analysis, in conjunction with the development of an experimental protocol for the measurement of the *Ft*PPK time courses as well as for assay measurement in end point format. The *Ft*PPK reaction was investigated applying the conditions used for the HTS (K_m concentration of substrates: 200 μM ADP and 1.5 μM $polyP_{25}$). However, to address possible issues of sensitivity, due to the low concentration of $polyP_{25}$ at K_m, the *Ft*PPK reaction was also investigated in the presence of saturating concentration of $polyP_{25}$ (30 μM $polyP_{25}$). To further improve the detection sensitivity by reducing the background signal, an alternative method, using TEA as ion pairing agent, was optimised. The quality of the HPLC-based *Ft*PPK assay in end point format was assessed by determination of the data variability (Mean ± SD and CV). Although in the presence of 1.5 μM $polyP_{25}$ a lower data variability was achieved, a better screening window and a greater potential for a more reliable detection of at least 20% inhibition was observed for the *Ft*PPK assays prepared with 30 μM $polyP_{25}$. Despite the likely lower sensitivity to competition for polyP in the presence of saturating $polyP_{25}$ concentration, the following conditions were applied for hit validation: 10 nM *Ft*PPK, 200 μM ADP and 30 μM $polyP_{25}$. The assays were stopped after 7 minutes (initial rate measurement) by addition of EDTA (50 mM).

Among the PKIS library initial active compounds, two were reselected as possible real hits: compound J07-4 and compound JOM-69. While compound JOM-69 was not readily available for further investigations, compound JO7-4 was re-tested and a 24.3 ± 3.3% inhibition was confirmed at the concentration of 50 μM.

Of the Reynolds library hits, inhibition of the *Ft*PPK for compounds RL42-Plt9 and RL41-Plt8 was initially detected at 10 μM and confirmed at 50 μM concentration (46 ± 8.6 % and 73.5 ± 0.1% inhibitions, respectively). Compounds RL42-Plt9 and RL41-Plt8 shared

some structural similarities at the naphthyl-methyl amide moiety. Similarities were also detected between compound RL41-Plt8 and compound RL60-Plt7 and RL37-Plt7, the latter two selected by thermal shift assay (section 4.2.2.3). Interestingly, neither compound RL42-Plt9 nor compound RL41-Plt8 were detected by thermal shift assay, further suggesting that perhaps the thermal shift assay was not conducted under ideal conditions.

At this point in the project, to allow a more detailed characterization of the identified inhibitors, further supplies of compound were required. Neither compound RL42-Plt9 nor RL41-Plt8 were commercially available, therefore it was necessary to engage into *in-house* synthesis. To rationalize the project workload, only compound RL42-Plt9, which showed the greater activity, was selected to take forward.

Chapter 5

Synthesis and Characterisation of the Validated Hit Compound RL42-Plt9

5.1. Introduction

Following the validation of hit compounds as real inhibitors of the chosen target, characterization studies to define the potency and the mode of action are undertaken. The first step entails IC_{50} measurements of the hit compounds derived from alternative sources, either re-synthesised or purchased, if commercially available. The IC_{50} determination, in addition to provide information about the compound potency, also allows to rule out possible inhibition due to unspecific binding or to aggregation.[86,444,445] Furthermore, investigation of the inhibition mode (e.g. reversible or covalent binding, competitive, non-competitive, uncompetitive, tight binding or slow binding inhibition) are required to clarify the mechanism of action. The latter, in conjunction with the determination of the binding affinity, constitutes a significant tool that complements structural information, both of which are crucial in guiding the hit to lead optimisation of inhibitor. Ideally, structural information derived from direct co-crystallization studies of the inhibitor in the active site, is desirable. Alternatively, computational modelling, aided by information on the mode of action and based on analogies with substrate occupancy, can be used. As part of the investigation leading to the hit to lead progression, a structure activity relationship (SAR) for a series of compounds can be developed. The SAR characterization involves the identification of a chemical scaffold essential for binding as well as the investigation on the effect that the introduction of various functional groups may have on the interaction with the active site. Initial SAR can often be developed based on the activity of structurally

related analogues identified during the HTS. The SAR is often further developed during the optimisation phase of the project when more analogues are synthesised and tested.

In this chapter, some preliminary characterization of the binding of compound RL42-Plt9 with the *Ft*PPK was reported. After being re-synthesised, compound RL42-Plt9 was investigated by biochemical assays, including measurement of potency by IC_{50}, mechanism of action and the spectrum of activity by testing with a PPK from a different microorganism. To follow, some SAR analysis and some structural characterization were attempted. Only those techniques that proved informative were described hereby; other techniques which gave problems or did not prove informative were reported in the Appendix (e.g. ITC studies and co-crystallization studies, section A5 1.3 and A5 2 respectively).

5.1.1. Inhibitor binding affinity: correlation between IC_{50}, K_i and mode of binding

The potency of an inhibitor for the target of interest is mostly expressed in terms of the concentration that causes 50% attenuation of the observed enzyme activity (IC_{50}). Despite being a convenient parameter to assess the inhibitor activity, due to the simple experimental determination, the IC_{50} values do not represent an absolute measure of the binding affinity.[272] Factors such as the mode of inhibition, substrate concentration and in some case the enzyme concentration (e.g. for tight binding inhibitors), strongly affect the IC_{50}.[272,374] To a lesser extent, small variation of the experimental conditions (e.g. pH, ionic strength, temperature)[272,374] can also result in variation of the observed IC_{50}. A more robust measure of an inhibitor potency is provided by the inhibitory constant K_i, a thermodynamic parameter that describes the affinity of the inhibitor for the target of interest (section 3.1.1, Eq. 3.1). Once the binding mode has been established, appropriate conditions can be set to derive an IC_{50} value that can be correlated to the K_i (Table 5.1 and Appendix, section A5 1.1).[446]

Table 5.1: IC_{50} – K_i relationship

[S] to K_m	Competitive	Uncompetitive	Non-competitive
[S] = K_m	$K_i = IC_{50}/2$	$K_i = IC_{50}/2$	$K_i = IC_{50}$
[S] >> K_m	$K_i << IC_{50}$	$K_i = IC_{50}$	$K_i = IC_{50}$
[S] << K_m	$K_i = IC_{50}$	$K_i << IC_{50}$	$K_i = IC_{50}$

5.1.1.1. IC_{50} determination

For an inhibitor that binds to the target of interest in a reversible manner and with a 1:1 stoichiometry, the binding is saturable.[272,374] In the presence of a fixed concentration of enzyme and substrate, an increase of inhibition can be observed with the increase of the inhibitor concentration, due to the increase of the amount of the EI complex over the ES complex (section 3.1.1, Figure 3.1). When all the enzyme available is engaged in the formation of the EI complex, hence saturation has been reached, no more activity is observed (100% inhibition). Titration curves of inhibitor concentrations (usually 11 concentrations, prepared by three fold or two fold dilutions) versus inhibition observed, are known as

concentration-response plots.[272] From these curves it is possible to derive the concentration at which 50% inhibition occurs, commonly known as IC_{50} (half-maximal inhibitory concentration). To define the level of inhibition at a specific concentration of inhibitor, the following equation can be applied:[374]

$$\%\ \text{Inhibition} = 100\left(1 - \frac{v_i}{v_0}\right)$$

Eq. 5.1: IC_{50} curve, percentage inhibition calculation

The ratio v_i/v_0 defines the fractional activity, which reflects the activity of the free enzyme. The relation (1-v_i/v_0) instead refers to the amount of enzyme bound. Experimentally, v_i is the rate measured in the presence of the inhibitor (hence due to the activity of the fraction of free enzyme), v_0 is the rate measured in the absence of inhibitor.

To define the IC_{50} value, the concentration-response plots, reported as inhibition observed against log of the inhibitor concentration, were fitted to a sigmoidal curve, described by a four-parameter equation (Eq. 5.2). The upper asymptote of the sigmoidal curve corresponds to the maximum of inhibition while the lower asymptote to the maximum of activity. The curve mid-point is equal to half response (the IC_{50}) and the mid-point slope describes the steepness of the curve (Hill coefficient (h), Appendix, section A5 1.1).[272,374]

$$\%\ \text{Inhibition} = y_{\text{min}} \frac{y_{\text{max}} - y_{\text{min}}}{1 + 10^{\text{h}(\log IC_{50} - \log[\text{I}])}}$$

Eq. 5.2: IC_{50} detemination, Hill equation

y_{min} is the response obtained when no inhibition occurs (or in the absence of inhibitor); y_{max} is the response obtained when 100% inhibition occurs; h is the Hill coefficient; I is the inhibitor concentration; IC_{50} is the concentration of inhibitor causing half response. .

5.1.1.2. Mechanism of action studies

An important step in the characterization of an inhibitor is the investigation of the mechanism of action (MOA), hence if the inhibitor binds in an irreversible or reversible manner, and in the latter instance if it is a competitive, non-competitive, uncompetitive, slow binding, tight binding or allosteric inhibitor. MOA studies provide information on how

an inhibitor interacts with the respective target and these information can be used to guide the medicinal chemistry optimisation and to interpret the inhibitor behaviour in cells.[380]

The first step of MOA studies consists in the investigation of reversibility.[374,379] Specifically, if an irreversible mechanism is detected, further investigation should focus on trying to define if the irreversible binding occurs by affinity labelling (e.g. by nucleophile-driven alkylation or acylation) or derives from the enzyme-dependent transformation of an unreactive compound into a highly reactive intermediate (mechanism-based inhibitor).[379,447,448] If the binding is characterised as reversible, experiments should be aimed to define if the inhibition mode is competitive, non-competitive or uncompetitive.

To test for reversibility, activity assays and mass spectrometry can be applied. In the first case, the reversibility can be assessed by investigation of displacement upon addition of substrate in high concentration and consequent effect on inhibition.[374,380,449] In the second case, irreversible binding can be confirmed by detection of species with mass corresponding to the inhibitor-enzyme adduct by mass spectrometry. Reversible binding inhibitors can be further characterised by biochemical assay, in view of the effect that inhibitors of specific modalities have on K_m and V_{max}.[272,273,374] The latter can be defined by measuring the apparent initial rate (v_0^{app}) at varying concentrations of substrate (usually 0.2 K_m to 5 K_m) and at varying concentrations of inhibitor (usually three concentrations causing low, medium and high degree of inhibition, plus a DMSO control with no inhibitor). Applying suitable graphical analysis (described in detail in Appendix, section A5 1.2), the K_i and mode of inhibition can be determined.

5.2. Results and discussion

5.2.1. Synthesis of the Reynolds library hit RL42-Plt9

Despite being part of a collection of nucleoside analogues donated by Prof. R. C. Reynolds (University of Alabama),[393–396] no synthetic routes have been reported to date in the literature for compound RL42-Plt9 (10). The convergent route described in Scheme 5.1 was proposed for the synthesis of the *E*/*Z* isomers of RL42-Plt9. The key step was the formation of the double bond by a Wittig reaction to link the naphthylmethyl amide moiety to the protected adenosine derivative.

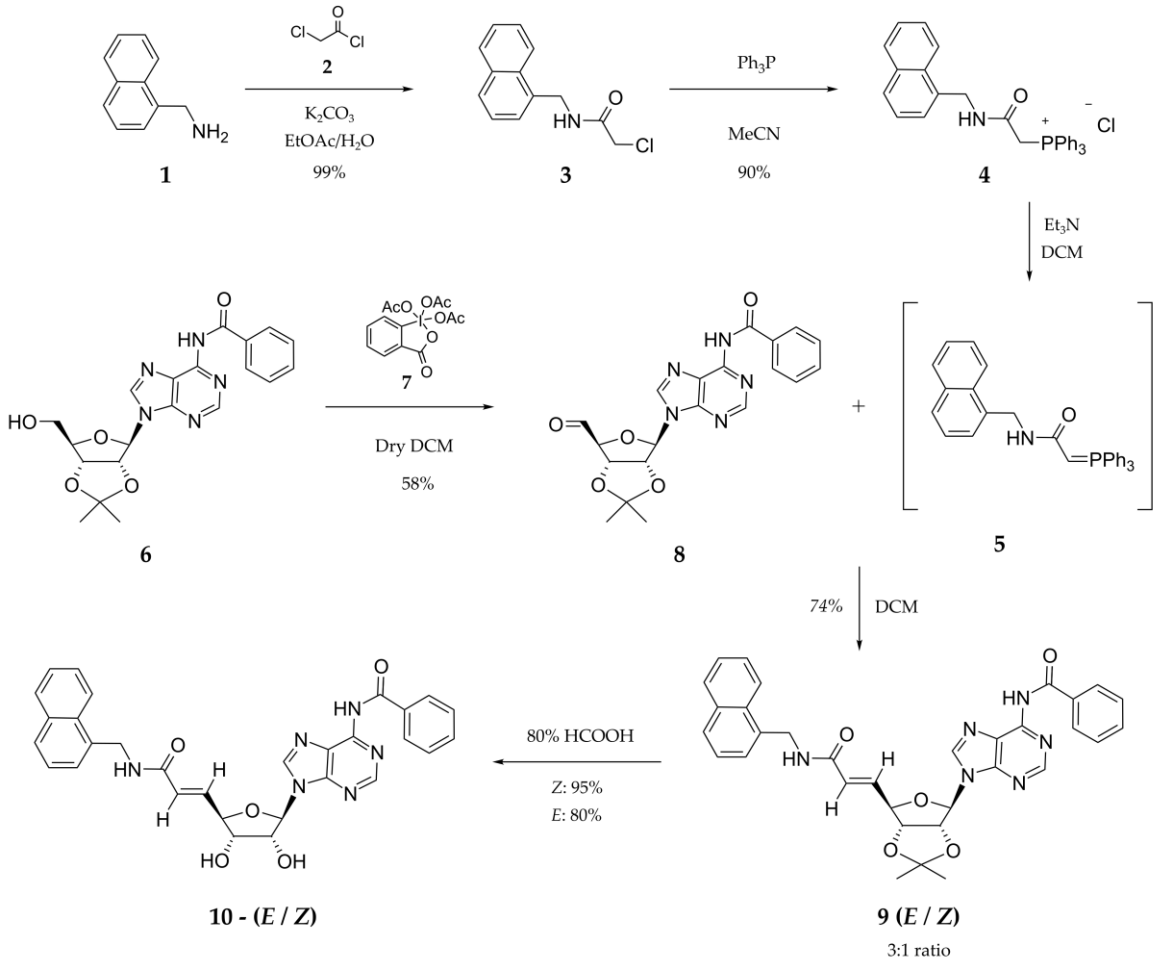

Scheme 5.1: RL42-Plt9 synthetic route

The first branch of the route consisted in a two-step procedure to synthesize the phosphonium salt (4). The 2-chloro-N-(naphthalen-1-ylmethyl)acetamide (3) was prepared by nucleophilic substitution of the 2-chloro-acetylchloride 2 with the amine 1. To drive the reaction to completion, K_2CO_3 was included in the reaction mixture.[450] The chloroacetamide

derivative (3) was then converted into the respective phosphonium salt by treatment with triphenylphosphine.[451,452] NMR analysis confirmed the formation of the phosphonium salt. Indeed, a change from a singlet into a doublet (J = 14.55 Hz) of the signal for the carbon in α– to the carbonyl was observed, due to the coupling with phosphorous.[453] Generation from the phosphonium salt and isolation of stabilized ylides with amide or ester functional groups in conjugation to the negatively charged carbon has been reported by treatment with either NaOH at pH 7[454,455] or trimethylamine (Et_3N).[456,457] Both conditions were tested to prepare ylide 5, however degradation to the acetamide derivative and triphenylphosphine oxide formation were observed.[454,458,459] To minimize ylide decomposition, it was decided to attempt in situ generation of the ylide in the presence of aldehyde, which was prepared in parallel. Preparation of the 5'-aldehyde from nucleosides has been reported in the literature, by oxidation under mild conditions by means of a diimide-activated Moffatt reaction,[460–469] by treatment with the iodo-compound Dess-Martin periodinane (DMP)[465,470–478] or by treatment with *o*-iodoxybenzoic acid (IBX, a precursor of DMP).[479–483]

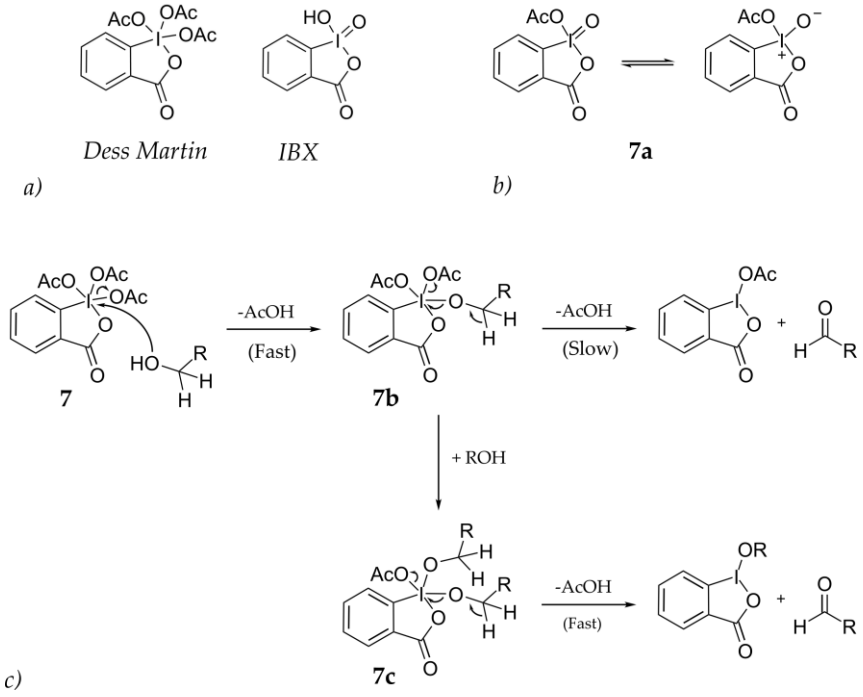

Scheme 5.2: Mechanism of Dess-Martin oxidation

For the synthesis of the adenosine 5'-aldehyde derivative 8, the Dess-Martin oxidation was selected. This choice was driven by the possibility of applying mild conditions, such as conducting the reaction at room temperature and at neutral pH.[484] The latter was particularly convenient to prevent possible depurination of the adenosine and/or loss of the protecting group at the 2' and 3' position. In comparison to other reactions (e.g. Swern oxidation), another reason for the selection of the Dess-Martin reagent lies in the greater retention of the configuration at stereogenic centres, observed following oxidation to epimerization-sensitive aldehydes.[484–487] The latter consideration is particularly relevant since the adenosine aldehyde 8 is potentially subjected to epimerization at the position α to the aldehyde function.

The Dess Martin oxidation is based on a two steps mechanism.[488–490] The first step consists of the displacement of an acetyl group from the iodine (I^V) upon alcohol attack (fast step). In the second step, driven by the removal of the α-proton of the alcohol, the carbonyl functional group is formed. The consequent breakage of the bond between the iodine and the oxygen results in the release of the carbonyl compound and into the reduction of the iodine compound to iodinane (I^{III}), accompanied by the release of another acetyl group (slow steps, Scheme 5.2).[488] It has been reported that in the presence of an excess of alcohol[491] or in the presence of water[492] the reaction proceeds faster, due to the formation of the intermediates 7c or 7a, respectively (Scheme 5.2). The increased rate was attributed to the greater electron donating character of the alkoxy group, which favours the dissociation of the acetyl group, making the intermediate 7c more labile than the intermediate 7b (Scheme 5.2). Although potentially increasing the reaction rate, excess of alcohol and exposure to water can negatively impact on the reaction yield by trapping part of the starting material in a periodinane intermediate or by formation of the aldehyde hydrate.

In the first attempt, the Dess-Martin reaction was prepared in reagent grade DCM and in the presence of 1.3 Eq DMP. Despite awareness of the possible side reaction, it was decided to add to the mixture 1.4% v/v of water, to test for the reactivity of the aldehyde towards the formation of the corresponding hydrate. Due to the similar R_f of the adenosine derivative 6 and the aldehyde 8, it was not possible to monitor the reaction by TLC. However, the conversion of 6 in the correspondent aldehyde 8 was confirmed by mass spectrometry ((M

$+ NH_4)^+$: 427 m/z; aldehyde 8 Mw: 409.14) and NMR (appearance of aldehyde H at δ 9.28, section 7.7.1.5). The NMR also revealed that about 30% of the starting material was unreacted. Therefore, to drive the reaction towards completion, more DMP (1.3 Eq) was added and the reaction time was extended to 24 h. No significant improvement was observed in the degree of conversion of the starting material. Since multiple products were detected on TLC analysis of the reaction mixture, the latter was purified by column chromatography ($CHCl_3$:MeOH – 95:5, spots R_f: 0.74, 0.55, 0.25) and each product analysed by NMR and mass spectrometry. The spots with R_f 0.74 and R_f 0.25 were identified as the 5'-carboxylic acid derivative of 8 and the product of depurination of the adenosine 6, respectively. The spot with R_f 0.55 was constituted by a mixture of unreacted starting material 6, the desired aldehyde 8 and the corresponding hydrate. In the presence of acetic acid, released during the DMP reaction, the addition of water to the reaction mixture certainly favoured the formation of the aldehyde hydrate, which in turn was oxidised to the carboxylic state, as well as the depurination reaction. To prevent or attenuate the formation of side products, the Dess-Martin reaction was repeated under dry conditions (anhydrous DCM and N_2 atmosphere). Since no significant effects were observed when more DMP reagent was added and the reaction time extended, the initial concentration of DMP (1.3 Eq) was applied and the reaction quenched after 6 hours. Again, upon analysis of the crude, the unreacted adenosine derivative 6 was detected by NMR (20%) and the same pattern of spots was observed on TLC analysis. The DMP reaction yield (58%) remained sub-optimal despite the anhydrous conditions. It is likely that the formation of the side products was mainly driven by the acidic conditions derived from the release of acetic acid. To prevent possible degradation/oxidation with time, it was decided to avoid the aldehyde purification by column chromatography and to attempt the Wittig reaction on the crude-aldehyde (stored at – 20°C).

Various examples of Wittig reaction applied to the synthesis of nucleoside derivative have been reported in the literature.[461,482,493–501] Due to the difficulties encountered with the isolation of ylide 5, for the synthesis of compound 9, an alternative approach was adopted. The ylide 5 was generated *in situ* by addition of Et_3N to the phosphonium salt 4 in the

presence of the crude aldehyde. Anhydrous conditions were applied, to prevent or limit both the ylide degradation and the formation of the aldehyde hydrate. It was anticipated that as soon as the ylide was produced, reaction with the aldehyde would occur and the desired Wittig product would be formed. An excess of phosphonium salt 4 (2 Eq) was used to compensate for possible ylide decomposition, in case of accidental introduction of moisture. The synthesis of the Wittig product was confirmed by both NMR and mass spectrometry. The reaction yielded a mixture of *E* and *Z* isomers which were separated by column chromatography (R_f 0.28 and 0.17, $CHCl_3$:EtOAc - 40:60). The overall yield, calculated with respect to the sum of the both isomers and from the crude aldehyde, was 74%. In accordance with the general stereoselectivity of a Wittig reaction wherein a stabilized ylide is used, the *E* isomer was the major product (75:25 ratio for *E:Z* isomers). The isomers were assigned by NMR, exploiting the characteristic difference of the coupling constant of two hydrogen involved in a double bond, with the coupling constant for the *E* isomer being higher than for the *Z* isomer (usually 15-18 Hz and about 10Hz, respectively). Accordingly, the isomer with R_f 0.28 was identified as the *Z* isomer (5' H: δ 5.7, $J = 10.3$ Hz) while the isomer with R_f 0.17 was identified as the *E* isomer (5' H: δ 6.9, $J = 15.3$ Hz). The final synthetic step consisted in the deprotection of OH in position 3' and 5' by removal of the 3',5'-isopropylidene group from the two isomers. Acid catalysed deprotection was initially investigated using the sulfonic resin Dowex 50Wx8 (hydrogen form) in methanol[502,503] but different ratios of compound 9:resin and variations of reaction time resulted in significant depurination. The deprotection was successfully achieved under milder conditions by treatment with 80% formic acid at room temperature[465] and appeared to be slightly faster for the *Z* isomer (6 hours) compared to the *E* isomer (8 hours). The deprotection yield was higher for the *Z* isomer (95%) than for the *E* isomer (80%). The total yield for the synthesis of the pure isomers 10 from the adenosine derivative 6 was: 29.5 % for the *E* isomer and 8% for the *Z* isomer.

5.2.2. Characterization of the confirmed hit compound RL42-Plt9

5.2.2.1. Investigation of the *E* and *Z* isomers activity by HPLC based assay

The binding of a specific isomer to an enzyme may be favoured or disfavoured (e.g. due to steric hindrance) because of the specific topography that the enzyme active site may have. The total synthesis of compound RL42-Plt9 (section 5.2.1) provided access to both the *E* and the *Z* isomers.

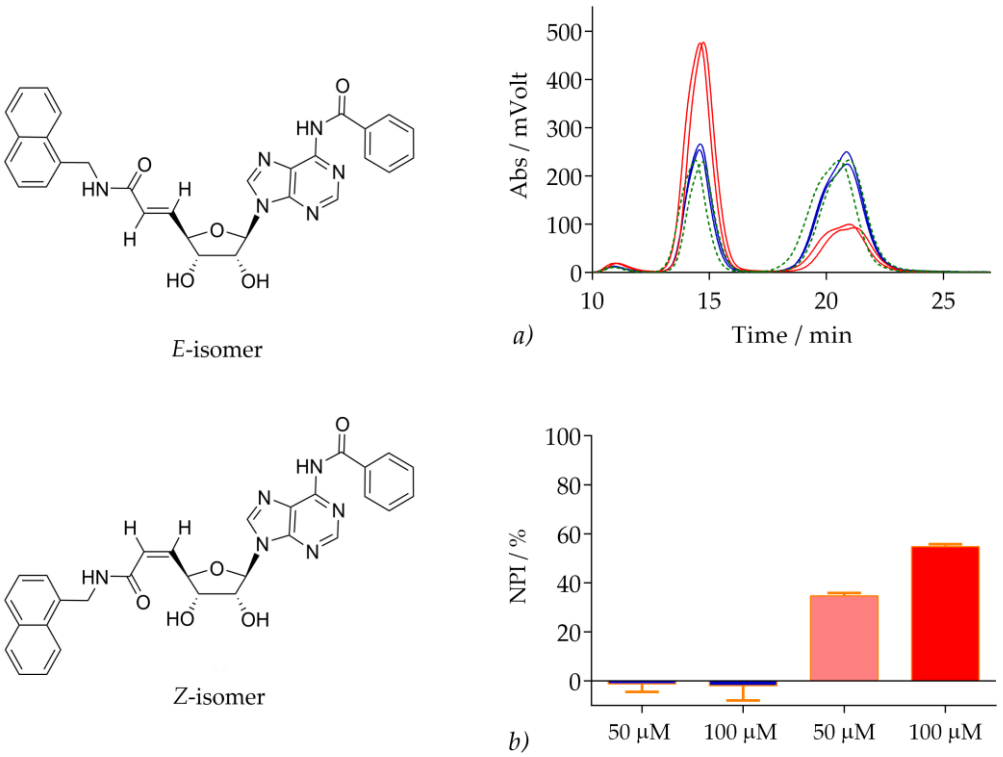

Figure 5.1: Activity of the *E* and *Z* isomer of the RL42-Plt9 inhibitor

a) Region of the HPLC chromatogram of assays containing no inhibitor (green dashed line positive), *E*-isomer RL42-Plt9 (red line) and *Z*-isomer RL42-Plt9 (blue line) at 100 µM concentration. Retention time: ADP 13-17 min, ATP 18-24 min. *b*) Percent inhibition of assays (in duplicate) containing 50 µM or 100 µM of *E*-isomer (blue blocks) or *Z*-isomer RL42-Plt9 (red blocks). Assay conditions: 100 µL volume, 10 nM *Ft*PPK, 10 mM $MgCl_2$, 30 µM $polyP_{25}$, 200 µM ADP, 50 µM or 100 µM RL42-Plt9, 5% DMSO.

The activity of the pure *E* and *Z* isomers on the *Ft*PPK was investigated by HPLC assay in end-point format (assays stopped after 420 minutes, section 4.2.3.1.4). No information were yet available with regard to the respective potency, hence assays were prepared with isomers at the arbitrarily chosen concentration of 50 µM and 100 µM. Control assays with

no inhibitor but containing only DMSO were also prepared alongside. The activity of the RL42-Plt9 isomers was reported in terms of % inhibition (derived according to Eq. 5.1). The *Ft*PPK activity observed in the presence of the *Z*-isomer was comparable to the activity observed in the absence of inhibitor (Figure 5.1*a*). When the *E*-isomer was tested, concentration dependent inhibition of the *Ft*PPK was observed (34.7 ± 1.2% at 50 μM, 54.8 ± 0.9% at 100 μM). The significant difference in activity of the two isomers could be possibly explained by the non rotatable nature of the double bond, which locks the *N*-naphthylmethyl-amide moiety either in a favourable or unfavourable orientation within the active site. The activity of the re-synthesised RL42-Plt9 appeared to be lower in comparison to the library stock tested for hit validation (section 4.2.3.3).

5.2.2.2. IC_{50} characterization by HPLC assay

Concentration-response curves for IC_{50} determination were prepared for both isomers: to assess the relative potency of the *E*-isomer and to investigate if the *Z*-isomer inhibited the *Ft*PPK at higher concentration. The IC_{50} curves were generated by the HPLC assay in end point format (assays stopped after 420 sec, section 4.2.3.1.4), in triplicate. The range of inhibitor concentration investigated was 0.78 μM – 400 μM, prepared by two fold serial dilution. Due to compound solubility limits, it was not possible to investigate the activity at higher concentration of RL42-Plt9. Negative control assays (5% DMSO, no RL42-Plt9,) and positive control assays (RL42-Plt9, no *Ft*PPK) were prepared to mimic no inhibition and 100% inhibition, respectively. The same substrate concentrations adopted for the hit validation by HPLC assay were maintained for the IC_{50} measurement: 200 μM ADP (K_m for ADP) and 30 μM $polyP_{25}$ (saturating concentration for $polyP_{25}$). Ideally, since the mode of inhibition was not yet clear, K_m concentration for both substrates should have been adopted. However, the $polyP_{25}$ concentration was maintained at 30 μM (K_m for $polyP_{25}$: 1.5 μM) to prevent issues due to the limited sensitivity of the HPLC. Furthermore, given the structure of compound RL42-Plt9 (a nucleotide analogue), inhibition by competition with ADP was judged as the most likely mode of action. The observed % inhibition (derived according to Eq. 5.1) was plotted against log of inhibitor concentration (Figure 5.2).

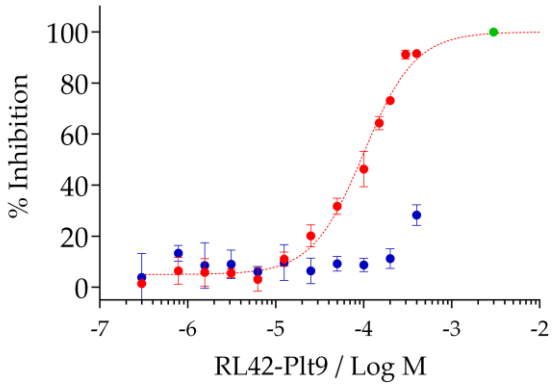

Figure 5.2: IC_{50} of *E* and *Z* isomer of inhibitor RL42-Plt9

E and *Z* isomer concentration-response plots. *E*-isomer: red circle; *Z*-isomer: blue circle. Higher concentration of RL42-Plt9 could not be investigated due to solubility issues. A data point corresponding to 100% inhibition was included (green circle) for comparison. Assay conditions: 100 µL volume, 10 nM *Ft*PPK, 10 mM $MgCl_2$, 30 µM $polyP_{25}$, 200 µM ADP, 0.78 - 400 µM RL42-Plt9 (either *E* or *Z* isomer), 5% DMSO.

Table 5.2: IC_{50} determination of RL42-Plt9

RL42-Plt9	IC_{50} (µM)	*h*	R^2
E-isomer	99 ± 9	1.5	0.98
Z-isomer	609 ± 300	3	0.47

To derive the IC_{50} values, the data were fitted to the four parameters symmetrical sigmoidal curve described by the Hill equation (Eq. 5.2), constraining the maximum asymptote (y_{max}) to 100% inhibition. An IC_{50} of 99 ± 9 µM was observed for the re-synthesised *E*-isomer (Table 5.2), which was weaker than previously anticipated (section 5.2.2.1 and 4.2.3.3). The Hill coefficient for the *E*-isomer was 1.5, which slightly deviates from the expected unit value for 1:1 stoichiometry. The activity of the *Z*-isomer towards the *Ft*PPK was confirmed to be negligible, with some marginal inhibition observed only at the top concentration tested (400 µM).

5.2.2.3. Mode of binding investigation

Given the presence of a Michael acceptor function in the structure of compound RL42-Plt9 (Figure 5.3), it was hypothesized that compound RL42-Plt9 could bind to the *Ft*PPK by a covalent mechanism. Various compounds containing a Michael acceptor function have been reported as covalent inhibitors,[448,504–507] with the formation of a covalent adduct (affinity labelling)[447,448] resulting from the attack of a nucleophilic residue to the β–C of the Michael acceptor function (Michael addition, Figure 5.3). Affinity labelling of inhibitors containing a Michael acceptor functional group has been reported most often for enzymes with a cysteine residue in their active site (e.g. for cysteine protease and for kinases)[504,508] and has also been observed for other nucleophilic amino acids such as serine and threonine.[448,508,509]

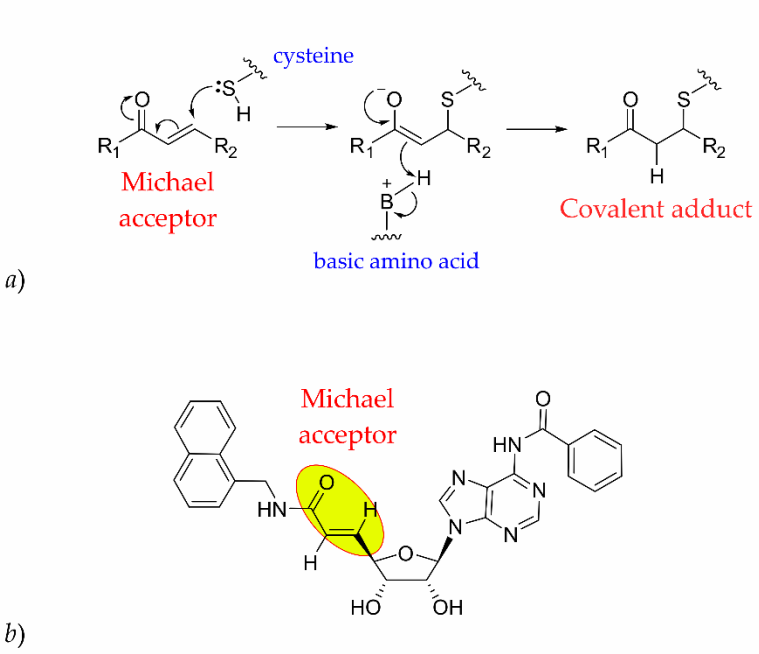

Figure 5.3: Michael acceptor function in RL42-Plt9

a) General affinity labelling mechanism of action: example of nucleophilic attack of a cysteine residue to a compound containing an electrophilic Michael acceptor function, resulting in the formation of a covalent adduct. *b*) Compound RL42-Plt9, Michael acceptor highlighted.

Michael addition reactions have been mainly exploited to create covalent irreversible inhibitors, although more recently, to address the problem of off-target effects, efforts have been directed towards the development of reversible covalent inhibitors, by addition of electron-withdrawing groups that increase the reactivity of the Michael acceptor.[510,511] For

the *Ft*PPK, no cysteine, serine or threonine residues are present in the catalytic pocket of the active site. However, numerous lysine and arginine residues are present within the active site cleft of the *Ft*PPK; in their deprotonated state, these could potentially act as nucleophiles, consistent with the hypothesis that compound RL42-Plt9 may function as a Michael acceptor.

5.2.2.3.1. Biochemical analysis of the reversibility of inhibitor binding

The first step in the characterization of RL42-Plt9 mediated inhibition was to investigate whether the binding to the *Ft*PPK occurred with a reversible or irreversible mode. A *jump dilution assay* was prepared to investigate the reversibility of binding.[374,449] Compound RL42-Plt9 was incubated with *Ft*PPK and $PolyP_{25}$ for 30 minutes at 300 μM (the highest concentration at which no issues of solubility were observed). The assay was then diluted by addition of ADP to yield a final concentration of 15 μM RL42-Plt9. The assay components were prepared to the appropriate concentrations that upon dilution by ADP resulted in the following final assay condition: 10 nM *Ft*PPK, 30 μM $polyP_{25}$, 200 μM ADP, 5% DMSO. Control assays were prepared alongside with no inhibitor, with 15 μM inhibitor (10% inhibition) and with 300 μM inhibitor (90% inhibition). If irreversible binding (either tight binding or covalent binding) occurs, inhibition comparable to the control assays containing 300 μM inhibitor should be observed, as the concentration of the EI complex would not be affected by the dilution step nor subjected to displacement by competition. On the other hand, if the inhibition detected after dilution is comparable to the inhibition detected in the presence of 15 μM inhibitor, a reversible binding profile is revealed. Indeed, upon dilution with ADP, a shift of the equilibrium between the EI complex and the free inhibitor will occur, increasing the free enzyme, with the observed result of no inhibition. The *Ft*PPK time course assays were initiated by addition of ADP and quenched at different time points by addition of EDTA. The *Ft*PPK activity was monitored over 30 minutes. The data were reported as ATP produced against time and each data set was empirically fitted to a one phase exponential association equation (Eq. 2.2). The activity detected after incubation and successive dilution with ADP was comparable to the activity measured for the control assay prepared with 15 μM RL42-Plt9 (Figure 5.4).

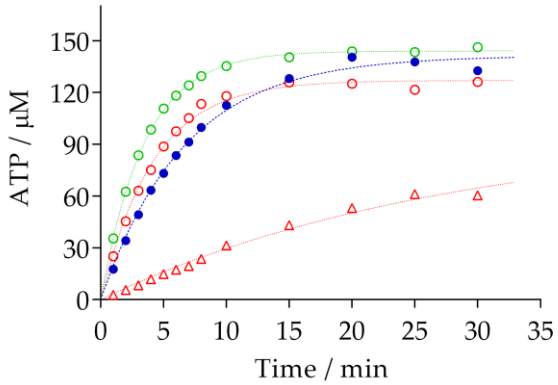

Figure 5.4: Reversible/irreversible binding investigation

Comparison of: *Ft*PPK time course measured after incubation with polyP$_{25}$ and 300 µM RL42-Plt9 followed by dilution to 15 µM (blue circles); *Ft*PPK time courses measured from control assays in the absence of inhibitor (green open circles), in the presence of 15 µM inhibitor (red open circles) and 300 µM inhibitor (red open triangles). The *Ft*PPK activity observed after dilution was comparable to the activity observed in the control assay with 15 µM RL42-Plt9. Assay conditions: 5 µL volume, 20x 10 nM *Ft*PPK, 20x 30 µM polyP$_{25}$, 300 µM RL42-Plt9, 5% DMSO, incubated for 30 min then diluted to 100 µL by addition of 95 µL 200 µM ADP. Control assay conditions: 100 µL volume, 10 nM *Ft*PPK, 30 µM polyP$_{25}$, 200 µM ADP, 0 or 15 or 300 µM RL42-Plt9, 5% DMSO.

Despite the pre-incubation with *Ft*PPK of compound RL42-Plt9 at a concentration that should have resulted in about 90% inhibition, the low degree of inhibition observed revealed that compound RL42-Plt9 was displaced upon dilution with ADP, hence suggesting binding by a reversible mechanism.

5.2.2.3.2. Investigation of irreversible binding by mass spectrometry

Alongside the jump assay, the reversibility of binding of compound RL42-Plt9 was also investigated by mass spectrometry. Aiming to uncover the possible formation of a covalent adduct and the requirement for Mg^{2+} ion and polyP$_{25}$, the conditions reported in Table 5.3 were tested. Control samples in which compound RL42-Plt9 was not included were also tested in parallel. The samples were analysed by ESI^+ mass spectrometry. The expected mass of the *Ft*PPK-RL42-Plt9 adduct was 33564.48 Da (*Ft*PPK mass: 33012.9 Da; RL42-Plt9 Mw: 550.58). A distinct peak for compound RL42-Plt9 (absent in the control samples) was observed in each spectrum, alongside the typical protein charge envelope resulting from different multi-protonated states of the enzyme, which corresponded to a species with mass

of 33017.4. No formation of the covalent adduct RL42-Plt9-*Ft*PPK was detected for any of the conditions tested. In accordance with the jump dilution assay (section 5.2.2.3.1), the mass spectrometric analysis suggested that RL42-Plt9 may bind to *Ft*PPK by a reversible mechanism.

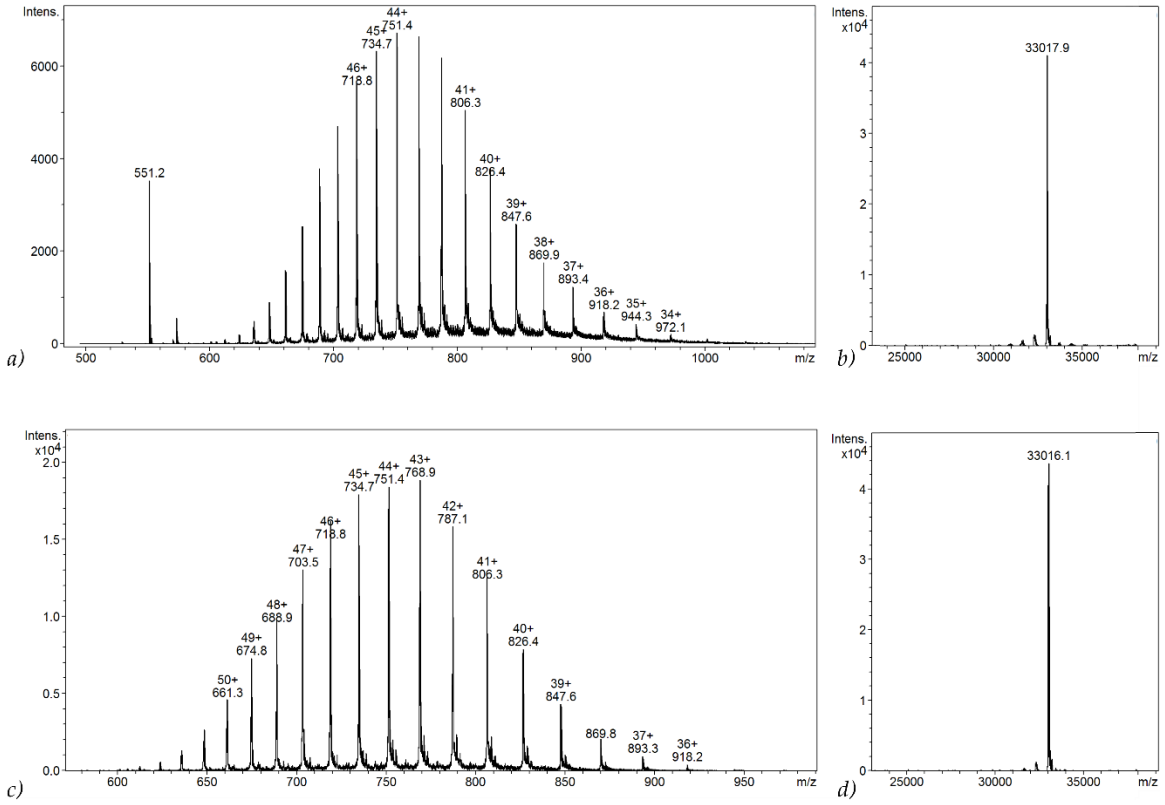

Figure 5.5: Covalent adduct investigation by mass spectrometry

a) ESI+ spectrum of *Ft*PPK in the presence of RL42-Plt9, $MgCl_2$ and $polyP_{25}$; *b*) Deconvoluted peak of *a*); *c*) ESI+ spectrum of control sample in which compound RL42-Plt9 was not included; *d*) Deconvoluted peak of *c*. RL42-Plt9 Mw: 550.58; *Ft*PPK Mw: 33012.9 Da; Expected mass for RL42-Plt9 covalent adduct: 33564.48 Da. Conditions: 60 µM *Ft*PPK, 10 mM $MgCl_2$, 100 µM $polyP_{25}$, 100 µM RL42-Plt9.

Table 5.3: Sample tested by mass spectrometry

Experiment	Conditions	Investigated
1	*Ft*PPK, RL42-Plt9, $MgCl_2$	Binding in the absence of $PolyP_{25}$
2	*Ft*PPK, $polyP_{25}$, RL42-Plt9, $MgCl_2$	Requirement of Mg^{2+} and $PolyP_{25}$ for binding
3	*Ft*PPK, RL42-Plt9	Binding in the absence of Mg^{2+} and $PolyP_{25}$
4	*Ft*PPK, $polyP_{25}$, RL42-Plt9	Binding in the absence of Mg^{2+}

5.2.2.3.3. Type of inhibition: competitive with ADP

Further characterization of the mode of binding of compound RL42-Plt9 was conducted, aiming to define if the binding occurs by competitive, non-competitive or uncompetitive mechanism. Given the structural analogy with a nucleotide, the investigation of a mode of binding competitive with ADP was prioritized. The apparent initial rate (v_0^{app}) was measured at a range of ADP concentrations between 30 μM and 2 mM and, per each concentration, in the absence of inhibitor and in the presence of 50 μM, 100 μM and 150 μM RL42-Plt9. The $polyP_{25}$ was maintained at a saturating concentration (30 μM), to ensure production of ATP within the HPLC detection range. The concentration of the *Ft*PPK was reduced to 2.5 nM, to slow down the reaction rate and therefore allow an accurate measurement of the v_0^{app} even at higher concentration of ADP. In light of the large number of individual observation required for this experiment and the relatively low throughput of the HPLC-based *Ft*PPK assay, it was not possible to conduct this experiment in replicates. For each concentration of substrate and inhibitor, a 10 points time course was measured (up to 6 minutes) and the v_0^{app} derived by fitting the linear phase to a linear regression equation (Eq. 2.4). Lineweaver-Burk plots and Dixon plots (Appendix, A5 1.2) were generated by plotting the reciprocate of rate against the reciprocate of concentration for each inhibitor concentration, or the reciprocate of rate against inhibitor concentration for each substrate concentration, respectively (Figure 5.6). In the Lineweaver-Burk plot, the lines, derived by fitting the data to a linear regression equation (Eq. 2.4), intercepted the $1/v_0^{app}$ axis and the 1/[ADP] axis at different points, indicating a variation of both the $V_{\max}^{app}$ and the K_{m}^{app}, a behaviour observed for non-competitive inhibitors (Figure 5.6*a*). The same mechanism of action was confirmed by the pattern observed in the Dixon plot, where the lines converged at $1/v_0^{app} = 0$ (Figure 5.6*b*). According to the Dixon plot, in the presence of K_{m} concentration of ADP (200 μM) and saturating concentration of polyP (30 μM), RL42-Plt9 binds to the *Ft*PPK with a K_{i} of approximately 50 μM and with a non-competitive mechanism with respect to ADP.

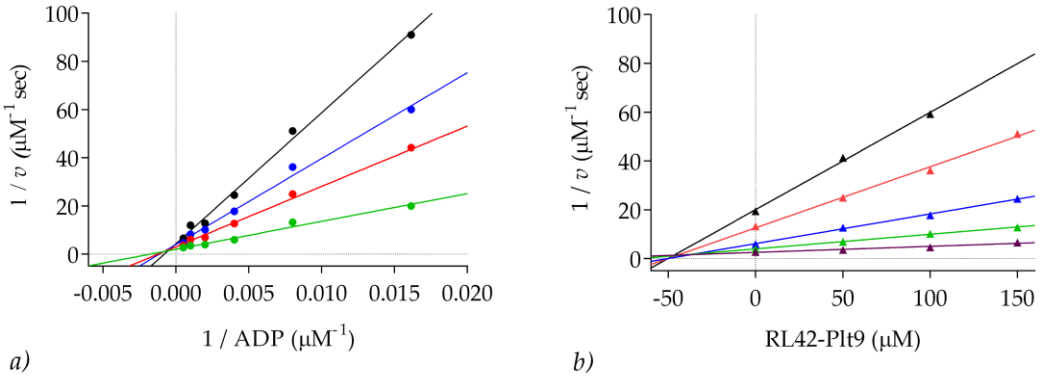

Figure 5.6: Mode of action investigation with respect to ADP

a) Lineweaver-Burk plot: reciprocate of v_0^{app} against reciprocate of ADP concentration, measured in the presence of 150 μM RL42-Plt9 (black dots), 100 μM RL42-Plt9 (blue dots), 50 μM RL42-Plt9 (red dots), DMSO (green dots). *b*) Dixon plot: reciprocate of v_0^{app} against RL42-Plt9 concentration, measured in the presence of 62 μM ADP (black triangles), 125 μM ADP (red triangles), 250 μM ADP (blue triangles), 500 μM ADP (green triangles), 1000 μM ADP (purple triangles). Assay conditions: 100 μL volume, 2.5 nM *Ft*PPK, 30 μM $polyP_{25}$, 62 μM - 2 mM ADP, 0 μM, 50 μM, 100 μM, 150 μM RL42-Plt9, 5% DMSO.

5.2.2.4. RL42-Plt9 activity with different PPK2-like enzymes

A broad spectrum of action is regarded as a very important property for an antibacterial agent. Although the major aim of this research project was to identify a new compound for the development of a new antibiotic for the biowarfare agent *Francisella tularensis*, or a compound that could act as a coadjuvant of currently available antibiotics, a molecule with a wider spectrum of action would be of greater interest and value. To investigate its potential as inhibitor for other PPK2 enzymes, the activity of compound RL42-Plt9 has been tested on the PPK2 from *Meiothermus ruber* (*Mr*PPK).[232]

According to the PPK2 classification proposed by Motomura, the *Ft*PPK belongs to class I, while the *Mr*PPK belongs to class III (section 1.3.3.1).[232] While *Ft*PPK prefers purine diphosphate as substrate,[260] *Mr*PPK can synthesize ATP by conversion of AMP into ADP and then by further phosphorylation of ADP, this last step being rate limiting.[232] The two enzymes are structurally closely related in overall fold, but specific sequence differences between the *Ft*PPK and the *Mr*PPK relate to those amino acid residues involved in nucleotide recognition.[512]

5.2.2.4.1. *Mr*PPK time course

*Mr*PPK was kindly donated by Dr J. N. Andexer, from the University of Freiburg (Germany). The activity of *Mr*PPK is being investigated in Andexer group and their optimal conditions use $MgCl_2$ as cofactor, at pH 8 (50 mM Tris buffer) and at 37°C, conditions slightly different than those reported by Motomura.[232] Data provided by Andexer supported the previous report[232] of a quicker phosphorylation of AMP in comparison to ADP: in the presence of 1.5 μM *Mr*PPK and 10 mM polyP, the conversion of AMP (2 mM) into ADP and ATP (produced in a 2:1 ratio, respectively) was faster (75% after 45 minutes) than the conversion of ADP (2 mM) into ATP (less than 30% after 45 minutes).[16] To date, only data relative to the substrate specificity but not a full kinetic characterization of *Mr*PPK has been published.[232] For the investigation of the RL42-Plt9 activity on the

[16] J. Alexander personal communication.

*Mr*PPK, the assay conditions were arbitrarily adapted based on the observations of the Andexer group and on the previous conditions used for the *Ft*PPK assay (Figure 4.15).

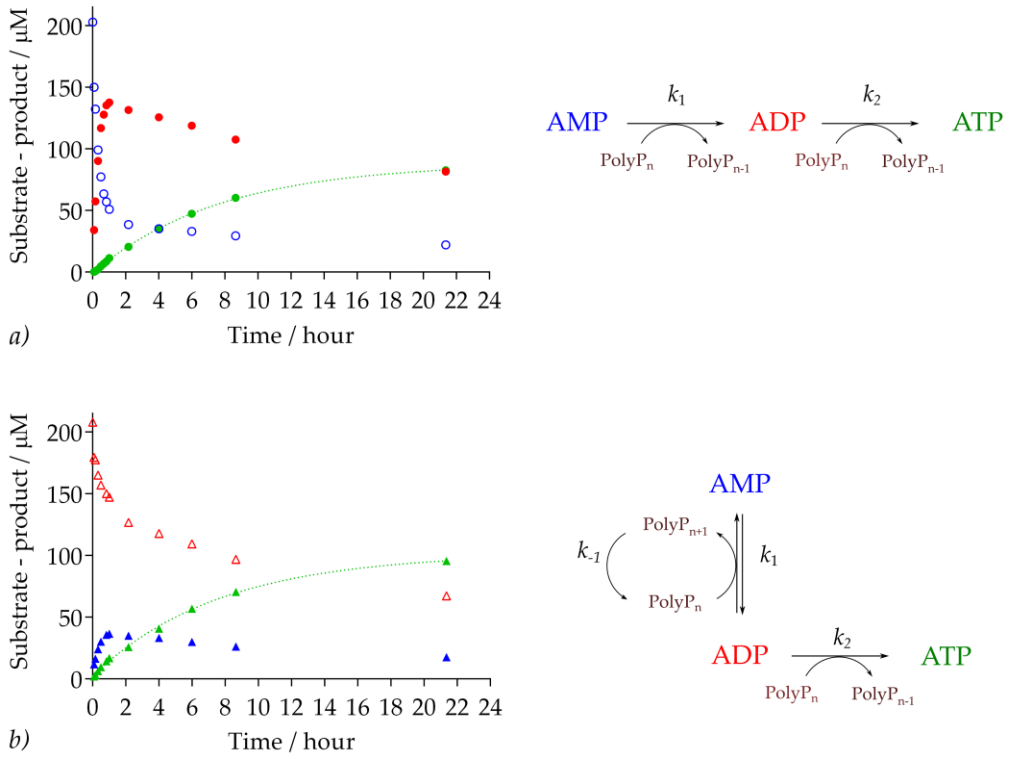

Figure 5.7: *Mr*PPK reaction time course

a) Time course using 200 µM AMP as substrate (blue open circles): ADP and ATP were produced (red and green circles, respectively); *b*) Time course using 200 µM ADP as substrate (red open triangles): AMP and ATP were produced (blue and green triangles, respectively). Assay conditions: 100 µL assay volume, 10 nM *Mr*PPK, 200 µM AMP or ADP, 1 mM polyP$_{25}$, 5% DMSO, 37°C. Due to time constraints, the assays were not prepared in replicate.

In particular, a concentration of enzyme and nucleotides comparable to the *Ft*PPK assay was adopted also for the *Mr*PPK activity measurement. Assays were prepared at pH 8.0 (Tris base), in the presence of 10 nM *Mr*PPK, 10 mM $MgCl_2$, 200 µM AMP or ADP. A concentration of 30 µM polyP$_{25}$ was showed to be enough to saturate the *Ft*PPK, however for *Mr*PPK the PolyP$_{25}$ was increased to 1 mM, given the high concentrations used by both Motomura and Andexer (5 mM and 10 mM respectively).[232] Prior to testing the RL42-Plt9 effect, the *Mr*PPK activity was investigated under the reported conditions by measuring two long time courses in parallel (over 22 hours), one with AMP as substrate the other with ADP. As previously for the *Ft*PPK, the *Mr*PPK was pre-incubated for 30 minutes at 37°C

in the presence of polyP$_{25}$, the assays were started by addition of the respective nucleotide substrate and quenched at each time point by EDTA (50 mM). The assays were analysed by HPLC, applying the method developed for the *Ft*PPK assay (section 4.2.3.1.2). In line with previous reports, the pattern of substrate consumption and product formation observed when using AMP as substrate was analogous to the kinetics of a consecutive reaction (Figure 5.7*a*).[271] The AMP was rapidly converted into ADP, which was then slowly converted into ATP (suggesting $k_1 >> k_2$). When ADP was used as substrate, not only ATP production was observed but also some AMP was produced and then partially consumed (Figure 5.7*b*). Whether AMP or ADP was used as substrate, the rate constant for ATP production was the same (0.13 ± 0.03 and 0.13 ± 0.07, respectively, derived by fitting the data to Eq. 2.2). Equally, when equilibrium was reached, the concentration of AMP, ADP and ATP were comparable independently from the initial substrate. The two time courses, initially measured to confirm that the *Mr*PPK received was active, provided a useful reference to set the condition for testing the effect of RL42-Plt9 on the *Mr*PPK activity.

5.2.2.4.2. Effect of compound RL42-Plt9 on *Mr*PPK activity

The activity of compound RL42-Plt9 on the *Mr*PPK was tested using both AMP and ADP as substrate and applying the same conditions adopted for the time course (section 5.2.2.4.1). The concentration used for compound RL42-Plt9 was 100 μM, the IC$_{50}$ value for *Ft*PPK (section 5.2.2.2). Time courses were measured in the absence and in the presence of compound RL42-Plt9. The data obtained were difficult to interpret, and should be confirmed by replicates (only single experiments were analysed for these time courses). A significant effect on the *Mr*PPK activity was observed mostly after 60 minutes and indeed was more evident in the time courses measured in the presence of ADP as substrate, which was left to run for longer. When using AMP as substrate, the concentration of AMP, ADP and ATP was comparable for the first 30 minutes, however after 60 minutes the concentration of ADP was lower in the presence of RL42-Plt9 while the ATP produced was higher (Figure 5.8*a*). The same pattern was observed when ADP was used as substrate (Figure 5.8*b*). In this case as well, the effect was more significant after 60 minutes. Not only a higher extent of ADP depletion and ATP synthesis was observed in the presence of RL42-Plt9 after 60 minutes,

but also the concentration of AMP was slightly lower. A possible explanation of the data observed could be that compound RL42-Plt9 interferes with the conversion of ADP into AMP, hence the lower concentration of AMP detected. Perhaps blocking of the dephosphorylation of ADP, the phosphorylation activity and therefore the synthesis of the ATP is favoured. It could be possible that the effect is more evident later during the time course as a consequence of a possible covalent mechanism when interacting with *Mr*PPK. Evidently these are just hypotheses and further investigation would be required, however it appeared clear that compound RL42-Plt9 was capable of exerting a certain effect on the *Mr*PPK activity.

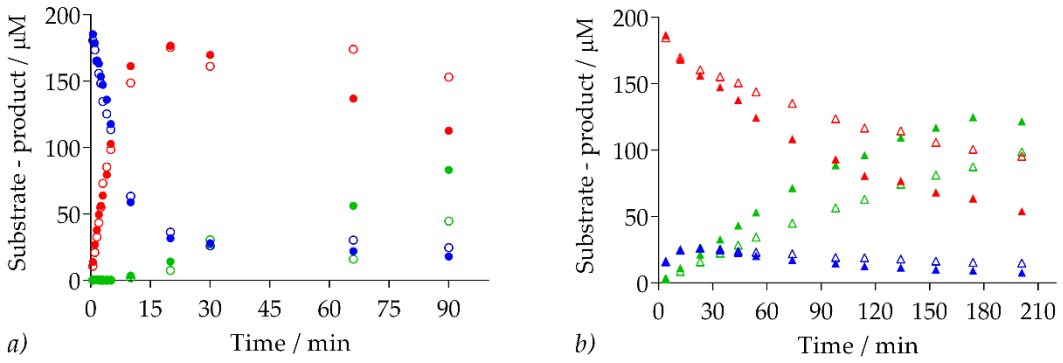

Figure 5.8: *Mr*PPK time course in the presence of RL42-Plt9

a) Time course using 200 µM AMP as substrate: in the presence of RL42-Plt9 (full circles) and in the absence of RL42-Plt9 (open circles); *b*) Time course using 200 µM ADP as substrate: in the presence of RL42-Plt9 (full triangles) and in the absence of RL42-Plt9 (open triangles). AMP: blue, ADP: red, ATP: green. Assay conditions: 100 µL assay volume, 10 nM *Mr*PPK, 200 µM AMP or ADP, 1 mM polyP$_{25}$, 100 µM RL42-Plt9, 5% DMSO, 37°C.

5.2.3. Structure activity relationship

Taking advantage of the presence in the library of a range of analogues of compound RL42-Plt9, a preliminary structure activity relation (SAR) investigation was undertaken. The analogues shared the nucleotide moiety (most of them were adenosine derivatives) and Michael acceptor moiety but differed in the functional group attached to the amide (Figure 5.9). The RL42-Plt9 analogues (from the library stock) were tested at the concentration of 100 µM, corresponding to the IC_{50} value determined for RL42-Plt9.

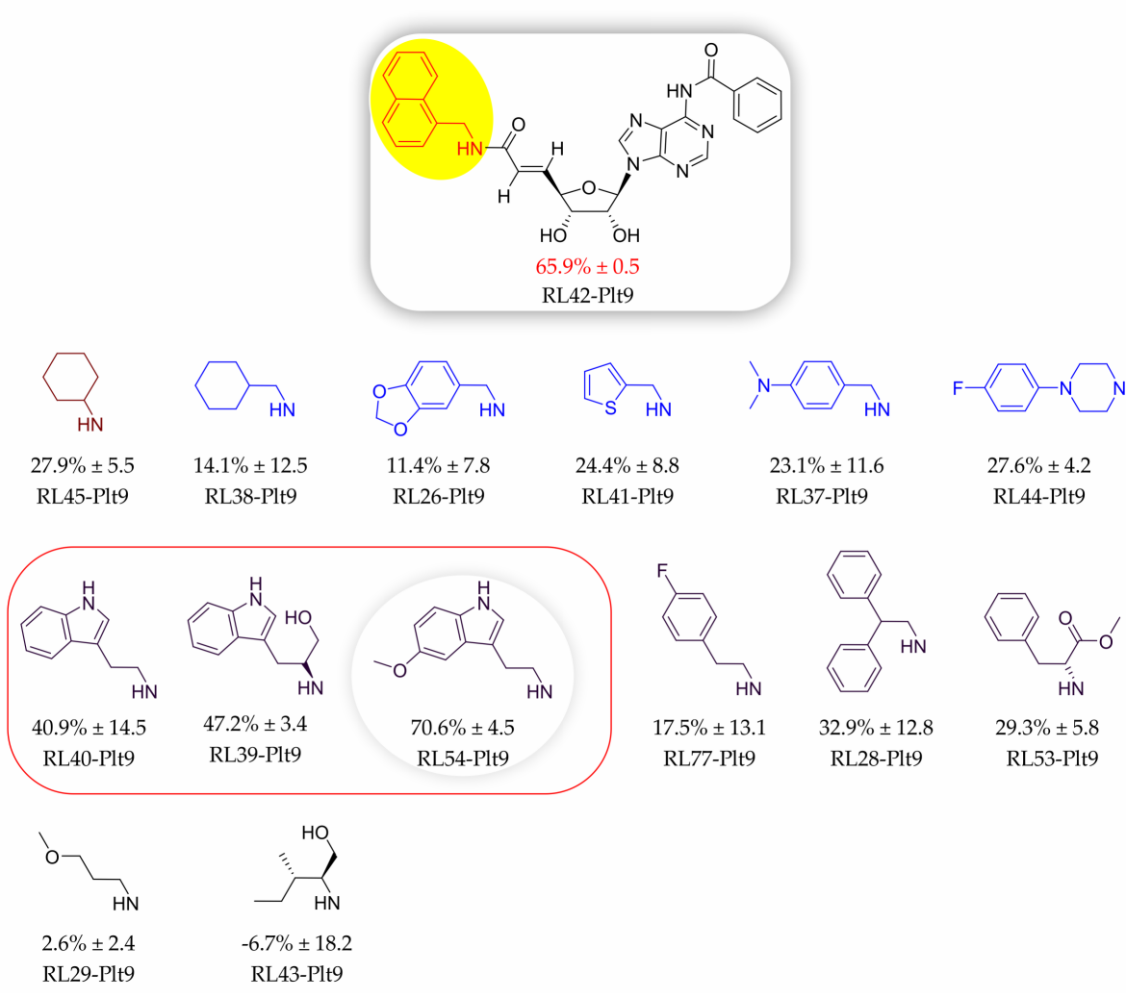

Figure 5.9: SAR

Variations of the amide side chain for RL42-Plt9. The analogues were tested at the concentration of 100 µM in duplicate.

A significant loss of activity was observed in the absence of the aromatic rings, suggesting their involvement in the interaction with the active site (compounds RL29-Plt9 and RL43-Plt9, Figure 5.9). The other differences among the analogues were: the presence of either a

single aromatic ring or a bicyclic aromatic system; the presence of either a methyl or an ethyl link between the amide function and the aromatic groups. Exceptions to these instances were compounds RL45-Plt9 and RL38-Plt9, in which a single non aromatic ring was attached to the methyl-amide function, and compound RL26-Plt9, in which the second cyclic ring was not aromatic. These compounds scored lower activity, suggesting the importance of the aromatic system for the interaction with the active site. A higher degree of inhibition was observed for molecules with two aromatic rings fused to form a bicyclic system (compounds RL40-Plt9, RL39-Plt9, RL54-Plt9, Figure 5.9). In comparison with compound RL42-Plt9, in place of the naphthyl system, these compounds have an indolic system, linked to the amide function by a C2 chain. Compound RL54-Plt9 also has an additional methoxy group in position 5 of the indolic system. The activity of compound RL54-Plt9 appeared comparable to the activity of compound RL49-Plt9. Furthermore, compounds RL54-Plt9 presents some additional structural features that may positively affect the interaction with the active site, namely a longer distance between the amide function and the aromatic system, and two sites which could engage in the formation of H-bonds: the methoxy group as H acceptor and the N-H of the indolic system as H-donor.

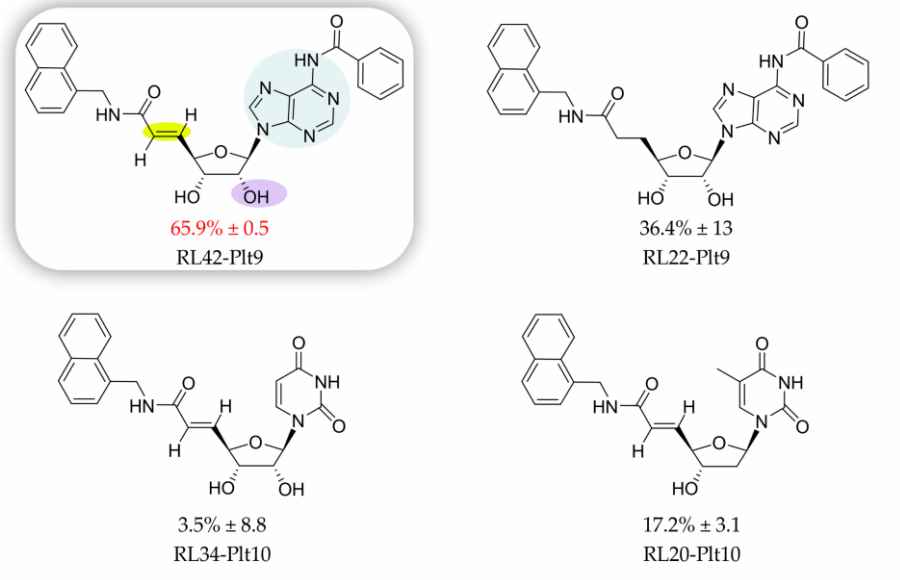

Figure 5.10: SAR, RL42-Plt9 nucleoside analogues

Analogues of RL42-Plt9 included in the Reynolds library with modification to the double bond and to the nucleoside moiety. The analogues were tested at the concentration of 100 μM in duplicate.

Within the Reynolds library a few analogues of compound RL42-Plt9 were found, two of which had a pyrimidine nucleobase, and one where the Michael acceptor function was removed by saturation of the double bond (Figure 5.10). Negligible activity was observed for the compounds with the pyrimidine in place of the adenine (compounds RL34-Plt9 and RL20-plt10, Figure 5.10), in line with the inability of the *Ft*PPK to use pyrimidine nucleotides as substrates (section 1.3.3.2.4). Interestingly, the activity of compound RL22-Plt9 (Figure 5.10) did not disappear in the absence of the double bond but was only attenuated. This data supported the hypothesis that compound RL42-Plt9 binds to *Ft*PPK by a mechanism that does not involve the Michael acceptor-mediated formation of a covalent bond (section 5.2.2.3.1 and 5.2.2.3.2).

5.2.4. Structural investigation of RL42-Plt9 binding to the active site

5.2.4.1. Modelling into the active site

Following the unsuccessful attempts to co-crystallize compound RL42-Plt9 with *Ft*PPK (Appendix, section A5 2), the compound was modelled in the *Ft*PPK active site using the crystallography model determined by A. Parnell[265] by co-crystallization of the *Ft*PPK with the non-hydrolysable ATP analogue AMPPCP.

5.2.4.1.1. *Ft*PPK structural features

The *Ft*PPK belongs to the P-loop family of kinases[513] and the structure, determined to a resolution of 2.2 Å, is constituted by four monomers, each consisting of six β-sheets and twelve α-helices (Figure 5.11*a* and *b*).[260] The β-sheets strands are centrally positioned, surrounded by ten α-helices. The two remaining helices (α-8 and α-9) fold above the β-sheets forming the lid loop module.[260] The three well conserved features of the PPK2-like family, the Walker A motif, the Walker B motif and the lid loop,[375] were identified for the *Ft*PPK by alignment with previously characterised PPK2 enzymes and confirmed by the apo structure (Figure 5.11*b* and *c*).[260] In *Ft*PPK, the conserved Walker B motif was identified with the amino acids 117-119 and is part of the sequence Asp117-Phe132 that is involved in the catalysis and defines the adenine binding pocket. The Walker A motif, corresponding to the amino acids 60-68, is located to the left of the Walker B motif and delimits the area of the binding pocket in which the di-phosphate or tri-phosphate chain binds. The binding cleft is defined by the flexible lid module, which was identified with the amino acids 168–198. A positively charged region, constituted by Arg and Lys residues, was recognized as the PolyP binding site (Figure 5.11*d*). The model generated by A. Parnell,[265] from the co-crystallization of the *Ft*PPK with $polyP_{25}$ and with the non-hydrolysable ATP analogue AMPPCP (Figure 5.12), allowed confirmation of the role of conserved amino acids within the Walker A and the lid module and to identify the residues within the adenine binding pocket involved in the nucleotide binding.

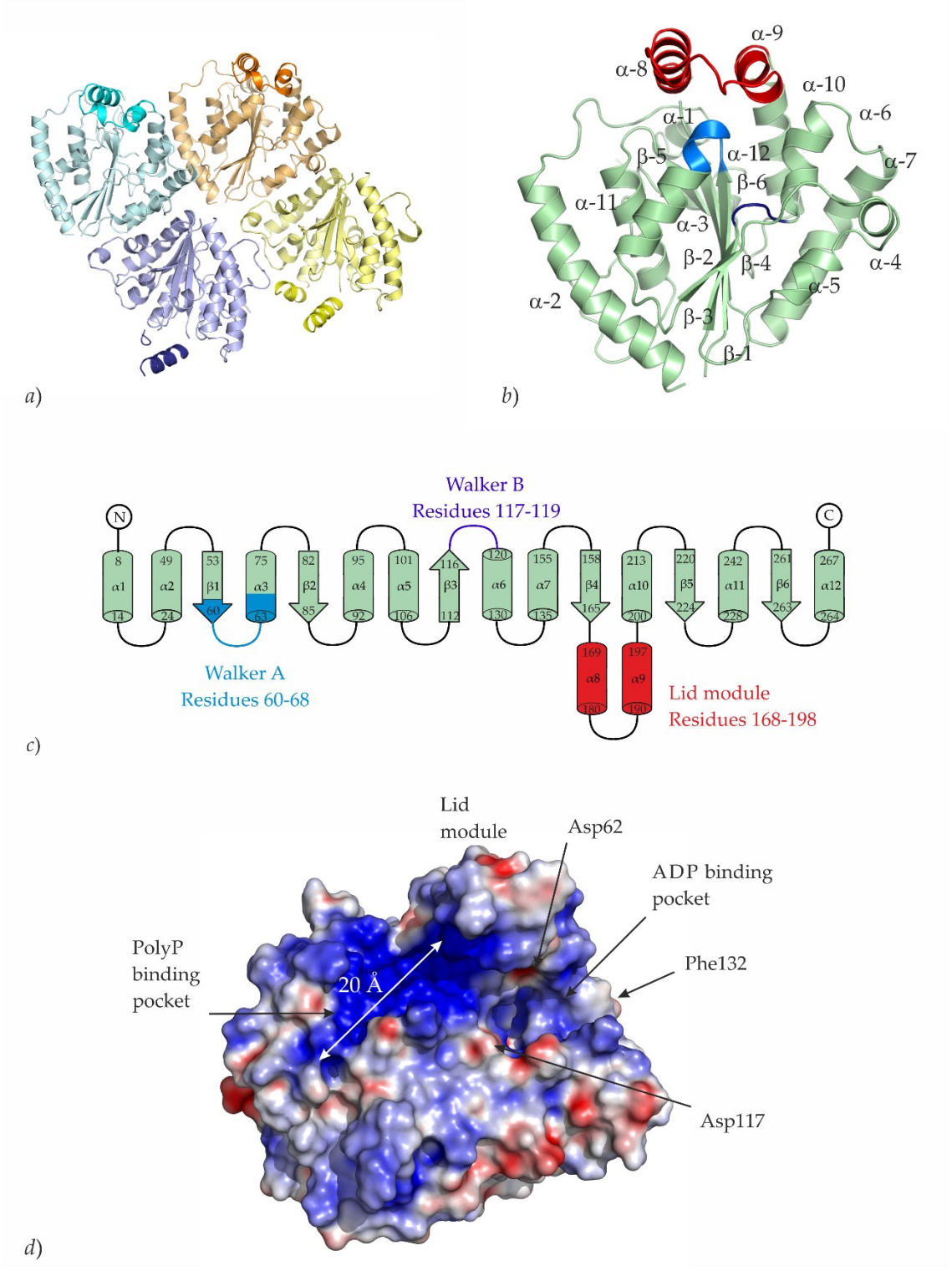

Figure 5.11: *Ft*PPK apo structure

a) *Ft*PPK monomers arrangement within the asymmetric unit. *b*) *Ft*PPK monomer with the respective β-sheet strands and α-helices labelled. The Walker A motive, the Walker B motive and the lid module were highlighted in blue, dark purple and red, respectively. *c*) *Ft*PPK monomer topology with colors corresponding to figure b. *d*) *Ft*PPK electrostatic surface model, showing the polyP binding pocket, the lid module, the ADP binding pocket and key amino acids. Figures taken with permission from Batten *et al*.[260]

In the first model proposed by A. Parnell, derived from the co-crystallization of $polyP_{25}$ with *Ft*PPK, the binding of the polyP in the positively charged channel below helix α-8 was confirmed.[265] The electron density map allowed the building of a model with a 9 unit polyP chain kept in place by interaction with several positively charged Arg and Lys residue, (Figure 5.13*a*).[265] Of particular relevance is the residue Arg178, belonging to the lid loop, which orientates the $polyP_{25}$ in the active site to a conformation favourable for the catalysis (Figure 5.14). In a second model elaborated by Parnell, the *Ft*PPK-AMPPCP model, an nucleotide derived from di-phosphorylation of the AMPPCP (AMPPCP-PP, Figure 5.12) was captured, providing insights in the nucleotide binding interactions and in the catalytic mechanism (Figure 5.13*b*).[265]

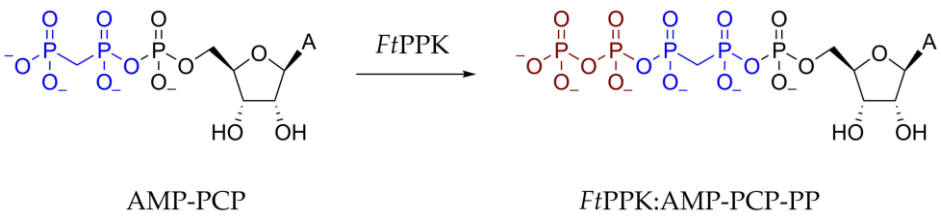

Figure 5.12: AMPPCP and AMPPCP-PP intermediate captured in the *Ft*PPK active site

The nucleotide binding pocket (Figure 5.13*b*) was confirmed to be shaped by the amino acids Asp117-Phe132 and by the base binding loop identified as helix 6 (amino acids 87-90).[265] The adenine was held in place by pi-stacking interactions with the Phe132 and by hydrophobic interaction with the Lys89 and with Pro90 from helix 6. The orientation of the ribose in the active site was defined by interactions of the 3'-OH with the Asn122, via a network of H-bonding, involving both 3' and 2'-OH and two molecules of water, and by van der Waals interaction of the ring oxygen with Val126 (Figure 5.13*b*). The residues Asp62 (from the Walker A motif) and Asp192 (from the lid module) were responsible for the coordination of the Mg^{2+} ion, essential for catalysis, which was in turn coordinated also to the α and the γ-phosphate of the nucleotide and to the first of the two phosphates presumably transferred from the $polyP_{25}$ to the AMPPCP analogue (Figure 5.13*c*).

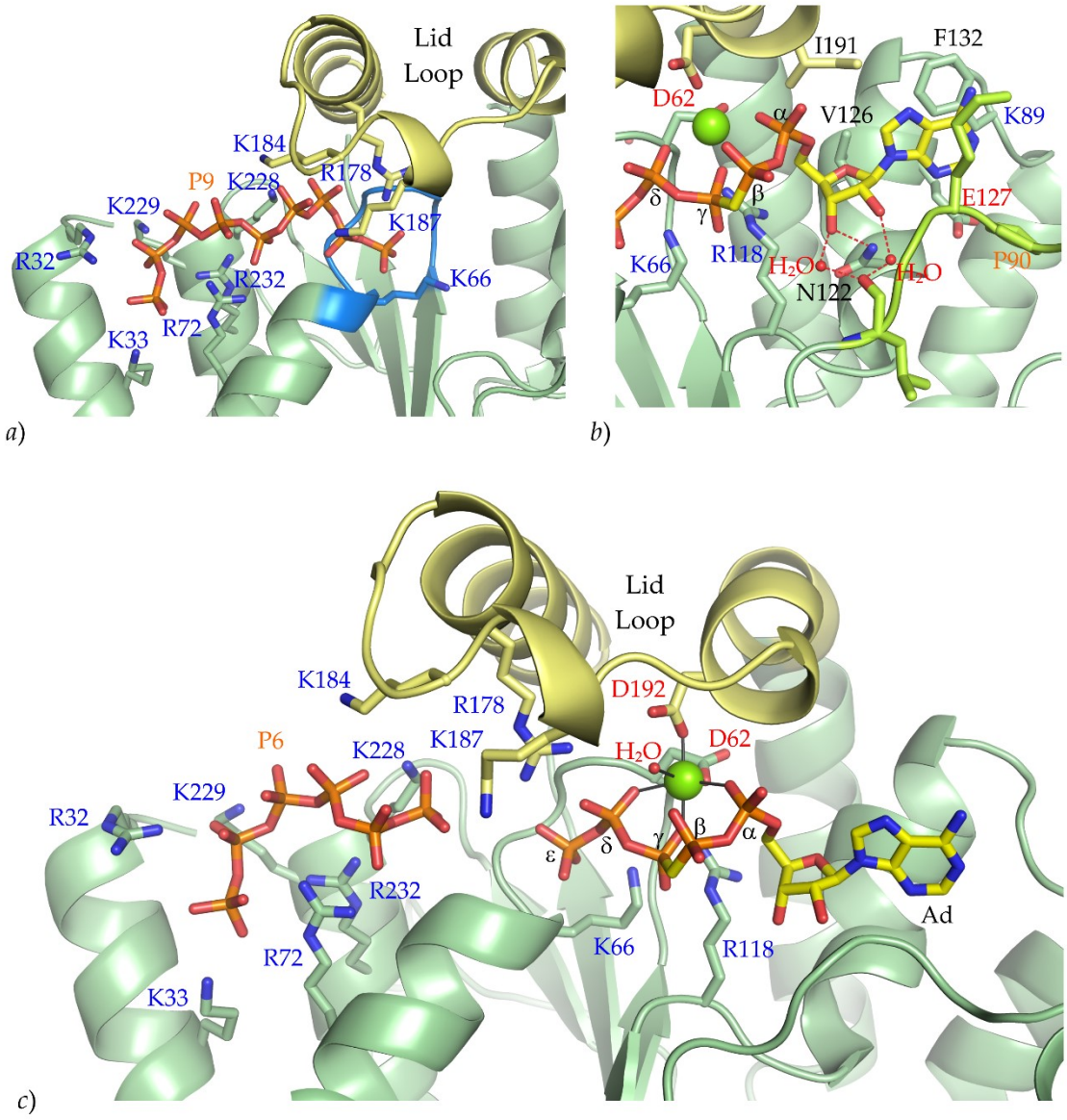

Figure 5.13: *Ft*PPK-polyP and AMPPCP model

a) *Ft*PPK-polyP$_{25}$ model; *b*) *Ft*PPK-AMPPCP-PP complex model: base interactions, *c*) *Ft*PPK-AMPPCP-PP complex model: Mg^{2+}-phosphate chain interactions. The lid loop was colored in yellow; the Mg^{2+} was represented by a green sphere; basic amino acid were colored in blue, acidic amino acids were colored in red. Figures taken with permission from A. Parnell thesis.[265]

The amino acids Asp117, Arg118 (from the Walker B motif) and Lys66 (from the Walker A motif) were confirmed to be involved in the catalysis.[265] Their role and a mechanism of action was inferred based on the observed interactions with the AMPPCP-PP intermediate (Figure 5.14*c*). It was proposed that the β-phosphate of the nucleotide participated in a nucleophilic attack to the terminal phosphate of the polyP chain, which was activated by coordination with the Mg^{2+} ion and by polarization of the P=O due to H-bonding with

Arg118. The latter was also proposed to be involved in the stabilization of the intermediate, in conjunction with a further H-bond to a water molecule bridging to Asp117. The following formation of ATP and $PolyP_{n-1}$ by collapse of the intermediate was proposed to be favoured by the Lys66 which stabilized the leaving polyP chain by H-bonding or by protonation. The mechanism proposed and the role of the amino acids Asp117, Arg118, Arg178 and Lys66 was supported by mutation studies.[265] Mutants of Arg178 and Lys66 showed a lower K_d for polyP, confirming their role in the polyP binding to the active site. A lower K_{cat} was reported for the Asp117 mutant while the *Ft*PPK activity was severely compromised for the Arg118 mutant.

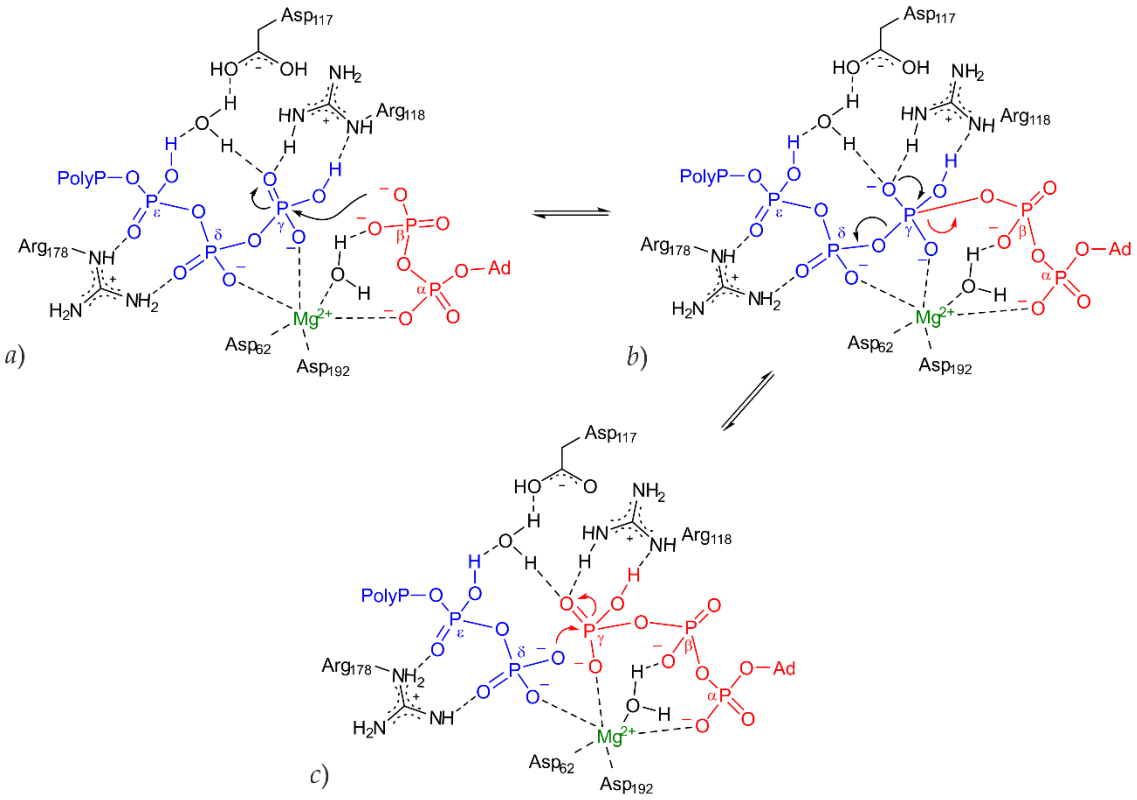

Figure 5.14: *Ft*PPK proposed mechanism of action

The proposed mechanism of action of the phosphate transfer from the polyP chain to the nucleotide and the opposite extension of the polyP chain was illustrated. *a*) nucleophilic attack; *b*) formation of intermediate followed by elimination of the $PolyP_{n-1}$ chain; *c*) nucleophilic attack of PolyP on the activated ATP γ-phosphate. The PolyP chain was highlighted in blue, the nucleotide in red. The black arrows refer to the nucleotide phosphorylation, the red arrows to the opposite polyP extension. Figure adapted from A. Parnell thesis.[265]

5.2.4.1.2. Modelling of compound RL42-Plt9 in the *Ft*PPK active site

The elaboration of a model of the binding of RL42-Plt9 into the *Ft*PPK active site would be of value for the understanding of the mechanism of action and for later medicinal chemistry optimisation. Due to the lack of success with the co-crystallization studies, molecular dynamic modelling of RL42-Plt9 was attempted on the basis of the *Ft*PPK-AMPPCPP complex model produced by A. Parnell.[265] Various software are available for simulation of ligand-protein interaction, such as AutoDock Vina, GOLD, eHiTS.[514–516] However, due to time constraints, to investigate the possible orientation of the RL42-Plt9 side chain in the active pocket, a preliminary study by manual docking followed by a brief perturbation was performed using the crystallography software Phenix[517] and visualized using either PyMOL,[518] or Coot[519] (Figure 5.15).

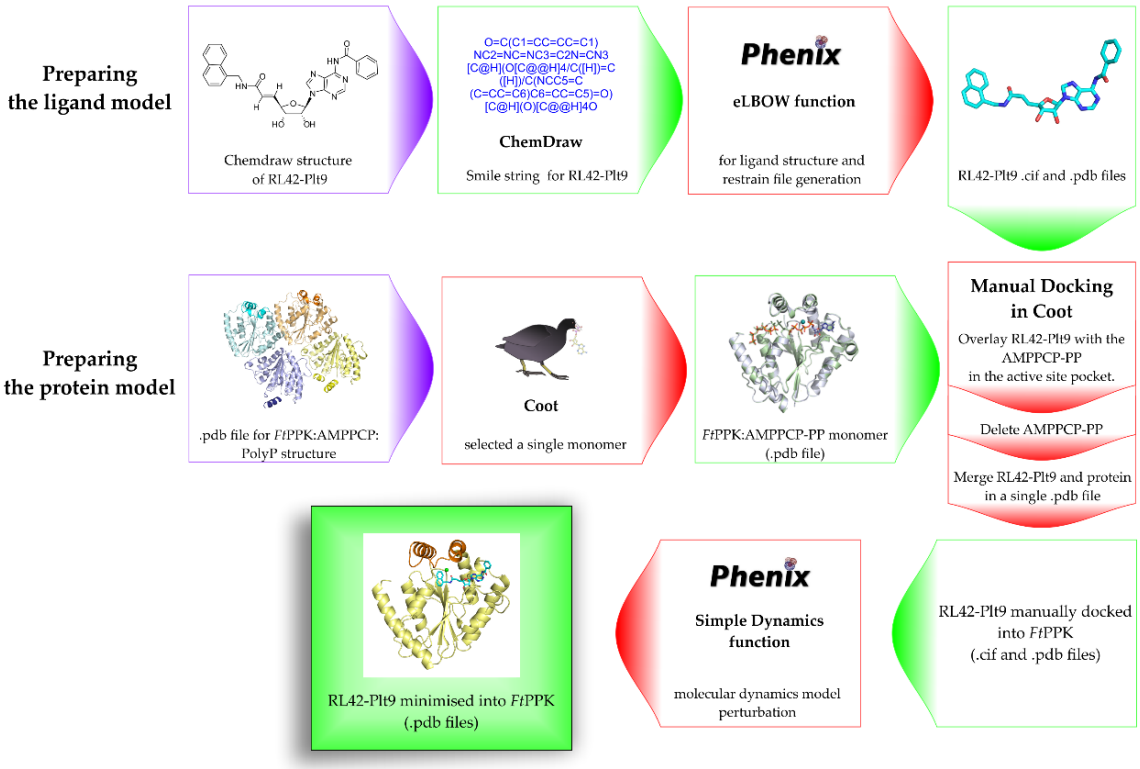

Figure 5.15: Modelling workflow diagram

The diagrams describe the steps applied for the modelling of compound RL42-Plt9 in the *Ft*PPK active site on the basis of the AMPPCP-PP interactions. The starting input, the .cdx file of the RL42-Plt9 structure and the .pdb file of the *Ft*PPK-AMPPCP-PP model were highlighted in a purple box; the inputs and the out puts were highlighted in a green box; the software and the operations applied were highlighted in a red box.

A .pdb file and respective restraint file (.cif) of the ligand were generated with Phenix eLBOW. One of the monomers from the *Ft*PPK-AMPPCP model (.pdb file kindly provided by A. Parnell)[265] was selected as a starting point for modelling. The ligand and the *Ft*PPK-AMPPCP .pdb files were opened in Coot and the RL42-Plt9 manually modelled by superimposition to the AMPPCP adenine and ribose. Due to structural rigidity, the side chain of the RL42-Plt9 was orientated in the binding pocket to loosely match the position of the PCP-PP chain of the AMPPCP-PP. The .pdb files of RL42-Plt9 and of the *Ft*PPK protein backbone were merged in a single .pdb file. The complex was then subjected to molecular dynamic perturbation by applying the Simple Dynamic function in Phenix. The operation allowed reciprocal adjustment of the ligand and of the protein conformation. The overall model of the single monomer *Ft*PPK:RL42-Plt9 complex and a zoomed image of the active site were shown in Figure 5.16. To compare the interactions of the RL42-Plt9 virtually docked in the active site with the interactions of the AMPPCP analogue determined by co-crystallization, the two models were overlaid (Figure 5.16 *c*). No significant differences were observed for the protein conformation. The ligand RL42-Plt9 appeared slightly displaced relatively to the position occupied by AMPPCP-PP with a consequent loose overlay of the adenines. Nonetheless, in the RL42-Plt9 model the pi-stacking interactions of the purine with the Phe132 and the ring staking with Cβ and Cε of the Lys89 appeared to be maintained (Figure 5.16*b* and *c*). The benzoyl group bound to the amino group in position 6 did not appear to be involved in any interactions with the active site. A significant difference was observed for the ribose conformation. The AMPPCP ribose presented a C-2 endo conformation while the conformation adopted by the ribose in the RL42-Plt9 appeared more similar to a C-3 endo conformation (Figure 5.16*c*). It is difficult to say whether the latter would have been naturally preferred by RL42-Plt9 or whether it was a modelling artefact. Indeed, during the initial manual structural overlay of RL42-Plt9, issues with the rigidity of the model, probably due to the C5'-C6' double bond, were encountered, which did not allow to change the ribose conformation to C-2 endo. In the RL42-Plt9 model the van der Waals contact of the ring oxygen with Val126 observed for the AMPPCP model was maintained, as well as the interactions of the OH groups with water and Asn122. However, opposite interactions were observed for the OH groups of RL42-Plt9, with the 3'-

OH interacting with a water molecule and Asn122 and the 2'-OH interacting with another water molecule, in turn bridging to residue Glu127 (Figure 5.16*b*).

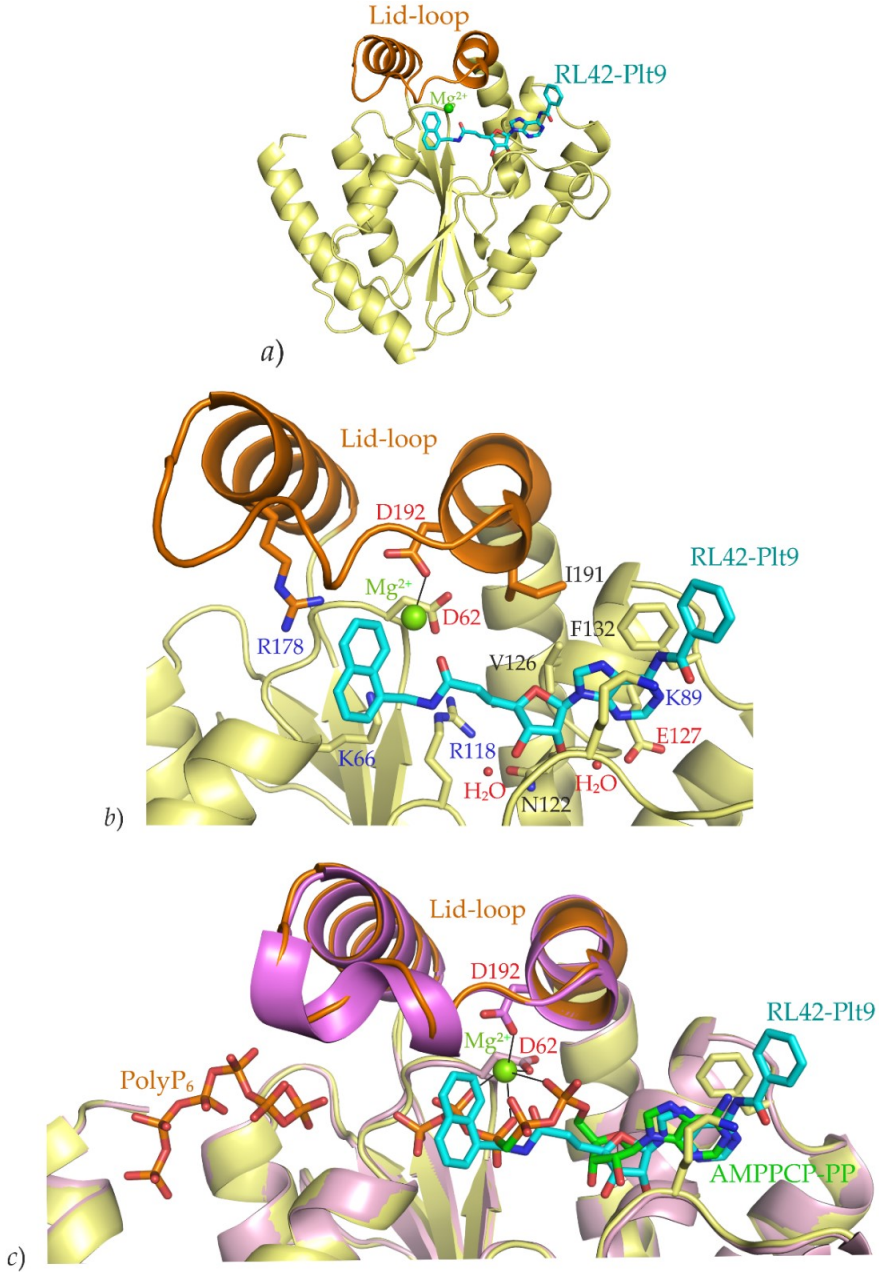

Figure 5.16: Model of the binding of RL42-Plt9 to *Ft*PPK

a) RL42-Plt9 orientation within the monomer; *b*) interactions of RL42-Plt9 with the active site region; *c*) overlay of the *Ft*PPK:RL42-Plt9 model with the *Ft*PPK:AMPPCP-PP structure determined by A Parnell.[265] For the *Ft*PPK:RL42-Plt9 complex, the protein is shown in pale yellow, the lid-loop in orange, the RL42-Plt9 in blue, Mg^{2+} in green. For the *Ft*PPK:AMPPCP-PP complex, the protein is shown in pink, the lid loop in violet, the AMPCPPP is shown in green.

The anticipated interactions between the Mg^{2+} ion and the C=O group of the RL42-Plt9 side chain were not observed. Although the carbonyl group pointed towards the right direction, the distance from the Mg^{2+} was greater than that required for coordination (typically 2.1-2.2 Å). However, it is worth noting that, following dynamic perturbation, the Mg^{2+} was slightly left-drifted in comparison to its original position within the *Ft*PPK:AMPPCP model (compare Figure 5.13*c* with Figure 5.16*c*). According to the preliminary SAR studies (section 5.2.2.4), the naphthyl-methyl amide functional group of compound RL42-Plt9 appears to be critical to retain significant activity towards the *Ft*PPK. The generated model does not indicate any likely interactions of the acrylamide moiety of compound RL42-Plt9 with the surrounding amino acids. Since the removal of the double bond resulted in a significant reduction of the activity (section 5.2.3), it could be hypothesized that the presence of the double bond may serve the purpose of maintaining a certain degree of rigidity that allows the positioning of the aromatic system in a favourable orientation within the active site. The preliminary SAR investigation revealed the relevance of a bicyclic aromatic system to preserve the activity, whereas loss of activity was observed in the presence of only one aromatic ring or in the presence of a second non aromatic ring (e.g. compounds RL37-Plt9, RL77-Pl9, RL26-Plt9, section 5.2.3). In the generated model, the aromatic system is placed at the center of the catalytic pocket, under the lid-loop (Figure 5.17*a*), a position corresponding approximately to the binding site of the terminal phosphates of the polyP chain (Figure 5.13*a*). It is possible to hypothesize that the naphthyl group could engage in pi-cation interactions with the Arg178 (hence rationalizing the requirement for an aromatic bi-cyclic system, Figure 5.16*b*), which has been proposed to be involved in the binding of the polyP in proximity to the catalytic site (Figure 5.11 and Figure 5.14).[265] Speculating that the different orientation of the adenosine moiety of RL42-Plt9 was a perturbation artefact, and assuming that in reality it would match the AMPPCP adenosine position in the active site, therefore being slightly left shifted, a possible additional interaction of the naphthyl group with the Trp186 by pi-stacking could be anticipated (Figure 5.17). For compound RL54-Plt9, the analogue that showed a comparable activity to RL42-Plt9 (section 5.2.3), in which an ethylene linker instead of a methylen linker connects the amide function with the aromatic bicyclic system, the latter could be in an

even more favourable position for the pi-stacking with the Trp186. Furthermore, the methoxy group of compound RL54-Plt9 could possibly engage in the formation of an H bond with some amino acid residues of the lid loop. On the basis of the obtained model, it is possible to speculate that the binding of compound RL42-Plt9 interferes with the binding of polyP in a position favourable to access the catalytic site, hence preventing the phosphorylation to occur.

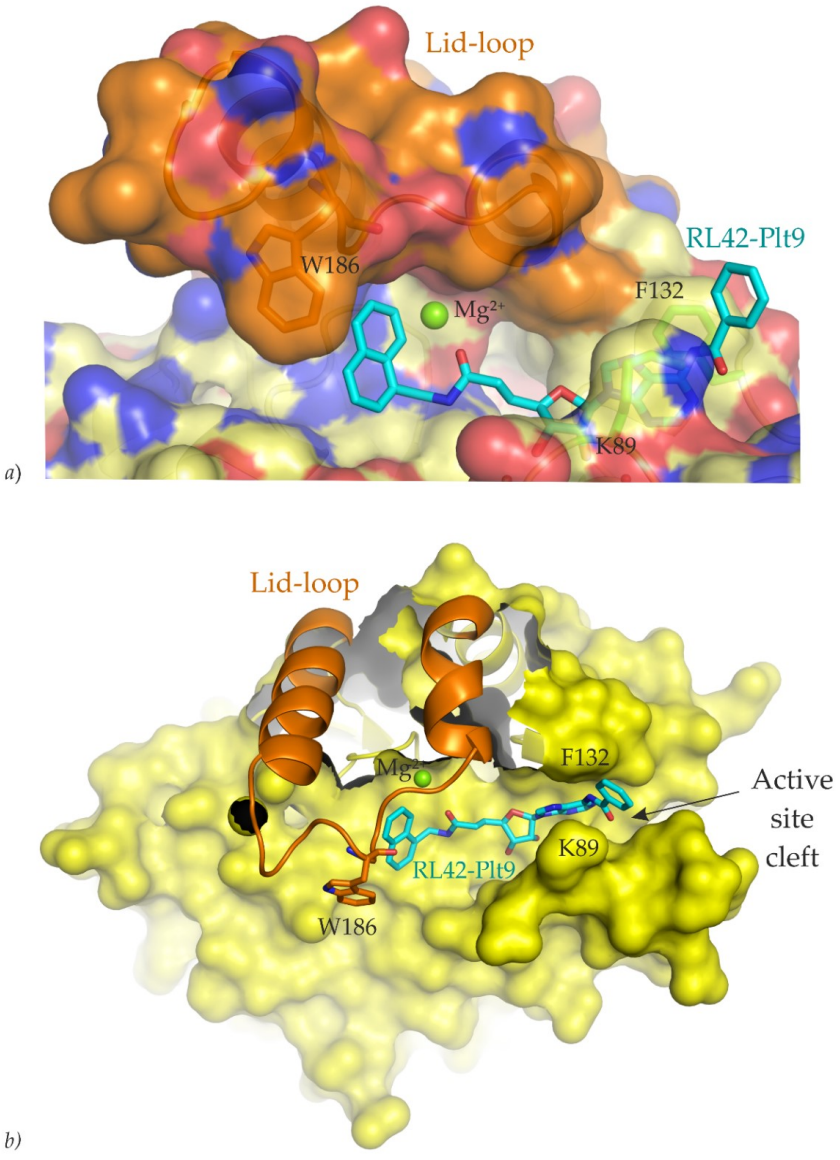

Figure 5.17: Model of the binding of RL42-Plt9 to *Ft*PPK, electron density surface

a) Model of the *Ft*PPK:RL42-Plt9 complex showing the active site surface; *b*) *Ft*PPK:RL42-Plt9 complex active site from a different angle. The uniform yellow surface was selected to emphasize the perspective of the active site cleft.

5.3. Summary

Compound RL42-Plt9, the confirmed hit from the Reynolds library screening, was re-synthesised via a concise convergent route. The double bond linking the adenosine moiety to the naphthyl-methyl amide moiety was prepared by Wittig reaction. The two isomers were obtained in a 75:25 ratio of *E*/*Z*-isomers. Overall, the active *E*-isomer was obtained in a 29.5% yield. The bottleneck of the synthetic procedure was the oxidation of the adenosine to the correspondent aldehyde by Dess-Martin reaction (58% yield). It was hypothesized that the low yield could be attributed to side reactions (hydrate formation and depurination of the starting material), favoured by the acidic environment due to acetic acid release during the reaction.

The activity of the pure *E* and *Z* isomers on the *Ft*PPK was tested by HPLC assay (at 50 μM and 100 μM). No significant activity was observed for the *Z* isomer while a concentration dependent activity was confirmed for the *E* isomer (34.7 ± 1.2% at 50 μM, 54.8 ± 0.9% at 100 μM). The *E* isomer of compound RL42-Plt9 was further characterised by IC_{50} measurement and the mechanism of binding investigated. Based on the preliminary assumption that compound RL42-Plt9 would compete with ADP for binding, derived from the structural analogy with adenosine, the experiments for RL42-Plt9 characterization were prepared at K_m concentration of ADP (200 μM) and in the presence of saturating concentration of $polyP_{25}$ (30 μM). The latter helped to maintain a good degree of sensitivity for the HPLC assay.

Under the conditions applied, the IC_{50} for *Ft*PPK was 99 ± 9 μM. Given the presence of a Michael acceptor functional group within the structure of compound RL42-Plt9, possible covalent binding was investigated by biochemical assay (jump dilution assay) and by mass spectrometry. However, in both cases evidence for a reversible mechanism of binding was provided. The mechanism of binding was further investigated with respect to ADP, testing the effect on the reaction rate of different concentration of RL42-Plt9 at different concentration of ADP. The data suggested that binding of RL42-Plt9 occurred in a non-competitive modality and a K_i of about 50 μM was estimated by Dixon plots. This data was not necessary in conflict with the estimated IC_{50}, but could be rationalized in view of the

conditions applied for the IC_{50} measurement, where an excess of $polyP_{25}$ was used. Indeed, in the hypothesis of a possible RL42-Plt9 competition with polyP, the use of polyP concentration $> K_m$ would result into the detection of a weaker binding, hence of an $IC_{50} > K_i$.

The activity of compound RL42-Plt9 was also tested on *Mr*PPK, a PPK2 enzyme belonging to class III. As opposed to *Ft*PPK (class I), which can only use nucleotide diphosphates for the synthesis of nucleotide triphosphates, the *Mr*PPK can also phosphorylate nucleotide monophosphates. In the presence of RL42-Plt9, an increase of the ATP produced, in correspondence to an increase of the ADP consumed, was observed at equilibrium, as well as an attenuation of the AMP concentration. It was hypothesized that the binding of RL42-Plt9 would interfere with the dephosphorylation of ADP, perhaps favouring the ATP synthesis. Although of difficult interpretation and certainly requiring further investigation, the effect of RL42-Plt9 on the *Mr*PPK activity anticipates the possibility of binding to other PPK2 enzymes.

Despite the attempts, the co-crystallization of compound RL42-Plt9 with the *Ft*PPK was not successful. To gain some insights into the possible interactions with the active site, the RL42-Plt9 was modelled into the *Ft*PPK binding pocket using Phenix (Simple Dynamics function), guided by a model derived by co-crystallization of the *Ft*PPK with the non-hydrolysable AMP-PCP. By superimposition of the adenosine moieties of RL42-Plt9 and AMP-PCP, it was possible to define the possible orientation of RL42-Plt9 within the active site. Although a more powerful modelling software would have probably provided a greater accuracy and reliability, the model generated by Phenix highlighted some potentially key interactions between compound RL42-Plt9 and the *Ft*PPK active site. In particular, the positioning of the aromatic bicyclic system at the catalytic active site and its possible interaction with Arg178 helped to rationalize the preliminary SAR and why the expected competition for binding with ADP was not confirmed by biochemical assays. Indeed, it was hypothesized that adenosine moiety contributes to the binding by anchoring the molecule to the nucleoside binding pocket, while the *N*-methyl-acrylamide moiety serves the purpose of protruding the aromatic bicyclic system slightly beyond the catalytic active site. But it

is actually the position of the bicyclic aromatic system under the lid-loop, potentially favoured by interactions with the Arg178 and the Trp186, that was considered to play the major role into RL42-Plt9 activity, possibly by preventing the polyP from binding or getting access to the catalytic site. The hereby formulated hypothesis certainly require validation by further biochemical investigation of the mode of action of RL42-Plt9 with respect to polyP (e.g. competitive, non-competitive or uncompetitive) but also by crystallographic model derived by co-crystallization of RL42-Plt9 with the *Ft*PPK.

Chapter 6

Conclusion and future work

6.1. Conclusion

6.1.1. *Ft*PPK-FLuc assay development and screening

A luminescence coupled assay was optimised to measure the activity of the *Ft*PPK (*Ft*PPK-FLuc assay) as a function of the polyP-driven phosphorylation of ADP. The optimisation of the *Ft*PPK concentration (primary enzyme) and of the FLuc concentration (secondary enzyme) constituted the critical step to ensure that the detection signal was a measure of *Ft*PPK activity (optimal concentrations: 10 nM *Ft*PPK and 300 nM FLuc). The optimised *Ft*PPK-FLuc assay was validated by kinetic characterization of the *Ft*PPK, where the K_m for ADP was defined as 206 ± 30.9 μM and the K_m for $polyP_{25}$ as 1.27 ± 0.15 μM.

The protocol for the *Ft*PPK-FLuc coupled assay was optimised in an end point format for HTS. The substrate conditions were adjusted to K_m concentrations for both the ADP and the $polyP_{25}$ (200 μM and 1.5 μM, respectively) to allow detection of possible competitive inhibitors. The *Ft*PPK activity was measured as a function of the apparent initial rate (v_0) by stopping the assay after 90 sec (a time point well within the linear progression of the *Ft*PPK time course). The end point format assay was adapted to a 384 well plate to an optimal standard for HTS (Z'-factor > 0.7).

The optimised *Ft*PPK-FLuc assay in end point format was applied for the screening of two small libraries: the PKIS library (a collection of 358 kinase inhibitors, competitive with ATP, provided by GSK) and the Reynolds library (a collection of 736 nucleoside and nucleotide analogues, provided by R. Reynolds from the University of Alabama). The libraries were screened at 10 μM concentration (5% DMSO). The hits cut-off criterion was

set in both cases as 2MAD, to allow selection of weak inhibitors although increasing the potential for a greater false positive rate. The hit rate was 11.1% for the PKIS screening and 4.5% for the Reynolds library screening.

6.1.2. Hit validation

The first step towards the validation of the obtained hits was a counter screening with the independent luminescence assay to identify compounds that inhibited the FLuc (false positive). Most of the hits, both from the PKIS and from the Reynolds library screening, showed activity towards the FLuc. Some of them were identified as possible real *Ft*PPK inhibitors by comparison of the performance in the coupled assay and in the independent luminescence assay.

Validation of the hits was attempted also by thermal shift assay at the concentration of 100 μM for the PKIS hits and at 50 μM and 100 μM for the RL42-Plt9 hits. None of the PKIS hits showed any significant T_m. Among the Reynolds library hits, compounds RL60-Plt7, RL37-Plt7 and RL20-Plt2 showed an increase of the T_m significant with respect to the remaining hits although not big in magnitude. Overall, the thermal shift assay was not judged suitable for hit validation and the development of an alternative biochemical assay was sought.

An HPLC-based *Ft*PPK assay in end point format was developed for hit validation, in which the *Ft*PPK reaction was monitored as a function of ATP production. Conditions analogous to the coupled assay were applied for hit validation (10 nM *Ft*PPK, 200 μM ADP), except for $polyP_{25}$, which was used at saturating concentrations (30 μM), due to issues with the detection sensitivity of HPLC analysis. An end point format of the HPLC-based assay was developed, where the activity of the *Ft*PPK was stopped by addition of EDTA after 7 minutes, a time point at the top although still within the linear phase of the *Ft*PPK time course. The format was validated by assessing the ability of reproducibly detect a 20% inhibition, hence proving suitable for hit validation.

The HPLC-based *Ft*PPK assay in end point format was applied for the validation of the hits (10 μM) from the PKIS and the Reynolds library screening. Among the PKIS library

hits, two compounds were identified as potential *Ft*PPK inhibitors: compound JO7-4 and compound JOM-69. However, none of them was followed up due to limited availability.

Among the Reynolds library hits, two compounds were selected: compound RL42-Plt9 and compound RL41-Plt8. Both compounds were re-tested at 50 μM, which allowed to confirm *Ft*PPK inhibition. Due to limited availability, it was necessary to re-synthesize the compound of interest for further characterization. Hence, it was decided to follow up only on compound RL42-Plt9, which appeared to be more potent.

6.1.3. Characterization of the confirmed hit RL42-Plt9

The key-step for the synthesis of compound RL42-Plt9 was the formation of the double bond between the naphthyl-methyl-amide moiety and the adenosyl moiety by Wittig reaction. In preparation for the Wittig reaction, a 5'-adenosine aldehyde was prepared by mild oxidation of the correspondent adenosine by Dess-Martin reagent and the ylide of the naphthyl-methyl-amide was generated *in situ* to attenuate decomposition. Compound RL42-Plt9 was synthesised as a couple of *E*:*Z* isomers in a 75:25 ratio. Overall, the yield of the *E* isomer, the active isomer, was only 29.5%.

The activity on the *Ft*PPK of both pure isomers of compound RL42-Plt9 were tested by HPLC assay at 50 μM and 100 μM. While concentration dependent activity was observed for the *E* isomer, the *Z* isomer did not show any significant inhibition. An IC_{50} of 99 ± 9 μM was determined for compound RL42-Plt9, in the presence of K_m concentration of ADP and saturating concentration of polyP. Investigation by biochemical assay and by mass spectrometry revealed reversible binding while the mechanism of binding was defined as non-competitive with respect to ADP. A K_i of 50 μM was determined by Dixon plots. For RL42-Plt9 characterization, polyP was maintained at saturating concentration while ADP at K_m for IC_{50} measurement or titrated for MOA studies, based on the assumption that RL42-Plt9, being an adenosine analogue, would compete with ADP.

By comparison with the activity of RL42-Plt9 analogues included in the Reynolds library, a preliminary SAR was formulated, which was rationalized with the support of a model of the RL42-Plt9 binding into the *Ft*PPK active site. According to the formulated model, the

adenosine moiety of RL42-Plt9 contributes in anchoring the molecule in the active site by interaction with the nucleoside binding pocket. No interactions were observed for the benzyl amide functional group at the N6 position of the adenine. Substitution of the adenine with a pyrimidine base resulted in the loss of activity. The acrylamide moiety did not appear to be involved in any significant interactions, although it was speculated that the carbonyl group could potentially be involved in the coordination of the Mg^{2+} ion. About a two-fold reduction, but not a complete loss of activity, was observed in the absence of the double bond, confirming that the Michael acceptor function is not involved in the mechanism of action. It was hypothesized that perhaps the double bond confers a certain degree of rigidity to the system, contributing to place the bicyclic aromatic system in a favourable position. Indeed, the naphthyl group was located to the left of the catalytic site, just under the lid-loop and interactions with the Arg178 and Trp186 were hypothesized. The bicyclic aromatic system proved to be essential for retention of activity, which was instead significantly attenuated in the presence of a single aromatic ring and completely lost in the presence of a non-aromatic ring. Activity was fully retained in the presence of an indole group in place of the naphthyl group. Whether a methyl group or an ethyl group as a linker to the acrylamide moiety favours the positioning of the aromatic system for the hypothesized interactions with Arg178 and Trp186 remains to be investigated.

It was speculated that the ability of compound RL42-Plt9 to inhibit the *Ft*PPK is ascribable to the interference with the binding of polyP into the active site. In particular, it has been hypothesized that the Arg178 is involved in the binding of the terminal phosphates of the polyP chain in proximity to the catalytic site. In the presence of compound RL42-Plt9, the access of the polyP into the active site is limited, probably due to either steric hindrance or to the limited availability of Arg178, which could potentially be engaged in interactions with the aromatic bicyclic system. If this will be confirmed to be the case, it is possible to envisage the possibility of using compound RL42-Plt9 as a scaffold for the development of a more potent inhibitor that not only can bind to the nucleoside pocket (a common feature for kinase inhibitors) but that also provides the potential for interactions with an area of the active site whose topography is potentially very specific for polyP binding enzymes.

6.2. Future work

6.2.1. Complementary MOA studies for RL42-Plt9 binding characterization

To improve our understanding of PPK2 inhibition, further characterization of the potency and mechanism of action of compound RL42-Plt9 should be undertaken. In particular, IC_{50} measurements should be repeated in the presence of K_m concentration of polyP and the mode of binding (competitive, non-competitive and uncompetitive) should be investigated with respect to polyP, while maintaining the concentration of ADP at saturating concentration. If the hypothesis formulated on the interactions of compound RL42-PLt9 with the active site are correct, it is likely that competition with polyP will be observed, and possibly a lower IC_{50} value.

For additional insights on RL42-Plt9 interaction within the active site, the ability of compound RL42-Ptl9 to bind directly to the apo enzyme or the requirement for either polyP or ADP (or both), possibly responsible for inducing conformational changes favourable to catalysis, can be investigated by ITC. The latter can be used also to clarify if interaction of compound RL42-Plt9 with the Mg^{2+} ion occurs during binding and to what extent they affect the affinity (e.g. if Mg^{2+} is required for binding or if it favours binding).

To validate the interaction of compound RL42-Plt9 with the Arg178 and Trp186, the activity of RL42-Plt9 could be tested with *Ft*PPK mutants where these amino acids are mutated in alanine residues. This study could include both single mutants (R178A already prepared by A. Parnell)[265] but also double mutants (R178A plus W186A mutants) could be tested. Attenuation or abrogation of the RL42-Plt9 activity should be observed for compound RL42-Plt9 if the interactions with these amino acids are important or essential, respectively, for activity.

6.2.2. Binding affinity determination by biophysical methods

Measurements of binding affinity by IC_{50} curves or by biochemical assays provide only an estimate of an inhibitor potency, due to the impact of experimental conditions (e.g. substrate concentration) on the activity displayed. An accurate measurement of potency is provided by the direct measurement of the binding event to the active site. The technique that is probably best suited to this purpose is ITC, which allows not only to directly measure the

binding affinity (K_a) but also to define the thermodynamic profile (ΔH and ΔS).[520,521] Some preliminary ITC experiments conducted during this project were not successful, principally due to issues with solubility of compound RL42-Plt9 in conjunction to the estimated low binding affinity (IC_{50} = 99 ± 9 μM, although this was measured in the presence of polyP excess). According to the modelling studies of the RL42-Plt9 interaction with the active site, the adenine N6-benzoyl amide is not involved in any binding interactions. The removal of this functional group may improve the molecule solubility, allowing investigation of the binding of the resultant inhibitor at higher concentrations. To address the difficulties to detect the binding due to the low affinity of compound RL42-Plt9, displacement experiments can be attempted.[522,523] Indeed, the binding of a ligand with low affinity can be characterised exploiting the binding of a ligand with higher affinity, by titration of a high affinity ligand into a solution of the respective target incubated with the inhibitor of low affinity (at concentrations comparable to the expected K_d). Knowing the K_a and the ΔH of the high affinity ligand, derived by a titration into a solution of only target, the corresponding parameters can also be derived for the ligand of low affinity.[522,523] If the competitive binding with respect to polyP is confirmed by MOA studies, the affinity of RL42-Plt9 can be determined from displacement experiments of polyP, whose binding to the *Ft*PPK (K_d: 0.6 μM) has succesfully been characterised by A. Parnell using ITC.[265]

Another biophysical method that can be applied for the investigation of the RL42-Plt9 binding to the *Ft*PPK is the Saturation Transfer Difference (STD) NMR.[524–526] STD is based on the nuclear Overhauser effect, where transfer of magnetization occurs through space via spin diffusion from the target to the bound ligand. STD can be used for determination of K_d and enable identification of the ligand atoms that are directly involved in the binding with the protein (binding epitope).[527] Investigation of RL42-Plt9 binding by STD would provide an alternative method to directly confirm the interaction with the active site, potentially validating the proposed binding model in case co-crystallization studies are not going to be succesful.

6.2.3. Optimisation of the synthetic route for the synthesis of RL42-Plt9 and respective analogues

The major problem encountered for the synthesis of compound RL42-Plt9 was the recovery of the desired isomer (*E* isomer) in a less than optimal yield (29.5%). In particular, the latter was affected by the adenosine oxidation step but also by the formation of the *Z* isomer.

It was hypothesized that yield of the adenosine oxidation suffered from the formation of aldehyde hydrates and depurination of the starting material, possibly favoured by the acidic environment due to the release of acetic acid during the reaction. To improve the yield of the oxidation step, buffering of the reaction mixture with $NaHCO_3$ could be attempted, although the concentration of $NaHCO_3$ should be carefully balanced to prevent possible elimination at C-3' with formation of a double bond with C-4', to which adenosine aldehyde are susceptible under basic conditions.[528]

To improve the selectively towards the *E* isomer of compound RL42-Plt9, the Horner-Wadsworth-Emmons reaction could be investigated as an alternative to the Wittig reaction. In the Horner-Wadsmorth Emmons (HWE) reaction the formation of a double bond occurs by reaction of an aldehyde with a phosphonate rather than with an ylide.[481,529,530] Although a stabilized ylide was used for the Wittig reaction, the recovery of the *E*:*Z* isomers was in a 75:25 ratio. If the HWE is reaction is applied, a range of phosphonates can be tested, where bulkier phosphonates have been reported to improve the selectivity towards the *E* isomer (Scheme 6.1).[531,532]

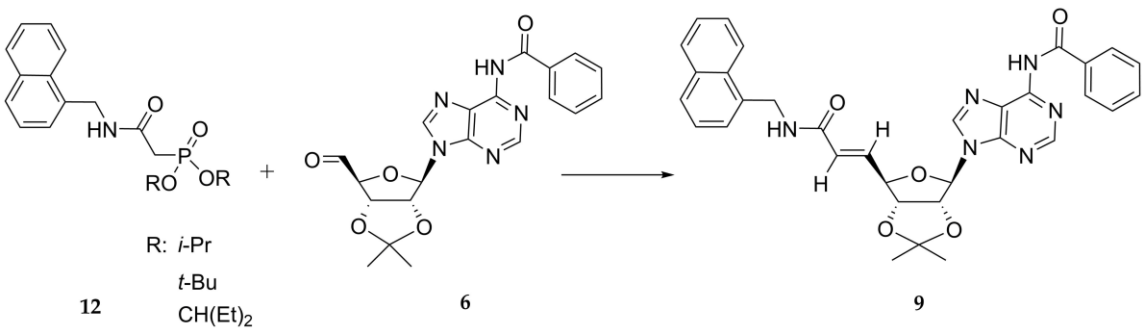

Scheme 6.1: **Horner-Wadsmorth Emmons reaction**

6.2.4. Medicinal chemistry optimisation of compound RL42-Plt9 and further SAR investigation

The following suggestions on possible structural modifications to investigate the role of specific moieties and in the attempt of improving the affinity for the active site are based on the *Ft*PPK:RL42-Plt9 model described in section 5.2.4.1.

In support of biochemical experiments and crystallography, to define the role of the naphthyl-methyl acetamide moiety, the adenosine moiety should be removed and the ability of the naphthyl-methyl acetamide to interact on its own with of RL42-Plt9 should be investigated. The removal of the adenosine moiety may result in significant attenuation of the activity, as observed for the RL42-Plt9 analogues with a pyrimidine in place of the adenine. Hence, the naphthyl-methyl acetamide could be dealt with as if it were a fragment (e.g. binding assessed at high concentration and by biophysical methods).

Investigation of the role of the bicyclic aromatic system in the binding should involve testing: the substitution with heteroatoms of the C in position *ortho* and *meta* of the ring attached to the methyl-amide function; the variation of the ring size (e.g. an indole system in place of the naphthyl, Figure 6.1). To build additional interactions, possibly with the region within the active site involved in the polyP binding, functional groups may be added in the second ring of the aromatic bicyclic system (e.g. to form H bonds with the Lys187).

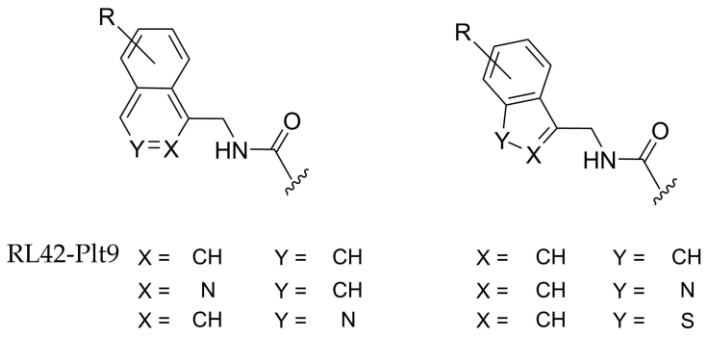

Figure 6.1: Possible aromatic bicyclic system substitutions

Modification of the linker between the naphthyl group and the acrylamide functional group could also result in the modulation of the enzyme activity. In particular, the following modifications may be investigated: the effect of the linker length (e.g. $(CH_2)_n$ with $1<n<4$),

with the purpose of locating the aromatic bicyclic system in a more favourable position for the potential interaction with Arg178 and the Trp186; introduction of a substituent with a negative charge (e.g. carboxylic acid) in α to the amide group, to target interaction with the Lys66 (involved in the polyP binding);[265] substitution of the linker with possible isosters (Figure 6.2).[533]

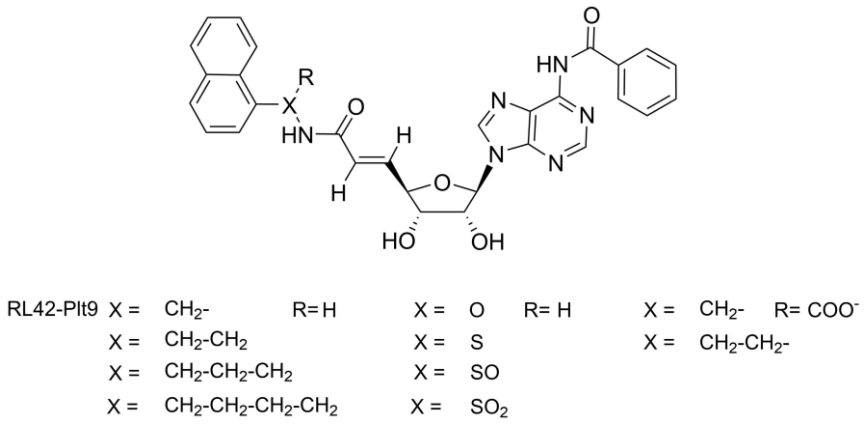

Figure 6.2: Possible linker substitutions

When modelled, the benzoylamide group at the N6 of the adenine did not appear to engage in any interactions with the active site but appeared to be protruding out from the nucleoside cleft. The removal of this functional group could be advantageous due to the potential increase of the overall polarity of compound RL42-Plt9, therefore improving the solubility in hydrophilic environment (including assay solution and cell culture). Finally, the substitution of the ribose and/or the adenine moiety with various bioisosters should be investigated to improve the binding affinity to the nucleoside cleft.

6.2.5. Optimisation of a crystal form for co-crystallization of compound RL42-Plt9 and respective analogues.

The co-crystallization of compound RL42-Plt9 with the *Ft*PPK is a critical objective, to help clarify the RL42-Plt9 mechanism of binding by identification of the key-interaction with the active site and to identify new possible interactions to increase the inhibitor potency. To achieve this goal two approaches can be taken: the identification of a new crystal form and soaking of compound RL42-Plt9 into known crystal forms of the protein.

Either way, the crystallization conditions, in terms of RL42-Plt9 concentration and substrate concentration, must be carefully defined based on the pre-determined binding parameters. In the preliminary co-crystallization experiments a 1:1 ratio of RL42-Plt9 and $polyP_{25}$ (500 μM) was used. However, under these conditions it is likely that the *Ft*PPK active site was saturated with $polyP_{25}$, given the high affinity of polyP (K_m: 1.5 μM) and the low affinity of RL42-Plt9 (estimated K_i: 50 μM), and in view of the newly hypothesized scenario where RL42-Plt9 may compete with the polyP for binding to the active site. Perhaps future co-crystallization and soaking experiments should be done in the absence of polyP and with an excess concentration of RL42-Plt9. However, the presence of $polyP_{25}$ at low concentration may be required for co-crystallization with RL42-Plt9. The latter hypothesis is formulated on the basis of the structural analogy of RL42-Plt9 with ADP and given the unsuccessful attempts of A. Parnell to co-crystallize ADP with *Ft*PPK in the absence of polyP, later rationalized with the requirement of polyP for the binding of ADP (investigated by ITC).[265]

6.2.6. Investigation of RL42-Plt9 activity on other PPK2s

The Arg178 and the Trp186, as well as the other amino acids constituting the lid-loop, are highly conserved in all the PPK2 enzymes.[229] If the hypothesized interaction with these amino acids is confirmed, then compound RL42-Plt9 hold a greater potential for binding to PPK2s from different subclasses and from a wide spectrum of microorganisms. To investigate the possible spectrum of action, the activity of compound RL42-Plt9 should be tested on other PPK2-like enzymes from relevant pathogens (e.g. PPKs from *P. aeruginosa*, *M. tuberculosis, Y. pestis, B. pseudomallei*), belonging to the same class as the *Ft*PPK (class I) but also to class II and III.

In conclusion, following the development of a suitable assay for HTS, an inhibitor of the *Ft*PPK was identified. Supported by some preliminary characterization, including insights into the mechanism of action, the elaboration of a preliminary SAR and of a model of the interactions with the active site, compound RL42-Plt9 constitutes a valid starting point for

the development of a more potent inhibitor with the potential to selectively target polyphosphate kinases due to the possible interactions with the polyP binding site.

Chapter 7

Experimental

7.1. Materials

Chemicals: biochemistry and molecular biology

All the reagents, unless otherwise specified were purchased from Sigma-Aldrich or Fischer Scientific. Bacto-tryptone and yeast extract was purchased from Oxoid. DTT, IPTG and antibiotics were purchased from Melford laboratory. EDTA-free Protease inhibitor cocktail (cOmplete^{TM}) was purchased from Roche. SYPRO® Orange Protein Gel Stain was purchased from ThermoFischer.

Chemicals: synthesis

All reagents were of synthetic grade (purchased from Sigma Aldrich, Fluka, Fisher Scientific). 1-naphthylmethylamine, triphenylphosphine and Dess-Martin periodinane were purchased from Sigma-Aldrich. N6-Benzoyl-2,3'-isopropylidene adenosine was purchased from Carbosynth. Anhydrous DCM and Et_3N were obtained from Prof. B. Linclau laboratory (University of Southampton).

Compound libraries

The Reynolds library was kindly donated by Prof. Robert C. Reynolds, Southern Research Institute (Birmingham, Alabama, USA). The PKIS library was obtained from GlaxoSmithKline.

Chromatography

Chelating sepharose Fast Flow resin, Superdex 75 resin and DEAE-sepharose Fast-Flow resin were purchased from GE Healthcare Life Sciences. Silica Gel 60 and pre-coated

aluminium sheets of Silica Gel 60 for TLC were purchased from Merck. Analytical HPLC column (Gemini C18 110A, 150 x 4.6 mm) and respective safety guard cartridges (Gemini C18, 4 x 3.00 mm) were purchased from Phenomenex. HPLC grade solvents were purchased from Fischer Scientific. Ion pairing agents DMHA and TEA were purchased from Sigma-Aldrich.

E. coli strains

E. coli K12 JM109 was purchased from New England Biolabs. BL21 Rosetta^{TM} pLysS (DE3) was purchased from Merck.

Enzymes

FLuc, *Ft*PPK and *Bp*PPX were expressed and purified in house from the correspondent plasmid. *Mr*PPK was expressed and purified by A. Parnell from the plasmid donated by Dr J. N. Andexer (University of Freiburg, Germany).

Luminescence assay and HTS

D-Luciferin was purchased from Apollo Scientific. ADP was purchased from Sigma and purified by anion exchange. PolyP was purchased from Merck and the average chain length was estimated to be 25 Pi units (by ^{31}P-NMR).[264] White 96 well plates (polystyrene, half are medium binding, max volume 170 µL) and white 384 well plate (polystyrene, flat bottom, lumitrac, medium binding, max volume 120 µL) were purchased from Greiner Bio-One. Tips for the liquid handling workstation were purchased from Beckman Coulter.

Plasmids and primers

The rLuc plasmid was purchased from GeneArt and the expression plasmid was prepared by J. Docherty.[352] The *Ft*PPK gene was amplified by PCR from the *F. tularensis* genome by L. Batten.[264] The *Ft*PPK expression plasmid was prepared by L. Batten.[264]

7.2. Equipment

Automated assay preparation

Assays were prepared in appropriate microplates by addition of working solution using Beckman Coulter Biomek3000 laboratory automation workstation at room temperature.

Centrifugation

Sorvall Evolution RC centrifuge (4°C), adapted with rotors of different size, were used to pellet cell culture and to clarify lysates prior protein purification. Small volume samples were centrifuged in a bench centrifuge Eppendorf 5415D at room temperature.

Data analysis

Row data were pre-analysed by using Microsoft Excel. For graphical representation and statistical analysis, GraphPad Prism 6 was used. To draw chemical structures ChemBioDraw Ultra 12.0 was used. For the crystallographic model, WinCoot and Phenix were used. PyMol was used for .pdb file visualization and to create images of the model.

Fast protein liquid purification (FPLC) chromatography

The ÄKTAPrime chromatography system (GE Healthcare) was used to operate Nickel chromatography (Ni-sepharose Fast Flow) and anion exchange chromatography (DEAE sepharose Fast Flow).

Gel imaging

The SynGene Genius Imager system was used for imagining of SDS-PAGE gels.

High pressure liquid chromatography (HPLC)

The HPLC analysis was carried out using a Gilson 321 Pump workstation, with H1 heads and a Gilson 234 Autoinjector system and a dual wavelength UV-vis 155 detector. Chromatograms were generated by Gilson Unipoint Software 5.11.

pH measurement

The pH was determined using a SevenCompact S220 Mettler Toledo pH meter connected to a Inlab Power PRO-ISM Mettler Toledo electrode. The equipment was calibrated at pH 4.0-7.0 or pH 7.0-10.0 before use.

Thermal shift assay

A real time PCR machine CFX96 Real-Time PCR detection system (Bio-rad) was used for thermal profiling of protein.

Spectroscopy

The plate reader POLARStar Omega (BMG LABTECH), equipped with two built in injectors (200 μL), was used for detection of luminescence and for absorbance measurements. The plate reader is operated by means of control protocols in which the type of measurement (luminescence, fluorescence, fluorescence polarisation and absorbance) and respective parameters can be set up. Scripts can be written to run a sequence of control protocols with the possibility to set delays in between consecutive protocols.

7.3. General methods and protocols

7.3.1. Microbiology and molecular biology techniques

7.3.1.1. General microbiology technique

Standard sterile technique was applied to microbiology experiments. Growth media was sterilised by autoclave. Heat labile components (e.g. glucose, IPTG, ampicillin) were filter sterilised and added to the media upon cooling (50°C). Antibiotics were added as required in the following concentrations: ampicillin 100 μg/mL, chloramphenicol 30 μg/mL (in ethanol).

7.3.1.2. 2x YT media

The media for liquid bacteria culture was prepared as reported in Table 7.1.

Table 7.1: 2x YT media

Component	Concentration	Quantity
Bacto-tryptone	1.6%	16 g
Bacto-yeast extract	1%	10 g
NaCl	0.5%	5 g
DI water		up to 1 L

7.3.1.3. 2x YT agar plate

Agar plates were prepared by supplementing 2x YT media with agar (Table 7.2). Following sterilisation by autoclave, the media was left to cool in the MSC to about 50°C and the required antibiotic added. The media was poured in Petri dishes and left to set. The plates were stored at 4°C.

Table 7.2: 2x YT agar plate

Component	Concentration	Quantity
Bacto-tryptone	1.6%	8 g
Bacto-yeast extract	1%	5 g
NaCl	0.5%	2.5 g
Agar	15%	7.5 g
DI water		up to 500 mL

7.3.1.4. Overnight culture

Overnight cultures were prepared by inoculation of a single well isolated colony from freshly transformed cells (section 7.3.1.7) or a loop of cells from a glycerol freeze (section 7.3.1.5) into 2xYT media (section 7.3.1.2) supplemented with the appropriate antibiotic (small scale: 10 mL 2x YT media; large scale: 100 mL 2x YT media). The culture was incubated overnight (37°C, 180 rpm) alongside a negative control constituted by 2x YT media supplemented with antibiotic.

7.3.1.5. Glycerol stock

Glycerol stocks were prepared from overnight cultures (500 μL, section 7.3.1.4) by addition of 75% glycerol solution (500 μL) previously sterilized by autoclave. The glycerol stocks were stored at -80°C.

7.3.1.6. Competent cells

Competent cells were chemically prepared with the RbCl method. Previously made competent cells of the desired *E. coli* strain (either JM109 or XL10 Gold) were plated on agar plate (section 7.3.1.3) and incubated overnight (37°C). A single well isolated colony was used to prepare an overnight culture in 2x YT media (10 mL, section 7.3.1.4) and this in turns was used as inoculum (1%) for a 100 mL culture in 2x YT media, supplemented with the required antibiotic. The culture was incubated (37°C, 180 rpm) until OD_{600} 0.6 was reached. The cells were placed on ice for 10 minutes and then centrifuged (4000 rpm, 10 min, 4°C). The supernatant was discarded and the cell pellet gently resuspended in ice cold TBF I buffer (10 mL, Table 7.3).

Table 7.3: TBF I buffer

Component	Concentration	Quantity
RbCl	100 mM	12.1 g
$MnCl_2$	50 mM	9.9 g
KOAc	30 mM	2.9 g
$CaCl_2$	10 mM	1.1 g
Glycerol	15%	150 mL
DI water		up to 1 L

Adjusted to pH 5.8 with acetic acid and filter sterilised. Stored at -80°C

The cells were incubated on ice for 15 minutes and then harvested by centrifugation (4000 rpm, 20 minutes, 4°C). The supernatant was discarded and the cell pellet resuspended in ice cold TBF II buffer (1 mL, Table 7.4). The competent cells were aliquoted (100 µl), flash frozen in liquid N_2 and stored at -80°C.

Table 7.4: TBF II

Component	Concentration	Quantity
MOPS	10 mM	2.1 g
RbCl	10 mM	1.2 g
$CaCl_2$	75 mM	8.3 g
Glycerol	15%	150 mL
DI water		up to 1 L

Adjusted to pH 6.8 with NaOH and filter sterilised. Stored at -80°C

7.3.1.7. Transformation of competent cells

Competent cells were thawed on ice (10 min) and gently resuspended. The plasmid DNA (1 µL to 100 µL cells) or the DNA from PCR reaction (40 µL to 150 µL cells) was added to the cells, which were gently mixed and incubated on ice for 30 minutes. Following heat shock (42°C, 40 sec), the cells were returned on ice for 2 minutes. SOC media was added (250 µL, Table 7.5) and the cells incubated with shaking at 37°C (180 rpm, 1 hour).

Table 7.5: SOC media

Component	Concentration	Quantity
Bacto-trypton	2 %	20 g
Bacto-yeast extract	0.5 %	5 g
NaCl	10 mM	0.5 g
KCl	2.5 mM	250 mM, 10 mL
$MgCl_2$	10 mM	2 M, 5 mL
Water		980 mL
Adjust to pH 7 with 5 M NaOH and autoclave. Leave to cool then add:		
Glucose*	20 mM	20 mL

*Filter sterilised

Agar plates supplemented with the appropriate antibiotic were also incubated at 37°C. The cells were plated out on the agar plates (60 µL cells transformed with plasmid DNA, 150 µL cells transformed with PCR product) and incubated overnight at 37°C. A single well

isolated colony was picked to prepare an overnight culture (section 7.3.1.4). Sealed plates were stored at 4°C up to two weeks.

7.3.1.8. Plasmid purification

Overnight culture (10 mL, section 7.3.1.4) of *E. coli* cells carrying the desired plasmid were harvested by centrifugation (8000 rpm, 10 min, 4°C). The plasmid was purified from cell pellet using the Miniprep kit (Promega), following the manufacturer instruction. The plasmid DNA was eluted from the column by deionized sterile nuclease-free water (50 μL). To maximize the yield, the plasmid sample was reloaded onto the column and eluted again. The DNA concentration was measured by Nanodrop (1.5 μL).

7.3.1.9. Restriction digest

The gene of interest was digested from the purified plasmid with the appropriate restriction enzymes. The analytical digestion assays were prepared using the recommended NEB buffer, applying the conditions reported in Table 7.6. Alongside the double digest (both restriction enzymes), two single digest assays (only one restriction enzyme) were prepared to monitor the activity of each restriction enzyme, as well as a negative control assay (no restriction enzymes). The restriction digest assays were incubated at 37°C for 1 hour. The product was analysed by 1% agarose gel (section 7.3.1.10).

Table 7.6: Restriction digest

Component	Stock concentration	Final concentration	Vol/10 μL
Plasmid		50 -250 ng/μL	5
NEB Buffer	10 x	1x	1
BSA	1 mg/mL	0.1 mg/mL	1
Restriction Enz 1	10 -20 U/μL	1-2 U/μL	1
Restriction Enz 2	10 -20 U/μL	1-2 U/μL	1
DI water			1

* The enzymes were added as last; ** Single digest and negative control assays: corresponding volume of water added in place of enzymes.

7.3.1.10. Agarose gel electrophoresis

DNA was analysed by 1% agarose gel electrophoresis. The gel was prepared by adding agarose (1% w/v, 0.4 g) to TAE buffer (40 mL, Table 7.7). The suspension was heated by microwave until a clear solution was obtained. The solution was left to cool and while still liquid the fluorescent stain Nancy-520 (0.05% v/v, 2.5 μL) was added. The agarose solution was poured into a gel tray with a comb inserted and left to set at room temperature.

Table 7.7: TAE buffer

Component	1x Stock	50x Stock*	Quantity/50x
Tris base	40 mM**	2 M**	242 g
Acetic acid (glacial)			57.1 mL
EDTA	1 mM	50 mM	500 mM, 100 mL (pH 8)
DI water			up to 1 L

* Communal 50x stock prepared, diluted to 1x stock working solution; ** Tris acetate concentration.

To the DNA sample (10 μL) the agarose gel loading buffer (2 μL, 6x stock solution, Table 7.8) was added. The gel was loaded and the electrophoresis run on 1x TAE buffer (Table 7.7) at 90 V for 45 minutes. The gel was visualized by SynGene Genius Imager under transluminator UV light.

Table 7.8: Agarose gel loading buffer

Component	6x Stock	Quantity
Sucrose	40% (w/v)	4 g
Bromophenol Blue	0.25%	25 mg
DI water		up to 10 mL

Stored at 4°C

7.3.2. Biochemistry techniques

7.3.2.1. Protein expression

Following transformation of *E. coli* cells (BL21 DE3 or Rosetta BL21 DE3 pLysS) with the expression plasmid (section 7.3.1.7), an overnight culture was prepared by inoculation of either a loop of glycerol stock or a single well isolated colony from a freshly transformed plate into 2xYT media supplemented with the required antibiotic (section 7.3.1.4). The overnight culture was in turn used as a 1% inoculum for either a small scale expression (1 mL inoculum into 100 mL 2xYT) or for a large scale expression (4x 12.5 mL inoculum into 4x 1.25 L 2xYT media). The cell culture was incubated at 37°C under shaking (180 rpm) and the growth monitored by OD_{600} measurements. The protein expression was induced by addition of IPTG at 0.6 OD_{600}. The temperature was dropped to 27°C and the culture incubated overnight under shaking (27°C, 180 rpm). The cells were harvested by centrifugation and the cell paste stored at -80°C. For details on the specific protein, refer to section 7.4.1.2 and 7.4.1.5.

7.3.2.2. Protein purification: Ni affinity chromatography

The cell paste was thawed and resuspended in lysis buffer at room temperature for 15 minutes. The cell suspension was moved to 4°C, lysozyme and protease inhibitor were added and the suspension stirred for 1 hour. The lysate was then sonicated on ice (20 cycles: 30 sec on/ 30 sec off). Extra cycles of sonication were applied until a concentration of 20 mg/mL protein was obtained (measured by Bradford assay, section 7.3.2.7). Cell debris was precipitated by centrifugation and the clear lysate applied to a Ni-IDA Sepharose Fast Flow Column (2 mL min^{-1}, 50 mL bed volume), pre-equilibrated with low imidazole buffer (Imidazole buffer A). To elute loosely bound proteins the column was washed with Imidazole buffer A (4 mL min^{-1}) until the baseline in the UV (Abs 280 nm) chromatogram was reached. The washing step was extended for two column volumes and a gradient of high imidazole buffer (Imidazole buffer B) was applied to elute the His_6-tagged protein (10 mL fractions). The protein fractions were analysed by Bradford assay (section 7.3.2.7) to estimate the concentration and by SDS-PAGE (section 7.3.2.5) to investigate purity. The fractions with the desired protein were pooled and dialyzed in Storage buffer (or Dialysis buffer). The final

protein concentration was measured by UV-vis (section 7.3.2.8). When required, the protein was concentrated by ultrafiltration (section 7.3.2.6) and then stored in aliquots at -80°C. For details on the specific protein, refer to section 7.4.1.3 and 7.4.1.6.

7.3.2.3. Imidazole removal by dialysis

Following Ni column purification (section 7.3.2.2), the high imidazole content in the purified protein sample was removed by dialysis. The dialysis membrane tubing were hydrated with deionized water, sealed at the bottom with appropriate clips and transferred into a cylinder with Storage buffer. Two cycle of dialysis were done (2x 1 L buffer, 1 hour, 4°C). After the first cycle the dialysis buffer was replaced with fresh buffer. The dialyzed protein was aliquoted and stored at – 80°C.

7.3.2.4. Protein purification: size exclusion chromatography

When a high degree of purity was required, following Ni-affinity chromatography the protein sample was further purified by size exclusion chromatography (or gel filtration). The gel filtration column, packed with Superdex-75 resin (200 mL bed volume), was pre-equilibrated with the Storage buffer (600 mL). The protein sample was concentrated by ultrafiltration (section 7.3.2.6) to a concentration of about 10 mg mL^{-1} and applied to the gel filtration column (2 mL, min^{-1}). The collected fractions (10 mL) were analysed by Bradford assay (section 7.3.2.7) to estimate the concentration and by SDS-PAGE to assess the purity (section 7.3.2.5). The fractions with pure protein were pooled and concentrated by ultrafiltration (section 7.3.2.6). The final protein concentration was measured by UV-vis (section 7.3.2.8). The protein was aliquoted and stored at -80°C.

7.3.2.5. Protein analysis by SDS-PAGE

The purity of protein fractions from column purification was analysed by Sodium Dodecyl Sulphate Polyacrylamide Gel Electrophoresis (15% acrylamide). The SDS-PAGE gels were prepared in house as reported in Table 7.9. The polymerizing agents ammonium persulfate (APS) and the TEMED were added just before assembling the gel. To assemble the gel, the resolving solution was quickly poured in the gel cassette. A layer of isopropanol was distributed above the resolving gel to create a flat and smooth surface and was left to set

for 1 hour. The isopropanol layer was removed and the stacking gel solution quickly pipetted on top of the resolving gel. A comb for shaping the sample wells was inserted and the gel left to set for further 45 minutes. After removing the comb, the gel was rinsed with deionised water and stored at 4°C.

Table 7.9: SDS-PAGE gel preparation

Component	15% acrylamide Resolving gel/20 mL	5% acrylamide Stacking gel/4 mL
30% Acrylamide/bis acrylamide	10 mL	670 μL
1.5 M Tris, pH 8.8	5 mL	-
1 M Tris, pH 6.8	-	500 μL
10% w/v SDS	200 μL	40 μL
10 % w/v APS*	200 μL	40 μL
TEMED**	8 μL	4 μL
DI water	4.6 mL	2.7 mL

* Freshly prepared; ** Added just before the gel solution was poured in the gel cassette

For SDS-PAGE analysis, unless otherwise stated, the protein samples were diluted to a concentration of 2 mg mL^{-1} (20 μL) and mixed in a 1:1 ratio with the 2x SDS-PAGE loading buffer (20 μL, Table 7.10). Samples more diluted than 2 mg mL^{-1} (20 μL) were mixed in a 1:1 ratio with the 2x SDS-PAGE loading buffer.

Table 7.10: SDS-PAGE loading buffer

Component	Concentration	Quantity
200 mM Tris HCl, pH 6.8	100 mM	50 mL
SDS	4% w/v	4 g
Bromophenol Blue	0.2% w/v	0.2 g
Glycerol	20% v/v	20 mL
DTT*	200 mM	-
DI water		up to 100 mL

* Added just before use (154 mg to 5 mL loading buffer)

The samples (1 mg mL^{-1} final concentration) were heat denatured (95°C, 5 min) and 10 μL loaded onto the gel. Electrophoresis separation was achieved by running the gel in the SDS-PAGE running buffer (Table 7.11) at 180V for 45 minutes.

Table 7.11: SDS-PAGE running buffer

Component	Concentration	Quantity
Glycine	250 mM	94 g
Tris base	25 mM	15.1 g
SDS	0.1% w/v	5 g
DI water		up to 5 L

The gel was visualized by staining with Coomassie Blue Brilliant Staining solution (microwave heated, 30-60 sec, Table 7.12) and destained with the Destaining solution (overnight, under rocking, Table 7.13)

Table 7.12: SDS-PAGE Coomassie Brilliant Blue Staining solution

Component	Concentration	Quantity
Methanol	45% v/v	450 mL
Glacial acetic acid	10% v/v	100 mL
Coomassie brilliant Blue	0.25 % w/v	2.5 g
DI water		up to 1 L

Table 7.13: SDS-PAGE Destaining solution

Component	Concentration	Quantity
Methanol	5% v/v	250 mL
Glacial acetic acid	7.5% v/v	375 mL
DI water		up to 5 L

7.3.2.6. Protein concentration and/or buffer exchange by ultrafiltration

In preparation for size exclusion chromatography or following column purification, the protein solution was concentrated by ultrafiltration. Ultrafiltration was also used for quick buffer exchange in preparation for ITC experiments or to test the stability of protein in alternative buffer. Cellulose membrane filters (specificity, 10 kDa cut-off), assembled in Amicon® stirred cells, were used for concentration of large volume of protein, driven by a constant flow of nitrogen applied (4°C). The sample was maintained under stir to prevent protein aggregation. For buffer exchange and for concentration of small volume of protein

solution (below 2 mL), centrifugation based concentration by means of spin-filters was used. Cycles of centrifugation (6000 rpm, 5 min, 4°C) were applied, taking care of thoroughly mixing the sample in between cycles, to reduce the extent of protein adhesion to the filter membrane or protein aggregation. The recovery by pressure-based ultrafiltration was always superior to the recovery by centrifugation based ultrafiltration. The first method was therefore preferentially used when possible.

7.3.2.7. Protein quantification by Bradford assay

The protein concentration of lysate or fractions collected from column chromatography was measured by Bradford assay.[534] The protein sample (20 µL) was added to the Bradford reagent (750 µL) and the absorbance measured at 595 nm. The protein concentration was determined by means of a BSA standard curve, prepared by two-fold dilution from a 1 mg mL^{-1} sample.

7.3.2.8. Protein and nucleotide quantification by UV-vis analysis

For an accurate determination of protein and nucleotide concentration, UV-vis spectroscopy was applied. The absorbance of a 50 µL sample was measured at 280 nm for proteins and at 256 nm for nucleotides (clear 96 well plate, half area). The sample was diluted with the respective buffer until an absorbance reading between 0.100 and 0.900 was obtained. Measurements were done in triplicate and at different concentrations (two fold serial dilutions). Protein concentration was calculated using the respective molar extinction coefficient (ε), according to the following relation.

$$c = \frac{Abs}{\varepsilon}$$

Eq 7.1: Lambert-Beer's law

c was the concentration of the sample and Abs the measured absorbance. The ε coefficients used were listed in Table 7.14.

Table 7.14: Molar extinction coefficients

	FLuc[535]	***Ft*PPK**[265]	**ADP/ATP**
ε coefficient/$M^{-1}cm$	4.556 x 10^4	5.787 x 10^4	1.54· x 10^4

7.3.3. *Ft*PPK assay: standard protocols

General protocols for the optimised independent luminescence assay, for the optimised *Ft*PPK-FLuc coupled assay and for the optimised *Ft*PPK-HPLC based assay were reported in the following section. During the optimisation process the protocols were often modified. When the conditions applied were different than what defined hereby, description of the alternative protocols were reported in the respective experimental section.

The optimised buffer composition for the *Ft*PPK activity assays was reported in Table 7.15. Only the concentrations of the each component in the final assay volume were reported, because of some differences in the preparation of the buffer stock to adapt to the assay protocol of interest (details reported in the specific sections).

Table 7.15: Optimised *Ft*PPK assay buffer

Component	Final concentration
Tris HCl	50 mM
$MgCl_2$	10 mM
NaCl	25 mM
$(NH_4)_2SO_4$	80 mM
Glycerol	20% v/v
DI water	

Adjusted to pH 7.8

7.3.3.1. Luminescence assay

The optimised luminescence assay was prepared in white 384 well microplates (unless otherwise stated) to a final volume of 100 µL. The following conditions, resulting from the assay optimisations, were applied: 300 nM FLuc/1.3 µM BSA, 70 µM luciferin, 5% DMSO, 30°C. The independent luminescence assay was routinely prepared alongside the coupled assay to derive an ATP standard curve and to monitor the activity of the FLuc. To prepare the standard curve, the following ATP concentrations were tested: 62.5 µM, 31.25 µM, 15.6 µM, 7.81 µM. The buffer for the luminescence assay was prepared as reported in Table 7.16. To limit adhesion of the FLuc to eppendorf tube surface, the FLuc was prepared in mixture with the BSA (Fluc/BSA). Due to possible precipitation of the FLuc at high concentration, the FLuc was first diluted to a 100x final concentration with FLuc storage buffer (which

favoured FLuc stability, section 7.4.1.3, Table 7.28) and then further diluted to 10x final concentration with a solution of BSA (1 mg/mL, 13 μM) in assay buffer (Table 7.16).

Table 7.16: optimised *Ft*PPK buffer for luminescence assay

Component	Component stock	Final concentration/100 μL	Amount/ Stock
Tris HCl	150 mM	45 mM	23.6 g
$MgCl_2$	33 mM	10 mM	1 M, 33 mL
NaCl	83 mM	25 mM	4.85 g
$(NH_4)_2SO_4$	266 mM	80 mM	5 M, 53.2 mL
Glycerol	40%	20%	400 mL
DI water			up to 1 L

Adjusted to pH 7.8

The luciferin reagent was prepared in the respective buffer (Table 7.17) to a 5x final concentration (350 μM).

Table 7.17: Luciferin buffer

Component	Component stock	Final concentration/100 μL	Amount/ Stock
Tris HCl	25 mM	5 mM	1.97 g
Glycerol	40%	20%	200 mL
DI water			up to 500 mL

Adjusted to pH 7.8

The ATP samples were prepared in water to a 10x final concentration, by two fold serial dilution from a top concentration of 10x 62.5 μM ATP. The assay solution were prepared as reported in Table 7.18. A master stock solution containing FLuc/BSA and DMSO in buffer (70 μL) was dispensed into the microplate by Biomek3000. Following addition of the ATP samples (10 μL), the microplate was incubated in the plate reader at 30°C for 20 minutes (unless otherwise stated). The luminescence reaction was started by addition of the luciferin reagent (20 μL), controlled by the plate reader built-in injector. The luminescence signal was measured 45 seconds after the addition of the luciferin (unless otherwise stated).

Table 7.18: Luminescence assay, ATP standard curve

Assay solution			
Component	**Component stock**	**Final concentration**	**Vol/ 100 µL**
Assay buffer	2x		10 µL
BSA**			10 µL
FLuc/BSA**	3 µM/13 µM	300 nM/1.3 µM	10 µL
DMSO	100%	5%	5 µL
DI water			35 µL
Later addition (by Biomek3000)			
ATP*	78 - 625 µM	7.8 – 62.5 µM	10 µL
To start the FLuc assay			
Luciferin**	350 µM	70 µM	20 µL

*Prepared in water; ** Prepared in assay buffer

7.3.3.2. *Ft*PPK-FLuc luminescence coupled assay

The optimised *Ft*PPK-FLuc luminescence assay was prepared in white 384 well microplates (unless otherwise stated) to a final volume of 100 µL. The following conditions, resulting from the assay optimisations and with substrate concentrations at K_m, were applied: 10 nM *Ft*PPK/1.3 µM BSA, 1.5 µM $polyP_{25}$, 200 µM ADP, 300 nM FLuc/1.3 µM BSA, 70 µM luciferin, 5% DMSO, 30°C. To prepare the *Ft*PPK/BSA solution, the *Ft*PPK was diluted to a 100x final concentration with assay buffer (Table 7.16) and then further diluted to a 10x final concentration with 1 mg/mL BSA solution prepared in assay buffer (Table 7.16). The FLuc/BSA solution was prepared as reported in section 7.3.3.1. The $polyP_{25}$ was prepared to a 10x final concentration in water, while the ADP and the luciferin to a 5x final concentration in water and luciferin buffer (Table 7.17), respectively. Unless otherwise stated, alongside the *Ft*PPK coupled assay, control assays were prepared, in which no *Ft*PPK but only BSA in buffer was added, and an ATP standard curve (section 7.3.3.1). The assays were prepared according to Table 7.19 (general example) and by the automated workstation, following the protocol reported below:

1. The coupled assay solution (60 µL, containing *Ft*PPK, FLuc, $polyP_{25}$, BSA and DMSO in assay buffer), the control assay solution (60 µL, containing FLuc, $polyP_{25}$, BSA and

DMSO in assay buffer), and the ATP standard curve solution (70 µL, containing FLuc, BSA and DMSO) were dispensed in the microplate.[q]

2. The ATP samples at the appropriate concentration (10 µL) were added to the ATP standard curve assays.
3. The microplate was incubated in the plate reader at 30°C for 10 minutes (unless otherwise stated).
4. The *Ft*PPK assay, including the negative control assays, were started by injection of ADP (20 µL, plate reader injector 2). After a variable delay, according to the time point measured, the luminescence assay was started by addition of the luciferin (20 µL, plate reader injector 1). The luminescence signal was measured after a constant delay of 16 seconds after the initiation of the luminescence assay.
5. For the ATP standard curves, the luminescence assay was started by addition of the luciferin (20 µL, plate reader injector 1). The luminescence signal was measured after a constant delay of 16 seconds (same as for the coupled assay) after the initiation of the luminescence assay.

For details on the reader control protocols refere to Appendix, section A2 3.3.

Table 7.19: *Ft*PPK-FLuc assay, general example

Assay solution			
Component	**Component stock**	**Final concentration**	**Vol/ 100 µL**
Assay buffer	2x		10 µL
$PolyP_{25}$*	150 µM	1.5 µM	10 µL
*Ft*PPK/BSA**	100 nM/13 µM	10 nM/1.3 µM	10 µL
FLuc/BSA**	3 µM/13 µM	300 nM/1.3 µM	10 µL
DMSO	100%	5%	5 µL
DI water			15 µL
To start the FtPPK assay			
ADP*	1 mM	200 µM	20 µL
To start the FLuc assay			
Luciferin**	350 µM	70 µM	20 µL

*Prepared in water; ** Prepared in assay buffer

[q] A variation of this protocol applied to the specific case of the HTS entails the injection into the microplate of the DMSO/library on its own before the addition of the assay solution (section 7.5.1.3)

7.3.3.3. HPLC-based *Ft*PPK assay

A RP IP chromatography was used for the HPLC analysis of ADP and ATP, the substrate and product of the *Ft*PPK reaction, respectively. For the nucleotide analysis a C18 reverse phase column (Gemini, 150 x 4.6 mm, 5 μm particle diameter) and a mobile phase of MeOH in water, supplied with the ion pairing agent TEAA (0.1 M), were used (unless otherwise stated). Alongside the *Ft*PPK assay, a nucleotide standard curve was always included in the chromatographic analysis, to extrapolate the concentration of the ADP and ATP in the assay solution and to account for possible variations due to experimental conditions (e.g. buffer variation). The following optimised standard conditions were applied to prepare the *Ft*PPK assay (unless otherwise stated): 10 nM *Ft*PPK, 30 μM polyP$_{25}$, 200 μM ADP, 2.6 μM BSA, 5% DMSO, 30°C. For the nucleotide standard curves, the following concentration of ADP and ATP were tested: 125 μM, 62.5 μM, 31.25 μM, 15.6 μM. The *Ft*PPK assays were stopped by addition of EDTA (50 mM final concentration), when prepared in end-point format, the assays were stopped after 7 minutes.

Table 7.20: *Ft*PPK buffer for HPLC based assay (2x stock)

Component	Component stock	Final concentration	Quantity/2x stock
Tris HCl	100 mM	50 mM	2.12 g
Tris			0.788 g
$MgCl_2$	20 mM	10 mM	1 M, 4 mL
$(NH_4)_2SO_4$	160 mM	80 mM	1 M, 32 mL
NaCl	50 mM	25 mM	0.584 g
Glycerol	40%	20%	80 mL
DI water			up to 200 mL

FtPPK time course for HPLC analysis: the *Ft*PPK assay was prepared according to Table 7.21, to a final volume of 100 μL. Control assays were prepared alongside in which no *Ft*PPK was added but only BSA. A *Ft*PPK reaction working solution with a total volume of *N*x 100 μL was prepared, where *N* was the number of *Ft*PPK assays plus 3. The working solution was constituted by:

a) Assay solution (*N*x 80 μL volume): prepared by addition to the assay buffer of a 10x final concentration stock of *Ft*PPK, polyP$_{25}$, BSA and DMSO, as reported in Table 7.21.

b) ADP solution (*N*x 20 μL volume): constituted by a 5x final concentration ADP solution.

Table 7.21: *Ft*PPK assays for HPLC analysis

Component	Component stock	Final concentration	Vol/ 100 μL
Assay buffer	2x		30 μL
$PolyP_{25}$*	300 μM	30 μM	10 μL
*Ft*PPK/BSA**	100 nM/13 μM	10 nM/1.3 μM	10 μL
BSA**	13 μM	1.3 μM	10 μL
DMSO	100%	5%	5 μL
DI water			15 μL
To start the FtPPK assay			
ADP*	1 mM	200 μM	20 μL

*Prepared in water; ** Prepared in assay buffer (Table 7.20)

The assays were prepared according to the following general protocol:

1. The assay solution (*N*x 80 μL) and the ADP solution were incubated at 30°C for 20 minutes in a water bath.
2. The assays were started by addition of the ADP (*N*x 20 μL).
3. The assays were stopped by addition of EDTA (10 μL, 550 mM stock, to a final concentration of 50 mM).

Minor variations applied the protocols based on whether the assay was used for time course measurement or in end-point format (refer to the specific sections for details).

Nucleotides standard analysis: For analysis of ADP or ATP in water, samples at the appropriated concentration were prepared to a 100 μL final volume, according to Table 7.22.

Table 7.22: Nucleotide standards in assay buffer for HPLC analysis

Component	Component stock	Final concentration	Vol/ 100 μL
Assay buffer	2x		30 μL
ADP/ATP*	10x	15.6 – 125 μM	10 μL
BSA**	1.3 μM	2.6 μM	20 μL
DMSO	100%	5%	5 μL
DI water			35 μL

*Prepared in water; **Prepared in assay buffer (Table 7.20)

The nucleotides were prepared to a 10x final concentration working solution. The standard curve samples were subjected to incubation at 30°C and EDTA was added to account for possible effect on the HPLC chromatography. The *Ft*PPK assay and standard curve assay solutions were stored at -80°C. On the day of HPLC analysis, the samples were thawed, heat denatured (95°C, 5 min) and centrifuged (12000 rpm, 5 min, 4°C) to precipitate protein. The supernatant (80 μL) was analysed by HPLC.

Standard HPLC analysis by TEAA method: for the analysis of the *Ft*PPK assay and related standard curves a RP IP HPLC system, where the TEAA was used as ion pairing agent and the analyte was eluted by a gradient of MeOH, obtained by mixing the mobile phase A and the mobile phase B was applied. The mobile phase composition was reported in Table 7.23, while the optimised elution method (flow rate: 0.8 mL min^{-1}) was reported in Table 7.24. The chromatographic separation was monitored by UV detection at the wavelength of 256 nm and 280 nm.

Table 7.23: TEAA mobile phase preparation for RP IP HPLC

	Component	Final concentration	Vol
Mobile phase A	TEA	0.1 M	27.8 mL
	Acetic acid (10 mM)		cca. 18 mL*
	DI water	100%	up to 2 L
Mobile phase B	TEA	0.1 M	7 mL
	Acetic acid (10 mM)		cca. 6 mL*
	MeOH	80%	400 mL
	DI water	20%	up to 500 mL

*approximate volume to adjust to pH 7

Table 7.24: HPLC analysis: TEAA elution method

Time / min	% Mobile phase B
0	5% B
24	5% B
25	10% B
36	10% B
37	100% B
42	100% B
43	5% B
53	5% B

7.4. Experimental for Chapter 2

7.4.1. Protein expression and purification

7.4.1.1. FLuc expression plasmid cloning

For cloning, the FLuc expression plasmid (pET16b::*luc*) was transformed into JM109 competent cells (section 7.3.1.7). An overnight culture was then prepared from a single isolated colony (section 7.3.1.4) and following cell harvesting the plasmid was purified (section 7.3.1.8). To verify that the cloning has been carried out successfully, the plasmid was analysed by restriction digest (section 7.3.1.9). To restrict the *luc* gene from the pET16 backbone, enzymes *Nco*I and *Xho*I in NEBuffer 4 were used. The restriction digest assays were analysed on 1% agarose gel (section 7.3.1.10).

7.4.1.2. FLuc expression

The FLuc was expressed from *E. coli* BL21 (DE3) Rosetta cells, freshly transformed with the pET16b::*luc* plasmid (section 7.3.1.7). An overnight culture was prepared by inoculation of a single well isolated colony into 2xYT media (100 mL) supplemented with ampicillin (100 μg/mL, section 7.3.1.4). The overnight culture was then used as inoculum for large scale growth (section 7.3.2.1). The protein expression was induced at 0.6 OD_{600} by addition of 400 μM IPTG. The cells were incubated overnight at 27°C and harvested by centrifugation (7500 rpm, 30 min, 4°C). Cell pellet was stored at -80°C.

7.4.1.3. FLuc purification – Ni column affinity chromatography

Cells paste (15 g) was thawed and resuspended in lysis buffer (5x w/v of cell paste, 1 hour, at 4°C, Table 7.25) supplemented with lysozyme (300 μg/mL), protease inhibitor (2x tablets) and benzonase (20 μL).

Table 7.25: FLuc purification – Lysis buffer

Component	Concentration	Quantity
Tris HCl	20 mM	0.315 g
NaCl	50 mM	0.292 g
Glycerol	10% v/v	10 mL
DI water		up to 100 mL

Adjusted to pH 7.8

The cells were lysed according to the protocol reported in section 7.3.2.2. To precipitate cell debris the lysate was centrifuged (20000 rpm, 45 min, 4°C) and the clear lysate applied to the Ni column pre-equilibrated in Imidazole buffer A (Table 7.26). To elute loosely bound protein the column was washed with 8 column volumes (8 x 50 mL) of Imidazole buffer A (Table 7.26). To elute the FLuc a gradient of imidazole was applied from 0% to 100% Imidazole buffer B (Table 7.27) over 250 mL. The fractions were analysed by Bradford assay (section 7.3.2.7) and by SDS-PAGE (section 7.3.2.5) and those containing FLuc pooled. To remove imidazole the FLuc solution was dialyzed in Storage buffer (Table 7.28 and section 7.3.2.3). The FLuc concentration was measured by UV-vis using the molar extinction coefficient of $4.556 \cdot 10^4\ M^{-1}cm^{-1}$ (7.3.2.8).[535] The FLuc was stored in aliquots at -80°C.

Table 7.26: FLuc purification - Imidazole Buffer A

Component	Concentration	Quantity
Tris HCl	20 mM	3.15 g
Imidazole	50 mM	3.4 g
NaCl	300 mM	17.55 g
NaH_2PO_4	100 mM	12 g
Glycerol	10% v/v	100 mL
DI water		up to 1 L

Adjusted to pH 7.8

Table 7.27: FLuc purification - Imidazole Buffer B

Component	Concentration	Quantity
Tris HCl	20 mM	3.15 g
Imidazole	500 mM	34 g
NaCl	300 mM	17.55 g
NaH_2PO_4	100 mM	12 g
Glycerol	10% v/v	100 mL
DI water		up to 1 L

Adjusted to pH 7.8

Table 7.28: FLuc purification – Storage buffer

Component	Concentration	Quantity
Tris acetate	25 mM	4.53 g
EDTA	2 mM	0.584 g
$(NH_4)_2SO_4$	200 mM	26.43 g
Ethylene glycol	30% v/v	300 mL
Glycerol	15% v/v	150 mL
DTT	5 mM	0.771 g
DI water		up to 1 L

Adjusted to pH 7.8

7.4.1.4. *Ft*PPK expression plasmid cloning

For cloning, the *Ft*PPK expression plasmid (pET16b::*Ftppk*) was transformed into JM109 competent cells (section 7.3.1.6 and 7.3.1.7). An overnight culture was then prepared from a single isolated colony (section 7.3.1.4) and following cell harvesting the plasmid was purified (section 7.3.1.8). To verify that the cloning has been carried out successfully, the plasmid was analysed by restriction digest (section 7.3.1.9). Restriction enzymes *Pst*I and *Nco*I in NEBuffer 3 were used to restrict the plasmid in correspondence of the amp^R gene and of the *ppk* gene, respectively. The restriction digest assays were analysed on 1% agarose gel (section 7.3.1.10).

7.4.1.5. *Ft*PPK expression

The *Ft*PPK was expressed from *E.coli* BL21 Rosetta^{TM} pLysS (DE3), either freshly transformed cells or glycerol freeze (section 7.3.1.7 and 7.3.1.5). An overnight culture was prepared by inoculation of either a single well isolated colony or a loop of glycerol freeze into 2xYT media (100 mL) supplemented with ampicillin (100 μg/mL, section 7.3.1.4). The overnight culture was then used as inoculum for large scale growth (section 7.3.2.1). The protein expression was induced at 0.6 OD_{600} by addition of 400 μM IPTG. The cells were incubated overnight at 27°C and were harvested by centrifugation (8000 rpm, 30 min, 4°C). Cell pellet was stored at -80°C.

7.4.1.6. *Ft*PPK purification – Ni column affinity chromatography

Cells paste was thawed and resuspended in lysis buffer (3x w/v of cell paste, 1 hour, at 4°C, Table 7.29) supplemented with lysozyme (5 mg per 50 mL) and protease inhibitor (1 tablet per 50 mL).

Table 7.29: *Ft*PPK purification – Lysis buffer

Component	Concentration	Quantity
Tris HCl	50 mM	1.27 g
Tris base		0.236 g
NaCl	500 mM	5.84 g
Glycerol	20% v/v	40 mL
DI water		up to 200 mL

Adjusted to pH 7.8

The cells were lysed according to the protocol reported in section 7.3.2.2. To precipitate cell debris the lysate was centrifuged (14000 rpm, 30 min, 4°C) and the clear lysate applied to the Ni column pre-equilibrated in Imidazole buffer A (Table 7.30). To elute loosely bound protein the column was washed with 5 column volumes (5 x 50 mL) of Imidazole buffer A (Table 7.30). To elute the *Ft*PPK a gradient of imidazole was applied from 0% to 100% Imidazole buffer B (Table 7.31) over 200 mL. The fractions were analysed by Bradford assay (section 7.3.2.7) and by SDS-PAGE (section 7.3.2.5) and those containing *Ft*PPK pooled.

Table 7.30: *Ft*PPK purification - Imidazole Buffer A

Component	Concentration	Quantity
Tris HCl	50 mM	6.35 g
Tris base		1.18 g
Imidazole	50 mM	3.4 g
NaCl	500 mM	29.22 g
Glycerol	20% v/v	200 mL
β-mercaptoethanol*	3 mM	200 µL
DI water		up to 1 L

Adjusted to pH 7.8; *Added before use

Table 7.31: *Ft*PPK purification - Imidazole Buffer B

Component	Concentration	Quantity
Tris HCl	50 mM	6.35 g
Tris base		1.18 g
Imidazole	500 mM	34 g
NaCl	500 mM	29.22 g
Glycerol	20% v/v	200 mL
β-mercaptoethanol*	3 mM	200 µL
DI water		up to 1 L

Adjusted to pH 7.8; *Added before use

To remove imidazole the *Ft*PPK solution was dialyzed in Storage buffer (Table 7.32 and section 7.3.2.3). After dialysis and in preparation for gel filtration, the *Ft*PPK was concentrated by membrane ultrafiltration in Amicon® apparatus (section 7.3.2.6) to a concentration of about 10 mg/mL and stored in aliquots of 3 mL at -80 C. The *Ft*PPK concentration was measured by UV-vis using the molar extinction coefficient of $5.787 \cdot 10^4$ $M^{-1}cm^{-1}$ (7.3.2.8).

Table 7.32: *Ft*PPK purification – Storage buffer

Component	Concentration	Quantity
Tris HCl	50 mM	6.35 g
Tris base		1.18 g
NaCl	300 mM	17.58 g
Glycerol	20% v/v	200 mL
DTT*	5 mM	0.077 g
DI water		up to 1 L

Adjusted to pH 7.8; *Added before use

7.4.1.7. *Ft*PPK purification – size exclusion chromatography

Following dialysis and protein concentration, the *Ft*PPK was further purified by size exclusion chromatography in *Ft*PPK storage buffer (Table 7.32) using the S75 resin (section 7.3.2.4). Up to three sample of *Ft*PPK (3 mL, about 10 mg/mL) were purified on a working day by consecutive injections. The new injection was started following elution of the last impurity after about 430 mL of washing.

7.4.2. Luminescence assay optimisation

7.4.2.1. Preliminary assay conditions

For the preliminary investigation of the FLuc activity, assays were manually prepared in white 96 well plate, full area. The final assay volume was 200 μL and the assays were prepared in triplicates. The FLuc activity was measured in the presence of 1 μM FLuc, 7.5 μM luciferin and a range of ATP concentrations between 150 μM and 5 mM. The buffer used for the luminescence assay was adopted from J. Docherty work[352] and is hereby defined "preliminary" because it was later subjected to optimisation. The FLuc and the luciferin were prepared in assay buffer (Table 7.33) to a 10x final concentration. ATP solutions were prepared by two fold serial dilutions from 10x 5 mM stock. The assays were prepared as reported in Table 7.34. The assay solution (180 μL) was manually injected in the microplate and the assays started by addition of ATP (20 μL). The luminescence was measured after 30 seconds at 37°C. The plate reader gain was 2050.

Table 7.33: Preliminary luminescence assay buffer – 2x stock

Component	2x Stock concentration	Final concentration	Quantity/ 2x stock
Tris HCl	100 mM	50 mM	15.75 g
$MgCl_2$	20 mM	10 mM	2 M, 10 mL
NaCl	600 mM	300 mM	35 g
$(NH_4)_2SO_4$	160 mM	80 mM	4 M, 42 mL
Glycerol	40% v/v	20% v/v	400 mL
DI water			up to 1 L

Adjusted to pH 7.8

Table 7.34: FLuc assay conditions

Component	Component stock	Final concentration	Vol/ 200 μL
Assay buffer	2x	1x	100 μL
FLuc	10 μM	1 μM	20 μL
Luciferin	75 μM	7.5 μM	20 μL
DI water			40 μL
To initiate the assay			
ATP	1.5 -50 mM	150 – 5000 μM	20 μL

7.4.2.2. Luminescence assay: optimisation of FLuc to rate limiting concentration

To identify conditions at which the FLuc concentration was rate limiting and the luminescence signal was proportional to the concentration of ATP, two sets of assays were prepared with either 1 μM or 100 nM FLuc, 7.5 μM luciferin and 15.5 – 500 μM ATP. The assays were prepared as described in section 7.4.2.1 and according to Table 7.35. The plate reader gain was 2550.

Table 7.35: FLuc assay optimisation to rate limiting concentration

Component	Component stock	Final concentration	Vol/ 200 μL
Assay buffer		50 mM	100 μL
FLuc	10 μM or 1 μM	1 μM or 100 nM	20 μL
Luciferin	75 μM	7.5 μM	20 μL
DI water			40 μL
To initiate the assay			
ATP	156 -5000 μM	15.6 – 500 μM	20 μL

7.4.2.3. Luminescence assay buffer: effect of BSA

To test the effect of the BSA on the FLuc activity two sets of assays were prepared with and without BSA (0.1 mg mL^{-1}) in the presence of 100 nM FLuc, 7.5 μM luciferin and 15.5 – 500 μM ATP. The assays were prepared as described in section 7.4.2.1 and according to Table 7.36.

Table 7.36: FLuc assay optimisation – Effect of BSA

Component	Component stock	Final concentration	Vol/ 200 μL
Assay buffer			100 μL
FLuc	1 μM	100 nM	20 μL
Luciferin	75 μM	7.5 μM	20 μL
BSA*	13 μM	1.3 μM	20 μL
DI water			20 μL
To initiate the assay			
ATP	156 -5000 μM	15.6 – 500 μM	20 μL

*Prepared in water

Working solutions at 10x final concentration were prepared for FLuc, luciferin and BSA in assay buffer (Table 7.33). For the assays with no BSA, the latter was replaced with water in equal volume. The plate reader gain was 2250.

7.4.2.4. Luminescence assay buffer: luciferin optimisation

To investigate the optimal concentration of luciferin, two sets of assay were prepared in the presence of 100 nM FLuc: *a*) 0.19-50 μM luciferin tested with 31.25, 62.5 and 125 μM ATP; *b*) 20-100 μM luciferin tested with 300 μM ATP. The assays were prepared in a white 96 well plate, full area, in a 200 μL volume (triplicates), according to Table 7.37. Working solutions at 10x final concentration were prepared for FLuc, BSA and luciferin in assay buffer (Table 7.33) and for ATP in water. The assay solution containing ATP (140 μL) was manually dispensed in the microplate, followed by addition of luciferin (20 μL) at the appropriate concentration. Control assays in which water was added in place of luciferin were prepared. The assays were started by addition of a mixture of FLuc/BSA (40 μL), using the automated injector built in the POLARstar Omega BMG plate reader. The luminescence was measured after 52 seconds from the injection of the FLuc/BSA reagent. The gain was 1650.

Table 7.37: FLuc assay optimisation – luciferin concentration

Component	Component stock	Final concentration	Vol/ 200 μL
Assay buffer	2x		100 μL
ATP*	0.312–1.25 mM or 3 mM	31.2-125 μM or 300 μM	20 μL
DI water			20 μL
Later addition			
Luciferin	1.9-500 μM or 200-1000 μM	0.19-50 μM or 20-100 μM	20 μL
To initiate the assay			
FLuc	1 μM	100 nM	20 μL
BSA*	13 μM	1.3 μM	20 μL

*Prepared in water

7.4.2.5. Luminescence assay buffer: temperature optimisation

To investigate the optimal temperature for the FLuc activity, assays were prepared in the presence of 100 nM FLuc, 70 μM luciferin and 3.9-62.5 μM ATP and the luminescence measured at 25°C, 30°C and 37°C. The assays were prepared in a white 96 well plate, half area. The final volume was reduced to 100 μL and the assays were prepared in triplicates according to (Table 7.38). Working solutions at 10x final concentration were prepared for FLuc, BSA and luciferin in assay buffer (Table 7.33). The assays were prepared by manually dispensing the buffer solution (60 μL) in the microplate, followed by addition of ATP (10 μL) at the appropriate concentration. Control assays in which water was added in place of ATP were prepared. The microplate was incubated at the temperature of interest for 20 minutes. The assays were started by addition of a mixture of FLuc/BSA/luciferin (30 μL), using the automated injector built in the POLARstar Omega BMG plate reader. The luminescence was measured after 43 seconds from the start of the reaction. The gain was 1500.

Table 7.38: FLuc assay optimisation – temperature investigation

Component	Component stock	Final concentration	Vol/ 100 μL
Assay buffer	2x		50 μL
DI water			10 μL
Later addition			
ATP*	39-625 μM	3.9-62.5 μM	10 μL
To initiate the assay			
FLuc	1 μM	100 nM	10 μL
BSA*	13 μM	1.3 μM	10 μL
Luciferin	700 μM	70 μM	10 μL

*Prepared in water

7.4.2.6. Luminescence assay buffer: ATP standard curve

To investigate the dynamic range of the luminescence assay an extended ATP standard curve (st curve) was prepared by merging the data from three separated standard curves in which the ATP samples were prepared by two-fold dilution from the following top concentrations: 2000 μM ATP, 1600 μM ATP and 600 μM ATP. The standard curves were

prepared in the presence of 100 nM FLuc, 70 μM luciferin and 15.6 - 2000 μM ATP (st curve 1) or 25 - 1600 μM ATP (st curve 2) or 9.37 - 600 μM ATP (st curve 3). As a control for the consistency of the FLuc activity across the curves, the sample containing 500 μM ATP used for the st curve 1 was included in the st curve 2 and 3. In the latter, the sample with 800 μM ATP used for the st curve 2 was also included.

Table 7.39: FLuc assay optimisation – ATP standard curve

Component	Component stock	Final concentration	Vol/ 100 μL
Assay buffer	2x		50 μL
DI water			10 μL
Later addition			
ATP*	0.156-20 mM or 0.250-16 mM or 0.093-6 mM	15.6-2000 μM or 25-1600 μM or 9.37-600 μM	10 μL
To initiate the assay			
FLuc	1 μM	100 nM	10 μL
BSA*	13 μM	1.3 μM	10 μL
Luciferin	700 μM	70 μM	10 μL

*Prepared in water

The assay were prepared as described in 7.4.2.5 and according to Table 7.39. The luminescence was measured at 30°C after 14 seconds from the start of the assays. The gain was 1500.

7.4.3. *Ft*PPK-FLuc coupled assay optimisation

7.4.3.1. *Ft*PPK-FLuc coupled assay optimisation: preliminary conditions

To investigate the suitability of a continuous and discontinuous format, the *Ft*PPK-FLuc coupled assay was prepared applying the following conditions: 300 nM *Ft*PPK, 200 μM $PolyP_{25}$, 1 mM ADP, 100 nM FLuc, 1.3 μM BSA, 70 μM luciferin, 30°C. The assays were prepared in triplicate to a 100 μL final volume (white 96 well plate, half area). Working solutions at 10x final concentration were prepared for *Ft*PPK and luciferin in assay buffer (Table 7.33). The FLuc/BSA solution was prepared as described in section 7.3.3.1. The *Ft*PPK assay was prepared according to Table 7.40 by means of the automated workstation Biomek3000. The assay solution (70 μL), containing $polyP_{25}$ and ADP, was dispensed in the microplate and the *Ft*PPK assay started by addition of the *Ft*PPK (10 μL).

Table 7.40: *Ft*PPK-FLuc coupled assay preliminary conditions

Component	Component stock	Final concentration	Vol/ 100 μL
Assay buffer	2x		20 μL
$PolyP_{25}$*	2 mM	200 μM	10 μL
ADP*	10 mM	1 mM	10 μL
DI water			30 μL
To start the FtPPK assay			
*Ft*PPK**	3 μM	300 nM	10 μL
To start the FLuc assay			
FLuc/BSA**	1 μM/13 μM	100 nM/1.3 μM	10 μL
Luciferin**	700 μM	70 μM	10 μL

*Prepared in water; ** Prepared in assay buffer

The microplate was transferred in the plate reader and the luminescence assay started by addition of the FLuc-BSA-luciferin reagent (20 μL), by means of the plate reader built in injector.

Continuous assay format: the luminescence assay was initiated 15 seconds after the start of the *Ft*PPK assay and the luminescence signal was measured every 3 seconds for 330 seconds (1500 gain). A single reader control protocol (BMG Omega Reader Control Software) was used to measure the luminescence.

Discontinuous assay format: a number of reader control protocols (BMG Omega Reader Control Software) equal to the number of time points measured were prepared. Each protocol controlled the injection of FLuc into a set of three assays (triplicate) and the measurement of the luminescence (14 seconds after the injection of FLuc). The protocols were linked by a script and delays corresponding to the *Ft*PPK assay time points were set between consecutive protocols (Appendix, section A2 3.1).

7.4.3.2. *Ft*PPK-FLuc coupled assay optimisation: effect of the temperature

To investigate the effect of the temperature on the *Ft*PPK-FLuc coupled assay, two time courses were prepared as reported in section 7.4.3.1. The microplate was incubated into the plate reader at 30°C and 37°C for 20 minutes before the *Ft*PPK assay was started. The assays were measured in a discontinuous format as described in section 7.4.3.1.

7.4.3.3. *Ft*PPK-FLuc coupled assay: preliminary optimisation of the *Ft*PPK concentration

For a preliminary optimisation of the *Ft*PPK concentration three time courses were prepared in parallel with the following concentration of *Ft*PPK: 300 nM, 100 nM, 30 nM. The assays were prepared as described in section 7.4.3.1 and according to Table 7.41.

Table 7.41: *Ft*PPK-FLuc coupled assay: preliminary *Ft*PPK concentration optimisation

Component	Component stock	Final concentration	Vol/ 100 µL
Assay buffer	2x		20 µL
$PolyP_{25}$*	2 mM	200 µM	10 µL
ADP*	10 mM	1 mM	10 µL
DI water			30 µL
To start the FtPPK assay			
*Ft*PPK**	3 µM or 1 µM or 300 nM	300 nM or 100 nM or 30 nM	10 µL
To start the FLuc assay			
FLuc/BSA**	1 µM/13 µM	100 nM/1.3 µM	10 µL
Luciferin**	700 µM	70 µM	10 µL

*Prepared in water; ** Prepared in assay buffer

The microplate was incubated at 30°C for 20 minutes prior addition of the *Ft*PPK at the desired concentration. The assays were measured in discontinuous format, as reported in section 7.4.3.1.

7.4.3.4. *Ft*PPK-FLuc coupled assay: effect of BSA

To investigate the effect of BSA on the *Ft*PPK activity, BSA was added to the *Ft*PPK reagent and a time course measured. The *Ft*PPK/BSA solution and the FLuc/BSA solution were prepared by dilution with assay buffer (Table 7.33) as reported in section 7.3.3.1. The assays were prepared as reported in section 7.4.3.1 and according to Table 7.42. The microplate was incubated for 20 minutes at 30°C prior addition of *Ft*PPK. The assays were measured in discontinuous format as reported in section 7.4.3.1.

Table 7.42: *Ft*PPK-FLuc coupled assay: BSA effect

Component	Component stock	Final concentration	Vol/ 100 µL
Assay buffer	2x		20 µL
$PolyP_{25}$*	2 mM	200 µM	10 µL
ADP*	10 mM	1 mM	10 µL
DI water			30 µL
To start the FtPPK assay			
*Ft*PPK**	300 nM/13 µM BSA or 300 nM	30 nM/1.3 µM BSA or 30 nM	10 µL
To start the FLuc assay			
FLuc/BSA**	1 µM/13 µM	100 nM/1.3 µM	10 µL
Luciferin**	700 µM	70 µM	10 µL

*Prepared in water; ** Prepared in assay buffer

7.4.3.5. *Ft*PPK-FLuc coupled assay: *Ft*PPK time course

A *Ft*PPK time course was prepared in the presence of 30 nM *Ft*PPK, 1 mM ADP and 200 µM $polyP_{25}$, to investigate the extent of the linear phase under the applied conditions and to investigate if the ATP produced was within the ATP standard curve dynamic range. The assay were prepared as reported in section 7.4.3.4 and according to Table 7.43. Negative control assays in which water was added in place of ADP were prepared. An ATP standard curve was prepared in the same microplate to monitor the activity of the FLuc with time,

as reported in Table 7.39. The microplate was incubated for 10 minutes at 30°C prior addition of *Ft*PPK. The assays were measured in discontinuous format as reported in section 7.4.3.1.

Table 7.43: *Ft*PPK-FLuc coupled assay: *Ft*PPK time course

Component	Component stock	Final concentration	Vol/ 100 µL
Assay buffer	2x		20 µL
$PolyP_{25}$*	2 mM	200 µM	10 µL
ADP*	10 mM	1 mM	10 µL
DI water			30 µL
To start the FtPPK assay			
*Ft*PPK/BSA**	300 nM/13 µM	30 nM/1.3 µM	10 µL
To start the FLuc assay			
FLuc/BSA**	1 µM/13 µM	100 nM/1.3 µM	10 µL
Luciferin**	700 µM	70 µM	10 µL

*Prepared in water; ** Prepared in assay buffer

7.4.3.6. *Ft*PPK-FLuc coupled assay: preliminary kinetics characterisation

7.4.3.6.1. K_m for ADP

To determine the *Ft*PPK K_m for ADP, a time course was measured at ADP concentrations between 7.81 µM and 2400 µM while the $polyP_{25}$ concentration was maintained constant (200 µM). The ADP samples were prepared by two fold serial dilutions from a 10x 2400 µM stock (Exp1) and from a 10x 1000 µM stock (Exp2). The assays were prepared as reported in section 7.4.3.4 and according to Table 7.44. Three sets of time courses and three set of ATP standard curve assays (ATP 3.90 – 62.5 µM) were prepared per microplate (in triplicate, 3 microplates in total). Negative control assays, in which water was added in place of ADP, were prepared for each set of time course. The microplate was incubated for 5 minutes at 30°C before to start the *Ft*PPK assay. The gain was 1500.

Two different assay formats were used to measure the K_m, differing for the injection step of the *Ft*PPK:

- *FtPPK injection by Biomek3000*: the *Ft*PPK assay and the FLuc assay were initiated and measured by discontinuous mode, as described in section 7.4.3.1 (Exp1).

- *FtPPK injection by the second injector of the BMG plate reader*: to improve the precision and the reproducibility of the *Ft*PPK time course measurement, a format in which the *Ft*PPK was injected by a second injector built in the BMG plate reader (injector 2) was developed (Appendix, section A2 3.2). The injection of *Ft*PPK (10 µL) was completed in all the assays belonging to the same time course, then the FLuc assay was started by addition of the FLuc/BSA/Luciferin mixture (20 µL, injection by injector 1) and the luminescence measured after 16 seconds (Exp2).

Table 7.44: *Ft*PPK-FLuc coupled assay: preliminary K_m with ADP

Component	Component stock	Final concentration	Vol/ 100 µL
Assay buffer	2x		20 µL
$PolyP_{25}$*	2 mM	200 µM	10 µL
ADP*	0.078 - 24 mM	7.8 - 2400 µM	10 µL
DI water			30 µL
To start the FtPPK assay			
*Ft*PPK/BSA**	300 nM/13 µM	30 nM/1.3 µM	10 µL
To start the FLuc assay			
FLuc/BSA**	1 µM/13 µM	100 nM/1.3 µM	10 µL
Luciferin**	700 µM	70 µM	10 µL

*Prepared in water; ** Prepared in assay buffer

7.4.3.6.2. K_m for $polyP_{25}$

To determine the appropriate concentration of ADP to use for the K_m measurement for $polyP_{25}$, a time course was measured at 1000 µM, 1500 µM, 2000 µM, 3000 µM ADP while the concentration of $polyP_{25}$ was set to 200 µM. The assays were prepared as reported in section 7.4.3.1 and according to Table 7.44, using the appropriate concentration of ADP.

To determine the K_m for $polyP_{25}$, time courses were measured titrating $polyP_{25}$ at concentrations between 6.25 µM and 600 µM, while the ADP concentration was maintained constant (1500 µM). The $polyP_{25}$ was prepared by two fold serial dilutions from a 10x 600 µM stock, 10x 500 µM stock and 10x 400 µM stock. The assays were prepared according to Table 7.45 and as reported for the experiment to determine the K_m with ADP (section 7.4.3.6.1), applying both the Exp1 format and the Exp2 format.

Table 7.45: *Ft*PPK-FLuc coupled assay: preliminary K_m with polyP

Component	Component stock	Final concentration	Vol/ 100 µL
Assay buffer	2x		20 µL
ADP*	1.5 mM	1500 µM	10 µL
$PolyP_{25}$*	0.062 - 6 mM	6.25 - 600 µM	10 µL
DI water			30 µL
To start the FtPPK assay			
*Ft*PPK/BSA**	300 nM/13 µM	30 nM/1.3 µM	10 µL
To start the FLuc assay			
FLuc/BSA**	1 µM/13 µM	100 nM/1.3 µM	10 µL
Luciferin**	700 µM	70 µM	10 µL

*Prepared in water; ** Prepared in assay buffer

7.4.3.7. *Ft*PPK-FLuc coupled assay: DMSO effect

To investigate the DMSO effect on the *Ft*PPK-FLuc assay, the initial rate in the presence of 0%, 1%, 2%, 4%, 6%, 8% and 10% DMSO was measured. Time courses were prepared applying the following conditions: 35 nM *Ft*PPK/1.3 µM BSA, 30 µM $PolyP_{25}$, 700 µM ADP, 100 nM FLuc/1.3 µM BSA, 70 µM luciferin, 0-10% (v/v) DMSO, 30°C. ATP standard curves were prepared alongside with the corresponding % of DMSO.

Table 7.46: *Ft*PPK-FLuc coupled assay: effect of DMSO – *Ft*PPK time course

Component	Component stock	Final concentration	Vol/ 100 µL
Assay buffer	2x		20 µL
$PolyP_{25}$*	300 µM	30 µM	10 µL
DMSO	10x	0 - 10 %	10 µL
DI water			10 µL
Later addition (by Biomek3000)			
*Ft*PPK/BSA**	350 nM/13 µM	35 nM/1.3 µM	10 µL
To start the FtPPK assay			
ADP*	3.5 mM	700 µM	20 µL
To start the FLuc assay			
FLuc/BSA**	1 µM/13 µM	100 nM/1.3 µM	10 µL
Luciferin**	700 µM	70 µM	10 µL

*Prepared in water; ** Prepared in assay buffer

The assay reagents were prepared as reported in 7.3.3.2, using the assay buffer described in Table 7.33. The assays were prepared in a white 96 well plate microplate, according to Table 7.46 and as reported in 7.3.3.2, with the difference that the luminescence assay was started by addition of a mixture of FLuc/BSA/luciferin. An optimised format (similar to the final optimal format) in which the *Ft*PPK assay was started by addition of ADP was applied. Different reader control protocols, linked in a script mode, were used to initiate the *Ft*PPK assay and the FLuc assay (Appendix, section A2 3.3). The gain was increased to 1700.

7.4.3.8. *Ft*PPK-FLuc coupled assay: format optimisation and incubation time

To determine the appropriate incubation time at 30°C prior the initiation of the assays, a *Ft*PPK-FLuc time course was measured following incubation of the microplate with the *Ft*PPK solution for 0, 60, 180, 300 and 600 seconds. The following conditions were applied to measure the time course: 35 nM *Ft*PPK/1.3 μM BSA, 30 μM $PolyP_{25}$, 700 μM ADP, 100 nM FLuc/1.3 μM BSA, 70 μM luciferin, 5% DMSO, 30°C. The assays were prepared as described in 7.4.3.7.

7.4.3.9. *Ft*PPK-FLuc coupled assay: optimisation of the FLuc concentration

For the optimisation of the FLuc concentration, the *Ft*PPK assay was coupled to the following FLuc concentrations: 50 nM, 100 nM, 125 nM, 166 nM, 200 nM, 250 nM, 290 nM, and 333 nM. Overall, the conditions applied to the coupled assay were: 35 nM *Ft*PPK/1.3 μM BSA, 30 μM $PolyP_{25}$, 700 μM ADP, 50 - 333 nM FLuc/1.3 μM BSA, 70 μM luciferin, 5% DMSO, 30°C. The assays were prepared in white 96 well plate, half area. Each microplate was prepared as follow: two ATP standard curves at a FLuc concentration of 100 nM (to monitor the loss of FLuc activity with time and from plate to plate) and two *Ft*PPK time courses coupled to a different FLuc concentration (respective ATP standard curve).

A further improvement to the assay protocol was introduced, consisting in the addition of the FLuc/BSA solution to the microplate and the initiation of the luminescence assay by injection of only luciferin. This protocol was very similar to the optimised standard protocol and together with the assay component preparation is described in section 7.3.3.2. The only difference to take into account consisted in the addition of *Ft*PPK/BSA and FLuc/BSA

solution, which were added in the microplate to the remaining assay solution by Biomek3000, as reported in Table 7.47.

Table 7.47: *Ft*PPK-FLuc coupled assay - optimisation of FLuc concentration

Component	Component stock	Final concentration	Vol/ 100 µL
Assay buffer	2x		10 µL
$PolyP_{25}$*	300 µM	30 µM	10 µL
DMSO	100%	5%	5 µL
DI water			15 µL
Later addition (by Biomek3000)			
*Ft*PPK/BSA**	350 nM/13 µM	35 nM/1.3 µM	10 µL
FLuc/BSA**	0.5 – 3.3 µM/13 µM	50 – 333 nM/1.3 µM	10 µL
To start the FtPPK assay			
ADP*	3.5 mM	700 µM	20 µL
To start the FLuc assay			
Luciferin**	350 µM	70 µM	20 µL

*Prepared in water; ** Prepared in assay buffer

7.4.3.10. *Ft*PPK-FLuc coupled assay: optimisation of the NaCl concentration

The effect of the NaCl on the activity of the FLuc and of the *Ft*PPK was investigated by testing a range of NaCl concentration (25 mM – 300 mM) on the independent luminescence assay and on the coupled assay. The following conditions were applied: 35 nM *Ft*PPK/1.3 µM BSA, 30 µM $PolyP_{25}$, 700 µM ADP, 300 nM FLuc/1.3 µM BSA, 70 µM luciferin, 5% DMSO, 30°C. The NaCl was included in the assay buffer. The assays were prepared as reported in section 7.4.3.9. Previously not only *Ft*PPK and FLuc have been prepared in assay buffer but luciferin as well, meaning that 40% of the assay components were supplied with the luciferin injection at the moment of the initiation of the luminescence assay. To allow the use of the same luciferin sample to start assays with a different concentration of NaCl, the luciferin was prepared in a Tris buffer containing only glycerol (called luciferin buffer, Table 7.17). As a consequence, the concentration of $MgCl_2$, NaCl and $(NH_4)_2SO_4$ in the assay buffer was adjusted so that the respective final concentration in 100 µL final volume would be obtained by addition of 30 µL buffer (in accordance to the protocol for the preparation of the coupled assay, which entails the injection of a total of 30 µL, section

7.3.3.2). The separation between a luciferin buffer and an assay buffer, containing all the components required for the assay, was adopted as standard (section 7.3.3.2).

7.4.3.11. *Ft*PPK-FLuc coupled assay: optimisation of the *Ft*PPK concentration

To ensure that the luminescence signal was a function of the *Ft*PPK activity, the relation between *Ft*PPK concentration and signal was investigated by titration of the *Ft*PPK while the FLuc was maintained constant. The *Ft*PPK concentrations tested were: 50 nM, 25 nM, 12.5 nM, 6.25 nM, 3.12 nM, 1.5 nM. Overall, the conditions applied to the coupled assay were: 1.5 - 50 nM *Ft*PPK/1.3 μM BSA, 30 μM $PolyP_{25}$, 700 μM ADP, 300 nM FLuc/1.3 μM BSA, 70 μM luciferin, 5% DMSO, 30°C. The assays were prepared in white 96 well plate, half area, as described in section 7.3.3.2 and according to Table 7.48.

Table 7.48: *Ft*PPK-FLuc coupled assay - optimisation of *Ft*PPK concentration

Component	Component stock	Final concentration	Vol/ 100 μL
Assay buffer	2x		10 μL
$PolyP_{25}$*	300 μM	30 μM	10 μL
DMSO	100%	5%	5 μL
DI water			15 μL
Later addition (by Biomek3000)			
*Ft*PPK/BSA**	15 - 500 nM/13 μM	1.5 – 50 nM/1.3 μM	10 μL
FLuc/BSA**	3 μM/13 μM	300 nM/1.3 μM	10 μL
To start the FtPPK assay			
ADP*	3.5 mM	700 μM	20 μL
To start the FLuc assay			
Luciferin**	350 μM	70 μM	20 μL

*Prepared in water; ** Prepared in assay buffer

7.4.3.12. *Ft*PPK-FLuc coupled assay: kinetics characterisation

The fully optimised *Ft*PPK-FLuc coupled assay was applied for the kinetic characterization of the *Ft*PPK. The coupled assay conditions were: 10 nM *Ft*PPK/1.3 μM BSA, ADP and $polyP_{25}$ as per respective experiment, 300 nM FLuc/1.3 μM BSA, 70 μM luciferin, 5% DMSO, 30°C.

Table 7.49: *Ft*PPK-FLuc coupled assay – K_m for ADP

Component	Component stock	Final concentration	Vol/ 100 µL
Assay buffer	2x		10 µL
ADP*	97.6 µM – 25 mM	9.76 - 2500 µM	10 µL
DMSO	100%	5%	5 µL
DI water			15 µL
Later addition (by Biomek3000)			
*Ft*PPK/BSA**	100 nM/13 µM	10 nM/1.3 µM	10 µL
FLuc/BSA**	3 µM/13 µM	300 nM/1.3 µM	10 µL
To start the FtPPK assay			
$PolyP_{25}$*	1 mM or 150 µM	200 µM or 30 µM	20 µL
To start the FLuc assay			
Luciferin**	350 µM	70 µM	20 µL

*Prepared in water; ** Prepared in assay buffer

Table 7.50: *Ft*PPK-FLuc coupled assay – K_m for polyP

Component	Component stock	Final concentration	Vol/ 100 µL
Assay buffer	2x		10 µL
$PolyP_{25}$*	7-8 µM – 4 mM	0.78 - 400 µM	10 µL
DMSO	100%	5%	5 µL
DI water			15 µL
Later addition (by Biomek3000)			
*Ft*PPK/BSA**	100 nM/13 µM	10 nM/1.3 µM	10 µL
FLuc/BSA**	3 µM/13 µM	300 nM/1.3 µM	10 µL
To start the FtPPK assay			
ADP*	7.5 mM or 12.5 mM	1500 µM or 2500 µM	20 µL
To start the FLuc assay			
Luciferin**	350 µM	70 µM	20 µL

*Prepared in water; ** Prepared in assay buffer

The K_m for ADP was measured by titration of ADP between 9.76 µM and 2500 µM, while the $polyP_{25}$ wad held constant at either 200 µM or 30 µM. The K_m for $polyP_{25}$ was measured by titration of $polyP_{25}$ between 0.78 µM and 400 µM, while the ADP was held constant at either 2500 µM or 1500 µM. The assays were prepared in white 96 well plate, half area, as described in section 7.3.3.2 and according to Table 7.49 and Table 7.50.

7.5. Experimental for Chapter 3

7.5.1. HTS format development

7.5.1.1. Preliminary investigation: rate measurement

A preliminary HTS format was designed in which replicates of *Ft*PPK time courses were prepared (three time points: 16 seconds, 23 seconds, 30 seconds) and the Z' factor measured to assess the assay quality. The effect of the FLuc concentration optimisation (section 2.2.4.3) was also investigated by preparing both assays coupled to 100 nM FLuc and assays coupled to 300 nM FLuc. The following assay conditions (not fully optimised) were applied: 35 nM *Ft*PPK/1.3 μM BSA, 30 μM $PolyP_{25}$, 700 μM ADP, 100 nM or 300 nM FLuc/1.3 μM BSA, 70 μM luciferin, 5% DMSO, 30°C. The assays were prepared on a 96 well plate, half are, with a total volume of 100 μL as follow: a total of 18 *Ft*PPK time courses (six sets of time courses in triplicate: three sets coupled to 100 nM FLuc and three sets coupled to 300 nM FLuc), 6 negative control assays (lacking *Ft*PPK, each measured in triplicate) and 3 sets of ATP standard curves (to monitor the activity of the FLuc with time). For the reagent preparation and the assay protocol refer to section 7.4.3.7 and Table 7.46 (adjusting for the appropriate DMSO and FLuc concentration).

7.5.1.2. End-point assay format in 96 and 384 well microplate

An end-point assay format was developed for HTS in which the activity of the *Ft*PPK was monitored by a single time point measurement within the linear phase of the *Ft*PPK time course (32 seconds). The end-point format was initially developed on a 96 well half area microplate and later transferred to a 384 well microplate, in both cases with a total volume of 100 μL. The following assay conditions (not fully optimised) were applied: 35 nM *Ft*PPK/1.3 μM BSA, 30 μM $PolyP_{25}$, 700 μM ADP, 300 nM FLuc/1.3 μM BSA, 70 μM luciferin, 5% DMSO, 30°C. The assays were prepared as described in section 7.4.3.9 and according to Table 7.47 (adjusting for the appropriate concentration of FLuc).

HTS end-point format in a 96 well plate: The 96 well microplate was prepared as follow: 40 *Ft*PPK-FLuc positive control assays, 40 negative control assays (no *Ft*PPK), two sets of ATP standard curve assays. The positive control assays and the negative control assays

were prepared in alternate columns (from columns 2 to 11), the ATP standard curve assays were prepared in column 1 and column 12 (refer to Appendix, section A3 1.1.1).

HTS end-point format in a 384 well plate: The 384 well microplate was prepared as follow: 160 *Ft*PPK-FLuc positive control assays, 160 negative control assays (no *Ft*PPK), 8 sets of ATP standard curve assays. For both the assay measurement and the data analysis, it was convenient to divide the microplate in four subsections, equivalent to a 96 well microplate and with analogous layout (40 positive control assays and 40 negative control assays in alternate position, plus 2 sets of ATP standard curve assays). The section including column 1 to column 12 and row A to row H was designated Q1 (quarter 1); the section including column 13 to column 24 and row A to row H was designated Q2; the section including column 1 to column 12 and row I to row P was designated Q3; the section including column 13 to column 24 and row I to row P was designated Q4 (refer to Appendix, section A3 1.1.2.

7.5.1.3. Z' factor reproducibility and screening layout determination

The layout for the HTS end-point format to apply for the screening was defined and the Z' day-to-day variability assessed by repeating the screening simulation over five different days. To reduce the signal drift across the microplate the following incubation times were investigated (30°C, prior initiation of the assays): 5 minutes, 15 minutes, 20 minutes, 25 minutes. The assays were prepared in a 384 well plate with a total volume of 100 µL. The following assay conditions (not fully optimised) were applied: 35 nM *Ft*PPK/1.3 µM BSA, 30 µM $PolyP_{25}$, 700 µM ADP, 300 nM FLuc/1.3 µM BSA, 70 µM luciferin, 5% DMSO, 30°C. The microplate was prepared as follow: 280 *Ft*PPK-FLuc assays, of which 40 assays to be used as negative control assays (no variation of the signal, 0% inhibition) and the remaining 240 to screen 80 library compounds in triplicate; 40 positive control assays (no *Ft*PPK, maximal variation of the signal. 100% inhibition); 8 sets of ATP standard curve assays.[r] The assay reagents were prepared as reported in section 7.3.3.2. To reduce the data

[r] So far, have been called positive controls those assays containing all the components, and negative controls those assays lacking *Ft*PPK. However, for the current experiment and when referring to the screening, those assays of which the activity was comparable to what observed in the presence of a strong inhibitor (no *Ft*PPK, 100% inhibition, no signal emitted) were labelled as positive controls.

variability that could derive from multiple injections with consequent increase of the experimental error, the *Ft*PPK/BSA and the FLuc/BSA solutions were included in the assay solution, as described in Table 7.19.

The assays components were dispensed into the microplate by the automated workstation according to the steps reported below. Per each step the injection of the assay components was performed in the order: Q1, Q3, Q2 and Q4. Only after completing the injection in each quarter the next step was started

1. To simulate the library compound addition step, 5 μL DMSO (100% stock) were dispensed in the wells due to contain the ATP standard curve assays, the positive control assays, the negative control assays and the assays due to contain the library compounds (in the reported order).
2. The ATP standard curve assays were prepared by dispensing 65 μL of the respective assay solution and then 10 μL ATP at the appropriate concentration (Table 7.18).
3. The positive control assays were prepared by dispensing 55 μL of the respective assay solution (no *Ft*PPK, comparable to 100% inhibition).
4. The negative control assays (no variation of the signal, comparable to 0% inhibition) and the assays due to contain the library compounds were prepared by dispensing 55 μL of the respective assay solution (Table 7.19).
5. The microplate plate was incubated into the BMG plate reader at 30°C for the appropriate time before to start the *Ft*PPK-FLuc assay.

For details on the plate reader control protocols set up for the assays measurement refer to Appendix, section A3 1.1.2

7.5.1.4. HTS format, optimised conditions

The final optimised conditions (section 2.2.4.4) were applied to the HTS format and the latter further improved to achieve a satisfactory and reproducible Z' factor. The assays were prepared in a 384 well plate with a total volume of 100 μL. The following optimal conditions were applied: 10 nM *Ft*PPK/1.3 μM BSA, 1.5 μM $PolyP_{25}$, 200 μM ADP, 300 nM FLuc/1.3

assays, while those assays containing DMSO but no inhibitors for which full activity was observed (0% inhibition, maximum signal emitted) were labelled as negative control assays.

μM BSA, 70 μM luciferin, 5% DMSO, 30°C. The assay reagent solutions were prepared as reported in section 7.3.3.2. The assays were prepared in the microplate applying the HTS layout and the protocol described in 7.5.1.3. Unless differently stated, the microplate was incubated for 20 minutes at 30°C, prior the start and the measurement of the assays. To define the final conditions for HTS, the assay performance was investigated at three different time points:

- *HTS 30 seconds end-point format*: the assays were measured applying the protocols and the script described in Appendix, section A3 1.1.2, Table A3 2.
- *HTS 60 seconds end-point format*: the assays were measured applying protocols similar to the 30 seconds end-point format protocols, modified with respect to the delay between the injection of the ADP and the injection of the FLuc, which was extended to 30 seconds (Appendix, section A3 1.1.2, Table A3 3).
- *HTS 90 seconds end-point format*: the assays were measured applying protocols similar to the 30 seconds end-point format protocols, modified with respect to the delay between the injection of the ADP and the injection of the FLuc, which was extended to 45 seconds (Appendix, section A3 1.1.2, Table A3 4).

7.5.2. PKIS library screening

The PKIS library was screened by the *Ft*PPK-FLuc coupled assay in end point format (30 seconds), applying the (not fully optimised) conditions: 35 nM *Ft*PPK/1.3 μM BSA, 30 μM $PolyP_{25}$, 700 μM ADP, 100 nM or 300 nM FLuc/1.3 μM BSA, 70 μM luciferin, 5% DMSO, 30°C (Table 3.1). The assay reagent solutions were prepared as reported in section 7.3.3.2. The assays were prepared in the microplate according to the layouts reported in section A3 1.1 (libraries plate layout and the screening plate layout) and following the protocol described in section 7.5.1.3 (end point: 30 seconds), with the difference that at step 1 not only DMSO but also the library compounds were added into the microplate. For details on the plate reader set up for the assay measurement refer to Appendix, section A3 1.1.2, Table A3 2.

7.5.3. Reynolds library screening

The Reynolds library was screened by the *Ft*PPK-FLuc coupled assay in end point format (90 seconds), applying the optimal conditions: 10 nM *Ft*PPK/1.3 μM BSA, 1.5 μM $PolyP_{25}$, 200 μM ADP, 300 nM FLuc/1.3 μM BSA, 70 μM luciferin, 10 μM library compound, 5% DMSO, 30°C (Table 3.2). The assay reagent solutions were prepared as reported in section 7.3.3.2. The assays were prepared in the microplate according to the layouts reported in section A3 1.1 (libraries plate layout and the screening plate layout) and following the protocol described in section 7.5.1.3 (end point: 90 seconds), with the difference that at step 1 not only DMSO but also the library compounds were added into the microplate. For details on the plate reader set up for the assay measurement refer to Appendix, section A3 1.1.2, Table A3 4.

7.6. Experimental for Chapter 4

7.6.1. Independent luminescence assays counter screen

The PKIS hits and the Reynolds library hits were counter screened with the independent luminescence assays to investigate their activity on the FLuc. The assays were prepared on a 96 well microplate with a total volume of 100 µL. The following assay conditions were applied: 300 nM FLuc/2.6 µM BSA, 70 µM luciferin, 10 µM ATP, 5% DMSO, 30°C. Each compound was tested in triplicate at the concentration of 10 µM. Alongside the assays containing the identified hits, the following control assays were prepared: negative control assays (0% inhibition): 3 assays in triplicate with only DMSO and 3 assays in triplicate with 10 µM library compound not selected as hit; positive control assays (100% FLuc inhibition): assays in which no FLuc was added. To monitor the activity of the FLuc with time, three standard curves were also prepared on the microplate. The assay were prepared as reported in section 7.3.3.1.

7.6.2. Thermal shift assay

7.6.2.1. Thermal shift assay optimisation

The optimisation of the conditions for thermal shift assay entailed the investigation of a suitable signal detection mode and optimal concentration of *Ft*PPK and SYPRO Orange. The thermal shift assay was measured by means of a real time PCR machine. Investigation of the detection mode (combined FAM/ROX channel vs FRET mode) proved the fluorescence measurement in FRET mode to be superior. The following concentration of *Ft*PPK and SYPRO Orange were tested for the identification of optimal conditions: 0.5 µM, 1 µM, 2 µM, 5 µM *Ft*PPK; 1x, 2x, 5x, 10x, 20x SYPRO Orange. Each concentration of *Ft*PPK was tested in the presence of each concentration of SYPRO Orange (in triplicate). Control assays with only *Ft*PPK (but not SYPRO Orange) and with only SYPRO Orange (but not *Ft*PPK) were prepared to measure background fluorescence. The assays were prepared in white PCR tubes in a 30 µL final volume, according to Table 7.51. The *Ft*PPK was prepared by dilution in assay buffer (Table 7.20) to a 10x final concentration. The assay solution (27 µL) was manually dispensed in the white PCR tube and incubated for 10 minutes at room temperature. The SYPRO Orange (3 µL) was added just before

measurement. The PCR tubes were sealed with appropriate caps to prevent evaporation and the solutions vortexed to ensure appropriate mixing (30 sec). The temperature was raised from 25°C to 95°C, at the rate of 0.5 °C min^{-1}. For data analysis, the T_m was defined by fitting the curve derived from the average of the triplicates to the Boltzmann equation. Because of the rapid decrease of the signal after the maximum of fluorescence was reached, the data beyond the third measurement were not considered for the fitting.

Table 7.51: Thermal shift assay, *Ft*PPK melting curve

Component	Component stock	Final concentration	Vol/ 30 µL
Assay buffer	2x		12 µL
*Ft*PPK	5 - 50 µM	0.5 - 5 µM	3 µL
DMSO	100%	5%	1.5 µL
DI water			10.5 µL
Added as last			
SYPRO Orange	10 - 200x	1 – 20x	3 µL

7.6.2.2. Hit validation by thermal shift assay

The thermal shift assay was applied for hit validation under the following conditions: 1 µM *Ft*PPK, 5x SYPRO Orange, 5% DMSO. The PKIS library hits were tested in duplicate at the concentration of 100 µM. The Reynolds library hits were tested in triplicate at the concentration of 10 µM, 50 µM and 100 µM. The assay solutions for the *Ft*PPK melting curve measurement in the presence of the hit compound were prepared were according to Table 7.52. The following control assays were also prepared: *Ft*PPK melting curve with 5% DMSO; control assays with *Ft*PPK assay but not SYPRO Orange; control assays with the library compound and SYPRO Orange but not *Ft*PPK. The hit compound or DMSO (1.5 µL) was dispensed into the PCR tube and then the assay solution containing the *Ft*PPK was added (25.5 µL). The assays solution was mixed by vortex and incubated at room temperature for 10 minutes. The SYPRO Orange was then added (3 µL), the PCR tube sealed and the solution mixed again by vortex (30 sec). The temperature was raised from 25°C to 95°C, at the rate of 0.5 °C min^{-1}. The assays were measured in FRET mode. The data analysed as reported in section 7.6.2.1.

Table 7.52: Thermal shift assay, *Ft*PPK melting curve in the presence of hit compound

Component	Component stock	Final concentration	Vol/ 30 µL
Assay buffer	2x		12 µL
*Ft*PPK	10 µM	1 µM	3 µL
Hit/DMSO	200 µM or 1 mM or 2 mM / 100%	10 µM or 50 µM or 100 µM / 5%	1.5 µL
DI water			10.5 µL
Added as last			
SYPRO Orange	50x	5x	3 µL

7.6.3. HPLC-based *Ft*PPK assay

7.6.3.1. HPLC method optimisation and *Ft*PPK assay quenching investigation

The first RP IP HPLC method applied for the analysis of the *Ft*PPK assay was a water/MeOH system, using DMHA as ion pairing agent. The mobile phases A was: 15 mM DMHA, 5% MeOH in water, pH 7; the mobile phase B was: 15 mM DMHA, 80% MeOH in water, pH 7. The pH was adjusted with acetic acid and the solution filtered prior use. The elution methods reported in Table 7.53 were investigated for optimal chromatographic separation of ADP and ATP (prepared as reported in section 7.3.3.3, Table 7.22). It should be noted that at this stage the final concentration of NaCl in the assays was 300 mM (assay buffer used: Table 7.33).

Table 7.53: DMHA-based RP IP HPLC, elution methods

Time	DMHA method 1	DMHA method 2	DMHA method 3
0 min:	25%B	25%B	25%B
5 min:	25%B	25%B	25%B
22 min	55%B	-	-
27 min	55%B	65%B	60%B
28 min	100%B	100%B	100%B
33 min	100%B	100%B	100%B
34 min	25%B	25%B	25%B
44 min	25%B	25%B	25%B

The DMHA method 3, which provided the best nucleotide resolution, was tested with three possible methods to stop the *Ft*PPK assay (prepared as reported in section 7.3.3.3, in the assay buffer Table 7.33):

- Heat quenching: the 100 μL assay solution were transferred into an PCR tube placed on a PCR machine at the constant temperature of 95°C for 5 minutes.
- Quenching by EDTA: the 100 μL assay solution were transferred into a PCR tube containing 10 μL of EDTA (550 mM, 50 mM final concentration in the final volume of 110 μL).
- Quenching by formic acid: the 100 μL assay solution were transferred into a PCR tube containing 10 μL of formic acid (1 M final assay concentration).

7.6.3.2. HPLC based-*Ft*PPK assay: time course to define a useful time point for the end-point format.

A *Ft*PPK time course was prepared and analysed by HPLC, in order to establish the assay linear phase and select a time point suitable for an end-point format. The conditions adopted for the screening were applied for the *Ft*PPK assay: 10 nM *Ft*PPK, 2.6 μM BSA, 200 μM ADP, 1.5 μM or 30 μM $polyP_{25}$, 5% DMSO, 30°C. The assays were prepared as reported in section 7.3.3.3, except for the assay buffer, which provided a 300 mM NaCl final concentration (Table 7.33). For the preparation of a *Ft*PPK time course, the *Ft*PPK reaction was stopped by addition of EDTA at the desired time point. The assays were prepared according to the general protocol described in section 7.3.3.3: step 1 and step 2 were executed exactly as reported; to stop the assay (step 3), 100 μL aliquots were taken out from the *Ft*PPK reaction solution and added at the desired time point to PCR tubes containing 10 μL EDTA (550 mM stock solution, giving a 50 mM final concentration in the total volume of 110 μL).The *Ft*PPK sample were analysed using the DMHA method 3 (Table 7.53).

7.6.3.3. HPLC based-*Ft*PPK assay: TEAA method development

To improve the peak shape and the resolution of the adenosine nucleotides, an HPLC method using TEAA as ion pairing agent was developed. Both a water/ACN system (Table

7.54) and a water/MeOH system (Table 7.23) were tested, applying a various range of elution methods (reported in section A4 3.2). The optimal system and elution gradient selected for the *Ft*PPK assay were described in the general section 7.3.3.3.

Table 7.54: TEAA/ACN system for RP IP HPLC

	Component	Final concentration	Vol
Mobile phase A	TEA	0.1 M	27.8 mL
	Acetic acid (10 mM)		cca. 18 mL*
	DI water	100%	up to 2 L
Mobile phase B	TEA	0.1 M	7 mL
	Acetic acid (10 mM)		cca. 6 mL*
	ACN	50%	250 mL
	DI water	20%	up to 500 mL

*approximate volume to adjust to pH 7

7.6.3.4. HPLC based-*Ft*PPK assay: end-point format analysed by the TEAA method

To establish the conditions for an HPLC-based assay in end-point format, suitable for hit validation, replicates of the *Ft*PPK assays, containing either 1.5 μM or 30 μM $polyP_{25}$ and stopped after 180 seconds or 300 seconds respectively, were tested and the data variation evaluated. The assays were prepared as described in section 7.3.3.3. To adapt for end-point format the protocol was slightly modified as reported below:

1. Aliquots (80 μL) of the assay solution (containing *Ft*PPK, $polyP_{25}$, BSA and DMSO) were dispensed in many PCR tubes as many assay replicates prepared.
2. The assay solution samples and the ADP solution were incubated at 30°C for 20 minutes in water bath.
3. The *Ft*PPK assay was started by addition of ADP (20 μL) to the assay solution contained in each PCR tube (precise record of the starting point was taken)
4. The *Ft*PPK were stopped by addition of EDTA (10 μL, 550 mM stock) after either 180 seconds or 300 seconds.

To achieve a good level of reproducibility among the replicates, it was of critical importance to stop the assays exactly after the set delay from the addition of ADP (a timer was used).

The *Ft*PPK samples were analysed applying the optimised TEAA method reported in section 7.3.3.3.

7.6.3.5. HPLC based-*Ft*PPK assay end-point format for hit validation

A long *Ft*PPK time course was measured in the presence of 30 μM $polyP_{25}$, to define the last time point useful for an end-point format assay. The *Ft*PPK conditions applied were: 10 nM *Ft*PPK, 2.6 μM BSA, 200 μM ADP, 30 μM $polyP_{25}$, 5% DMSO, 30°C. The assays were prepared as reported in section 7.3.3.3 and according to the protocol described in section 7.6.3.2. The sample were analysed by the TEAA method reported in section 7.3.3.3.

7.6.3.6. PKIS and Reynolds library hit validation by HPLC assay

The HPLC-based *Ft*PPK assay in end point format (assays stopped after 7 minutes) was applied for hit validation. A good summary of the *Ft*PPK assay conditions was reported in Table 4.8. The hits were tested in duplicate at 10 μM concentration. The assays were prepared as reported in section 7.3.3.3, with the minor variation of not including the DMSO in the assay solution, which resulted in a small variation also in the protocol for the assay preparation (Table 7.55).

Table 7.55: HPLC-based *Ft*PPK assays for hit validation

Component	Component stock	Final concentration	Vol/ 100 μL
Assay buffer	2x		30 μL
$PolyP_{25}$*	300 μM	30 μM	10 μL
*Ft*PPK/BSA**	100 nM/13 μM	10 nM/1.3 μM	10 μL
BSA**	13 μM	1.3 μM	10 μL
DI water			15 μL
In PCR tube			
Hit/DMSO	200 μM/100%	10 μM/5%	5 μL
To start the FtPPK assay			
ADP*	1 mM	200 μM	20 μL

*Prepared in water; ** Prepared in assay buffer (Table 7.20)

To prepare the assays in end point format, the protocol described in section 7.6.3.4 was applied, with a small variation in the preparation of the assay solution and in step 1. No

DMSO was included in the assay solution but only *Ft*PPK, $polyP_{25}$ and BSA (tot volume: *N*x 75 µL). The hit compound (or DMSO for the control assays, 5 µL) was added into the PCR tubes, followed by addition of the assay solution (75 µL). Step 2, 3 and 4 were maintained unmodified (assays stopped after 420 seconds). The samples were analysed by TEAA method (section 7.3.3.3).

7.7. Experimental for Chapter 5

7.7.1. Synthesis of the Reynolds library hit RL42-PLT9

7.7.1.1. 2-Chloro-N-(naphthalen-1-ylmethyl)acetamide (3)

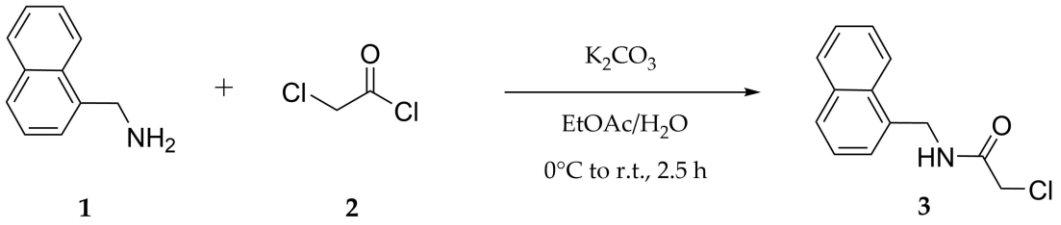

1 **2** **3**

A solution of compound 2 (1.21 mL, 15.2 mmol, 1.6 Eq) in ethyl acetate (50 mL) was added dropwise to a solution of compound 1 (1.4 mL, 9.5 mmol, 1 Eq) and K_2CO_3 (5.34 g, 38 mmol, 4 Eq) in a mixture of ethyl acetate (250 mL) and water (250 mL). The reaction was left to stir vigorously at room temperature for 2.5 h. The organic phase was separated from the aqueous phase and dried over $MgSO_4$. The solvent was removed by rotary evaporation and the residue triturated with hexane. A colourless crystalline solid (R_f: 0.80 in $CHCl_3$:MeOH - 9:1; 0.38 in DCM:MeOH – 1:9) was recovered (2.15 g, 99% yield).

^{1}H NMR (400 MHz, $CDCl_3$): δ 7.92 (1H, d, J = 8.1 Hz, Ar H), 7.83 (1H, d, J = 7.5 Hz, Ar H), 7.77 (1H, dd, J = 6.6, 2.9 Hz, Ar H), 7.48 (2H, m, Ar H) 7.38 (2H, m, Ar H), 6.74 (1H, br. s, N<u>H</u>), 4.88 (2 H, d, J = 5.5 Hz, C<u>H</u>$_2$NH), 4.04 (2H, s, C<u>H</u>$_2$Cl).

^{13}C NMR (400 MHz, $CDCl_3$): δ 165.59 (NH<u>C</u>O), 133.91 (Ar C), 132.54 (Ar C), 131.32 (Ar C), 128.97 (Ar CH), 128.91 (Ar CH), 126.85 (Ar CH), 126.78 (Ar CH), 126.14 (Ar CH), 125.40 (Ar CH), 123.19 (Ar CH), 42.60 (<u>C</u>H$_2$NH), 42.01 (<u>C</u>H$_2$Cl).

LRMS (ESI$^+$) m/z: 234.17, 235.25, 236.13 $(M+H)^+$, 256.11 $(M+Na)^+$.

7.7.1.2. {2-[(Naphthalen-1-ylmethyl)amino]-2-oxoethyl}triphenylphosphonium salt (4)

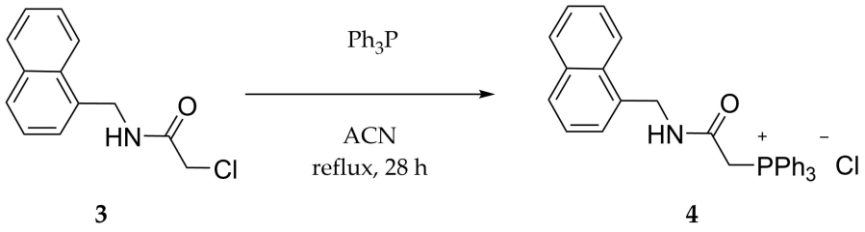

To a solution of compound 3 (2 g, 8.55 mmol, 1 Eq) in acetonitrile (60 mL) triphenylphosphine (3.36 g, 12.8 mmol, 1.5 Eq) was added. The reaction mixture was refluxed until the starting material completely disappeared (28 h). The phosphonium salt (4) precipitated during reflux in the reaction mixture. The solid residue was filtered and washed with ethyl acetate. A fine white-pink powder was recovered (3.84 g, 90% yield).

^{1}H NMR (400 MHz, $CDCl_3$): δ 10.5 (1H, br t, J = 5.56 Hz x2, $CH_2N\underline{H}CO$), 8.03 (1H, d, J = 7.3 Hz, Ar H), 7.74 (1H, d, J = 6.9 Hz, Ar H), 7.65 (7H, m, Ar H), 7.55 (3H, m, Ar H), 7.39 (8H, m, Ar H), 7.33 (1H, d, J = 6.7 Hz, Ar H), 7.23 (1H, m, Ar H), 5.04 (2H, d, J = 14.5 Hz, $COC\underline{H}_2P$), 4.69 (2H, d, J = 6.1 Hz, $C\underline{H}_2NHCO$).

^{13}C NMR (400 MHz, $CDCl_3$): δ 162.42 ($\underline{C}OCH{=}P$), 162.32 ($\underline{C}OCH_2P$), 134.78 ($\underline{C}$H, Ar phenyl), 134.74 ($\underline{C}$H Ar phenyl), 134.02 ($\underline{C}$H Ar phenyl), 133.91 ($\underline{C}$H, Ar phenyl), 133.66 (C, Ar naphthyl), 133.33 (C, Ar naphthyl), 131.32 (C, Ar naphthyl), 129.99 (CH, Ar phenyl), 129.86 ($\underline{C}$H, Ar phenyl), 128.30 ($\underline{C}$H, Ar naphthyl), 127.74 ($\underline{C}$H, Ar naphthyl), 126.75 ($\underline{C}$H, Ar naphthyl), 126.36 ($\underline{C}$H, Ar naphthyl), 125.55 ($\underline{C}$H, Ar naphthyl), 125.40 ($\underline{C}$H, Ar naphthyl), 124.03 ($\underline{C}$H, Ar naphthyl), 118.72 ($COCH{=}P\underline{C}$), 117.84 ($COCH_2P\underline{C}$), 41.49 ($\underline{C}H_2NH$), 32.27 ($CO\underline{C}H{=}P$), 31.73 ($CO\underline{C}H_2P$).

LRMS (ESI^+) m/z: 460.26 $(M)^+$, 461.24, 462.25 $(M{+}H)^+$.

7.7.1.3. {2-[(Naphthalen-1-ylmethyl)amino]-2-oxoethyl}triphenylphosphonium ylide (5)a

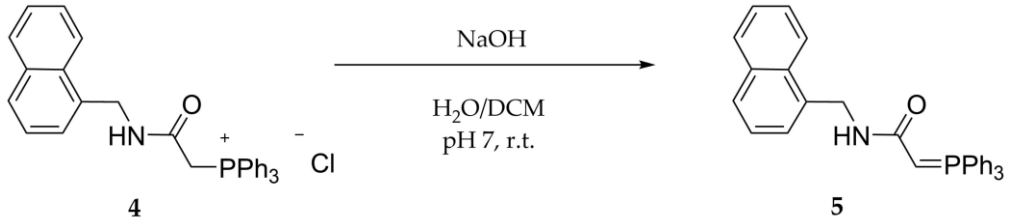

4 5

The phosphonium salt 4 (150 mg, 0.3 mmol, 1 Eq) was dissolved into a mixture of water (2.5 mL) and DMC (2.5 mL).[455] The reaction was stirred vigorously to avoid separation of the phases and NaOH (1 mL, 2 M) was added. The pH was adjusted by addition of HCl (1M) to 7-8. The reaction was monitored by TLC ($CHCl_3$:MeOH – 9:1). After 30 minutes no starting material (R_f 0.34) was left but two new spots appeared (R_f 0.58 and 0.68). The two phases were separated and the aqueous layer extracted with DCM (3 x 10 mL). The combined organic phases were washed with brine and then dried over $MgSO_4$. The reaction mixture was purified by silica chromatography and the spots analysed by mass spectrometry and NMR. The two spots were identified as:

Spot R_f 0.68: triphenylphosphine oxide. ^{1}H NMR (400 MHz, $CDCl_3$): δ 7.6 (6 H, m, Ar), 7.47 (3 H, m, Ar), 7.39 (6 H, m, Ar). LRMS (ESI^+) m/z: 279.16, $(M+H)^+$.

Spot R_f 0.58: N-(1-naphthylmethyl)-acetamide. ^{1}H NMR (400 MHz, $CDCl_3$): δ 7.94 (1H, d, J = 8.07 Hz, naphthyl H), 7.8 (1H, m, 1H, naphthyl H), 7.74 (1H, m, naphthyl H), 7.46 (2H, m, naphthyl H), 7.37 (2H, m, naphthyl H),[s] 5.72 (1H, br s, $CH_2N\underline{H}CO$), 4.81 (2H, d, J = 5.4 Hz, $C\underline{H}_2NHCO$), 1.93 (3H, s, $NHCOC\underline{H}_3$).[t] LRMS (ESI^+) m/z: 200.15 $(M+H)^+$, 222.16 $(M+Na)^+$.

[s] The integral for the peaks at 7.46 and 7.37 δ were 3.5 and 5 respectively, from which the number of H assigned to the triphenylphosphine oxide (refer to note c) were subtracted.

[t] In the spectrum the following signals were assigned to H from the phenyl groups of triphenylphosphine oxide: 7.58 (3H, m, phenyl H), 7.46 (1.5H, m, phenyl H), 7.37 (3H, m, phenyl H). In the analysed sample the ratio between the acetamide derivative and the triphenylphosphine oxide was 2:1

7.7.1.4. {2-[(Naphthalen-1-ylmethyl)amino]-2-oxoethyl}triphenylphosphonium ylide (5)b

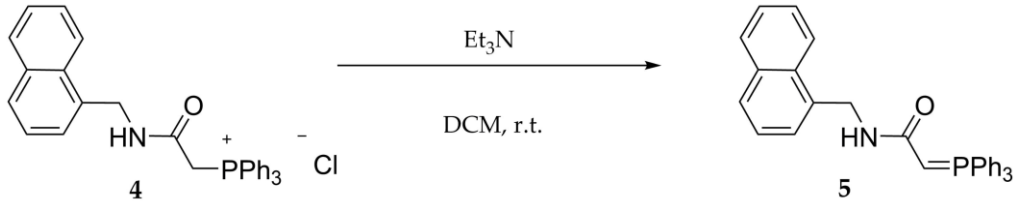

The phosphonium salt 4 (80 mg, 0.16 mmol, 1 Eq) was dissolved in DCM (1.6 mL) and Et_3N (15 µl, 0.177 mmol, 1.1 Eq) was added. The reaction was monitored by TLC. Spots with a similar R_f as for the reaction reported on section 7.7.1.3 were detected. The starting material consumption was much slower, however only degradation products were obtained as confirmed by mass spectrometry.

7.7.1.5. N-{9-[(3aR,4R,6S,6aS)-6-Formyl-2,2-dimethyltetrahydrofuro[3,4-d][1,3]dioxol-4-yl] -9H-purin-6-yl}benzamide (8)

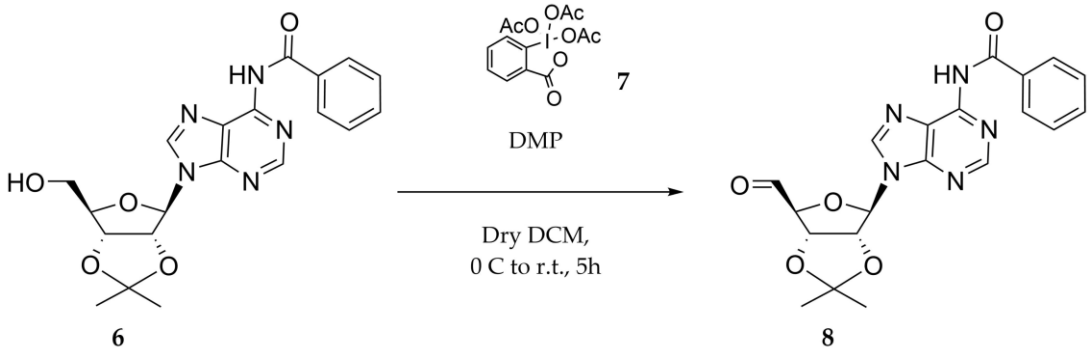

The DMP reagent (1.32 g, 3.11 mmol, 1.3 Eq) was suspended in freshly distilled DCM (5 mL) and cooled on ice. To the suspension of DMP a solution of adenosine 6 (1 g, 2.43 mmol, 1 Eq) in freshly distilled DCM (15 mL) was added. The reaction mixture was prepared under N_2, stirred on ice for the first hour then gradually warmed to room temperature and left to stir for 6 hours. It was not possible to monitor the reaction by TLC because of the similar R_f of the adenosine derivative (R_f: 0.58, $CHCl_3$:MeOH – 95:5) and the bigger spot detected in the reaction mixture (R_f between 0.41 and 0.60, spots with R_f 0.74 and 0.25 were also detected). The formation of the aldehyde derivative was confirmed by NMR

analysis. After 6 hours no significant changes were observed on the TLC and NMR showed that only about 18 % of the starting material remained unreacted (same amount remained after leaving the reaction overnight). To quench the excess of DMP a 10% solution of $Na_2S_2O_3$ in a saturated $NaHCO_3$ solution was prepared. The reaction mixture was diluted with ethyl acetate (50 mL) and the $Na_2S_2O_3$ solution added until the two phases became clear. The two layers were separated and the organic washed with a $NaHCO_3$ saturated solution (3 x 50 mL) and brine (30 mL) and then dried over $MgSO_4$. The solvent was removed and the obtained crude mixture (oily residue) was used for the Wittig reaction without prior purification (580 mg, 58% yield).

^{1}H NMR (400 MHz, $CDCl_3$):[u] δ 9.28 (1H, s, CHC<u>H</u>O), 8.92 (1H, s, N<u>H</u>COPh), 8.60 (1H, s, adenine-pyrimidine ring CNC<u>H</u>NC), 8.06 (1H, s, adenine-imidazole ring, NC<u>H</u>N), 7.95 (2H, br d, J = 7.3, *o*-benzoyl H), 7.55 (1H, m, *p*-benzoyl H), 7.47 (2H, m, *m*-benzoyl H), 6.21 (1H, s, ribose ring, OC<u>H</u>(N)CH(O)CH(O)), 5.5 (1H, dd, J = 6.1, 1.6 Hz, ribose ring, OCH(N)CH(O)C<u>H</u>(O)), 5.29 (1H, d, J = 6 Hz, ribose ring, OCH(N)C<u>H</u>(O)CH(O)), 4.64 (1H, d, J = 1.34 Hz, ribose ring, CH(O)CH(O)C<u>H</u>(CHO)O), 1.55 (3H, s, OCC<u>H</u>$_3$), 1.35 (3H, s, OCC<u>H</u>$_3$).

^{13}C NMR (400 MHz, $CDCl_3$):[v] δ 199.37 (<u>C</u>HO), 164.51 (NH<u>C</u>OPh), 152.66 (adenine-pyrimidine ring CN<u>C</u>HNC), 150.55 (adenine C), 149.93 (benzoyl C), 142.47 (adenine-imidazole ring, NC<u>H</u>N), 133.32 (adenine C), 133.00 (adenine C), 128.95 (benzoyl CH), 127.91 (benzoyl CH), 123.65 (benzoyl CH), 114.21 (<u>C</u>(CH$_3$)$_2$), 93.16 (ribose, O<u>C</u>H(N)CH(O)), 92.43 (ribose OCH(N)CH(O)<u>C</u>H(O)), 84.73 (ribose OCH(N)<u>C</u>H(O) CH(O)), 83.60 (ribose CH(O)CH(O)<u>C</u>H(CHO)O), 26.59 (OC<u>C</u>H$_3$), 25.03 (OC<u>C</u>H$_3$).

LRMS (ESI$^+$) m/z: 427.14 $(M+NH_4)^+$.

[u] The assignment has been done by comparison with the spectrum of the starting material N6-Benzoyl-2',3'-Isoproylidene-adenosine, which in turn has been assigned by referring to Ciuffreda P.,[568] and by comparison with the spectrum reported by Thompson S.[460]

[v] Some degree of uncertainty applies to the assignment of the aromatic carbons.

7.7.1.6. N-{9-[(3aR,4R,6R,6aR)-2,2-Dimethyl-6-((*E*/*Z*)-3-((naphthalen-1-ylmethyl)amino)-3-oxoprop-1-en-1-yl)tetrahydrofuro[3,4-d][1,3]dioxol-4-yl]-9H-purin-6-yl}benzamide (9)

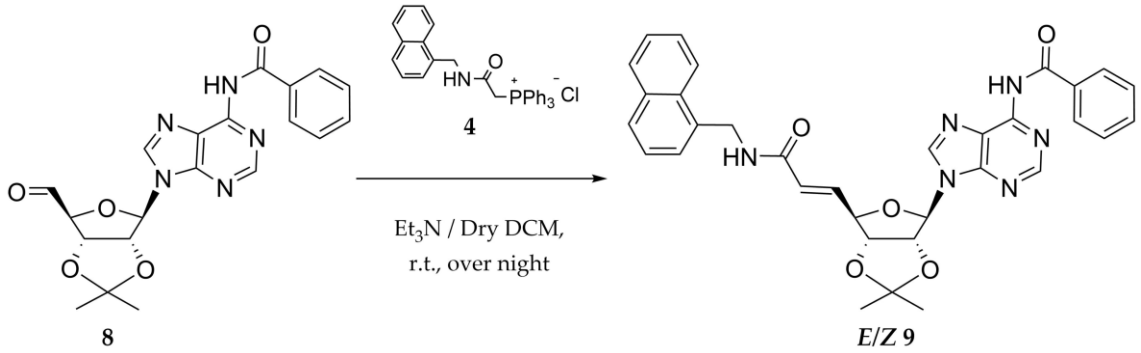

To a solution of phosphonium salt 4 (1.57 g, 2.7 mmol, 2 Eq) in DCM (10 mL) a solution of crude aldehyde 8 (570 mg, 1.38 mmol, 1 Eq) in DCM (25 mL) was added. The reaction was started by *in situ* generation of the ylide 5 upon addition of Et_3N (1.5 mL, 11 mmol, 8 Eq). To ensure anhydrous condition and prevent degradation of the ylide, the reaction was done under N_2 and freshly distilled DCM and Et_3N were used. As soon as the Et_3N was added, a change of colour from light yellow to an intense yellow-orange was observed. The intense colour faded after about half an hour. The reaction mixture was left to stir at room temperature overnight. The solvent was removed by rotary evaporation and the crude oil was purified by column chromatography ($CHCl_3$:EtOAc - 40:60). To improve the separation of the two isomers (*Z*-isomer R_f 0.28, *E*-isomer R_f 0.17, $CHCl_3$:EtOAc - 40:60) a gradient from 60% to 40% $CHCl_3$ was applied. Overall, 605 mg of Wittig product were recovered (90 mg *Z*-isomer, 420 mg *E*-isomer, 95 mg *Z/E* isomer mixture). The overall yield was 74% (*Z*/*E* isomers: 1:3 ratio).

<u>*Z*-isomer</u> ^{1}H NMR (400 MHz, $CDCl_3$): δ 8.95 (1H, s, N<u>H</u>COPh), 8.70 (1H, s, adenine-pyrimidine ring CNC<u>H</u>NC), 7.97 (1H, s, adenine-imidazole ring, NC<u>H</u>N), 7.93 (3H, m, naphthyl 1H, *o*-benzoyl 2H), 7.8 (1H, d, J = 7.4 Hz, naphthyl H), 7.74 (1H, d, J = 7.4 Hz, naphthyl H), 7.54 (1H, m, *p*-benzoyl H), 7.46 (4H, m, naphthyl 2H, *m*-benzoyl 2H), 7.35 (2H, m, naphthyl H), 6.02 (1H, d, J = 2 Hz, ribose ring, OC<u>H</u>(N)CH(O)CH(O)), 5.95 (1H, br t, J = 5.1x 2 Hz, CH_2N<u>H</u>CO), 5.83 (2H, m, NHCOCH=C<u>H</u>CH; 1H, ribose ring,

CH(O)CH(O)C<u>H</u>(CH=CH)O)),[w] 5.66 (1H, d, J = 10.3 Hz, *Z*-isomer NHCOC<u>H</u>=CHCH), 5.61 (1H, dd, J = 6.1, 1.8 Hz, OCH(N)C<u>H</u>(O)CH(O)), 5.11 (1H, dd, J = 6.2, 2.3 Hz, OCH(N)CH(O)C<u>H</u>(O), 4.89 (2H, m, C<u>H</u>$_2$NHCO), 1.58 (3H, s, OCC<u>H</u>$_3$), 1.37 (3H, s, OCC<u>H</u>$_3$).

<u>*Z*-isomer</u> ^{13}C NMR (400 MHz, $CDCl_3$): 164.67 (C, NH<u>C</u>OPh), 164.56 (C, NH<u>C</u>OCH=CH), 152.73 (CH, adenine), 151.08 (C, adenine), 149.72 (C, benzoyl), 142.85 (CH, adenine), 141.76 (CH),[x] 133.87 (C, adenine and naphthyl),[y] 133.51 (CH, COCH=<u>C</u>H),[x] 133.15 (C, adenine and naphthyl),[y] 132.90 (CH, CO<u>C</u>H=CH), 131.38 (C, naphthyl), 128.92 (CH, benzoyl), 128.81 (CH, naphthyl), 128.77 (CH, naphthyl), 127.84 (CH, benzoyl), 126.94 (CH, naphthyl), 126.72 (CH, naphthyl), 126.07 (CH, naphthyl), 125.41 (CH, naphthyl), 124.60 (CH, benzoyl), 123.52 (CH, naphthyl), 114.35 (<u>C</u>(CH$_3$)$_2$), 91.88 (CH, ribose), 86.59 (CH, ribose), 84.85 (CH, ribose), 83.73 (CH, ribose), 41.86 (<u>C</u>H$_2$NHCOCH=CH), 27.05 (OC<u>C</u>H$_3$), 25.44 (OC<u>C</u>H$_3$).

<u>*E*-isomer</u> ^{1}H NMR (400 MHz, $CDCl_3$): δ 8.71 (1H, s, N<u>H</u>COPh), 8.65 (1H, s, adenine-pyrimidine ring CNC<u>H</u>NC), 8.06 (1H, s, adenine-imidazole ring, NC<u>H</u>N), 7.86 (3H, m, naphthyl 1H, *o*-benzoyl 2H), 7.74 (1H, d, J = 7.4 Hz, naphthyl H), 7.66 (1H, d, J = 7.1 Hz, naphthyl H), 7.53 (1H, m, *p*-benzoyl H), 7.42 (4H, m, naphthyl 2H, *m*-benzoyl 2H), 7.27 (2H, m, naphthyl H), 6.86 (1H, dd, J = 15.3, 4.8 Hz, NHCOCH=C<u>H</u>CH), 6.13 (1H, d, J = 1.8 Hz, ribose ring, OC<u>H</u>(N)CH(O)CH(O)), 5.72 (1H, br t, J = 5.3x 2 Hz, CH$_2$N<u>H</u>CO), 5.56 (1H, dd, J = 6.2, 1.71 Hz, ribose ring, OCH(N)C<u>H</u>(O)CH(O)), 5.52 (1H, dd, J = 15.2, 1.8 Hz, *E*-isomer NHCOC<u>H</u>=CHCH), 5.06 (1H, dd, J = 6.1, 3.4 Hz, OCH(N)CH(O)C<u>H</u>(O), 4.79 (3H, m, C<u>H</u>$_2$NHCO 2H, ribose ring, CH(O)CH(O) C<u>H</u>(CH=CH)O), 1.56 (3H, s, OCC<u>H</u>$_3$), 1.34 (3H, s, OCC<u>H</u>$_3$).

---

[w] The peak is recognized by the software as a multiplette, however it is possible to distinguish the signal from the H at 5' position of the ribose and the H at position 4' despite the overlapping. Coupling constants were also manually calculated: J = 10.6 Hz (coupling of the 5' H with the *cis* H of the double bond, J = 7.5 Hz (coupling of the 5' H with the 4' H), J = 7.3 Hz (coupling of the 4' H with the 5' H).

[x] Difficulties in the assignment, some degree of uncertainty applies.

[y] Based on previous NMR.

E-isomer ^{13}C NMR (400 MHz, $CDCl_3$): 164.67 (C, NHCOPh), 164.08 (C, NHCOCH=CH), 152.80 (CH, adenine), 151.74 (C, adenine), 149.61 (C, benzoyl), 142.52 (CH, adenine), 139.67 (CH, COCH=CH), 133.79 (C, adenine and naphthyl),[z] 133.16 (C, adenine and naphthyl),[f] 132.93 (CH, COCH=CH), 131.31 (C, naphthyl), 128.86 (CH, benzoyl), 128.73 (CH, naphthyl), 128.55 (CH, naphthyl), 127.89 (CH, benzoyl), 126.67 (CH, naphthyl), 126.65 (CH, naphthyl), 125.94 (CH, naphthyl), 125.35 (CH, naphthyl), 123.99 (CH, benzoyl), 123.41 (CH, naphthyl), 114.81 ($C(CH_3)_2$), 90.74 (CH, ribose), 86.47 (CH, ribose), 84.16 (CH, ribose), 83.53 (CH, ribose), 41.73 (CH, CH_2NHCOCH=CH), 27.07 (OCCH_3), 25.37 (OCCH_3).

LRMS (ESI$^+$) m/z: 591.31 $(M+H)^+$, 613.28 $(M+Na)^+$.

7.7.1.7. N-{9-[(2R,3R,4S,5R)-3,4-Dihydroxy-5-((*E*/*Z*)-3-((naphthalen-1-yl methyl)amino)-3-oxoprop-1-en-1-yl)tetrahydrofuran-2-yl]-9H-purin-6-yl} benzamide (10)

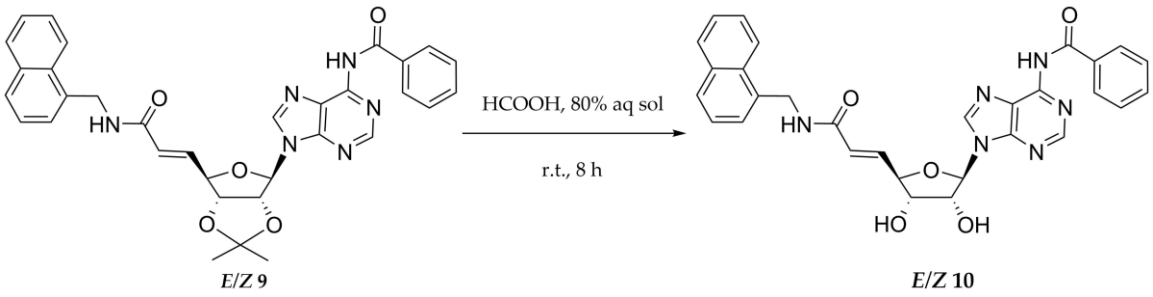

E/*Z* 9 *E*/*Z* 10

The pure isomer *Z* or *E* (*Z*-isomer: 78.5 mg, 0.13 mmol, 1 Eq; *E*-isomer: 276 mg, 0.46 mmol, 1 Eq) was dissolved in formic acid 80% aqueous solution (*Z*-isomer: 4 mL; E-isomer 14 mL) and left to stir at room temperature. The reaction was monitored by TLC (CH_3Cl:MeOH – 9:1, Wittig products: *Z*-isomer R_f 0.71, *E*-isomer R_f 0.63; Deprotection products: *Z*-isomer R_f 0.36, *E*-isomer R_f 0.30) and quenched by co-evaporation with toluene of formic acid under high vacuum when no starting material was detect on TLC (*Z*-isomer: 6 hours, *E*-isomer: 8 hours). The reaction crude was purified by column chromatography (CH_3Cl:MeOH – 3:97). For the *E*-isomer purification after the impurities were washed off (R_f: 0.43 and 0.36, CH_3Cl:MeOH – 9:1) the solvent system was changed to CH_3Cl:MeOH – 5:95 to speed up

[z] Based on previous NMR

the elution of the desired product. For the *Z*-isomer 72 mg (95% yield) were recovered, while for the *E*-isomer 210 mg (80% yield).

Z-isomer ^{1}H NMR (400 MHz, DMSO-d_6): δ 11.27 (1H, br s, NHCOPh), 8.85 (1H, s, adenine-pyrimidine ring CNCHNC), 8.82 (1H, s, adenine-imidazole ring, NCHN), 8.79 (1H, t, J = 5.6 x 2 Hz, NHCOCH=CH), 8.13 (3H, m, naphthyl 1H, *o*-benzoyl 2H), 8.02 (1H, d, J = 7.3 Hz, naphthyl H), 7.94 (1H, d, J = 7.6 Hz, naphthyl H), 7.71 (1H, m, *p*-benzoyl H), 7.63 (4H, m, naphthyl 2H, *m*-benzoyl 2H), 7.55 (2H, m, naphthyl H), 6.49 (1H, dd, J = 11.6, 8.2 Hz, NHCOCH=CH), 6.15 (1H, d, J = 6.2 Hz, ribose ring, OCH(N)CH(OH)CH(OH)), 6.09 (1H, dd, J = 11.7 Hz, *Z*-isomer NHCOCH=CH), 5.78 (1H, m, ribose ring CH(OH)CH(OH)CH(CH=CH)O), 5.65 (2H, d, J = 4.4 Hz, ribose ring, OCH(N)CH(OH)CH(OH)), 4.97 (1H, m, OCH(N)CH(OH)CH(OH)), 4.87 (2H, d, J = 5.6 Hz, CH_2NHCO), 4.2 (1H, m, OCH(N)CH(OH)CH(OH)).

Z-isomer ^{13}C NMR (400 MHz, DMSO-d_6): δ 165.21 (2C, NHCOPh and NHCOCH=CH),[aa] 150.94 (CH, benzoyl), 144.42 (C, adenine), 142.59 (CH, COCH=CH), 134.74 (C, adenine and naphthyl), 133.8 (C, adenine and naphthyl), 131.14 (C, naphthyl), 129.01 (CH, benzoyl), 128.96 (CH, naphthyl), 128.23 (CH, benzoyl), 126.81 (CH, naphthyl), 126.39 (CH, naphthyl), 126.34 (CH, naphthyl), 125.92 (CH, naphthyl), 124.41 (CH, naphthyl), 124 (CH, benzoyl), 111.38 (CH, COCH=CH), 88.18 (CH, ribose), 81.40 (CH, ribose), 79.64 (CH, ribose), 76.02 (CH, ribose), 73.5 (CH, ribose), 46.96 (CH, CH_2NHCOCH=CH).

E-isomer ^{1}H NMR (400 MHz, DMSO-d_6): δ 11.22 (1H, br s, NHCOPh), 8.75 (1H, s, adenine-pyrimidine ring CNCHNC), 8.71 (1H, s, adenine-imidazole ring, NCHN), 8.63 (1H, t, J = 5.7 x 2 Hz, NHCOCH=CH), 8.06 (3H, m, Naphthyl 1H, *o*-benzoyl 2H), 7.95 (1H, d, J = 7.3 Hz, naphthyl H), 7.86 (1H, d, J = 7.6 Hz, naphthyl H), 7.65 (1H, m, *p*-benzoyl H), 7.56 (4H, m, naphthyl 2H, *m*-benzoyl 2H), 7.46 (2H, m, naphthyl H), 6.89 (1H, dd, J = 15.34, 5.56 Hz, NHCOCH=CH), 6.22 (1H, dd, J = 15.41, 1.47 Hz, *E*-isomer NHCOCH=CH), 6.11 (1H, d, J = 4.8 Hz, ribose ring, OCH(N)CH(OH)CH(OH)), 5.69 (1H, d, J = 5.5 Hz,

[aa] Only one peak was observed at δ 165.21 with higher relative intensity than observed for the Wittig product. In the latter case the signal for the two C=O was very close. Therefore, it was hypothesised that the signal at δ 165.21 derive from both the C=O groups.

ribose ring, OCH(N)CH(O<u>H</u>)CH(OH)), 5.58 (1H, d, J = 5.7 Hz, ribose ring, OCH(N)CH(OH)CH(O<u>H</u>)), 4.81 (2H, d, J = 5.6 Hz, C<u>H</u>$_2$NHCO), 4.75 (1H, q, J = 5.1 x 3 Hz, OCH(N)C<u>H</u>(OH)CH(OH)), 4.55 (1H, m, ribose ring, CH(OH)CH(OH) C<u>H</u>(CH=CH)O), 4.29 (1H, q, J = 5.3 x 3 Hz, OCH(N)CH(OH)C<u>H</u>(OH)).

<u>*E*-isomer</u> ^{13}C NMR (400 MHz, DMSO-d_6):[bb] δ 166.10 (C, NH<u>C</u>OPh), 164.64 (C, NH<u>C</u>OCH=CH), 150.94 (C, benzoyl), 143.95 (C, adenine), 139.81 (CH, COCH=<u>C</u>H), 134.88 (C, adenine and naphthyl), 133.77 (C, adenine and naphthyl), 132.93 (CH, CO<u>C</u>H=CH), 131.37 (C, naphthyl), 129.03 (CH, benzoyl), 128.99 (CH, naphthyl), 128.86 (CH, naphthyl), 128.12 (CH, benzoyl), 126.75 (CH, naphthyl), 126.37 (CH, naphthyl), 126.29 (C, naphthyl), 126.23 (CH, naphthyl), 125.89 (CH, naphthyl), 125.19 (CH, naphthyl), 124.00 (CH, benzoyl), 88.40 (CH, ribose), 83.35 (CH, ribose), 74.15 (CH, ribose), 73.26 (CH, ribose), 49.06 (CH, <u>C</u>H$_2$NHCOCH=CH).

LRMS (ESI$^+$) m/z: 551.44 $(M+H)^+$, 573.31 $(M+Na)^+$.

HRMS (ESI$^+$) m/z: calculated for $C_{30}H_{26}N_6O_5$ $(M+H)^+$ 551.2043, found 551.2037.

[bb] Some degree of uncertainty applies to the assignment of the aromatic carbons.

7.7.2. Characterisation of compound RL42-Plt9

7.7.2.1. Isomers activity and IC_{50} measurement by HPLC assay

The activity of the pure re-synthesised isomers *E* and *Z* was tested by HPLC-based *Ft*PPK assay in end point format (assays stopped after 7 minutes), applying the following conditions: 10 nM *Ft*PPK, 30 μM $polyP_{25}$, 200 μM ADP, 2.6 μM BSA, 5% DMSO, 30°C. The two isomers were tested at the final concentrations of 50 μM and 100 μM (the working solutions were prepared to a 20x final concentration), and by determination of IC_{50} curves. In the latter case, a 13 point curve was prepared for each isomer. The different concentration of inhibitors were prepared by two-fold serial dilution from 300 μM and 400 μM top concentration. (prepared as 20x final concentration working solution). Assays with *Ft*PPK and DMSO and assays with no *Ft*PPK were prepared alongside, as 100% activity and 100% inhibition control respectively. The assays were prepared as described in section 7.6.3.5. and analysed by the TEAA method (section 7.3.3.3).

7.7.2.2. Investigation of binding reversibility

7.7.2.2.1. *Ft*PPK HPLC-based assay: jump assay

To investigate the ability of the RL42-Plt9 to bind to the *Ft*PPK with a reversible or irreversible mechanism, the *E* isomer of compound RL42-Plt9 was incubated in high concentration (300 μM) with the *Ft*PPK and then displacement was attempted by competition with ADP (condition A). The activity of the *Ft*PPK after addition of ADP was compared to the activity of controls in which: no inhibitor was added (condition B); inhibitor was added in a concentration (15 μM) that inhibited the *Ft*PPK as if displacement occurred (condition C); inhibitor was added in a concentration (300 μM) that inhibited the *Ft*PPK as if no displacement occurred (condition D). The following assay conditions were applied: 10 nM *Ft*PPK, 30 μM $polyP_{25}$, 200 μM ADP, 2.6 μM BSA, 5% DMSO, 30°C. The assays were prepared as reported in Table 7.56 and in Table 7.57. For condition A, a concentrated solution of *Ft*PPK with RL42-Plt9 and $polyP_{25}$ was prepared (5 μL). Each component was at a concentration such as to match the corresponding concentrations in the control assays after dilution (Table 7.56). The solution of condition A was incubated for 30 minutes at 30°C and then diluted by addition of an ADP solution (95 μL) to a final volume

of 100 µL. In the occurrence of reversible binding, the addition of ADP not only started the *Ft*PPK reaction but also caused a displacement from the *Ft*PPK by direct competition or as a consequence of the dilution. A time course was measured, as described in section 7.6.3.2.

Table 7.56: *Ft*PPK/RL42-Plt9 binding - jump assay: condition A

Component	Component stock	Concentration/5µL	Final Concentration/100µL	Vol/ 100µL
*Ft*PPK**	900 nM	200 nM	10 nM	1.1 µL
RL42-Plt9	6 mM	300 µM/5% DMSO	15 µM	0.25 µL
$PolyP_{25}$*	3 mM	600 µM	30 µM	1 µL
Buffer				2.65 µL
Displacement solution				
Buffer				26.25 µL
BSA**	1 mg/mL		0.2 mg/mL	20 µL
DMSO				4.75 µL
ADP*	1 mM		200 µM	20 µL
DI water				24 µL

*Prepared in water; ** Prepared in assay buffer (Table 7.20)

Conditions B, C and D (Table 7.57) were prepared in parallel according to the standard procedure and a time course measured as described in section 7.6.3.2.

Table 7.57: *Ft*PPK/RL42-Plt9 binding - jump assay: condition B, C, D

Component	Component stock	Final concentration	Vol/ 100 µL
Assay buffer	2x		30 µL
$PolyP_{25}$*	300 µM	30 µM	10 µL
*Ft*PPK/BSA**	100 nM/13 µM	10 nM/1.3 µM	10 µL
BSA**	13 µM	1.3 µM	10 µL
DMSO or RL42-Plt9	100% or 10x	5% or 15 µM or 300 µM	5 µL
DI water			15 µL
To start the FtPPK assay			
ADP*	1 mM	200 µM	20 µL

*Prepared in water; ** Prepared in assay buffer (Table 7.20)

The assays were analysed by the TEAA method (section 7.3.3.3).

7.7.2.2.2. Investigation of RL42-Plt9 binding by mass spectrometry

Potential binding with covalent mechanism was investigated by protein mass spectrometry (ESI^+). The following conditions were applied: 60 μM *Ft*PPK, 100 μM RL42-Plt9, 100 μM $polyP_{25}$, 10 mM $MgCl_2$. To investigate requirement of $MgCl_2$ for possible covalent binding, the *Ft*PPK was prepared in buffer with and without $MgCl_2$ (Table 7.15). To investigate requirement of $polyP_{25}$ for possible covalent, assays were prepare with and without $polyP_{25}$. For each condition tested (Table 7.58), control assays were prepared in which no RL42-Plt9 but only DMSO was added.

Table 7.58: *Ft*PPK/RL42-Plt9 binding – mass spectrometry analysis

Component	[stock]	[Final]	Vol/ 200 μL	Vol/ 200 μL
			Condition 1	**Condition 2**
*Ft*PPK + $MgCl_2$*	66 μM	60 μM	180 μL	180 μL
$PolyP_{25}$*	2 mM	100 μM	-	10 μL
RL42-Plt9	2 mM	100 μM	10 μL	10 μL
DI water			10 μL	-
			Condition 3	**Condition 4**
*Ft*PPK**	66 μM	60 μM	180 μL	180 μL
$PolyP_{25}$*	2 mM	100 μM	-	10 μL
RL42-Plt9	2 mM	100 μM	10 μL	10 μL
DI water			10 μL	

*Prepared in buffer containing $MgCl_2$; ** Prepared in buffer without $MgCl_2$

The sample were analysed by protein mass spectrometry in ESI^+ mode, coupled to HPLC for RP chromatography (column C4) to remove buffer salts.

7.7.2.3. Investigation of RL42-Plt9 mechanism of binding with respect to ADP

To define if compound RL42-Plt9 binds to the *Ft*PPK with competitive, non-competitive or uncompetitive mechanism with respect to the ADP, time courses were prepared at a range of ADP concentrations and in the presence of different concentrations of RL42-Plt9. The concentration of ADP tested were: 62.5 μM, 125 μM, 250 μM, 500 μM, 1000 μM and 2000 μM ADP. Each of this concentration was tested in the presence of: 0 μM (only DMSO), 50 μM, 100 μM and 150 μM RL42-Plt9. To ensure that the linear phase of the time course could be accurately measured also at high concentration of ADP, the *Ft*PPK conditions

applied were: 2.5 nM *Ft*PPK, 30 μM $polyP_{25}$, 2.6 μM BSA, 5% DMSO, 30°C. To prepare the time course, the activity was measured at 90 seconds and then every 30 seconds up to 360 seconds. The assays and the time course were prepared as described in section 7.6.3.2. The assays were analysed by the TEAA method (section 7.6.3.4).

7.7.2.4. Investigation of RL42-Plt9 binding by ITC

ITC experiments were prepared to investigate the binding of compound RL42-Plt9 to the *Ft*PPK. A direct titration of RL42-Plt9 into *Ft*PPK and an inverse titration of *Ft*PPK into R42-Plt9 was attempted, applying in both cases a 1:10 ratio (200 μM titrant/20 μM titrated solution). The *Ft*PPK was exchanged in HEPES buffer (Table 7.59), either by size-exclusion chromatography or by repeated cycles of ultrafiltration by spin-filters (section 7.3.2.6) and stored at -80°C in aliquots. On the day of the experiment, working solutions of RL42-Plt9 (or ligand) and *Ft*PPK were prepared by dilution with ITC buffer.

Table 7.59: ITC buffer

Component	Final concentration	Quantity
HEPES	50 mM	4.76 g
$MgCl_2$	10 mM	1 M, 4 mL
$(NH_4)_2SO_4$	80 mM	1 M, 32 mL
NaCl	25 mM	0.584 g
β-mercaptoethanol*	0.15 mM	4 μL
Glycerol	20%	80 mL
DI water		up to 400 mL
Adjusted to pH 7.8		

*Added before use

For each experiment, 5 mL buffer with 5% DMSO (cell washing and buffer run), 140 μL ligand (2 injections, 40 μL syringe volume plus excess for syringe filling) and 350 μL protein solution (280 μL cell volume plus excess for cell filling) were prepared as reported in Table 7.60 and Table 7.61. All the solutions were degassed prior to use. At the beginning of each experiment, the titration cell and the ligand syringe were rinsed with ultrapure water and then with ITC buffer containing 5% DMSO. To detect possible buffer mismatching and to define the heat of dilution, a titration ligand/buffer was done before the titration

ligand/protein. If mismatching were observed, 0.5% DMSO was added to the buffer and the ligand/buffer titration repeated. If the mismatch was attenuated, the same amount of DMSO was also added to the protein solution prior ligand/protein titration. If the mismatch was not solved, the solution were reprepared. In the occurrence of precipitation during the experiment the titration cell was soaked with detergent for 30 minutes and then rinsed with water and buffer.

Table 7.60: ITC reagent preparation, direct titration

Component	Component stock	Final concentration	Volume
Buffer (5% DMSO)			Vol/5000 µL
ITC Buffer	1x	1x	4750 µL
DMSO	100%	5%	250 µL
RL42-Plt9 (5% DMSO)			Vol/140 µL
ITC Buffer	1x	1x	133 µL
Ligand/DMSO	25 mM/100% DMSO	200 µM	1.1 µL
DMSO	100%	5%	5.9 µL
FtPPK (5% DMSO)			Vol/350 µL
ITC Buffer	1x	1x	219.5 µL
*Ft*PPK	62 µM	20 µM	113 µL
DMSO	100%	5%	17.5 µL

Table 7.61: ITC reagent preparation, inverse titration

Component	Component stock	Final concentration	Volume
FtPPK (5% DMSO)			Vol/140 µL
ITC Buffer	1x	1x	5 µL
*Ft*PPK*	220 µM	200 µM	128 µL
DMSO	100%	5%	7 µL
RL42-Plt9 (5% DMSO)			Vol/350 µL
ITC Buffer	1x	1x	332.5 µL
Ligand/DMSO	7 mM /100% DMSO	20 µM	1 µL
DMSO	100%	5%	16.5 µL

*Concentrated by spin filters

The ITC experiment was run at the temperature of 30°C. A total number of 40 injections of the titrant (syringe) into the titrated solution (titration cell) was performed. The injection volume was 0.4 µL for the first injection and 2 µL for the following injections. The following

settings were applied: injection duration 5 sec, the spacing between injection 150 sec, the filter period 5 sec. The data were analysed by MicroCal iTC_{200} – Origin 7.0 software. Following subtraction of the ligand dilution heat, the measured μcal/sec (injection peaks) versus time (min) were converted into kcal mol^{-1} of injection versus molar ratio and the data fitted to the appropriated model.

7.7.3. RL42-Plt9 activity on *Mr*PPK

The activity of compound RL42-Plt9 was tested on the *Mr*PPK, expressed and purified by A. Parnell.[265] *Mr*PPK accepts both ADP and AMP as substrate. The activity of RL42-Plt9 was tested by comparing time courses prepared in the presence and in the absence of RL42-Plt9 (tested at 100 μM), using either ADP or AMP as substrate.

Table 7.62: *Mr*PPK assay

Component	Component stock	Final concentration	Vol/ 100 μL
Assay buffer	2x		55 μL
$PolyP_{25}$*	10 mM	1 mM	10 μL
*Mr*PPK**	100 nM/13 μM	10 nM/1.3 μM	10 μL
RL42Plt9/DMSO	2 mM/100%	100 μM/5%	5 μL
DI water			15 μL
To start the FtPPK assay			
ADP or AMP*	1 mM	200 μM	20 μL

*Prepared in water; ** Prepared in assay buffer (Table 7.63)

Table 7.63: *Mr*PPK buffer

Component	Component stock	Final concentration	Quantity/2x stock
Tris HCl	100 mM	50 mM	2.12 g
Tris			0.788 g
$MgCl_2$	40 mM	20 mM	5 M, 1.6 mL
NaCl	200 mM	100 mM	2.33 g
Glycerol	40%	20%	80 mL
DI water			up to 200 mL

The pH was adjusted to 8; The buffer composition was advised by Andexer.[265]

The following conditions were applied: 10 nM *Mr*PPK, 200 μM ADP or AMP, 1 mM $polyP_{25}$, 2.6 μM BSA, 5% DMSO, 30°C. The *Mr*PPK assays and time courses were prepared

following the protocols applied for the *Ft*PPK (section 7.6.3.2), according to Table 7.62. The assays were analysed by the TEAA method (section 7.3.3.3).

Appendix

Appendix to Chapter 2

A2 1. Coupled assay optimisation: theoretical calculation of the optimal concentration of the coupled enzyme.

The concentration of the coupled enzyme required to remove the lag phase can be theoretically calculated by means of the equation Eq A2 1, derived by Storer and Cornish-Bowden:[278]

$$t_{99\%} = \frac{\phi\, K_{m2}}{v_2}$$

Eq A2 1: Storer and Cornish-Bowden equation for the derivation of the coupled enzyme

$t_{99\%}$ is the time required to reach the condition $v_2/v_1 = 0.99$ and corresponds to the lag phase; K_{m2} is the K_m of the coupled enzyme with respect to B; v_1 = is the rate of the conversion A to B; ϕ is a coefficient that depends on v_2/v_1 and on v_1/V_{max2}.

For $v_2/v_1 = 0.99$, the value of the ratio v_1/V_{max2} for different values of ϕ has been calculated.[272,278] Knowing the K_{m2}, the expected v_1 (which should be set in excess compared to the expected value) and the value of $t_{99\%}$, it is possible to derive ϕ and from it V_{max2}, hence the concentration of the coupled assay, according to Eq. 2.6.

A2 2. Plasmid maps and protein sequence

A2 2.1. FLuc plasmid

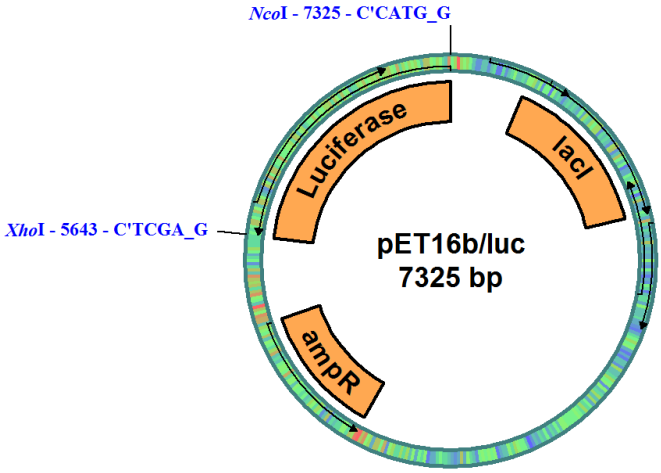

Figure A2 1: rLuc expression vector

Luc gene ligated into the pET16b plasmid. The restriction enzymes and the antibiotic resistance gene were reported.

A2 2.2. *Ft*PPK plasmid

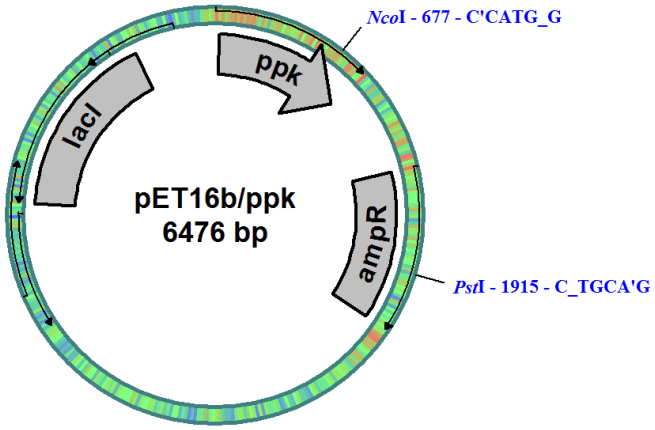

Figure A2 2: *ftppk*::pET16b plasmid

The restriction enzymes and the antibiotic resistance gene were reported.

A2 2.3. FLuc sequence

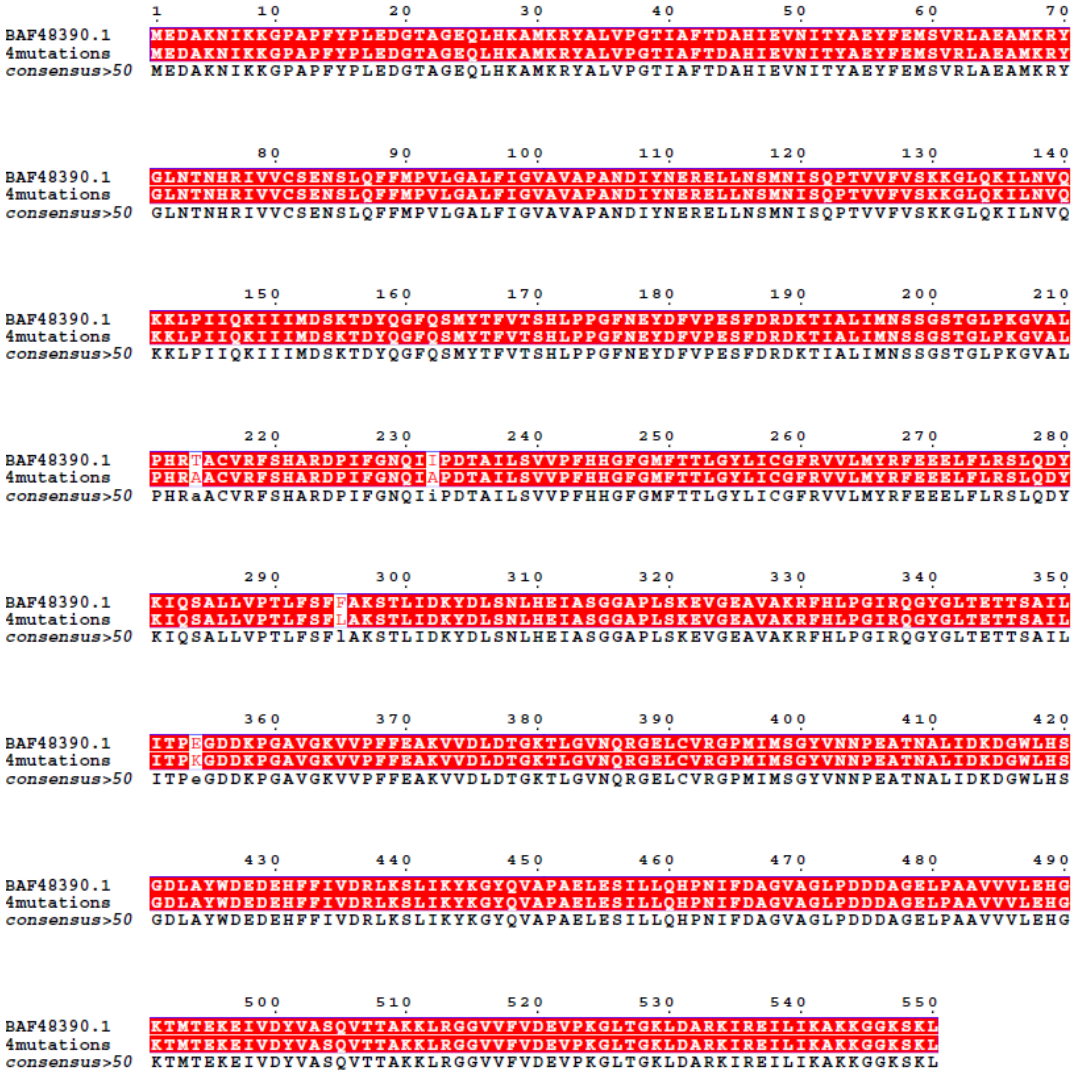

A2 3. Optimisation of the assay format and of the plate reader control protocols for the coupled assay

The control protocols (BMG Omega Reader Control Software) applied for the various stages of the *Ft*PPK-FLuc assay were reported in this section.

A2 3.1. *Ft*PPK-FLuc coupled assay: time course – Format 1

This format was applied for the *Ft*PPK time course measurement in the preliminary phases of the coupled assay optimization and for preliminary kinetics characterisation. The assay solutions were dispensed in the microplate by the Biomek3000 (8 probes tool), including the addition of the *Ft*PPK to start the reaction. Assays in the same column were started at the same time (triplicates of the same time point were prepared in the same column) while assays in adjacent s were started after a delay of 24 seconds from each other (the time required to unload/load used/clean tips and to dispense *Ft*PPK solution, Figure A2 3).

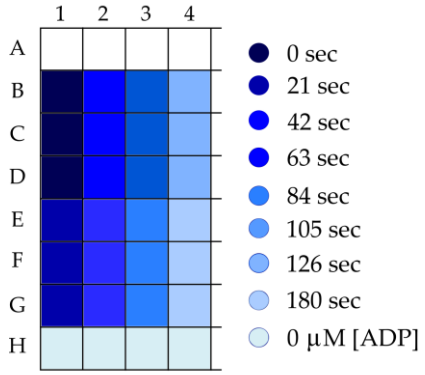

Figure A2 3: Plate layout, assay format 1

The time points reported in the figure refer to the start of the luminescence assay (injection of the luminescence/BSA/luciferin mixture), according to the sequence defined by the script.

To start the luminescence assay the plate was moved into the plate reader and the FLuc-BSA-luciferin mixture injected into the first set of triplicate (first time point measured). This operation entailed a further delay of 18 seconds between the completion of the *Ft*PPK addition and the start of the luminescence assay to measure the first time point. To minimise the delay between the start of the *Ft*PPK assay (PPK injection) and the measurement of

the first time point, while the *Ft*PPK was dispensed from column 4 to column 1, the luminescence assay was started in the inverse order (from column 1 to column 4).

For each *Ft*PPK time point (set of triplicate assay), a single reader control protocol was used to start and measure the luminescence. The mixture FLuc-BSA-luciferin (20 μL) was added by means of the automated injector built in the plate reader (injector 1). After the injection was completed, following a delay of 7 seconds the luminescence was measured and then again after a further delay of 14 seconds (the latter measurement was considered for data analysis). A number of protocols with the same settings but with a different layout were prepared in equal number to the time points to measure. The protocols were then linked in script mode (Table A2 1). The latter ensured that the plate reader temperature was maintained constant until the end of the experiment and that the protocols would be started one after the other. No delays were set between consecutive protocols.

Table A2 1: Reader control protocol script – format 1

Protocol*	*Ft*PPK added**	Reader control protocol started***	Time point measured****
B1-D1	0 s	0 s	32 s
E1-G1	0 s	21 s	53 s
B2-D2	24 s earlier	42 s	98 s
E2-G2	24 s earlier	63 s	119 s
B3-D3	48 s earlier	84 s	164 s
E3-G3	48 s earlier	105 s	185 s
B4-D4	72 s earlier	126 s	230 s
E4-G4	72 s earlier	180 s	284 s
B5-D5	96 s earlier	230 s	481 s
E5-G5	96 s earlier	260 s	681 s
B6-D6	120 s earlier	290 s	881 s
E6-G6	120 s earlier	320 s	1031 s

*position on the microplate; ** Injection by BIOMEK3000, earlier refers to the column with the first and second time point (called *0 sec*); *** 18 s delay between the injection of *Ft*PPK on *0 s* column the start of control protocol *0 s*, the name of the following protocols refer to the delay from the *0 s* protocol; **** final time point measurement, calculated accounting for the 14 s delay between the start of the FLuc assay and the respective delays form the start of the *Ft*PPK assay

Each time point of the *Ft*PPK time course was defined taking into account: the delay between the *Ft*PPK additions in adjacent columns, the 18 seconds delay between the completion of the *Ft*PPK addition and the start of the luminescence assay, the delay between the FLuc addition and the *Ft*PPK addition, the 14 seconds delay between the

addition of the FLuc and the measurement of the luminesce. The *Ft*PPK time point derived accordingly were reported in Table A2 1

A2 3.2. *Ft*PPK-FLuc coupled assay: time course – Format 2

To be able to measure early time points of the *Ft*PPK time course, the assay format was modified: the *Ft*PPK-BSA reagent was injected by means of the seconds injector built in the plate reader (injector 2). A maximum of three time courses, including respective negative control assays and ATP standard curve, could be prepared for each microplate (Figure A2 4). The injection of the *Ft*PPK and of the FLuc/luciferin, to start the respective reactions, were controlled by different reader control protocols. A single protocol was used to inject the *Ft*PPK in all the assays following the direction pointed by the arrows in Figure A2 4. To complete the injection 16 seconds were required.

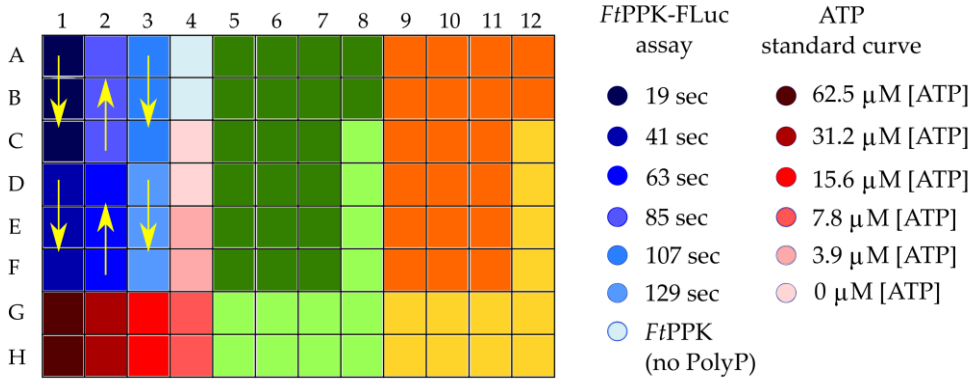

Figure A2 4: Plate layout, assay format 2

The time points reported in the figure refer to the start of the luminescence assay (injection of the FLuc/luciferin), according to the sequence defined by the script.

To inject the FLuc/luciferin and to measure the luminescence, a number of reader control protocols equal to the number of time points were prepared. The FLuc/luciferin injection and luminescence reading protocol performed 1 injection cycle (addition of FLuc/luciferin) followed by 3 reading cycles (luminescence measurement), requiring 5 second each. The last luminescence measurement (16 seconds after the addition of the FLuc/luciferin) was considered for the data analysis. The protocols were linked in script mode, as reported in Table A2 2.

Each time point of the *Ft*PPK time course was defined taking into account: the delay between the injection of the *Ft*PPK (start of the *Ft*PPK reaction) and the FLuc/luciferin injection (start of the luminescence assay), and the 16 seconds delay between the injection of the FLuc/luciferin and the luminescence measurement considered for the analysis. For the ATP standard curve, copies of the protocol used to inject the /luciferin and measure the luminescence were used. In the script, after the protocols to measure the ATP standard curve belonging to the first time course, a sequence of protocols (with same settings as for the first time course but different layout) was included for the measurement of the second and the third time courses (prepared on the same microplate).

Table A2 2: Reader control protocol script – format 2

Protocol sequence	Protocol starting time*	Time point measured**
*Ft*PPK injection	0 s	-
delay	*3 s*	-
FLuc: A1-C1	19 s	35 s
FLuc: D1-F1	41 s	55 s
FLuc: D2-F2	63 s	75 s
FLuc: A2-C2	85 s	95 s
FLuc: A3-C3	107 s	115 s
FLuc: D3-F3	129 s	135 s
BNK A4-B4		
ATP st curve protocols		

*Compared to the start of the script; **derived following correction for the delays between *Ft*PPK injection, FLuc injection and luminescence reading

A2 3.3. *Ft*PPK-FLuc coupled assay: time course – Format 3

Uncertainty regarding the accuracy of the time points measured with the assay format 2 (section A2 3.2) in conjunction with the observed increase of the experimental error upon injection of the *Ft*PPK by the plate reader injector (compared to the injection by Biomek3000), led to the investigation of alternative formats. It was hypothesised that the variability observed when injecting the *Ft*PPK/BSA solution by the plate reader injector was possibly being affected by some unfavourable flow properties of the solution (e.g. high content of glycerol). It was decided to swap the viscous *Ft*PPK solution for an ADP solution prepared by dilution with water. Hence, the *Ft*PPK was included in the assay solution

dispensed in the plate by Biomek3000 and the *Ft*PPK reaction was started by addition of ADP by means of the injector 2 of the plate reader.

Several advantages derived from this exchange: the *Ft*PPK was pre-incubated with the $MgCl_2$ and the $polyP_{25}$ prior initiation of the assay; a better equilibration of the *Ft*PPK at the assay temperature was allowed, negative control assays in which the *Ft*PPK was left out but the ADP included could be easily prepared without detriment of the assay throughput and allowing to detect background luminescence due to ATP impurities in the ADP sample. The decision to start the assay by addition of ADP rather than $polyP_{25}$ was driven by data generated by A. Parnell,[265] showing that incubation of the *Ft*PPK with $polyP_{25}$ favoured the activity while ADP did not bind to the *Ft*PPK in the absence of $polyP_{25}$.

To measure the *Ft*PPK time course a new format was developed in which, for each time point, the start of the *Ft*PPK assay (by addition of ADP), the start of the FLuc assay (by addition of the FLuc/luciferin or of the luciferin)[cc] and the measurement of the luminesce signal was controlled by a single protocol. The plate layout and the settings of the reader control protocols were reported in Figure A2 5 and in Table A2 3, respectively.

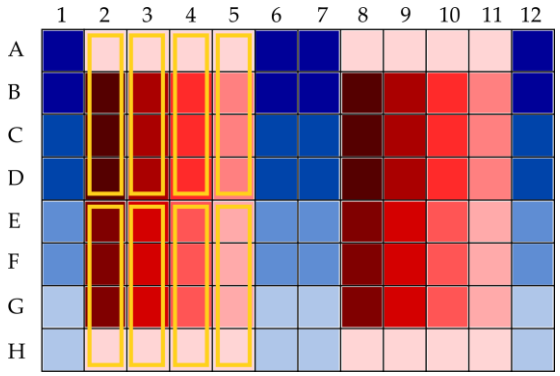

Figure A2 5: Plate layout, assay format 3

The assays in the wells grouped by the orange rectangles were started (addition of ADP and luciferin) and the luminescence measured using the same reader control protocol.

[cc] In the first version of the assay format 3 the luminescence reaction was started by addition of a mixture of FLuc/BSA/luciferin. Later, the FLuc/BSA was included in the assay solution dispensed by Biomek3000 (together with the *Ft*PPK and the other assay components) and the luminescence reaction started by addition of luciferin.

Each protocol was designed to include a triplicate of the time point of interest and a control assay in which no *Ft*PPK was added. The protocol was constituted by three kinetic windows (kw): kw1 controlling the addition of ADP, kw2 controlling the addition of FLuc/luciferin or luciferin, kw3 controlling the measurement of the luminescence. A different delay between kw1 and kw2 was set according to the time point to measure. The consistent and precise delays between injections of reagents and measurement of luminescence, applied to all the assays, allowed to achieve a great accuracy in the measurement of each point of the time course.

Table A2 3: Plate reader control protocol settings – format 3

Protocols for FtPPK time course			
General setting for each kinetic window			
Plate layout	4 wells (#A-D or #E-H)		
Positioning delay*	0.5 s		
Injection start time*	0.5 s		
Measurement start time*	0.5 s		
Measurement interval time*	1s		
Number of cycle	1		
Number of kinetics window	3		
Kinetics window (kw)	**kw1: ADP injection**	**kw2: FLuc injection**	**kw3: Luminescence measurement**
Injector	1	2	-
Total Injection time**	8 s	8 s	-
Total Measuring time**	8 s	8 s	8 s
Minimum cycle time	8 s	8 s	8 s
Cycle time	8 s + delay***	8 s	8 s

*referring to each well; ** referring to 4 wells, simultaneous injection and measurement; ***according to time point to measure

For the measurement of the ATP standard curve assays, similar protocols where prepared in which only the kw 2 and 3 were active. The protocols were linked in script mode, as reported in Table A2 4.

Table A2 4: Plate reader script mode – format 3

Step	Protocol sequence	Delay after ADP injection	Delay FLuc injection-measurement	Time point measured
1) Incubation at 30°C for 5 minutes				
2) ATP st curve 1	A1-D1	-	8 s	-
	E1-H1	-	8 s	-
3) FtPPK time course 1	A2-D2*	4 s + 0 s	8 s	12 s
	E2-D2	8 s + 0 s	8 s	16 s
	A3-D3	8 s + 4 s	8 s	20 s
	E3-D3	8 s + 14 s	8 s	30 s
	A4-D4	8 s + 24 s	8 s	40 s
	E4-D4	8 s + 34 s	8 s	50 s
	A5-D5	8 s + 44 s	8 s	60 s
	E5-D5	8 s + 54 s	8 s	70 s
4) ATP st curve 2	As for st curve 1 but different layout (refer to Figure A2 5)			
5) ATP st curve 3	As for st curve 1 but different layout (refer to Figure A2 5)			
6) FtPPK time course 1	As for *Ft*PPK time course 1 but different layout (refer to Figure A2 5)			
7) ATP st curve 4	As for st curve 1 but different layout (refer to Figure A2 5)			

*To measure a 12 s time point the protocol was split in 2, with a layout of 2 wells. The time required for injection in 2 wells was 4 s. Hence, the cycle time for the kinetic window was 4 sec but for kinetic window 2 and 3 was set to 8 s, for consistency with the other time points measured.

A2 4. *Ft*PPK-FLuc coupled assay: ADP concentration for the measurement of K_m for polyP$_{25}$

The concentration of ADP to apply for the measurement of the K_m with polyP$_{25}$ was experimentally determined. The polyP$_{25}$ concentration was maintained at 200 µM while the following ADP concentration were tested: 1000 µM, 1500 µM, 2000 µM and 3000 µM. Inhibition of the luminescence was observed at 3000 µM while a comparable luminescence intensity was observed at 1500 µM and 2000 µM (Figure A2 6).

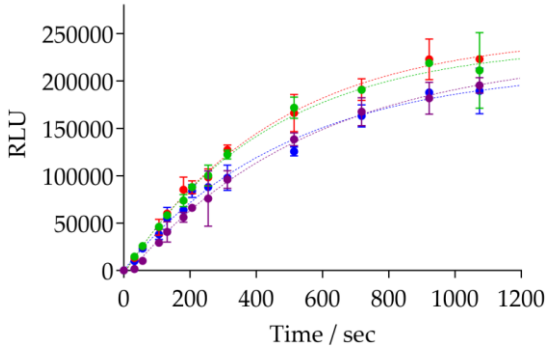

Figure A2 6: Optimal concentration of ADP to measure K_m for polyP$_{25}$

Time courses measured in the presence of: 1000 µM ADP (blue circles), 1500 µM ADP (red circles), 2000 µM ADP (green circles), 3000 µM ADP (purple circles). Assay conditions: 100 µL assay volume, 30 nM *Ft*PPK /1.3 µM BSA, 200 µM polyP$_{25}$, 1000 – 3000 µM ADP, 100 nM FLuc/1.3 µM BSA, 70 µM luciferin, 30°C. Gain: 1500.

A2 5. ADP purification by anion exchange chromatography

Widening the assay dynamic range by increasing the difference between the signal produced by assays in which full activity is observed (positive control assays) and assays in which no activity is observed (negative control assays) can positively contribute towards the improvement of the Z' factor (Eq. 2.11). One way of accomplishing this task would be to reduce the background signal, namely the signal that can not be attributed to the *Ft*PPK activity. A relatively significant luminescence has been detected from control assays in which ADP and polyP$_{25}$ but not *Ft*PPK were present. This was tracked down to ATP impurities in the commercial ADP sample.

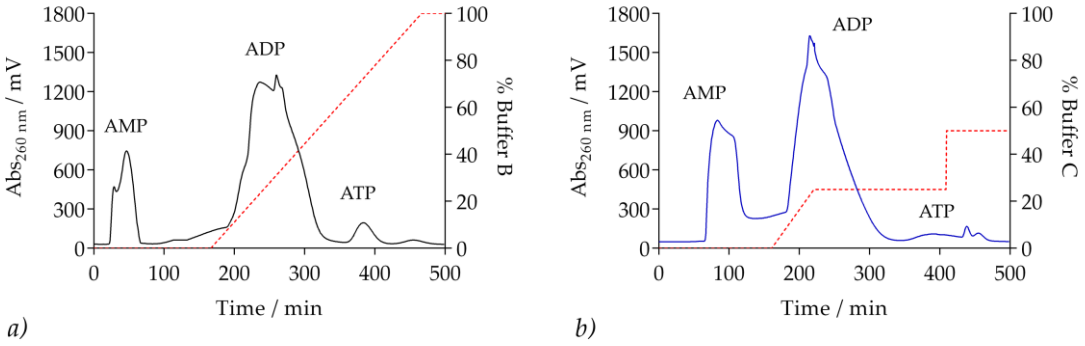

Figure A2 7: ADP purification by ion exchange chromatography

a) Nucleotides elution by gradient of NaH_2PO_4 (0-100% buffer B, pH 6). AMP eluted between 30 mL and 80 mL, ADP between 180 mL and 350 mL, ATP after 350 mL. *b*) Nucleotides elution by steep gradient of NH_4HCO_3 (0-25% buffer B1-C1, pH 8) followed by prolonged washing and step gradient (25-50% buffer C1, pH 8). AMP and some ADP co-eluted between 50 mL and 120 mL, the remaining ADP eluted between 180 mL and 330 mL and ATP after 340 mL.

To reduce the ATP contaminants, the purification of ADP by anion exchange chromatography (DEAE sepharose) was investigated. For elution of the nucleotides a gradient of either NaH_2PO_4 at pH 6 or a gradient of NH_4HCO_3 at pH 8 has been applied (Figure A2 7). In both cases, the column (30 mL) was pre-equilibrated in Tris buffer (pH 6) and the ADP sample (300 mg/4 mL), dissolved in water, was applied without prior adjustment of the pH (pH 4). The AMP impurities were eluted by washing with the Tris buffer. For ADP and ATP elution either a gradient of high concentration NaH_2PO_4 buffer (buffer B: 0.5 M NaH_2PO_4, pH 6; or the combination of a gentle gradient followed by a step gradient of high concentration NH_4HCO_3 buffer (buffer C1: 0.5 M NH_4HCO_3, pH 8) were applied. In the latter case, after being equilibrated in Tris buffer and before applying the gentle gradient of high content NH_4HCO_3 buffer (buffer C1), the column was washed with a buffer containing a low concentration of NH_4HCO_3 (buffer B1: 5 mM NH_4HCO_3) to elute AMP.[dd] The two methods were comparable in terms of purification efficiency, allowing to remove most of the ATP contaminants from the ADP sample. However, the purification by NH_4HCO_3 offered the advantage of recovering a salt-free sample after freeze-drying, which

[dd] Previously the column has been equilibrate directly in buffer B1. Following repeating washing of the column with buffer B1 it was not possible to elute AMP which instead co-eluted with ADP when the gradient of buffer C1 was applied.

was not possible for the NaH_2PO_4 method unless a de-salting step was added. The concentration of the purified ADP and its degree of purity were determined by ion-pair reversed-phase HPLC chromatography. The method used by L. Batten for the *Ft*PPK HPLC-based assay was adopted.[264] N,N-dimethylhelxylamine (DMHA) was used as ion pairing agent, which was added to both the aqueous eluent (A, 15 mM DMHA, 5% MeOH, pH 7) and the organic eluent (B, 15 mM DMHA, 80% MeOH, pH 7). The method applied for elution of the nucleotides consisted of an isocratic elution at 9% eluent B (5 min) followed by a gradient to 80% eluent B (59.1 min).

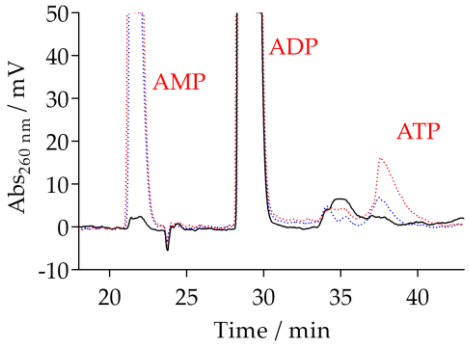

Figure A2 8: ADP analysis by RP-IP HPLC

HPLC chromatogram of a sample of the purified ADP (500 µM, black line) and two non-purified ADP controls (1 mM, red dotted line; 500 µM blue dotted line). AMP and ATP peaks were detected in the non-purified ADP samples while were not detected in the purified ADP sample. HPLC method: DMHA 1 (Experimental, section 7.6.3.1). Retention time: AMP eluted at 21-23 min, ADP at 28-31 min, ATP at 37-40 min.

The HPLC analysis confirmed removal of a high proportion of the contaminating ATP (Figure A2 8), although some residual luminescence was still observed in the control assays of the coupled assay.

A2 6. *Ft*PPK-FLuc coupled assay: improvement of the luminescence signal by optimisation of the NaCl concentration

The assay buffer used for the *Ft*PPK-FLuc coupled, adopted from the previous work of L. Batten and J. Docherty,[264,352] contained 300 mM NaCl, which was supposedly included to stabilise the *Ft*PPK and/or the FLuc. No references or investigation of the effect on the activity of both enzymes were reported.[264,352] Although delayed within the optimisation process, a range of NaCl concentrations (0-300 mM) was tested on the independent FLuc assay and on the *Ft*PPK coupled assay to define the optimal concentration. A dramatic increase of the FLuc activity (five-fold) was observed when the concentration of NaCl was reduced from 300 mM to 25 mM (Figure A2 9).

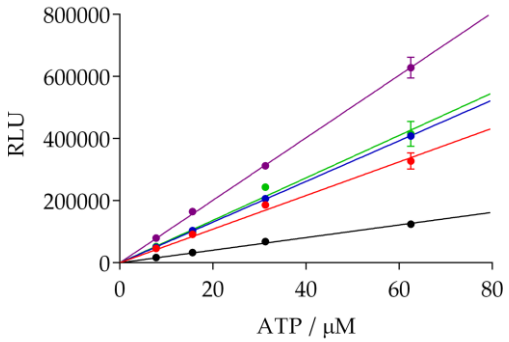

Figure A2 9: *Ft*PPK-FLuc coupled assay: NaCl optimisation, effect on the FLuc activity

Effect of NaCl on the FLuc activity tested on ATP standard curves at the following concentration: 300 mM NaCl (black dots), 150 mM NaCl (red dots), 100 mM NaCl (blue dots), 50 mM NaCl (green dots), 25 mM NaCl (purple dots). An increase of the luminescence intensity was observed with the reduction of the NaCl concentration. Assay conditions: 100 µL assay volume, 300 nM FLuc/1.3 µM BSA, 70 µM luciferin, 15.6 – 62.5 µM ATP, 5% DMSO, 30°C. Gain: 1700.

When the experiment was repeated on the *Ft*PPK-FLuc coupled assay the effect of completely removing the NaCl was also investigated (Figure A2 10). The removal of the NaCl was detrimental for the activity of the *Ft*PPK, which otherwise appeared to be less sensitive to variation of the NaCl concentration (Figure A2 10*b*). The concentration of 25 mM NaCl was identified as optimal for both the FLuc and the *Ft*PPK activity and therefore was adopted as standard for the *Ft*PPK-FLuc coupled assay.

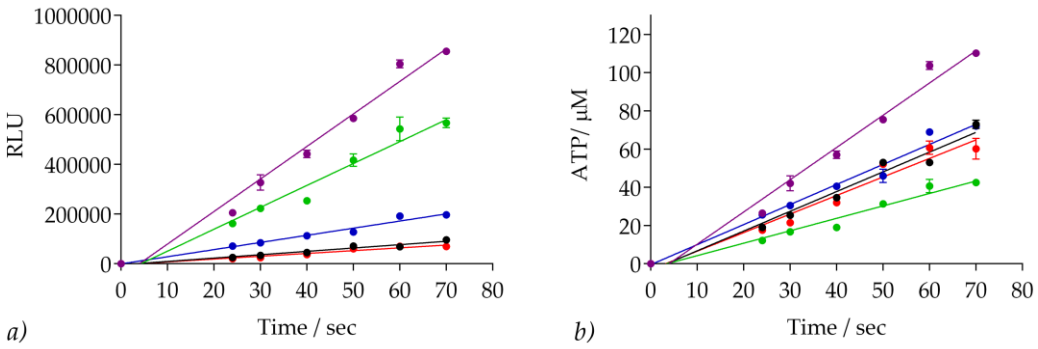

Figure A2 10: *Ft*PPK-FLuc coupled assay: NaCl optimisation, *Ft*PPK-FLuc coupled assay

Effect of NaCl on the activity of the FLuc and of the *Ft*PPK activity tested on the *Ft*PPK-FLuc coupled assay at the following concentration: 300 mM NaCl (black dots), 150 mM NaCl (red dots), 75 mM NaCl (blue dots), 25 mM NaCl (purple dots), 0 mM NaCl (green dots). *a*) *Ft*PPK time course reported in terms of the luminescence produced. The signal detected was affected by the effect of NaCl on both the FLuc and the *Ft*PPK; *b*) *Ft*PPK time course reported in terms of the ATP produced. The data were generated by extrapolation by means of an ATP standard curve with corresponding NaCl content, hence they reflect the effect of NaCl on the *Ft*PPK activity only. Assay conditions: 100 µL assay volume, 35 nM *Ft*PPK /1.3 µM BSA, 700 µM ADP, 30 µM $polyP_{25}$, 300 nM FLuc/1.3 µM BSA, 70 µM luciferin, 0-300 mM NaCl, 5% DMSO, 30°C. Gain: 1700.

Appendix to Chapter 3

A3 1. Measuring the coupled assay: plate layouts, plate reader control protocols and script mode

It appeared meaningful to report a detailed account of plate layouts and protocols used for the measurement of the coupled assays, in view of a better understanding of the experimental description and to provide maximum support for the possible attempt in reproducing the experiments, since the fine adjustment of the measuring parameters of the BMG control protocols was critical for the achievement of a good assay quality.

A3 1.1. Protocols and plate layout used for HTS format development

A3 1.1.1 HTS format development: end-point format in 96 well plate

The layout used for the HTS end-point format in a 96 well microplate (section 3.2.1.1) was reported in Figure A3 1. Positive control assays (full signal) and negative control assays (no *Ft*PPK, only background signal) were prepared in alternate columns. Two ATP standard curves were prepared in column 1 and column 12 to monitor the activity of the FLuc.

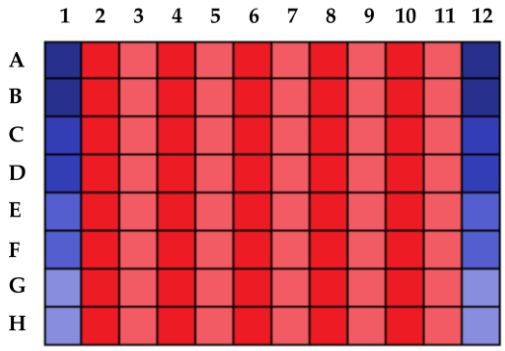

Figure A3 1: HTS format, 96 wells end-poin format - plate layout

Blue wells: ATP standard curves (decreasing concentration of ATP corresponding to colour fading); dark red wells: positive control assays (maximum signal); light red wells: negative control assays (background signal).

A single control protocol was used for the assays prepared in the same column (e.g. A2-H2, A3-H3) to start the *Ft*PPK assay, to start the respective FLuc assay, and to measure the

luminescence signal produced. The general protocol settings (Table A3 1) were analogous to the settings of the protocols designed for the time course measurement (Appendix, section A2 3.3, Table A2 3). The only differences was the layout (8 wells rather than 4) and consequently the cycle time (time required to perform the injection or the measurement in the 8 wells on a 96 well plate was 16 seconds, refer to Table A3 1). Overall the *Ft*PPK activity was measured after 32 seconds (16 seconds kw1, ADP injection + 16 seconds kw2, luciferin injection).[ee] To measure the ATP standard curves, a single control protocol was used for the assays prepared in the same column (A1-H1 or A12-H12), in which the luminescence signal was measured 16 seconds after the start of the FLuc assay. The control protocols were linked by a script, as reported in Table A3 2.

A3 1.1.2 HTS format development: end-point format in 384 well plate

- *HTS 30 seconds end-point format*: the 384 well microplate was divided into 4 subsections (or quarters) each comparable to a 96 well microplate (Figure A3 2).

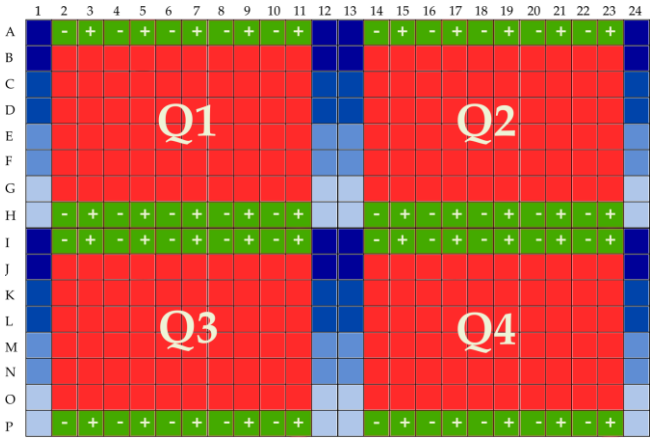

Figure A3 2: HTS format, 384 wells end-point format - plate layout

Blue wells: ATP standard curves (decreasing concentration of ATP corresponding to colour fading); green wells: negative control assays (minus symbol) and positive control assays (plus symbol); red wells: assays due to contain the library compounds.

[ee] The only difference between the protocols used for the format in 96 wells and in 384 wells was the cycle time, hence the time required to measure a column of 8 wells (e.g. from A till H or from I till P). In a 96 well plate the cycle time was 16 seconds, in the 384 well plate the cycle time was 15 seconds.

For each quarter the following assays were prepared: negative control assays (maximum signal, comparable to 0% inhibition) and positive control assays (no *Ft*PPK, background signal, comparable to 100% inhibition) in row A and H from column 2 to 11, in alternate positions; 60 assays due to contain the library compounds in triplicate (3 x 20) in row B to G, column 2 to 11; 2 sets of ATP standard curve assays column 1 and column 12 from row A to H. The assays were prepared in the following order: assays in Q1, then Q3, Q2 and Q4. As for the 96 well format, a single reader control protocol was used to start the *Ft*PPK assay, the FLuc assay and to measure the luminescence for the assays prepared on the same column of a subsection (e.g. A2-H2, A10-H10, I2-P2, I10-P10). The general protocol settings (Table A3 1) were analogous to the setting of the protocols designed for the time course measurement (Appendix, section A2 3.3, Table A2 3). The only differences was the layout (8 wells rather than 4) and consequently the cycle time (time required to perform the injection or the measurement in the 8 wells).

Table A3 1: HTS end-point format 384 well, control protocol settings

Protocols for HTS end-point format in 384 well plate			
General setting for each kinetic window			
Plate layout	8 wells (e.g. #A2-H2 or # I2-P2)		
Positioning delay*	0.5 s		
Injection start time*	0.5 s		
Measurement start time*	0.5 s		
Measurement interval time*	1s		
Number of cycle	1		
Number of kinetics window	3		
Kinetics window (kw)	**kw1: ADP injection**	**kw2: FLuc injection**	**kw3: Luminescence measurement**
Injector	1	2	-
Total Injection time**	15 s	15 s	-
Total Measuring time**	15 s	15 s	15 s
Minimum cycle time	15 s	15 s	15 s
Cycle time	15s	15 s	15 s

*referring to each well; ** referring to 8 wells, simultaneous injection and measurement

To measure the whole plate in the shortest time possible, the *Ft*PPK activity was recorded at the quickest time point: 30 seconds, derived from the sum of the delay between the start

of the *Ft*PPK assay and the start of the FLuc assay (15 seconds, delay between kw1 and kw2) and the delay between the latter and the measurement of the luminescence (15 seconds, delay between kw2 and kw3, Table A3 1). A number of protocols equal to the number of columns (from row A until H and from row I until P) containing *Ft*PPK assays in the 384 well plate were prepared, differing only for the layout. The protocols to measure the ATP standard curves lacked the kw1 while the kw2 and kw3 were unchanged. The protocols were linked by a script, as reported in Table A3 2. The overall time required to measure the whole microplate was 40 minutes.

Table A3 2: Plate reader script mode – HTS 30 seconds end-point format

Step		Protocol sequence	Delay after ADP injection	Delay FLuc injection-measurement	Time point measured
1)	*Incubation at 30°C for 20 minutes*				
2)	*Q1: Column AH2-6*	2AH	15 s	15 s	30 s
	Control assays and assays due to contain the library compound	3AH	15 s	15 s	30 s
		4AH	15 s	15 s	30 s
		5AH	15 s	15 s	30 s
		6AH	15 s	15 s	30 s
3)	*ATP st curve 1*	1AH	-	15 s	-
4)	*Q1: Column AH7-11*	7AH	15 s	15 s	30 s
	Control assays and assays due to contain the library compound	8AH	15 s	15 s	30 s
		9AH	15 s	15 s	30 s
		10AH	15 s	15 s	30 s
		11AH	15 s	15 s	30 s
5)	*ATP st curve 2*	12AH	-	15 s	-
6)	*Q2: Column AH14-18*	As for Q1, protocols 14AH to 18AH			
7)	*ATP st curve 3*	13AH	-	15 s	-
8)	*Q2: Column AH19-23-*	As for Q1, protocols 19AH to 23AH			
9)	*ATP st curve 4*	24AH	-	15 s	-
10)	*Q3: Column IP2-6*	As for Q1, protocols 2IP to 6IP			
11)	*ATP st curve 5*	1IP	-	15 s	-
12)	*Q3: Column AH19-23-*	As for Q1, protocols 7IP to 11IP			
13)	*ATP st curve 6*	12IP	-	15 s	-
14)	*Q4: Column AH14-18*	As for Q1, protocols 14IP to 18IP			
15)	*ATP st curve 7*	13IP	-	15 s	-
16)	*Q4: Column AH19-23-*	As for Q1, protocols 19IP to 23IP			
17)	*ATP st curve 8*	24IP	-	15 s	-

- *HTS 60 seconds end-point format*: to measure the *Ft*PPK assay after 60 seconds the control protocols were modified as follow: the cycle time of kw1, kw2 and kw3 was extended to 30 seconds (refer to Table A3 1 and Table A3 3) and the protocol layout included the whole column, from row A till row P. The protocols were linked by a script, as reported in Table A3 3.

Table A3 3: Plate reader script mode – HTS 60 seconds end-point format

Step	Protocol sequence		Delay after ADP injection	Delay FLuc injection-measurement	Time point measured
1)	*Incubation at 30°C for 20 minutes*				
2)	*Q1 and Q3: Column AP2-6*	2AP	30 s	30 s	60 s
	Control assays and assays due to contain the library compound	3 AP	30 s	30 s	60 s
		4 AP	30 s	30 s	60 s
		5 AP	30 s	30 s	60 s
		6 AP	30 s	30 s	60 s
3)	*ATP st curve 1*	1 AP	-	30 s	-
4)	*Q1 and Q3: Column AP7-11*	7AP	30 s	30 s	60 s
	Control assays and assays due to contain the library compound	8 AP	30 s	30 s	60 s
		9 AP	30 s	30 s	60 s
		10 AP	30 s	30 s	60 s
		11 AP	30 s	30 s	60 s
5)	*ATP st curve 2*	12 AP	-	30 s	-
6)	*Q2 and Q3: Column AP13-18*	As for Q1 and Q3, protocols 13AP to 18AP			
7)	*ATP st curve 3*	13AP	-	30 s	-
8)	*Q2 and Q3: Column AP19-23-*	As for Q1 and Q3, protocols 19AP to 23AP			
9)	*ATP st curve 4*	24AP	-	30 s	-

- *HTS 90 seconds end-point format*: to measure the *Ft*PPK assay after 90 seconds the control protocols were modified as follow: the cycle time of kw1, kw2 and kw3 was extended to 45 seconds (refer to Table A3 1 and Table A3 4) and the protocol layout included three consecutive columns within the same quarter (e.g. first protocol: 2AH, 3AH, 4AH; second protocol: 5AH, 6AH, 7AH, *etc.*). This allowed to start and to measure the assays in the same order as the order of preparation on the microplate (Q1, then Q2, Q3, Q4). The protocols were linked by a script, as reported in Table A3 4.

Table A3 4: Plate reader script mode – HTS 90 seconds end-point format

Step		Protocol sequence	Delay after ADP injection	Delay FLuc injection-measurement	Time point measured
1)	*Incubation at 30°C for 15 minutes*				
2)	*Q1 and Q2: Column AH2-10*	2-4AH	45 s	45 s	90 s
	Control assays and assays due to contain the library compound	5-7AH	45 s	45 s	90 s
		8-10AH	45 s	45 s	90 s
3)	*ATP st curve 1 and 2*	1AH and 12AH	-	45 s	-
4)	*Q1 and Q3: Column AH11-23*	11AH and 13-15AH	45 s	45 s	90 s
	Control assays and assays due to contain the library compound	16-18AH	45 s	45 s	90 s
		19-21AH	45 s	45 s	90 s
		21-23AH	45 s	45 s	90 s
5)	*ATP st curve 3 and 4*	13AH and 24AH	-	45 s	-
6)	*Q3 and Q4: Column IP2-10*	As for Q1 and Q2, protocols 2-4IP to 8-10IP			
7)	*ATP st curve 5-6*	1IP and 12IP	-	45 s	-
8)	*Q3 and Q4: Column IP11-23-*	As for Q1 and Q3, protocols 11AP and 13-15IP to 23IP			
9)	*ATP st curve 7-8*	13IP and 24IP	-	45 s	-

A3 1.2. Protocols and plate layout used during the screening

A3 1.2.1 PKIS and Reynolds library: plate layout

The layout of the PKIS plates (200 μM, 100% DMSO) and the layout of the Reynolds library plates (200 μM, 100% DMSO) were reported below. For a full list of the compounds (with corresponding label provided with the library) contained in each plate refer to Table A3 5 for the PKIS library and to Table A3 6 for the Reynolds library. The following labelling system were adopted to refer to a specific compound. PKIS library: compound 6 of plate JOL was identified as JOL-6. Reynolds library: compound 25 of plate 7 was identified as RL25-Plt7.

	1	2	3	4	5	6	7	8	9	10	11	12
A	1	9	17	25	33	41	49	57	65	73		
B	2	10	18	26	34	42	50	58	66	74		
C	3	11	19	27	35	43	51	59	67	75		
D	4	12	20	28	36	44	52	60	68	76		
E	5	13	21	29	37	45	53	61	69	77		
F	6	14	22	30	38	46	54	62	70	78		
G	7	15	23	31	39	47	55	63	71	79		
H	8	16	24	32	40	48	56	64	72	80		

Figure A3 3: PKIS library plate layout

PKIS library layout. To each compound it was assigned a number based on the position on the microplate. Column 11 and 12 were empty.

	1	2	3	4	5	6	7	8	9	10	11	12
A		1	9	17	25	33	41	49	57	65	73	
B		2	10	18	26	34	42	50	58	66	74	
C		3	11	19	27	35	43	51	59	67	75	
D		4	12	20	28	36	44	52	60	68	76	
E		5	13	21	29	37	45	53	61	69	77	
F		6	14	22	30	38	46	54	62	70	78	
G		7	15	23	31	39	47	55	63	71	79	
H		8	16	24	32	40	48	56	64	72	80	

Figure A3 4: Reynolds library plate layout

Reynolds library layout. To each compound it was assigned a number based on the position on the microplate. Column 1 and 12 were empty.

Table A3 5: PKIS library compounds

Compound #	Plate JOL	Plate JOM	Plate JON	Plate JO7	Plate JO8
1	SB-592602	GSK586581B	GI261520A	GW580496A	GW804482X
2	GSK1392956A	GSK1023156A	GW300660X	GW568377B	SB-738482
3	GW830365A	GW352430A	GSK248233A	GW811761X	GW296115X
4	SB-220455	SB-630812	GW683768X	GW693917X	GW804482X
5	SB-278539	GW620972X	GW427984X	GSK635416A	SB-738482
6	SB-437013	GW829055X	SB-409513	SB-693162	GW296115X
7	GSK317354A	GW829115X	GSK949675A	GW824645A	GW435821X
8	SB-735465	GW809897X	GSK317315A	GI98581X	GSK1030058A
9	GW549390X	GW874091X	GW410563A	SB-707548-A	SB-239272
10	GW282974A	GW829906X	GW641155B	GW683134A	GSK299115A
11	GW581744X	GSK620503A	GW572738X	GSK2219385A	GW827396X
12	GW429374A	GSK204925A	GSK605714A	GW305074X	GW568326X
13	GSK2213727A	GW301789X	GW284372X	GSK2110236A	GW861893X
14	SB-242717	GW627834A	GW574782A	SB-251527	GW275944X
15	GW784307A	GSK180736A	GW684626B	GW701427A	GW575533A
16	GSK182497A	SB-736290	GW589961A	GW416469X	GW278681X
17	GW781673X	GSK571989A	GW701032X	GW830263A	SB-657836-AAA
18	GSK238583A	GW574783B	GW819230X	GSK938890A	SB-711237
19	GW827105X	GW700494X	GW642138X	GW810372X	GW807930X
20	GW441756X	GW578748X	GSK605714A	GSK718429A	GW305178X
21	GW589933X	GSK237700A	GSK625137A	GW567808A	GSK943949A
22	GW810576X	GW833373X	GW806290X	SB-744941	GW445017X
23	GW853606X	GW680908A	SB-216385	GW622055X	GW659386A
24	GW576484X	GW796920X	GR269666A	GW612286X	GW440139B
25	GW778894X	GSK2163632A	GW621431X	GW290597X	GSK1511931A
26	SB-347804	SB-814597	GW561436X	SB-253228	GW651576X
27	SB-739452	GW678313X	GW575808A	SKF-86055	GSK969786A
28	SB-476429-A	GSK1173862A	GW445012X	GSK1751853A	GW566221B
29	GW817396X	GSK270822A	GW439255X	GSK1713088A	GR105659X
30	GW784752X	GW805758X	GW711782X	GW445015X	SB-750140
31	GW683109X	GW280670X	GW569293X	GW627512B	GW772405X
32	GW616030X	GW549034X	GW769076X	GW284408X	SB-732941
33	GW775608X	GSK2186269A	GW820759X	SB-242721	SB-742864
34	GW405841X	SB-223133	GW782612X	GW644007X	GW806742X
35	GW837331X	SB-251505	GW559768X	GW300653X	GW458344A
36	GW301888X	SB-242718	GW801372X	GW680975X	SB-431533
37	GW782912X	GW817394X	GW618013X	SB-682330-A	SB-221466
38	GW708893X	GW396574X	GW416981X	GW643971X	GW435821X
39	GW407323A	GW458787A	GW607117X	GW853609X	-
40	SB-698596-AC	GW708336X	GW654652X	SB-360741	-

PKIS library compounds

Comp #	Plate JOL	Plate JOM	Plate JON	Plate JO7	Plate JO8
1	GW785404X	GW279320X	GSK466317A	GW450241X	-
2	SB-737198	GW811168X	GW276655X	GW831090X	-
3	GW768505A	GW442130X	GW819077X	GW695874X	-
4	GW809885X	GW275616X	GW680191X	SB-242719	-
5	GW572401X	SB-736302	GSK554170A	SB-614067-R	-
6	GW406731X	GW830900A	GW576609A	SB-400868-A	-
7	SB-732881-H	GSK711701A	GSK1326255A	GW580509X	-
8	SB-376719	GW786460X	GW673715X	GSK300014A	-
9	GW432441X	GW782907X	GSK192082A	SB-409514	-
10	SB-264865	SB-735467	GSK579289A	SB-285234-W	-
11	SB-245392	SB-358518	SB-675259-M	SB-333612	-
12	GSK619487A	SB-772077-B	GW576924A	GW694590A	-
13	GW632046X	GSK269962B	GW633459A	SB-739245-AC	-
14	GSK953913A	GW785804X	GSK466314A	GW631581B	-
15	GW693881A	GW445014X	GSK237701A	GW770220A	-
16	SB-741905	SB-743899	GW615311X	GW794726X	-
17	SB-390527	GW632580X	GW621823A	GSK1030061A	-
18	SB-751399	SB-725317	GW583373A	SB-278538	-
19	GW831091X	GSK980961A	GSK1220512A	SB-226879	-
20	SB-686709-A	SKF-86002	GSK978744A	GSK1000163A	-
21	SB-734117	GW607049B	GW779439X	GW785974X	-
22	SB-361058	GW693481X	GW771127A	GW827099X	-
23	SB-738561	GW642125X	GW795493X	GSK317314A	-
24	GW572399X	GSK319347A	SB-250715	GSK1030059A	-
25	GW577921A	GW876790X	SB-284847-BT	SB-390523	-
26	SB-236687	SB-678557-A	GW513184X	GSK1030062A	-
27	GW796921X	GW743024X	SB-254169	GW703087X	-
28	SB-431542-A	GSK994854A	GW335962X	GW828525X	-
29	GW659893X	GSK238063A	SB-253226	GW827106X	-
30	SKF-62604	GSK312948A	GW682841X	GSK1819799A	-
31	GW434756X	GW459057A	GW734508X	GW799251X	-
32	GW856804X	SB-590885-R	SB-210313	GSK200398A	-
33	GSK561866B	GW843682X	GSK614526A	GW300657X	-
34	GW813360X	GW694234A	GW770249A	GW869810X	-
35	GW780056X	GW282449A	GSK1007102B	GW406108X	-
36	SB-264866	GW759710A	GSK2220400A	GW846105X	-
37	SB-742865	GW794607X	SB-610251-B	GW832467X	-
38	GW784684X	GW829874X	GW301784X	GW829877X	-
39	GW461104B	GW679410X	GW282536X	SB-633825	-
40	GW621970A	GW569530A	GW852849X	GW780159X	-

Table A3 6: RL library compounds

Comp #	Plate 1 – SRI#	Plate 2 – SRI#	Plate 3 – SRI#	Plate 4 – SRI#	Plate 5 – SRI#	Plate 6 – SRI#	Plate 7 – SRI#	Plate 8 – SRI#	Plate 9 – SRI#	Plate 10 – SRI#
1	25509	25560	27117	27749	28045	27202	26151	25521	25438	27704
2	25732	26208	27116	27547	28044	27201	25549	25523	25373	27699
3	25600	26207	27115	27546	28043	27200	26098	25556	25371	27698
4	25607	26205	27114	27545	28042	27198	26099	25544	27735	27697
5	25482	26204	27113	27544	28041	27196	26100	25514	27736	27696
6	25481	26203	27111	27543	28040	27195	26101	25572	27737	27693
7	25479	26202	27110	27539	28039	27194	26102	25527	27738	27692
8	25684	26201	27109	27538	28038	27193	26106	25524	27739	27690
9	25588	26200	27108	27537	28037	27190	26135	25548	27740	27691
10	25606	26189	27099	27527	28025	27089	26122	25777	28071	27673
11	25583	26190	27100	27528	28027	27090	26128	25779	28059	27674
12	25593	26191	27101	27529	28028	27091	26111	25780	27747	27677
13	25474	26192	27102	27530	28029	27092	26110	25787	27746	27678
14	25505	26193	27103	27531	28030	27093	26109	25783	27745	27679
15	25477	26194	27104	27533	28031	27187	26108	25659	27744	27680
16	25680	26195	27105	27534	28032	27188	26152	25642	27742	27683
17	25734	26198	27106	27535	28035	27189	25566	25525	27741	27685
18	25738	26199	27107	27536	28036	27191	26126	25545	28129	27686
19	25502	26188	27098	27525	28024	27088	26103	25785	28072	27672
20	25480	26187	27097	27524	28023	27086	25645	25765	28073	27671
21	25483	26184	25902	27523	28022	27085	25774	25668	28074	27670
22	25501	26183	25901	27522	28021	27084	26119	25778	28075	27669
23	25585	26180	25900	27521	27770	27083	26120	25655	28076	27668
24	25599	27182	25899	27520	27769	27082	25526	25775	28070	27667
25	25563	27181	25898	27519	27762	27081	26153	25660	28080	27666
26	25476	27180	25897	27518	27767	27080	25516	25669	28081	27665
27	25586	27179	25896	27517	27766	27079	26125	25648	28086	27662
28	25605	27169	25887	27506	27757	27070	25666	25543	28100	27652
29	25562	27170	25888	27507	27758	27071	25671	25531	28099	27653
30	25561	27171	25889	27510	27760	27192	26096	25567	28097	27654
31	25473	27172	258910	27511	27761	27073	26105	25568	28095	27655
32	25590	27173	25891	27512	27755	27074	26150	25520	28094	27656
33	25475	27174	25892	27513	27754	27075	26123	25664	28090	27657
34	25592	27175	25893	27514	27764	27076	26121	25354	28089	27658
35	25736	27176	25894	27515	27765	27077	26107	25564	28087	27659
36	25608	27178	25895	27516	27118	27078	25662	25518	28067	27661
37	25603	27168	25886	27505	27750	27068	25766	25656	28101	27651
38	25598	27167	25885	27504	25570	27067	26149	25661	28102	27650
39	25601	27166	25883	27502	25368	27066	26139	25764	28103	27648
40	25468	27165	27821	27501	-	27065	26154	25647	28104	27647

Reynolds library compounds

Comp #	Plate 1 – SRI#	Plate 2 – SRI#	Plate 3 – SRI#	Plate 4 – SRI#	Plate 5 – SRI#	Plate 6 – SRI#	Plate 7 – SRI#	Plate 8 – SRI#	Plate 9 – SRI#	Plate 10 – SRI#
41	25587	27164	27820	27500	-	27064	25786	25776	28105	27646
42	25735	27163	27819	27499	-	27061	26129	25652	28107	27644
43	25739	27162	27818	27498	-	27060	25584	25646	28108	27645
44	25559	27161	27817	27497	-	27048	26130	25663	28109	27643
45	25589	27159	27816	27496	-	27047	25538	25654	28110	27642
46	25591	27150	27797	27759	-	27038	25537	25437	28123	27632
47	25472	27151	27798	28033	-	27039	25670	25366	28122	27633
48	25506	27152	27799	28034	-	27040	25769	25351	28121	27635
49	25679	27153	27801	28050	-	27041	26117	25356	28120	27636
50	25478	27154	27803	28051	-	27042	26127	25355	28117	27637
51	25470	27155	27804	28052	-	27043	25737	25650	28116	27638
52	25504	27156	27802	28053	-	27044	26114	25658	28113	27639
53	25469	27157	27814	28046	-	27045	26118	25667	28112	27640
54	25687	27158	27815	27494	-	27046	26104	25771	28111	27641
55	25604	27148	27796	27830	-	27037	26124	25441	28124	27630
56	25683	27147	27795	28196	-	27034	25533	25463	28125	27631
57	25685	27146	27794	28195	-	27033	25547	25450	28126	27006
58	25681	27145	27793	28194	-	27032	25535	25454	28127	26581
59	26179	27144	27792	28193	-	27031	26138	25460	25446	26580
60	26178	27143	27780	28192	-	27030	25782	25445	25784	26549
61	26173	27142	27789	28191	-	27029	26133	25365	27207	26454
62	26174	27139	27788	28190	-	27028	26134	25352	27186	25791
63	26172	27138	27787	28189	-	27026	25651	25361	27213	26146
64	26162	27127	27777	28179	-	25644	26097	25363	25529	25789
65	26163	27128	27778	28180	-	27018	25653	25360	25539	25794
66	26164	27129	27779	28181	-	27017	25557	25369	27212	25790
67	26165	27130	27781	28182	-	26159	26116	25367	27208	26141
68	26171	27131	27782	28184	-	27021	25551	25358	-	26142
69	26167	27133	27783	28185	-	27022	25767	25451	-	26143
70	26168	27134	27784	28186	-	27023	26132	25370	-	26144
71	26169	27136	27785	28187	-	27024	25781	25458	-	-
72	26170	27137	27786	28188	-	27015	25532	25442	-	-
73	26197	27126	27776	28177	-	25641	25550	25440	-	-
74	26206	27125	27775	28176	-	26161	25552	25353	-	-
75	26186	27124	27774	28175	-	26160	25517	25457	-	-
76	26182	27123	27773	28183	-	26158	26113	25372	-	-
77	26166	27122	27771	28054	-	26157	25665	25455	-	-
78	26181	27121	27753	28049	-	26155	25565	25364	-	-
79	26196	27120	27752	28048	-	26156	25657	25448	-	-
80	26177	27119	27751	28047	-	27025	25554	25362	-	-

A3 1.2.2 PKIS and Reynolds library screening: 384 plate layout

The plate layout adopted for both the PKIS and the Reynolds library screening was reported in Figure A3 5. Each number refers to a specific compound (screened in triplicates), according to the labelling reported in Figure A3 3 and in Figure A3 4. The green wells correspond to the negative and positive controls, the blue wells to the ATP standard controls (different shade: different concentration of ATP).

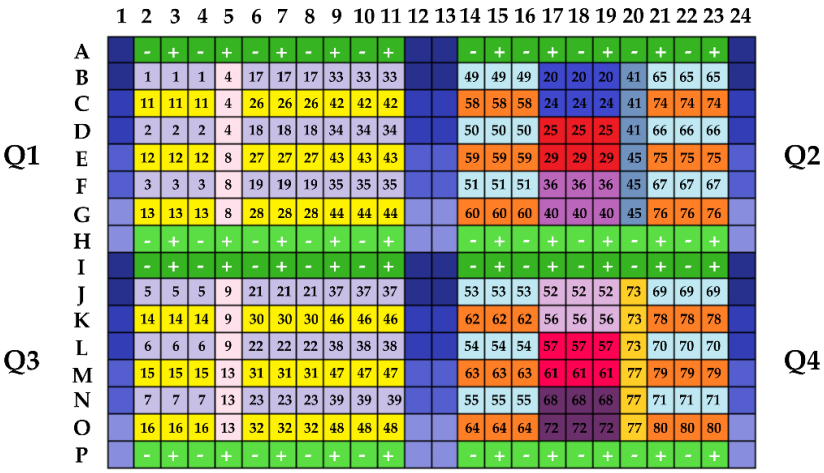

Figure A3 5: PKIS and Reynolds library screening, plate layout

A3 2. The *B-score* normalization

The B-score is based on the application of robust statistical analysis[387] in conjunction with a two-way median polish.[388] The *B-score* normalization can be applied according to the following equation:

$$B\text{-}score = \frac{r_{ijp}}{MAD_p}$$

Eq A3 1: B-score

where r_{ijp} is the residual of the signal measured on row *i* and column *j* of plate *p*, and MAD_p is the median absolute deviation calculate from the derived r_{ijp}.

The signal residual r_{ijp} is defined as reported in the following equation:

$$r_{ijp} = y_{ijp} - \hat{y}_{ijp} = y_{ijp} - (\hat{\mu}_p + \hat{r}_{ip} + \hat{c}_{jp})$$

Eq A3 2: nominator of the B-score (residual of the signal in row *i* and colum *j* of plate *p*)

where y_{ijp} is the raw signal measured in row *i* and column *j* of plate *p*, $\hat{y}_{ijp}$ is the value obtained by the sum of $\hat{\mu}_p$ (the plate average) of $\hat{r}_{ip}$(the row effect) and $\hat{c}_{jp}$ (the column effect), each computed by application of the median polish.[ff]

[ff] The $\hat{}$ sign indicates that the values are estimates of the median polish.

A3 3. HTS format development and screening

A3 3.1. Z'-factor: day-to-day data variability

The Z' factor day-to-day variability for the HTS format optimisation was assessed by repeating the screening simulation in different days. In the following sections the data obtained from the coupled assay in its pre-optimal conditions (section 2.2.4.3 and 3.2.1.3) and its final optimal conditions (2.2.4.4 and 3.2.1.4) were reported.

A3 3.1.1 HTS end-point format, 384 well plate: pre-optimal conditions

The assay conditions applied and the description of the format were reported in section 3.2.1.3. To assess the Z' variability, the mock screening was repeated in 5 different days, in conjunction to the investigation of different incubation times to reduce the drifting effect along the microplate (Figure A3 6*a, b, c, d, f*). An increase of the signal across the different quarters was observed when incubating between 5 and 15 minutes while a decrease occurred when incubating for 25 minutes. The incubation for 20 minutes at 30°C yielded a better stability of the signal across the microplate (Figure A3 6*d*). The screening simulation was repeated on a further different day incubating the microplate for 20 minutes at 30°C (Figure A3 6*e,* also reported in Figure 3.6). A satisfactory consistency of the signal across the microplate was confirmed, hence 20 minutes adopted as standard incubation time for the HTS format. Overall, the Z' of the whole microplate was consistently above 0.55, despite the variation in the incubation time. The performance for each individual quarter was mostly above 0.65, in some cases approaching 0.80 (Table A3 7).

Table A3 7: HTS end-point format, day-to-day variability

Plate	Z'	Plate	Z'	Plate	Z'	Plate	Z'	Plate	Z'	Plate	Z'
a)	**0.59**	***b)***	**0.76**	***c)****	**-**	***d)***	**0.69**	***e)*** **	**0.70**	***f)****	**0.69**
Q1	0.54	Q1	0.83	Q1	0.84	Q1	0.69	Q1	0.68	Q1	0.74
Q2	0.75	Q2	0.82	Q2	0.80	Q2	0.73	Q2	0.75	Q2	0.72
Q3	0.64	Q3	0.82	Q3	0.84	Q3	0.68	Q3	0.70	Q3	0.69
Q4	0.77	Q4	0.82	Q4	-	Q4	0.73	Q4	0.70	Q4	0.70

*a problem with the injection of ADP occurred for the Q4 (Figure A3 6*c*) hence a Z' for Q4 and for the whole plate was not calculated; ** also reported in Figure 3.6.

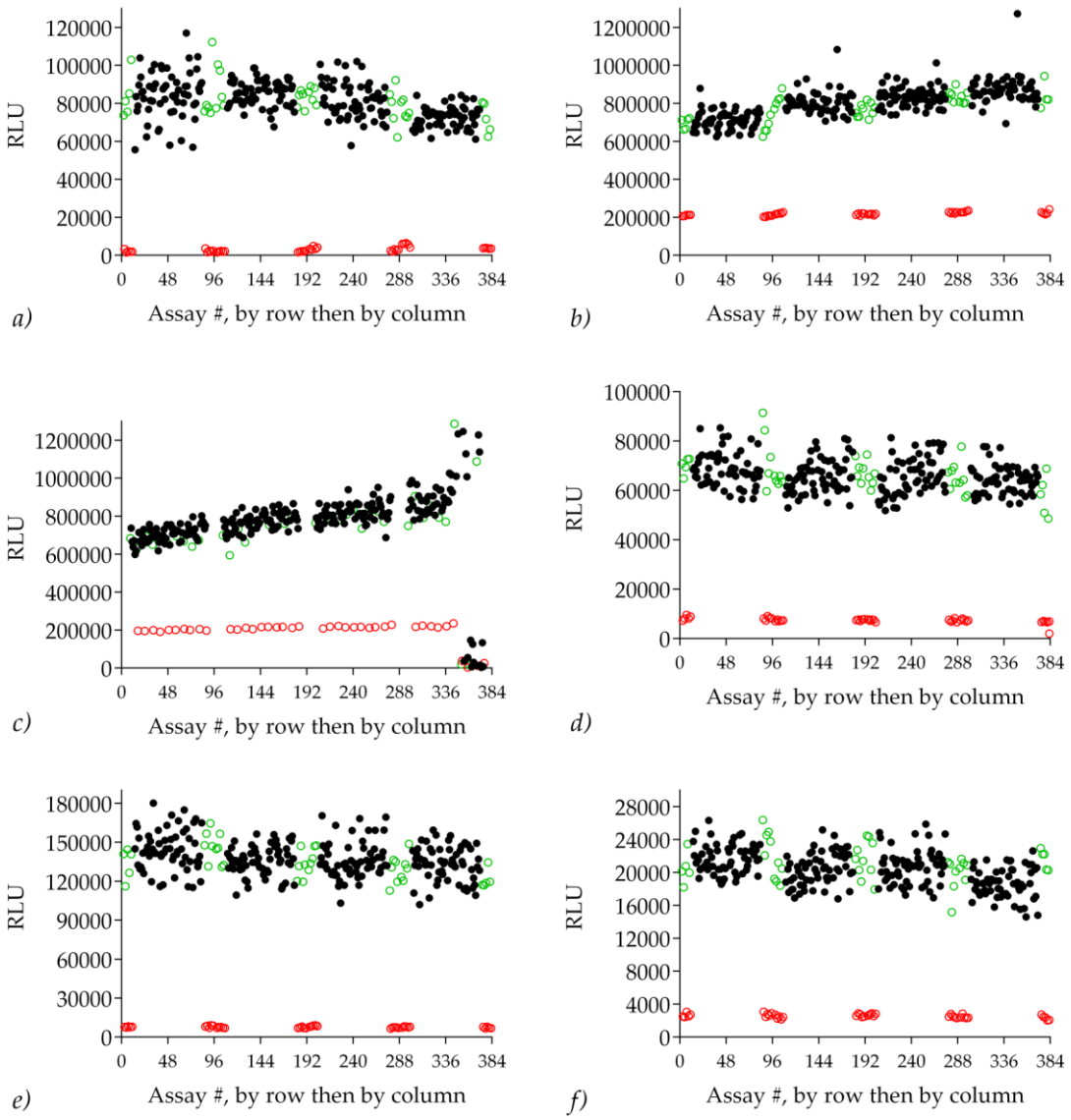

Figure A3 6: HTS format – Z'factor, day-to-day reproducibility

The data reported refers to screening simulation repeated in different days and varying the incubation time: *a*) 5 minutes; *b*) 10 minutes, gain 1700; *c*) 15 minutes, gain 1700; *d*) 20 minutes, gain 1600, e) 20 minutes, gain 1700 (reported also in Figure 3.6, section 3.2.1.3); f) 20 minutes, gain 1300. The different intensity of the signal was due to adjustments of the plate reader gain due to the unexpected and not reproducible high luminescence obtained for the experiment reported in *d* and *c*. Nonetheless, the data were considered valid for the purpose of evaluating the drift as a consequence of incubation time and for the Z' variability assessment.

A3 3.1.2 HTS end-point format, 384 well plate: optimal conditions

The data and respective Z' factor from the day-to-day variability test of the 30 seconds end-point format (section 3.2.1.4.) were reported in Figure A3 7 and Table A3 8. The Z' factor significantly deteriorated when a greater data variability occurred, as for the experiment reported in Figure A3 7*d*. The small separation of the negative and positive control bands, due to the low luminescence derived from the ATP produced after 30 seconds, was further negatively affecting the Z' factor when a greater data variability was observed. Furthermore, the drift across the microplate had the effect of increasing the variation band of the negative control assays when a single Z' factor was computed for the whole microplate, as showed by the discrepancy between the latter and the Z' calculated for a single quarter (Table A3 8).

Table A3 8: HTS end-point format, day-to-day variability, optimised conditions

Plate	Z'	Plate	Z'	Plate	Z'	Plate	Z'	Plate	Z'
a)	**0.65**	***b)***	**0.64**	***c)***	**0.63**	***d)***	**0.26**	***e)***	**0.69**
Q1	0.74	Q1	0.78	Q1	0.73	Q1	0.66	Q1	0.66
Q2	0.79	Q2	0.69	Q2	0.76	Q2	0.59	Q2	0.79
Q3	0.75	Q3	0.78	Q3	0.68	Q3	0.52	Q3	0.84
Q4	0.60	Q4	0.81	Q4	0.80	Q4	0.52	Q4	0.83

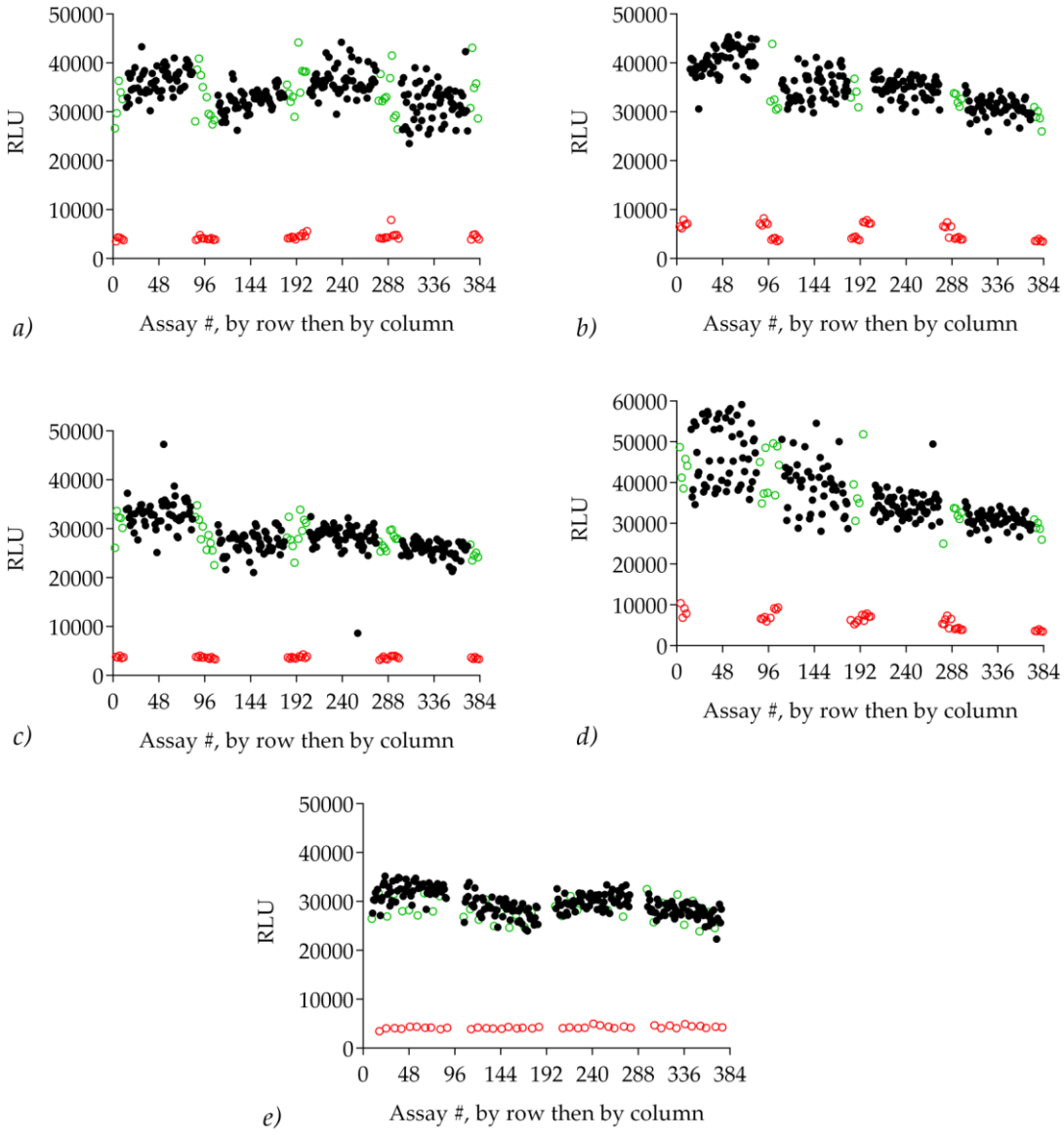

Figure A3 7: HTS format – Z'factor, day-to-day reproducibility, optimal conditions

The data reported refers to screening simulation repeated in different days for the HTS end-point format for which the *Ft*PPK activity was measured after 30 seconds. The following conditions were applied: Assay conditions: 100 µL volume, 10 nM *Ft*PPK /1.3 µM BSA, ADP 200, polyP$_{25}$ 1.5 µM, 300 nM FLuc/1.3 µM BSA, 70 µM luciferin, 5% DMSO, 20 minutes incubation, 30°C. Gain: 1700.

A3 3.2. PKIS screening

The raw data of the PKIS library screen were reported in Figure A3 8. The statistical analysis (Z'-factor and Z-factor) to assess the performance of each microplate was reported in Table A3 9.

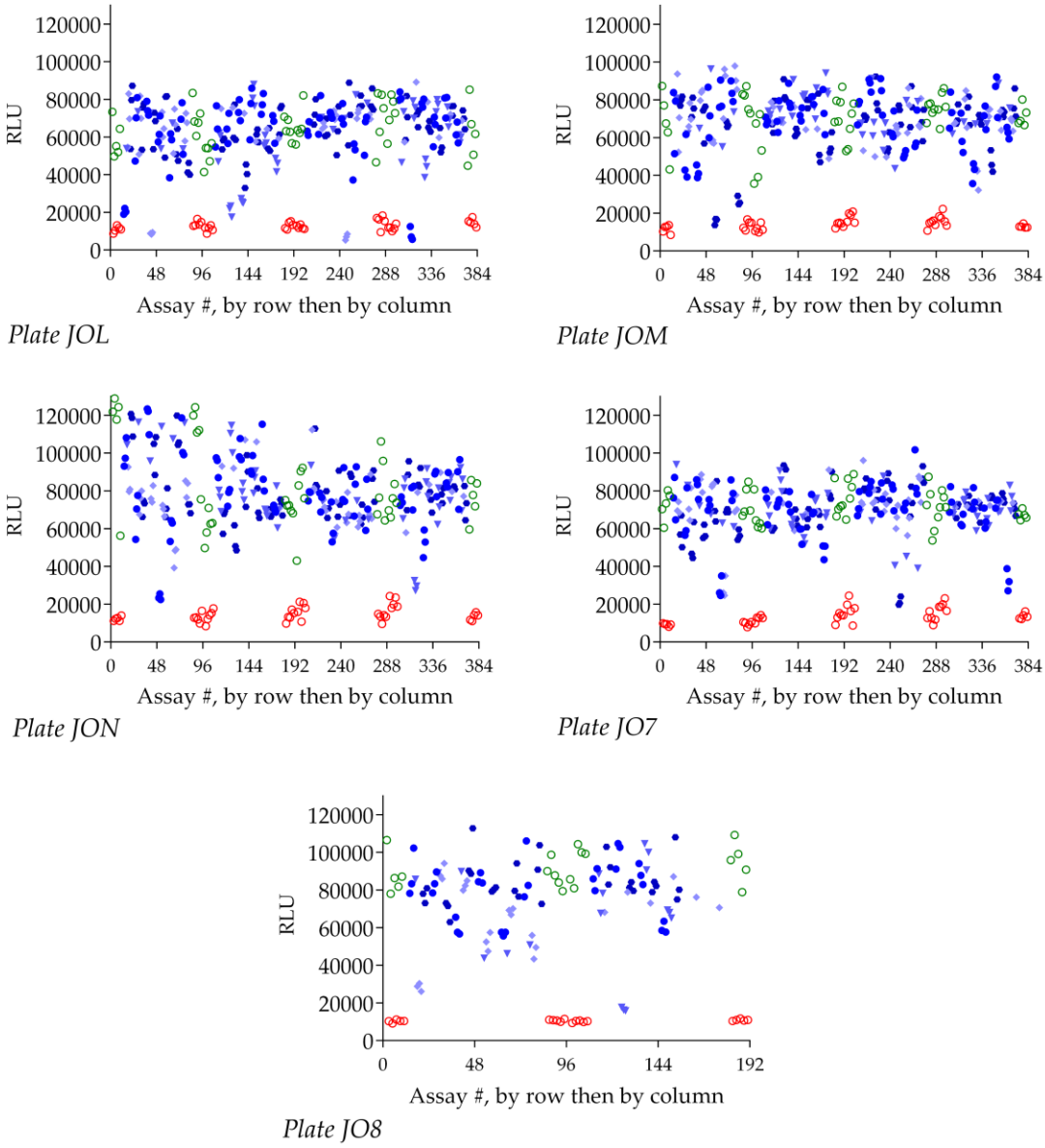

Figure A3 8: PKIS screening, raw data

Assays containing the inhibitors: various shade of blue (a different symbol and shade of blue was used for each triplicate); negative control assays (containing DMSO): green open circles; positive control assays (no *Ft*PPK): red open circles.

Table A3 9: Quality control of the assay during the PKIS screening

Plate	Z'- value	Z- value	Plate	Z'- value	Z- value
J00B-JOL	**0.39**	**0.42**	**J00B-JOM**	**0.63**	**0.46**
Q1	0.52	0.42	Q1	0.53	0.52
Q2	0.50	0.31	Q2	0.32	0.41
Q3	0.45	0.34	Q3	0.67	0.39
Q4	0.58	0.44	Q4	0.61	0.57
J00B-JON	**0.38**	**0.43**	**J00B-JO7**	**0.51**	**0.50**
Q1	0.80	0.41	Q1	0.72	0.66
Q2	0.65	0.58	Q2	0.68	0.46
Q3	0.32	0.54	Q3	0.38	0.56
Q4	0.49	0.39	Q4	0.69	0.62
J00B-JO8	**0.74**	**0.63**			
Q1	0.82	0.51			
Q3	0.83	0.78			

The hits selected from the PKIS library screening were reported in Table A3 10. The compounds were reported ranked by Z_R-*score*. Each compound was identified by a label denoting the plate of origin and the position within the plate (e.g.: compound JO7-54 was taken from plate JO7, position 54), the compound label provided by GSK (table with GSK list), the corresponding Z_R-*score* and NPI_R and the IC_{50} concentration with respect to the FLuc reported in Dranchak *et al.*[392]. The hits selected by the Z_R-*score* were reported in the first section of the table, the hit selected by NPI_R were reported in the second section of the table, in order of Z_R-*score*.

The structures of the PKIS hits were reported in Figure A3 9 until Figure A3 13, grouped according to structure similarities. Within each figure, the hit were reported in order of Z_R-*score*, from top left to bottom right. In particular, the anilino aryloxazole analogues (Figure A3 9), the benzimidazole-urea analogues (Figure A3 10) and the pyrrolopyrimidine analogues (Figure A3 11) have been reported as FLuc inhibitors with IC_{50} in the low micromolar range.[392]

Table A3 10: PKIS library, hits selected ranked by *ZR-score*

Ranked	Plate position	GSK Reg N.	*ZR-score*	*NPIR*	FLuc IC_{50}*
1	JO7-54	GW631581B	-7.46 ± 0.3	85.2 ± 3.9	6.51 µM
2	JO8-26	GR105659X	-6.99 ± 0.1	90.9 ± 1.4	5.17 µM
3	JOL-53	GW632046X	-6.76 ± 0.18	110.9 ± 2.9	0.58 µM
4	JOL-65	GW577921A	-6.6 ± 0.40	108.3 ± 6.6	1.03 µM
5	JOL-9	GW549390X	-6.54 ± 0.06	107.4 ± 1	-
6	JOM-14	GW627834A	-6.49 ± 0.20	97.2 ± 3.1	1.03 µM
7	JO7-15	GW701427A	-6.4 ± 0.84	73.2 ± 9.6	0.12 µM
8	JON-66	GW513184X	-5.96 ± 0.35	74.6 ± 4.5	-
9	JO7-78	GW829877X	-5.79 ± 0.87	66.2 ± 9.9	-
10	JO8-3	GW296115X	-5.7 ± 0.23	73.6 ± 4.5	-
11	JOL-1	SB-592602	-5.24 ± 0.17	86 ± 2.9	-
12	JOM-20	GW578748X	-5.22 ± 0.28	78.2 ± 4.2	3.66 µM
13	JOL-26	SB-347804	-5.19 ± 0.34	85.1 ± 5.6	0.92 µM
14	JON-11	GW572738X	-4.7 ± 0.1	86.7 ± 1.8	0.82 µM
15	JOL-29	GW817396X	-4.64 ± 0.13	76.1 ± 2.2	33 µM
16	JO7-52	GW694590A	-4.45 ± 0.48	50.8 ± 5.6	14.6 µM
17	JON-16	GW589961A	-3.86 ± 0.72	48.4 ± 9.1	> 30 µM
18	JOM-69	GSK238063A	-3.7 ± 0.74	55.4 ± 11	-
19	JO8-12	GW575533A	-3.69 ± 0.38	46.6 ± 5.2	5.8 µM
20	JO7-38	GW643971X	-3.44 ± 0.62	39.3 ± 7.1	-
21	JOM-68	GSK994854A	-3.42 ± 0.63	51.3 ± 9.5	-
22	JOL-30	GW784752X	-3.11 ± 0.69	51.1 ± 11.4	6.5 µM
23	JOM-8	GW809897X	-3.41 ± 0.40	51 ± 6	0.58 µM
24	JO8-19	GW445017X	-3.4 ± 0.68	42.7 ± 9.2	-
25	JO8-13	GW278681X	-3.09 ± 0.54	38.6 ± 7.3	-
26	JON-68	GW335962X	-2.97± 0.97	37.2 ± 12.2	3.66 µM
27	JO7-7	GW824645A	-2.96 ± 1.55	33.8 ± 17.8	-
28	JOM-74	GW694234A	-2.8 ± 0.68	41.9 ± 10.3	-
29	JOL-20	GW441756X	-2.79 ± 0.37	45.8 ± 6.1	-
30	JON-27	GW575808A	-2.78 ± 0.45	40.7 ± 6.7	1.46 µM
31	JOM-5	GW620972X	-2.69 ± 1.4	40.24 ± 21.4	-
Selected only NPIR					
32	JOL-69	GW659893X	-2.66 ± 0.54	43.7 ± 8.9	-
33	JO8-15	SB-711237	-2.61 ± 0.12	32.1 ± 1.64	2.31 µM
34	JOL-39	GW407323A	-2.46 ± 0.4	40.4 ± 6.5	-
35	JOM-43	GW442130X	-2.32 ± 0.22	34.8 ± 3.3	-
36	JOM-55	GW445014X	-2.31 ± 0.22	34.6 ± 3.3	-
37	JO8-31	GW806742X	-2.29 ± 0.33	27.8 ± 4.5	9.19 µM
38	JO8-8	GW827396X	-2.28 ± 0.53	27.7 ± 7.2	-
39	JO7-20	GSK718429A	-2.21 ± 0.41	25.3 ± 4.7	-
40	JO7-4	GW693917X	-2 ± 1.26	22.9 ±14.5	-

Hit selected: compounds with mean + standard deviation falling beyond the hit selection criterion; *Values reported by Dranchak P *et al.*

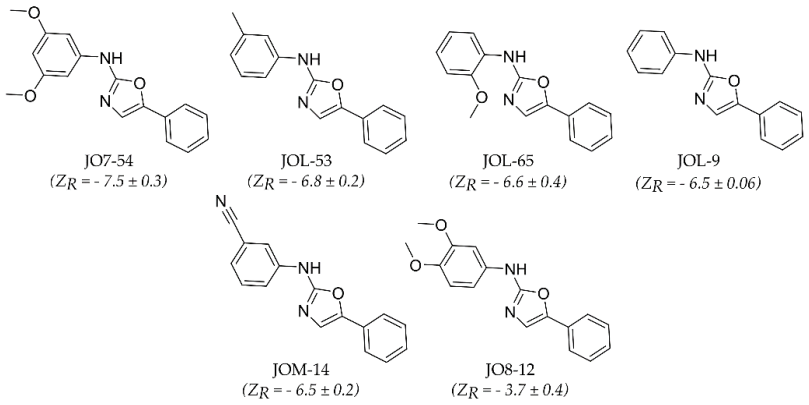

Figure A3 9: PKIS hits: anilino aryloxazole analogues

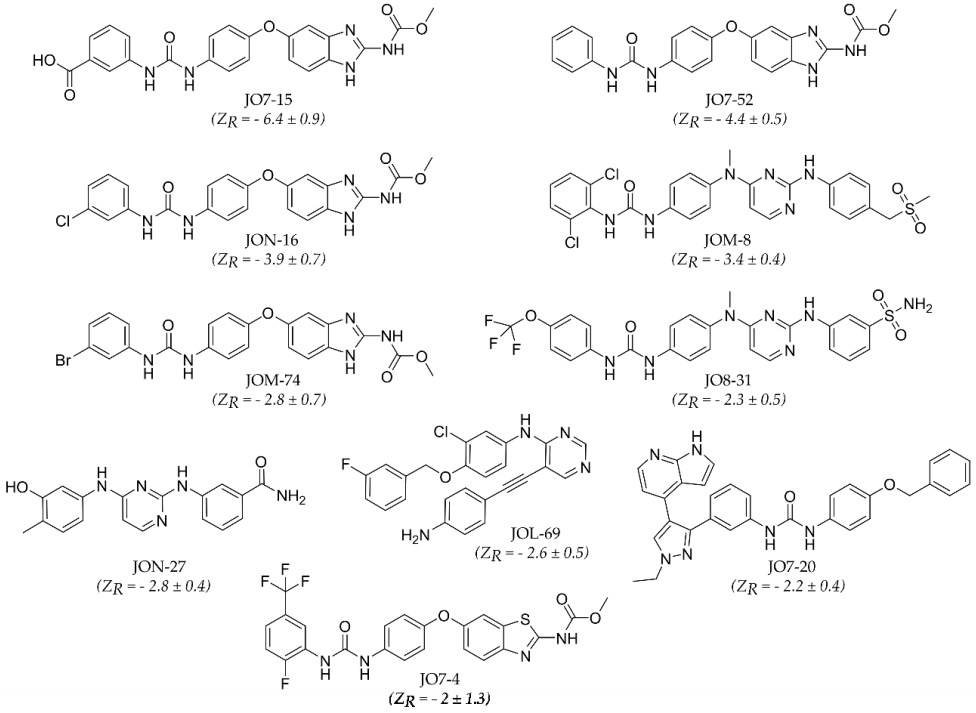

Figure A3 10: PKIS hits: benzimidazole-urea analogues

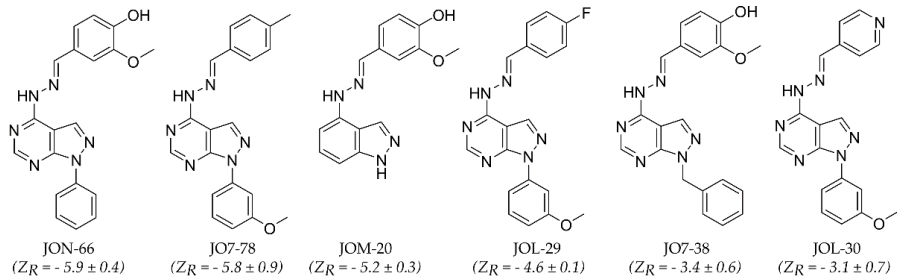

Figure A3 11: PKIS hits: pyrrolopyrimidine analogues

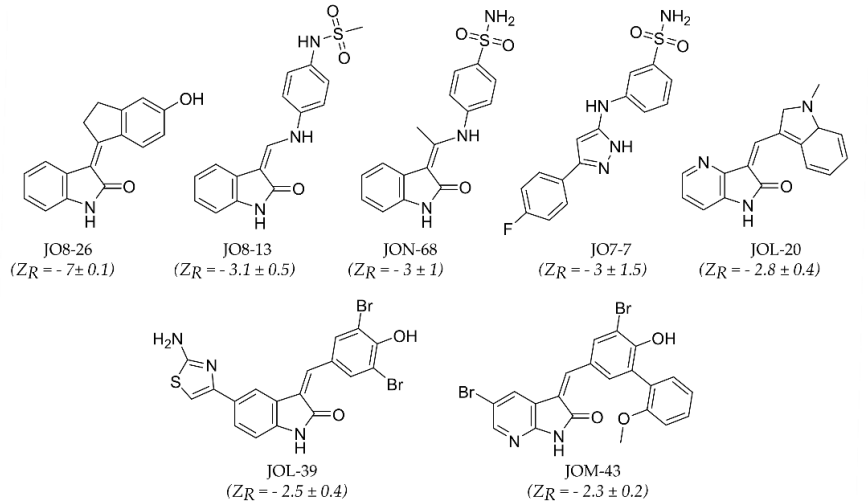

Figure A3 12: PKIS hits

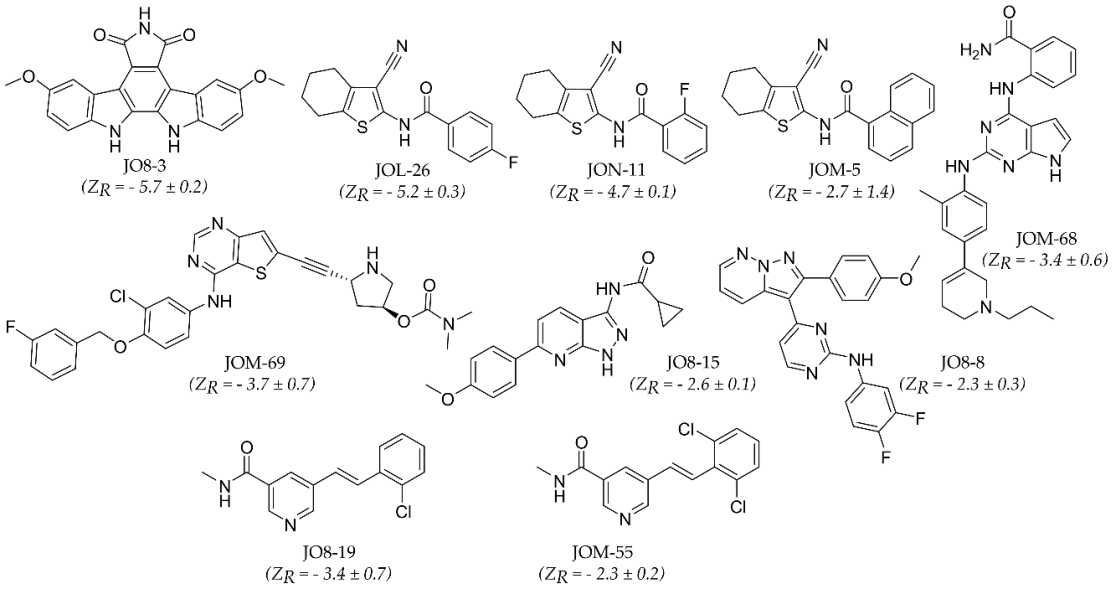

Figure A3 13: PKIS hits

A3 3.3. Reynolds library screening

The raw data of the Reynolds library screen were reported in Figure A3 14 and in Figure A3 15. The Z-factor (based on classic and robust statistical analysis) derived to assess the performance of each microplate was reported in Table A3 11.

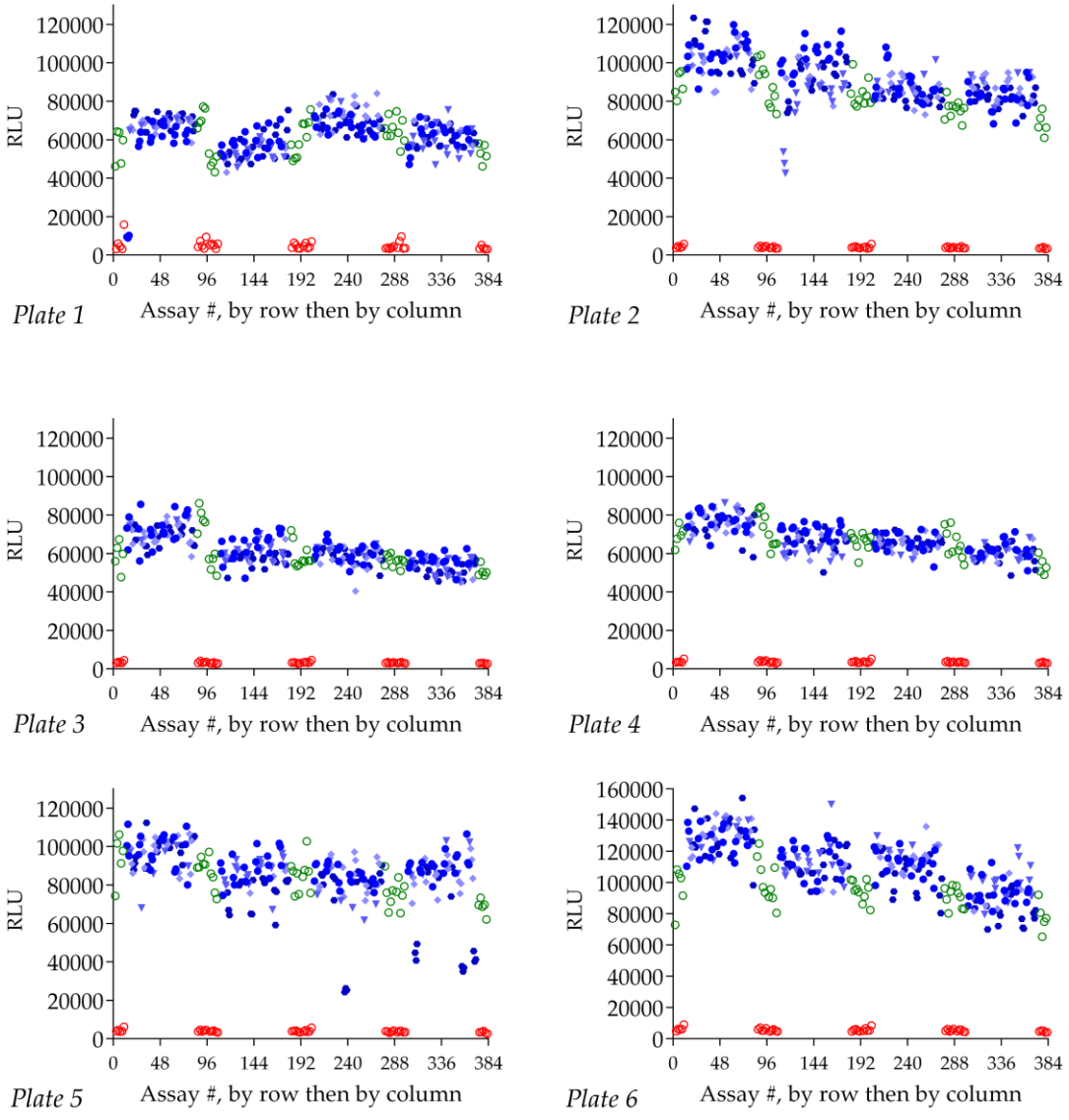

Figure A3 14: Reynolds library screening, raw data, plate 1-6

Assays containing the inhibitors: various shade of blue (a different symbol and shade of blue was used for each triplicate); negative control assays (containing DMSO): green open circles; positive control assays (no *Ft*PPK): red open circles.

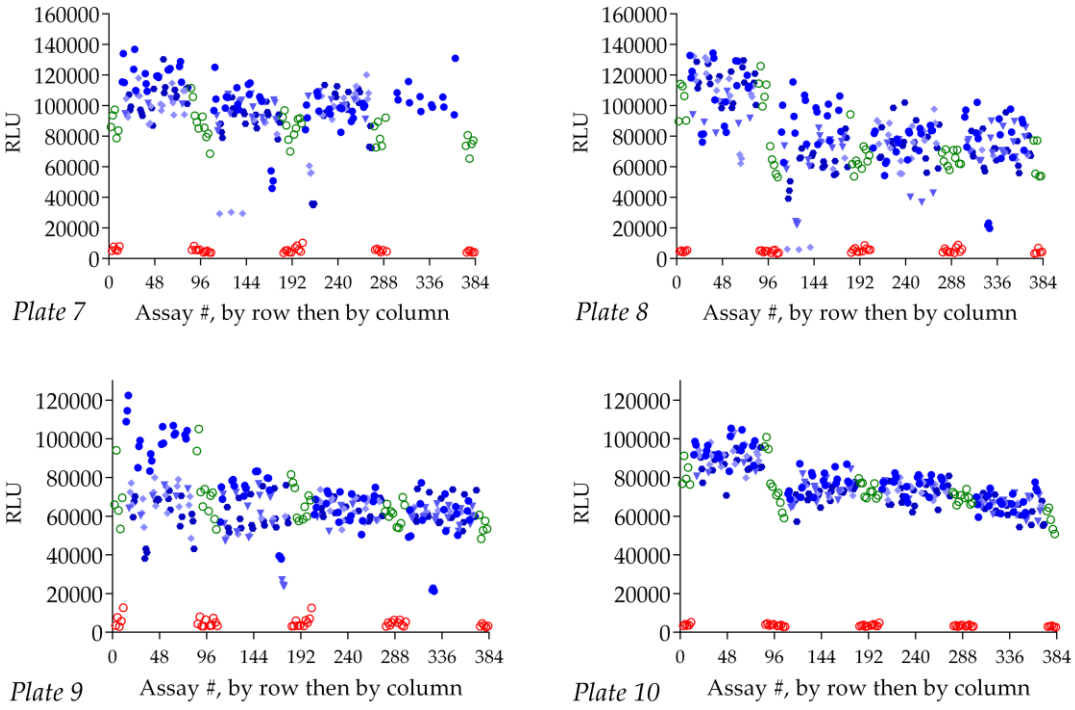

Figure A3 15: Reynolds library screening, raw data, plate 7-10

Assays containing the inhibitors: various shade of blue (a different symbol and shade of blue was used for each triplicate); negative control assays (containing DMSO): green open circles; positive control assays (no *Ft*PPK): red open circles.

The hits selected from the Reynold library screening were reported in Table A4 2. The compounds were reported ranked by Z_R-*score*. Each compound was identified by a label denoting the plate of origin and the position within the plate (e.g.: compound RL56-Plt2 was taken from plate 2, position 56), the compound label provided for each compound of the library and the corresponding Z_R-*score* and NPI_R. The hits selected by the Z_R-*score* were reported in the first section of the table, the hit selected by NPI_R were reported in the second section of the table, in order of Z_R-*score*.

The structure of the hits selected were reported in Figure A3 16 until Figure A3 18.

Table A3 11: Quality control of the assay during the RL screening

Plate	Zc- value	ZR- value	Plate	Zc- value	ZR- value
#1	**0.35**	**0.66**	**#6**	**0.49**	**0.67**
Q1	0.10	0.78	Q1	0.72	0.80
Q2	0.55	0.69	Q2	0.69	0.80
Q3	0.66	0.79	Q3	0.66	0.79
Q4	0.55	0.73	Q4	0.71	0.59
#2	**0.56**	**0.70**	**#7**	**0.36**	**0.65**
Q1	0.70	0.80	Q1	0.61	0.73
Q2	0.50	0.74	Q2	0.30	0.74
Q3	0.72	0.84	Q3	0.30	0.74
Q4	0.74	0.84	Q4	-	-
#3	**0.55**	**0.73**	**#8**	**0**	**0.44**
Q1	0.70	0.82	Q1	0.46	0.71
Q2	0.68	0.82	Q2	-0.18	0.44
Q3	0.71	0.83	Q3	0.36	0.64
Q4	0.72	0.82	Q4	0.21	0.64
#4	**0.61**	**0.74**	**#9**	**0.15**	**0.62**
Q1	0.74	0.84	Q1	0.03	0.48
Q2	0.70	0.77	Q2	0.17	0.44
Q3	0.77	0.87	Q3	0.56	0.70
Q4	0.75	0.86	Q4	0.36	0.78
#5	**0.43**	**0.76**	**#10**	**-0.11**	**0.70**
Q1	0.70	0.81	Q1	0.75	0.84
Q2	0.64	0.77	Q2	0.74	0.83
Q3	0.39	0.79	Q3	0.77	0.85
Q4	0.28	0.81	Q4	0.73	0.80

Table A3 12: RL library, hits selected ranked by Z_R-score

Ranked	Plate position	SRI#	Z_R-score	NPI_R
1	RL1-PLT1	25509	-18.41 ± 0.21	92.23 ± 1.07
2	RL54-PLT9	28111	-11.16 ± 0.23	67.45 ± 1.38
3	RL38-PLT5	25570	-11.06± 0.19	72.60 ± 1.22
4	RL71-PLT7	25781	-10 ± 0.28	60.03 ± 1.65
5	RL37-PLT7	25766	-9.06 ± 0.08	68.04 ± 0.62
6	RL80-PLT7	25554	-8.83 ± 0.58	53.00 ± 3.49
7	RL41-PLT7	25786	-8.70 ± 0.06	71.89 ± 0.52
8	RL69-PLT7	25767	-8.32 ± 0.86	49.96 ± 5.13
9	RL54-PLT8	25771	-6.99 ± 0.25	74.34 ± 2.68
10	RL20-PLT2	26187	-6.22 ± 0.75	50.78 ± 6.14
11	RL21-PLT7	25774	-5.93 ± 0.4	44.54 ± 2.98
12	RL60-PLT7	25782	-5.84 ± 0.76	48.19 ± 6.29
13	RL41-PLT8	25776	-5.58 ± 0.06	97.21 ± 1.13
14	RL13-PLT8	25787	-4.86 ± 0.41	51.20 ± 4.29
15	RL19-PLT8	25785	-4.71 ± 0.29	44.00 ± 2.73
16	RL24-PLT8	25775	-4.18 ± 0.09	72.74 ± 1.51
17	RL40-PLT9	28104	-3.37 ± 0.16	62.27 ± 2.99
18	RL10-PLT8	25777	-3.28 ± 0.30	30.63 ± 2.82
19	RL48-PLT6	27040	-3.16 ± 1.58	20.37 ± 10.17
20	RL42-PLT9	28107	-3.14 ± 0.26	45.29 ± 3.79
21	RL18-PLT2	26199	-3.12 ± 0.04	18.64 ± 0.25**
22	RL48-PLT7	25769	-3.10 ± 1.15	23.29 ± 8.65
23	RL13-PLT5	28029	-3.01 ± 0.86	19.78 ± 5.64
24	RL54-PLT2	27158	-2.80 ± 0.88	14.31 ± 4.47**
25	RL46-PLT6	27038	-2.47 ± 1.23	15.93 ± 7.93
26	RL2-PLT1	25732	-2.42 ± 1.18	12.14 ± 5.93**
Selected only by NPI				
27	RL4-PLT8	25544	-2.40 ± 0.6	22.47 ± 5.58
28	RL22-PLT8	25778	-2.39 ± 0.64	25.22 ± 6.77
29	RL65-PLT8	25360	-2.35 ± 0.48	40.97 ± 8.39
30	RL47-PLT6	27039	-2.35 ± 1.4	15.16 ± 9.03
31	RL65-PLT2	27128	-2.29 ± 0.4	18.73 ± 3.26
32	RL47-PLT1	25472	-2.22 ± 0.95	18.20 ± 7.75
33	RL11-PLT8	25779	-2.20 ± 1.04	20.54 ± 9.75

*Hit selected: compounds with mean + standard deviation falling beyond the hit selection criterion;
**compound selected only by Z_R-score normalization

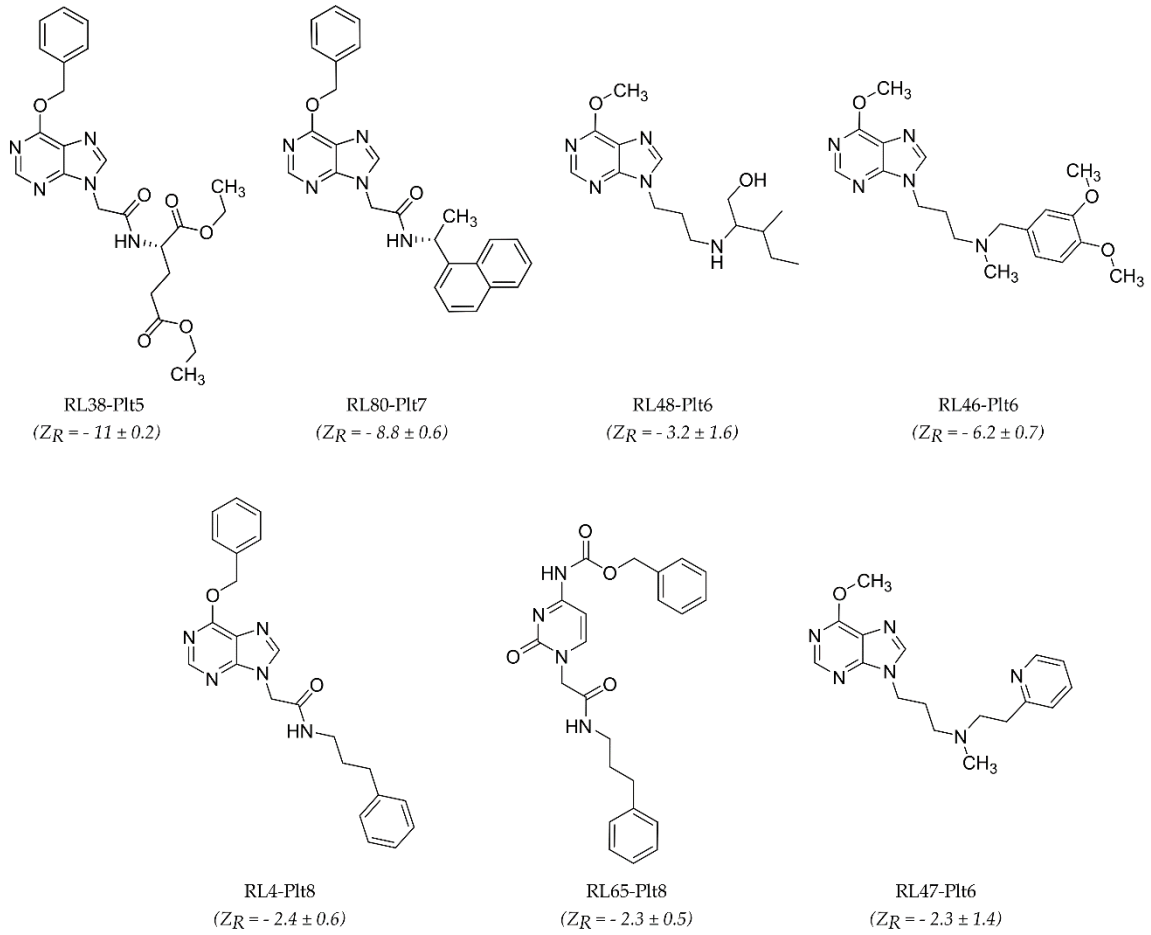

Figure A3 16: Reynolds library hits: nucleoside acetamide analogues

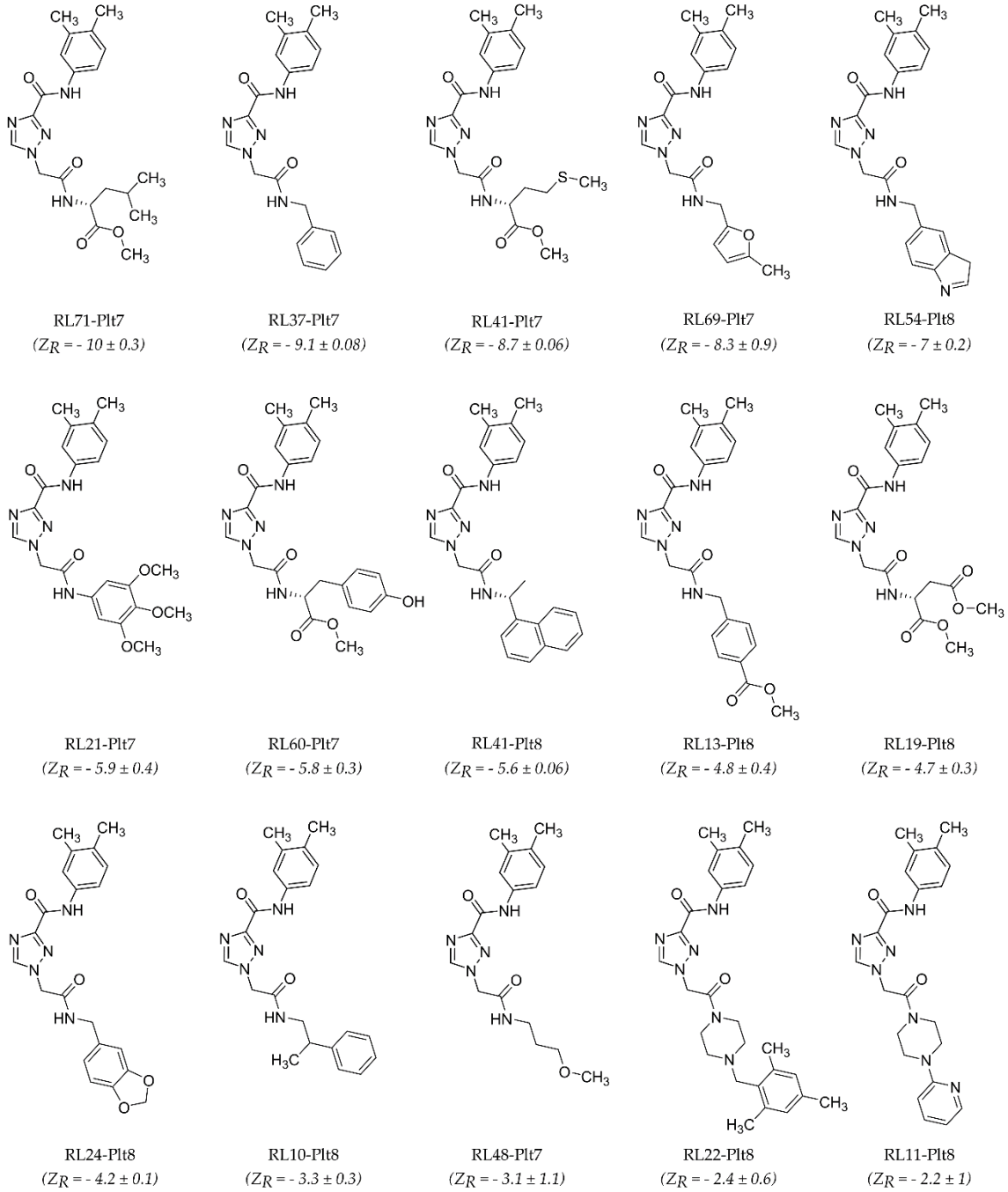

Figure A3 17: Reynolds library hits: triazole-acetamide analogues

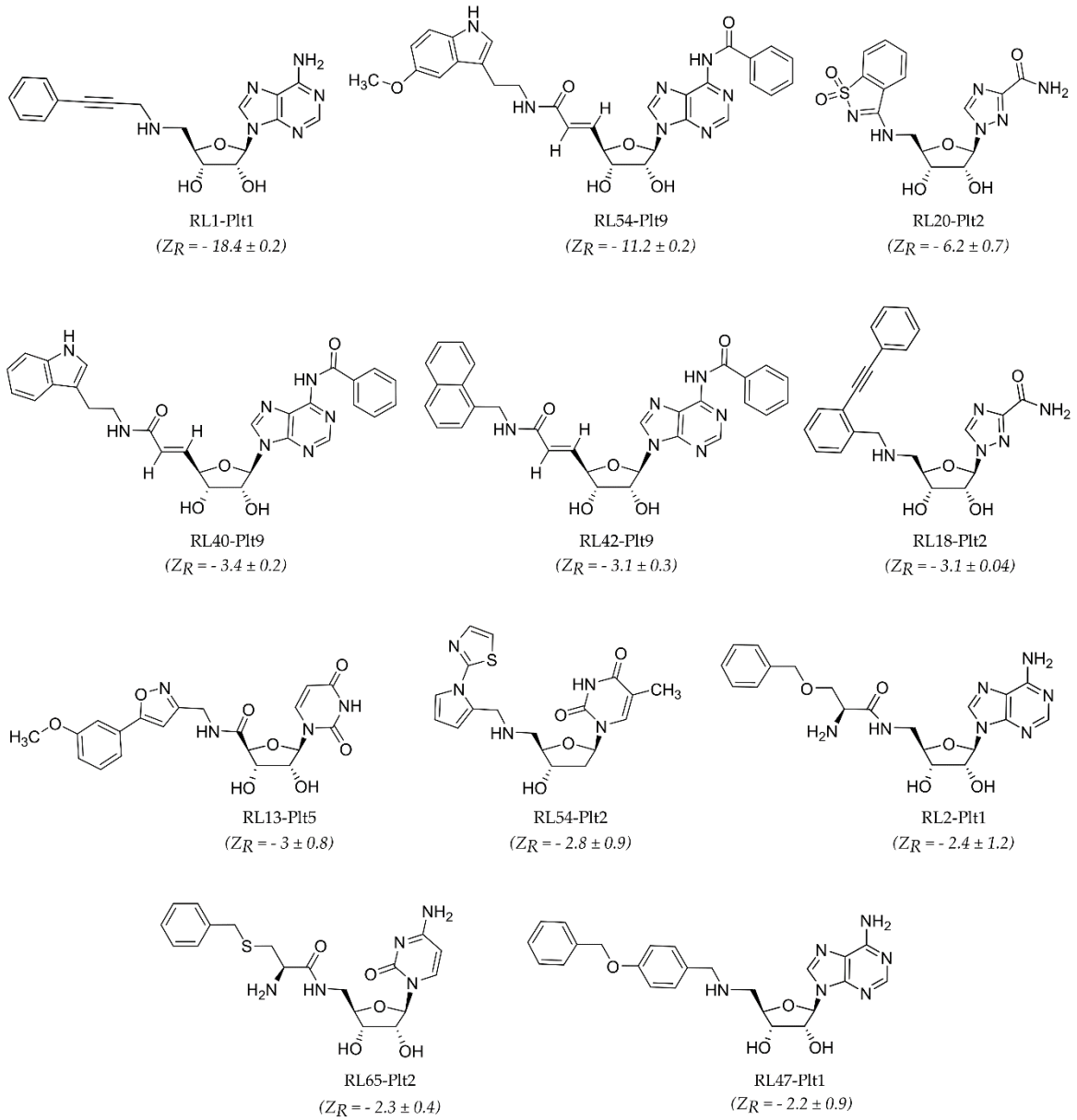

Figure A3 18: Reynolds library hits: nucleotide analogues

Appendix to Chapter 4

A4 1. Thermal shift assay

A4 1.1. DSF assay: *Ft*PPK and SYPRO Orange concentration optimisation

To optimise the condition for DSF, different concentration of SYPRO Orange (1x – 20x) were tested against different concentration of *Ft*PPK (0.5 – 5 µM).

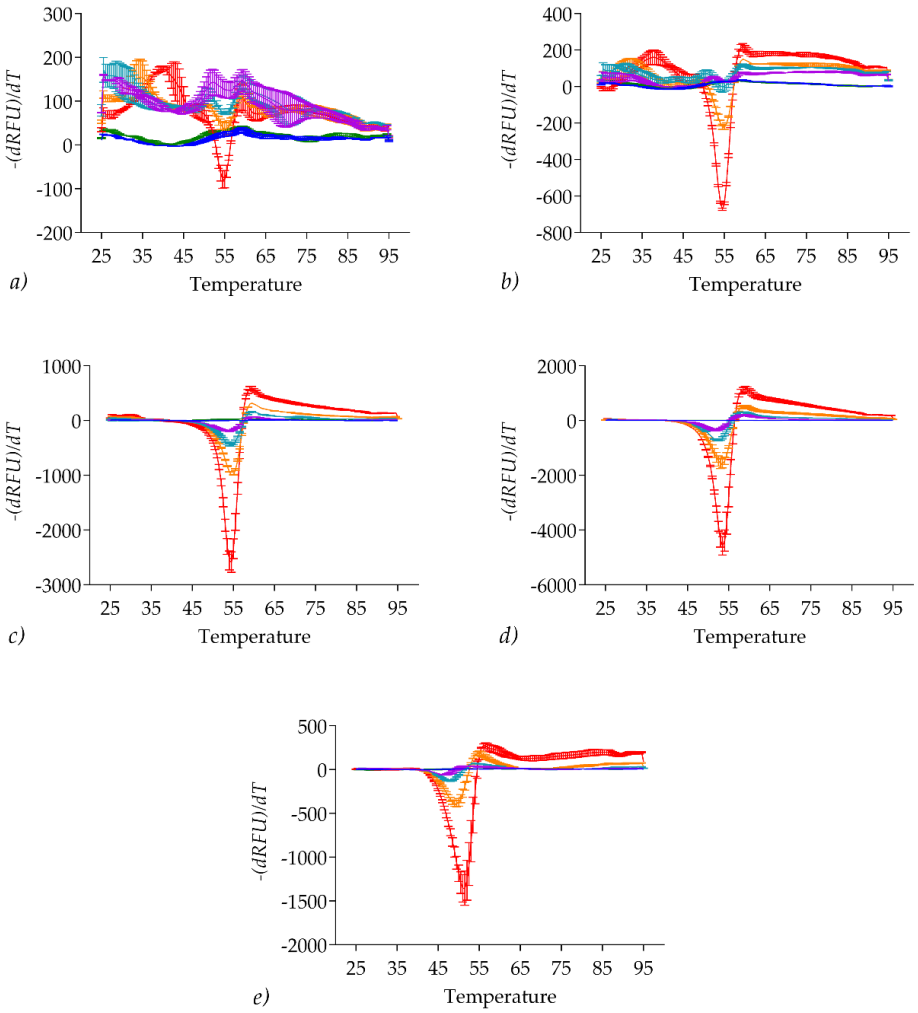

Figure A4 1: DSF assay, *Ft*PPK and SYPRO Orange concentration optimisation

Different concentration of SYPRO Orange were tested against a range of *Ft*PPK concentrations (0.5 - 5 µM). *a*) 1x SYPRO Orange; *b*) 2x SYPRO Orange; c) 5x SYPRO Orange; d) 10x SYPRO Orange; e) 20x SYPRO Orange. Per each concentration of SYPRO Orange, the following *Ft*PPK concentration were tested: 0.5 µM *Ft*PPK (purple), 1 µM *Ft*PPK (light blue), 2 µM *Ft*PPK (orange), 5 µM *Ft*PPK (red). Control assays were also

prepared, in which the RFU of the *Ft*PPK without dye (green) and of the dye without *Ft*PPK (blue) was measured.

A4 1.2. DSF assay: PKIS hit validation

A negative downshift of the melting temperature was caused by most of the PKIS library hits. A significant positive shift of the T_m was observed only in the presence of compound JO8-3. The melting curve of *Ft*PPK in the presence of compound JO8-3 was reported in Figure A4 2. The graphs included the *Ft*PPK melting curve measured in the presence of 5% DMSO and the JO8-3 background signal measured in the absence of *Ft*PPK

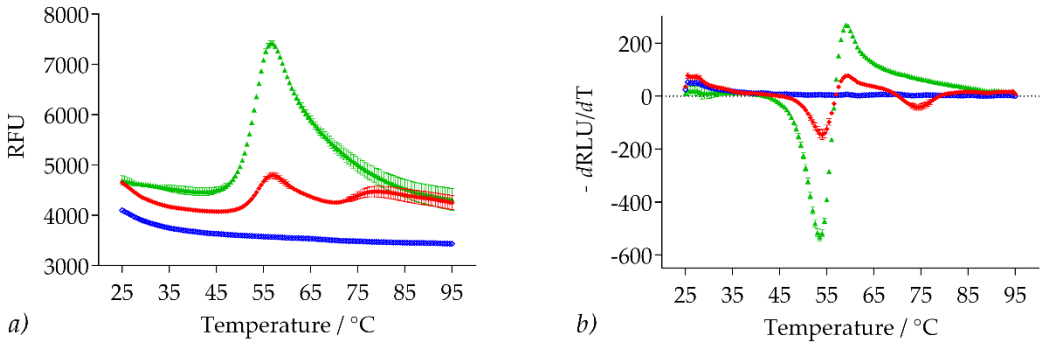

Figure A4 2: DSF assay, JO8-3 melting curves

*Ft*PPK melting curve in the presence of 100 μM JO8-3 (red), *Ft*PPK melting curve in the presence of 5% DMSO (green), background signal generated by JO8-3 in the presence of SYPRO Orange and in the absence of *Ft*PPK (blue). The data were reported as: *a*) Fluorescence intensity RLU against temperature; *b*). negative first derivative of fluorescence intensity (RFU) versus temperature.

A4 1.3. DSF assay: Reynolds library hit validation

A negative downshift of the melting temperature was caused by most of the Reynolds library hits at the concentration of 100 μM. The only compounds for which a significant positive shift of the *Ft*PPK T_m was observed were: RL60-Plt7, RL20-Plt2, and RL37-Plt7. The *Ft*PPK melting curves measured in the presence of these compounds were reported in Figure A4 3, in conjunction with the respective background signal measured in the absence of *Ft*PPK and of a *Ft*PPK melting curve measured in the presence of 5% DMSO.

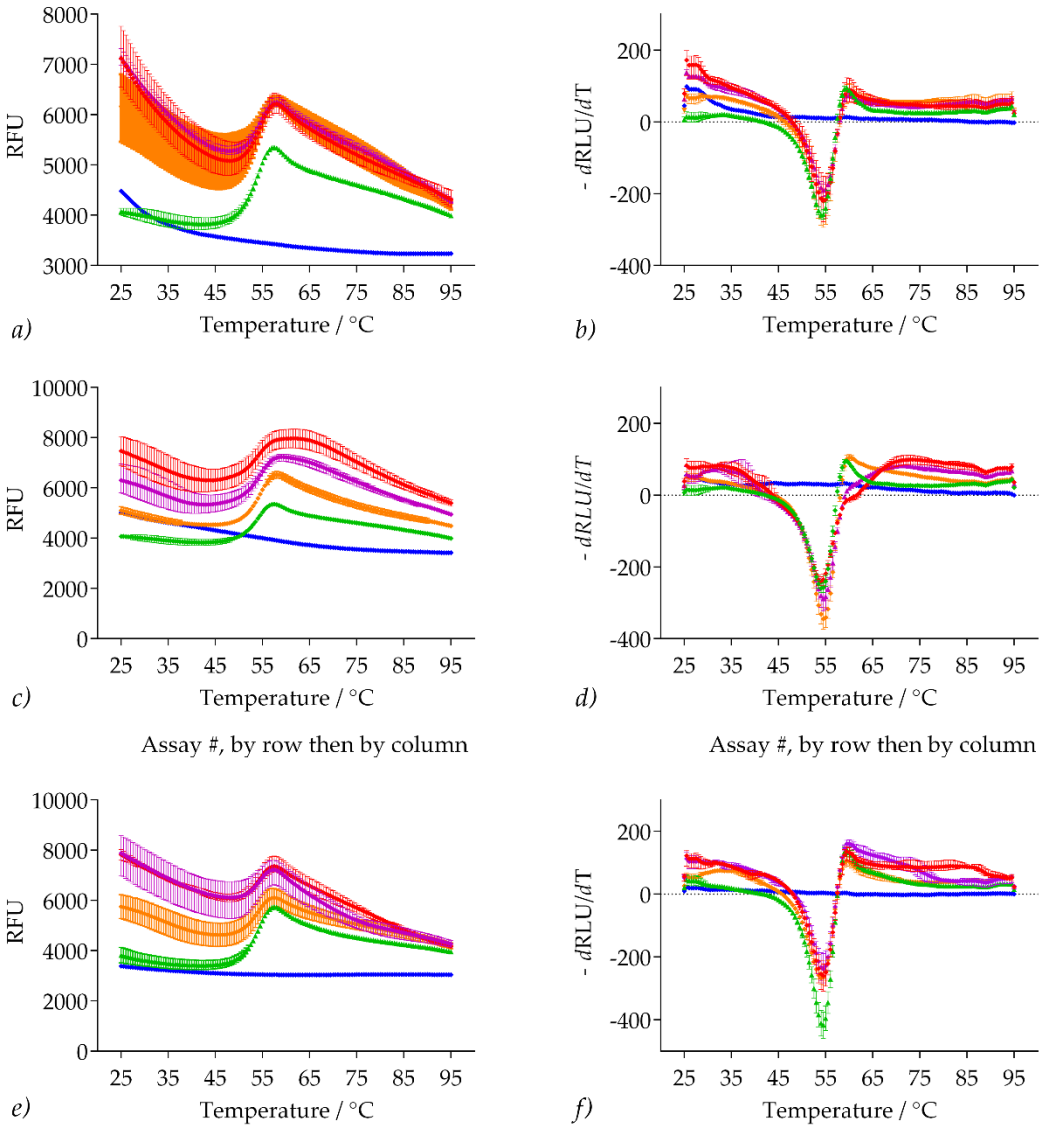

Figure A4 3: RL hits tested by DSF

a) and *b*) *Ft*PPK melting curve in the presence of RL60-PLT7; *c*) and *d*) *Ft*PPK melting curve in the presence of RL20-PLT2; *e*) and *f*) *Ft*PPK melting curve in the presence of RL37-PLT7. For each graph the following melting curve were reported: *Ft*PPK melting curve in the presence of 100 µM hit (red), 50 µM hit (purple), 10 µM hit (orange); *Ft*PPK melting curve in the presence of 5% DMSO (green), background signal generated by 100 µM hit in the presence of SYPRO Orange and in the absence of *Ft*PPK (blue). The data were reported as: *a*), *c*), *d*) fluorescence intensity (RLU) against temperature; *b*), *d*), *e*) negative first derivative of fluorescence intensity (RFU) versus temperature.

A4 2. Development of a *Ft*PPK-PPX-malachite green assay for polyP measurement

For the development of an alternative biochemical assay, the possibility of monitoring the *Ft*PPK activity as a function of either polyP synthesis or degradation was considered. Despite the widespread distribution in cells, few methods are available for the polyP quantitative analysis.[536,537] For polyP chain size investigation, polyacrylamide gel electrophoresis[537,538] and phosphorous NMR (^{31}P-NMR) have been used.[536] The first method relies on the different mobility of chains of different lengths, which allows for size determination by comparison with the retention factors (R_f) of known standards.[538] Determination of polyP size by ^{31}P-NMR instead is possible based on the differences in the resonance of intermediate and terminal phosphates.[264],[260] For polyP quantification, the staining of polyP with the fluorescent dye DAPI (4',6-diamidino-2-phenylindole) has been used.[539] Upon binding to polyP, a shift in the fluorescence peak of DAPI occurs, with a correlation between polyP concentration and fluorescence intensity that is independent from the polyP chains length.[540] Alternatively, polyP quantification has involved the hydrolysis into inorganic phosphate (P_i), either by treatment with hydrochloric acid or catalysed by exopolyphosphatase (PPX).[537,541,542] The P_i units derived from this hydrolysis step have then been quantified by either the metachromatic assay with Toluidine Blue O (TBO)[536,537,543,544] or by the colorimetric malachite green assay.[545–550] Finally, the PPK itself has been used for polyP quantification, by determination of the ATP produced upon polyP-driven ADP phosphorylation.[169,537,543] None of these methods can be universally applied for the analysis of polyP, but limitations may arise due to the heterogeneity in terms of chain length of polyP samples, towards which each method has a different sensitivity.[536,537] Enzyme based methods are the most sensitive and specific, although subjected to enzyme specificity to certain chain lengths.[537] The DAPI method is effective only on polyP chains between 15 and 130 P_i residues and does not distinguish between chains of different length.[540] The gel electrophoresis provides a good description of the sample heterogeneity but is not suitable for precise quantitative analysis. Metachromatic and colorimetric assays require hydrolysis of polyP chains. Once more, limitations to accurate quantitative analysis may arise from either hydrolysis of other phosphate-containing compounds upon treatment with acid, or from uncomplete hydrolysis upon enzyme catalysed reaction, due to chain

length specificity. Finally, restriction to the application of ^{31}P-NMR analysis may derive from the low throughput and the large amount of sample required for analysis.

A metachromatic assay, in which polyP was quantified by means of Toluidine Blue, has been reported for the PPK activity measurement.[424] The method is based on the shift of the absorbance peak of Toluidine upon interaction with polyP. The shift is proportional to the polyP concentration but is also affected by the polyP chain length, hence providing a semi-quantitative analysis.[424] In the attempt to develop a fully quantitative method for the measurement of the *Ft*PPK reaction as a function of either polyP synthesis or degradation, the development of an exopolyphosphatase coupled assay was investigated. The *Ft*PPK reaction was coupled to polyP hydrolysis catalysed by the PPX from *Burkholderia pseudomallei* (*Bp*PPX). The polyP concentration was then derived by quantification of the released P_i by means of the malachite green assay.

A4 2.1. Malachite green assay

The malachite green assay (MG assay) is a colorimetric assay that allows detection of P_i upon formation of a chromogenic complex.

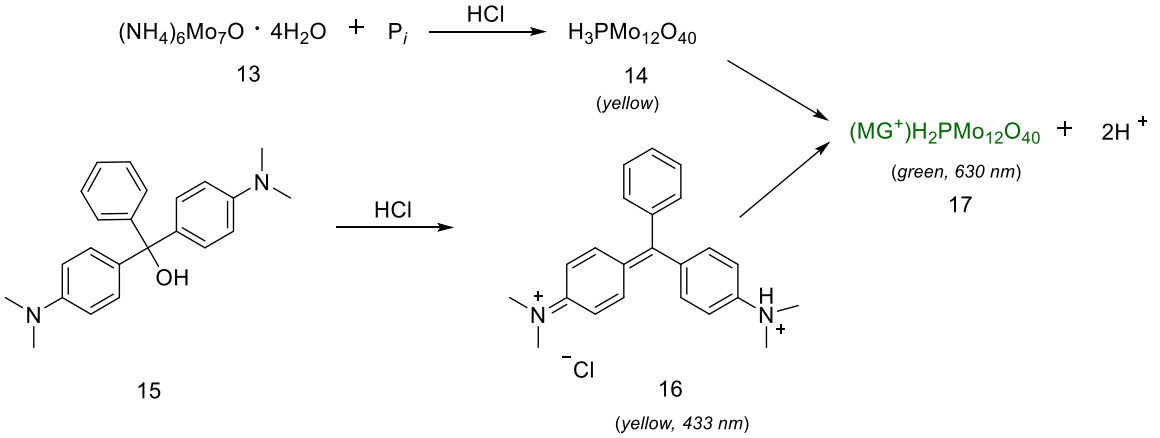

Scheme A4 1: Malachite green - reaction scheme

Malachite green reagent composition: 1 volume of 4.2% ammonium molybdate (14) in 4M HCl; 3 volumes of 0.045% MG carbinol dye (15) in water; 0.01% Tween 20.

The malachite green reagent (MG reagent) is constituted by ammonium molybdate tetrahydrate (14) and malachite green carbinol base (MG, 15). Under acidic conditions (HCl) and in the presence of the P_i, ammonium phosphomolybdate is formed (16, yellow)

and the MG carbinol base is converted into the cation HMG^{2+} (16, yellow, 446 nm). The phosphomolybdate anion associates with the HMG^{2+} cation and the MG-phosphomolybdate complex 17 is generated. The assay solution turns from yellow to green and a shift in the absorbance peak from 443 nm to 630 nm is observed. Within a certain range, the intensity of the absorbance signal measured at 630 nm is proportional to the concentration of P_i.

A4 2.2. MG assay: P_i standard curve

The malachite green assay conditions adopted by C. Saunders for the characterization of *Burkholderia pseudomallei* PPX (*Bp*PPX),[551] in turn adapted from Sherwood,[548] were applied for the *Ft*PPK-PPX-malachite green assay. A P_i standard curve was prepared to investigate the correlation between P_i concentration and absorbance signal.

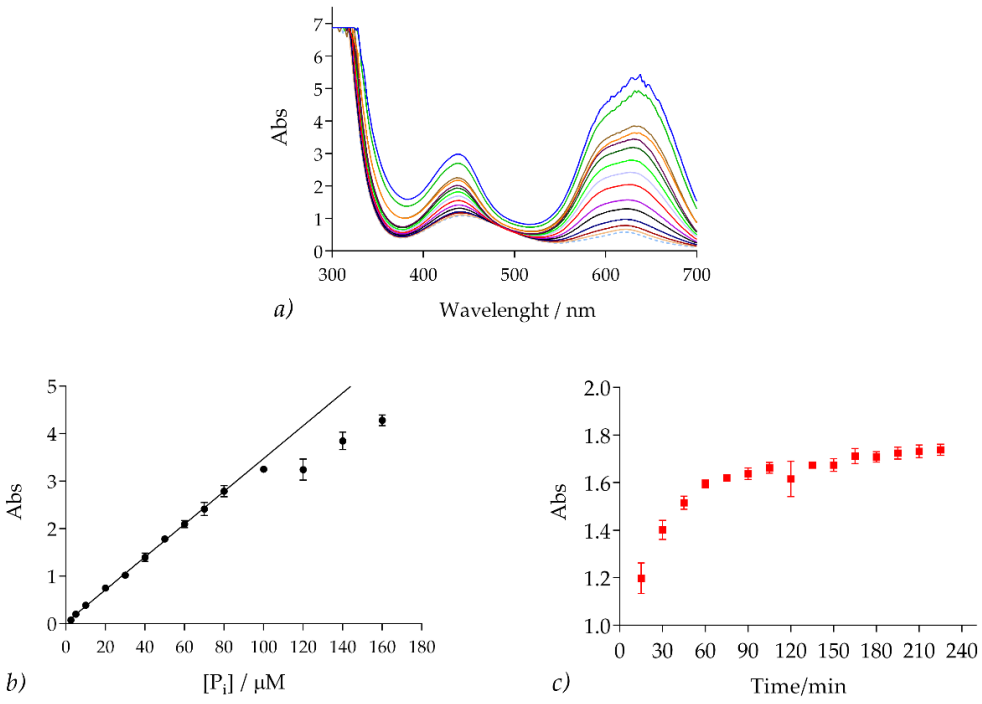

Figure A4 4: MG assay – P_i standard curve

a) Absorption spectra; *b*) Standard curve measured at λ 630 nm. The signal was blank-corrected; *c*) Variation of the signal with time (40 µM Na_2HPO_4). Assay conditions: P_i assay volume 50 µL (*Ft*PPK assay buffer, 2.5 – 160 µM Na_2HPO_4, 1.3 µM BSA, 5% DMSO); MG reagent 50 µL (1 volume of 4.2% ammonium molybdate in 4M HCl, 3 volumes of 0.045% MG carbinol dye in water, 0.01% Tween 20). The assays were prepared in triplicate at room temperature.

The standard curve was prepared using Na_2HPO_4 (2.5 μM – 160 μM) in the *Ft*PPK assay buffer and in the presence of DMSO (in anticipation of the conditions that would be applied to the coupled *Ft*PPK2-PPX assay). To measure the background signal due to P_i traces in the assay buffer, control assays (no Na_2HPO_4) were also prepared. The P_i assays were prepared in 50 μL volume, to which 50 μL of MG reagent were added. The full spectrum was recorded for each P_i concentration, to confirm that, under the conditions applied, the maximum absorbance signal occurs between 625 nm and 640 nm (Figure A4 4*a*). To generate the P_i standard curve, the assays were measured at 630 nm after 10 minutes from the addition of the MG reagent, and then every 15 minutes to determine the stability of the signal with time (Figure A4 4*b* and *c*). A relation of linearity was observed between 2.5 μM and 80 μM P_i, above which a deviation from linearity was detected. The signal intensity increased with time during the first 50-60 minutes, after which it became approximately stable.

A4 2.3. MG assay: stability of ATP and ADP under acidic conditions

A possible limitation in using the MG assay as readout method for the *Ft*PPK-PPX coupled assay might derive from the strongly acidic conditions (4 M, HCl) required for the preparation of the MG reagent. Under acidic conditions, the hydrolysis of the terminal phosphate of the *Ft*PPK substrates, ATP and ADP, might be favoured, hence interfering with the *Ft*PPK assay measurement. The stability with time of ATP and ADP in the presence of the MG reagent was investigated. Assays with different concentrations of P_i with and without ADP (70 μM) or ATP (350 μM) were prepared, alongside controls with only P_i, ADP or ATP. The assays were measured after 10 minutes from the addition of the MG reagent and then monitored for 3.30 hours. Following the first measurement, a comparable signal was detected from the assays containing P_i and ATP or ADP, and the assays containing only P_i (Figure A4 5*a*). However, after the second measurement, a increase of the signal from the assays containing ATP was observed in comparison to the assays containing only P_i or including ADP, consistent with hydrolytic release of P_i (Figure A4 5*b*). Because of the observed ATP hydrolysis under the malachite green assay conditions, the measurement of *Ft*PPK activity using ADP as substrate should be preferred.

Alternatively, if a format using ATP as substrate provides significant advantages for the *Ft*PPK activity measurement, a control assay to monitor ATP hydrolysis should be prepared alongside the *Ft*PPK assay. Furthermore, the signal should be measured soon after the addition of the MG reagent, to limit the extent of ATP hydrolysis.

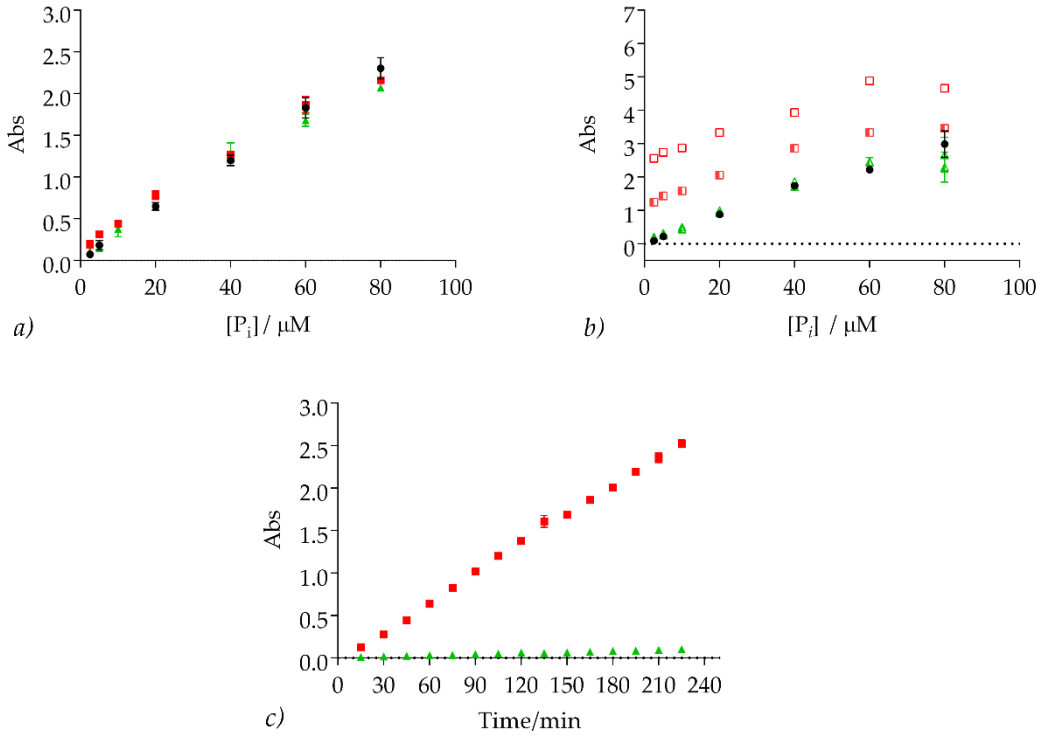

Figure A4 5: MG assay –stability of ATP and ADP under acidic conditions

Standard curves prepared with only P_i (black circles), with P_i and ATP (red squares) and with P_i and ADP (green triangles). *a*) Measurement after 10 min. *b*) Measurements after 1.30 h (ATP: half squares, ADP: half triangles) and after 3.30 h (ATP: empty squares, ADP: empty triangles). *c*) Negative control assays containing only ATP (red squares) or ADP (green triangles). Assay conditions: 2.5 – 80 µM Na_2HPO_4, 1.3 µM BSA, 5% DMSO; P_i – ATP assays: included 350 µM ATP; P_i – ADP assays: included 70 µM ADP. MG reagent: 1 volume of 4.2% ammonium molybdate in 4M HCl, 3 volumes of 0.045% MG carbinol dye in water, 0.01% Tween 20.

A4 2.4. Development of the *Bp*PPX-MG assay

Purified *B. pseudomallei* PPX was available in-house (courtesy of A. Parnell)[265] and was used for the development of a *Bp*PPX-*Ft*PPK coupled assay. The PPX catalyses the hydrolysis of polyP into P_i units. To measure the activity of the PPX, the MG assay was applied for the quantification of the P_i produced. A *Bp*PPX time course was prepared, using

100 nM *Bp*PPX and 30 µM polyP$_{25}$. While the concentration of *Bp*PPX was arbitrarily chosen, the concentration used for the *Ft*PPK screening was adopted for polyP. The *Bp*PPX assays were initiated by addition of polyP$_{25}$ and stopped at the desired time points by addition of the MG reagent. A P_i standard curve (5 – 70 µM) was prepared alongside the *Bp*PPX assay, to convert the absorbance signal into P_i concentration.

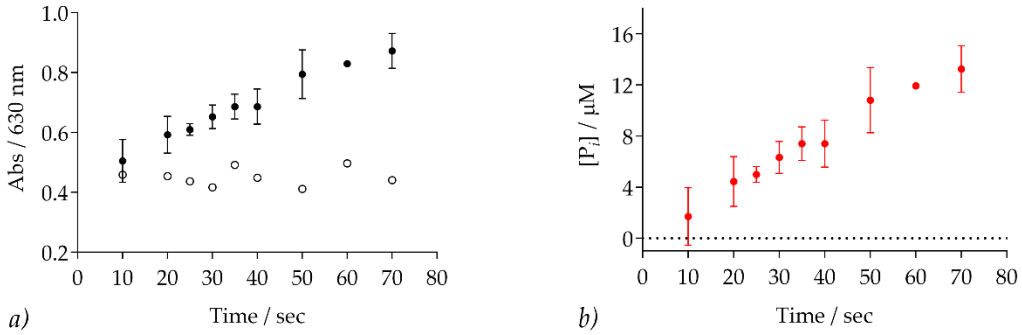

Figure A4 6: *Bp*PPX – MG time course

a) Raw data plotted as absorbance signal versus time; *b*) background corrected data, converted into P_i produced by means of the P_i standard curve. The assays were prepared in triplicate. *Bp*PPX- MG assay conditions: 100 nM *Bp*PPX, 30 µM polyP$_{25}$, 1.3 µM BSA, 5% DMSO; MG reagent: 1 volume of 4.2% ammonium molybdate in 4M HCl, 3 volumes of 0.045% MG carbinol dye in water, 0.01% Tween 20.

Under the conditions applied, a linear increase with time of P_i was observed, which validated the MG assay as a readout method for the *Bp*PPX activity assay. However, the rate of product formation was judged too slow to couple the *Bp*PPX assay for the measurement of the *Ft*PPK activity. Ideally, for the *Ft*PPK coupled assay, a concentration of *Bp*PPX that catalyses immediate conversion of polyP into P_i is required. A range of *Bp*PPX concentrations between 25 nM and 1.2 µM was investigated, measuring time courses in the presence of 30 µM polyP$_{25}$ (excess of polyP). A concentration of 800 nM *Bp*PPX was chosen, in the presence of which the P_i produced at plateau (80 µM) was within the linear range of the MG standard curve (Figure A4 7*b*).

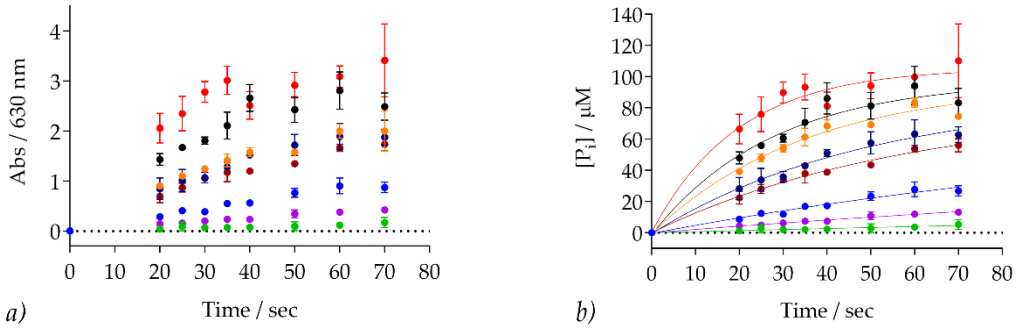

Figure A4 7: Optimisation of the *Bp*PPX concentration

Time courses measured at different concentrations of *Bp*PPX: 25 nM green circles,100 nM purple circles, 200 nM blue circles, 400 nM bordeaux circles, 600 nM dark blue circles, 800 nM orange circles, 1000 nM black circles, 1200 nM red circles. *a*) data plotted as absorbance signal versus time; *b*) data reported as P_i produced with time. *Bp*PPX- MG assay conditions: 25 - 1200 nM *Bp*PPX, 30 µM $polyP_{25}$, 1.3 µM BSA, 5% DMSO; MG reagent: 1 volume of 4.2% ammonium molybdate in 4M HCl, 3 volumes of 0.045% MG carbinol dye in water, 0.01% Tween 20.

A4 2.5. Development of the *Ft*PPK-*Bp*PPX-MG assay in a continuous format

The coupling of the *Ft*PPK assay to the *Bp*PPX-MG assay was attempted in continuous format. The *Ft*PPK reaction was investigated in the direction of the polyP synthesis, in view of the better sensitivity provided by a product formation format. The concentrations applied for the screening were adopted for *Ft*PPK (10 nM) and for $polyP_{25}$ (1.5 µM), whereas for ATP the K_m concentration (350 µM) was chosen.[264] A format similar to the *Ft*PPK-FLuc assay was investigated, in which the *Bp*PPX (800 nM) was added after a variable delay from the start of the *Ft*PPK assay to measure different time points. In turn, for each time point, the MG reagent was added at the same time interval after the addition of *Bp*PPX assay (63 seconds), to inactivate the *Bp*PPX and start the colorimetric assay. An increase of the absorbance signal with time was expected, as a function of the hydrolysis of growing polyP chains, derived from the *Ft*PPK catalysed polyP synthesis. In fact, the signal from the *Ft*PPK-*Bp*PPX coupled assay was equal to the signal from *Bp*PPX control assays, in which no *Ft*PPK was included (Figure A4 8). The data obtained suggested that the rate of the polyP hydrolysis catalysed by *Bp*PPX was sufficiently slow to mask any *Ft*PPK activity.

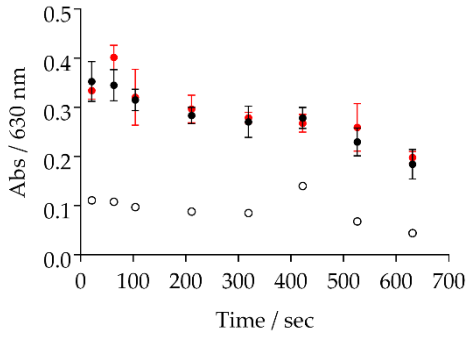

Figure A4 8: *Ft*PPK-*Bp*PPX-MG coupled assay, continuous format

*Ft*PPK-*Bp*PPX coupled assay time course: red circles; independent *Bp*PPX time course: black circles; control assays (no *Ft*PPK and *Bp*PPX): black open circles. *Ft*PPK-*Bp*PPX-MG assay conditions: 10 nM *Ft*PPK, 1.5 μM $polyP_{25}$, 350 μM ATP, 800 nM *Bp*PPX, 1.3 μM BSA, 5% DMSO; *Bp*PPX-MG assay conditions: 800 nM *Bp*PPX, 1.5 μM $polyP_{25}$, 350 μM ATP, 1.3 μM BSA, 5% DMSO; MG reagent: 1 volume of 4.2% ammonium molybdate in 4M HCl, 3 volumes of 0.045% MG carbinol dye in water, 0.01% Tween 20.

A4 2.6. *Ft*PPK-*Bp*PPX-MG assay in discontinuous format: polyP synthesis

Following the failure to measure a *Ft*PPK time course using a *Bp*PPX-MG coupled assay in continuous format, the development of a discontinuous format was attempted. The latter involved the following steps: preparation of a *Ft*PPK time course by stopping the reaction at the desired time points by heat denaturation; precipitation of the inactivated *Ft*PPK by centrifugation; incubation of the *Ft*PPK reaction supernatant with *Bp*PPX to allow complete hydrolysis of $polyP_{25}$ (Figure A4 9); incubation of the *Bp*PPX reaction with the MG reagent for the P_i detection. The *Ft*PPK assay was prepared using 1.5 μM $polyP_{25}$ and both the polyP synthesis reaction (in the presence of 350 μM ATP) and the polyP degradation reaction (in the presence of 200 μM ADP) were investigated. To ensure that the polyP hydrolysis reached completion, the product of the *Ft*PPK reaction was incubated with *Bp*PPX for 1.5 hours. Although an upward trend was observed, a correct interpretation of the data from the polyP synthesis format was compromised by their poor quality (Figure A4 10). The latter was possibly due to the abundant protein precipitation caused by the acidic environment.

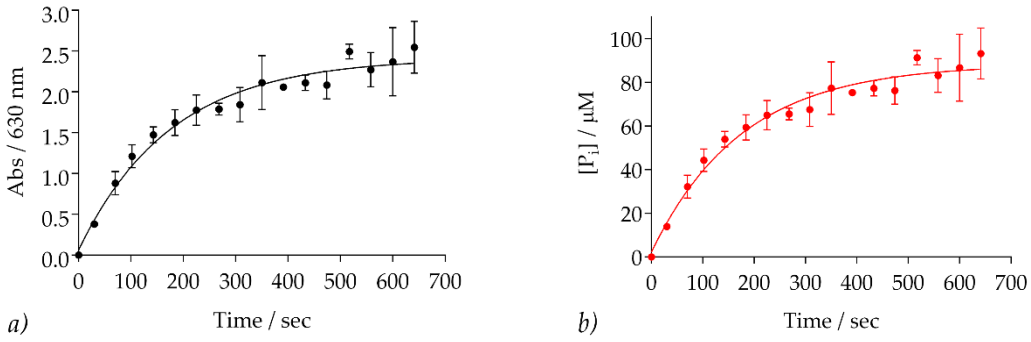

Figure A4 9: *Bp*PPX long time course

The time course showed that PPX saturation was reached after 10 minutes. *a*) Absorbance with time; *b*) P_i with time. *Bp*PPX-MG assay conditions: 800 nM *Bp*PPX, 1.5 µM polyP, 350 µM ATP, 1.3 µM BSA, 5% DMSO; MG reagent: 1 volume of 4.2% ammonium molybdate in 4M HCl, 3 volumes of 0.045% MG carbinol dye in water, 0.01% Tween 20.

The absorbance signal derived from the hydrolysis of 1.5 µM $polyP_{25}$ (control assays, Figure A4 10) approached the top limit of the MG assay standard curve. Hence, the polyP degradation format, for which a decrease of the signal with time was expected, was judged better suitable.

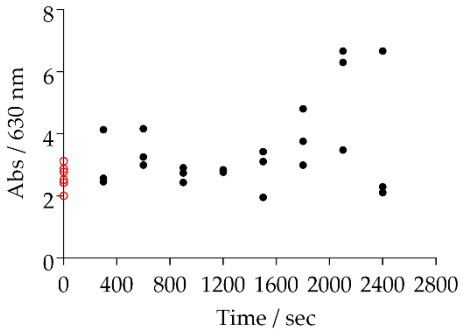

Figure A4 10: *Ft*PPK-*Bp*PPX-MG coupled assay, discontinuous format, polyP synthesis

*Ft*PPK-*Bp*PPX discontinuous format time course: black circles; control assays (*Ft*PPK but not *Bp*PPX): red empty circles. *Ft*PPK was removed by precipitation and centrifugation before addition of *Bp*PPX. Assay conditions: 10 nM *Ft*PPK, 1.5 µM polyP, 350 µM ATP, 800 nM *Bp*PPX, 1.3 µM BSA, 5% DMSO; MG reagent: 1 volume of 4.2% ammonium molybdate in 4M HCl, 3 volumes of 0.045% MG carbinol dye in water, 0.01% Tween 20.

Although a greater variability than desirable was observed also for the data derived from the polyP degradation assay, in the latter instance a clear decrease of the signal with time was observed (Figure A4 11). However, further to the requirement of significant

optimisation, the assay was judged not adequate for hit validation, in view of the limited screening window provided. According to the obtained data (Figure A4 11), the estimated linear range of the polyP degradation reaction extended for only 0.2 Abs units. Indeed, starting from a signal of 1.9 Abs units, derived from the hydrolysis of the initial concentration of $polyP_{25}$ (1.5 μM), an apparent plateau was reached after about 25 minutes, to which a signal of about 1.65 Abs units corresponded. It was anticipated that this limited window would most likely make particular difficult a sensible detection of the *Ft*PPK inhibition.

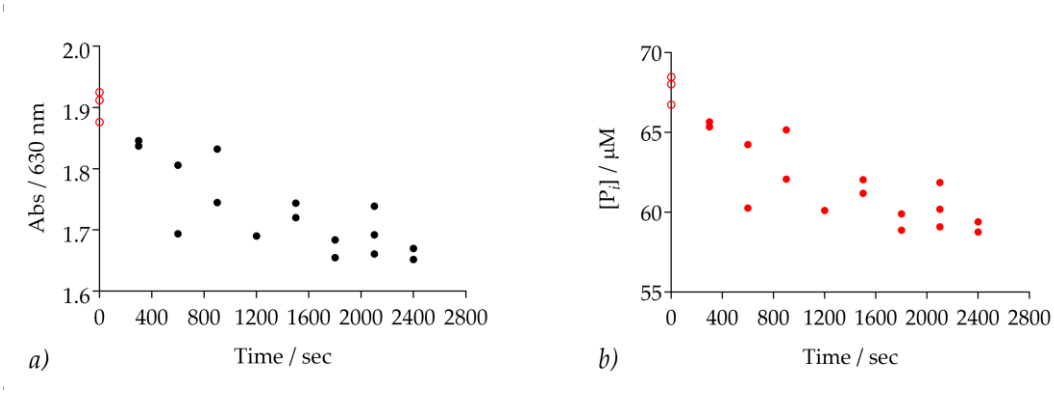

Figure A4 11: *Ft*PPK-*Bp*PPX-MG coupled assay, discontinuous format, polyP degradation

a) Absorbance with time; *b*) P_i with time. *Ft*PPK was removed by precipitation and centrifugation before addition of *Bp*PPX. Assay conditions: 10 nM *Ft*PPK, 1.5 μM polyP, 200 μM ADP, 800 nM *Bp*PPX, 1.3 μM BSA, 5% DMSO; MG reagent: 1 volume of 4.2% ammonium molybdate in 4M HCl, 3 volumes of 0.045% MG carbinol dye in water, 0.01% Tween 20.

A4 3. HPLC based *Ft*PPK assay

A4 3.1. DMHA method optimisation and compatibility with *Ft*PPK assay quenching methods

The starting point for the HPLC assay development was the DMHA method adopted from L. Batten work,[264] in which the nucleotides were eluted applying the following program: 0 min 25% B, 5 min 25% B, 22 min 55% B, 27 min 55% B, 28 min 100% B (DMHA method 1, mobile phase composition reported in section 4.2.3.1.1). The retention time and the peak shape of AMP, ADP and ATP were investigated in water and later in assay buffer. The method allowed a good resolution of the adenosine nucleotides monophosphate, diphosphate and triphosphate prepared in water (Figure A4 12*a*).

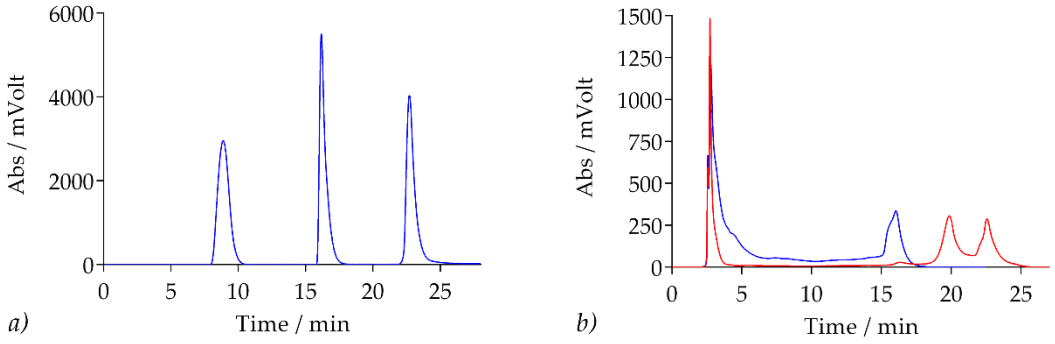

Figure A4 12: Nucleotides analysis by HPLC (RP IP chromatography)

HPLC UV-vis traces measured at 260 nm *a*) Nucleotides analysis (1 mM, prepared in water). Retention time: 8-10 min AMP; 16-18 min ADP; 22-25 min ATP. *b*) Analysis of ADP and ATP (500 µM) prepared in assay buffer and in the presence of 1 M formic acid. Retention time: 15-18 min ADP (blue trace), 18.5 – 25 min ATP (double peak, red trace). Mobile phase A: 15 mM DMHA, 5% MeOH, pH 7; Mobile phase B: 15 mM DMHA, 80% MeOH, pH 7. The DMHA method 1 (Experimental, Table 7.53) was applied.

The nucleotide resolution was then investigated in the assay buffer and in the presence of formic acid (1 M), which was considered as a quenching agent for the *Ft*PPK assay. The nucleotide separation strongly deteriorated with a double peak observed for ATP and, as a consequence, a poor resolution from ADP (Figure A4 12*b*). Furthermore, a big injection peak appeared in the chromatogram while the ADP and ATP (500 µM) peaks were considerably small. The "injection peak" was hypothesized to arise from the formic acid with the retention of the nucleotides, due to the shift of the equilibrium towards the protonated form. Consequently, only a low fraction of nucleotides was retained in the column in complex

with the DMHA, which would also justify the small peaks. The first step towards the improvement of the HPLC method was the investigation of an alternative elution gradient to increase the retention of the ATP without greatly extend the overall length of the method. The isocratic elution at 55% B from minute 22 to minute 27 (DMHA method 1) was replaced with an extension of the gradient to 27 min at 65% B (DMHA method 2) and 60% B (DMHA method 3). An increased retention of the ATP was observed when the DMHA method 3 was applied (Figure A4 13).

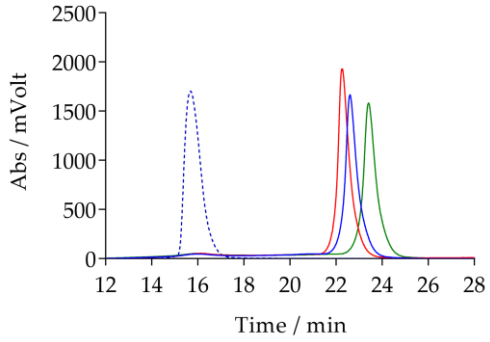

Figure A4 13: Nucleotides analysis by HPLC, method optimisation

Optimisation of the DMHA method to delay the ATP elution (500 µM, prepared in water) by the extending the gradient of solvent B: method 1, 22 min 55% B (blue), method 2, 27 min 65% B (red); method 3, 27 min 60% B (green). Mobile phase A: 15 mM DMHA, 5% MeOH, pH 7; Mobile phase B: 15 mM DMHA, 80% MeOH, pH 7.

The DMHA method 3 was then tested for the analysis of ADP and ATP in assay buffer and the effect of formic acid (1 M), heat treatment (95°C, 5 min) and EDTA (50 mM), the possible assay quenching methods, on the retention time and peak shape was investigated. Applying the DMHA method 3, a satisfactory resolution of ADP and ATP was achieved (Figure A4 14). No significant effect on the nucleotide retention was observed upon heat treatment or in the presence of EDTA (Figure A4 14*a* and *c*). The previously detected decrease of the peak area, in parallel to the appearance of a big injection peak, was confirmed in presence of formic acid (Figure A4 14*b*).

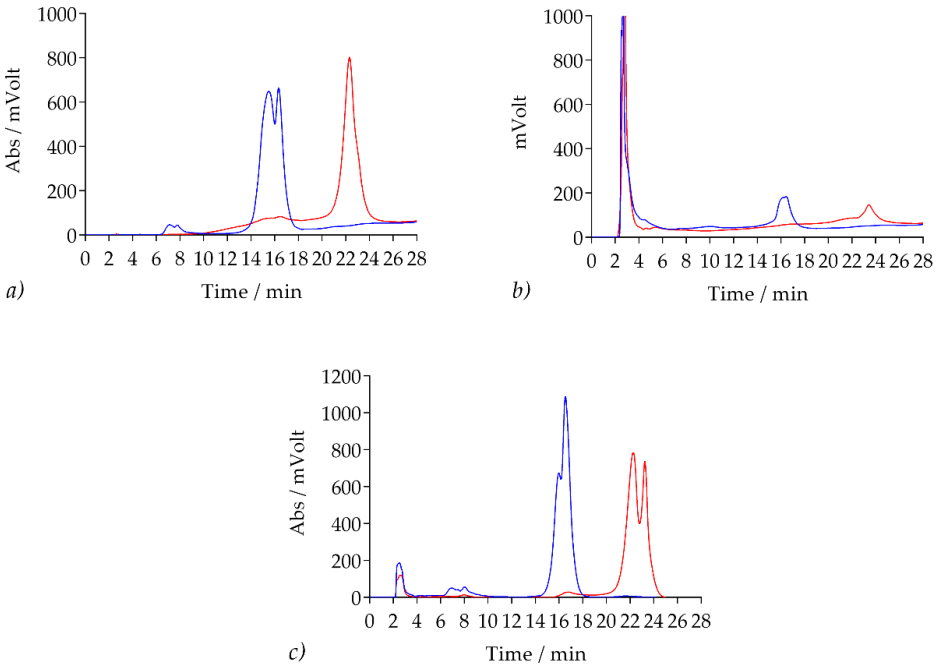

Figure A4 14: Nucleotides analysis by HPLC, quenching methods

HPLC traces showing the effect of different quenching methods on the retention of ADP (blue) and ATP (red, 500 µM) prepared in buffer: *a*) quenching by heat, *b*) quenching by formic acid (1 M), *c*) quenching by EDTA (50 mM). HPLC analysis method: DMHA method 3 (Experimental, Table 7.53).

By comparison of ADP prepared in water and in buffer, it was confirmed that the widening and the splitting of the elution peaks was caused by the assay buffer (Figure A4 15*a*).[gg] It was hypothesized that the high content of salt in the assay buffer might favour the formation of different salt-nucleotide-DMHA complex with a slightly different retention time. The hypothesis was supported by the sharpening of the elution peaks observed by reduction of the NaCl content from 300 mM to 25 mM (Figure A4 15*b*). Both the heat step and the addition of EDTA proved to be compatible with the nucleotides analysis and their effectiveness in quenching the *Ft*PPK assay was tested by preparing a time course (section 4.2.3.1.1).

[gg] At the time of this experiment, the *Ft*PPK buffer composition included 300 mM NaCl, which was later reduced to 25 mM NaCl (section 2.2.2.3 and A2 6).

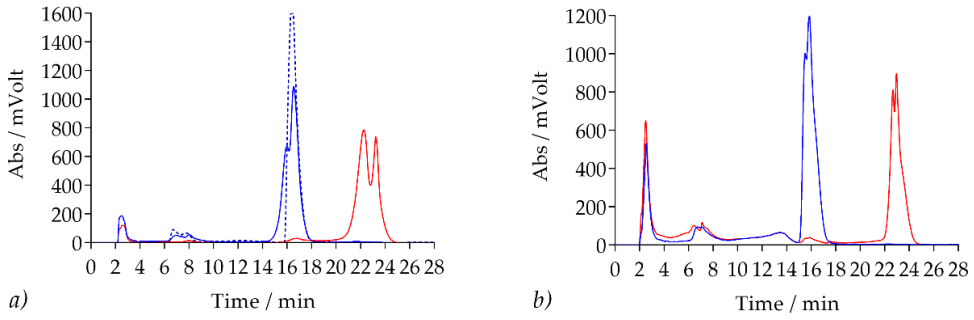

Figure A4 15: Nucleotides analysis by HPLC, effect of NaCl

Comparison of the HPLC traces of nucleotides analysis in buffer containing 300 mM and 25 mM NaCl. *a*) 300 mM NaCl: ADP (blue) and ATP (red) prepared in buffer in the presence of EDTA, ADP (blue dashed line) prepared in water in the presence of EDTA; *b*) 25 mM NaCl: ADP (blue) and ATP (red) prepared in buffer in the presence of EDTA. HPLC analysis method: DMHA method 3 (Experimental, Table 7.53).

A4 3.2. TEAA method development

To improve the analysis of nucleotides in *Ft*PPK assay buffer, an IP RP HPLC method in which the TEA was used as ion pairing agent was optimised. The aqueous and the organic mobile phase were supplemented with 0.1 M TEAA. Both acetonitrile (ACN) and methanol (MeOH) were investigated as organic component of the mobile phase.

A4 3.2.1. TEAA method development: water/acetonitrile system

For the investigation of a water/ACN system the following mobile phases were used. Mobile phases A: 0.1 M TEAA, water; mobile phases B: 0.1 M TEAA, 50% water/50% ACN, pH 7. The first elution program investigated consisted of an isocratic elution at 10%B followed by a gradient to 60% B, which resulted into the immediate elution of the unresolved mixture ADP/ATP (Figure A4 16*a*). Next, the effect of a 5 minutes isocratic at 0% B and 5% B to 20% B and 15% B respectively over 20 minutes was investigated (Figure A4 16*a*). The best ADP/ATP resolution in conjunction with a convenient elution time was obtained when applying a 5 minutes isocratic at 5% B and a gradient to 15% B (Figure A4 16*a*). After investigating slight variations of the gradient (Figure A4 16*b* and *c*), the best method for

ADP/ATP resolution which allowed to maintain the length of the method under 30 minutes was: 5 min 5% B, 20 min 10% B.

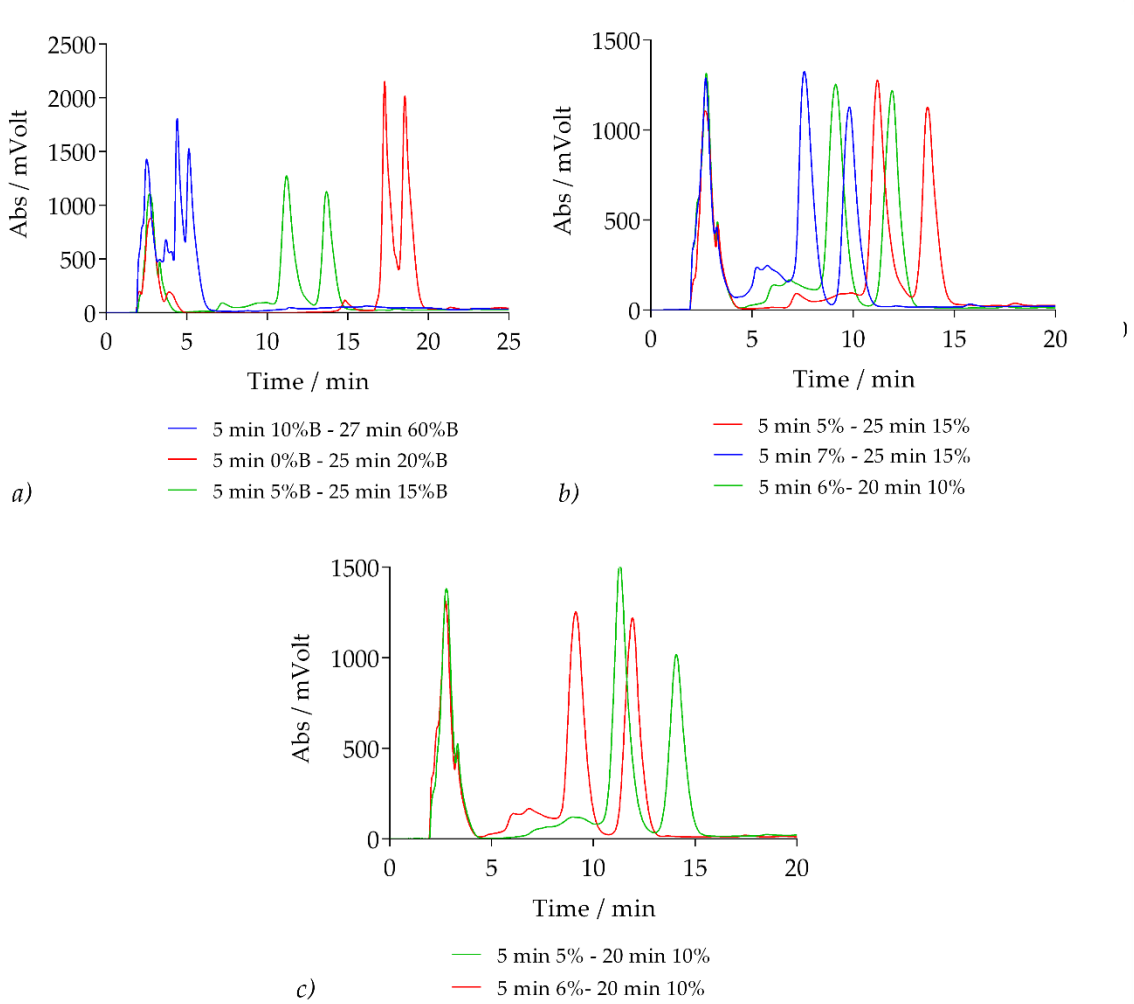

Figure A4 16: TEAA method, water/acetonitrile mobile phase

Mobile phase A: 0.1 M TEAA, water, pH 7; mobile phase B: 0.1 M TEAA, 50% ACN in water, pH 7. The first peak eluting was ADP, the second was ATP. The best method for ADP/ATP resolution was 5 min 5% B, 20 min 10% B (figure c).

A4 3.2.2. TEAA method development: water/methanol system

For the investigation of a water/methanol system the same percentage of organic component as for the water/acetonitrile system (50%) was used for the mobile phase B, of which the composition was: 0.1 M TEAA, 50% MeOH in water, pH 7. Isocratic elution and gradient elution methods were investigated (Figure A4 17). The best ADP/ATP resolution was

obtained when an isocratic at 10% B was applied (Figure A4 17*b*). However the ADP/ATP resolution was comparable to that observed when the best water/acetonitrile system was applied (Figure A4 16*c*).

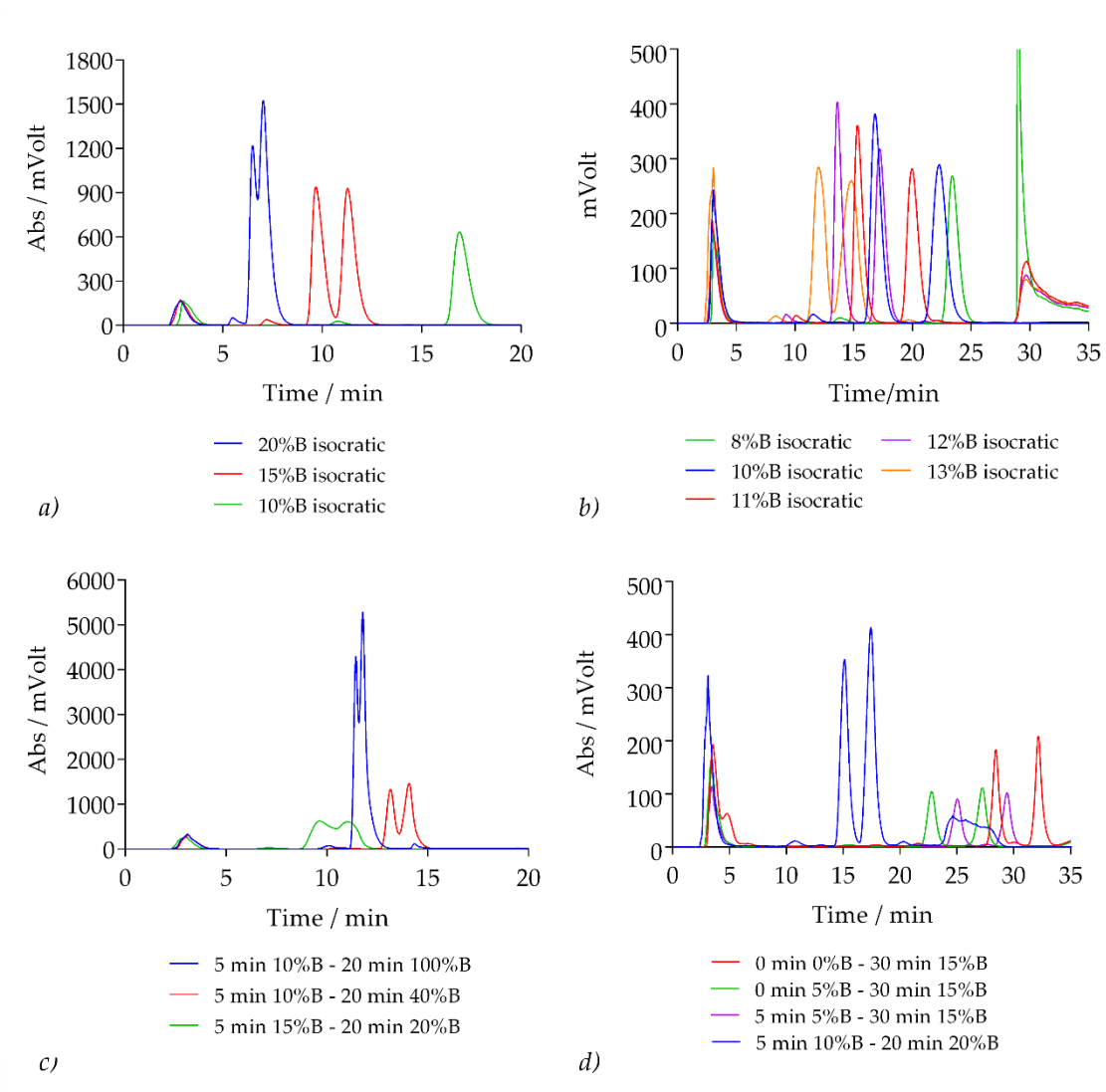

Figure A4 17: TEAA method, water/50% methanol mobile phase

a and *b*: isocratic elutions; *c* and *d*: gradient elutions. Mobile phase A: 0.1 M TEAA, water, pH 7; mobile phase B: 0.1 M TEAA, 50% MeOH in water, pH 7. The first peak eluting was ADP, the second peak was ATP. The best method for ADP/ATP resolution was 10%B isocratic (figure b).

With the purpose of further improving the separation of ADP and ATP, the percentage of methanol in the mobile phase B was increased to 80% and isocratic elution and gradient elution methods were investigated (Figure A4 18). A good ADP/ATP resolution was obtained when isocratic elution at 5% B followed by a step gradient to 10% B was applied In particular, the best method was: 26 min 5% B, 27 min 10% B (Figure A4 18*e*).

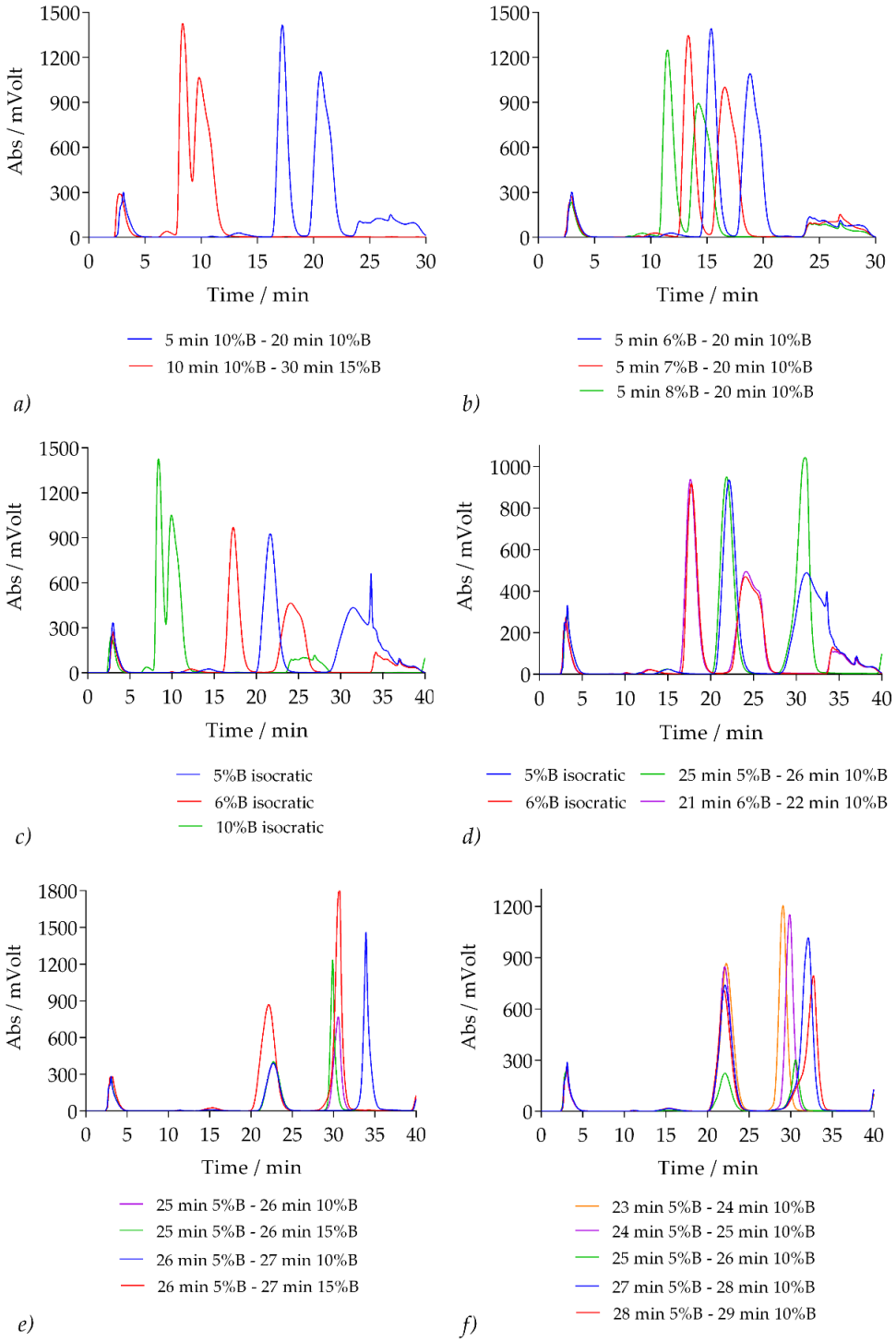

Figure A4 18: TEAA method, water/80% methanol mobile phase

Mobile phase A: 0.1 M TEAA, water, pH 7; mobile phase B: 0.1 M TEAA, 80% MeOH in water, pH 7. The first peak eluting was ADP, the second peak was ATP. The best method for ADP/ATP resolution was: 26 min 5% B, 27 min 10% B (figure *e*).

This method was validated with the measurement of ADP/ATP standard curves (Figure A4 19*a*). The appearance of shoulders was observed at higher concentrations of ATP,

possibly due to the ATP elution starting already at 5% B. The anticipation or the delay of the step gradient to 10% B was investigated (Figure A4 18*f*) and the isocratic elution at 5%B for 24 minutes followed by step increase to 10% B at 25 minutes was chosen as standard, given that no shoulder were observed for the ATP peak (Figure A4 19*f*).

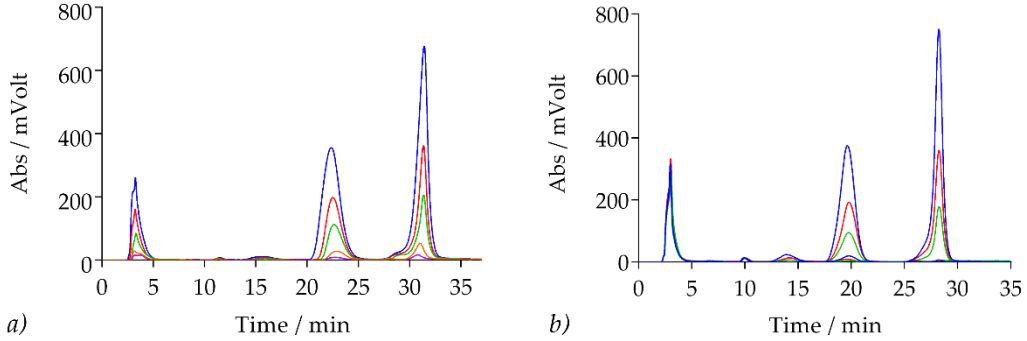

Figure A4 19: TEAA method, water/80% methanol mobile phase, standard curves

ADP/ATP standards analysed by the TEAA/80%MeOH method applying the following gradients: *a*) 26 min 5% B, 27 min 10% B; *b*) 24 min 5% B, 25 min 10% B.

A4 3.2.3. TEAA method optimisation: summary

To summarise, the best ADP/ATP resolution was achieved applying the following methods: water/acetonitrile system, isocratic elution at 5% B for 5 min followed by a gradient to 10% B over 15 min; water/methanol system, isocratic elution at 5% B for 24 min followed by a step gradient to 10% B over 1 min and isocratic elution at 10% B over 10 minutes. A considerable improvement of the chromatogram with a baseline resolution of the nucleotides and elution as single sharp peaks was observed applying both TEAA systems. The background signal was strongly reduced, particularly for the water/methanol system, allowing a more reliable estimation of low concentration of ATP. Furthermore, a better control over the reproducibility of the chromatogram was observed, possibly due to the buffering power of TEAA, which allowed a better stability of the pH. Both methods provided a good resolution of AMP, ADP and ATP (Figure A4 20). The advantage of a quicker analysis (method length: 37 minutes, Figure A4 20*a*) was provided by the water/acetonitrile system. The water methanol system on the other hand allowed a better

resolution of ADP and ATP although to the detriment of the analysis length (method length: 53 minutes, Figure A4 20*b*). In anticipation of possible variation of the nucleotides retention time, due to subtle variation of the buffer preparation, it was decided to adopt the TEAA/MeOH method as standard for the development of an HPLC-based format for hit validation. Furthermore, given the composition of the Reynolds library (nucleotide analogues) the better resolution between the ADP and the ATP obtained with the TEAA/MeOH method appeared to reduce the chances of co-elution with ADP and ATP of hit molecules with possible similar properties of polarity.

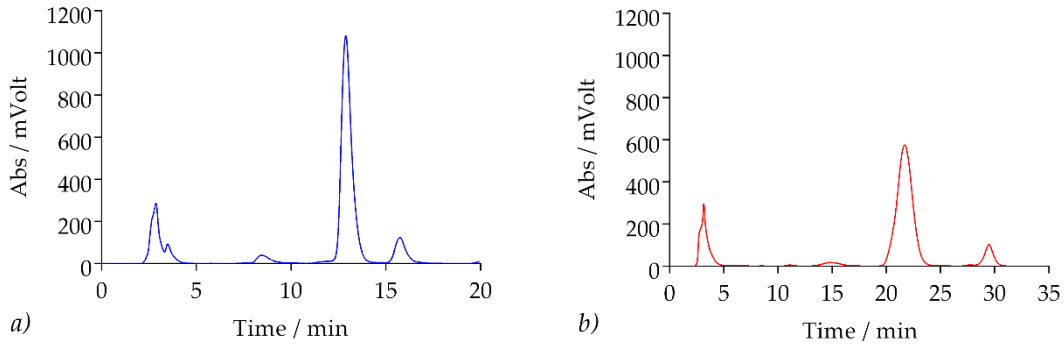

Figure A4 20: TEAA based RP IP, comparison between acetonitrile and methanol system

*Ft*PPK assay (200 μM ADP, 1.5 μM polyP$_{25}$) quenched by EDTA (180 sec) and analysed by the TEAA method: *a*) water/acetonitrile system, mobile phase A: 0.1M TEAA, water pH 7, mobile phase B: 0.1M TEAA, 50% acetonitrile in water, pH 7; method: 0 min 5% B, 5 min 5% B, 20 min 10% B; ADP retention time: 12-14 min; ATP retention time: 15-17 min; *b*) water/methanol system, mobile phase A: 0.1M TEAA, water pH 7; mobile phase B: 0.1 M TEAA, 80% methanol in water, pH 7; method: 0 min 5% B, 24 min 5% B, 25 min 10%, 35 min 10% B; ADP retention time: 19-24 min; ATP retention time: 28-31 min.

A4 4. Hit validation: data summary

Table A4 1: PKIS library hits validation

Ranked (by Z_R)	Plate position	Z_R-score	Coupled assay NPI_R	FLuc assay NPI^*	Thermal shift assay	HPLC assay
1	JO7-54	-7.5 ± 0.3	85.2 ± 3.9	59.3 ± 12.1	-0.11 ± 0.2	-7 ± 2.6
2	JO8-26	-7 ± 0.1	90.9 ± 1.4	34.7 ± 0.9	-0.59 ± 0.1	-8.4 ± 1.9
3	JOL-53	-6.7 ± 0.2	110.9 ± 2.9	97.7 ± 0.06	0.015 ± 0.07	-3.7 ± 0.1
4	JOL-65	-6.6 ± 0.4	108.3 ± 6.6	96.8 ± 0.02	-0.23 ± 0.09	14.6 ± 3.4
5	JOL-9	-6.5 ± 0.06	107.4 ± 1	n/a	-0.27 ± 0.13	-0.5 ± 6.3
6	JOM-14	-6.5 ± 0.2	97.2 ± 3.1	84.8 ± 0.08	-0.44 ± 0.19	-8.5 ± 0.2
7	JO7-15	-6.4 ± 0.8	73.2 ± 9.6	93 ± 0.3	-0.28 ± 0.34	-3.8 ± 2.7
8	JON-66	-6 ± 0.3	74.6 ± 4.5	66.1 ± 3.8	-0.10 ± 0.21	5.2 ± 13.3
9	JO7-78	-5.8 ± 0.9	66.2 ± 9.9	63.8 ± 1.8	-0.01 ± 0.08	-7.8 ± 15.7
10	JO8-3	-5.7 ± 0.23	73.6 ± 4.5	50.6 ± 1.4	0.51 ± 0.13	18.4 ± 10.9
11	JOL-1	-5.2 ± 0.2	86 ± 2.9	62.2 ± 1.2	-0.15 ± 0.26	4.5 ± 0.05
12	JOM-20	-5.2 ± 0.3	78.2 ± 4.2	70.5 ± 0.5	-0.34 ± 0.18	-15.8 ± 0.5
13	JOL-26	-5.2 ± 0.3	85.1 ± 5.6	65.7 ± 1.2	0.03 ± 0.18	-7 ± 0.9
14	JON-11	-4.7 ± 0.1	86.7 ± 1.8	73.2 ± 3.2	-0.00 ± 0.17	-25.3 ± 6.8
15	JOL-29	-4.6 ± 0.2	76.1 ± 2.2	66.7 ± 2	-0.31 ± 0.26	-1.7 ± 15.9
16	JO7-52	-4.5 ± 0.5	50.8 ± 5.6	35.6 ± 0.8	0.035 ± 0.15	-3.43 ± 6.1
17	JON-16	-3.8 ± 0.7	48.4 ± 9.1	51.6 ± 1.5	-0.17 ± 0.22	-20.6 ± 3.5
18	JOM-69	-3.7 ± 0.7	55.4 ± 11	25.6 ± 7.3	-0.20 ± 0.39	43.3 ± 7.2
19	JO8-12	-3.7 ± 0.4	46.6 ± 5.2	41.2 ± 0.2	-0.65 ± 0.18	-21 ± 23.3
20	JO7-38	-3.4 ± 0.6	39.3 ± 7.1	24.8 ± 0.4	-0.28 ± 0.35	-10.9 ±-0.01
21	JOM-68	-3.4 ± 0.6	51.3 ± 9.5	49.9 ± 0.5	-0.79 ± 0.17	-8.2 ± 9.6
22	JOL-30	-3.1 ± 0.7	51.1 ± 11.4	38.9 ± 1.5	-0.74 ± 0.3	-14.8 ± 23.4
23	JOM-8	-3.4 ± 0.4	51 ± 6	46.2 ± 2	-0.11 ± 0.64	-5.4 ± 10.9
24	JO8-19	-3.4 ± 0.7	42.7 ± 9.2	16.1 ± 2.1	-0.41 ± 0.53	12.4 ± 1.2
25	JO8-13	-3.1 ± 0.5	38.6 ± 7.3	35.6 ± 0.7	-0.07 ± 0.37	3.8 ± 3.7
26	JON-68	-3 ± 1	37.2 ± 12.2	55.6 ± 0.8	-0.18 ± 0.2	-7.8 ± 1.5
27	JO7-7	-3 ± 1.5	33.8 ± 17.8	22.1 ± 2.8	-0.14 ± 0.32	10.9 ± 9.3
28	JOM-74	-2.8 ± 0.7	41.9 ± 10.3	38.3 ± 6.6	-0.26 ± 0.22	8.8 ± 6.6
29	JOL-20	-2.8 ± 0.4	45.8 ± 6.1	35.3 ± 2.8	-0.26 ± 0.18	9.8 ± 2.5
30	JON-27	-2.8 ± 0.4	40.7 ± 6.7	58.2 ± 1.9	-0.35 ± 0.16	-38.5 ± 0.8
31	JOM-5	-2.7 ± 1.4	40.24 ± 21.4	48.3 ± 2.5	-0.25 ± 0.2	6.3 ± 9.7
Selected only NPI_R						
32	JOL-69	-2.6 ± 0.5	43.7 ± 8.9	44.6 ± 2.1	-0.5 ± 0.15	6.7 ± 7.1
33	JO8-15	-2.6 ± 0.1	32.1 ± 1.64	24.2 ± 0.9	-0.47 ± 0.14	10.3 ± 0.07
34	JOL-39	-2.5 ± 0.4	40.4 ± 6.5	42.7 ± 3.6	-1.93 ± 0.22	13.7 ± 12.2
35	JOM-43	-2.3 ± 0.2	34.8 ± 3.3	47.9 ± 0.5	n/a	10 ± 3.3
36	JOM-55	-2.3 ± 0.2	34.6 ± 3.3	13 ± 4.2	-1.05 ± 0.14	-35.5 ± 16.5
37	JO8-31	-2.3 ± 0.3	27.8 ± 4.5	0.2 ± 2.3	n/a	6.9 ± 4
38	JO8-8	-2.2 ± 0.5	27.7 ± 7.2	22.1 ± 4.9	n/a	12.4 ± 10.1
39	JO7-20	-2.2 ± 0.4	25.3 ± 4.7	-7.1 ± 3.9	n/a	-0.8 ±1.3
40	JO7-4	-2 ± 1.3	22.9 ±14.5	2.7 ± 11.1	n/a	17.6 ± 2

Table A4 2: Reynolds library hits validation

Ranked	Plate position	Z_R-*score*	Coupled assay NPI_R	FLuc assay *NPI*	Thermal shift assay	HPLC assay
1	RL1-PLT1	-18.4 ± 0.2	92.2 ± 1.1	85.7 ± 0.5	-0.14 ± 0.21	-16.3 ± 0.5
2	RL54-PLT9	-11.2 ± 0.2	67.4 ± 1.4	60.3 ± 0.7	-0.05 ± 0.15	10.3 ± 12.5
3	RL38-PLT5	-11.1± 0.2	72.6 ± 1.22	69.9 ± 0.5	-0.4 ± 0.12	5.2 ± 0.6
4	RL71-PLT7	-10 ± 0.3	60 ± 1.6	50.2 ± 1.2	-0.47 ± 0.4	-12.2 ± 0.01
5	RL37-PLT7	-9.1 ± 0.1	68 ± 0.6	63.8 ± 0.9	0.70 ± 0.3	-12.3 ± 3.4
6	RL80-PLT7	-8.8 ± 0.6	53 ± 3.5	47.4 ± 2.4	-10.5 ± 2.09	-8.6 ± 14.9
7	RL41-PLT7	-8.7 ± 0.1	71.9 ± 0.5	69.5 ± 1.1	0.02 ± 0.2	4 ± 1.6
8	RL69-PLT7	-8.3 ± 0.7	50 ± 5.1	47.3 ± 1.5	-28.8 ± 10	-15.3 ± 20.4
9	RL54-PLT8	-7 ± 0.2	74.3 ± 2.7	75.2 ± 1.1	-0.05 ± 0.46	-6.34 ± 0.6
10	RL20-PLT2	-6.2 ± 0.7	50.8 ± 6.1	-4.9 ± 1.6	0.30 ± 0.42	-2.6 ± 4.1
11	RL21-PLT7	-5.9 ± 0.4	44.5 ± 3	46.7 ± 0.7	-9.5 ± 0.24	5 ± 13.5
12	RL60-PLT7	-5.8 ± 0.8	48.2 ± 6.3	42.8 ± 1.5	1.22 ± 0.4	-13.8 ± 1.2
13	RL41-PLT8	-5.6 ± 0.1	97.2 ± 1.2	92.5 ± 0.1	-17.2 ± 0.3	8.1 ± 1.1
14	RL13-PLT8	-4.9 ± 0.4	51.2 ± 4.3	51 ± 4.6	-2.6 ± 0.3	-0.5 ± 0.7
15	RL19-PLT8	-4.7 ± 0.3	44 ± 2.7	42.7 ± 1.3	-0.02 ± 0.12	-13.5 ± 10.5
16	RL24-PLT8	-4.2 ± 0.1	72.7 ± 1.5	71.9 ± 0.6	-0.4 ± 0.32	9.1 ± 5.3
17	RL40-PLT9	-3.4 ± 0.2	62.3 ± 3	59.1 ± 1.3	-1.6 ± 0.2	7.1 ± 6.7
18	RL10-PLT8	-3.2 ± 0.3	30.6 ± 2.8	32.1 ± 0.3	-0.79 ± 0.3	0.6 ± 8.9
19	RL48-PLT6	-3.2 ± 1.6	20.4 ± 10.2	-4.3 ± 2.6	-1.37 ± 0.2	-21.9 ± 24.4
20	RL42-PLT9	-3.1 ± 0.3	45.3 ± 3.8	10.1 ± 1.6	-0.2 ± 0.28	29.1 ± 1.7
21	RL18-PLT2	-3.1 ± 0.04	18.6 ± 0.2**	5.2 ± 2.4	-3.2 ± 0.3	8.1 ± 9.5
22	RL48-PLT7	-3.1 ± 1.1	23.3 ± 8.6	29 ± 0.5	-0.56 ± 0.3	6.7 ± 4.7
23	RL13-PLT5	-3 ± 0.9	19.8 ± 5.6	-6.8 ± 3.3	-0.23 ± 0.36	5 ± 7.6
24	RL54-PLT2	-2.8 ± 0.9	14.3 ± 4.5**	27 ± 3.3	-0.56 ± 0.28	0.6 ± 8.4
25	RL46-PLT6	-2.5 ± 1.2	15.9 ± 7.9	5.3 ± 1.9	-0.20 ± 0.27	0.2 ±7.7
26	RL2-PLT1	-2.4 ± 1.2	12.1 ± 5.9**	-1.9 ± 3.4	-0.25 ± 0.32	-10 ± 2.1
Selected only by NPI						
27	RL4-PLT8	-2.4 ± 0.6	22.5 ± 5.6	27.2 ± 1.5	-0.5 5± 0.23	-5.3 ± 10.9
28	RL22-PLT8	-2.4 ± 0.6	25.2 ± 6.7	26.3 ± 0.9	n/a	14.5 ± 5.3
29	RL65-PLT8	-2.3 ± 0.5	41 ± 8.4	-4.2 ± 1.8	-5.58 ± 0.28	-14.2 ± 3.6
30	RL47-PLT6	-2.3 ± 1.4	15.2 ± 9	6.1 ± 4.5	-0.27 ± 0.16	7.9 ± 7.3
31	RL65-PLT2	-2.3 ± 0.4	18.7 ± 3.3	2.3 ± 2.2	-0.61 ± 0.16	-7.3 ± 16.8
32	RL47-PLT1	-2.2 ± 0.9	18.2 ± 7.7	22.1 ± 2.4	-0.28 ± 0.18	4 ± 9.9
33	RL11-PLT8	-2.2 ± 1.	20.5 ± 9.7	-7.2 ± 1.4	-0.05 ± 0.33	-12.1 ± 1.9

**selected by Z_R-*score* only

Appendix to Chapter 5

A5 1. Mode of binding investigation

A5 1.1. IC_{50} measurement: the significance of the Hill coefficient and the relationship between IC_{50} and K_i.

The Hill coefficient is a parameter linked to the stoichiometry of the inhibitor-enzyme binding interaction and can therefore provide interesting insight into the mechanism of binding[272,374,552] For a 1:1 inhibitor:enzyme stoichiometry, the Hill coefficient is usually close to 1. Hill coefficients greater than 1 may suggest binding to multiple sites with positive cooperativity (e.g. within oligomeric enzymes), tight binding or irreversible binding.[374] On the other hand, an Hill coefficient much smaller than 1 may indicate binding to more than one non-equivalent binding site.[374] Anomalous behaviour of the inhibitor may also lead to Hill coefficient much greater or smaller than 1, in the first case due to unspecific binding (e.g. due to promiscuous inhibitor or denaturing agents), in the second case due to compound aggregation or issues of solubility.[374]

The IC_{50} value provides only a relative estimation of an inhibitor potency, nonetheless it is frequently used to rank inhibitors, especially when dealing with a high number of hits derived from screening campaigns or to assess and compare the effect of medicinal chemistry optimisation. This approach can be justified, given the relation between IC_{50} and K_i defined by the Cheng-Prusoff equations (Eq. A5 1, Eq. A5 2, Eq. A5 3).[272,446,553]

$$K_i = \frac{IC_{50}}{1 + \frac{[S]}{K_m}}$$

Eq. A5 1: IC_{50} – K_i relationsh

ip for competitive inhibitors

K_i is the inhibitor dissociation constant, IC_{50} is the concentration of inhibitor at which 50% inhibition is observed, S is the concentration of substrate, K_m is the concentration of substrate at which ½ V_{max} is reached.

$$K_i = \frac{IC_{50}}{1 + \frac{K_m}{[S]}}$$

Eq. A5 2: IC_{50} – K_i relationship for uncompetitive inhibitors

K_i is the inhibitor dissociation constant, IC_{50} is the concentration of inhibitor at which 50% inhibition is observed, S is the concentration of substrate, K_m is the concentration of substrate at which ½ V_{max} is reached.

$$IC_{50} = \frac{[S] + K_m}{\frac{K_m}{K_i} + \frac{[S]}{\alpha K_i}}$$

Eq. A5 3: IC_{50} – K_i relationship for non-competitive inhibitors

K_i is the inhibitor dissociation constant, IC_{50} is the concentration of inhibitor at which 50% inhibition is observed, S is the concentration of substrate, K_m is the concentration of substrate at which ½ V_{max} is reached, α is a constant which describes how the affinity of the substrate for the enzyme is affected by the inhibitor.

According to these equations, the relation between IC_{50} and K_i is determined by the substrate concentration and by the mode of action and requires the knowledge of the K_m for the substrate (Table 5.1).

A5 1.2. Graphical analysis of Lineweaver-Burk and Dixon plots K_i and mode of inhibition determination

The inhibitor modality can be determined from experiments where the apparent initial rate (v_0^{app}) is measured at varying concentrations of substrate (usually 0.2 K_m to 5 K_m) and at varying concentrations of inhibitor. By plotting the obtained data in a double reciprocal plot of $1/v_0^{app}$ against 1/[S] (Lineweaver - Burk plots), it is possible to identify the inhibitor modality based on the pattern of the straight lines obtained at each concentration of inhibitor (Figure A5 1).[272,554] Within the Lineweaver - Burk plots, the slope represents the ratio K_m/V_{max}, the intercept to the y axis is equal to $1/V_{max}$, and the intercept to the x axis is equal to the K_m.[272] In accordance with the effect on K_m and V_{max}, for competitive inhibitors, the lines intercept the y axis on the same point (no changes in V_{max}^{app}) while the slope varies with the inhibitor concentration (increase of K_m^{app}, Figure A5 1*a*). Lines intercepting the y axis at different points and with a variation in slope (corresponding to

decrease in $V_{\max}^{app}$ while K_{m}^{app} remains unchanged) indicates non-competitive modality (Figure A5 1*b*). Uncompetitive modality is instead identified by parallel lines that intercept the y axis at different points (decrease of $V_{\max}^{app}$ and K_{m}^{app} and consequent constant slope, Figure A5 1*c*).

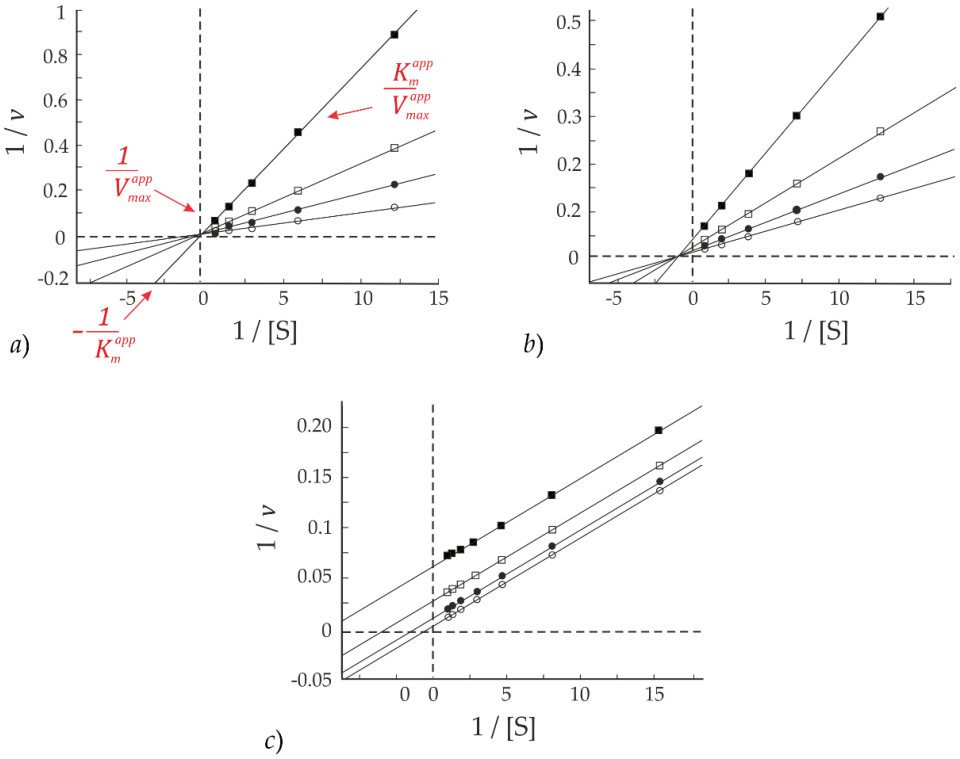

Figure A5 1: Mechanism of action determination by Lineweaver-Burk plots

Black squares: high inhibitor concentration [I]; clear squares: medium [I]; black circles: low [I]; clear circles: no inhibitor. *a*) Competitive inhibitor mode: $1/V_{max}$ intercepts the y axis at the same point (equal V_{max} at different [I]), variable K_m/V_{max} (different K_m at different [I]); *b*) noncompetitive inhibitor mode: $1/V_{max}$ intercepts the y axis at the different points (different V_{max} at different [I]), variable K_m/V_{max} (different K_m at different [I]); c) uncompetitive inhibitor mode: $1/V_{max}$ intercepts the y axis at the different points (different V_{max} at different [I]), same K_m/V_{max} (same K_m at different [I]). The intercept of the line to the x axis corresponds to K_m. Figure adapted from Copeland.[374]

By rearrangement of the same data, where the reciprocal of the rate ($1/v_0^{app}$), measured at a fixed concentration of substrate, is plotted against varying concentration of inhibitors, the Dixon plots can be generated, which provide an alternative way of estimating the K_i, which is defined by the point of convergence of the generated lines (Figure A5 2).

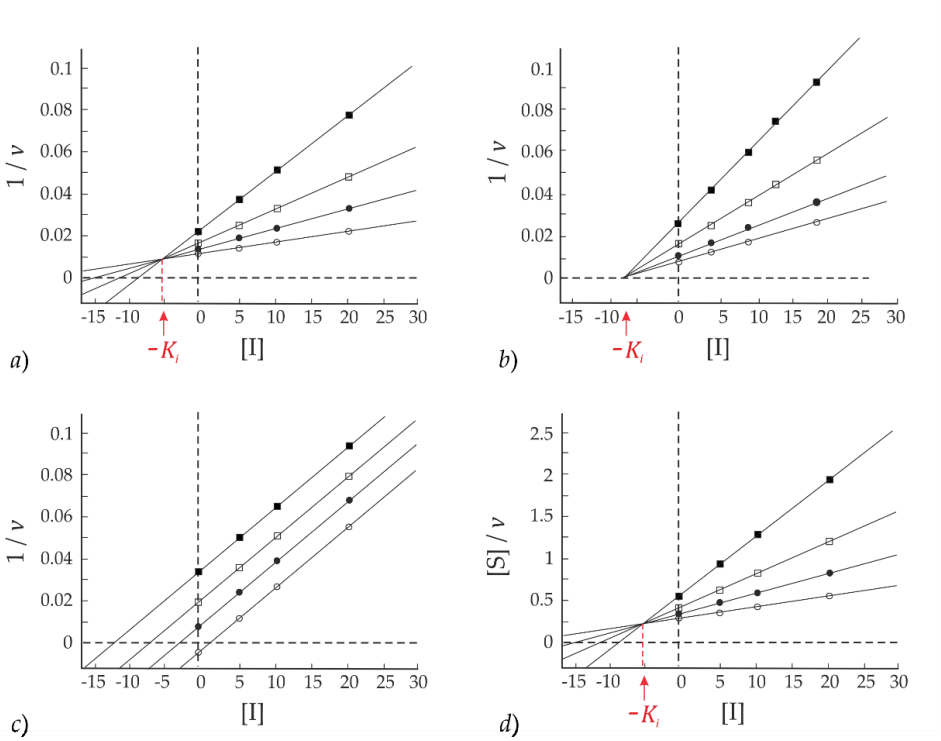

Figure A5 2: K_i determination by Dixon plots and Cornish-Bowden

Black squares: low substrate concentration [S]; clear squares and black circles: intermediate [S]; clear circles: high [S]. *a*) Dixon plot, competitive inhibitor; *b*) Dixon plot, non-competitive inhibitor; *c*) Dixon plot, uncompetitive inhibitor; *d*) Cornish-Bowden plot, uncompetitive inhibitor. The point of convergence of the lines graphically defines the K_i.

While for competitive and non-competitive inhibitors (where $1/v_0^{app} = 1/V_{max}$ and $1/v_0^{app} = 0$, respectively) a convergence of the lines is observed (Figure A5 2*a* and *b*), for uncompetitive inhibitors parallel lines are obtained, preventing the graphical determination of K_i (Figure A5 2*c*). In this case, it is convenient to re-plot the data as $[S]/v$ against inhibitor concentration (Cornish-Bowden plot),[555] which transforms the parallel lines in convergent lines, of which the point of interception correspond to the K_i (Figure A5 2*d*).

A5 1.3. Binding affinity studies by biophysical methods

Biophysical methods constitute a valid tool to characterise binding interactions, and are increasingly finding application within drug discovery campaigns.[81,556] In particular, ITC, NMR and SPR have been applied for both screening and hit validation, offering the advantage of allowing detection of weak inhibitors (e.g. fragments).[524–526,556–560] The other

advantage provided by these techniques is the possibility to characterise the binding in terms of binding affinity, described either by the affinity constant K_a or by the dissociation constant K_d ($K_d = 1/K_a$).[556] Furthermore, in some cases (e.g. ITC and SPR) a thermodynamic profile can also be derived, permitting characterisation the binding with respect to enthalpy (ΔH) and entropy (ΔS).[520,521] The latter constitutes an important resource, since a connection between affinity and selectivity of binding and increase/decrease of the enthalpy and entropy has been identified.[520,561]

Isothermal Titration Calorimetry (ITC) is widely regarded as the "gold standard" for observing the thermodynamic signature of binding based on the detection of heat released or taken up upon ligand binding to the target.[562,563]

The ITC provides a thermodynamic characterisation of the binding event by direct measurement of Gibbs energy (and therefore K_a), enthalpy and entropy (which are linked by Eq. A5 4) and information on the stoichiometry of binding (n).

$$\Delta G = \Delta H - T\Delta S = - RT\ln(K_a)$$

Eq. A5 4: Relation between $\Delta G_{binding}$ and K_a

ΔG is the Gibbs energy of binding, ΔH is the enthalpy of binding, ΔS is the entropy of binding, T is the temperature, R is the gas constant, K_a is the binding affinity.

ITC experimental protocol consists in the ligand titration into a target solution by multiple injections of a constant volume. For each injection the heat of binding is measured, which decreases with the increase of the number of injections, in correspondence to the target saturation. Under optimal conditions of ligand and protein concentration, the variation of the heat released per injection plotted against the ratio ligand/target, fit a sigmoidal curve from which K_a, ΔH and the stoichiometry can be derived. As opposed to the determination of the potency by biochemical assays, which is significantly affected by the condition applied, investigation of binding by ITC (and in general of biophysical methods) provides an absolute measurement of an inhibitor potency, hence it should be applied in conjunction with the other MOA studies for inhibitor characterization.

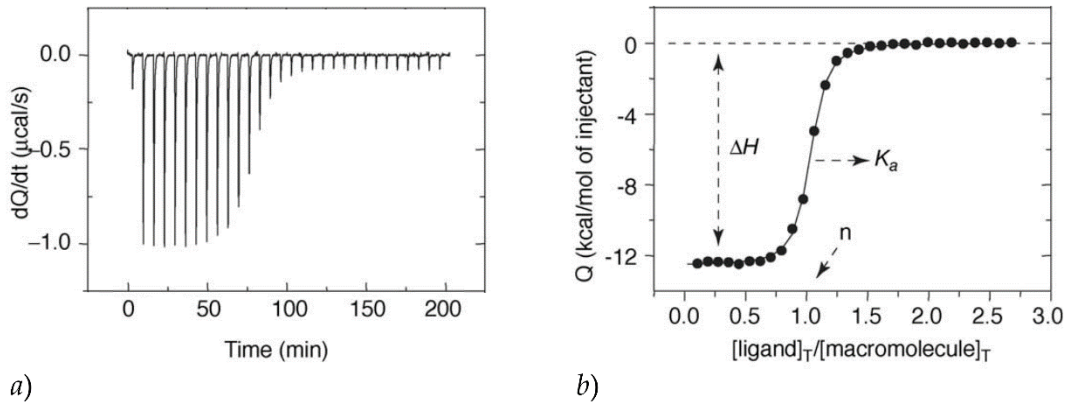

Figure A5 3: Binding studies by ITC

a) ITC data generated by ligand titration into the target solution. *b*) ITC data derived from the integration of the injection peaks, plotted against the ratio of ligand/target. Figure adapted from Freire.[561]

A5 1.3.1. Binding affinity investigation by ITC

In addition to the biochemical characterization, the determination of the binding affinity of compound RL42-Plt9 with respect to the *Ft*PPK was attempted by ITC. Although Tris buffer has been used for *Ft*PPK storage and activity assays, for ITC the *Ft*PPK was transferred in HEPES buffer, to prevent possible interference due high enthalpy of ionization of Tris. To avoid buffer mismatches due to the presence of DMSO (5%) in the RL42-Plt9 solution, the same amount of DMSO was included also in the *Ft*PPK solution. The binding of RL42-Plt9 was investigated starting from a ten-fold excess of inhibitor (200 µM) in comparison to the *Ft*PPK solution (20 µM). After a number of 10 injection, a severe deterioration of the signal was observed, due to precipitation of the ligand in the cell, as confirmed by the cloudiness of the solution removed from the cell. To circumvent the issues of RL42-Plt9 solubility (precipitation above 400 µM in solution containing 5% DMSO), an inverse titration was attempted, in which the *Ft*PPK (200 µM) was injected into the ligand solution (20 µM). Once again, deterioration of the injection signal was observed due to precipitation, this time most probably of the *Ft*PPK.

A5 2. Structural investigation of the complex *Ft*PPK-Rl42-Plt9

A5 2.1. Strategies for protein crystallisation and co-crystallisation studies

Structural information on the binding of an inhibitor to the active site constitutes a valuable tool to complement a biochemically derived model of the mechanism of action. The access to structural information enables the improvement of the binding affinity by rational design of additional favourable interactions with the target. Hence, co-crystallization studies of the inhibitor with the target are usually undertaken in parallel to MOA studies.

The crystallization process consists in the transition from the soluble phase to a highly ordered solid state, driven by the change of protein solubility in the presence of precipitating agents (salts, polymers or organic solvents).[564,565] The phase transition is a function of the protein and precipitant concentration and is affected by multiple factors such as purity and homogeneity of the protein sample and by temperature, pH and possible additives. [564–566] Crystal growth entails three stages: nucleation, growth and growth arrest. The nucleation process consists in the formation of small clusters of protein, on which surface ordered apposition of macromolecule leads to crystal growth. The depletion of protein from the solution eventually causes arrest of the growth. The phase diagram illustrates the relation between the different stages of crystal growth and the concentration of protein and precipitant while other variables are held constant.[567] For crystallization to occur, the protein solution must reach the supersaturated state (protein concentration beyond the limit of solubility) from which three possible scenarios can derive based on the degree of supersaturation.[564] Rapid formation of an amorphous precipitate occurs when a high degree of supersaturation is reached (precipitation zone). When the combination of protein concentration and precipitant concentration results in a degree of supersaturation corresponding to the stable zone, the system has enough energy to allow nucleation and crystal growth. Instead, within the metastable zone, the energy of the system is not sufficient to promote nucleation but only crystal growth can take place.

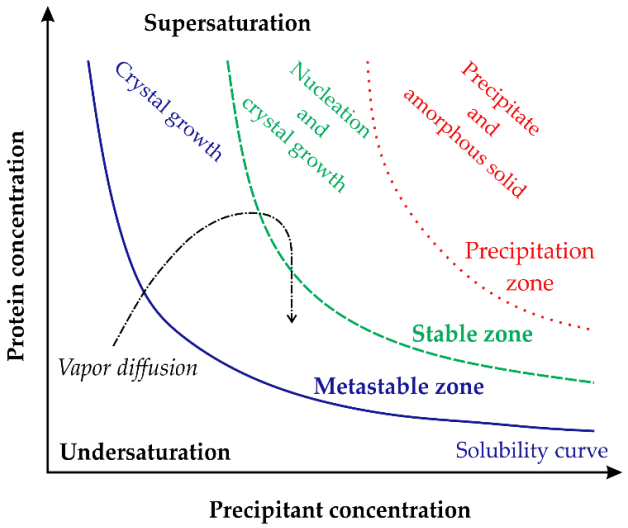

Figure A5 4: Crystallisation phase diagram

The solubility curve defines the threshold of solubility beyond which the solution is supersaturated. Based on the degree of supersaturation, three zones were identified in which crystal growth (metastable zone), nucleation and growth (stable zone) and precipitation (precipitation zone) occur. The ideal phase transition during crystallisation by vapour diffusion is traced by the black discontinuous arrow: the increase of protein and precipitant concentration due to the drop shrinking brings the system to the stable zone allowing nucleation. The consequent protein depletion shift the system to the metastable zone in which growth around the existing nuclei occurs. Adapted from Asherie N.[567]

Various crystallisation methods have been developed in which the protein solution, in the presence of a precipitant solution, is brought to the supersaturation state.[565,566] Vapour diffusion is the most commonly used method, in which the supersaturation state is achieved by concentration of a protein-precipitant solution by evaporation. The protein solution, at a concentration close to the solubility limit, is diluted with the precipitant solution (usually in a 1:1 ratio) and is equilibrated in a close system with the same precipitant solution, of which the concentration is just below what required to cause protein precipitation. Transfer of vapour from the protein-precipitant solution (drop) to the precipitant solution (reservoir) occurs until equilibrium is reached between the respective vapour pressures. The consequent drop shrinking leads to the increase of the precipitant and protein concentration promoting nucleation and crystal growth (stable zone). The depletion of the protein due to nucleation and crystal growth causes the transition to the metastable zone in which no further nucleation but only enlargement of the existing crystals occurs. This ideal behaviour is not always observed and often the system is highly supersaturated, although still within the

stable zone. In this case the formation of many nuclei with consequent protein depletion results in many small crystals, while ideally few but bigger crystals are desirable. To address this problem, the seeding technique can be used, where a crystal fragment or a small crystal is placed in the protein-precipitant drop under conditions that, following equilibration, bring the system to the metastable zone.[565] Crystal growth by apposition to the seed leads to the formation of big crystals while no more nucleation occurs. Two different set up can be used for vapour diffusion crystallisation: the hanging drop and the sitting drop system (Figure A5 5).[565]

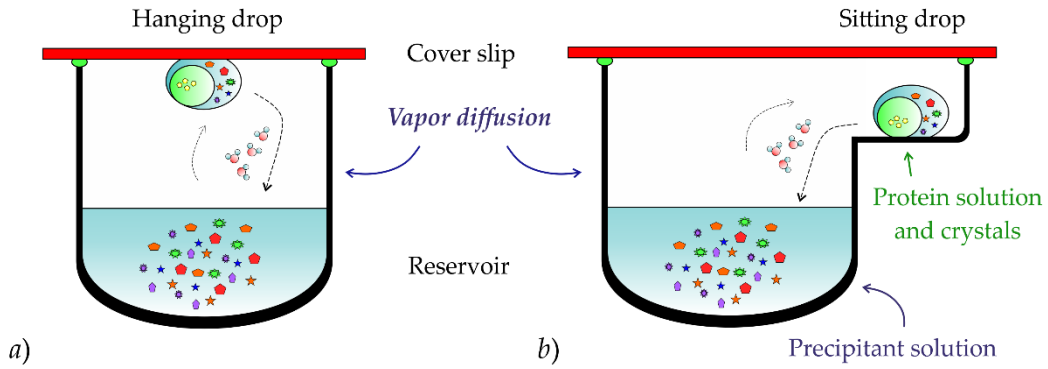

Figure A5 5: Crystallisation by vapour diffusion

a) Hanging drop method; *b*) sitting drop method. Evaporation of water from the drop to the precipitant solution, driven by equilibration of the respective vapour pressure, causes shrinking of the drop. The consequent concentration of protein and precipitant bring the system to supersaturation allowing crystal growth.

In the first case, a drop of protein-precipitant is set up on a cover slip which is then placed on top of the reservoir filled with corresponding precipitant solution. For the sitting drop method, the drop is set up on a side chamber communicating with the reservoir containing the precipitant solution. Practical aspects usually dictate the choice of one or the other method. The sitting drop method is preferred when plates are prepared by means of crystallography robots, particularly useful when many conditions are investigated and drops of a small size are set up. On the other hand, the hanging drop method is usually adopted for manual set up and offers the advantage of an easier fishing of the crystals, which gather in proximity of the drop surface due to gravity.

A5 2.2. Identification of a *Ft*PPK:RL42-Plt9 complex crystal form by screening

Co-crystallization studies of compound RL42-Plt9 with the *Ft*PPK were undertaken in parallel to the biochemical characterization of the mechanism of action. To identify a crystal form of the *Ft*PPK: RL42-Plt9 complex, the conditions provided by the screens JCSG-*plus*™ (sparse matrix), PACT *premier*™ (systematic) and Morpheus® (containing low molecular weight ligand) were investigated.

Table A5 1: Screens condition yielding crystal forms

Screen	Well position	Condition
with polyP$_{25}$		
JCSG-*plus*	A1	0.1 M Sodium acetate (pH 4.5), 0.2 M Li_2SO_4; 50% w/v PEG 400
	A6	0.1 M Phosphate/citrate (pH 4.2), 0.2 M Li_2SO_4, 20% w/v PEG 1000
	F8	2.1 M DL-Malic acid (pH 7)
	F9	2.4 M Sodium malonate dibasic monohydrate (pH 7)
	F10	0.1 M HEPES, 1.1 M Sodium malonate dibasic monohydrate (pH 7), 0.5% v/v Jeffamine® ED-2003
	G12	0.1 M BIS-Tris (pH 5.5), 3 M NaCl
PACT *premier*	A8	0.1 M Sodium acetate (pH 5), 0.2 M NH_4Cl; 20% w/v PEG 6000
	H12	0.1 M Bis-Tris propane (pH 8.5), 0.2 M Sodium malonate dibasic monohydrate tartrate; 20% w/v PEG 3350
Morpheus	C10	0.1 M Tris base, BICINE (pH 8.5); 0.09 NPS*; 50% v/v precipitant mix (40% v/v Ethylene glycol, 20% w/v PEG 8000)
without polyP$_{25}$		
PACT *premier*	F9	0.1 M Bis-Tris propane (pH 6.5), 0.2 M Potassium sodium tartrate tetrahydrate; 20% w/v PEG 3350
	H9	0.1 M Bis-Tris propane (pH 8.5), 0.2 M Potassium sodium tartrate tetrahydrate; 20% w/v PEG 3350
Morpheus	A3	0.1 M Imidazole, MES monohydrate acid (pH 6.5); 0.03 M $MgCl_2{\cdot}6H_2O$, 0.03 M $CaCl_2{\cdot}2H_2O$; 50% v/v precipitant mix (40% v/v Glycerol, 20% w/v PEG 4000)
	F3	0.1 M Imidazole, MES monohydrate acid (pH 6.5); 0.02 M D-Glucose, 0.02 M D-Mannose, 0.02 M D-Galactose, 0.02 M L-Fucose, 0.02 M D-Xylose, 0.02 M N-Acetyl-D-Glucosamine; 50% v/v precipitant mix (40% v/v Glycerol, 20% w/v PEG 4000)

*0.09 M NPS: 0.03 M $NaNO_3$, 0.03 M Na_2HPO_4, 0.03 M $(NH_4)_2SO_4$

The information derived by biochemical studies on the mechanism of action were not available at the time when the co-crystallization experiments were undertaken. On the assumption that compound RL42-Plt9 was competitive with ADP and that $polyP_{25}$ was required for the ADP binding, the three screens were tested for co-crystallization of the *Ft*PPK:RL42-Plt9 complex in the absence and in the presence of $polyP_{25}$, in the latter case applying a 1:1 ratio of polyP:inhibitor. The vapour diffusion method in sitting drops was used for the screens. *Ft*PPK solutions (10 mg/mL) containing a final concentration of 500 μM RL42-Plt9 (5% DMSO) were prepared, with and without $polyP_{25}$ (500 μM). The crystallography plates (96 wells) were set up by means of the automated robot, which enabled the preparation of 0.2-0.3 μL size drops, in 1:2, 1:1 and 2:1 ratio of protein:precipitant, equilibrated with a 40 μL reservoir. Some conditions yielding initial crystal forms, both in the presence and in the absence of $polyP_{25}$, were identified (Table A5 1). Only crystals from the conditions PACT-A8, PACT-B7, JCSG-A6, JCSG-F8, JCSG-F9, JCSG-F10 and Morpheus-C10, grown in the presence of $polyP_{25}$, could be harvested and were tested on the beamline IO2 of the Diamond Light Source synchrotron. All the crystals were confirmed to be protein, although the diffraction was poor (above 3.5 Å). The only exception were the crystals from condition JCSG-F8 (2.1 M DL-Malic acid, pH 7) which diffracted at 2-2.5 Å. However, due to the morphology of two double plates superimposed, the corresponding double diffraction pattern acquired could not be processed.

A5 2.3. Optimisation of the identified *Ft*PPK:RL42-Plt9 crystal form

The crystal forms obtained from the screens by co-crystallization of *Ft*PPK with RL42-Plt9 in the absence of $polyP_{25}$ (needles and small prisms with common nucleation point) were judged more difficult to optimize in comparison to other crystal forms obtained by co-crystallization in the presence of $polyP_{25}$. In view of this fact and because of the initial assumption that $polyP_{25}$ was required for binding, the crystallization conditions in the absence of $polyP_{25}$ were discarded while the optimisation of crystal forms obtained in the presence of $polyP_{25}$ was attempted. The reproducibility of the crystal form and the optimisation of the conditions JCSG-A1, JCSG-A6 and PACT-A8 were investigated in 96 wells plate by sitting drops (1 or 1.5 μL, in 1:2, 1:1, 2:1 ratio protein:precipitant),

equilibrated against 50 μL precipitant in the reservoir. Probably due to the different ratio between the drop size and the precipitant volume in the reservoir, it was not possible to reproduce the crystal forms. Condition JCSG-A1 was also tested by hanging drop in 24 well plate (drop size: 3 and 2 μL, 1:2, 1:1 and 2:1 protein:precipitant ratio), equilibrated against 500 μL reservoir. No protein crystallization was observed but salt crystallized in negative control drops (only precipitant). Optimisation of the conditions JCSG-F8, JCSG-F9, JCSG-F10 and Morpheus-C10 was also attempted by hanging drop crystallization in 24 well plate. Only very small and not reproducible crystals were obtained from condition JCSG-F8. The optimisation of JCSG-F9 and JCSG-F10 resulted in the identification of an improved condition (0.1M HEPES, 1.4 M sodium malonate dibasic monohydrate, 0.5% Jeffamine, pH 8.5), which yielded the formation of small cubic crystals requiring further optimisation. Crystal growth was consistently observed from condition Morpheus-C10. The latter was further optimised by investigation of various concentration of salt (NPS: nitrate, phosphate, sulfate) and precipitant (40% v/v Ethylene glycol, 20% w/v PEG 8000). The best condition identified was: 0.1 M Tris base, BICINE, 0.15 M NPS, 40% precipitant mix, pH 8.5 (condition Morpheus_C10a). However, the obtained crystals did not diffracted below 3.5 Å and further optimisation of the crystal form was carried out. Drop size and ratio protein:precipitant were investigated, as well as the effect of each component of the NPS salt mixture. The optimal drop size was 3 μL in a 1:1 ratio of protein:precipitant (1.5 μL + 1.5 μL) and the phosphate salt was identified essential for crystallization, while precipitation occurred in the presence of either nitrate or sulfate. The best crystals were obtained under the condition 0.1 M Tris base, BICINE, 0.05 M Sodium phosphate dibasic, 45% precipitant mix, pH 8.5 (condition M_C10b). The optimisation of the conditions led to the formation of fewer, bigger and ticker plates with a more regular shape, quite often clustered with a common nucleation axis, despite extending on different planes. Once again, the obtained crystals did not diffracted below 3.5 Å. Due to time constraint, it was not possible to attempt growth by seeding or to investigate alternative crystallization conditions, including soaking of the ligand into the protein or co-crystallization in the absence of $polyP_{25}$.

References

(1) Piddock, L. J. (2012) The crisis of no new antibiotics—what is the way forward? *Lancet Infect. Dis. 12*, 249–253.

(2) World Health Organization (Ed.). (2015) Global action plan on antimicrobial resistance.

(3) Bush, K., Courvalin, P., Dantas, G., Davies, J., Eisenstein, B., Huovinen, P., Jacoby, G. A., Kishony, R., Kreiswirth, B. N., Kutter, E., Lerner, S. A., Levy, S., Lewis, K., Lomovskaya, O., Miller, J. H., Mobashery, S., Piddock, L. J. V., Projan, S., Thomas, C. M., Tomasz, A., Tulkens, P. M., Walsh, T. R., Watson, J. D., Witkowski, J., Witte, W., Wright, G., Yeh, P., and Zgurskaya, H. I. (2011) Tackling antibiotic resistance. *Nat. Rev. Microbiol. 9*, 894–896.

(4) Levy, S. B., and Marshall, B. (2004) Antibacterial resistance worldwide: causes, challenges and responses. *Nat. Med. 10*, S122–S129.

(5) Falagas, M. E., and Bliziotis, I. A. (2007) Pandrug-resistant Gram-negative bacteria: the dawn of the post-antibiotic era? *Int. J. Antimicrob. Agents 29*, 630–636.

(6) Falagas, M. E., Bliziotis, I. A., Kasiakou, S. K., Samonis, G., Athanassopoulou, P., and Michalopoulos, A. (2005) Outcome of infections due to pandrug-resistant (PDR) Gram-negative bacteria. *BMC Infect. Dis. 5*, 24.

(7) Davies, J., and Davies, D. (2010) Origins and Evolution of Antibiotic Resistance. *Microbiol. Mol. Biol. Rev. 74*, 417–433.

(8) Laxminarayan, R., Duse, A., Wattal, C., Zaidi, A. K. M., Wertheim, H. F. L., Sumpradit, N., Vlieghe, E., Hara, G. L., Gould, I. M., Goossens, H., Greko, C., So, A. D., Bigdeli, M., Tomson, G., Woodhouse, W., Ombaka, E., Peralta, A. Q., Qamar, F. N., Mir, F., Kariuki, S., Bhutta, Z. A., Coates, A., Bergstrom, R., Wright, G. D., Brown, E. D., and Cars, O. (2013) Antibiotic resistance—the need for global solutions. *Lancet Infect. Dis. 13*, 1057–1098.

(9) Giske, C. G., Monnet, D. L., Cars, O., and Carmeli, Y. (2008) Clinical and Economic Impact of Common Multidrug-Resistant Gram-Negative Bacilli. *Antimicrob. Agents Chemother. 52*, 813–821.

(10) Brown, E. D., and Wright, G. D. (2016) Antibacterial drug discovery in the resistance era. *Nature 529*, 336–343.

(11) D'Costa, V. M., King, C. E., Kalan, L., Morar, M., Sung, W. W. L., Schwarz, C., Froese, D., Zazula, G., Calmels, F., Debruyne, R., Golding, G. B., Poinar, H. N., and Wright, G. D. (2011) Antibiotic resistance is ancient. *Nature 477*, 457–461.

(12) Rodríguez-Rojas, A., Rodríguez-Beltrán, J., Couce, A., and Blázquez, J. (2013) Antibiotics and antibiotic resistance: a bitter fight against evolution. *Int. J. Med. Microbiol. 303*, 293–7.

(13) Laxminarayan, R., and Heymann, D. (2012) Challenges of drug resistance in the

developing world. *BMJ 344*, e1567.

(14) Hughes, D. (2003) Microbial genetics: Exploiting genomics, genetics and chemistry to combat antibiotic resistance. *Nat. Rev. Genet. 4*, 432–441.

(15) Boucher, H. W., Talbot, G. H., Bradley, J. S., Edwards, J. E., Gilbert, D., Rice, L. B., Scheld, M., Spellberg, B., and Bartlett, J. (2009) Bad Bugs, No Drugs: No ESKAPE! An Update from the Infectious Diseases Society of America. *Clin. Infect. Dis. 48*, 1–12.

(16) Boucher, H. W., Talbot, G. H., Benjamin, D. K., Bradley, J., Guidos, R. J., Jones, R. N., Murray, B. E., Bonomo, R. A., and Gilbert, D. (2013) 10 x '20 Progress--Development of New Drugs Active Against Gram-Negative Bacilli: An Update From the Infectious Diseases Society of America. *Clin. Infect. Dis. 56*, 1685–1694.

(17) Payne, D. J., Gwynn, M. N., Holmes, D. J., and Pompliano, D. L. (2007) Drugs for bad bugs: confronting the challenges of antibacterial discovery. *Nat. Rev. Drug Discov. 6*, 29–40.

(18) Tommasi, R., Brown, D. G., Walkup, G. K., Manchester, J. I., and Miller, A. A. (2015) ESKAPEing the labyrinth of antibacterial discovery. *Nat. Rev. Drug Discov. 14*, 529–542.

(19) Payne, D. J., Gwynn, M. N., Holmes, D. J., and Pompliano, D. L. (2007) Drugs for bad bugs: confronting the challenges of antibacterial discovery. *Nat. Rev. Drug Discov. 6*, 29–40.

(20) Lewis, K. (2017, June 15) New approaches to antimicrobial discovery. *Biochem. Pharmacol.* Elsevier Inc.

(21) Woodford, N., and Livermore, D. M. (2009) Infections caused by Gram-positive bacteria: a review of the global challenge. *J. Infect. 59*, S4–S16.

(22) Thomson, J. M., and Bonomo, R. A. (2005) The threat of antibiotic resistance in Gram-negative pathogenic bacteria: β-lactams in peril! *Curr. Opin. Microbiol. 8*, 518–524.

(23) Rennie, R. P. (2012) Current and future challenges in the development of antimicrobial agents. *Handb. Exp. Pharmacol.* 45–65.

(24) Jain, A., and Mondal, R. (2008) Extensively drug-resistant tuberculosis: current challenges and threats. *FEMS Immunol. Med. Microbiol. 53*, 145–150.

(25) Dorman, S. E., and Chaisson, R. E. (2007) From magic bullets back to the Magic Mountain: the rise of extensively drug-resistant tuberculosis. *Nat. Med. 13*, 295–298.

(26) Swinney, D. C., and Anthony, J. (2011) How were new medicines discovered? *Nat. Rev. Drug Discov. 10*, 507–19.

(27) Projan, S. J. (2003) Why is big Pharma getting out of antibacterial drug discovery? *Curr. Opin. Microbiol. 6*, 427–430.

(28) Chellat, M. F., Raguž, L., and Riedl, R. (2016) Targeting Antibiotic Resistance. *Angew. Chemie Int. Ed. 55*, 6600–26.

(29) Gwynn, M. N., Portnoy, A., Rittenhouse, S. F., and Payne, D. J. (2010) Challenges of antibacterial discovery revisited. *Ann. N. Y. Acad. Sci. 1213*, 5–19.

(30) Lewis, K. (2013) Platforms for antibiotic discovery. *Nat. Rev. Drug Discov. 12*, 371–387.

(31) Pankey, G. A., and Sabath, L. D. (2004) Clinical Relevance of Bacteriostatic versus Bactericidal Mechanisms of Action in the Treatment of Gram-Positive Bacterial Infections. *Clin. Infect. Dis. 38*, 864–870.

(32) Kohanski, M. A., Dwyer, D. J., and Collins, J. J. (2010) How antibiotics kill bacteria: from targets to networks. *Nat. Rev. Microbiol. 8*, 423–35.

(33) Kotra, L. P., Haddad, J., and Mobashery, S. (2000) Aminoglycosides: Perspectives on mechanisms of action and resistance and strategies to counter resistance. *Antimicrob. Agents Chemother. 44*, 3249–3256.

(34) Davis, B. D., Chen, L. L., and Tai, P. C. (1986) Misread protein creates membrane channels: an essential step in the bactericidal action of aminoglycosides. *Proc. Natl. Acad. Sci. U. S. A. 83*, 6164–8.

(35) Courvalin, P. (2006) Vancomycin Resistance in Gram-Positive Cocci. *Clin. Infect. Dis. 42*, S25–S34.

(36) Tran, T. T., Munita, J. M., and Arias, C. A. (2015) Mechanisms of drug resistance: daptomycin resistance. *Ann. N. Y. Acad. Sci. 1354*, 32–53.

(37) Falagas, M. E., Rafailidis, P. I., and Matthaiou, D. K. (2010) Resistance to polymyxins: Mechanisms, frequency and treatment options. *Drug Resist. Updat. 13*, 132–138.

(38) Huovinen, P. (2001) Resistance to trimethoprim-sulfamethoxazole. *Clin. Infect. Dis. 32*, 1608–14.

(39) Connell, S. R., Tracz, D. M., Nierhaus, K. H., and Taylor, D. E. (2003) Ribosomal Protection Proteins and Their Mechanism of Tetracycline Resistance. *Antimicrob. Agents Chemother. 47*, 3675–3681.

(40) Chopra, I., and Roberts, M. (2001) Tetracycline antibiotics: mode of action, applications, molecular biology, and epidemiology of bacterial resistance. *Microbiol. Mol. Biol. Rev. 65*, 232–60 ; second page, table of contents.

(41) Garneau-Tsodikova, S., and Labby, K. J. (2016) Mechanisms of resistance to aminoglycoside antibiotics: overview and perspectives. *Med. Chem. Commun. 7*, 11–27.

(42) Leclercq, R. (2002) Mechanisms of resistance to macrolides and lincosamides: nature of the resistance elements and their clinical implications. *Clin. Infect. Dis. 34*, 482–92.

(43) Long, K. S., and Vester, B. (2012) Resistance to Linezolid Caused by Modifications at Its Binding Site on the Ribosome. *Antimicrob. Agents Chemother. 56*, 603–612.

(44) Schwarz, S., Kehrenberg, C., Doublet, B., and Cloeckaert, A. (2004) Molecular basis of bacterial resistance to chloramphenicol and florfenicol. *FEMS Microbiol. Rev. 28*, 519–542.

(45) Mast, Y., and Wohlleben, W. (2014) Streptogramins – Two are better than one! *Int. J. Med. Microbiol. 304*, 44–50.

(46) Jacoby, G. A. (2005) Mechanisms of resistance to quinolones. *Clin. Infect. Dis. 41*

Suppl 2, S120-6.

(47) Goldstein, B. P. (2014) Resistance to rifampicin: a review. *J. Antibiot. (Tokyo). 67*, 625–30.

(48) Fischbach, M. A., and Walsh, C. T. (2009) Antibiotics for emerging pathogens. *Science 325*, 1089–93.

(49) Andriole, V. T. (2005) The Quinolones: Past, Present, and Future. *Clin. Infect. Dis. 41*, S113–S119.

(50) Fu, L., Liu, X., Ling, C., Cheng, J., Guo, X., He, H., Ding, S., and Yang, Y. (2012) Design, synthesis, and structure–activity relationship studies of conformationally restricted mutilin 14-carbamates. *Bioorg. Med. Chem. Lett. 22*, 814–819.

(51) Wright, G. D. (2011) Molecular mechanisms of antibiotic resistance. *Chem. Commun. 47*, 4055.

(52) Fernández, L., Breidenstein, E. B. M., and Hancock, R. E. W. (2011) Creeping baselines and adaptive resistance to antibiotics. *Drug Resist. Updat. 14*, 1–21.

(53) Silver, L. L. (2011) Challenges of Antibacterial Discovery. *Clin. Microbiol. Rev. 24*, 71–109.

(54) Bapteste, E., and Boucher, Y. (2009) Epistemological Impacts of Horizontal Gene Transfer on Classification in Microbiology, in *Horizontal Gene Transfer: Genomes in Flux* (Gogarten, M. B., Gogarten, J. P., and Olendzenski, L. C., Eds.), pp 55–72. Humana Press, Totowa, NJ.

(55) Kojima, S., and Nikaido, H. (2013) Permeation rates of penicillins indicate that Escherichia coli porins function principally as nonspecific channels. *Proc. Natl. Acad. Sci. 110*, E2629–E2634.

(56) Fernandez, L., and Hancock, R. E. W. (2012) Adaptive and Mutational Resistance: Role of Porins and Efflux Pumps in Drug Resistance. *Clin. Microbiol. Rev. 25*, 661–681.

(57) Lambert, P. A. (2005) Bacterial resistance to antibiotics: modified target sites. *Adv. Drug Deliv. Rev. 57*, 1471–85.

(58) Katayama, Y., Ito, T., and Hiramatsu, K. (2000) A new class of genetic element, staphylococcus cassette chromosome mec, encodes methicillin resistance in Staphylococcus aureus. *Antimicrob. Agents Chemother. 44*, 1549–55.

(59) Long, K. S., Poehlsgaard, J., Kehrenberg, C., Schwarz, S., and Vester, B. (2006) The Cfr rRNA methyltransferase confers resistance to Phenicols, Lincosamides, Oxazolidinones, Pleuromutilins, and Streptogramin A antibiotics. *Antimicrob. Agents Chemother. 50*, 2500–5.

(60) Cattoir, V., and Nordmann, P. (2009) Plasmid-mediated quinolone resistance in gram-negative bacterial species: an update. *Curr. Med. Chem. 16*, 1028–1046.

(61) Beceiro, A., Llobet, E., Aranda, J., Bengoechea, J. A., Doumith, M., Hornsey, M., Dhanji, H., Chart, H., Bou, G., Livermore, D. M., and Woodford, N. (2011) Phosphoethanolamine Modification of Lipid A in Colistin-Resistant Variants of

Acinetobacter baumannii Mediated by the pmrAB Two-Component Regulatory System. *Antimicrob. Agents Chemother. 55*, 3370–3379.

(62) Wright, G. D. (2005, July 29) Bacterial resistance to antibiotics: Enzymatic degradation and modification. *Adv. Drug Deliv. Rev.*

(63) Livermore, D. M. (2008) Defining an extended-spectrum β-lactamase. *Clin. Microbiol. Infect. 14*, 3–10.

(64) Balaban, N. Q., Merrin, J., Chait, R., Kowalik, L., and Leibler, S. (2004) Bacterial persistence as a phenotypic switch. *Science 305*, 1622–5.

(65) Lewis, K. (2007) Persister cells, dormancy and infectious disease. *Nat. Rev. Microbiol. 5*, 48–56.

(66) Maisonneuve, E., Castro-Camargo, M., and Gerdes, K. (2013) (p)ppGpp controls bacterial persistence by stochastic induction of toxin-antitoxin activity. *Cell 154*, 1140–50.

(67) Keren, I., Kaldalu, N., Spoering, A., Wang, Y., and Lewis, K. (2004) Persister cells and tolerance to antimicrobials. *FEMS Microbiol. Lett. 230*, 13–18.

(68) Losick, R., and Desplan, C. (2008) Stochasticity and cell fate. *Science 320*, 65–8.

(69) Veening, J. W., Smits, W. K., and Kuipers, O. P. (2008) Bistability, epigenetics, and bet-hedging in bacteria. *Annu. Rev. Microbiol 62*, 193–210.

(70) Kussell, E., and Leibler, S. (2005) Phenotypic diversity, population growth, and information in fluctuating environments. *Science 309*, 2075–8.

(71) Clatworthy, A. E., Pierson, E., and Hung, D. T. (2007) Targeting virulence: a new paradigm for antimicrobial therapy. *Nat. Chem. Biol. 3*, 541–8.

(72) Joyce, A. R., Reed, J. L., White, A., Edwards, R., Osterman, A., Baba, T., Mori, H., Lesely, S. A., Palsson, B. Ø., and Agarwalla, S. (2006) Experimental and computational assessment of conditionally essential genes in Escherichia coli. *J. Bacteriol. 188*, 8259–71.

(73) Autret, N., and Charbit, A. (2005) Lessons from signature-tagged mutagenesis on the infectious mechanisms of pathogenic bacteria. *FEMS Microbiol. Rev. 29*, 703–717.

(74) Gill, E. E., Franco, O. L., and Hancock, R. E. W. (2015) Antibiotic Adjuvants: Diverse Strategies for Controlling Drug-Resistant Pathogens. *Chem. Biol. Drug Des. 85*, 56–78.

(75) Sintim, H. O., Smith, J. a I., Wang, J., Nakayama, S., and Yan, L. (2010) Paradigm shift in discovering next-generation anti-infective agents: targeting quorum sensing, c-di-GMP signaling and biofilm formation in bacteria with small molecules. *Future Med. Chem. 2*, 1005–1035.

(76) Fox, S., Farr-Jones, S., Sopchak, L., Boggs, A., Nicely, H. W., Khoury, R., and Biros, M. (2006) High-throughput screening: update on practices and success. *J. Biomol. Screen. 11*, 864–869.

(77) Macarron, R., Banks, M. N., Bojanic, D., Burns, D. J., Cirovic, D. A., Garyantes, T., Green, D. V. S., Hertzberg, R. P., Janzen, W. P., Paslay, J. W., Schopfer, U., and Sittampalam, G. S. (2011) Impact of high-throughput screening in biomedical research. *Nat.*

Rev. Drug Discov. 10, 188–195.

(78) Bleicher, K. H., Böhm, H., Müller, K., and Alanine, A. I. (2003) Hit and lead generation: beyond high-throughput screening. *Nat. Rev. Drug Discov. 2*, 369–78.

(79) Gribbon, P., and Sewing, A. (2005) High-throughput drug discovery: what can we expect from HTS? *Drug Discov. Today 10*, 17–22.

(80) Paul, S. M., Mytelka, D. S., Dunwiddie, C. T., Persinger, C. C., Munos, B. H., Lindborg, S. R., and Schacht, A. L. (2010) How to improve R&D productivity: the pharmaceutical industry's grand challenge. *Nat. Rev. Drug Discov. 9*, 203–14.

(81) Mayr, L. M., and Bojanic, D. (2009) Novel trends in high-throughput screening. *Curr. Opin. Pharmacol. 9*, 580–588.

(82) Hughes, J. P., Rees, S., Kalindjian, S. B., and Philpott, K. L. (2011) Principles of early drug. *Br. J. Pharmacol. 162*, 1239–1249.

(83) Yang, Y., Adelstein, S. J., and Kassis, A. I. (2009) Target discovery from data mining approaches. *Drug Discov. Today 14*, 147–154.

(84) Zhang, J.-H., Chung, T. D. Y., and Oldenburg, K. R. (1999) A Simple Statistical Parameter for Use in Evaluation and Validation of High Throughput Screening Assays. *J. Biomol. Screeningreening 4*, 67–73.

(85) Ciulli, A. (2013) Biophysical screening for the discovery of small-molecule ligands. *Methods Mol. Biol. 1008*, 357–388.

(86) Baell, J. B., and Holloway, G. A. (2010) New substructure filters for removal of pan assay interference compounds (PAINS) from screening libraries and for their exclusion in bioassays. *J. Med. Chem. 53*, 2719–40.

(87) Harris, C. J., Hill, R. D., Sheppard, D. W., Slater, M. J., and Stouten, P. F. W. (2011) The design and application of target-focused compound libraries. *Comb. Chem. High Throughput Screen. 14*, 521–31.

(88) Folmer, R. H. A. (2016) Integrating biophysics with HTS-driven drug discovery projects. *Drug Discov. Today 21*, 491–498.

(89) Simon, G. M., Niphakis, M. J., and Cravatt, B. F. (2013) Determining target engagement in living systems. *Nat. Chem. Biol. 9*, 200–205.

(90) Durham, T. B., and Blanco, M. J. (2015) Target engagement in lead generation. *Bioorg. Med. Chem. Lett. 25*, 998–1008.

(91) Danhof, M., de Lange, E. C. M., Della Pasqua, O. E., Ploeger, B. A., and Voskuyl, R. A. (2008) Mechanism-based pharmacokinetic-pharmacodynamic (PK-PD) modeling in translational drug research. *Trends Pharmacol. Sci. 29*, 186–91.

(92) Sierra, H., Cordova, M., Chen, C.-S. J., and Rajadhyaksha, M. (2015) Confocal Imaging–Guided Laser Ablation of Basal Cell Carcinomas: An Ex Vivo Study. *J. Invest. Dermatol. 135*, 612–615.

(93) Singh, S. S. (2006) Preclinical pharmacokinetics: an approach towards safer and

efficacious drugs. *Curr. Drug Metab. 7*, 165–182.

(94) Chung, T. D. Y., Terry, D. B., and Smith, L. H. (2004) In Vitro and In Vivo Assessment of ADME and PK Properties During Lead Selection and Lead Optimization – Guidelines, Benchmarks and Rules of Thumb. *Assay Guid. Man.*

(95) Kornberg, A., Rao, N. N., and Ault-Riché, D. (1999) Inorganic polyphosphate: a molecule of many functions. *Annu. Rev. Biochem. 68*, 89–125.

(96) Kulaev, I. S., Vagabov, V. M., and Kulakovskaya, T. V. (2004) The Biochemistry of Inorganic Polyphosphates (Wiley, Ed.) 2nd ed. John Wiley & Sons, Ltd, Chichester, UK.

(97) Rao, N. N., Gómez-García, M. R., and Kornberg, A. (2009) Inorganic Polyphosphate: Essential for Growth and Survival. *Annu. Rev. Biochem. 78*, 605–647.

(98) Wood, H. G., and Clark, J. E. (1988) Biological Aspects of Inorganic Polyphosphates. *Annu. Rev. Biochem. 57*, 235–260.

(99) Harold, F. M. (1966) Inorganic polyphosphates in biology: structure, metabolism, and function. *Bacteriol. Rev. 30*, 772–94.

(100) Yoshida, A. (1955) Metaphosphate. II. Heat of hydrolysis of metaphosphate extracted from yeast cells. *J. Biochem. 42*, 163–168.

(101) Schmidt, G., Hecht, L., and Thannhauser, S. J. (1946) The enzymatic formation and the accumulation of large amounts of a metaphosphate in bakers' yeast under certain conditions. *J. Biol. Chem. 166*, 775.

(102) Wiame, J. M. (1947) Étude d'une substance polyphosphorée, basophile et métachromatique chez les levures. *Biochim. Biophys. Acta 1*, 234–255.

(103) Wiame, J. (1949) The occurrence and physiological behavior of two metaphosphate fractions in yeast. *J. Biol. Chem. 178*, 919–929.

(104) Widra, A. (1959) Metachromatic granules of microorganisms. *J. Bacteriol. 78*, 664–670.

(105) Wilkinson, J. F., and Duguid, J. P. (1960) The influences of cultural conditions on bacterial cytology. *Intern. Rev. Cytol. 9*, 1–76.

(106) Tzeng, C., and Kornberg, A. (1998) Polyphosphate kinase is highly conserved in many bacterial pathogens. *Mol. Microbiol. 29*, 381–382.

(107) Kulaev, I. S., and Vagabov, V. M. (1983) Polyphosphate metabolism in micro-organisms. *Adv. Microb. Physiol. 24*, 83–171.

(108) Ahn, K., and Kornberg, A. (1990) Polyphosphate kinase from Escherichia coli. Purification and demonstration of a phosphoenzyme intermediate. *J. Biol. Chem. 265*, 11734–9.

(109) Kornberg, A. (1995) Inorganic polyphosphate: toward making a forgotten polymer unforgettable. *J. Bacteriol. 177*, 491–6.

(110) Kuroda, A., and Kornberg, A. (1997) Polyphosphate kinase as a nucleoside diphosphate kinase in Escherichia coli and Pseudomonas aeruginosa. *Proc. Natl. Acad. Sci.*

U. S. A. 94, 439–42.

(111) Akiyama, M., Crooke, E., and Kornberg, A. (1992) The polyphosphate kinase gene of Escherichia coli. Isolation and sequence of the ppk gene and membrane location of the protein. *J. Biol. Chem. 267*, 22556–61.

(112) Crooke, E., Akiyama, M., Rao, N. N., and Kornberg, A. (1994) Genetically altered levels of inorganic polyphosphate in Escherichia coli. *J. Biol. Chem. 269*, 6290–5.

(113) Rashid, M. H., Rao, N. N., and Kornberg, A. (2000) Inorganic Polyphosphate Is Required for Motility of Bacterial Pathogens. *J. Bacteriol. 182*, 225–227.

(114) Zhang, H., Ishige, K., and Kornberg, A. (2002) A polyphosphate kinase (PPK2) widely conserved in bacteria. *Proc. Natl. Acad. Sci. U. S. A. 99*, 16678–83.

(115) Ishige, K., Zhang, H., and Kornberg, A. (2002) Polyphosphate kinase (PPK2), a potent, polyphosphate-driven generator of GTP. *Proc. Natl. Acad. Sci. U. S. A. 99*, 16684–8.

(116) Kulakovskaya, T., and Kulaev, I. (2013) Enzymes of inorganic polyphosphate metabolism. *Prog. Mol. Subcell. Biol. 54*, 39–63.

(117) Akiyama, M., Crooke, E., and Kornberg, A. (1993) An exopolyphosphatase of Escherichia coli. The enzyme and its ppx gene in a polyphosphate operon. *J. Biol. Chem. 268*, 633–9.

(118) Bolesch, D. G., and Keasling, J. D. (2000) Polyphosphate Binding and Chain Length Recognition of Escherichia coli Exopolyphosphatase. *J. Biol. Chem. 275*, 33814–33819.

(119) Miyake, T., Shiba, T., Kameda, A., Ihara, Y., Munekata, M., Ishige, K., and Noguchi, T. (1999) The gene for an exopolyphosphatase of Pseudomonas aeruginosa. *DNA Res. 6*, 103–108.

(120) Kuroda, A., Murphy, H., Cashel, M., and Kornberg, A. (1997) Guanosine tetra- and pentaphosphate promote accumulation of inorganic polyphosphate in Escherichia coli. *J. Biol. Chem. 272*, 21240–3.

(121) Kulaev, I., Vagabov, V., and Kulakovskaya, T. (1999) New aspects of inorganic polyphosphate metabolism and function. *J. Biosci. Bioeng. 88*, 111–29.

(122) Brown, M. R. W., and Kornberg, A. (2004) Inorganic polyphosphate in the origin and survival of species. *Proc. Natl. Acad. Sci. U. S. A. 101*, 16085–7.

(123) Brown, M. R. W., and Kornberg, A. (2008) The long and short of it - polyphosphate, PPK and bacterial survival. *Trends Biochem. Sci. 33*, 284–90.

(124) Roszak, D. B., and Colwell, R. R. (1987) Survival strategies of bacteria in the natural environment. *Microbiol. Rev. 51*, 365–379.

(125) Siegele, D. A., and Kolter, R. (1992) Life after log. *J. Bacteriol. 174*, 345–8.

(126) Bohannon, D. E., Connell, N., Keener, J., Tormo, A., Espinosa-Urgel, M., Zambrano, M. M., and Kolter, R. (1991) Stationary-phase-inducible “gearbox” promoters: differential effects of katF mutations and role of sigma 70. *J. Bacteriol. 173*, 4482–92.

(127) Hengge-Aronis, R. (1993) Survival of hunger and stress: The role of rpoS in early stationary phase gene regulation in E. coli. *Cell 72*, 165–168.

(128) Kolter, R., Siegele, D. A., and Tormo, A. (1993) Annu. Rev. Microbiol. *Annu. Rev. Microbiol. 47:*, 855–874.

(129) Loewen, P. C., and Hengge-Aronis, R. (1994) The role of the sigma factor sigma S (KatF) in bacterial global regulation. *Annu. Rev. Microbiol. 48*, 53–80.

(130) Wösten, M. M. (1998) Eubacterial sigma-factors. *FEMS Microbiol. Rev. 22*, 127–50.

(131) Mulvey, M. R., and Loewen, P. C. (1989) Nucleotide sequence of katF of Escherichia coli suggests KatF protein is a novel s transcription factor. *Nucleic Acids Res. 17*, 9979–9991.

(132) Wagner, R. (2002) Regulation of ribosomal RNA synthesis in E. coli: effects of the global regulator guanosine tetraphosphate (ppGpp). *J. Mol. Microbiol. Biotechnol. 4*, 331–40.

(133) Ross, W., Vrentas, C. E., Sanchez-Vazquez, P., Gaal, T., and Gourse, R. L. (2013) The magic spot: a ppGpp binding site on E. coli RNA polymerase responsible for regulation of transcription initiation. *Mol. Cell 50*, 420–9.

(134) Hengge-Aronis, R. (2002) Signal transduction and regulatory mechanisms involved in control of the sigma(S) (RpoS) subunit of RNA polymerase. *Microbiol. Mol. Biol. Rev. 66*, 373–95, table of contents.

(135) Dong, T., and Schellhorn, H. E. (2010) Role of RpoS in virulence of pathogens. *Infect. Immun. 78*, 887–897.

(136) Dalebroux, Z. D., and Swanson, M. S. (2012) ppGpp: magic beyond RNA polymerase. *Nat. Rev. Microbiol. 10*, 203–212.

(137) Gentry, D. R., Hernandez, V. J., Nguyen, L. H., Jensen, D. B., and Cashel, M. (1993) Synthesis of the stationary-phase sigma factor sigma s is positively regulated by ppGpp. *J. Bacteriol. 175*, 7982–9.

(138) Österberg, S., del Peso-Santos, T., and Shingler, V. (2011) Regulation of alternative sigma factor use. *Annu. Rev. Microbiol. 65*, 37–55.

(139) Hirsch, M., and Elliott, T. (2002) Role of ppGpp in rpoS Stationary-Phase Regulation in Escherichia coli Role of ppGpp in rpoS Stationary-Phase Regulation in Escherichia coli. *J. Bacteriol. 184*, 5077–5087.

(140) Rao, N. N., and Kornberg, A. (1996) Inorganic polyphosphate supports resistance and survival of stationary-phase Escherichia coli. *J. Bacteriol. 178*, 1394–400.

(141) Shiba, T., Tsutsumi, K., Yano, H., Ihara, Y., Kameda, A., Tanaka, K., Takahashi, H., Munekata, M., Rao, N. N., and Kornberg, A. (1997) Inorganic polyphosphate and the induction of rpoS expression. *Proc. Natl. Acad. Sci. U. S. A. 94*, 11210–5.

(142) Kusano, S., and Ishihama, A. (1997) Functional interaction of Escherichia coli RNA polymerase with inorganic polyphosphate. *Genes Cells 2*, 433–41.

(143) Hauryliuk, V., Atkinson, G. C., Murakami, K. S., Tenson, T., and Gerdes, K. (2015) Recent functional insights into the role of (p)ppGpp in bacterial physiology. *Nat. Rev. Microbiol. 13*, 298–309.

(144) Wu, J., and Xie, J. (2009) Magic spot: (p)ppGpp. *J. Cell. Physiol. 220*, 297–302.

(145) Potrykus, K., and Cashel, M. (2008) (p)ppGpp: Still Magical? *Annu. Rev. Microbiol. 62*, 35–51.

(146) Magnusson, L. U., Farewell, A., and Nyström, T. (2005) ppGpp: a global regulator in Escherichia coli. *Trends Microbiol. 13*, 236–242.

(147) Cashel, M. (1975) ppGpp and pppGpp. *Annu. Rev. Microbiol. 29*, 301–318.

(148) Xiao, H., Kalman, M., Ikehara, K., Zemel, S., Glaser, G., and Cashel, M. (1991) Residual guanosine 3',5'-bispyrophosphate synthetic activity of relA null mutants can be eliminated by spoT null mutations. *J. Biol. Chem. 266*, 5980–90.

(149) Rojiani, M. V., Jakubowski, H., and Goldman, E. (1989) Effect of variation of charged and uncharged tRNA(Trp) levels on ppGpp synthesis in Escherichia coli. *J. Bacteriol. 171*, 6493–6502.

(150) Wendrich, T. M., Blaha, G., Wilson, D. N., Marahiel, M. A., and Nierhaus, K. H. (2002) Dissection of the Mechanism for the Stringent Factor RelA. *Mol. Cell 10*, 779–788.

(151) Haseltine, W. A., and Block, R. (1973) Synthesis of guanosine tetra and pentaphosphate requires the presence of a codon-specific uncharged transfer ribonucleic acid in the acceptor site of ribosomes. *Proc. Natl. Acad. Sci. USA 70*, 1564–1568.

(152) Murray, K. D., and Bremer, H. (1996) Control of spoT-dependent ppGpp synthesis and degradation in Escherichia coli. *J. Mol. Biol. 259*, 41–57.

(153) Hogg, T., Mechold, U., Malke, H., Cashel, M., and Hilgenfeld, R. (2004) Conformational antagonism between opposing active sites in a bifunctional RelA/SpoT homolog modulates (p)ppGpp metabolism during the stringent response [corrected]. *Cell 117*, 57–68.

(154) Hernandez, V. J., and Bremer, H. (1991) Escherichia coli ppGpp synthetase II activity requires spoT. *J. Biol. Chem. 266*, 5991–9.

(155) Battesti, A., and Bouveret, E. (2006) Acyl carrier protein/SpoT interaction, the switch linking SpoT-dependent stress response to fatty acid metabolism. *Mol. Microbiol. 62*, 1048–1063.

(156) Gong, L., Takayama, K., and Kjelleberg, S. (2002) Role of spoT-dependent ppGpp accumulation in the survival of light-exposed starved bacteria. *Microbiology 148*, 559–70.

(157) Seyfzadeh, M., Keener, J., and Nomura, M. (1993) spoT-dependent accumulation of guanosine tetraphosphate in response to fatty acid starvation in Escherichia coli. *Proc. Natl. Acad. Sci. U. S. A. 90*, 11004–8.

(158) Spira, B., Silberstein, N., and Yagil, E. (1995) Guanosine 3',5'-bispyrophosphate (ppGpp) synthesis in cells of Escherichia coli starved for Pi. *J. Bacteriol. 177*, 4053–8.

(159) Vinella, D., Albrecht, C., Cashel, M., and Ari, R. D. (2005) Iron limitation induces SpoT-dependent accumulation of ppGpp in Escherichia coli. *Mol. Microbiol. 56*, 958–970.

(160) Potrykus, K., Murphy, H., Philippe, N., and Cashel, M. (2011) ppGpp is the major source of growth rate control in E. coli. *Environ. Microbiol. 13*, 563–575.

(161) Kriel, A. et al. (2012) Direct regulation of GTP homeostasis by (p)ppGpp: a critical component of viability and stress resistance. *Mol Cell 48*, 231–241.

(162) Durfee, T., Hansen, A.-M., Zhi, H., Blattner, F. R., and Jin, D. J. (2008) Transcription profiling of the stringent response in Escherichia coli. *J. Bacteriol. 190*, 1084–96.

(163) Bougdour, A. (2006) Modulating RssB activity: IraP, a novel regulator of S stability in Escherichia coli. *Genes Dev. 20*, 884–897.

(164) Paul, B. J., Barker, M. M., Ross, W., Schneider, D. A., Webb, C., Foster, J. W., and Gourse, R. L. (2004) DksA: a critical component of the transcription initiation machinery that potentiates the regulation of rRNA promoters by ppGpp and the initiating NTP. *Cell 118*, 311–22.

(165) Paul, B. J., Berkmen, M. B., and Gourse, R. L. (2005) DksA potentiates direct activation of amino acid promoters by ppGpp. *Proc. Natl. Acad. Sci. USA 102*, 7823–7828.

(166) Barker, M. M., Gaal, T., Josaitis, C. A., and Gourse, R. L. (2001) Mechanism of regulation of transcription initiation by ppGpp. I. Effects of ppGpp on transcription initiation in vivo and in vitro. *J. Mol. Biol. 305*, 673–88.

(167) Jishage, M., Kvint, K., Shingler, V., and Nyström, T. (2002) Regulation of sigma factor competition by the alarmone ppGpp. *Genes Dev. 16*, 1260–70.

(168) Srivatsan, A., and Wang, J. D. (2008) Control of bacterial transcription, translation and replication by (p)ppGpp. *Curr. Opin. Microbiol. 11*, 100–105.

(169) Ault-Riché, D., Fraley, C. D., Tzeng, C. M., and Kornberg, A. (1998) Novel assay reveals multiple pathways regulating stress-induced accumulations of inorganic polyphosphate in Escherichia coli. *J. Bacteriol. 180*, 1841–7.

(170) Kuroda, A., Tanaka, S., Ikeda, T., Kato, J., Takiguchi, N., and Ohtake, H. (1999) Inorganic polyphosphate kinase is required to stimulate protein degradation and for adaptation to amino acid starvation in Escherichia coli. *Proc. Natl. Acad. Sci. U. S. A. 96*, 14264–9.

(171) Mandelstam, J. (1958) Turnover of protein in growing and non-growing populations of Escherichia coli. *Biochem. J. 69*, 110–9.

(172) Sussman, A. J., and Gilvarg, C. (1969) Protein turnover in amino acid-starved strains of Escherichia coli K-12 differing in their ribonucleic acid control. *J. Biol. Chem. 244*, 6304–6306.

(173) Maurizi, M. R. (1992) Proteases and protein degradation in Escherichia coli. *Experientia 48*, 178–201.

(174) Kuroda, A., Nomura, K., Ohtomo, R., Kato, J., Ikeda, T., Takiguchi, N., Ohtake, H., and Kornberg, A. (2001) Role of inorganic polyphosphate in promoting ribosomal protein

degradation by the Lon protease in E. coli. *Science 293*, 705–8.

(175) Nomura, K., Kato, J., Takiguchi, N., Ohtake, H., and Kuroda, A. (2004) Effects of Inorganic Polyphosphate on the Proteolytic and DNA-binding Activities of Lon in Escherichia coli. *J. Biol. Chem. 279*, 34406–34410.

(176) Anderson, D. G., and Kowalczykowski, S. C. (1998) Reconstitution of an SOS response pathway: derepression of transcription in response to DNA breaks. *Cell 95*, 975–9.

(177) McKenzie, G. J., Lee, P. L., Lombardo, M. J., Hastings, P. J., and Rosenberg, S. M. (2001) SOS mutator DNA polymerase IV functions in adaptive mutation and not adaptive amplification. *Mol. Cell 7*, 571–9.

(178) Smith, B. T., and Walker, G. C. (1998) Mutagenesis and more: umuDC and the Escherichia coli SOS response. *Genetics 148*, 1599–610.

(179) Patel, M., Jiang, Q., Woodgate, R., Cox, M. M., and Goodman, M. F. (2010) A new model for SOS-induced mutagenesis: how RecA protein activates DNA polymerase V. *Crit. Rev. Biochem. Mol. Biol. 45*, 171–84.

(180) Tsutsumi, K., Munekata, M., and Shiba, T. (2000) Involvement of inorganic polyphosphate in expression of SOS genes. *Biochim. Biophys. Acta 1493*, 73–81.

(181) Goodman, M. F. (2002) Error-prone repair DNA polymerases in prokaryotes and eukaryotes. *Annu. Rev. Biochem. 71*, 17–50.

(182) Stumpf, J. D., and Foster, P. L. (2005) Polyphosphate kinase regulates error-prone replication by DNA polymerase IV in Escherichia coli. *Mol. Microbiol. 57*, 751–761.

(183) Fuchs, R. P., Fujii, S., and Wagner, J. (2004) Properties and functions of Escherichia coli: Pol IV and Pol V. *Adv. Protein Chem. 69*, 229–264.

(184) Maisonneuve, E., and Gerdes, K. (2014) Molecular Mechanisms Underlying Bacterial Persisters. *Cell 157*, 539–548.

(185) Van Melderen, L., and Saavedra De Bast, M. (2009) Bacterial Toxin–Antitoxin Systems: More Than Selfish Entities? *PLoS Genet. 5*, e1000437.

(186) Black, D. S., Kelly, A. J., Mardis, M. J., and Moyed, H. S. (1991) Structure and organization of hip, an operon that affects lethality due to inhibition of peptidoglycan or DNA synthesis. *J. Bacteriol. 173*, 5732–9.

(187) Korch, S. B., Henderson, T. A., and Hill, T. M. (2003) Characterization of the hipA7 allele of Escherichia coli and evidence that high persistence is governed by (p)ppGpp synthesis. *Mol. Microbiol. 50*, 1199–1213.

(188) Maisonneuve, E., Shakespeare, L. J., Jorgensen, M. G., and Gerdes, K. (2011) Bacterial persistence by RNA endonucleases. *Proc. Natl. Acad. Sci. 108*, 13206–13211.

(189) Keren, I., Shah, D., Spoering, A., Kaldalu, N., and Lewis, K. (2004) Specialized persister cells and the mechanism of multidrug tolerance in Escherichia coli. *J. Bacteriol. 186*, 8172–80.

(190) Gerdes, K., and Maisonneuve, E. (2012) Bacterial persistence and toxin-antitoxin loci.

Annu. Rev. Microbiol. 66, 103–23.

(191) Pedersen, K., Christensen, S. ., and Gerdes, K. (2002) Rapid induction and reversal of a bacteriostatic condition by controlled expression of toxins and antitoxins. *Mol. Microbiol. 45*, 501–510.

(192) Germain, E., Castro-Roa, D., Zenkin, N., and Gerdes, K. (2013) Molecular mechanism of bacterial persistence by HipA. *Mol. Cell 52*, 248–54.

(193) Kaspy, I., Rotem, E., Weiss, N., Ronin, I., Balaban, N. Q., and Glaser, G. (2013) HipA-mediated antibiotic persistence via phosphorylation of the glutamyl- tRNA-synthetase. *Nat. Commun. 4*, 3001.

(194) Germain, E., Roghanian, M., Gerdes, K., and Maisonneuve, E. (2015) Stochastic induction of persister cells by HipA through (p)ppGpp-mediated activation of mRNA endonucleases. *Proc. Natl. Acad. Sci. 112*, 5171–5176.

(195) Verstraeten, N., Knapen, W. J., Kint, C. I., Liebens, V., Van den Bergh, B., Dewachter, L., Michiels, J. E., Fu, Q., David, C. C., Fierro, A. C., Marchal, K., Beirlant, J., Versées, W., Hofkens, J., Jansen, M., Fauvart, M., and Michiels, J. (2015) Obg and Membrane Depolarization Are Part of a Microbial Bet-Hedging Strategy that Leads to Antibiotic Tolerance. *Mol. Cell 59*, 9–21.

(196) Gerdes, K., and Maisonneuve, E. (2015) Remarkable Functional Convergence: Alarmone ppGpp Mediates Persistence by Activating Type I and II Toxin-Antitoxins. *Mol. Cell 59*, 1–3.

(197) Schumacher, M. A., Min, J., Link, T. M., Guan, Z., Xu, W., Ahn, Y.-H., Soderblom, E. J., Kurie, J. M., Evdokimov, A., Moseley, M. A., Lewis, K., and Brennan, R. G. (2012) Role of unusual P loop ejection and autophosphorylation in HipA-mediated persistence and multidrug tolerance. *Cell Rep. 2*, 518–25.

(198) Rashid, M. H., Rumbaugh, K., Passador, L., Davies, D. G., Hamood, A. N., Iglewski, B. H., and Kornberg, A. (2000) Polyphosphate kinase is essential for biofilm development, quorum sensing, and virulence of Pseudomonas aeruginosa. *Proc. Natl. Acad. Sci. U. S. A. 97*, 9636–41.

(199) Rashid, M. H., and Kornberg, A. (2000) Inorganic polyphosphate is needed for swimming, swarming, and twitching motilities of Pseudomonas aeruginosa. *Proc. Natl. Acad. Sci. U. S. A. 97*, 4885–90.

(200) Davies, D. G., Parsek, M. R., Pearson, J. P., Iglewski, B. H., Costerton, J. W., and Greenberg, E. P. (1998) The involvement of cell-to-cell signals in the development of a bacterial biofilm. *Science 280*, 295–8.

(201) Diggle, S. P., Crusz, S. A., and Cámara, M. (2007) Quorum sensing. *Curr. Biol. 17*, R907–R910.

(202) Smith, R. S., and Iglewski, B. H. (2003) P. aeruginosa quorum-sensing systems and virulence. *Curr. Opin. Microbiol. 6*, 56–60.

(203) Costerton, J. W., Lewandowski, Z., Caldwell, D. E., Korber, D. R., and Lappin-Scott,

H. M. (1995) Microbial biofilms. *Annu. Rev. Microbiol. 49*, 711–45.

(204) O'Toole, G. A., and Kolter, R. (1998) Flagellar and twitching motility are necessary for Pseudomonas aeruginosa biofilm development. *Mol. Microbiol. 30*, 295–304.

(205) Ryder, C., Byrd, M., and Wozniak, D. J. (2007) Role of polysaccharides in Pseudomonas aeruginosa biofilm development. *Curr. Opin. Microbiol. 10*, 644–8.

(206) Kim, H. Y., Schlictman, D., Shankar, S., Xie, Z., Chakrabarty, A. M., and Kornberg, A. (1998) Alginate, inorganic polyphosphate, GTP and ppGpp synthesis co-regulated in Pseudomonas aeruginosa: implications for stationary phase survival and synthesis of RNA/DNA precursors. *Mol. Microbiol. 27*, 717–25.

(207) Høiby, N., Bjarnsholt, T., Givskov, M., Molin, S., and Ciofu, O. (2010) Antibiotic resistance of bacterial biofilms. *Int. J. Antimicrob. Agents 35*, 322–332.

(208) Stewart, P. S., and William Costerton, J. (2001) Antibiotic resistance of bacteria in biofilms. *Lancet 358*, 135–138.

(209) Parks, Q. M., and Hobden, J. A. (2005) Polyphosphate kinase 1 and the ocular virulence of Pseudomonas aeruginosa. *Invest. Ophthalmol. Vis. Sci. 46*, 248–51.

(210) Fraley, C. D., Rashid, M. H., Lee, S. S. K., Gottschalk, R., Harrison, J., Wood, P. J., Brown, M. R. W., and Kornberg, A. (2007) A polyphosphate kinase 1 (ppk1) mutant of Pseudomonas aeruginosa exhibits multiple ultrastructural and functional defects. *Proc. Natl. Acad. Sci. U. S. A. 104*, 3526–31.

(211) Ortiz-Severín, J., Varas, M., Bravo-Toncio, C., Guiliani, N., and Chávez, F. P. (2015) Multiple antibiotic susceptibility of polyphosphate kinase mutants (ppk1 and ppk2) from Pseudomonas aeruginosa PAO1 as revealed by global phenotypic analysis. *Biol. Res. 48*, 22.

(212) Kim, K.-S., Rao, N. N., Fraley, C. D., and Kornberg, A. (2002) Inorganic polyphosphate is essential for long-term survival and virulence factors in Shigella and Salmonella spp. *Proc. Natl. Acad. Sci. U. S. A. 99*, 7675–80.

(213) McMeechan, A., Lovell, M. A., Cogan, T. A., Marston, K. L., Humphrey, T. J., and Barrow, P. a. (2007) Inactivation of ppk differentially affects virulence and disrupts ATP homeostasis in Salmonella enterica serovars Typhimurium and Gallinarum. *Res. Microbiol. 158*, 79–85.

(214) Candon, H. L., Allan, B. J., Fraley, C. D., and Gaynor, E. C. (2007) Polyphosphate kinase 1 is a pathogenesis determinant in Campylobacter jejuni. *J. Bacteriol. 189*, 8099–8108.

(215) Gangaiah, D., Liu, Z., Arcos, J., Kassem, I. I., Sanad, Y., Torrelles, J. B., and Rajashekara, G. (2010) Polyphosphate Kinase 2: A Novel Determinant of Stress Responses and Pathogenesis in Campylobacter jejuni. *PLoS One 5*, e12142.

(216) Shirai, M., Kakada, J., Shibata, K., Morshed, M. G., Matsushita, T., and Nakazawa, T. (2000) Accumulation of polyphosphate granules in Helicobacter pylori cells under anaerobic conditions. *J. Med. Microbiol. 49*, 513–9.

(217) Tan, S., Fraley, C. D., Zhang, M., Dailidiene, D., Kornberg, A., and Berg, D. E. (2005) Diverse phenotypes resulting from polyphosphate kinase gene (ppk1) inactivation in different strains of Helicobacter pylori. *J. Bacteriol. 187*, 7687–95.

(218) Ayraud, S., Janvier, B., Labigne, A., Ecobichon, C., Burucoa, C., and Fauchère, J.-L. (2005) Polyphosphate kinase: a new colonization factor of Helicobacter pylori. *FEMS Microbiol. Lett. 243*, 45–50.

(219) Shi, X., Rao, N. N., and Kornberg, A. (2004) Inorganic polyphosphate in Bacillus cereus: motility, biofilm formation, and sporulation. *Proc. Natl. Acad. Sci. U. S. A. 101*, 17061–5.

(220) Sureka, K., Dey, S., Datta, P., Singh, A. K., Dasgupta, A., Rodrigue, S., Basu, J., and Kundu, M. (2007) Polyphosphate kinase is involved in stress-induced mprAB-sigE-rel signalling in mycobacteria. *Mol. Microbiol. 65*, 261–276.

(221) Sureka, K., Sanyal, S., Basu, J., and Kundu, M. (2009) Polyphosphate kinase 2: A modulator of nucleoside diphosphate kinase activity in mycobacteria. *Mol. Microbiol. 74*, 1187–1197.

(222) Chuang, Y.-M., Belchis, D. A., and Karakousis, P. C. (2013) The Polyphosphate Kinase Gene ppk2 Is Required for Mycobacterium tuberculosis Inorganic Polyphosphate Regulation and Virulence. *MBio 4*, e00039-13.

(223) Ogawa, N., Tzeng, C. M., Fraley, C. D., and Kornberg, A. (2000) Inorganic polyphosphate in Vibrio cholerae: genetic, biochemical, and physiologic features. *J. Bacteriol. 182*, 6687–93.

(224) Tunpiboonsak, S., Mongkolrob, R., Kitudomsub, K., Thanwatanaying, P., Kiettipirodom, W., Tungboontina, Y., and Tungpradabkul, S. (2010) Role of a Burkholderia pseudomallei polyphosphate kinase in an oxidative stress response, motilities, and biofilm formation. *J. Microbiol. 48*, 63–70.

(225) Wrench, A. P., Gardner, C. L., Siegel, S. D., Pagliai, F. A., Malekiha, M., Gonzalez, C. F., and Lorca, G. L. (2013) MglA/SspA Complex Interactions Are Modulated by Inorganic Polyphosphate. *PLoS One 8*, e76428.

(226) Guina, T., Radulovic, D., Bahrami, A. J., Bolton, D. L., Rohmer, L., Jones-Isaac, K. A., Chen, J., Gallagher, L. A., Gallis, B., Ryu, S., Taylor, G. K., Brittnacher, M. J., Manoil, C., and Goodlett, D. R. (2007) MglA Regulates Francisella tularensis subsp. novicida (Francisella novicida) Response to Starvation and Oxidative Stress. *J. Bacteriol. 189*, 6580–6586.

(227) Richards, M. I., Michell, S. L., and Oyston, P. C. F. (2008) An intracellularly inducible gene involved in virulence and polyphosphate production in Francisella. *J. Med. Microbiol. 57*, 1183–1192.

(228) Leipe, D. D., Koonin, E. V., and Aravind, L. (2003) Evolution and classification of P-loop kinases and related proteins. *J. Mol. Biol. 333*, 781–815.

(229) Nocek, B., Kochinyan, S., Proudfoot, M., Brown, G., Evdokimova, E., Osipiuk, J., Edwards, A. M., Savchenko, A., Joachimiak, A., and Yakunin, A. F. (2008) Polyphosphate-

dependent synthesis of ATP and ADP by the family-2 polyphosphate kinases in bacteria. *Proc. Natl. Acad. Sci. U. S. A. 105*, 17730–5.

(230) Ishige, K., and Noguchi, T. (2000) Inorganic polyphosphate kinase and adenylate kinase participate in the polyphosphate:AMP phosphotransferase activity of Escherichia coli. *Proc. Natl. Acad. Sci. U. S. A. 97*, 14168–71.

(231) Ishige, K., and Noguchi, T. (2001) Polyphosphate:AMP phosphotransferase and polyphosphate:ADP phosphotransferase activities of Pseudomonas aeruginosa. *Biochem. Biophys. Res. Commun. 281*, 821–6.

(232) Motomura, K., Hirota, R., Okada, M., Ikeda, T., Ishida, T., and Kuroda, A. (2014) A New Subfamily of Polyphosphate Kinase 2 (Class III PPK2) Catalyzes both Nucleoside Monophosphate Phosphorylation and Nucleoside Diphosphate Phosphorylation. *Appl. Environ. Microbiol. 80*, 2602–2608.

(233) Nahálka, J., and Pätoprstý, V. (2009) Enzymatic synthesis of sialylation substrates powered by a novel polyphosphate kinase (PPK3). *Org. Biomol. Chem. 7*, 1778–1780.

(234) Hilleman, M. R. (2002) Overview: cause and prevention in biowarfare and bioterrorism. *Vaccine 20*, 3055–67.

(235) Zapanta, P. E., and Ghorab, S. (2014) Age of Bioterrorism: Are You Prepared? Review of Bioweapons and Their Clinical Presentation for Otolaryngologists. *Otolaryngol. Head. Neck Surg. 151*, 208–14.

(236) Riedel, S. (2004) Biological warfare and bioterrorism: a historical review. *Proc. (Bayl. Univ. Med. Cent). 17*, 400–6.

(237) Carus, W. S. (2015) The History of Biological Weapons Use: What We Know and What We Don't. *Heal. Secur. 13*, 219–55.

(238) Anderson, P. D., and Bokor, G. (2012) Bioterrorism: pathogens as weapons. *J. Pharm. Pract. 25*, 521–9.

(239) Dire, D. J. (2016) CBRNE-Biological Warfare Agents http://emedicine.medscape.com.

(240) Gilligan, P. H. (2002) Therapeutic challenges posed by bacterial bioterrorism threats. *Curr. Opin. Microbiol. 5*, 489–495.

(241) Ellis, J., Oyston, P. C. F., Green, M., and Titball, R. W. (2002) Tularemia. *Clin. Microbiol. Rev. 15*, 631–46.

(242) Cronquist, S. D. (2004) Tularemia: the disease and the weapon. *Dermatol. Clin. 22*, 313–320.

(243) Dennis, D. T., Inglesby, T. V., Henderson, D. A., Bartlett, J. G., Ascher, M. S., Eitzen, E., Fine, A. D., Friedlander, A. M., Hauer, J., Layton, M., Lillibridge, S. R., McDade, J. E., Osterholm, M. T., O'Toole, T., Parker, G., Perl, T. M., Russell, P. K., Tonat, K., and for the Working Group on Civilian Biodefense. (2001) Tularemia as a Biological Weapon. *JAMA 285*, 2763.

(244) Oyston, P. C. F. (2008) Francisella tularensis: unravelling the secrets of an

intracellular pathogen. *J. Med. Microbiol. 57*, 921–930.

(245) Enderlin, G., Morales, L., Jacobs, R. F., and Cross, J. T. (1994) Streptomycin and alternative agents for the treatment of tularemia: review of the literature. *Clin. Infect. Dis. 19*, 42–47.

(246) Limaye, A. P., and Hooper, C. J. (1999) Treatment of tularemia with fluoroquinolones: two cases and review. *Clin. Infect. Dis. 29*, 922–4.

(247) Reilly, T. J., Baron, G. S., Nano, F. E., and Kuhlenschmidt, M. S. (1996) Characterization and Sequencing of a Respiratory Burst-inhibiting Acid Phosphatase from Francisella tularensis. *J. Biol. Chem. 271*, 10973–10983.

(248) Santic, M., Asare, R., Skrobonja, I., Jones, S., and Abu Kwaik, Y. (2008) Acquisition of the Vacuolar ATPase Proton Pump and Phagosome Acidification Are Essential for Escape of Francisella tularensis into the Macrophage Cytosol. *Infect. Immun. 76*, 2671–2677.

(249) Lai, X. H., Golovliov, I., and Sjöstedt, A. (2001) Francisella tularensis induces cytopathogenicity and apoptosis in murine macrophages via a mechanism that requires intracellular bacterial multiplication. *Infect. Immun. 69*, 4691–4.

(250) Ray, K., Marteyn, B., Sansonetti, P. J., and Tang, C. M. (2009) Life on the inside: the intracellular lifestyle of cytosolic bacteria. *Nat. Rev. Microbiol. 7*, 333–340.

(251) Baron, G. S., and Nano, F. E. (1998) MglA and MglB are required for the intramacrophage growth of Francisella novicida. *Mol. Microbiol. 29*, 247–59.

(252) Charity, J. C., Costante-Hamm, M. M., Balon, E. L., Boyd, D. H., Rubin, E. J., and Dove, S. L. (2007) Twin RNA Polymerase–Associated Proteins Control Virulence Gene Expression in Francisella tularensis. *PLoS Pathog. 3*, e84.

(253) Lauriano, C. M., Barker, J. R., Yoon, S.-S., Nano, F. E., Arulanandam, B. P., Hassett, D. J., and Klose, K. E. (2004) MglA regulates transcription of virulence factors necessary for Francisella tularensis intraamoebae and intramacrophage survival. *Proc. Natl. Acad. Sci. 101*, 4246–4249.

(254) Nano, F. E., Zhang, N., Cowley, S. C., Klose, K. E., Cheung, K. K. M., Roberts, M. J., Ludu, J. S., Letendre, G. W., Meierovics, A. I., Stephens, G., and Elkins, K. L. (2004) A Francisella tularensis pathogenicity island required for intramacrophage growth. *J. Bacteriol. 186*, 6430–6.

(255) Bröms, J. E., Sjöstedt, A., and Lavander, M. (2010) The Role of the Francisella Tularensis Pathogenicity Island in Type VI Secretion, Intracellular Survival, and Modulation of Host Cell Signaling. *Front. Microbiol. 1*, 136.

(256) Charity, J. C., Blalock, L. T., Costante-Hamm, M. M., Kasper, D. L., and Dove, S. L. (2009) Small molecule control of virulence gene expression in Francisella tularensis. *PLoS Pathog. 5*, e1000641.

(257) Rohlfing, A. E., and Dove, S. L. (2014) Coordinate control of virulence gene expression in Francisella tularensis involves direct interaction between key regulators. *J. Bacteriol.*

196, 3516–3526.

(258) Dean, R. E., Ireland, P. M., Jordan, J. E., Titball, R. W., and Oyston, P. C. F. (2009) RelA regulates virulence and intracellular survival of Francisella novicida. *Microbiology 155*, 4104–4113.

(259) Faron, M., Fletcher, J. R., Rasmussen, J. A., Long, M. E., Allen, L.-A. H., and Jones, B. D. (2013) The Francisella tularensis migR, trmE, and cphA Genes Contribute to F. tularensis Pathogenicity Island Gene Regulation and Intracellular Growth by Modulation of the Stress Alarmone ppGpp. *Infect. Immun. 81*, 2800–2811.

(260) Batten, L. E., Parnell, A. E., Wells, N. J., Murch, A. L., Oyston, P. C. F., and Roach, P. L. (2016) Biochemical and structural characterization of polyphosphate kinase 2 from the intracellular pathogen Francisella tularensis. *Biosci. Rep. 36*, e00294–e00294.

(261) Morrissey, J. H., Choi, S. H., and Smith, S. a. (2012) Polyphosphate: an ancient molecule that links platelets, coagulation, and inflammation. *Blood 119*, 5972–9.

(262) Smith, S. A., and Morrissey, J. H. (2014) Polyphosphate. *Curr. Opin. Hematol. 21*, 388–394.

(263) Azevedo, C., and Saiardi, A. (2014) Functions of inorganic polyphosphates in eukaryotic cells: a coat of many colours. *Biochem. Soc. Trans. 42*, 98–102.

(264) Batten, L. E. (2013) Bacterial Kinases as Potential Targets for Broad-sprectrum Antibiotics. Doctoral thesis. University of Southampton.

(265) Parnell, A. E. (2017) Mechanistic and structural analysis of the enzymes polyphosphate kinase and exopolyphosphatase from biothreat agents. Doctoral thesis. University of Southampton.

(266) Richards, M. I., Michell, S. L., and Oyston, P. C. F. (2008) An intracellularly inducible gene involved in virulence and polyphosphate production in Francisella. *J. Med. Microbiol. 57*, 1183–92.

(267) Haouz, A., Vanheusden, V., Munier-Lehmann, H., Froeyen, M., Herdewijn, P., Van Calenbergh, S., and Delarue, M. (2003) Enzymatic and structural analysis of inhibitors designed against Mycobacterium tuberculosis thymidylate kinase: New insights into the phosphoryl transfer mechanism. *J. Biol. Chem. 278*, 4963–4971.

(268) Shum, K. T., Lui, E. L. H., Wong, S. C. K., Yeung, P., Sam, L., Wang, Y., Watt, R. M., and Tanner, J. A. (2011) Aptamer-mediated inhibition of Mycobacterium tuberculosis polyphosphate kinase 2. *Biochemistry 50*, 3261–71.

(269) Minor, L. K. (2006) Handbook of Assay Development in Drug Discovery (Minor, L., Ed.). CRC Press, Boca Raton, FL.

(270) Acker, M. G., and Auld, D. S. (2014) Considerations for the design and reporting of enzyme assays in high-throughput screening applications. *Perspect. Sci. 1*, 56–73.

(271) Fersht, A. (1999) Structure and Mechanism in Protein Science: A Guide to Enzyme Catalysis and Protein Folding. Freeman, W H.

(272) Copeland, R. A. (2000) Enzymes: A Practical Introduction to Structure, Mechanism,

and Data Analysis. Wiley-VCH.

(273) Segel, I. H. (1975) Enzyme Kinetics: Behavior and Analysis of Rapid Equilibrium and Steady-State Enzyme Systems. Wiley-Interscience.

(274) Cornish-Bowden, A. (2012) Fundamentals of Enzyme Kinetics 4th ed. Wiley-Blackwell.

(275) Michaelis, L., and Menten, M. L. (2013) The kinetics of invertin action: Translated by T.R.C. Boyde, Submitted 4 February 1913. *FEBS Lett. 587*, 2712–2720.

(276) Johnson, K. A., and Goody, R. S. (2011) The Original Michaelis Constant: Translation of the 1913 Michaelis–Menten Paper. *Biochemistry 50*, 8264–8269.

(277) Briggs, G. E., and Haldane, J. B. S. (1925) A Note on the Kinetics of Enzyme Action. *Biochem. J. 19*, 338–339.

(278) Storer, A. C., and Cornish-Bowden, A. (1974) The kinetics of coupled enzyme reactions. Applications to the assay of glucokinase, with glucose 6-phosphate dehydrogenase as coupling enzyme. *Biochem. J. 141*, 205–9.

(279) Tipton, K. F. (2002) Principles of enzyme assay and kinetic studies, in *Enzyme Assays: A practical Approach* (Eisenthal, R., and Danson, M. J., Eds.) 2nd ed. IRL Press, Oxford.

(280) McClure, W. R. (1969) A Kinetic Analysis of Coupled Enzyme Assays. *Biochemistry 8*, 2782–2786.

(281) Fersht, A. (1985) Enzyme structure and mechanism 2nd ed. W. H. Freeman and Company.

(282) Marques, S. M., and Esteves da Silva, J. C. G. (2009) Firefly bioluminescence: A mechanistic approach of luciferase catalyzed reactions. *IUBMB Life 61*, 6–17.

(283) Inouye, S. (2010) Firefly luciferase: an adenylate-forming enzyme for multicatalytic functions. *Cell. Mol. Life Sci. 67*, 387–404.

(284) Fraga, H. (2008) Firefly luminescence: A historical perspective and recent developments. *Photochem. Photobiol. Sci. 7*, 146–158.

(285) Lee, R. T., Denburg, J. L., and McElroy, W. D. (1970) Substrate-binding properties of firefly luciferase. II. ATP-binding site. *Arch. Biochem. Biophys. 141*, 38–52.

(286) Tanega, C., Shen, M., Mott, B. T., Thomas, C. J., MacArthur, R., Inglese, J., and Auld, D. S. (2009) Comparison of bioluminescent kinase assays using substrate depletion and product formation. *Assay Drug Dev. Technol. 7*, 606–14.

(287) Fan, F., and Wood, K. V. (2007) Bioluminescent Assays for High-Throughput Screening. *Assay Drug Dev. Technol. 5*, 127–136.

(288) Valeur, B. (2006) Molecular Fluorescence: principles and applications 2nd ed. Wiley-VCH.

(289) Deo, S. K. (2011) Chemiluminescence and bioluminescence: past, present and future, in *Analytical and Bioanalytical Chemistry* (Roda, A., Ed.), pp 1457–1458. RSC Publishing.

(290) Lakowicz, J. R. (2006) Principles of Fluorescence Spectroscopy 3rd Ed. Springer, Berlin.

(291) O' Brien, M. A. (2006) A comparison of homogeneous bioluminescent and fluorescent methods for protease assays, in *Handbook of assay development in drug discovery*, pp 125–139. CRC Press, Taylor & Francis Group.

(292) Simeonov, A., Jadhav, A., Thomas, C. J., Wang, Y., Huang, R., Southall, N. T., Shinn, P., Smith, J., Austin, C. P., Auld, D. S., and Inglese, J. (2008) Fluorescence spectroscopic profiling of compound libraries. *J. Med. Chem. 51*, 2363–2371.

(293) Auld, D. S., Southall, N. T., Jadhav, A., Johnson, R. L., Diller, D. J., Simeonov, A., Austin, C. P., and Inglese, J. (2008) Characterization of chemical libraries for luciferase inhibitory activity. *J. Med. Chem. 51*, 2372–2386.

(294) Hastings, J. W., and Johnson, C. H. (2003) Bioluminescence and chemiluminescence. *Methods Enzymol. 360*, 75–104.

(295) Shimomura, O. (2012) Bioluminescence: chemical principles and methods. World Scientific Publishing Co. Pte. Ltd.

(296) Wilson, T., and Hastings, J. W. (1998) Bioluminescence. *Annu. Rev. Cell Dev. Biol. 14*, 197–230.

(297) Hastings, J. W., and Wood, K. V. (2001) Photobiology for the 21st Century (Valenzeno, D. P., and Coohil, T. P., Eds.). Valdenmar Publishing.

(298) Thorne, N., Inglese, J., and Auld, D. S. (2010) Illuminating insights into firefly luciferase and other bioluminescent reporters used in chemical biology. *Chem. Biol. 17*, 646–57.

(299) Singh, P., Harden, B. J., Lillywhite, B. J., and Broad, P. M. (2004) Identification of kinase inhibitors by an ATP depletion method. *Assay Drug Dev. Technol. 2*, 161–9.

(300) Hoshino, H. (2009) Current advanced bioluminescence technology in drug discovery. *Expert Opin. Drug Discov. 4*, 373–389.

(301) Lundin, A. (2014) Optimisation of the firefly luciferase reaction for analytical purposes, in *Bioluminescence: Fundamentals and applications in biotechnology* (Thouand, G., and Marks, R., Eds.), pp 31–62. Springer-Verlag.

(302) Srikantha, T., Klapach, A., Lorenz, W. W., Tsai, L. K., Laughlin, L. A., Gorman, J. A., and Soll, D. R. (1996) The sea pansy Renilla reniformis luciferase serves as a sensitive bioluminescent reporter for differential gene expression in Candida albicans. *J. Bacteriol. 178*, 121–129.

(303) Roda, A., Guardigli, M., Michelini, E., and Mirasoli, M. (2009) Bioluminescence in analytical chemistry and in vivo imaging. *Trends Anal. Chem. 28*, 307–322.

(304) Bronstein, I., Fortin, J., Stanley, P. E., Stewart, G. S. A. B., and Kricka, L. J. (1994) Chemiluminescent and Bioluminescent Reporter Gene Assays. *Anal. Biochem. 219*, 169–181.

(305) Greer, L. F., and Szalay, A. A. (2002) Imaging of light emission from the expression

of luciferases in living cells and organisms: a review. *Luminescence 17*, 43–74.

(306) Gulick, A. M. (2009) Conformational Dynamics in the Acyl-CoA Synthetases, Adenylation Domains of Non-ribosomal Peptide Synthetases, and Firefly Luciferase. *ACS Chem. Biol. 4*, 811–827.

(307) McElroy, W. D., DeLuca, M., and Travis, J. (1967) Molecular uniformity in biological catalyses. The enzymes concerned with firefly luciferin, amino acid, and fatty acid utilization are compared. *Science 157*, 150–60.

(308) Berg, P. (1956) Acyl adenylates; an enzymatic mechanism of acetate activation. *J. Biol. Chem. 222*, 991–1013.

(309) de Wet, J. R., Woodt, K. V, Helinski, D. R., and Delucat, M. (1985) Cloning of firefly luciferase cDNA and the expression of active luciferase in Escherichia coli. *Proc. Natl. Acad. Sci. USA 82*, 7870–7873.

(310) de Wet, J. R., Wood, K. V, Deluca, M., and Helinski, D. R. (1987) Firefly Luciferase Gene : Structure and Expression in Mammalian Cells. *Mol. Cell. Biol. 7*, 725–737.

(311) Conti, E., Franks, N. P., and Brick, P. (1996) Crystal structure of firefly luciferase throws light on a superfamily of adenylate-forming enzymes. *Structure 4*, 287–98.

(312) Conti, E., Lloyd, L. F., Akins, J., Franks, N. P., and Brick, P. (1996) Crystallization and preliminary diffraction studies of firefly luciferase from Photinus pyralis. *Acta Crystallogr. Sect. D Biol. Crystallogr. 52*, 876–878.

(313) Sundlov, J. A., Fontaine, D. M., Southworth, T. L., Branchini, B. R., and Gulick, A. M. (2012) Crystal Structure of Firefly Luciferase in a Second Catalytic Conformation Supports a Domain Alternation Mechanism. *Biochemistry 51*, 6493–6495.

(314) White, E. H., McCapra, F., and Field, G. F. (1963) The Structure and Synthesis of Firefly Luciferin. *J. Am. Chem. Soc. 85*, 337–343.

(315) Blank, G. E., Pletcher, J., and Sax, M. (1971) The molecular structure of firefly D-(−)-luciferin: A single crystal x-ray analysis. *Biochem. Biophys. Res. Commun. 42*, 583–588.

(316) McElroy, W. D., and Green, A. (1956) Function of adenosine triphosphate in the activation of luciferin. *Arch. Biochem. Biophys. 64*, 257–271.

(317) Rhodes, W. C., and McElroy, W. D. (1958) Enzymatic synthesis of adenyl-oxyluciferin. *Science 128*, 253–4.

(318) Rhodes, W. C., and McElroy, W. D. (1958) The synthesis and function of luciferyl-adenylate and oxyluciferyl-adenylate. *J. Biol. Chem. 233*, 1528–37.

(319) Seliger, H. H., McElroy, W. D., White, E. H., and Field, G. F. (1961) Stereo-specificity and firefly bioluminescence, a comparison of natural and synthetic luciferins. *Proc. Natl. Acad. Sci. U. S. A. 47*, 1129–34.

(320) Seliger, H. H., and McElroy, W. D. (1962) Chemiluminescence of firefly luciferin without enzyme. *Science 138*, 683–5.

(321) McCapra, F., Chang, Y. C., and Francois, V. P. (1968) The chemiluminescence of a firefly luciferin analogue. *Chem. Commun.* 22–23.

(322) Hopkins, T. A., Seliger, H. H., White, E. H., and Cass, M. W. (1967) Chemiluminescence of firefly luciferin. Model for the bioluminescent reaction and identification of the product excited state. *J. Am. Chem. Soc. 89*, 7148–7150.

(323) Wannlund, J., DeLuca, M., Stempel, K., and Boyer, P. D. (1978) Use of 14C-carboxyl-luciferin in determining the mechanism of the firefly luciferase catalyzed reactions. *Biochem. Biophys. Res. Commun. 81*, 987–992.

(324) Shimomura, O., Goto, T., and Johnson, F. H. (1977) Source of oxygen in the CO(2) produced in the bioluminescent oxidation of firefly luciferin. *Proc. Natl. Acad. Sci. U. S. A. 74*, 2799–802.

(325) White, E. H., Miano, J. D., and Umbreit, M. (1975) Mechanism of firefly luciferin luminescence. *J. Am. Chem. Soc. 97*, 198–200.

(326) Suzuki, N., and Goto, T. (1972) Studies on firefly bioluminescence—II. *Tetrahedron 28*, 4075–4082.

(327) Gates, B. J., and DeLuca, M. (1975) The production of oxyluciferin during the firefly luciferase light reaction. *Arch. Biochem. Biophys. 169*, 616–621.

(328) White, E. H., Steinmetz, M. G., Miano, J. D., Wildes, P. D., and Morland, R. (1980) Chemi- and bioluminescence of firefly luciferin. *J. Am. Chem. Soc. 102*, 3199–3208.

(329) McCapra, F. (1977) Alternative mechanism for dioxetan decomposition. *J. Chem. Soc. Chem. Commun.* 946–948.

(330) Koo, J. A., Schmidt, S. P., and Schuster, G. B. (1978) Bioluminescence of the firefly: key steps in the formation of the electronically excited state for model systems. *Proc. Natl. Acad. Sci. U. S. A. 75*, 30–33.

(331) Seliger, H. H., and McElroy, W. D. (1964) The colors of firefly bioluminescence: enzyme configuration and species specificity. *Proc. Natl. Acad. Sci. U. S. A. 52*, 75–81.

(332) Seliger, H. H., and McElroy, W. D. (1960) Spectral emission and quantum yield of firefly bioluminescence. *Arch. Biochem. Biophys. 88*, 136–141.

(333) White, E. H., Steinmetz, M. G., Miano, J. D., Wildes, P. D., and Morland, R. (1980) Chemi- and bioluminescence of firefly luciferin. *J. Am. Chem. Soc. 102*, 3199–3208.

(334) Branchini, B. R., Murtiashaw, M. H., Magyar, R. A., Portier, N. C., Ruggiero, M. C., and Stroh, J. G. (2002) Yellow-green and red firefly bioluminescence from 5,5-dimethyloxyluciferin. *J. Am. Chem. Soc. 124*, 2112–2113.

(335) McCapra, F. (2000) Chemical generation of excited states: the basis of chemiluminescence and bioluminescence. *Methods Enzymol. 305*, 3–47.

(336) Branchini, B. R., Southworth, T. L., Murtiashaw, M. H., Magyar, R. A., Gonzalez, S. A., Ruggiero, M. C., and Stroh, J. G. (2004) An alternative mechanism of bioluminescence color determination in firefly luciferase. *Biochemistry 43*, 7255–62.

(337) Nakatsu, T., Ichiyama, S., Hiratake, J., Saldanha, A., Kobashi, N., Sakata, K., and Kato, H. (2006) Structural basis for the spectral difference in luciferase bioluminescence. *Nature 440*, 372–376.

(338) Hosseinkhani, S. (2011) Molecular enigma of multicolor bioluminescence of firefly luciferase. *Cell. Mol. Life Sci. 68*, 1167–1182.

(339) Ando, Y., Niwa, K., Yamada, N., Enomoto, T., Irie, T., Kubota, H., Ohmiya, Y., and Akiyama, H. (2008) Firefly bioluminescence quantum yield and colour change by pH-sensitive green emission. *Nat. Photonics 2*, 44–47.

(340) DeLuca, M., and McElroy, W. D. (1974) Kinetics of the firefly luciferase catalyzed reactions. *Biochemistry 13*, 921–5.

(341) Ribeiro, C., and Esteves da Silva, J. C. G. (2008) Kinetics of inhibition of firefly luciferase by oxyluciferin and dehydroluciferyl-adenylate 1085–1090.

(342) Lemasters, J. J., and Hackenbrock, C. R. (1977) Kinetics of Product Inhibition during Firefly Luciferase Luminescence. *Biochemistry 16*, 445–447.

(343) Fraga, H., Esteves Da Silva, J. C. G., and Fontes, R. (2004) Identification of Luciferyl Adenylate and Luciferyl Coenzyme A Synthesized by Firefly Luciferase. *ChemBioChem 5*, 110–115.

(344) Fraga, H., Fernandes, D., Novotny, J., Fontes, R., and Silva, J. C. G. E. da. (2006) Firefly Luciferase Produces Hydrogen Peroxide as a Coproduct in Dehydroluciferyl Adenylate Formation. *ChemBioChem 7*, 929–935.

(345) Fontes, R., Dukhovich, A., Sillero, A., and Sillero, M. a. (1997) Synthesis of dehydroluciferin by firefly luciferase: effect of dehydroluciferin, coenzyme A and nucleoside triphosphates on the luminescent reaction. *Biochem. Biophys. Res. Commun. 237*, 445–450.

(346) Fontes, R., Fernandes, D., Peralta, F., Fraga, H., Maio, I., and Esteves da Silva, J. C. G. (2008) Pyrophosphate and tripolyphosphate affect firefly luciferase luminescence because they act as substrates and not as allosteric effectors. *FEBS J. 275*, 1500–1509.

(347) McElroy, W. D., Hastings, J. W., Coulombre, J., and Sonnenfeld, V. (1953) The mechanism of action of pyrophosphate in firefly luminescence. *Arch. Biochem. Biophys. 46*, 399–416.

(348) Fraga, H., Fernandes, D., Fontes, R., and Esteves da Silva, J. C. G. (2005) Coenzyme A affects firefly luciferase luminescence because it acts as a substrate and not as an allosteric effector. *FEBS J. 272*, 5206–5216.

(349) Airth, R. L., Rhodes, W. C., and McElroy, W. D. (1958) The function of coenzyme A in luminescence. *Biochim. Biophys. Acta 27*, 519–532.

(350) Meiering, E. M., Serrano, L., and Fersht, A. R. (1992) Effect of active site residues in barnase on activity and stability. *J. Mol. Biol. 225*, 585–589.

(351) Tisi, L. C., White, P. J., Squirrell, D. J., Murphy, M. J., Lowe, C. R., and Murray, J. A. H. (2002) Development of a thermostable firefly luciferase. *Anal. Chim. Acta 457*, 115–123.

(352) Docherty, J. (2012) The expression and purification of Firefly luciferase for use as a luminometric indicator in a biological assay, measuring the impact of various inhibitors on the stringent response of intracellular pathogens. M.Chem Project Report, University of Southampton.

(353) Norton, P. T., Merz, R. L., and Leach, F. R. (1981) The inactivation of firefly luciferase by proteolytic enzymes — an assay for proteases. *Biochem. Int. 3*, 457–462.

(354) Ford, S. R., Hall, M. S., and Leach, F. R. (1992) Comparison of properties of commercially available crystalline native and recombinant firefly luciferases. *J. Biolumin. Chemilumin. 7*, 185–193.

(355) Hall, M. S., and Leach, F. R. (1988) Stability of firefly luciferase in Tricine buffer and in a commercial enzyme stabilizer. *J. Biolumin. Chemilumin. 2*, 41–44.

(356) Leach, F. R., and Webster, J. J. (1986) Commercially available firefly luciferase reagents. *Methods Enzym. 133*, 51–70.

(357) Ugarova, N., and Koksharov, M. (2012) Thermostabilization of Firefly Luciferases Using Genetic Engineering, in *Genetic Engineering - Basics, New Applications and Responsibilities* (Prof. Hugo A. Barrera-Saldaña, Ed.), pp 61–92. InTech.

(358) Wood, K. V. (1994) Luciferase assays method. Patent US 5283179 A.

(359) Novy, R., Drott, D., Yaeger, K., and Mierendorf, R. (2001) Overcoming the codon bias of E. coli for enhanced protein expression. *Innovations 12*, 1–3.

(360) Novy, R., Yaeger, K., Monsma, S., and Scott, M. (1999) pTriEx-1 Multisystem Vector for protein expression in E.coli, mammalian, and insect cells. *Innovations 10*, 2–5.

(361) Webster, J. J., Chang, J. C., Manley, E. R., Spivey, H. O., and Leach, F. R. (1980) Buffer effects on ATP analysis by firefly luciferase. *Anal. Biochem. 106*, 7–11.

(362) Lundin, A., Rickardsson, A., and Thore, A. (1976) Continuous monitoring of ATP-converting reactions by purified firefly luciferase. *Anal. Biochem. 75*, 611–620.

(363) Nichols, W. W., Curtis, G. D. W., and Johnston, H. H. (1981) Choice of buffer anion for the assay of adenosine 5'-triphosphate using firefly luciferase. *Anal. Biochem. 114*, 396–397.

(364) Denburg, J. L., and McElroy, W. D. (1970) Anion inhibition of firefly luciferase. *Arch. Biochem. Biophys. 141*, 668–675.

(365) DeLuca, M. (1969) Hydrophobic nature of the active site of firefly luciferase. *Biochemistry 8*, 160–166.

(366) Matthews, J. C., Hori, K., and Cormier, M. J. (1977) Purification and properties of Renilla reniformis luciferase. *Biochemistry 16*, 85–91.

(367) Deluca, M., Wirtz, G. W., and McElroy, W. D. (1964) Role of sulfhydryl groups in firefly luciferase. *Biochemistry 3*, 935–9.

(368) Li, S., Schöneich, C., and Borchardt, R. T. (1995) Chemical instability of protein pharmaceuticals: Mechanisms of oxidation and strategies for stabilization. *Biotechnol.*

Bioeng. 48, 490–500.

(369) Bisswanger, H. (2008) Enzyme kinetics: Principles and methods. Wiley-VCH.

(370) Lemasters, J. J., and Hackenbrock, C. R. (1977) Kinetics of product inhibition during firefly luciferase luminescence. *Biochemistry 16*, 445–447.

(371) Leitão, J. M. M., and Esteves da Silva, J. C. G. (2010) Firefly luciferase inhibition. *J. Photochem. Photobiol. B Biol. 101*, 1–8.

(372) da Silva, L. P., and Esteves da Silva, J. C. G. (2011) Kinetics of inhibition of firefly luciferase by dehydroluciferyl-coenzyme A, dehydroluciferin and l-luciferin. *Photochem. Photobiol. Sci. 10*, 1039–1045.

(373) Ribeiro, C., and Esteves da Silva, J. C. G. (2008) Kinetics of inhibition of firefly luciferase by oxyluciferin and dehydroluciferyl-adenylate. *Photochem. Photobiol. Sci. 7*, 1085–1090.

(374) Copeland, R. A. (2013) Evaluation of Enzyme Inhibitors in Drug Discovery: A Guide for Medicinal Chemists and Pharmacologists 2nd ed. John Wiley & Sons, Inc.

(375) Nocek, B., Kochinyan, S., Proudfoot, M., Brown, G., Evdokimova, E., Osipiuk, J., Edwards, A. M., Savchenko, A., Joachimiak, A., and Yakunin, A. F. (2008) Polyphosphate-dependent synthesis of ATP and ADP by the family-2 polyphosphate kinases in bacteria. *Proc. Natl. Acad. Sci. U. S. A. 105*, 17730–5.

(376) Iversen, P. W., Beck, B., Chen, Y.-F., Dere, W., Devanarayan, V., Eastwood, B. J., Farmen, M. W., Iturria, S. J., Montrose, C., Moore, R. a., Weidner, J. R., and Sittampalam, G. S. (2012) HTS Assay Validation, in *Assay Guidance Manual [Internet]* (Sittampalam GS, Coussens NP, Nelson H, et al, Ed.), pp 1–31. Eli Lilly & Company and the National Center for Advancing Translational Sciences.

(377) Robertson, J. G. (2005) Mechanistic basis of enzyme-targeted drugs. *Biochemistry 44*, 5561–71.

(378) Copeland, R. A., Harpel, M. R., and Tummino, P. (2007) Targeting enzyme inhibitors in drug discovery. *Expert Opin. Ther. Targets 11*, 967–978.

(379) Copeland, R. A. (2003) Mechanistic considerations in high-throughput screening. *Anal. Biochem. 320*, 1–12.

(380) Strelow, J., Dewe, W., Iversen, P. W., Brooks, H. B., Radding, J. A., McGee, J., and Weidner, J. (2012) Mechanism of Action assays for Enzymes, in *Assay Guidance Manual [Internet]* (Sittampalam GS, Coussens NP, Nelson H, et al, Ed.), pp 1–27. Eli Lilly & Company and the National Center for Advancing Translational Sciences.

(381) Bogoyevitch, M., and Fairlie, D. (2007) A new paradigm for protein kinase inhibition: blocking phosphorylation without directly targeting ATP binding. *Drug Discov. Today 12*, 622–633.

(382) Wu, G., Yuan, Y., and Hodge, C. N. (2003) Determining Appropriate Substrate Conversion for Enzymatic Assays in High-Throughput Screening. *J. Biomol. Screen. 8*, 694–700.

(383) Wu, G., Yuan, Y., and Hodge, C. N. (2003) Determining appropriate substrate conversion for enzymatic assays in high-throughput screening. *J. Biomol. Screen. Off. J. Soc. Biomol. Screen. 8*, 694–700.

(384) Malo, N., Hanley, J. a, Cerquozzi, S., Pelletier, J., and Nadon, R. (2006) Statistical practice in high-throughput screening data analysis. *Nat. Biotechnol. 24*, 167–175.

(385) Brideau, C., Gunter, B., Pikounis, B., and Liaw, A. (2003) Improved statistical methods for hit selection in high-throughput screening. *J. Biomol. Screen. 8*, 634–647.

(386) Goktug, A. N., Chai, C. S., and Che, T. (2013) Data Analysis Approaches in High Throughput Screening, in *Drug Discovery* (El-Shemy, H. A., Ed.), pp 201–226. InTech.

(387) Huber, P. J., and Ronchetti, E. M. (2009) Robust Statistics 2nd ed. John Wiley & Sons, Inc., Hoboken, NJ, USA.

(388) Tukey, J. W. (1977) Exploratory Data Analysis. Addison-Wesley, Reading, MA, USA.

(389) Zhang, X. D., Yang, X. C., Chung, N., Gates, A., Stec, E., Kunapuli, P., Holder, D. J., Ferrer, M., and Espeseth, A. S. (2006) Robust statistical methods for hit selection in RNA interference high-throughput screening experiments. *Pharmacogenomics 7*, 299–309.

(390) Sittampalam, G. S., Coussens, N. P., Nelson, H., Arkin, M. R., Auld, D. S., Austin, C., Bejcek, B., Glicksman, M., Inglese, J., Iversen, P. W., Li, Z., McGee, J., McManus, O., Minor, L., Napper, A., Peltier, J. M., Riss, T., Trask, O. J. J., and Weidner, J. (2004) Assay Guidance Manual. *[Internet]* (Sittampalam, G. S., Coussens, N. P., Nelson, H., Arkin, M. R., Auld, D. S., Austin, C., Bejcek, B., Glicksman, M., Inglese, J., Iversen, P. W., Li, Z., McGee, J., McManus, O., Minor, L., Napper, A., Peltier, J. M., Riss, T., Trask, O. J. J., and Weidner, J., Eds.). Eli Lilly & Company and the National Center for Advancing Translational Sciences.

(391) Macarron, R., Banks, M. N., Bojanic, D., Burns, D. J., Cirovic, D. A., Garyantes, T., Green, D. V. S., Hertzberg, R. P., Janzen, W. P., Paslay, J. W., Schopfer, U., and Sittampalam, G. S. (2011) Impact of high-throughput screening in biomedical reseaarch. *Nat. Rev. Drug Discov. 10*, 188–195.

(392) Dranchak, P., MacArthur, R., Guha, R., Zuercher, W. J., Drewry, D. H., Auld, D. S., and Inglese, J. (2013) Profile of the GSK Published Protein Kinase Inhibitor Set Across ATP-Dependent and-Independent Luciferases: Implications for Reporter-Gene Assays. *PLoS One* (Jung, M., Ed.) *8*, e57888.

(393) Moukha-chafiq, O., and Reynolds, R. C. (2013) Parallel solution-phase synthesis of an adenosine antibiotic analog library. *ACS Comb. Sci. 15*, 147–52.

(394) Moukha-Chafiq, O., and Reynolds, R. C. (2014) Synthesis and General Biological Activity of a Small Adenosine-5′-(Carboxamide and Sulfanilamide) Library. *Nucleosides, Nucleotides and Nucleic Acids 33*, 709–729.

(395) Moukha-Chafiq, O., and Reynolds, R. C. (2014) Parallel solution-phase synthesis and general biological activity of a uridine antibiotic analog library. *ACS Comb. Sci. 16*, 232–237.

(396) Moukha-Chafiq, O., and Reynolds, R. C. (2014) Synthesis of novel Peptidyl adenosine antibiotic analogs. *Nucleosides, Nucleotides and Nucleic Acids 33*, 53–63.

(397) Harpel, M. R. (2009) Wheat from Chaff: General and Mechanistic Triage of Screening Hits for Enzyme Targets, in *In Handbook of Drug Screening* (Seethala, R., and Zhang, L., Eds.) 2nd ed., pp 269–297. Informa Healthcare.

(398) Feng, B. Y., Simeonov, A., Jadhav, A., Babaoglu, K., Inglese, J., Shoichet, B. K., and Austin, C. P. (2007) A high-throughput screen for aggregation-based inhibition in a large compound library. *J. Med. Chem. 50*, 2385–2390.

(399) Lo, M. C., Aulabaugh, A., Jin, G., Cowling, R., Bard, J., Malamas, M., and Ellestad, G. (2004) Evaluation of fluorescence-based thermal shift assays for hit identification in drug discovery. *Anal. Biochem. 332*, 153–159.

(400) Pantoliano, M. W., Petrella, E. C., Kwasnoski, J. D., Lobanov, V. S., Myslik, J., Graf, E., Carver, T., Asel, E., Springer, B. a, Lane, P., and Salemme, F. R. (2001) High-Density Miniaturized Thermal Shift Assays as a General Strategy for Drug Discovery. *J. Biomol. Screen. 6*, 429–440.

(401) Niesen, F. H., Berglund, H., and Vedadi, M. (2007) The use of differential scanning fluorimetry to detect ligand interactions that promote protein stability. *Nat. Protoc. 2*, 2212–2221.

(402) Bergsdorf, C., and Ottl, J. (2010) Affinity-based screening techniques: their impact and benefit to increase the number of high quality leads. *Expert Opin. Drug Discov. 5*, 1095–1107.

(403) Simeonov, A. (2013) Recent developments in the use of differential scanning fluorometry in protein and small molecule discovery and characterization. *Expert Opin. Drug Discov. 8*, 1071–1082.

(404) Schellman, J. A. (1997) Temperature, stability, and the hydrophobic interaction. *Biophys. J. 73*, 2960–4.

(405) Holdgate, G. A., and Ward, W. H. J. (2005) Measurements of binding thermodynamics in drug discovery. *Drug Discov. Today 10*, 1543–1550.

(406) Poklar, N., Lah, J., Salobir, M., Maček, P., and Vesnaver, G. (1997) pH and Temperature-Induced Molten Globule-Like Denatured States of Equinatoxin II: A Study by UV-Melting, DSC, Far- and Near-UV CD Spectroscopy, and ANS Fluorescence †. *Biochemistry 36*, 14345–14352.

(407) Senisterra, G. A., Markin, E., Yamazaki, K., Hui, R., Vedadi, M., and Awrey, D. E. (2006) Screening for Ligands Using a Generic and High-Throughput Light-Scattering-Based Assay. *J. Biomol. Screen. 11*, 940–948.

(408) Vedadi, M., Niesen, F. H., Allali-Hassani, A., Fedorov, O. Y., Finerty, P. J., Wasney, G. A., Yeung, R., Arrowsmith, C., Ball, L. J., Berglund, H., Hui, R., Marsden, B. D., Nordlund, P., Sundstrom, M., Weigelt, J., and Edwards, A. M. (2006) Chemical screening methods to identify ligands that promote protein stability, protein crystallization, and structure determination. *Proc. Natl. Acad. Sci. U. S. A. 103*, 15835–40.

(409) Matulis, D., Kranz, J. K., Salemme, F. R., and Todd, M. J. (2005) Thermodynamic Stability of Carbonic Anhydrase: Measurements of Binding Affinity and Stoichiometry Using ThermoFluor. *Biochemistry 44*, 5258–5266.

(410) Waldron, T. T., and Murphy, K. P. (2003) Stabilization of proteins by ligand binding: application to drug screening and determination of unfolding energetics. *Biochemistry 42*, 5058–64.

(411) Fedorov, O., Niesen, F. H., and Knapp, S. (2012) Kinase inhibitor selectivity profiling using differential scanning fluorimetry. *Methods Mol. Biol. 795*, 109–118.

(412) Layton, C. J., and Hellinga, H. W. (2011) Quantitation of protein-protein interactions by thermal stability shift analysis. *Protein Sci. 20*, 1439–1450.

(413) Zubriene, A., Matuliene, J., Baranauskiene, L., Jachno, J., Torresan, J., Michailoviene, V., Cimmperman, P., and Matulis, D. (2009) Measurement of nanomolar dissociation constants by titration calorimetry and thermal shift assay - radicicol binding to Hsp90 and ethoxzolamide binding to CAII. *Int. J. Mol. Sci. 10*, 2662–80.

(414) Vivoli, M., Novak, H. R., Littlechild, J. A., and Harmer, N. J. (2014) Determination of Protein-ligand Interactions Using Differential Scanning Fluorimetry. *J. Vis. Exp.* 1–13.

(415) Garbett, N. C., and Chaires, J. B. (2012) Thermodynamic studies for drug design and screening. *Expert Opin. Drug Discov. 7*, 299–314.

(416) Hau, J. C., Fontana, P., Zimmermann, C., De Pover, A., Erdmann, D., and Chène, P. (2011) Leveraging the contribution of thermodynamics in drug discovery with the help of fluorescence-based thermal shift assays. *J. Biomol. Screen. 16*, 552–6.

(417) Au, J. L., Su, M. H., and Wientjes, M. G. (1989) Extraction of intracellular nucleosides and nucleotides with acetonitrile. *Clin. Chem. 35*, 48–51.

(418) Giannattasio, S., Gagliardi, S., Samaja, M., and Marra, E. (2003) Simultaneous determination of purine nucleotides, their metabolites and beta-nicotinamide adenine dinucleotide in cerebellar granule cells by ion-pair high performance liquid chromatography. *Brain Res. Protoc. 10*, 168–174.

(419) Huang, D., Zhang, Y., and Chen, X. (2003) Analysis of intracellular nucleoside triphosphate levels in normal and tumor cell lines by high-performance liquid chromatography. *J. Chromatogr. B 784*, 101–109.

(420) Volonté, M. G., Yuln, G., Quiroga, P., and Consolini, A. E. (2004) Development of an HPLC method for determination of metabolic compounds in myocardial tissue. *J. Pharm. Biomed. Anal. 35*, 647–653.

(421) Czarnecka, J., Cieślak, M., and Michał, K. (2005) Application of solid phase extraction and high-performance liquid chromatography to qualitative and quantitative analysis of nucleotides and nucleosides in human cerebrospinal fluid. *J. Chromatogr. B 822*, 85–90.

(422) Vela, J. E., Olson, L. Y., Huang, A., Fridland, A., and Ray, A. S. (2007) Simultaneous quantitation of the nucleotide analog adefovir, its phosphorylated anabolites and 2′-deoxyadenosine triphosphate by ion-pairing LC/MS/MS. *J. Chromatogr. B 848*, 335–343.

(423) Yeung, P., Ding, L., and Casley, W. L. (2008) HPLC assay with UV detection for determination of RBC purine nucleotide concentrations and application for biomarker study in vivo. *J. Pharm. Biomed. Anal. 47*, 377–382.

(424) Jagannathan, V., Kaur, P., and Datta, S. (2010) Polyphosphate Kinase from M. tuberculosis: An Interconnect between the Genetic and Biochemical Role. *PLoS One* (Ojcius, D. M., Ed.) *5*, e14336.

(425) Cohen, S., Megherbi, M., Jordheim, L. P., Lefebvre, I., Perigaud, C., Dumontet, C., and Guitton, J. (2009) Simultaneous analysis of eight nucleoside triphosphates in cell lines by liquid chromatography coupled with tandem mass spectrometry. *J. Chromatogr. B 877*, 3831–3840.

(426) Coulier, L., Gerritsen, H., van Kampen, J. J. A., Reedijk, M. L., Luider, T. M., Osterhaus, A. D. M. E., Gruters, R. A., and Brüll, L. (2011) Comprehensive analysis of the intracellular metabolism of antiretroviral nucleosides and nucleotides using liquid chromatography–tandem mass spectrometry and method improvement by using ultra performance liquid chromatography. *J. Chromatogr. B 879*, 2772–2782.

(427) Ganzera, M., Vrabl, P., Wörle, E., Burgstaller, W., and Stuppner, H. (2006) Determination of adenine and pyridine nucleotides in glucose-limited chemostat cultures of Penicillium simplicissimum by one-step ethanol extraction and ion-pairing liquid chromatography. *Anal. Biochem. 359*, 132–140.

(428) Cichna, M., Daxecker, H., and Raab, M. (2003) Determination of 18 nucleobases, nucleosides and nucleotides in human peripheral blood mononuclear cells by isocratic solvent-generated ion-pair chromatography. *Anal. Chim. Acta 481*, 245–253.

(429) Cichna, M., Raab, M., Daxecker, H., Griesmacher, A., Müller, M. ., and Markl, P. (2003) Determination of fifteen nucleotides in cultured human mononuclear blood and umbilical vein endothelial cells by solvent generated ion-pair chromatography. *J. Chromatogr. B 787*, 381–391.

(430) Uesugi, T., Sano, K., Uesawa, Y., Ikegami, Y., and Mohri, K. (1997) Ion-pair reversed-phase high-performance liquid chromatography of adenine nucleotides and nucleoside using triethylamine as a counterion. *J. Chromatogr. B Biomed. Sci. Appl. 703*, 63–74.

(431) Apffel, A., Chakel, J. a, Fischer, S., Lichtenwalter, K., and Hancock, W. S. (1997) Analysis of Oligonucleotides by HPLC—Electrospray Ionization Mass Spectrometry. *Anal. Chem. 69*, 1320–1325.

(432) Ghorbaniaghdam, A., Chen, J., Henry, O., and Jolicoeur, M. (2014) Analyzing Clonal Variation of Monoclonal Antibody-Producing CHO Cell Lines Using an In Silico Metabolomic Platform. *PLoS One 9*, e90832.

(433) Cordell, R. L., Hill, S. J., Ortori, C. A., and Barrett, D. A. (2008) Quantitative profiling of nucleotides and related phosphate-containing metabolites in cultured mammalian cells by liquid chromatography tandem electrospray mass spectrometry. *J. Chromatogr. B 871*, 115–124.

(434) Pruvost, A., Théodoro, F., Agrofoglio, L., Negredo, E., and Bénech, H. (2008)

Specificity enhancement with LC-positive ESI-MS/MS for the measurement of nucleotides: application to the quantitative determination of carbovir triphosphate, lamivudine triphosphate and tenofovir diphosphate in human peripheral blood mononuclear cells. *J. Mass Spectrom. 43*, 224–233.

(435) Qian, T., Cai, Z., and Yang, M. S. (2004) Determination of adenosine nucleotides in cultured cells by ion-pairing liquid chromatography-electrospray ionization mass spectrometry. *Anal. Biochem. 325*, 77–84.

(436) Henneré, G., Becher, F., Pruvost, A., Goujard, C., Grassi, J., and Benech, H. (2003) Liquid chromatography–tandem mass spectrometry assays for intracellular deoxyribonucleotide triphosphate competitors of nucleoside antiretrovirals. *J. Chromatogr. B 789*, 273–281.

(437) Cai, Z., Song, F., and Yang, M. . (2002) Capillary liquid chromatographic–high-resolution mass spectrometric analysis of ribonucleotides. *J. Chromatogr. A 976*, 135–143.

(438) Steinberg, T. H., Jones, L. J., Haugland, R. P., and Singer, V. L. (1996) SYPRO orange and SYPRO red protein gel stains: one-step fluorescent staining of denaturing gels for detection of nanogram levels of protein. *Anal. Biochem. 239*, 223–37.

(439) Steinberg, T. H., White, H. M., and Singer, V. L. (1997) Optimal filter combinations for photographing SYPRO orange or SYPRO red dye-stained gels. *Anal. Biochem. 248*, 168–72.

(440) Steinberg, T. H., Haugland, R. P., and Singer, V. L. (1996) Applications of SYPRO orange and SYPRO red protein gel stains. *Anal. Biochem. 239*, 238–245.

(441) Cherry, J. J., Rietz, A., Malinkevich, A., Liu, Y., Xie, M., Bartolowits, M., Davisson, V. J., Baleja, J. D., and Androphy, E. J. (2013) Structure Based Identification and Characterization of Flavonoids That Disrupt Human Papillomavirus-16 E6 Function. *PLoS One* (Zheng, Z.-M., Ed.) *8*, e84506.

(442) Huttu, J., Singh, B. K., Bhargav, S. P., Sattler, J. M., Schüler, H., and Kursula, I. (2010) Crystallization and preliminary structural characterization of the two actin-depolymerization factors of the malaria parasite. *Acta Crystallogr. Sect. F Struct. Biol. Cryst. Commun. 66*, 583–587.

(443) Krishna, S. N., Luan, C.-H., Mishra, R. K., Xu, L., Scheidt, K. a., Anderson, W. F., and Bergan, R. C. (2013) A Fluorescence-Based Thermal Shift Assay Identifies Inhibitors of Mitogen Activated Protein Kinase Kinase 4. *PLoS One* (Jung, M., Ed.) *8*, e81504.

(444) McGovern, S. L., Caselli, E., Grigorieff, N., and Shoichet, B. K. (2002) A Common Mechanism Underlying Promiscuous Inhibitors from Virtual and High-Throughput Screening. *J. Med. Chem. 45*, 1712–1722.

(445) Brian Y Feng, Anang Shelat, Thompson N Dorman, R Kip Guy, and Brian K Shoichet. (2005) High-throughput assays for promiscuous inhibitors. *Nat. Chem. Biol. 1*, 146–148.

(446) Brandt, R. B., Laux, J. E., and Yates, S. W. (1987) Calculation of inhibitor Ki and inhibitor type from the concentration of inhibitor for 50% inhibition for Michaelis-Menten

enzymes. *Biochem. Med. Metab. Biol. 37*, 344–349.

(447) Silverman, R. B., and Holladay, M. W. (2004) Enzyme Inhibition and Inactivation, in *The Organic Chemistry of Drug Design and Drug Action* 3rd ed., pp 227–321. Elsevier.

(448) Singh, J., Petter, R. C., Baillie, T. a, and Whitty, A. (2011) The resurgence of covalent drugs. *Nat. Rev. Drug Discov. 10*, 307–317.

(449) Copeland, R. A., Basavapathruni, A., Moyer, M., and Scott, M. P. (2011) Impact of enzyme concentration and residence time on apparent activity recovery in jump dilution analysis. *Anal. Biochem. 416*, 206–210.

(450) Jung, J. H., Lee, M. H., Kim, H. J., Jung, H. S., Lee, S. Y., Shin, N. R., No, K., and Kim, J. S. (2009) Metal ion induced FRET On–Off in naphthyl-pyrenyl pendent tetrahomodioxacalix[4]arene. *Tetrahedron Lett. 50*, 2013–2016.

(451) Kand, D., Chauhan, D. P., Lahiri, M., and Talukdar, P. (2013) δ-Unsaturated γ-amino acids: enantiodivergent synthesis and cell imaging studies. *Chem. Commun. 49*, 3591.

(452) Wube, A. a, Hüfner, A., Thomaschitz, C., Blunder, M., Kollroser, M., Bauer, R., and Bucar, F. (2011) Design, synthesis and antimycobacterial activities of 1-methyl-2-alkenyl-4(1H)-quinolones. *Bioorg. Med. Chem. 19*, 567–579.

(453) Kayser, M. M., Hatt, K. L., and Hooper, D. L. (1991) An NMR study of the structure and reactivity of phosphonium ylides stabilized by a carbonyl function. *Can. J. Chem. 69*, 1929–1939.

(454) Guiney, D., Gibson, C. L., and Suckling, C. J. (2003) Syntheses of highly functionalised 6-substituted pteridines. *Org. Biomol. Chem. 1*, 664–75.

(455) Manley, D. W., McBurney, R. T., Miller, P., Walton, J. C., Mills, A., and O'Rourke, C. (2014) Titania-promoted carboxylic acid alkylations of alkenes and cascade addition-cyclizations. *J. Org. Chem. 79*, 1386–98.

(456) Brovarets, V. S., Golovenko, A. V, Sviripa, V. N., Zyuz, K. B., Chernega, A. N., and Drach, B. S. (2004) New transformations of the reaction product f 4-(Dichloromethylene)-2-phenyl-1,3-oxazol-5(4H)-one with Triphenylphosphine. *Russ. J. Gen. Chem. 74*, 1328–1334.

(457) Schlindwein, H., and Diehl, K. (1989) Intramolekulare Diels-Alder-Reaktion bei Allencarboxaniliden; Konkurrenz des Anilinkerns mit ,,benzylisch-gebundenen" Aromaten 577–584.

(458) Byrne, P. A., and Gilheany, D. G. (2016) The Mechanism of Phosphonium Ylide Alcoholysis and Hydrolysis: Concerted Addition of the O—H Bond Across the P=C Bond. *Chem. - A Eur. J. 22*, 9140–9154.

(459) Schnell, A., Dawber, J. G., and Tebby, J. C. (1976) The mechanism of hydrolysis of phosphonium ylides. *J. Chem. Soc. Perkin Trans. 2 0*, 633.

(460) Thompson, S., McMahon, S. A., Naismith, J. H., and O'Hagan, D. (2016) Exploration of a potential difluoromethyl-nucleoside substrate with the fluorinase enzyme. *Bioorg. Chem. 64*, 37–41.

(461) Liu, W., Bodlenner, A., and Rohmer, M. (2015) Hemisynthesis of deuteriated adenosylhopane and conversion into bacteriohopanetetrol by a cell-free system from Methylobacterium organophilum. *Org. Biomol. Chem. 13*, 3393–3405.

(462) Zhang, X., Bernet, B., and Vasella, A. (2006) Oligonucleotide analogues with integrated bases and backbone. Part 13. Synthesis and association of ethynylene-linked self-complementary dimers. *Helv. Chim. Acta 89*, 2861–2917.

(463) Wang, J.-F., Yang, X.-D., Zhang, L.-R., Yang, Z.-J., and Zhang, L.-H. (2004) Synthesis and biological activities of 5′-ethylenic and acetylenic modified L-nucleosides and isonucleosides. *Tetrahedron 60*, 8535–8546.

(464) Rozners, E., Katkevica, D., Bizdena, E., and Strömberg, R. (2003) Synthesis and properties of RNA analogues having amides as interuridine linkages at selected positions. *J. Am. Chem. Soc. 125*, 12125–12136.

(465) Gunji, H., and Vasella, A. (2000) Oligonucleosides with a nucleobase-including backbone, Part 2. Synthesis and structure determination of adenosine-derived monomers. *Helv. Chim. Acta 83*, 1331–1345.

(466) Chen, X., Wiemer, A. J., Hohl, R. J., and Wiemer, D. F. (2002) Stereoselective Synthesis of the 5‘-Hydroxy-5‘-phosphonate Derivatives of Cytidine and Cytosine Arabinoside. *J. Org. Chem. 67*, 9331–9339.

(467) Danishefsky, S. J., DeNinno, S. L., Chen, S. H., Boisvert, L., and Barbachyn, M. (1989) Fully synthetic stereoselective routes to the differentially protected subunits of the tunicamycins. *J. Am. Chem. Soc. 111*, 5810–5818.

(468) Vrudhula, V. M., Kappler, F., Afshar, C., Ginell, S. L., Lessinger, L., and Hampton, A. (1989) Approaches to isozyme-specific inhibitors. 16. A novel methyl-C5’ covalent adduct of L-ethionine and beta,gamma-imido-ATP as a potent multisubstrate inhibitor of rat methionine adenosyltransferases. *J. Med. Chem. 32*, 885–890.

(469) Ranganathan, R., Jones, G. H., and Moffatt, J. G. (1974) Novel analogs of nucleoside 3’,5’-cyclic phosphates. I. 5’-Mono- and dimethyl analogs of adenosine 3’,5’-cyclic phosphate. *J. Org. Chem. 39*, 290–298.

(470) Gibbons, G. S., Showalter, H. D., and Nikolovska-Coleska, Z. (2015) Novel Carboxaldehyde Mediated Synthetic Pathway for 5′-Amino Adenosine Analogues. *Nucleosides, Nucleotides and Nucleic Acids 34*, 348–360.

(471) Salinas, J. C., Migawa, M. T., Merner, B. L., and Hanessian, S. (2014) Alternative Syntheses of (S)-cEt-BNA: A Key Constrained Nucleoside Component of Bioactive Antisense Gapmer Sequences. *J. Org. Chem. 79*, 11651–11660.

(472) Sun, T., Deutsch, C., and Krause, N. (2012) Combined coinage metal catalysis in natural product synthesis: total synthesis of (+)-varitriol and seven analogs. *Org. Biomol. Chem. 10*, 5965–70.

(473) Shen, F., Li, X., Zhang, X., Yin, Q., Qin, Z., Chen, H., Zhang, J., and Ma, Z. (2011) Microwave-assisted synthesis of dinucleoside analogues containing a thiazolidin-4-one linkage via one-pot tandem Staudinger/aza-Wittig/cyclization. *Org. Biomol. Chem. 9*,

5766–72.

(474) Wong, J. H., Sahni, U., Li, Y., Chen, X., and Gervay-Hague, J. (2009) Synthesis of sulfone-based nucleotide isosteres: identification of CMP-sialic acid synthetase inhibitors. *Org. Biomol. Chem. 7*, 27–29.

(475) Douglass, J. G., DeCamp, J. B., Fulcher, E. H., Jones, W., Mahanty, S., Morgan, A., Smirnov, D., Boyer, J. L., and Watson, P. S. (2008) Adenosine analogues as inhibitors of P2Y12 receptor mediated platelet aggregation. *Bioorg. Med. Chem. Lett. 18*, 2167–2171.

(476) Groziak, M. P., and Thomas, D. W. (2002) Synthesis of New Transglycosidically Tethered 5‘-Nucleotides Constrained to a Highly Biologically Relevant Profile. *J. Org. Chem. 67*, 2152–2159.

(477) Groziak, M., and Ronghui, L. (2000) The 5′,6-Oxomethylene Transglycosidic Tether for Conformational Restriction of Pyrimidine Ribonucleosides. Investigation of 6-Formyl- and 6-(Hydroxymethyl)uridine 5′-Carboxaldehydes. *Tetrahedron 56*, 9885–9893.

(478) Dess, D. B., and Martin, J. C. (1983) Readily accessible 12-I-5 oxidant for the conversion of primary and secondary alcohols to aldehydes and ketones. *J. Org. Chem. 48*, 4155–4156.

(479) Wang, G., Deval, J., Hong, J., Dyatkina, N., Prhavc, M., Taylor, J., Fung, A., Jin, Z., Stevens, S. K., Serebryany, V., Liu, J., Zhang, Q., Tam, Y., Chanda, S. M., Smith, D. B., Symons, J. A., Blatt, L. M., and Beigelman, L. (2015) Discovery of 4′-Chloromethyl-2′-deoxy-3′,5′-di- O -isobutyryl-2′-fluorocytidine (ALS-8176), A First-in-Class RSV Polymerase Inhibitor for Treatment of Human Respiratory Syncytial Virus Infection. *J. Med. Chem. 58*, 1862–1878.

(480) Ragab, A. E., Grüschow, S., Tromans, D. R., and Goss, R. J. M. (2011) Biogenesis of the Unique 4′,5′-Dehydronucleoside of the Uridyl Peptide Antibiotic Pacidamycin. *J. Am. Chem. Soc. 133*, 15288–15291.

(481) Nencka, R., Sinnaeve, D., Karalic, I., Martins, J. C., and Van Calenbergh, S. (2010) Synthesis of C-6-substituted uridine phosphonates through aerobic ligand-free Suzuki–Miyaura cross-coupling. *Org. Biomol. Chem. 8*, 5234.

(482) Lerner, C., Masjost, B., Ruf, A., Gramlich, V., Jakob-Roetne, R., Zürcher, G., Borroni, E., and Diederich, F. (2003) Bisubstrate inhibitors for the enzyme catechol-O-methyltransferase (COMT): influence of inhibitor preorganisation and linker length between the two substrate moieties on binding affinity. *Org. Biomol. Chem. 1*, 42–9.

(483) More, J. D., and Finney, N. S. (2002) A simple and advantageous protocol for the oxidation of alcohols with o-iodoxybenzoic acid (IBX). *Org. Lett. 4*, 3001–3003.

(484) Zhdankin, V. V, and Stang, P. J. (2002) Recent developments in the chemistry of polyvalent iodine compounds. *Chem. Rev. 102*, 2523–84.

(485) Leonori, D., and Seeberger, P. H. (2012) De Novo Synthesis of the Bacterial 2-Amino-2,6-Dideoxy Sugar Building Blocks d -Fucosamine, d -Bacillosamine, and d -Xylo-6-deoxy-4-ketohexosamine. *Org. Lett. 14*, 4954–4957.

(486) Davis, F. A., Kasu, P. V. N., Sundarababu, G., and Qi, H. (1997) Nonracemic α-Fluoro Aldehydes: Asymmetric Synthesis of 4-Deoxy-4-fluoro-D-arabinopyranose. *J. Org. Chem. 62*, 7546–7547.

(487) Davis, F. A., Srirajan, V., and Titus, D. D. (1999) Efficient Asymmetric Synthesis of β-Fluoro α-Amino Acids. *J. Org. Chem. 64*, 6931–6934.

(488) Tojo, G., and Fernandez, M. (2006) Hypervalent Iodine Compounds, in *Oxidation of alcohols to aldehydes and ketones: a guide to current common practice*, pp 181–214. Springer-Verlag.

(489) Munari, S. De, Frigerio, M., and Santagostino, M. (1996) Hypervalent Iodine Oxidants: Structure and Kinetics of the Reactive Intermediates in the Oxidation of Alcohols and 1,2-Diols by o-Iodoxybenzoic Acid (IBX) and Dess-Martin Periodinane. A Comparative 1H-NMR Study. *J. Org. Chem. 61*, 9272–9279.

(490) Nicolaou, K. C., Baran, P. S., Kranich, R., Zhong, Y., Sugita, K., and Zou, N. (2001) Mechanistic Studies of Periodinane-Mediated Reactions of Anilides and Related Systems. *Angew. Chem. Int. Ed. Engl. 40*, 202–206.

(491) Dess, D. B., and Martin, J. C. (1991) A useful 12-I-5 triacetoxyperiodinane (the Dess-Martin periodinane) for the selective oxidation of primary or secondary alcohols and a variety of related 12-I-5 species. *J. Am. Chem. Soc. 113*, 7277–7287.

(492) Meyer, S. D., and Schreiber, S. L. (1994) Acceleration of the Dess-Martin Oxidation by Water. *J. Org. Chem. 59*, 7549–7552.

(493) Majik, M., Tilvi, S., and Parvatkar, P. (2014) Recent Developments Towards the Synthesis of Varitriol: An Antitumour Agent from Marine Derived Fungus Emericella Variecolor. *Curr. Org. Synth. 11*, 268–287.

(494) Sarabia, F., Vivar-García, C., García-Ruiz, C., Martín-Ortiz, L., and Romero-Carrasco, A. (2012) Exploring the Chemistry of Epoxy Amides for the Synthesis of the 2″-epi -Diazepanone Core of Liposidomycins and Caprazamycins. *J. Org. Chem. 77*, 1328–1339.

(495) Kumamoto, H., Ogamino, J., Tanaka, H., Suzuki, H., Haraguchi, K., Miyasaka, T., Yokomatsu, T., and Shibuya, S. (2001) Radical-mediated furanose ring reconstruction from 2′,3′- seco -uridine. *Tetrahedron 57*, 3331–3341.

(496) Hatanaka, Y., Hashimoto, M., I.-P. Jwa Hidari, K., Sanai, Y., Nagai, Y., and Kanaoka, Y. (1996) Synthesis of a Carbon-linked CMP-NANA Analog and Its Inhibitory Effects on GM3 and GD3 Synthases. *Heterocycles 43*, 531.

(497) Jun-Dong, Z., and Li-He, Z. (1990) Application of Wittig Reaction to Adenosine Derivatives. *Synthesis (Stuttg). 1990*, 909–911.

(498) Suzuki, Y., Matsuda, A., and Ueda, T. (1987) Synthesis of 6,5'-cyclo-5'-deoxy-5'(R and S)-(2-hydroxyethyl)-uridines (Nucleosides and Nucleotides. LXXIII). *Chem. Pharm. Bull. 35*, 1808–1811.

(499) Matsuda, A., and Ueda, T. (1986) Synthesis of 8,6'-cyclo-6'-deoxyhexofuranosyladenines: adenosines fixed in an anti-conformation (Nucleosides and

nucleotides. LXVI). *Chem. Pharm. Bullettin 34*, 1578.

(500) Walker, T. E., Follmann, H., and Hogenkamp, H. P. C. (1973) The synthesis of 5′-C-alkyl analogs of adenosine. *Carbohydr. Res. 27*, 225–234.

(501) Jones, G. H., and Moffatt, J. G. (1968) The synthesis of 6'-deoxyhomonucleoside 6'-phosphonic acids. *J. Am. Chem. Soc. 90*, 5337–5338.

(502) Lesiak, K., Watanabe, K. A., Majumdar, A., Seidman, M., Vanderveen, K., Goldstein, B. M., and Pankiewicz, K. W. (1997) Synthesis of Nonhydrolyzable Analogues of Thiazole-4-carboxamide and Benzamide Adenine Dinucleotide Containing Fluorine Atom at the C2‘ of Adenine Nucleoside: Induction of K562 Differentiation and Inosine Monophosphate Dehydrogenase Inhibitory Activity. *J. Med. Chem. 40*, 2533–2538.

(503) Hun Park, K., Jin Yoon, Y., and Gyeong Lee, S. (1994) Efficient cleavage of terminal acetonide group: Chirospecific synthesis of 2,5-dideoxy-2,5-imino-D-mannitol. *Tetrahedron Lett. 35*, 9737–9740.

(504) Santos, M. M. M., and Moreira, R. (2007) Michael acceptors as cysteine protease inhibitors. *Mini Rev. Med. Chem. 7*, 1040–50.

(505) Hernandez, A. A., and Roush, W. R. (2002) Recent advances in the synthesis, design and selection of cysteine protease inhibitors. *Curr. Opin. Chem. Biol. 6*, 459–465.

(506) Bauer, R. A. (2015) Covalent inhibitors in drug discovery: from accidental discoveries to avoided liabilities and designed therapies. *Drug Discov. Today 20*, 1061–1073.

(507) González-Bello, C. (2016) Designing Irreversible Inhibitors-Worth the Effort? *ChemMedChem 11*, 22–30.

(508) Liu, Q., Sabnis, Y., Zhao, Z., Zhang, T., Buhrlage, S. J., Jones, H., and Gray, N. S. (2013) Developing irreversible inhibitors of the protein kinase cysteinome. *Chem. Biol. 20*, 146–159.

(509) Powers, J. C., Asgian, J. L., Ekici, Ö. D., and James, K. E. (2002) Irreversible Inhibitors of Serine, Cysteine, and Threonine Proteases. *Chem. Rev. 102*, 4639–4750.

(510) Lee, C.-U., and Grossmann, T. N. (2012) Reversible Covalent Inhibition of a Protein Target. *Angew. Chemie Int. Ed. 51*, 8699–8700.

(511) Serafimova, I. M., Pufall, M. A., Krishnan, S., Duda, K., Cohen, M. S., Maglathlin, R. L., McFarland, J. M., Miller, R. M., Frödin, M., and Taunton, J. (2012) Reversible targeting of noncatalytic cysteines with chemically tuned electrophiles. *Nat. Chem. Biol. 8*, 471–476.

(512) Loasby, A. E., Mordhorst, S., Kemper, F., Giurrandino, M., Schwarzer, N., Hofer, A., Jessen, H. J., Gerhardt, S., Einsle, O., Oyston, P. C. F., Andexer, J. N., and Roach, P. L. Substrate Recognition and Mechanism Revealed by Ligand-Bound Polyphosphate Kinase 2 Structures. *Manuscr. Prep.*

(513) Leipe, D. D., Koonin, E. V, and Aravind, L. (2003) Evolution and Classification of P-loop Kinases and Related Proteins. *J. Mol. Biol. 333*, 781–815.

(514) Plewczynski, D., Łaźniewski, M., Augustyniak, R., and Ginalski, K. (2011) Can we

trust docking results? Evaluation of seven commonly used programs on PDBbind database. *J. Comput. Chem. 32*, 742–755.

(515) Corbeil, C. R., and Moitessier, N. (2009) Docking Ligands into Flexible and Solvated Macromolecules. 3. Impact of Input Ligand Conformation, Protein Flexibility, and Water Molecules on the Accuracy of Docking Programs. *J. Chem. Inf. Model. 49*, 997–1009.

(516) Englebienne, P., and Moitessier, N. (2009) Docking Ligands into Flexible and Solvated Macromolecules. 4. Are Popular Scoring Functions Accurate for this Class of Proteins? *J. Chem. Inf. Model. 49*, 1568–1580.

(517) Adams, P. D., Afonine, P. V, Bunkóczi, G., Chen, V. B., Davis, I. W., Echols, N., Headd, J. J., Hung, L.-W., Kapral, G. J., Grosse-Kunstleve, R. W., McCoy, A. J., Moriarty, N. W., Oeffner, R., Read, R. J., Richardson, D. C., Richardson, J. S., Terwilliger, T. C., and Zwart, P. H. (2010) PHENIX: a comprehensive Python-based system for macromolecular structure solution. *Acta Crystallogr. Sect. D 66*, 213–221.

(518) Schrödinger, L. The PyMOL Molecular Graphics System, Version 1.8. LLC.

(519) Emsley, P., Lohkamp, B., Scott, W. G., and Cowtan, K. (2010) Features and development of Coot. *Acta Crystallogr. Sect. D 66*, 486–501.

(520) Garbett, N., and Chaires, J. (2012) Thermodynamic studies for drug design and screening. *Expert Opin. Drug Discov. 7*, 299–314.

(521) Retra, K., Irth, H., and van Muijlwijk-Koezen, J. E. (2010) Surface Plasmon Resonance biosensor analysis as a useful tool in FBDD. *Drug Discov. Today Technol. 7*, e181–e187.

(522) Zhang, Y.-L., and Zhang, Z.-Y. (1998) Low-Affinity Binding Determined by Titration Calorimetry Using a High-Affinity Coupling Ligand: A Thermodynamic Study of Ligand Binding to Protein Tyrosine Phosphatase 1B. *Anal. Biochem. 261*, 139–148.

(523) Sigurskjold, B. W. (2000) Exact analysis of competition ligand binding by displacement isothermal titration calorimetry. *Anal. Biochem. 277*, 260–266.

(524) Viegas, A., Manso, J., Nobrega, F. L., and Cabrita, E. J. (2011) Saturation-transfer difference (STD) NMR: A simple and fast method for ligand screening and characterization of protein binding. *J. Chem. Educ. 88*, 990–994.

(525) Meyer, B., and Peters, T. (2003) NMR Spectroscopy Techniques for Screening and Identifying Ligand Binding to Protein Receptors. *Angew. Chemie Int. Ed. 42*, 864–890.

(526) Krishnan, V. V. (2005) Ligand Screening by Saturation-Transfer Difference (STD) NMR Spectroscopy. *Curr. Anal. Chem. 1*, 307–320.

(527) Mayer, M., and Meyer, B. (2001) Group Epitope Mapping by Saturation Transfer Difference NMR To Identify Segments of a Ligand in Direct Contact with a Protein Receptor. *J. Am. Chem. Soc. 123*, 6108–6117.

(528) Jones, G. H., Taniguchi, M., Tegg, D., and Moffatt, J. G. (1979) 4'-Substituted nucleosides. 5. Hydroxymethylation of nucleoside 5'-aldehydes. *J. Org. Chem. 44*, 1309–1317.

(529) Blackburn, G. M., and Rashid, A. (1989) Enantiospecific syntheses of the methylene- and α-fluoromethylene-phosphonate analogues of 3-phospho-D-glyceric acid. *J. Chem. Soc., Chem. Commun.* 40–41.

(530) Stec, W. J. (1983) Wadsworth-Emmons reaction revisited. *Acc. Chem. Res. 16*, 411–417.

(531) Nagaoka, H., and Kishi, Y. (1981) Further synthetic studies on rifamycin s. *Tetrahedron 37*, 3873–3888.

(532) Boschelli, D., Takemasa, T., Nishitani, Y., and Masamune, S. (1985) Synthesis of amphotericin B. 2. fragment C-D of the aglycone. *Tetrahedron Lett. 26*, 5239–5242.

(533) Meanwell, N. A. (2011) Synopsis of some recent tactical application of bioisosteres in drug design. *J. Med. Chem. 54*, 2529–91.

(534) Bradford, M. M. (1976) A rapid and sensitive method for the quantitation of microgram quantities of protein utilizing the principle of protein-dye binding. *Anal. Biochem. 72*, 248–254.

(535) Green, A. A., and McElroy, W. D. (1956) Crystalline firefly luciferase. *Biochim. Biophys. Acta 20*, 170–6.

(536) Majed, N., Li, Y., and Gu, A. Z. (2012) Advances in techniques for phosphorus analysis in biological sources. *Curr. Opin. Biotechnol. 23*, 852–9.

(537) Ohtomo, R., Sekiguchi, Y., Kojima, T., and Saito, M. (2008) Different chain length specificity among three polyphosphate quantification methods. *Anal. Biochem. 383*, 210–216.

(538) Clark, J. E., and Wood, H. G. (1987) Preparation of standards and determination of sizes of long-chain polyphosphates by gel electrophoresis. *Anal. Biochem. 161*, 280–90.

(539) Aschar-Sobbi, R., Abramov, A. Y., Diao, C., Kargacin, M. E., Kargacin, G. J., French, R. J., and Pavlov, E. (2008) High Sensitivity, Quantitative Measurements of Polyphosphate Using a New DAPI-Based Approach. *J. Fluoresc. 18*, 859–866.

(540) Diaz, J. M., and Ingall, E. D. (2010) Fluorometric Quantification of Natural Inorganic Polyphosphate. *Environ. Sci. Technol. 44*, 4665–4671.

(541) Werner, T. P., Amrhein, N., and Freimoser, F. M. (2005) Novel method for the quantification of inorganic polyphosphate (iPoP) in Saccharomyces cerevisiae shows dependence of iPoP content on the growth phase. *Arch. Microbiol. 184*, 129–136.

(542) Rao, N. N., Liu, S., and Kornberg, A. (1998) Inorganic polyphosphate in Escherichia coli: the phosphate regulon and the stringent response. *J. Bacteriol. 180*, 2186–93.

(543) Ezawa, T., Cavagnaro, T. R., Smith, S. E., Smith, F. A., and Ohtomo, R. (2004) Rapid accumulation of polyphosphate in extraradical hyphae of an arbuscular mycorrhizal fungus as revealed by histochemistry and a polyphosphate kinase/luciferase system. *New Phytol. 161*, 387–392.

(544) Mullan, A., Quinn, J. P., and McGrath, J. W. (2002) A nonradioactive method for the assay of polyphosphate kinase activity and its application in the study of polyphosphate

metabolism in Burkholderia cepacia. *Anal. Biochem. 308*, 294–299.

(545) Baykov, A. A., Evtushenko, O. A., and Avaeva, S. M. (1988) A malachite green procedure for orthophosphate determination and its use in alkaline phosphatase-based enzyme immunoassay. *Anal. Biochem. 171*, 266–270.

(546) Zhou, X., and Arthur, G. (1992) Improved procedures for the determination of lipid phosphorus by malachite green. *Lipid Res. 33*, 1233–1236.

(547) Feng, J., Chen, Y., Pu, J., Yang, X., Zhang, C., Zhu, S., Zhao, Y., Yuan, Y., Yuan, H., and Liao, F. (2011) An improved malachite green assay of phosphate: Mechanism and application. *Anal. Biochem. 409*, 144–149.

(548) Sherwood, A. R., Paasch, B. C., Worby, C. a., and Gentry, M. S. (2013) A malachite green-based assay to assess glucan phosphatase activity. *Anal. Biochem. 435*, 54–56.

(549) Pegan, S., Tian, Y., Sershon, V., and Mesecar, A. (2010) A Universal, Fully Automated High Throughput Screening Assay for Pyrophosphate and Phosphate Release from Enzymatic Reactions. *Comb. Chem. High Throughput Screen. 13*, 27–38.

(550) Wu, Z. L. (2011) Phosphatase-Coupled Universal Kinase Assay and Kinetics for First-Order-Rate Coupling Reaction. *PLoS One* (Uversky, V. N., Ed.) *6*, e23172.

(551) Saunders, C. (2013) Burkholderia pseudomallei Exopolyphosphatase enzyme (BpPpx) purification and Malachite Green assay development. M.Chem Project Report, University of Southampton.

(552) Prinz, H. (2010) Hill coefficients, dose–response curves and allosteric mechanisms. *J. Chem. Biol. 3*, 37–44.

(553) Cheng, Y.-C., and Prusoff, W. H. (1973) Relationship between the inhibition constant (KI) and the concentration of inhibitor which causes 50 per cent inhibition (I50) of an enzymatic reaction. *Biochem. Pharmacol. 22*, 3099–3108.

(554) Lineweaver, H., and Burk, D. (1934) The determination of enzyme dissociation constants. *J. Am. Chem. Soc. 56*, 658–666.

(555) Cornish-Bowden, A. (1974) A simple graphical method for determining the inhibition constants of mixed, uncompetitive and non-competitive inhibitors. *Biochem. J. 137*, 143–144.

(556) Holdgate, G., Geschwindner, S., Breeze, A., Davies, G., Colclough, N., Temesi, D., and Ward, L. (2013) Biophysical methods in drug discovery from small molecule to pharmaceutical. *Methods Mol Biol. 1008*, 327–55.

(557) Genick, C. C., Barlier, D., Monna, D., Brunner, R., Bé, C., Scheufler, C., and Ottl, J. (2014) Applications of Biophysics in High-Throughput Screening Hit Validation. *J. Biomol. Screen. 19*, 707–714.

(558) Renaud, J.-P., and Delsuc, M.-A. (2009) Biophysical techniques for ligand screening and drug design. *Curr. Opin. Pharmacol. 9*, 622–628.

(559) Silvestre, H. L., Blundell, T. L., Abell, C., and Ciulli, A. (2013) Integrated biophysical approach to fragment screening and validation for fragment-based lead discovery. *Proc.*

Natl. Acad. Sci. U. S. A. 110, 12984–9.

(560) Turnbull, W. B., and Daranas, A. H. (2003) On the value of c: can low affinity systems be studied by isothermal titration calorimetry? *J. Am. Chem. Soc. 125*, 14859–66.

(561) Freire, E. (2004) Isothermal titration calorimetry: controlling binding forces in lead optimization. *Drug Discov. Today Technol. 1*, 295–299.

(562) Freyer, M. W., and Lewis, E. a. (2008) Isothermal Titration Calorimetry: Experimental Design, Data Analysis, and Probing Macromolecule/Ligand Binding and Kinetic Interactions, in *Methods in Cell Biology*, pp 79–113.

(563) Chaires, J. B. (2008) Calorimetry and Thermodynamics in Drug Design. *Annu. Rev. Biophys. 37*, 135–151.

(564) Rhodes, G. (2006) Crystallography Made Crystal Clear (Rhodes, G., Ed.) 3rd ed. Academic Press.

(565) Ducruix, A., and Giegé, R. (1999) Crystallization of Nucleic Acids and Proteins: a Practical Approach (Ducruix, A., and Giegé, R., Eds.) 2nd ed. Oxford University Press.

(566) Russo Krauss, I., Merlino, A., Vergara, A., and Sica, F. (2013) An Overview of Biological Macromolecule Crystallization. *Int. J. Mol. Sci. 14*, 11643–11691.

(567) Asherie, N. (2004) Protein crystallization and phase diagrams. *Methods 34*, 266–272.

(568) Ciuffreda, P., Casati, S., and Manzocchi, A. (2007) Complete1H and13C NMR spectral assignment of α- and β-adenosine, 2′-deoxyadenosine and their acetate derivatives. *Magn. Reson. Chem. 45*, 781–784.